Neurovascular Sonography

Wendy C. Ziai
Christy L. Cornwell
Editors

Springer

Neurovascular Sonography

Wendy C. Ziai • Christy L. Cornwell
Editors

Neurovascular Sonography

Springer

Editors
Wendy C. Ziai
Departments of Neurology
Neurosurgery, Anesthesiology
and Critical Care Medicine
The Johns Hopkins University
School of Medicine
Baltimore, MD, USA

Christy L. Cornwell
Neurosonology Consultant
Cardiovascular Ultrasound
Services, Inc.
Columbus, OH, USA

ISBN 978-3-030-96892-2 ISBN 978-3-030-96893-9 (eBook)
https://doi.org/10.1007/978-3-030-96893-9

This Springer imprint is published by the registered company Springer Nature Switzerland AG
The registered company address is: Gewerbestrasse 11, 6330 Cham, Switzerland

Foreword

Transcranial Doppler has been the forerunner neuroimaging modality long before CT scans and MRIs became the "go to" imaging for structural evaluation of the brain. TCDs and carotid ultrasound continue to be the "doctor's stethoscope for the brain," providing sophisticated physiological information about cerebrovascular hemodynamics complementing structural imaging. Over the last few years, our body of knowledge in neurosonology has dramatically expanded with the discovery of new clinical applications. This has pushed transcranial Doppler from being a technically burdensome cheaper alternative to vascular imaging into the mainstream of stroke and neurocritical care.

A decade ago, I had wandered into the neurocritical care unit as an eager fellow to begin my fellowship training in neuro critical care. Very few units had dedicated TCD programs at that time. I was curiously introduced to transcranial Doppler at the Cleveland Clinic, starting a journey leading to Wake Forest School of Medicine that has been at the forefront of neurovascular ultrasound education since 1974. As a young faculty, I had much to learn about intracranial hemodynamics and had no idea at that time how dramatically it would change my approach to evaluation of the brain in the coming years.

It has been delightful to see things changing considerably across the globe with regards to noninvasive evaluation of the brain across multiple clinical settings like intensive care, inpatient care, outpatient clinics, and perioperative monitoring. Neurovascular ultrasound has brought several clinical specialties under the same umbrella with focus towards reducing acute brain injury and

secondary brain injury prevention. The use of neuroultrasound has expanded from evaluation of classical cerebrovascular diseases to critical care and other medical diseases like traumatic brain injury, sepsis, infective endocarditis, and post-cardiac arrest management. No longer is TCD viewed as a harmless distraction, but rather as a tool, which takes advantage of the major assets of ultrasound – portability, cost-consciousness, and flexibility – for serial examination, giving us new perspectives into mechanisms of brain injury, serving as a true window to the brain.

Most academic centers now have or want a neurovascular ultrasound program. There is a formal certification in neurovascular ultrasound allowing physicians the designation of Registered Physician in Neurovascular Interpretation (RPNI), and nonphysician providers the designation of Neurovascular Specialist (NVS). Many critical care ultrasound educational resources and guidelines now introduce neuroultrasound as a core skill for the general intensivist, encouraging further education. Our integrated ultrasound curriculum at Wake Forest School of Medicine now includes transcranial Doppler to get medical students excited about the brain and teach cerebrovascular physiology.

Neurovascular Sonography is designed to fill this important niche. It is comprehensive in scope with the objective of providing a practical reference that focuses on basic interpretation and state-of-the-art guidance for using TCD in clinical decision-making for patients at risk of brain injury. We hope this book triggers further education and investigation in your clinical evaluation since there is much to be learned about the brain through cerebrovascular ultrasound. We are indebted to the authors for facilitating this work and convey our sincere gratitude to Dr. Wendy Ziai and Christy Cornwell, BS, NVS, RVT, for leading this effort as editors.

Aarti Sarwal, MD, FNCS, FAAN, FCCM, RPNI
Professor, Neurology, Section Chief
Neurocritical Care, Medical Director, Neurocritical Care Unit
Atrium Wake Forest School of Medicine
Winston-Salem, NC, USA

Preface and Acknowledgments

Neurosonology has come of age in the era of critical care ultrasound and is now considered as a separate discipline with applications continuing to expand both for the inpatient and outpatient setting and for a wide variety of neurological conditions. Transcranial Doppler provides a unique diagnostic tool which is dynamic and complex, requiring mastery of ultrasound techniques and interpretation, but which is within the grasp of any healthcare provider who has a curiosity for how ultrasound can be used to interpret cerebral hemodynamics and improve the management of cerebrovascular disease.

This book represents the culmination of an idea originally discussed during the 2019 meeting of the Neurocritical Care Society. It was then apparent that there was no comprehensive handbook of neurosonology for clinicians that could be utilized as a bedside reference for technicians and providers. This work was initially envisioned as a true handbook, and is now condensed in an over 500 page textbook to encompass the rapidly growing volume of neurosonology information over the past few decades. Our goal is to provide a practical source of pertinent information, particularly for those beginning their investigation into this fascinating field.

We are indebted to the commitment and efforts of many professionals who contributed significantly to the completion of this book. This work would not have been possible without the dedication and love for teaching of each of our esteemed colleagues who contributed chapters to this work. We would like to especially thank Bahattin (Bobby) Ergin, RVT, for his invaluable help with illustrations and organizational tasks. We owe enormous appreci-

ation to our publishers at Springer, particularly our editor Josephine Fabiola whose patience and support were so essential to the preparation of this book. Finally, we bestow our deepest gratitude to our spouses and children who provided continual encouragement and support and without whom this work would not have been possible.

Baltimore, MD, USA — Wendy C. Ziai, MD, MPH
Columbus, OH, USA — Christy L. Cornwell, BS, NVS, RVT

Contents

Contributors

Francisco Abecasis, MD, PhD Pediatric Intensive Care Unit, Centro Hospitalar Universitário Lisboa Norte, Hospital de Santa Maria, Lisbon, Portugal

Andrei V. Alexandrov Department of Neurology, University of Tennessee Health Science Center, Memphis, TN, USA

John Bennet Department of Neurology, Wake Forest School of Medicine, Winston-Salem, NC, USA

Jan Bittar Division of Cerebrovascular Diseases and Neurocritical Care, Department of Neurology, The Ohio State University, Columbus, OH, USA

Creagh Boulger Department of Emergency Medicine, The Ohio State University Wexner Medical Center, Columbus, OH, USA

Eder Caceres Translational Science in Infectious Disease and Critical Care Research Group, Clínica Universidad de La Sabana, Chía, Cundinamarca, Colombia

Danilo Cardim Department of Neurology and Neurotherapeutics, University of Texas Southwestern Medical Center, Dallas, TX, USA

Armando Mario Cacciatori Castro National Institute of Donations and Transplants, Clinic Hospital, Montevideo, Uruguay

Toufic Chaaban Division of Stroke and Neurocritical Care, Department of Neurology, The Ohio State University, Columbus, OH, USA

Christy L. Cornwell, BS, NVS, RVT Neurosonology Consultant, Cardiovascular Ultrasound Services, Inc., Columbus, OH, USA

William K. Cornwell III Medicine-Cardiology, Advanced Heart Failure, LVAD and Cardiac Transplant, Wilderness and Environmental Medicine, University of Colorado Anschutz Medical Campus, Aurora, CO, USA

William K. Cornwell Cardiovascular Ultrasound Services, Inc., Columbus, OH, USA

Colleen Douville Swedish Vascular Ultrasound, Swedish Neuroscience Institute, Swedish Health Services, Seattle, WA, USA

Richard Genova Neurovascular Ultrasound Laboratory, Weill Cornell Medicine—New York Presbyterian Hospital, New York, NY, USA

Alwyn Gomez Section of Neurosurgery, Department of Surgery, Rady Faculty of Health Sciences, University of Manitoba, Winnipeg, MB, Canada

Deepak Gulati The Ohio State University Wexner Medical Center, Columbus, OH, USA

Ryan Hakimi Neuro ICU and TCD Services Prisma Health-Upstate, Department of Medicine (Neurology) University of South Carolina School of Medicine-Greenville, Greenville, SC, USA

Yousef Hannawi Division of Cerebrovascular Diseases and Neurocritical Care, Department of Neurology, The Ohio State University, Columbus, OH, USA

Megan F. Hunt School of Medicine, Johns Hopkins, Baltimore, MD, USA

Omar Hussein University of New Mexico, Albuquerque, NM, USA

Kerri L. LaRovere Department of Neurology, Boston Children's Hospital and Harvard Medical School, Boston, MA, USA

Shraddha Mainali Department of Neurology, Virginia Commonwealth University, Richmond, VA, USA

Nicole F. O'Brien Department of Pediatrics, The Ohio State University/Nationwide Children's Hospital, Columbus, OH, USA

Amanda K. Phillips Vascular Sonographer Sr., Vascular Lab, Prisma Health–Upstate, Greenville, SC, USA

Pirouz Piran Departments of Neurology, Neurosurgery, Anesthesiology and Critical Care Medicine, Johns Hopkins University, Baltimore, MD, USA

Larry N. Raber RMDS-RVT Clinical Manager Ultrasound-Neurovascular Laboratory, Imaging Institute, Cleveland Clinic, Cleveland, OH, USA

Alexander Razumovsky TCD Global, Inc., York, PA, USA

TCD Consultant, SpecialtyCare, Inc., Brentwood, TN, USA

Becky J. Riggs Department of Anesthesiology and Critical Care, Division of Pediatric Anesthesiology & Critical Care Medicine, Charlotte Bloomberg Children's Center, Baltimore, MD, USA

Oregon Health Science University, Doernbecher Children's Hospital, Portland, OR, USA

Brenda Rinsky Neurovascular Ultrasound Laboratory, Department of Neurology, Cedars-Sinai Medical Center, Los Angeles, CA, USA

Lucia Rivera-Lara Division of Neurosciences Critical Care, Department of Neurology and Neurosurgery, Anesthesia and Critical Care Medicine, Johns Hopkins University School of Medicine, Baltimore, MD, USA

Mark N. Rubin Neurology, University of Tennessee Health Science Center, Memphis, TN, USA

Aarti Sarwal Neurology, Neurocritical Care, Wake Forest Baptist Medical Center, Winston Salem, NC, USA

Varun Shah College of Medicine, The Ohio State University Wexner Medical Center, Columbus, OH, USA

Sanjeev Sivakumar USC School of Medicine-Greenville, Greenville, SC, USA

Tamara Strohm Neurology, The Ohio State University Wexner Medical Center, Columbus, OH, USA

Pam Young Vascular Lab Services, Prisma Health–Upstate, Greenville, SC, USA

Frederick A. Zeiler Section of Neurosurgery, Department of Surgery, Rady Faculty of Health Sciences, University of Manitoba, Winnipeg, MB, Canada

Department of Human Anatomy and Cell Science, Rady Faculty of Health Sciences, University of Manitoba, Winnipeg, MB, Canada

Biomedical Engineering, Faculty of Engineering, University of Manitoba, Winnipeg, MB, Canada

Division of Anaesthesia, Department of Medicine, Addenbrooke's Hospital, University of Cambridge, Cambridge, UK

Wendy C. Ziai, MD, MPH Departments of Neurology, Neurosurgery, Anesthesiology and Critical Care Medicine, The Johns Hopkins University School of Medicine, Baltimore, MD, USA

Principles of Transcranial Doppler Sonography

Andrei V. Alexandrov and John Bennet

Introduction

Instruments used to perform Transcranial Doppler (TCD) come in a variety of configurations and degrees of complexity. All utilize *pulsed-wave* Doppler technology alone (TCD) or, in combination with real-time B-mode imaging, what we will refer to as Transcranial Color Doppler Imaging (TCDI). While each has features which render the modality particularly well suited for certain applications, by far, the most commonly used outputs provided by transcranial Doppler instruments are the *audible sound* and the *FFT spectral waveform. These are the result of* processing *Doppler shift* information from a *single sample volume (gate)* placed along an *ultrasound beam*. The time averaged mean of the maximum velocity envelope (TAMM, TAMV, Mean) and the pulsatility index (PI) are the values most widely used clinically.

A. V. Alexandrov
Department of Neurology, University of Tennessee Health Science Center, Memphis, TN, USA

J. Bennet (✉)
Department of Neurology, Wake Forest School of Medicine, Winston-Salem, NC, USA
e-mail: jbbennet@wakehealth.edu

W. C. Ziai, C. L. Cornwell (eds.), *Neurovascular Sonography*,
https://doi.org/10.1007/978-3-030-96893-9_1

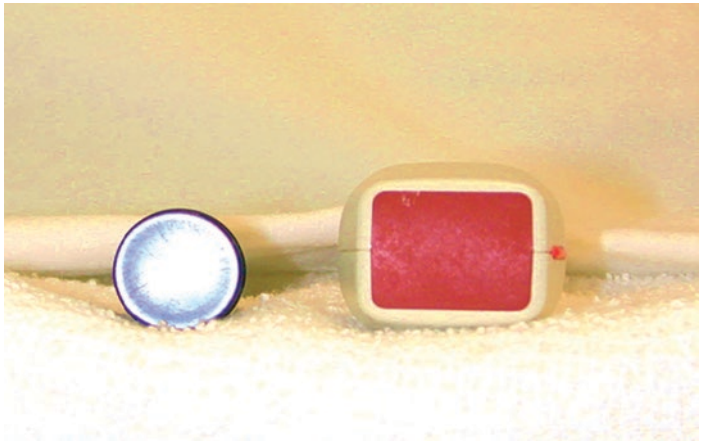

Fig. 1 Transducers used in performing TCD (left) and TCDI (right). (Photo courtesy of Charles H Tegeler)< MD, RPNI

The *pulsed* ultrasound beam may be generated in one of two ways: (1) by means of a single element mechanically focused transducer or; (2) by means of a multi-element, electronically steered and focused transducer (Fig. 1).

In either case, a *piezoelectric* material within the transducer is excited by a *voltage* determined by a user adjustable *transmit power* or, as it is commonly labelled, *Power.* It is this *power* which will determine the *amplitude of the transmitted ultrasound and*, in combination with beam area, spatial *pulse length (SPL)* and *pulse repetition frequency (PRF)* (kHz), which will determine the *intensity* of the ultrasound energy delivered into the body.

In the case of a single element transducer, the size and shape of the ultrasound beam is determined by the diameter, frequency and focus of the transducer and the direction of propagation is perpendicular to the transducer surface. The *excitation voltage* as determined by the Power setting is delivered by the *pulser.*

In comparison, a multi-element transducer beam is significantly more complex. The shape and direction of the sound beam

is determined by the shape or type of transducer (linear, sector, convex) and the *beam former. The beam former is responsible for coordination of the recruitment, delay and excitation of groups of tiny piezoelectric elements within the transducer.* The ultrasound beam is not always perpendicular to the transducer surface. The excitation voltage is still delivered by the *pulser,* which in this case, is incorporated into the *beam former.* Such instruments are capable of producing two-dimensional real-time B-mode and color Doppler images.

Additional methods for processing *Doppler shift* information will be discussed in more detail later in this chapter and those which follow. First, however, attention will be directed toward obtaining and processing Doppler shift information using a single ultrasound beam with a single gate.

It is the purpose of this chapter to present a practical review of the physical principles of ultrasound and more specifically, Doppler ultrasound. For a more comprehensive review of the subject material the reader is referred to several textbooks dedicated to this subject [1–5].

Ultrasound

Special thanks: Several of the concepts presented in this chapter are adapted from Kremkau [1] with permission.

Ultrasound is sound consisting of frequencies higher than the range of human hearing. The audible range commonly used in textbooks is:

$$> 20\,\text{Hz to} < 20\,\text{kHz}$$

Sound of frequencies greater than 20 kHz is described as *ultrasound*. Sound of frequencies less than 20 Hz is described as *infrasound*.

It is much to the benefit of those of us who use Doppler ultrasound that *Doppler shift* frequencies from moving blood fall within the *audible range.* Many experienced sonographers con-

sider the audible signal the key to performing the TCD examination.

A basic understanding of the nature of sound waves and the terminology used when describing them is essential to the art and science of sonography.

Sound

Sound is a *mechanical compressional wave* which travels through a medium in a series of repeating variations consisting of *pressure*, *density*, *temperature* and *particle motion*. Referred to as *acoustic variables,* their movement through a medium, in our case human tissue, results in a pushing and pulling or *vibrating* effect. Positive amplitude or peaks correspond to regions of high density or *compression* while negative amplitude or troughs correspond to regions of low density or *rarefaction.* Zero amplitude corresponds to an *undisturbed* state. Sound is also described as a *longitudinal wave* because the acoustic variables travel parallel to the direction of wave propagation.

Acoustic Variables **include:**

- Pressure
- Density
- Temperature
- Particle Motion

Wave Parameters (Fig. 2)

Wave parameters are terms used to describe waves.

- *Cycle*

Each complete repetition of the wave process as it transitions from zero to peak positive; back to zero; to peak negative; and, back to zero constitutes a *cycle.* The cycle is an important parameter as *pulses* are comprised of cycles.

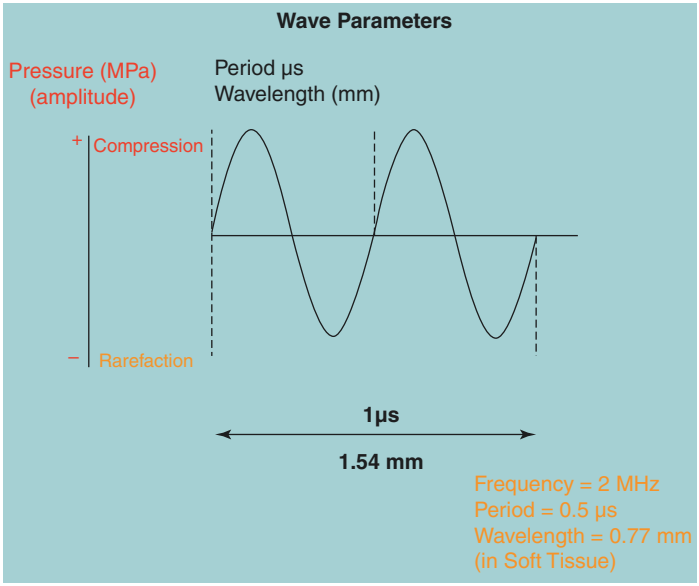

Fig. 2 Wave parameters include frequency, wavelength, period and amplitude. One complete wave from any point to the same point on the following wave represents 1 *cycle*

- *Frequency*

The number of cycles which occur in 1 second determines the *frequency of the wave* and is expressed in units of hertz (Hz). One cycle per second equals 1 Hz.

In ultrasound, the units most often used are kilohertz and megahertz.

$$\text{One kilohertz}\,(\text{kHZ})\,\text{equals}\,1,000\,\text{Hz}.$$
$$\text{One megahertz}\,(\text{MHz})\,\text{equals}\,1,000,000\,\text{Hz}.$$

- *Wavelength*

Wavelength λ (mm) is the *distance* over which 1 cycle occurs (mm). Wavelength may be measured from any point along a wave

cycle to that same point upon an adjacent wave cycle. Wavelength is a distance measurement.

Wavelength (λ) (mm) = *c* (*mm*/(*μs*))/*f* (*MHz*) where *c* is the propagation speed of sound. For our purposes, *c* is the propagation speed of sound in *soft tissue*, 1540 m/s or *1.54 mm/μs*. The latter results in simplification of units of expression. For example, the wavelength of a 2 MHz transducer as is commonly used in transcranial Doppler is:

$$wavelength = \frac{c}{f}\frac{\frac{uS}{mm}}{MHz} = \frac{1.54\frac{uS}{mm}}{2\,MHz} = 0.77\,\text{mm}$$

As frequency increases the wavelength decreases. Resolution, both axial and lateral, increases at the expense of penetration which decreases.

- *Period*

Period (T) (μS) is the *time* which it takes to complete one cycle. The period of a wave is in units of time what the wavelength is in units of distance. For our 2 MHz wave:

$$\mathrm{T}(\mu s) = \frac{1}{f\,MHz} = \frac{1}{2\,MHz} = 0.5\,us$$

- *Amplitude*

Amplitude is the vertical deviation of a wave *from zero* or the height of the wave. Amplitude is most often expressed as pressure in units of megapascals (MPa). However, it is applicable to the other *wave variables* as well. Amplitude may be expressed as:

$$maximum\ positive - maximum\ negative\ /\ 2$$

Propagation Speed

P*ropagation speed* is the speed at which a wave travels through a medium. Propagation speed is determined by the medium, primarily its *stiffness*. The *stiffer* or less compressible the medium, the faster the sound travels through it. In general, sound travels faster in solids than liquids and faster in liquids than gases. Or, in anatomical terms, ultrasound waves travel faster through bone than soft tissue and faster through soft tissue than lung (or air). Units for expressing propagation speed include meters per second (m/s) and millimeters per microsecond (mm/μs).

An appreciation of propagation speed is necessary to understanding ultrasound and how ultrasound devices work. The propagation speed in soft tissue, and that assumed by ultrasound devices, is 1540 m/s. Kremkau [1] reduces this to 1.54 μs/mm which results in simplification of units as we will see later.

As will be discussed next, *propagation speed* also plays a significant role in determining the *acoustic impedance* of a tissue and thus the *amplitude* of echoes returning from tissue boundaries or *interfaces*.

Impedance

Acoustic impedance (z) is a function of a tissue's *density (kg/m^3)* times the *propagation speed (m/s)* or,

$$z = p \times c\left(\text{expressed in units of } \textit{rayls}\right)$$

The average acoustic impedance of *soft tissue is 1,630,000 rayls (K).*

Acoustic impedance is an important concept because it is the differences in "z" or, *impedance mismatches,* which, along with *intensity* and *angle of incidence*, determine the amplitudes (inten-

sities) of echoes returning to the transducer and those continuing to propagate. The reflected intensity can be calculated as follows:

$$\mathrm{IRC} = \frac{Ir}{Ii}\frac{\left(\frac{mW}{cm^2}\right)}{\left(\frac{mW}{cm^2}\right)} \times \left(z1 - z2 / z1 + z2\right)^2 .$$

where IRC is the *intensity reflection coefficient*, IR is the reflected intensity, Ii is the incident intensity, z1 is the acoustic impedance of the first medium and z2 is the acoustic impedance of the second medium.

Since IRC + ITC (intensity transmission coefficient) = 100% (incident intensity):

$$\mathrm{ITC} = 1 - \mathrm{IRC}$$

In imaging, the amplitudes of echoes returning to the transducer are displayed as different shades of gray or *brightness* in B-mode imaging. B-mode is excellent at differentiating between adjacent tissues with even small differences in acoustic impedance. It is this capability which results in B-mode imaging being a useful tool for identifying tissue boundaries and textures encountered during imaging of the carotid arteries including plaque features and thrombus.

The role of acoustic impedance in Doppler is usually less obvious than in imaging, the important exception being in *emboli detection*. It is the differences in impedance between blood and embolic materials (gaseous and solid) which result in significant differences in the amplitude of echoes and in the audible signal. Emboli detection will be discussed in detail in chapter "Monitoring for Emboli Detection (Without and With Microbubbles)". Otherwise, in Doppler, aside from the interface between the intima and blood, acoustic impedance contributes to attenuation, primarily as a result of interface(s) with bone.

Reflection and Scatter

At an interface a portion of the *incident* wave is *reflected* or *scattered* back toward the transducer (or refracted) while a portion is

transmitted onward along the same or altered path at an intensity reduced by the amount reflected or scattered. The extent to which the ultrasound is reflected back along the same path is determined by the angle of the *incident* wave relative to the interface, the angle of incidence.

Reflection, especially *specular reflection*, requires that the boundary of an interface be oriented perpendicular to the incident wave. A beneficial example of specular reflection is the common carotid artery oriented perpendicular to the sound beam on the display to allow measurement of intimal-medial thickness. A not so beneficial example would be a TCD transducer positioned on the skin perpendicular to the temporal bone resulting in reflection approaching 100%. This is one of the reasons a small amount of angle between the transducer and the temporal bone can be helpful in achieving a signal.

The majority of tissue interfaces, however, are not aligned perpendicular to the incident sound wave but at some angle. The paths of the reflected waves and transmitted waves are determined by *the reflection angle* and *the transmitted angle,* respectively.

The intensity at which the wave is reflected or transmitted is determined by the *impedance mismatch* of the interface tissues as determined by the *intensity reflection coefficient* and *intensity transmission coefficient*, respectively. If there is no impedance mismatch, meaning the impedances are equal on either side of an interface, there is no reflection. However, there may be scattering.

Refraction refers to redirection of a transmitted wave as a result of oblique angle of incidence and different propagation speeds on either side of an interface. Refraction can result in artifacts within images.

Scattering

Scattering occurs at interfaces which are small relative to the wavelength of the ultrasound and, or have non-uniform surfaces (*scatterers*). As the term implies, scattering occurs in many directions. Echoes scattered back in the direction of the incident beam are termed *backscatterers*. Unlike specular reflection, scattering is not as dependent on the angle of incidence. Such interfaces are

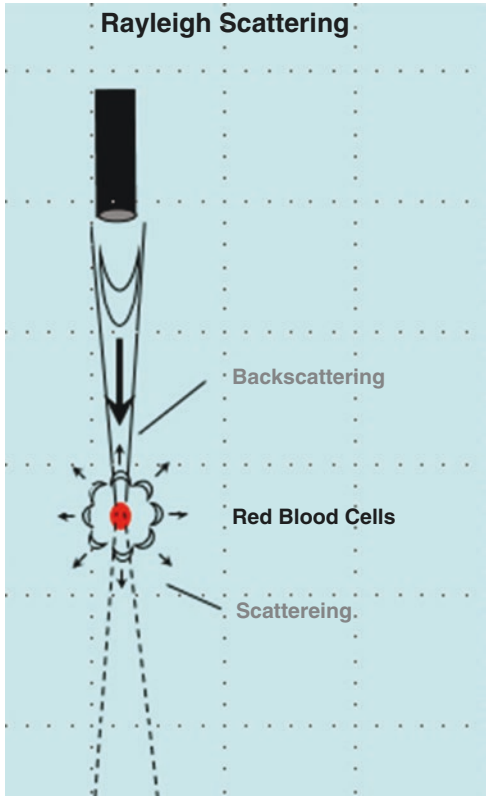

Fig. 3 Scattering

common in diagnostic ultrasound as they include echoes from organ parenchyma as well as blood (Fig. 3)

In the case of blood, the scatterers are predominantly red blood cells *(RBCs)* suspended in plasma, the concentration of which is described by the *hematocrit*. The amount of "backscatter" and, therefore the intensity of the returning echoes, is determined by the volume of RBCs within the sample volume and the impedance mismatch between the blood and the intima. The small size of these scatterers relative to the wavelength of the ultrasound beam and their non-uniform distribution result in their being described as *Rayleigh scatterers,* the same phenomenon responsible for the blue of the sky.

The intensity of backscattered echoes is proportional to frequency to the fourth power. In imaging, it is not unusual to visualize spontaneous echo contrast using transducer frequencies in the 10 MHz range and higher. However, with lower frequency transducers such as 2 MHz used in TCD, the result is weak backscatter, compounding the challenge which already exists due to high attenuation.

Introduction to Doppler Ultrasound

Doppler instruments generate either continuous wave (CW) or pulsed-wave (PW) ultrasound or both. In CW Doppler, the transducer consists of two crystals with one transmitting continuously and the other receiving continuously. The focus is determined by the crossing points of the two beams.

Pulsed-wave Doppler uses a single beam to both transmit and receive. The transducer may be in the form of a single large element (TCD) or many small ones acting together (TCDI) to form the ultrasound beam (Fig. 4).

Frequencies used for Doppler ultrasound are lower than those used for imaging. Lower frequency results in less rapid attenuation which results in better sensitivity at depth and less aliasing in comparison with higher frequencies. As previously mentioned, 2 MHz is commonly used for transcranial Doppler although frequencies as low as 1 MHz are sometimes used. Frequencies as high as 20 MHz may be used intraoperatively where the transducer is in direct contact with the vessel such as during open repair of cerebral aneurysms.

Transducer

The source of ultrasound is the transducer. Ultrasound transducers incorporate a piezoelectric material meaning it changes shape when an electrical voltage is applied. The transducer functions to convert electrical voltages into mechanical vibrations and mechanical vibrations into electrical voltages. The frequency of the sound produced depends on the type and thickness of the crystal. Performance is optimized by the use of damping and matching

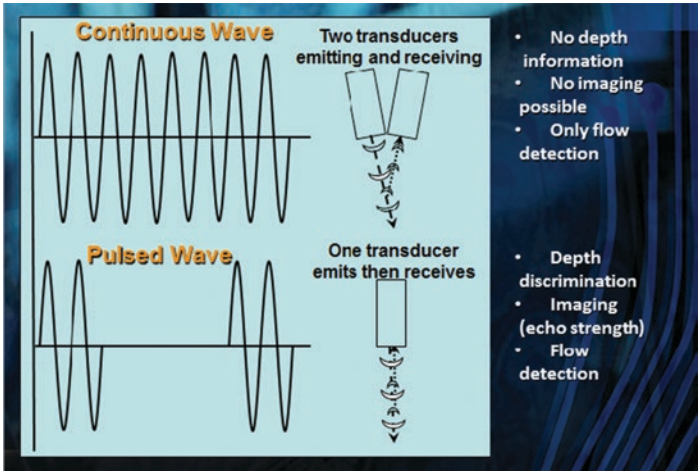

Fig. 4 *Continuous wave (CW) Doppler* consists of two piezo-electric components, one of which is *transmitting* and one of which is *receiving* continuously, hence the name. *Pulsed wave (PW) Doppler* utilizes one piezo-electric component which both transmits and receives and is a *sampling* technique. The rate at which sampling takes place is determined by the *pulse repetition frequency (PRF).* Transcranial Doppler and most vascular applications of Doppler utilize the pulsed wave technique. (With permission, Alexandrov AV. *Neurovascular Ultrasound Examination*. Wiley: 2013)

layers in back and in front of the piezoelectric element, respectively. The damping layer acts to *dampen* or shorten the pulse. While a shorter pulse improves image resolution it also dampens amplitude resulting in reduced sensitivity to weak scatterers which is not desirable in Doppler. Most TCD instruments utilize undampened transducers. The *matching layer* serves to adapt the impedance of the transducer to that of the skin. Use of an aqueous based gel provides coupling to the skin which along with a reasonable amount of pressure acts to maximize energy transfer.

- **Pulser/Receiver**

The transducer is connected to both a *pulser* and a *receiver*. The pulser and transducer function together on the transmit side

of the ultrasound beam while the transducer and receiver work in combination on *the receive side.* The *pulser* delivers the appropriate voltage at the resonant frequency to drive the piezoelectric crystal(s) in the transducer. The *receiver* amplifies and measures the returning echoes and, in the case of Doppler instruments, compares them with the transmitted pulse in determining frequency, amplitude and phase (direction).

Ultrasound Beam

In the case of *pulse echo imaging* and *pulsed-wave Doppler*, the transducer is the source of *pulses* or *bursts* of ultrasound cycles interspersed with periods of no ultrasound or listening. For imaging, the pulses consist of 1–3 pulses while for Doppler they consist of 2–30 pulses. This *stream of pulses* results in a three dimensional beam of ultrasound. The *near zone length* (NZL or Fresnel zone) of this beam originates from the transducer with an area equal to the transmitting element(s). The beam converges at the depth at which the beam is *focused, either mechanically or electronically*. The diameter of the beam at any given depth is referred to as the *beam width.* The beam width and area are smallest at the focus, approximating half that at the transducer. The far zone *length* (FZL or Fraunhofer zone) diverges from the focal point returning to the original beam width at a depth approximately 2× that of the focal depth or near zone length. In water, in which the characteristics of ultrasound beams are typically measured, the intensity of the beam will be greatest at the depth where the area is smallest, at the focus. Intensity is expressed as:

$$I\left(mw/cm^2\right) = Power\left(mw\right)/Area\left(cm^2\right)$$

Intensity is expressed in many ways. The measure most commonly cited and by which ultrasound devices are regulated is Ispta where *sp* is the spatial peak (the highest intensity across the beam, usually in the center) and *ta* is temporal average, the average of all intensities within the pulse including the pulse repetition period (PRP) or, "listening time," during which no pulses are being gener-

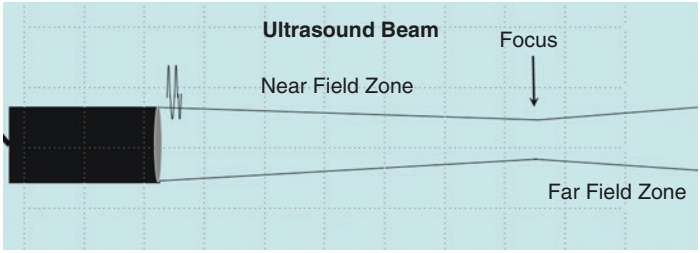

Fig. 5 The ultrasound beam consists of a *near field (Fresnel)* and a *far field (Fraunhofer)*. Typically, the *intensity* of the ultrasound beam is greatest at the focus where the beam area is smallest. This is not always the case, however, with TCD due to the high attenuation coefficient of bone

ated. In vivo, and as is certainly the case with transcranial Doppler, the maximum intensity is often found closer to the transducer where amplitude is highest and before significant attenuation has occurred (despite the larger beam diameter) (Fig. 5).

Attenuation

Attenuation is the weakening in the *amplitude* and *intensity* of a sound wave as it propagates. Attenuation is expressed using a logarithmic scale and is expressed in units of decibels (dB).

Processes contributing to attenuation include *absorption, reflection, refraction and scattering*. *Absorption* involves the conversion of mechanical energy to heat and accounts for the majority of attenuation. It will be discussed again later as it is important in safety.

Attenuation is dependent upon both the *source* and the *medium*. An example of the *source* contributing to attenuation is *frequency.* Attenuation increases with increasing *frequency.* For this reason, as frequency increases, penetration decreases.

The amount of attenuation which occurs per centimeter is termed the *coefficient of attenuation (ac)* and is expressed in units of decibels per centimeter (dB/cm). The coefficient of attenuation is different for different tissues and frequencies. The average coefficient of attenuation (dB/cm) in soft tissue is approximately equal to one-half of the frequency. Therefore, the coefficient of

attenuation (ac) for our 2 MHz wave traveling through soft tissue is approximately:

$$\text{ac} = 2\,MHz / 2 = 1\,dB / cm$$

To calculate attenuation, the attenuation coefficient is multiplied by the path length:

$$a\left(dB\right) = ac\left(\frac{dB}{cm}\right) \times L\left(cm\right)$$

Attenuation of 3 dB corresponds to a reduction of *intensity* of 50% while 10 dB is equivalent to a 90% reduction in *intensity* [1]. In other words, in soft tissue, our 2 MHz wave could reach our 5 cm focal depth, which is approximately the mid M1 segment, and return to the transducer at 10% of its original intensity.

However, attenuation is much higher in bone (and air) than in soft tissue. In the case of transcranial Doppler performed through the temporal window (and, to a lesser extent other windows), the sound waves must pass through thin portions of bone in both directions. The coefficient of attenuation (ac) for a 2 MHz wave passing through bone is approximately 20 dB/cm or 2 dB/mm. A tendency toward increasing amounts of air within the temporal squama with increasing age and osteoporosis further complicates calculation. It becomes readily apparent why a population dependent percentage of individuals have inadequate temporal *windows for insonation. Temporal window thickness greater than 3.6 mm or 2.9 mm and heterogeneous have been reported to be associated with inadequate or absent temporal windows* [6, 9].

Methods of Compensating for Attenuation

Fortunately, transcranial Doppler and diagnostic ultrasound in general tends to outperform theoretical limitations.

As previously discussed, attenuation increases with frequency. Therefore, using a *lower frequency* is one method to compensate for attenuation.

As previously described, intensity is the amplitude of the wave divided by the area of the ultrasound beam and amplitude is determined by the *power* output of the instrument. Fifty percent (−3 dB) of a "stronger" ultrasound beam is greater than fifty percent of a

"weaker" ultrasound beam. The use of higher acoustic output is another method for compensating for the attenuation coefficient encountered with transcranial Doppler. However, higher amplitude and intensity are associated with increased safety concerns in the form of bioeffects (see Safety and Amplitude and Intensity).

Gain is yet another tool for compensating for attenuation. Gain amplifies the signals returning to the receiver. It is analogous to volume on your radio. The caveat with Gain is that, if the signal is weak (poor signal-to-noise) both are amplified equally. Increasing the Gain can be useful in helping to find a signal. Unlike Power, increasing the Gain does not affect the amplitude or intensity of the ultrasound beam.

In addition to overall gain, imaging instruments are equipped with *Time Gain Compensation* (*TGC*) which allows for selective amplification or suppression of echoes returning from various depths along the sound beam. TGC allows the sonographer to fine tune the image such that echoes from like tissues (z) are displayed at the same brightness.

Doppler Effect

The *Doppler Effect* is the change in the observed frequency of a wave due to *motion*. There are variations depending on whom or what is doing the moving.

Blood as Moving Scatterers

For our purposes, the Doppler shift is a change in frequency between the transmitted or *operational frequency* of the ultrasound transducer and the frequency of echoes returning to the transducer from the motion of blood (see Scatterers, Rayleigh).

The Doppler shift frequency (fD) is the difference between the *operational frequency* (fo) and the *received frequency* (frequencies, actually) (fR):

$$\mathrm{fD}\left(\mathrm{kHz}\right) = fR\left(MHz\right) - \mathrm{fo}\left(\mathrm{MHz}\right)$$

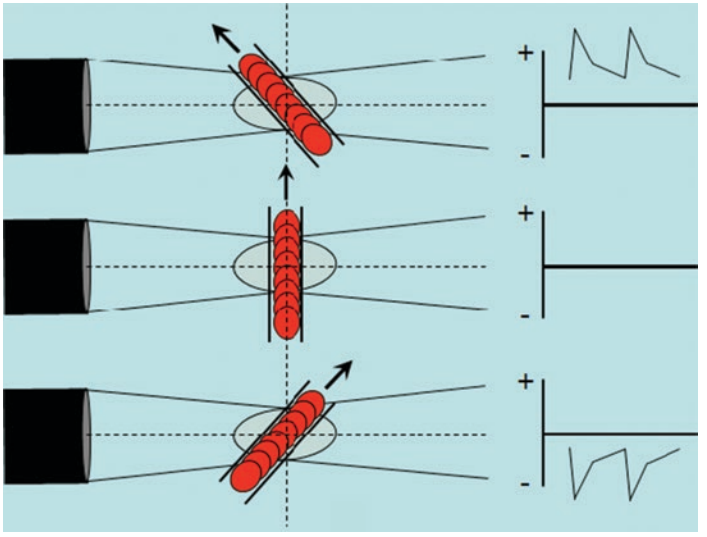

Fig. 6 Top: The scatterers are moving relatively toward the ultrasound beam resulting in a positive *Doppler shift* or, fR > fo. Middle: At an *angle of 90°*, motion is neither toward nor away relative to the ultrasound beam resulting in no *Doppler shift* or, fo = fR. Bottom: The scatterers are moving away relative to the ultrasound beam resulting in a negative Doppler shift or, fR < fo. (With permission, Alexandrov AV. *Neurovascular Ultrasound Examination*. Wiley: 2013)

The *operating frequency (fo)* and the *received* frequenc(ies) (fR) are within the megahertz range. *Doppler shift frequencies* (fD) are within the kilohertz range and audible range of human hearing.

If the received frequency (fR) is greater than the operational frequency it is considered a positive Doppler shift. If the Doppler shift frequency is less than the operational frequency it is considered to be a negative Doppler shift. If there is no difference detected between the operating frequency and the received frequency, as is the case when there is no motion relative to the direction of propagation of the ultrasound beam, there is no Doppler shift (Fig. 6).

Table 1 Examples of Doppler Shift frequencies and velocities commonly encountered in TCD

fo (MHz)	fR (MHz)	Doppler Shift (KHz)	Velocity (cm/s)
2.0	2.0013	+1.3	+50
2.0	2.0026	+2.6	+100
2.0	2.0052	+5.2	+200

The received frequencies are higher than the transmitted frequency of 2 MHz resulting in these being positive Doppler shifts. The Doppler shift frequency is proportional to speed. Assuming angle of 0°, the *direction* of motion is directly toward the transducer and is displayed as a velocity

Doppler Equation

For a moving scatterer such as blood, assuming an angle of *zero degrees* (cosine θ = 0), the equation is:

$$fD\left(kHz\right) = fo\left(kHz\right) \times 2 \times \frac{v\left(\frac{cm}{s}\right)}{\frac{cm}{s}}$$

Rearranging to place velocity on left and using the speed of sound in tissue and appropriate units [1], results in the following simplified equation:

$$\mathrm{v}\left(\mathrm{cm}/\mathrm{s}\right) = \frac{77\left(\frac{cm}{ms}\right) \times f\left(D\right)\left(KHz\right)}{f\left(\mathrm{o}\right)\left(MHz\right)}$$

Examples of Doppler shifts and corresponding velocities commonly found in TCD are found in (Table 1). A zero degree angle of insonation is assumed.

Doppler Angle

The term "relative" to the ultrasound beam was used previously because, unlike the example above, in which the direction of blood flow is directly toward the transducer (0°), blood flow is not always

directly toward or away from the ultrasound beam but at an angle (θ). The angle at which the ultrasound beam intersects with the moving blood is termed the *angle of insonation*. When the angle of insonation is not zero, that is, neither directly toward nor away from the direction of the transmitted sound waves, the Doppler shift is not maximum. In order to "correct" for the resulting underestimation, the cosine of the angle of insonation (θ) is introduced into the Doppler Equation in order to calculate what the Doppler shift would be if the angle of insonation were zero. Angle correction is routinely used in carotid duplex and other vascular applications.

Rewriting the Doppler Equation to "correct" for an angle of insonation other than zero, it becomes:

$$\mathrm{v}(\mathrm{cm/s}) = \frac{77\left(\frac{cm}{ms}\right) \times f(D)(KHz)}{f(\mathrm{o})(MHz) \times cosine\varnothing}$$

This is the function which is performed when the angle cursor is adjusted on the display of an imaging system. While it is standard of practice to angle correct when performing carotid duplex and other vascular ultrasound, it is currently not the case when performing TCDI. As with TCD, an angle of 0° is assumed accepting this may not always be achieved. However, by always striving to obtain the highest Doppler shift, this approach has been demonstrated useful for clinical applications [7]. By assuming an angle of zero degrees, the velocity cannot be overestimated, only underestimated.

Pulsed-Wave Doppler

Pulsed-wave Doppler is a sam*pling Doppler technique* consisting of a series of short bursts or *pulses* of ultrasound interspersed with periods of no ultrasound or *listening*. *Pulses* consist of multiple *cycles*. In comparison with imaging for which short (dampened) pulses of 1–3 cycles are used in order to achieve greater resolution, Doppler utilizes longer pulses consisting of 2–30 cycles due to the need for adequate sampling to improve sensitivity and signal-to-noise.

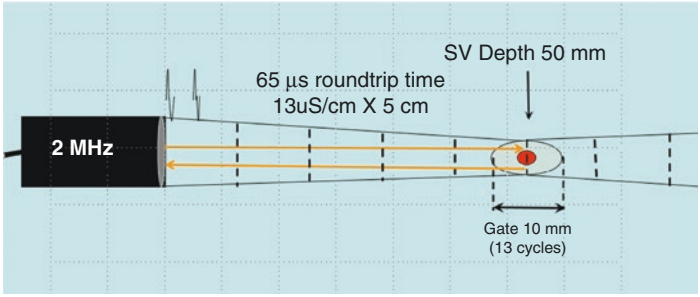

Fig. 7 For a 10 mm *sample volume* (SV) (*gate*) at a selected depth of 50 mm, the gate would open 29.25 uS and close 35.75 uS following the beginning of the pulse resulting in the center of the gate occurring 32.5 uS following the beginning of the pulse. The time for the pulse to travel to the selected depth range and for Doppler shift echoes to return to the transducer would be 65 µS (Kremkau's rule of 13)

Range Gating

Pulsed –wave Doppler provides the means by which echoes from operator selected depth ranges along the ultrasound beam may be *received* and *processed* using the technique of *range gating*. The *gate* is opened and closed at times corresponding to the selected depth and length. Using the principle described by *Kremkau in the Rule of 13, whereby roundtrip travel time* of ultrasound in soft tissue equals *13 us/cm* (6.5 us/cm one way), the instrument determines the depth and length of time the gate is open. It is common that the selected gate depth corresponds to the center of the gate Fig. 7.

Exercise

A 10 mm SV would typically be associated with an equal SPL of 10 mm. A transducer with an operating frequency of 2 MHz has a wavelength = c/f or, 1.54 us/2 = 0.77 mm. Since SPL = wavelength × number of cycles, by dividing the SPL (10 mm) by the wavelength (0.77 mm) we arrive at the number of cycles in the pulse or, 10 mm/0.77 mm = 13. Taking it a step further, if we take the period or $T = \frac{1}{2}$ = 0.5 uS, we see that 13 cycles × 0.5 uS/

cycle = 6.5 Ss = the time it takes sound to travel 1 cm (10 mm) in soft tissue which is the length (in time) of our gate.

Additional Parameters Inherent to Pulsed-Wave Doppler

Pulse Duration and Spatial Pulse Length

Pulse Duration (PD)(uS), is the time it takes for one pulse to occur while spatial pulse length (SPL) is the length (mm) of one pulse or,

$$\mathrm{PD}(\mathrm{uS}) = \mathrm{Period}(\mathrm{T})(\mathrm{uS}) \times \text{number of cycles and,}$$

$$\mathrm{SPL}(\mathrm{mm}) = \text{wavelength} \times \text{number of cycles}$$

It is typical that the spatial pulse length is equal to the length of the sample gate. Therefore, the larger the sample gate, the longer the SPL (more cycles) and pulse duration and the greater the intensity of the ultrasound beam.

Pulse Repetition Frequency, Pulse Repetition Period and Duty Factor

Pulse Repetition Period (PRP) (uS) is the length of time between the beginnings of successive pulses which means it includes the "listening" time. Since several thousand pulses are transmitted each second, PRP is expressed in kHz.

Duty Factor (DF) refers to the percentage of time the ultrasound is on, that pulses are being emitted.

$$\mathrm{DF}\% = \frac{PD}{PRP}$$

In the case of CW Doppler, the duty factor is 100% because the ultrasound is continuously on. The DF for Imaging ranges from 0.1% to 1.0% while the DF of pulsed-wave Doppler ranges from 0.5% to 5.0% due to the pulses consisting of more cycles [1].

Pulse Repetition Frequency (PRF)

The Pulse Repetition Frequency (PRF) (kHz) is the number of *pulses* transmitted per second. The *PRF* determines the maximum Doppler shift frequency (fD) that can be detected without experiencing *aliasing*. Aliasing is an artifact due to under sampling which results in higher frequencies of a waveform being cut off and displayed in the opposite direction. As previously described, pulsed wave Doppler is a sampling technique. In order to achieve accurate representation, the *sampling rate* must be at least 2× the frequency of the maximum Doppler shift frequency. If the Doppler shifted frequency exceeds this limit it will result in aliasing. The frequency at which this occurs is known as the Nyquist Limit after the engineer who described the phenomenon. It is written as:

$$\text{Nyquist Limit}\left(\text{kHz}\right) = \frac{1}{2} \times \text{PRF}\left(\text{kHz}\right)$$

In modern instruments, *PRF* is linked to the velocity *Scale* on the vertical axis of the spectral Doppler display. As the scale is increased, the PRF will increase in order to accurately sample the resulting higher frequency shifts (velocities). Options for correcting for aliasing include increasing the PRF or changing to a lower operating frequency transducer while an option for compensating for aliasing consists of lowering the baseline (cutting and pasting) in order to provide additional scale in the appropriate direction to display more of the waveform.

Range Ambiguity

In addition to aliasing, there is another artifact which can be explained using Kremkau's "R*ule of 13"* whereby all of the echoes from the previous pulse do not have time to return from the depth of the SV before the next pulse begins (PRP). This results in *range ambiguity* as there is no way to be certain from exactly where along the beam the returning echoes originated. While high PRF may be useful in certain cases, due to the many potential sources within the brain, many TCD instruments elect not to process echoes beyond the limit of ambiguity. Instruments which

allow PRFs beyond the limit of ambiguity typically display additional sample volumes to alert the sonographer to the possibility of ambiguous signals.

In performing transcranial Doppler, it is not unusual that high velocity signals are detected at depths beyond the limit of ambiguity using a PRF which would not result in aliasing. In these cases, the sonographer has the option to decrease the PRF (scale) and accept aliasing in favor of ambiguity.

Doppler Processes and Instruments

To briefly review, Doppler instruments transmit a known frequency (fo) of ultrasound, receive and amplify returning echoes to determine the difference (shift) in the frequencies and the phase (direction). From that point on, it is a matter of how the Doppler shift information is processed and displayed (Fig. 8)

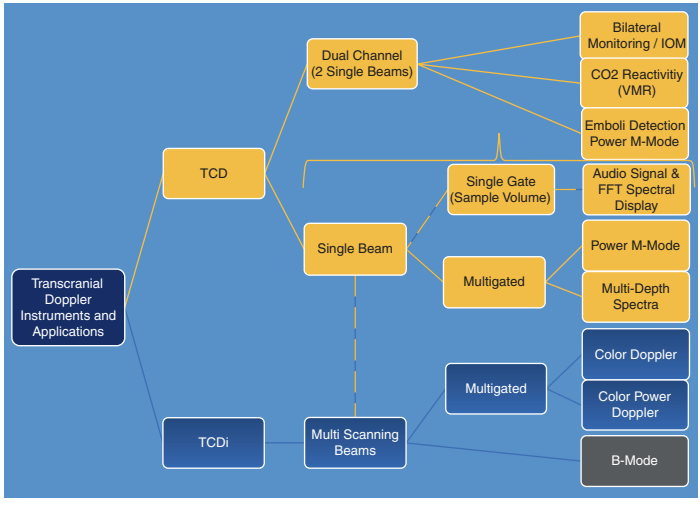

Fig. 8 Transcranial Doppler Instruments. Conventional Instruments (TCD) consist of a single ultrasound beam with one (single gate) or many (multigate) sample volumes. Instruments used for TCDI consist of multiple multigate beams scanned at a rate which appears as real-time. Two Channel TCD Instruments essentially consist of two Single Channel TCD machines combined in one instrument

The *audio signal* and *FFT spectral waveform* representing *Doppler shifted* echoes from a single *sample volume* remain the primary sources of diagnostic information provided by TCD instruments.

Audio

The primary means by which Doppler shift information is presented is as an *audio output.*

It is much to our benefit that Doppler shifted frequencies from moving blood fall within the *audible range.* The audio signals lend themselves nicely to presentation in stereo with flow toward the transducer (positive shifts) in one channel and flow away from the transducer (negative shifts) in the other using either loudspeakers or headphones. Many experienced sonographers consider the audio signal to be of the highest importance when performing a TCD examination.

Spectral Analysis

The audible Doppler signal consists of a *spectrum* of Doppler shift frequencies representing complex backscattered echoes from moving blood and possibly adjacent tissues. The spectrum analyzer, originally debuted as a "sound spectrum analyzer," uses a mathematical process known as the fast Fourier transform in an effort to represent visually what our ears hear in the audible signal. The result is the *Doppler spectral waveform*, either in color or gray scale, with *frequency distribution and intensity* displayed on the vertical axis and *time* on the horizontal axis. While several parameters and indices may be measured or derived from the spectral waveform, by far, that most widely used in transcranial Doppler is the *time averaged mean of the maximum velocity* envelope (TAMM) and commonly referred to as *Mean*.

Because the sample volume is large in comparison with the intracranial arteries, it is not uncommon that echoes from branches and vessel segments in close proximity may appear within the

spectrum. The spectral waveform is helpful in identifying these as well as bruits and musical murmurs.

Additional Methods of Doppler Signal Processing

Thus far, our attention has been limited to the processing of Doppler shift echoes returning from a single sample volume (gate) along a single ultrasound beam. This is the technology used in the original transcranial Doppler devices and which remains the primary end point of transcranial Doppler instruments today. Advances in digital technology have, however, resulted in several processing techniques which provide beneficial adjuncts to *single-gate* Doppler technology.

Recall that pulsed-wave Doppler consists of rapidly (PRF) transmitted series of *pulses* consisting of several *cycles*. While *range- gating* allows for the selective processing of returning echoes from a discrete depth range, echoes continue to return to the transducer from pulses all along the course of the sound beam. Faster processing speeds and expanded memory allow for these echoes to be processed and displayed in a variety of ways using the technique of *multi–gating*. Modern TCD instruments incorporate both single-gate and multi-gate processing (Fig. 9).

Transcranial Color Doppler Imaging (TCDI)

Multi-gated pulsed Doppler is at the core of *color Doppler* imaging and therefore *TCDI*. TCDI utilizes existing color Doppler imaging technology, most similar to that used in echocardiography whereby B-mode imaging is combined with color Doppler imaging. Color Doppler or color flow imaging, as it is sometimes called, is the result of displaying multiple multi-gate scan lines (sound beams) in sequence to create a two dimensional image in the same way a real-time B-mode image is created. Doppler shifts are processed using the technique of *autocorrelation* to determine

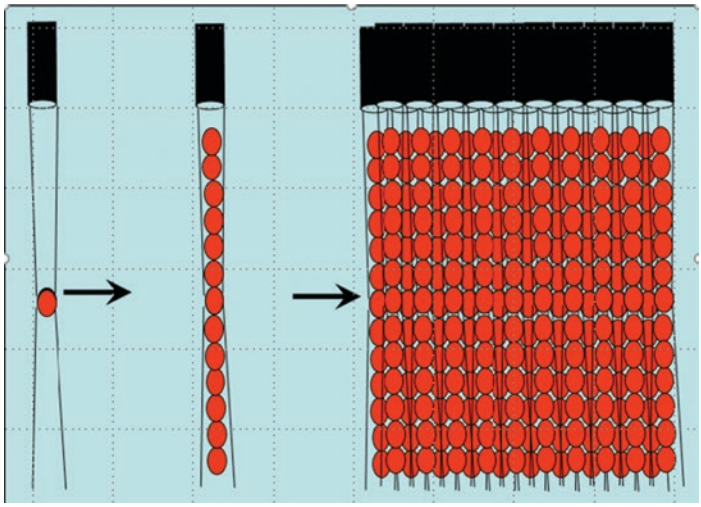

Fig. 9 Left: Single beam with single sample gate; Middle: Single beam with multiple sample gates (multi-gate); Right: multiple beams with multiple gates with capability for scanning at rates which appear as real-time (TCDI)

the direction and mean (and in cardiac, variance) of Doppler shifted echoes along a scan line. This information is displayed according to a particular *color map* which appears on the display. The color map is essential to understanding and interpreting flow direction, relative speed of motion and aliasing. Multiple pulses or *ensembles* are required to produce each scan line, typically 10–20, and many scan lines are required to produce a cross-sectional image. More scan lines result in improved accuracy and color filling as well as sensitivity to slower flow. However, more scan lines result in slower frame rates, the number of times per second which the cross-sectional image is updated. The size of the *color box,* that portion of the display selected for processing as *color flow imaging,* also has an effect on frame rate. The larger the color box, the slower the frame rate.

The color box (parallelogram) may be *"steered"* to the right or left using *phased array technology.* This aids in achieving a more favorable angle of insonation for vessels oriented more perpendicular to the sound beam such as $\leq 60°$ in the case of carotid arteries or identifying flow with TCDI.

For carotid imaging, *phased linear array* transducers of a variety of broad band frequency combinations ranging anywhere from 3 to 13 MHz are typically used. TCDI utilizes *phased array sector* transducers with broadband frequencies of 1–5 MHz, the same used for adult echocardiography.

In both carotid ultrasound and transcranial Doppler imaging, the spectral waveform originating from a single-gate remains the Doppler presentation used as diagnostic criteria. It remains an area of some discussion whether the same TAMM criteria used for TCD are applicable for TCDI.

Two Channel TCD

Two channel TCD instruments are effectively two TCD instruments in one. Such instruments drive two transducers in a synchronized fashion allowing for real-time presentation of multiple waveforms, the most common being the bilateral MCA or PCA segments. These instruments operate in single-gate and multi-gate modes and are capable of displaying TCD parameters trended over extended periods of time. Additional channels allow display of physiologic information such as CO_2, MAP, ICP, ECG, and others making them well suited for ICU and surgical monitoring (IOM) as well as for specialized diagnostic studies such as emboli monitoring and CO_2 reactivity where bilateral data acquisition is of benefit.

Power M-mode

Power M-mode allows the sonographer to visualize Doppler shifts along the path of the sound beam as an 'ice pick" view or single scan line. *Direction* and *intensity* of Doppler shift echoes from many gates along the sound beam are displayed corresponding to depth on the vertical axis. Time is represented on the scrolling horizontal axis resulting in real-time display of echoes returning from all along the sound beam. At depths at which Doppler shifts are detected, the positive shifts are displayed in shades of red and the negative shifts in shades of blue while *inten-*

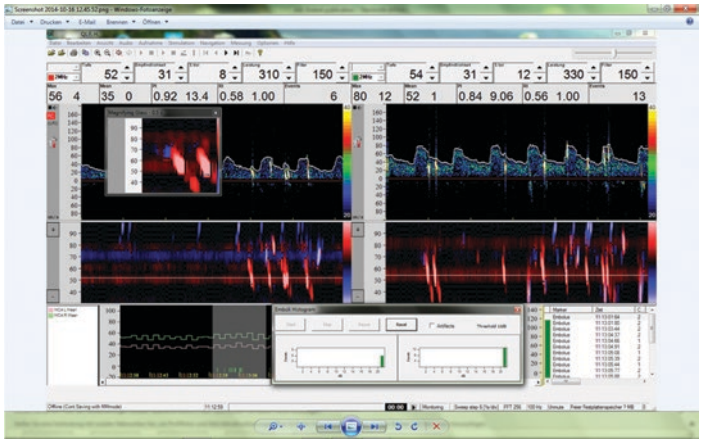

Fig. 10 Two channel display of bilateral MCA spectral waveforms and Power M-mode with trends of Mean velocity following injection of agitated saline for detection of right-to-left shunt

sity is represented by lighter shades of each. Power M-mode is of particular value for emboli detection as well as an aid to spatial orientation (Fig. 10).

Multi-depth

Multi-depth is a feature of available displays spectral waveforms from multiple, commonly eight, equal depth ranges from along the sound beam in addition to the primary sample volume.

Safety

A *bioeffect* is any effect on biological tissue caused by an outside source. We have acknowledged that ultrasound waves produce bioeffects in the form of pressure, particle motion and heat, the latter as a result of absorption. It is therefore important to distinguish between bioeffects and harmful bioeffects. Fortunately, the conditions are few and will be discussed later.

While no harmful bioeffects have been reported associated with the intensities used in diagnostic ultrasound (K) we must be cognizant of the fact that the potential exists for thermal (heating) and mechanical (cavitation) bioeffects.

In addition to power (amplitude), sample volume (due to pulse duration (PD) and spatial pulse length (SPL)) and pulse repetition frequency (PRF) contribute to the intensity of the ultrasound beam. These are parameters over which the sonographer can exercise control in observing the ALARA (As Low As Reasonably Achievable) Principle. Several safety precautions are incorporated into modern ultrasound instruments which aid the sonographer. An overall upper limit for Ispta of 720 mW/cm^2 has been established by the FDA along with the requirement to present acoustic output information on the instrument display. Modern instruments are designed not to exceed the maximal power limit regardless of operator settings. For example, if the spatial pulse length, which typically is equal to the sample volume or gate length, and the PRF are increased by the user to settings which would result in exceeding 720 mW/cm^2, the software will reduce the transmit power in order that the intensity does not exceed 720 mW/cm^2. Nonetheless, the sonographer should exercise vigilance in observing the ALARA Principle and limiting insonation time.

Mechanical Index (MI)

Mechanical Index (MI) is an indicator of pressure or cavitation potential. Thus far, the clinical application has been in bubble maintenance or destruction when using ultrasound contrast agents. The AIUM Practice Standards suggest not exceeding an MI >0.23 when insonating through the orbital window.

Thermal Index (TIS, TIB, TIC)

Thermal Index is based on estimates of the amount of power necessary to increase tissue temperature 1 °C. Three of these have

been established which are specific to the path of the ultrasound beam through tissue and whether bone is present and where.

- ***TIS*** is an estimate for an ultrasound beam passing through soft tissue without encountering bone;
- ***TIB*** is an estimate for a beam passing through soft tissue and then encountering bone near the region of focus and;
- ***TIC*** is an estimate for a beam which encounters bone near the transducer. TIC is the acronym for *Thermal Index Cranial* (*TIC*) and is that which applies directly to TCD.

Conditions Specific to Transcranial Doppler

In the case of TCD using the transtemporal approach, the bone is separated from the transducer only by the skin. As previously mentioned, the intensity of a sound beam is typically greatest at the focus, where area is at its minimum, and directly in front of the transducer where amplitude is greatest.

Bone has high *acoustic impedance* and a high *coefficient of attenuation* which results in a significant portion of the intensity of the ultrasound beam being attenuated within the first few millimeters, predominantly due to reflection, refraction and absorption, the latter resulting in conversion to heat. Early work by Grolimund [8] reported a reduction in intensity of the sound beam entering the brain tissue of at least 65–80%.

Due to initial attenuation and the fact the brain is highly perfused with blood flow acting as a radiator to rapidly dissipate heat, the potential for brain warming is usually not an issue. The skin is typically well vascularized, however, with age and conditions such as diabetes, cutaneous blood flow may be compromised. This is important to remember, especially during prolonged monitoring with TCD, as this may exacerbate warming of the skin and even bone. The potential for thermal injury can be minimized by limiting the time of insonation. When monitoring, limiting the time the transducer(s) are active (transmitting), using adequate gel and replenishing often and checking the skin periodically minimizes the risk of thermal injury.

Transorbital Approach

Special attention is required when insonating through the transorbital window. Power should be adjusted not to exceed an Ispta of 17 mW/cm^2 or 10% of the maximum output of the device. TIC is not applicable to transorbital insonation. AIUM Practice Parameters include an MI $\leq$0.23.

Suggested power settings for specific procedures and anatomical approaches will appear as relevant in those chapters.

As always, the best way to minimize exposure is by following the ALARA Principle and by limiting exam time.

References

1. Kremkau FW. Sonography: principles and instruments. 10th ed. St Louis: Elsevier; 2020.
2. Kremkau FW. Doppler ultrasound: principles and instruments. Philadelphia: Saunders; 1990.
3. Alexandrov AV. Neurovascular examination: the rapid evaluation of stroke patients using ultrasound waveform interpretation. Hoboken: Wiley; 2013.
4. Evans DH, McDicken WN, Skidmore R, Woodcock JP. Doppler ultrasound: physics, instrumentation, and clinical applications. Chichester: Wiley; 1991.
5. Atkinson P, Woodcock JP. Doppler ultrasound and it's use in clinical measurement. London: Academic; 1982.
6. Tegeler CH, Eicke M. Physics and principles of transcranial Doppler ultrasonography. In: Babikian VL, Wechsler LR, editors. Transcranial Doppler ultrasonography. St Louis: Mosby; 1993.
7. Aaslid R. Development and principles of transcranial Doppler. In: Newell DW, Aaslid R, editors. Transcranial Doppler. New York: Raven; 1992. p. 1–8.
8. Grolimund P. Transmission of ultrasound through the temporal bone. In: Aaslid R, editor. Transcranial Doppler sonography. Vienna: Springer; 1986.
9. Del Brutto OH, Mera RM, de la Luz Andrade M, Espinosa V, Castillo PR, Zambrano M, Nader JA. Temporal bone thickness and texture are major determinants of the high rate of insonation failures of transcranial Doppler in Amerindians (The Atahualpa Project). J Clin Ultrasound: JCU. 2015;44:55–60. https://doi.org/10.1002/jcu.22284.

Overview of Pertinent Cerebral Vascular Anatomy

Pirouz Piran and Wendy C. Ziai

Performing and interpreting cerebrovascular ultrasound studies requires a basic understanding of the anatomy of the vessels involved. You should make yourself familiar with the normal course and appearance of both arteries and veins.

From the heart, two pairs of arteries supply the brain: 1- internal carotid arteries (anterior circulation) and 2- vertebral arteries (posterior circulation). Anterior and posterior circulations ultimately anastomose with each other at the base of the brain forming a circle of arteries known as the circle of Willis.

The common carotid arteries (CCAs) branch from the aortic arch and ascend on both sides of the neck. The CCA bifurcates into an internal and an external branch. The internal carotid artery (ICA) enters the skull at the level of the petrous bone and gives off the ophthalmic artery as its first intracranial branch. The ICA terminates into anterior cerebral artery (ACA) and middle cerebral artery (MCA) on both sides. Right before terminating to ACA and MCA, the ICA gives off two branches: 1- anterior choroidal artery and 2- posterior communicating artery.

P. Piran
Departments of Neurology, Neurosurgery, Anesthesiology and Critical Care Medicine, Johns Hopkins University, Baltimore, MD, USA

W. C. Ziai (✉)
Departments of Neurology, Neurosurgery, Anesthesiology and Critical Care Medicine, The Johns Hopkins University School of Medicine, Baltimore, MD, USA
e-mail: weziai@jhmi.edu

W. C. Ziai, C. L. Cornwell (eds.), *Neurovascular Sonography*,
https://doi.org/10.1007/978-3-030-96893-9_2

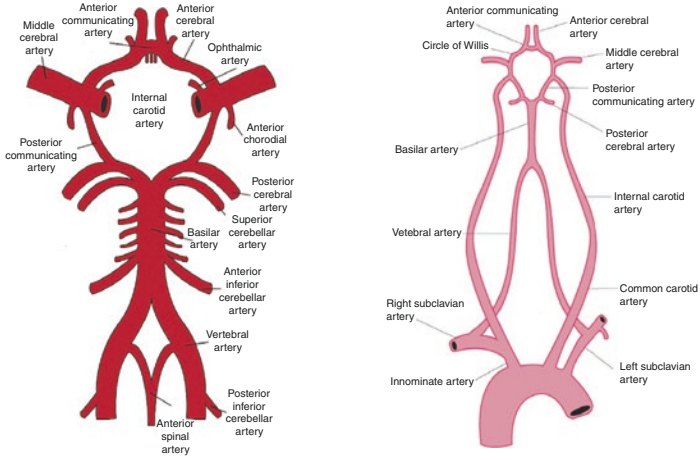

Fig. 1 Intracranial arteries and their origination from the heart. Note the anastomosis of blood between the anterior and posterior intracranial circulations by way of the circle of Willis (picture on the left) and the origination of the internal carotid arteries and vertebral arteries from the aortic arch (picture on the right)

The vertebral arteries (VA) originate from the right and left subclavian arteries (from the aortic arch) [1]. The vertebral arteries ascend through the cervical vertebrae and join each other to form the basilar artery which later terminates into the posterior cerebral arteries (PCA) (Fig. 1).

Anatomical Variations

Fewer than half of the normal population have a complete circle of Willis. There are many anatomical variations to this circle [2] however, some are relevant to cerebrovascular studies (Fig. 2). The most common anatomical variation is hypoplasia of one of the components of the circle of Willis which is present in up to 25% of patients.

Of all the anomalies, hypoplasia of the posterior communication artery is the most common followed by hypoplasia of the P1 segment of PCA, A1 segment of ACA and the anterior communicating artery.

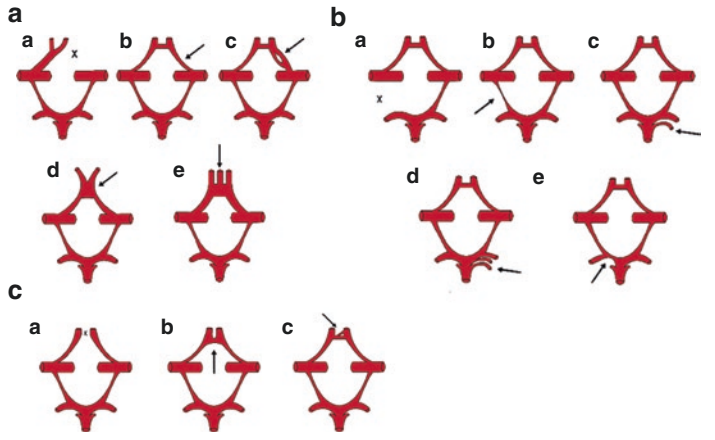

Fig. 2 (**a**) Anterior cerebral artery common anatomical variations. (a) absent ACA; (b) hypoplastic ACA; (c) splitting ACA; (d) joint ACA; (e) triple ACA. (**b**) (a, b): Posterior communicating artery variations. (a) absent PcomA; (b) hypoplastic PcomA; (c–e): PCA anatomical variations, (c) duplicate PCA; (d) triple PCA; (e) hypoplastic PCA. (**c**) Anterior communicating artery common anatomical variations. (a) Absent AcomA; (b) Joint/absent variation; (c) Duplicate AcomA

The other less common anatomical variations are; presence of accessory vessels, anomalous origin and absent vessels [3].

Internal Carotid Artery Segments [4] (Fig. 3)

- Cervical (C1): begins at the level of CCA bifurcation and ends where it enters the petrous bone via carotid canal.
- Petrous (C2): this segment refers to the part of ICA that runs through the carotid canal within the petrous bone. The ICA is considered intracranial at this level.
- Lacerum (C3): this segment of ICA is between the petrous segment and the cavernous segment. The ICA passes superior to the foramen lacerum, but doesn't pass through the foramen.
- Cavernous (C4): this segment is surrounded by the cavernous sinus and usually has a vertical segment, a posterior bend (medial loop of the ICA), a horizontal segment and an anterior

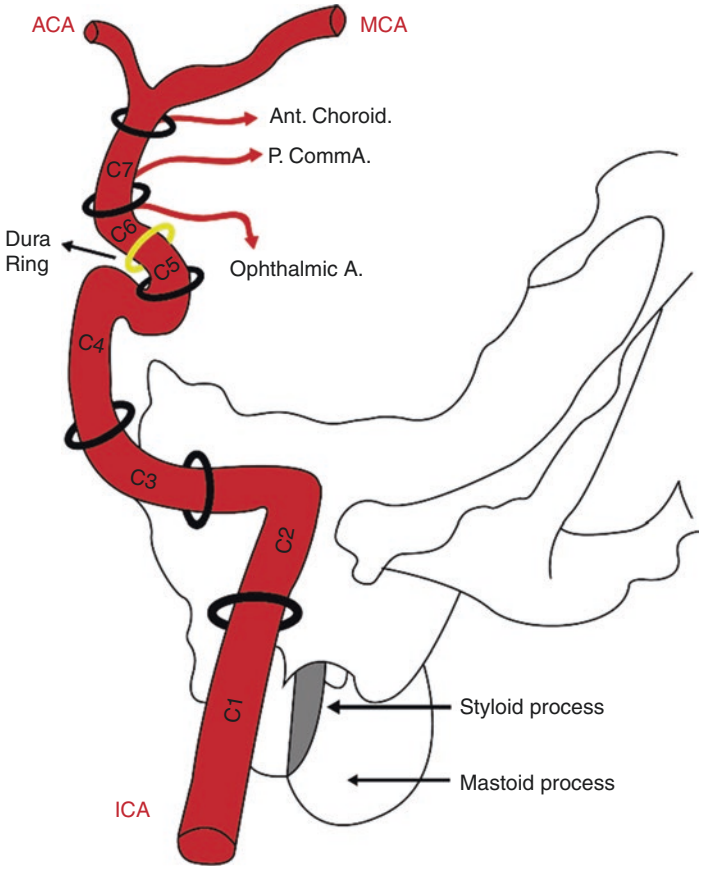

Fig. 3 Internal carotid artery segments. C1: cervical, C2: Petrous, C3: Lacerum, C4: Cavernous, C5: Clinoid, C6: Ophthalmic, C7: Communicating

bend (anterior loop of the ICA) which together give the siphon shape to this segment of the ICA (carotid siphon).

- Clinoid (C5): this short segment is the continuation of the anterior loop of the cavernous segment.
- Ophthalmic (C6): this segment begins when the anterior loop of the ICA becomes intradural. The ophthalmic artery which is the first intracranial branch of the ICA arises from this segment in most people.

- Communicating (C7): this segment begins proximal to the area where the posterior communicating artery joins the ICA and ends where ICA bifurcates into MCA and ACA.

Middle Cerebral Artery

MCA is the largest terminal branch of the ICA. The MCA divides into four main segments, denominated M1 to M4.

1. M1 segment originates at the carotid bifurcation and terminates as the middle cerebral artery.
2. M2 segment bifurcates or occasionally trifurcates. It travels laterally to the Sylvian fissure, and its branches end in the cerebral cortex.
3. M3 segment travels externally through the insula into the cortex.
4. M4 segments are thin and extend from the Sylvian fissure to the cortex [5].

M1 segment is the main segment of the MCA that is insonated in TCD through the temporal window. The blood is flowing towards the transducer (Fig. 4).

Anterior Cerebral Artery (Proximal Segments)

As mentioned above, the ACA is part of the circle of Willis and perfuses the medial parts of the frontal lobe and medial superior parts of the parietal lobes.

ACA consist of five segments however, only the first two segments are relevant to TCD studies (Fig. 5)

1. A1 segment: originates from the ending of internal carotid artery and extends to the anterior communicating artery
2. A2 segment: originates at the anterior communicating artery and extends anterior to the lamina terminalis and along the rostrum of the corpus callosum, terminating either at the genu of the corpus callosum or at the origin of the callosomarginal artery [6]

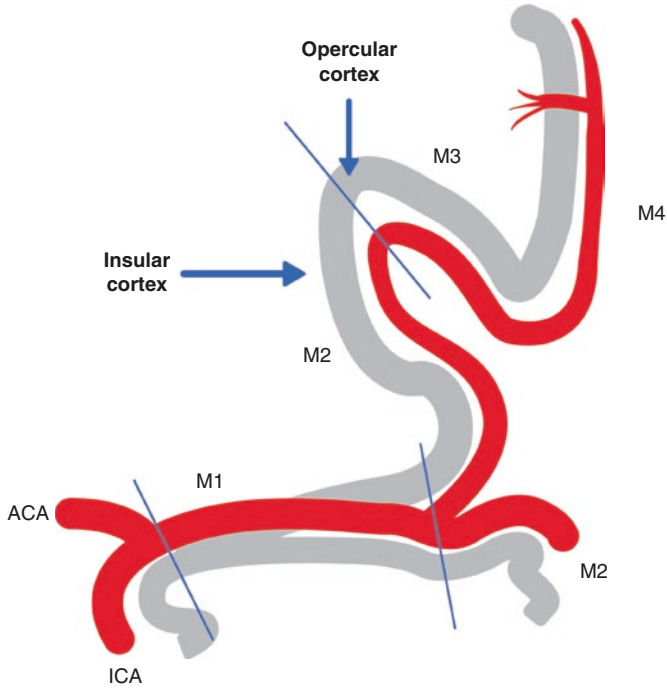

Fig. 4 Schematic illustration of the Middle Cerebral Artery (MCA) segments

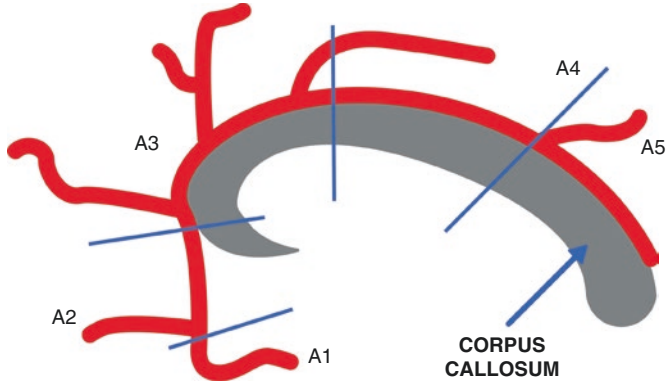

Fig. 5 Schematic illustration of the Anterior Cerebral Artery (ACA) segments

Basilar Artery

As mentioned above posterior circulation to the brain consist of the two vertebral arteries joining together to form the basilar artery. Basilar artery terminates into two posterior cerebral arteries (PCAs).

Posterior Cerebral Artery [7]

PCAs curve around the midbrain and supply the midbrain, inferior portions of the temporal lobes, occipital lobes and the thalamus. This artery is divided into 5 segments, however only the P1 and P2 segments can be insonated by TCD (Fig. 8).

- P1: The P1 segment is located within the interpeduncular cistern and starts from the termination of the basilar artery to the posterior communicating artery, passing over the oculomotor nerve (CN III).
- P2: The P2 segment begins at the posterior communicating artery and curves around the ambient cistern of the midbrain, and courses above the tentorium cerebelli. The main branch of this segment is the posterior choroidal artery.
- P3: The P3 segment of the PCA refers to the part of the artery that runs through the quadrigeminal cistern.
- P4: The P4 segment is the last segment of the PCA as it ends in the calcarine sulcus.
- P5: The terminal branches of the parieto-occipital and the calcarine arteries are included as the P5 segment.

Venous System

The venous drainage back to the heart is through the internal jugular veins. Cerebral veins can be divided to 1- superficial and 2- deep veins.

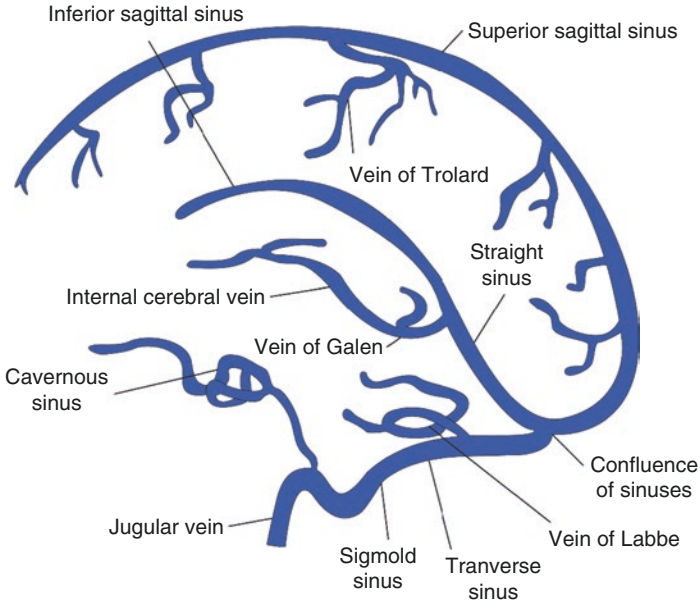

Fig. 6 Schematic illustration of the intracranial venous system

In normal individuals the deep cerebral veins, especially the basal vein of Rosenthal and vein of Galen can be visualized with ultrasound. Unfortunately, ultrasound is not sensitive enough to be used for screening of venous sinus thrombosis (Fig. 6).

Vein of Galen is a deep vein that is formed by two internal cerebral veins (Fig. 6). A vein of Galen malformation is the most frequent arteriovenous malformation (AVM) in neonates and can be diagnosed with TCD.

Locations for Transcranial Doppler Probes

The ultrasound frequencies are not able to penetrate through the bones of the skull sufficiently and therefore, areas with soft tissue or thinner bone are typically used to place the probe (Fig. 7).

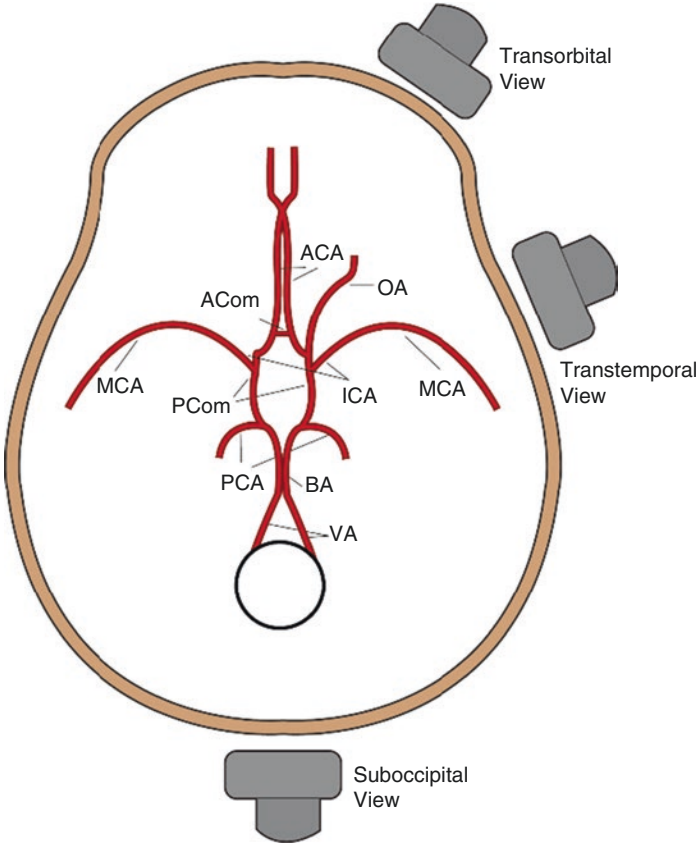

Fig. 7 Schematic illustration of intracranial arteries in respect to various locations of transcranial Doppler probes

These areas are:

1. **Temporal window:** located right above the zygomatic arch. The temporal window can be used to insonate MCAs, proximal ACAs, ICA bifurcations and the PCAs.
2. **Orbital window:** used to insonate the ophthalmic arteries as well as the siphon of the ICAs.
3. **Suboccipital window:** used to insonate intracranial portions of the vertebral arteries and the basilar artery.

Identifying Intracranial Vessels

Now that you are familiar with the cerebrovascular anatomy of the vessels. It is useful to know how to identify different vessels based on the window and the depth that you are insonating with the probe based on previous studies in adult patients aged between 18 to 80 years [8, 9] (Table 1 and Fig. 8).

Evaluating Collateral Circulations

When an artery is blocked or severely narrowed an alternate route of circulation will be formed through the nearby smaller vessels; this is called collateral circulation formation. Usually these collateral pathways are dormant in healthy individuals however, when there is an occlusion or severe stenosis, the pressure gradient between the anastomosed vessels changes and a new collateral circulation is formed. As mentioned above, anterior and posterior communicating arteries are the main collateral systems in the brain.

Table 1 Identifying the arteries based on the depth of insonation

Artery	Window	Direction	Depth (mm)	Mean Flow Velocity
MCA	Temporal	Towards probe	30–60 mm	55 ± 12 cm/s
OA	Orbital	Towards probe	40–60 mm	20 ± 10 cm/s
Terminal ICA	Temporal	Towards probe	55–65 mm	39 ± 09 cm/s
ACA	Temporal	Away	60–85 mm	50 ± 11 cm/s
PCA	Temporal	Bidirectional	60–70 mm	40 ± 10 cm/s
ICA	Orbital	Bidirectional	60–80 mm	45 ± 15 cm/s
VA	Occipital	Away	60–80 mm	38 ± 10 cm/s
BA	Occipital	Away	80–110 mm	41 ± 10 cm/s

MCA middle cerebral artery, *OA* ophthalmic artery, *ICA* internal carotid artery, *ACA* anterior cerebral artery, *PCA* posterior cerebral artery, *VA* vertebral artery, *BA* basilar artery

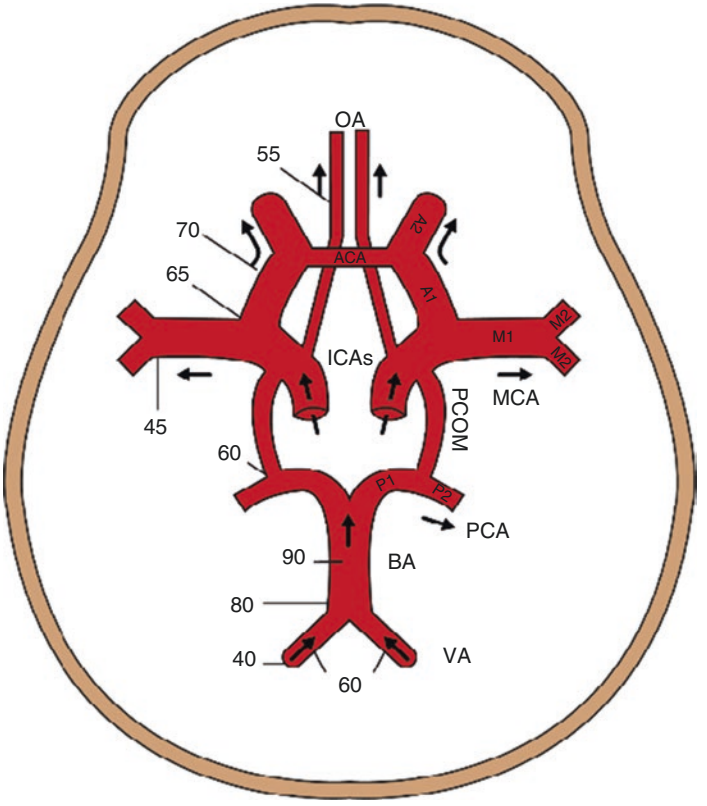

Fig. 8 Flow directions of the intracranial arteries with depths of insonation (in mm) for an average human skull are shown. Please note that the direction of the flow may change in the setting of active collateral circulations. MCA middle cerebral artery, OA ophthalmic artery, ICA internal carotid artery, ACA anterior cerebral artery, PCA posterior cerebral artery, VA vertebral artery, BA basilar artery

TCD is very useful for evaluation of these collateral circulations. It can assess collateral flow with good sensitivity via the (1) circle of Willis and reversed ophthalmic artery flow in the case of proximal internal carotid artery occlusion/severe stenosis; (2) flow to leptomeningeal collaterals anastomosing ACA or PCA with the distal MCA branches in middle cerebral artery occlusion.

This flow diversion has been defined by an increase of 30% in velocities in the ACA or PCA (in comparison to the contralateral same vessels) and was associated with good leptomeningeal vessels on angiography in 88% of cases in a study of 51 patients with MCA occlusion [10]; (3) reversed basilar artery flow in proximal basilar occlusion and; (4) reversed vertebral artery flow in proximal subclavian or innominate artery occlusion (Fig. 8).

References

1. Moini J, Piran P. Functional and clinical neuroanatomy: a guide for health care professionals. Elsevier Science & Technology; 2020.
2. Gunnal SA, Farooqui MS, Wabale RN. Anatomical variations of the circulus arteriosus in cadaveric human brains. Neurol Res Int. 2014;2014:687281.
3. Iqbal S. A comprehensive study of the anatomical variations of the circle of willis in adult human brains. J Clin Diagn Res. 2013;7(11):2423.
4. Bouthillier A, Van Loveren HR, Keller JT. Segments of the internal carotid artery: a new classification. Neurosurgery. 1996;38(3):425–33.
5. Navarro-Orozco D, Sánchez-Manso JC. Neuroanatomy, middle cerebral artery. In: InStatPearls [Internet]. StatPearls Publishing; 2019.
6. Perlmutter D, Rhoton AL. Microsurgical anatomy of the distal anterior cerebral artery. J Neurosurg. 1978;49(2):204–28.
7. Javed K, Reddy V, Das JM. Neuroanatomy, Posterior Cerebral Arteries. In: InStatPearls [Internet]. StatPearls Publishing; 2020.
8. Ringelstein EB, Kahlscheuer B, Niggemeyer E, Otis SM. Transcranial Doppler sonography: anatomical landmarks and normal velocity values. Ultrasound Med Biol. 1990;16(8):745–61.
9. Alexandrov AA, Neumyer MM. Intracranial cerebrovascular ultrasound examination techniques. In: Cerebrovascular ultrasound in stroke prevention and treatment. Blackwell Publishing.
10. Kim Y, Sin DS, Park HY, Park MS, Cho KH. Relationship between flow diversion on transcranial Doppler sonography and leptomeningeal collateral circulation in patients with middle cerebral artery occlusive disorder. J Neuroimaging. 2009;19(1):23–6.

Cerebral Waveforms for Hemodynamic Assessment

Aarti Sarwal

Qualitative waveform analysis is a key component of interpretation of Transcranial Doppler (TCD) studies in addition to evaluation via quantitative metrics like mean flow velocity (MFV) or pulsatility index (PI) [1]. Normative values for MFVs for intracranial vasculature and PIs are described in literature and mentioned in other chapters of this book [2]. This chapter will focus on qualitative assessment of cerebral hemodynamic waveforms and describe patterns in spectral waveforms that help in assessing cerebrovascular pathology. Many of these characteristic spectral patterns need to be taken in context of the clinical setting, patient presentation, underlying anatomy and pathology being evaluated and should be used as complementary information with disease specific evidence elsewhere in this book.

Vital organs like brain, heart, liver, placenta and kidney all maintain a low resistance circulation to allow preferential blood flow to them in times of shock compared to the rest of the body like the musculoskeletal system and gut where blood vessels feed a high peripheral vascular resistance circulation. Cerebral circulation in addition is unique in its complete dependency on available

A. Sarwal (✉)
Neurology, Neurocritical Care, Wake Forest Baptist Medical Center, Winston Salem, NC, USA
e-mail: asarwal@wakehealth.edu

W. C. Ziai, C. L. Cornwell (eds.), *Neurovascular Sonography*,
https://doi.org/10.1007/978-3-030-96893-9_3

inflow of an oxygenated blood supply to feed the metabolism of neurons and supporting cells with no inbuilt glucose or glycogen sources in the brain. Neurovascular coupling and cerebral autoregulation respond to changes in systemic circulation to preserve cerebral perfusion and ensure blood flow to the brain throughout the cardiac cycle especially diastole. These factors inherently affect the appearance of the spectral waveform on TCD. Transcranial insonation can be performed by imaging Doppler (duplex or B mode guided Doppler) or non-imaging Doppler but for simplicity, all figures will focus on spectral waveforms only when describing pathology, irrespective of accompanying B mode color imaging.

Components of the waveforms Spectral waveforms acquired from pulse wave Doppler imaging of intracranial vessels correspond to the phases of the cardiac cycle with initial 1/3rd of the waveforms representing systole with two components- an up going or acceleration phase and a latter down going deceleration phase (Fig. 1a, b). The following 2/3rd of the waveform represents the diastole or diastolic runoff. The overall waveform has three main characteristics: (1) direction of flow - towards the probe or away from the probe, (2) velocity- time average mean flow velocity, peak systolic velocity and end diastolic velocity and (3) systolic flow acceleration and deceleration slopes (Fig. 1a). A classical intracranial waveform has a sharp early systolic flow acceleration, stepwise late systolic deceleration followed by a robust diastolic run off that maintains 1/4–1/2 of velocities with peak systolic flow throughout the diastole. Systolic phase of systole may manifest three different peaks - P1 (percussion wave triggered by myocardial contractility), P2 (tidal wave created by Windkessel effect or distensibility of arterial wall and subsequent volume displacement), and P3 (dicrotic wave marking the beginning of the diastolic phase and usually follows dicrotic notch (Fig. 1c). These waveforms have been well described in intracranial waveforms visualized on intracranial pressure (ICP) monitors and represent the same hemodynamic phenomena. Pulsations of major arteries and choroid plexus contribute to P1 component. P2

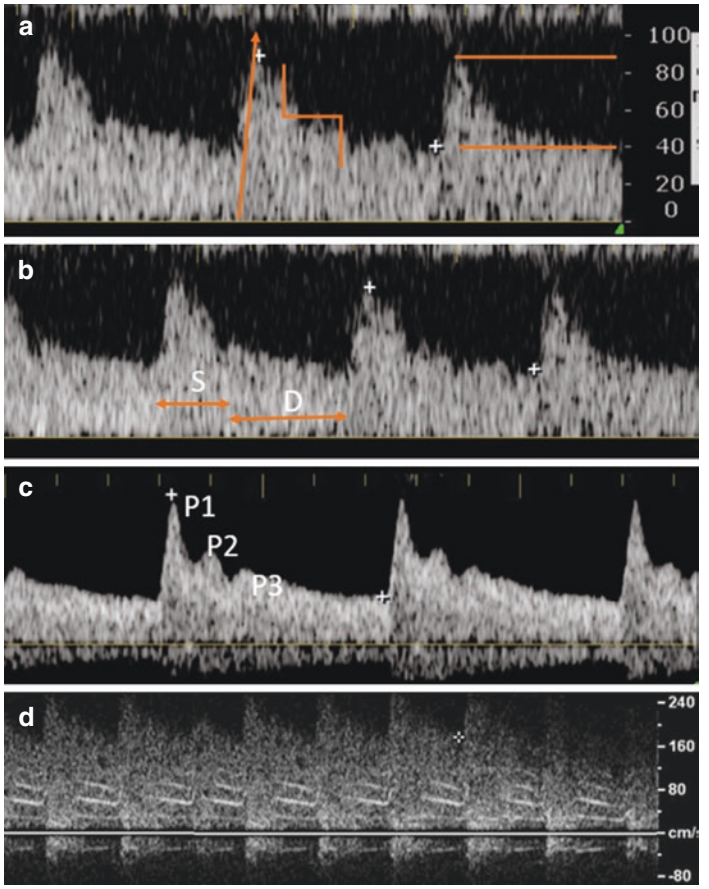

Fig. 1 Normal cerebral circulation represents a low resistance circuit with a rapid upstroke in initial systolic phase followed by a stepwise deceleration (**a**). The initial hump or initial third of the waveform represents the systole (S) and latter 2/3rd represents the diastole (D) in (**b**). The systolic phase has three peaks – P1 representing myocardial contractility, P2 representing arterial distensibility or Windkessel effect and P3 that follows the dicrotic notch hallmarking beginning of diastole (**c**). Figure (**d**) represents an abnormal Doppler spectrum with high mean flow velocity but preserved spectral patterns seen in (**a**–**c**). Bright white lines represent bruits or harmonics that may be created by laminar flow through stenosis

is dependent upon the intracranial compliance and is typically lower than P1 in normal brain. P3 component follows the dicrotic notch of the arterial waveform [3].

On the contrary, the typical wave form of the peripheral circulation or high resistance circulation has a sharp upstroke corresponding to systole but there is reversed flow during early and late diastole giving the classical triphasic oscillating appearance. Such waveforms can be seen in insonation of the external carotid artery or femoral artery [4].

Effect of Cerebral Vascular Resistance on waveforms Many cerebrovascular diseases manifest as changes in resistance of the cerebral vessels or the distal vascular bed (Table 1). Quantitative measures of distal resistance include pulsatility index of Gosling & King - [Peak Systolic Velocity- End Diastolic velocity]/ Mean flow Velocity; and Pourcelot's resistive index - [Peak Systolic Velocity-End Diastolic Velocity]/Peak Systolic Velocity. Resistance changes can have variable effect on the flow and velocity of the blood through the insonated segment dictated by the Spencer and Reid curve (Fig. 2) [5, 6]. This hemodynamic model was classically described for the carotid but is applicable to most vascular lesions in the brain [5]. The correlation of waveforms with the Spencer Reid curve can help understand changes in velocity, flow and resistance and their transitions with progressive lesions.

Qualitatively distal resistance can be assessed by the relationship of the diastolic part of the waveform with the systolic flow. Higher than normal resistance can be seen typically distally in the intracranial circulation during distal vasospasm, hyperventilation, increased

Table 1 Pathological states that affect resistance characteristics of waveforms

Resistance of the cerebral vessels	Resistance of the distal vascular bed
Increased in intracranial stenosis, cerebral vasospasm/ vasoconstriction	Increased in increased intracranial pressure or distal atherosclerotic disease
Decreased in arteriovenous shunting	Decreased in peripheral vasodilatation as in hypercarbia or reperfusion of ischemic brain

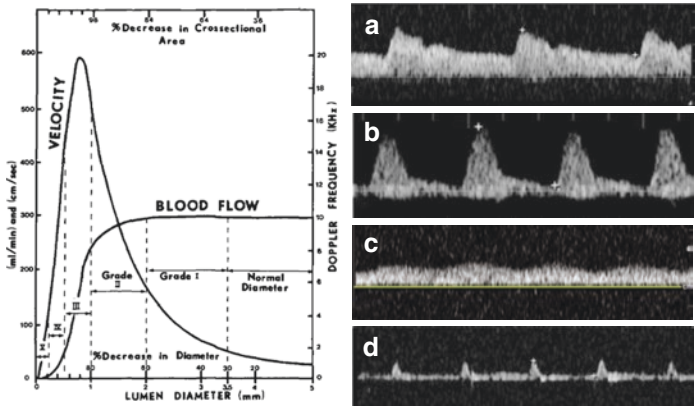

Fig. 2 Spencer and Reid first described a hemodynamic model that explains to a large extent the spectral patterns observed with variations in flow and resistance in progressive stenosis of the carotid artery [5, 6]. This hemodynamic model stands true for most cerebrovascular phenomena observed in transcranial Doppler. (Spencer Reid curve used with permission from Stroke.1979;10:326–330 [6]). (**a**) represents normal cerebral waveforms on right lower corner of the graph with normal diameter, normal flow and normal velocity. (**b**) represents the resistive waveforms expected to be seen in grade II stenosis where velocities are elevated, diastolic flow is compromised and waveforms appear resistive with high pulsatility index. (**c**) represents blunted waveforms in higher grade III stenosis where flow is significantly compromised and velocities are dropping and (**d**) represents near occlusion where minimal flow is seen mostly during systole with significantly low velocities

ICP or as a result of diffuse intracranial atherosclerotic disease (Fig. 3a–3c). Velocity elevation may be the early and only sign of increased vascular resistance in many instances but as luminal stenosis affects flow, different patterns emerge guided by the Spencer Reid curve. Figure 3a, b represents cases where diastolic flow is significantly lower than a 1/4th of systolic, approaches zero or can even be reversed while Fig. 3c represents a relatively normal resistance where elevated MFV is the initial sign of vasospasm. A PI greater than 1.2 in proximal vessels reflects increased distal resistance. Resistance index of 1 denotes no diastolic flow and RI >1 shows reversed EDF and intracranial circulation typically shows RI <1. Distal insonation of the vessels close to the skull may cause physiological changes similar to high resistance especially in the distal MCA and intracranial vertebral insonation that show falsely high PI and RI.

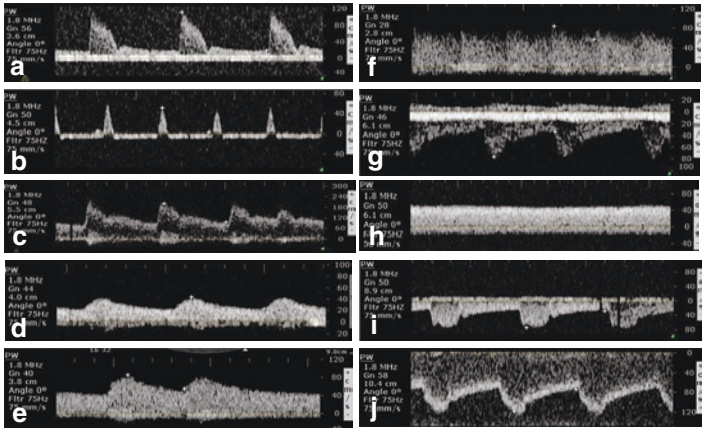

Fig. 3 Resistive waveforms with intact systolic upstroke, downward deceleration can be seen in pre-stenotic segments of focal stenosis or increased intracranial pressure (**a**). Intracranial pressure significantly higher than patient's diastolic pressure can cause reversal of cerebral blood flow during diastole (**b**). Normal cerebral waveforms with physiological relationships of spectral shapes may have elevated velocities, spectral narrowing (white envelope at the upper end of the spectral wave) and bruit (white signal on the baseline at the peak of each systole); such patterns show increased resistance (**c**). Insonation of segments distal to stenosis may show parvus et tardus waveforms (**d**, **e**). Cardiac irregularity can sometimes be noticeable on Doppler studies (**e**) and should be reported. Increased diastolic to systolic ratio can be seen in hyperemic waveforms (**f**). Basilar veins of Rosenthal (white bands with venous waveforms close to the baseline) can often be insonated along with distal posterior cerebral artery (spectral wave below the baseline) (**g**). (**h**) represents the non-pulsatile waveforms seen in patients on coronary bypass. Vertebral and basilar insonation often shows non-compliant waveforms with P2 higher in amplitude than P1 in physiological states (**i**). Spectral narrowing (white envelope at the bottom of the waveform) may be an early sign of increased resistance but has fallen out of diagnostic criteria (**j**)

Lower than normal distal resistance in intracranial vessels manifests in spectral Doppler when flow during diastole exceeds more than 50% of the peak systolic flow. This can be seen diffusely in hypercarbia causing distal vasodilatation-hyperemic waveforms (Fig. 3f). When MFVs are high, analysis of PIs and the spectral waveforms helps distinguish whether vasospasm (high resistance) or hyperemia (low resistance) is causing elevated

velocities. Lindegaard ratios (intracranial middle cerebral artery MFV/ extracranial internal carotid artery MFV) can also help. When lower than normal resistance is seen focally, it usually represents arteriovenous shunting distal to the insonated area (Fig. 3f) or insonation occurring distal to the stenotic lesion (Fig. 3d). Post-stenotic waveforms specifically manifest delayed systolic flow acceleration and deceleration with lower peak velocities classically called *parvus (small) et tardus (late)* (Figs. 3d and 5b) that distinguish them from hyperemic waveforms that may have elevated MFV with normal systolic upstroke but comparatively higher diastolic flow. Severe aortic stenosis could cause all intracranial waveforms to look post-stenotic in the absence of other intracranial lesions. Low resistance waveforms will have a low PI typically <0.6 and very low RI.

Observing qualitative waveform changes in obstructive sleep apnea can be remarkable for low resistance hyperemic waveforms at the end of apneic spells coinciding with hypercarbia which return to normal with initiation of the hyperventilation phase of Cheyne-Stokes breathing. Vasoreactivity test involving inhalation of CO2 or administration of acetazolamide are based on changes in distal vasodilatation caused by hypercarbia driving hyperemic waveforms. Patients with severe anemia or with sickle cell crisis may also demonstrate hyperemic waveforms and looks similar to low resistance waveforms.

Malignant cerebral edema and cerebral circulatory arrest present a unique pattern of increased distal resistance from increased ICPs. Waveforms transition with changes in ICP quite predictably. Resistive waveforms emerge with gradual increase in distal resistance affecting the diastolic component (Fig. 4b). When ICP significantly elevates above patient's diastolic pressure, spectral waveforms may have a reversal of diastolic flow (Fig. 3b). If underlying brain injury progresses and is not amenable to therapy, this waveform classically named oscillating waveforms cannot sustain cerebral perfusion due to lack of diastolic run off necessary for sustaining cerebral oxygenation (Fig. 3b). Anecdotal reports of reversal of this pattern exist when underlying pathology was addressed even if temporarily. Figure 4 represents a hemorrhage with increased ICP patterns on ipsilateral middle cerebral

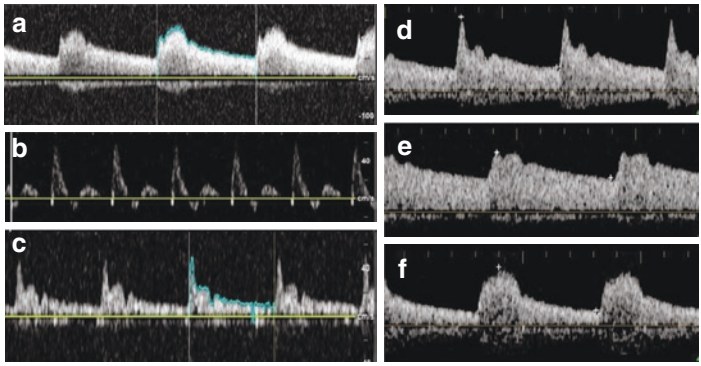

Fig. 4 A young patient with hemorrhagic stroke with insonation of middle cerebral artery ipsilateral to the lesion. Initial waveforms showed a non-compliant waveform with P2 higher in amplitude than P1 (**a**). During an intracranial pressure crisis, the same vessel showed reversal of flow during early and late diastole (**b**). After osmotic therapy administration, the waveforms restored to positive diastolic flow but maintained resistive patterns (**c**). (**d**) represents a normal cerebral waveform in a young compliant brain as a comparison. P2 is same amplitude as P1 in (**e**) whereas it consistently stays higher than P1 in (**f**). Such change in patterns of compliance may be early signs of an impending increased intracranial pressure and need further research

artery insonation (Fig. 4b) that resolved to some extent after hemorrhage evacuation (Fig. 4c) with restoration of forward diastolic flow but ongoing ICP issues. Such cases have elucidated the value of serial TCDs as non-invasive markers of increased ICPs in neurocritical care patients at risk of cerebral edema [7, 8]. Such patterns may be extremely helpful in patients with hepatic encephalopathy who are liver transplant candidates due to challenges in invasive monitoring [9]. Persistence of this pattern despite therapy, however, portends cerebral circulatory arrest [10]. If ICPs continue to rise, oscillating pattern is replaced by systolic hump or spike followed by no flow. Details of cerebral circulatory arrest are described in more detail in another chapter.

Increased resistance localized to a segment of cerebral blood vessels as in intracranial stenosis may produce a sequential transition of spectral waveforms that can help localize the lesion (Fig. 5). Patients may manifest high resistance waveforms when

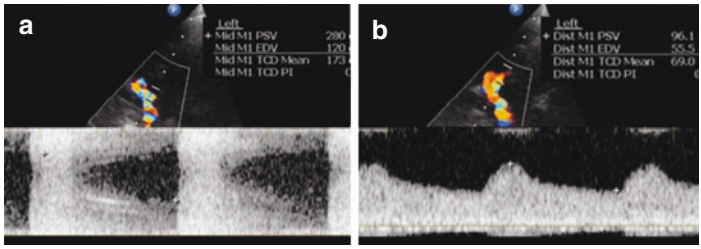

Fig. 5 Patient with subarachnoid hemorrhage complicated by vasospasm had sustained elevation in left middle cerebral artery velocities (**a**) on serial examinations performed daily and was being managed with induced hypertension. During this particular insonation on day 12, no change in mean flow velocity occurred in the left MCA from the previous day (**a**, mean flow velocity 173 cm/s) but the patient had a subtle deterioration in exam. Waveform analysis revealed new finding of a post-stenotic pattern on distal middle cerebral artery insonation (**b**) not seen on prior transcranial Doppler studies suggesting a focal acute MCA flow limiting lesion. Cerebral angiogram revealed a thrombus, and emergent thrombectomy was performed with complete recanalization

insonated proximal to the stenotic segment and low resistance post-stenotic waveforms when insonated distal to the segment with stenosis. Proximal stenotic lesions in the intracranial ICA can cause post-stenotic waveforms in downstream MCA. Due to difficulties in insonation of ICA sometimes this can be the only evidence of hemodynamically significant intracranial ICA stenosis. Figure 5 describes the waveforms in a young patient with subarachnoid hemorrhage on day 12 of her vasospasm watch with high mean flow velocities in the range of moderate-severe vasospasm (173 cm/s, mid segment of middle cerebral artery) but this could be attributable to hyperemia as well, given a favorable relationship between systolic and diastolic flow that points towards low resistance (Fig. 5a). While Lindegaard ratios will be additionally helpful in differentiating these two, the presence of post-stenotic waveforms just distal to the insonated segment directed attention to an acute hemodynamically significant stenosis that incited emergent cerebral angiography (Fig. 5b). Another descriptive example in the follow up of patients being monitored for vasospasm where spectral doppler analysis is helpful, would be progression of waveform patterns to show increased distal

resistance due to increased ICP. Presence of vasospasm with high velocities as seen in Fig. 3c progressing to resistive waveforms in Fig. 3a with apparent normalization of velocities could be a non-invasive marker for diffuse cerebral edema. In both of these cases, assessment of quantitative measures such as velocity alone on serial TCDs would have neglected to bring attention to an acute MCA thrombus discovered on follow up angiogram that was amenable to thrombectomy or diffuse cerebral edema that sequentially decreased diastolic flow in presence of vasospasm without affecting MFV. In these cases, if the neurological exam is limited or confounded, TCD can be a key non-invasive tool to assess patient's cerebral hemodynamics.

Typical flow in a patent vessel is laminar and this may produce clustering of velocities of flowing red blood cells in the vessel lumen. Such clustering is commonly seen in peripheral vessels due to high resistance and called spectral narrowing. In the intracranial circulation, spectral narrowing can be seen in waveforms insonated in stenosed or proximal to high resistance segments (Fig. 3c, j). Extreme cases of spectral narrowing can create harmonics or bruits in the spectral waveforms (Fig. 5a). Spectral broadening is a typical phenomenon seen in turbulent flow downstream of stenosis where laminar flow is interrupted and is a hallmark feature of post-stenotic flow (Fig. 5b). Due to variability of angle of insonation and limitations in adjusting sample size gates to vessel lumen, spectral broadening or narrowing may not be a consistent phenomenon in the intracranial circulation as it is in carotid or peripheral vascular ultrasound and is no longer recommended as a diagnostic criteria. When present, spectral narrowing can be a sign of stenosis (Fig. 3c, j). Another spectral change in stenosed segments could be turbulence- the sonographic correlate of a murmur which can be seen superimposed on the systolic component on the waveform (Fig. 3c).

Effect of cerebral blood flow on cerebral waveforms Flow may be variably affected by resistance. Hence resistive waveforms may progress from preserved to decreased flow as luminal stenosis progresses or vice versa (Fig. 2). Cerebral autoregulation typically targets preserving cerebral blood flow downstream hence presence

of absence of autoregulation may affect changes in spectral waveforms. Patients on systemic vasopressors with intact autoregulation may not manifest any significant change in intracranial waveforms whereas patients with impaired autoregulation may show hyperemic waveforms with induced hypertension or presumed normotension attempted with pressors (Fig. 3f). Such hyperemic injury and its correlate in TCDs is being investigated in post cardiac arrest resuscitation where hyperemic waveforms have been observed during therapeutic temperature modulation and may be a surrogate of reperfusion injury [11]. Another application of ability to distinguish high resistance and high flow states in patients with impaired autoregulation using spectral Doppler is in subarachnoid hemorrhage with vasospasm where induced hypertension continues to be a mainstay. A subset of these patients with impaired autoregulation may continue to have indeterminate velocity elevations with indeterminate ranges in Lindegaard ratios and may be at risk of reperfusion injury after the supposed phase of perfusion dependent delayed cerebral ischemia is over. In post stroke care, emerging reports of flow augmentation across flow limiting lesions not amenable to acute revascularization manifesting as change in spectral patterns on systemic hemodynamic augmentation provide a clinical application and benefit to emergent point of care spectral analysis when existing radiological and clinical information may be insufficient [12].

Collateralization may augment flow in cerebral vessels to compensate for flow limiting lesions. TCD spectral waveforms can be valuable in detecting collateralization patterns [13]. Such collateralization may manifest high velocity waveforms with higher than normal diastolic component or hyperemia waveforms where flow patterns change without obvious change in resistance. Ipsilateral MCA stenosis will often result in hyperemia waveforms in contralateral ACA through AComm recruitment, reversal of ipsilateral ACA and hyperemia in ipsilateral PCA through PComm recruitment eventually leading to reversed ophthalmic recruiting external carotid circulation of the same side. Such patterns of reversal and hyperemia can be a hallmark sign of MCA or intracranial ICA stenosis when either of the vessels cannot be insonated for any reason.

Traumatic brain injury typically shows phasic responses on cerebral blood flow patterns that need more characterization [14]. Limited angiographic studies have shown a hypoperfusion phase followed by hyperemia reperfusion tailed by vasospasm phase in patients with severe TBI [15]. Sonographic characterization of these phases with regard to cerebral blood flow changes and its impact on brain injury needs to be investigated.

Effect of Intracranial compliance effect on cerebral waveforms Lundberg waves and changes in pattern on ICP waves have been long described in the neurocritical care literature [3]. Given the closed compartment created by skull, changes in brain compliance that manifest in ICP waveforms also can be seen in TCD waveforms. The three systolic peaks P1, P2 and P3 can be visualized in spectral waveforms and show similar changes (Fig. 1c). After an ICP crisis, ICP waveforms may have a higher plateau and may manifest decrease in compliance as evidenced by the P2 wave with an equal or greater amplitude than P1 wave (Fig. 4e, f). This results from decrease in the Windkessel effect where decreasing brain compliance decreases the distensability of cerebral blood vessels [9]. This decreased compliance can be seen in TCD waveforms in the anterior circulation in patients who have cerebral edema [9]. It is hypothesized that these patients may have a neurological decline at a lower delta for increased ICP and may need closer monitoring or lower ICP thresholds. Waveforms from insonation of the intracranial vertebrobasilar arteries often show features of decreased compliance in physiological conditions due to the anatomical constraints created by the posterior fossa and do not represent pathology (Fig. 3i). Figure 4 demonstrates a descriptive case with intracranial hemorrhage showing this transition in pattern of P2 relationship with P1 with a compliant waveform (Fig. 4d) on serial assessments on insonation of the middle cerebral artery on the same side as the hemorrhage. Hemorrhage expansion and increase in peri-lesional edema, possibly affected compliance with increase in amplitude of P2 (Fig. 4e, f). Patient suffered an ICP crisis during which the waveforms were noted to be resistive with reversal of flow in early diastole and minimal diastolic flow due to increased distal resistance (Fig. 4b).

Escalating medical therapy and surgical evacuation transitioned the waveforms to positive flow throughout the cardiac cycle though waveforms continue to be relatively high resistance (Fig. 4c). Further investigation needs to be performed in research trials whether addition of spectral Doppler waveform analysis can assist in goal directed therapy in patients at risk of cerebral edema.

Effect of recanalization on cerebral waveforms With wider applications of thrombectomy, recanalization of large vessel occlusions is confirmed by cerebral angiogram and graded by the TICI (Thrombolysis In Cerebral Infarction) score. A similar sonographic grading was proposed to assess recanalization rates after thrombolysis called the Thrombolysis in Brain Ischemia (TIBI) classification [16]. TIBI waveforms are graded as follows: 0, absent; 1, minimal (Fig. 2d); 2, blunted (Fig. 2c); 3, dampened; 4, stenotic (Fig. 2b); and 5, normal (Fig. 2a). In failed recanalization after angiogram, gradual recanalization of thrombosed vessels as evidenced by TCD spectral waveforms can be a correlate of better prognosis. Incidental recurrent thrombosis can be also recognized in high risk patients with confounded exams using spectral waveforms.

Systemic effects on cerebral waveforms Qualitative analysis of the waveforms can be affected in conditions like irregular heart rate (Fig. 3e) or variable pulse pressure. Systemic hemodynamic states such as severe aortic stenosis, presence of heart bypass circuit, can also affect the patterns of spectral waveforms on transcranial Doppler. Patients with severe aortic stenosis may demonstrate post-stenotic waveforms in bilateral anterior and posterior circulation (Fig. 3d). Patient with veno-arterial extracorporeal membrane oxygenation, left ventricular assist devices or undergoing cardiopulmonary bypass intraoperatively for cardiac surgery may have non-pulsatile waveforms (Fig. 3h). In such cases the velocity measured represents the mean flow velocity since the systolic and diastolic phases of the cardiac cycle are missing. Patients with distal atherosclerotic disease especially in advanced age may have higher resistance in distal vessels from non-compliant vessels (Fig. 2b).

Effect of steal of cerebral waveforms Classical description of steal involving vertebral arteries have been extensively studied in relationship to manifest changes in spectral waveforms in neck insonation of vertebral arteries [17]. When steal is severe, changes can also be seen in the intracranial insonation of vertebral arteries through sub-occipital windows. High grades of steal may have complete reversal of vertebral waveforms on affected side with collateralization from opposite vertebral arteries (Fig. 6). Complete reversal of flow in basilar is relatively rare occurrence but has been transiently reported. Rarely, patients with carotid-

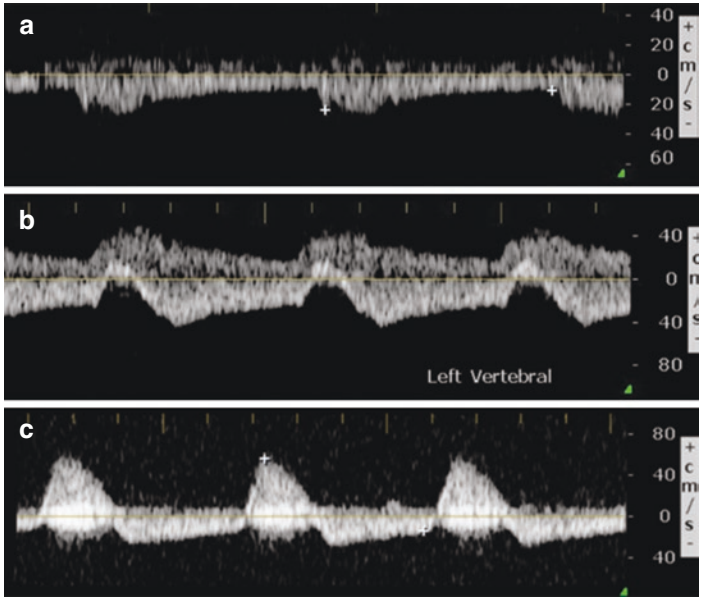

Fig. 6 Vertebral artery waveforms show characteristic waveform changes in presence of subclavian steal syndrome which have been well characterized in literature [17]. Top panel (**a**) shows vertebral vessel insonated via the suboccipital window with flow away from probe showing systolic deceleration. Middle panel (**b**) shows reversal of flow during mid systole that represents a higher grade steal; vertebral artery waveforms are below the baseline with ipsilateral posterior inferior cerebellar artery waveforms superimposed above the baseline. The bottom panel (**c**) shows complete systolic reversal

subclavian bypass procedures with ineffective collateralization across cerebral hemispheres may have intracranial steal waveforms [18]. It is key to note that steal phenomena can be dynamic and triggered by physiological maneuvers like inflating a blood pressure cuff on the same side reducing steal followed by deflation invoking post ischemic reperfusion that may trigger the steal.

Venous compartment of cerebral waveforms Most of the components of the deep cerebral venous system are amenable to insonation by spectral Doppler and show characteristic venous waveforms that appear similar to the blunted waveforms seen in post-stenotic areas on arterial Doppler. The characteristic sound on audible insonation is the *venous hum*. Incidental insonation of basilar veins of Rosenthal is not uncommon during insonation of the distal PCA (Fig. 3g) where a superimposed band of venous spectral Doppler can be seen on the PCA spectrum [18]. The deep middle cerebral veins, basilar vein of Rosenthal, straight sinus, petrosal sinus and transverse sinuses can be insonated via the temporal windows more readily on transcranial duplex with guided B mode. The straight sinus can in addition be insonated via the suboccipital window. More investigations are needed on changes in venous spectral patterns and velocities in different pathologies.

References

1. Alexandrov AV. Extra- and intracranial waveform analysis algorithm, descriptions, classifications, and differential diagnosis. J Vasc Ultrasound. 2015;39(4):192–202.
2. D'Andrea A, Conte M, Scarafile R, Riegler L, Cocchia R, Pezzullo E, et al. Transcranial Doppler ultrasound: physical principles and principal applications in Neurocritical care unit. J Cardiovasc Echogr. 2016;26(2):28–41.
3. Cardoso ER, Rowan JO, Galbraith S. Analysis of the cerebrospinal fluid pulse wave in intracranial pressure. J Neurosurg. 1983;59(5):817–21.
4. Hwang JY. Doppler ultrasonography of the lower extremity arteries: anatomy and scanning guidelines. Ultrasonography. 2017;36(2):111–9.
5. Alexandrov AV. The Spencer's curve: clinical implications of a classic hemodynamic model. J Neuroimaging. 2007;17(1):6–10.

6. Spencer MP, Reid JM. Quantitation of carotid stenosis with continuous-wave (C-W) Doppler ultrasound. Stroke. 1979;10(3):326–30.
7. Cardona P, Quesada H, Cano L, Campelacreu J, Escrig A, Mora P, et al. Oscillating transcranial Doppler patterns of brain death associated with therapeutic maneuvers. Pers Med. 2012;1(1):321–4.
8. Kumar G, Alexandrov AV. Vasospasm surveillance with transcranial Doppler sonography in subarachnoid hemorrhage. J Ultrasound Med. 2015;34(8):1345–50.
9. Aggarwal S, Brooks DM, Kang Y, Linden PK, Patzer JF II. Noninvasive monitoring of cerebral perfusion pressure in patients with acute liver failure using transcranial doppler ultrasonography. Liver Transpl. 2008;14(7):1048–57.
10. Ducrocq X, Hassler W, Moritake K, Newell DW, von Reutern GM, Shiogai T, et al. Consensus opinion on diagnosis of cerebral circulatory arrest using Doppler-sonography: Task Force Group on cerebral death of the Neurosonology Research Group of the World Federation of neurology. J Neurol Sci. 1998;159(2):145–50.
11. Iordanova B, Li L, Clark RSB, Manole MD. Alterations in cerebral blood flow after resuscitation from cardiac arrest. Front Pediatr. 2017;5:174.
12. Gomez J, Wolfe S, Sarwal A. Sonographic demonstration of a perfusion-dependent stroke with negative MRI and a flow-limiting stenosis. Neurocrit Care. 2020;32(3):883–8.
13. Muller M, Hermes M, Bruckmann H, Schimrigk K. Transcranial Doppler ultrasound in the evaluation of collateral blood flow in patients with internal carotid artery occlusion: correlation with cerebral angiography. Am J Neuroradiol. 1995;16(1):195–202.
14. Ziegler D, Cravens G, Poche G, Gandhi R, Tellez M. Use of transcranial Doppler in patients with severe traumatic brain injuries. J Neurotrauma. 2017;34(1):121–7.
15. Inoue Y, Shiozaki T, Tasaki O, Hayakata T, Ikegawa H, Yoshiya K, et al. Changes in cerebral blood flow from the acute to the chronic phase of severe head injury. J Neurotrauma. 2005;22(12):1411–8.
16. Demchuk AM, Burgin WS, Christou I, Felberg RA, Barber PA, Hill MD, et al. Thrombolysis in brain ischemia (TIBI) transcranial Doppler flow grades predict clinical severity, early recovery, and mortality in patients treated with intravenous tissue plasminogen activator. Stroke. 2001;32(1):89–93.
17. Kliewer MA, Hertzberg BS, Kim DH, Bowie JD, Courneya DL, Carroll BA. Vertebral artery Doppler waveform changes indicating subclavian steal physiology. Am J Roentgenol. 2000;174(3):815–9.
18. Baumgartner RW, Gönner F, Arnold M, Müri RM. Transtemporal power- and frequency-based color-coded duplex sonography of cerebral veins and sinuses. AJNR Am J Neuroradiol. 1997;18(9):1771–81.

Transcranial Doppler for Monitoring in the Neurocritical Care Unit

Toufic Chaaban, Danilo Cardim, and Shraddha Mainali

Introduction

Transcranial Doppler (TCD) is a valuable noninvasive tool for bedside monitoring in Neurocritical care. It is most commonly used in the Neurocritical Care unit (NCCU) for assessment of cerebral blood flow (CBF), cerebral artery vasospasm, vasomotor reactivity (VMR)/Cerebral autoregulation (CA), emboli detection and as a tool for indirect measurement of intracranial pressure (ICP). While absolute TCD values have limited utility, TCD trends provide important insight into the dynamics of intracranial pathophysiology. TCD should be an integral component of

T. Chaaban
Division of Stroke and Neurocritical Care, Department of Neurology, The Ohio State University, Columbus, OH, USA

D. Cardim
Department of Neurology and Neurotherapeutics, University of Texas Southwestern Medical Center, Dallas, TX, USA

S. Mainali (✉)
Department of Neurology, Virginia Commonwealth University, Richmond, VA, USA
e-mail: shraddha.mainali@vcuhealth.org

W. C. Ziai, C. L. Cornwell (eds.), *Neurovascular Sonography*,
https://doi.org/10.1007/978-3-030-96893-9_4

multimodal monitoring in the NCCU as it can be frequently used at the bedside due to its non-invasive and cost-effective nature. Available TCD values should be considered in regard to hemodynamic parameters including heart rate, blood pressure, hemoglobin/hematocrit and partial pressure of carbon dioxide ($PaCO_2$) as these factors can alter CBF and hence TCD parameters.

Transcranial Color-Coded Duplex (TCCD) enables color-coded imaging of intracranial arterial blood flow in red and blue, respectively, indicating flow toward and away from the probe. Besides its usefulness in identifying the insonated vessels during vasospasm monitoring, it has also shown to be helpful in screening for midline shift, hematoma volume assessment and to follow evolution of hydrocephalus.

Advantages of TCD/TCCD include non-invasive technology, bedside application, absence of ionizing radiation and cost-effectiveness. On the other hand, some of the challenges include requirement of specific skills for data acquisition and interpretation, interrater-variability and technical challenges due to poor TCD windows. In this chapter, we will focus on the utility of TCD/TCCD in the Neurocritical Care Unit. The role of TCD in specific diseases is discussed separately.

I. **Common indications of TCD in the NCCU**
   1. Vasospasm monitoring
   2. Monitoring of cerebral autoregulation and cerebrovascular reactivity
   3. Assessment of intracranial pressure
   4. Cerebral emboli detection
   5. To assess patency of cerebrovascular bypass graft
   6. Ancillary testing for brain death
   7. Assessment of cerebral vascular occlusion or revascularization post thrombolysis

II. **Common indications of TCCD in the NCCU**
   1. Vasospasm monitoring
   2. Assessment of hydrocephalus
   3. Assessment of hematoma volume
   4. Assessment of midline shift

Transcranial Doppler

1. **Vasospasm monitoring**

   TCD is routinely used in the NCCU for vasospasm monitoring in patients with subarachnoid hemorrhage as well as traumatic brain injury (TBI). Mean flow velocities (mFV) are measured in the anterior and posterior circulation bilaterally in the following vessels:

   (a) Middle cerebral artery (MCA)
   (b) Anterior cerebral artery (ACA)
   (c) Carotid siphon (SIPH)
   (d) Ophthalmic artery (OA)
   (e) Posterior cerebral artery (PCA)
   (f) Vertebral artery (VA)
   (g) Basilar artery (BA)
   (h) Terminal internal carotid artery (TICA)

TCD velocities, in addition to Lindegaard ratio (LR) is used to predict the degree of vasospasm. The LR represents the ratio between the velocity of the MCA or ACA and the ipsilateral extracranial ICA and can help differentiate changes caused by generalized hyperemia from vasospasm. A similar ratio can also be obtained between the basilar artery and the extracranial vertebral artery.

Normal mFV in the MCA in adults range from 50 to 80 cm/s (Fig. 1a); in the ACA, 35 to 60 cm/sec; in the PCA, 30 to 50 cm/sec; and in the basilar artery, 25 to 50 cm/s. In general, the veloc-

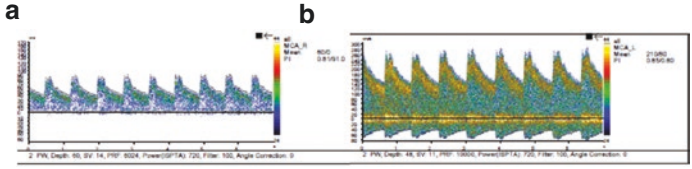

Fig. 1 (**a**) Normal spectral waveform (MCA). (**b**) Severe vasospasm (MCA)

ity in the OA is roughly one-fourth the velocity in the MCA whereas the velocity in the PCAs, VAs and BA is about one-half the velocity in the MCA.

Use of TCD is known to most reliably predict vasospasm in the proximal MCAs (Fig. 1b) in 97% of SAH patients with 67% sensitivity and 99% specificity. An MFV <120 cm/s in the MCA has a 94% negative predictive value, while an MFV >200 cm/s has an 87% positive predictive value [1]. For ACAs absolute values are less reliable with sensitivity and specificity of only 42% and 76%, respectively [1]. More specific measures for ACA vasospasm are findings of ≥50% increase in mFV or increase by >50 cm/s within a 24-hour period. For PCAs, rising velocity trends may be more predictive of vasospasm than absolute values. In the BA, vasospasm is estimated by the ratio of BA to extracranial VA (ECVA), also known as Soustiel's ratio [2].

- BA/ECVA >2: Basilar artery vasospasm
- BA/ECVA >2.5: Moderate to severe spasm
- BA/ECVA >3: Severe vasospasm

In addition, vasospasm is known to occur in 35 to 61% of traumatic brain injury patients [3] and can lead to secondary brain injury. Vasospasm in the BA has been reported to occur more commonly after traumatic SAH than aneurysmal SAH. In the ICU, TCD based evaluation of vasospasm may help guide management including optimization of CPP.

It is important to note that elevated velocities can also occur in the setting of hyperemia. Therefore, clinical context and the LR should be taken into account while interpreting TCD velocities. Table 1 represents the vasospasm grading criteria based on mFV and LR.

2. **TCD for Intracranial Pressure Estimation**

   Monitoring of intracranial pressure (ICP) is an important aspect of NCCU management in patients with acute brain injury. In the Neuro ICU, ICP is typically measured by an intra-parenchymal probe or intraventricular catheter. In circumstances where invasive ICP monitoring is not possible,

Table 1 American Society of Neuroimaging TCD Grading criteria for MCA vasospasm [4, 5]

Mean flow velocity (MFV) (cm/s)	MCA/ICA MFV ratio (Lindegaard)	Interpretation
<120	<3	Hyperemia
>80	3–4	Hyperemia + possible mild spasm
>120	3–4	Mild spasm + hyperemia
>120	4–5	Moderate spasm + hyperemia
>120	5–6	Moderate spasm
>180	6	Moderate-to-severe spasm
>200	>6	Severe spasm
>200	4–6	Moderate spasm + hyperemia
>200	3–4	Hyperemia + mild (often residual) spasm
>200	<3	Hyperemia

TCD may be used for indirect ICP estimation. Several TCD based methods can be used for indirect assessment of ICP as described below:

Gosling Pulsatility Index:
Pulsatility index (PI) is the ratio derived from the difference between systolic velocity (FVs) and diastolic velocity (FVd) divided by mean velocity (FVm)

$$\text{PI} = \frac{\boldsymbol{FVs - FVd}}{\boldsymbol{FVm}}$$

In patients with raised ICP, the passive flow or diastolic flow is significantly impacted compared to the systolic flow, which leads to a characteristic high resistance flow pattern with elevation of PI >1.2 (Fig. 2). This measure is independent of angle of insonation, hence is not operator dependent. However, it is important to note that PI is also dependent on other variables like cerebral perfusion pressure (CPP), arterial blood pressure (ABP), arterial pulsatility/compliance of the cerebral arterial bed, heart rate and the variation in partial pressure of CO_2 (PCO_2). The normal PI ranges from 0.7 to 1.1. Although elevation of PI may indicate rise in ICP [6–8],

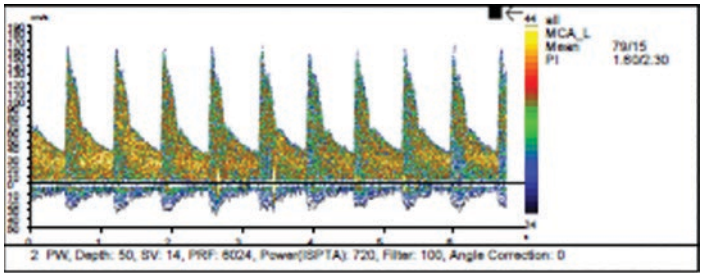

Fig. 2 High resistance flow pattern with elevation of PI

Table 2 Causes of elevated Pulsatility Index. PI: Pulsatility Index, ICP: Intracranial Pressure

PI>1.2, End diastolic flow present	PI>2, End diastolic flow absent
All arteries: Hyperventilation Increased cardiac output Hypertension Increased ICP	All arteries: Distal arterial occlusions Extremely high ICP Arrest of cerebral circulation
Unilateral: Compartmental increase in ICP Distal stenosis	Unilateral: Compartmental increase in ICP Distal stenosis
One artery: Distal obstruction (spasm, stenosis, edema)	One artery: Distal obstruction (spasm, stenosis, edema)

it is important to note the PI may be elevated due to increase in distal vascular resistance (e.g., hypocapnia with related vasoconstriction) with associated *decrease* in ICP. Hence, use of PI based ICP estimation is mostly helpful to assess trends and elevated PI should not be used as an absolute indicator of rise in ICP. When interpreting abnormal values, it is important to consider whether arterial involvement is diffuse or focal and whether end diastolic flow is present or absent in addition to the overall clinical picture. Examples of causes of elevated PI are summarized in Table 2.

Non-invasive Cerebral Perfusion Pressure based ICP estimation

This method for noninvasive cerebral perfusion pressure (nCPP) measurement using TCD was originally described by Czosnyka et al. in 1998 [9].More recently, Schmidt et al. demonstrated a good correlation between nCPP and invasive CPP measurement using the formula [10]

$$\text{nCPP} = \boldsymbol{MAP} * \frac{\boldsymbol{FVd}}{\boldsymbol{FVm}} + \mathbf{14}\,\text{mm}\,Hg$$

Where, FVd (diastolic flow velocity); FVm (mean flow velocity); MAP (mean arterial pressure)

The FVd and FVm are measured in bilateral MCAs at a depth of 4.5–6 cm.

Once nCPP is calculated, nICP (non-invasive ICP) is derived by using the formula:

$$\text{nICP} = \text{MAP} - \text{nCPP}$$

This method has shown satisfactory correlation with direct CPP measurement within the CPP range of 60–100 mm Hg. However, it is important to note that local mass effect and auto-regulatory dysfunction can significantly alter measurements between the two sides.

Several other methods for nCPP based ICP calculation have also been suggested [6, 7]

nICP Measurement based on Ophthalmic Artery Insonation:

In this method, both internal and external segments of the ophthalmic artery (OA) are insonated. The intracranial segment is pathologically compressed by raised ICP thereby affecting blood flow. The extracranial segment is artificially compressed by applying graded external pressure (Pe) around the eyeball. Pressure is increased gradually until flow in the extracranial segment equals flow in the intracranial segment. This Pe is assumed to reflect ICP;

i.e. Pe = ICP. Certain devices (e.g Cerepress or Vittamed 205 devices) have been used for external pressure application. This method has fair sensitivity and specificity in the order of around 70% and 80% respectively [11, 12]

Optic Nerve Sheath Diameter (ONSD)

CSF circulates in the optic nerve sheath postero-anteriorly. Due to the trabeculated nature of the retrobulbar part of the nerve sheath, it is distensible and ICP changes are quickly reflected (within seconds) as the nerve sheath dilates. ONSD measured 3 mm behind the retina has better accuracy for detection of increased ICP when compared to other TCD based methods [13, 14]. However, the diameter cutoff for detection of intracranial hypertension is still debatable and ranges somewhere between 5–6 mm [15].

3. **Vasomotor Reactivity and Cerebral Autoregulation Monitoring:**

Cerebral Autoregulation:

Cerebral autoregulation (CA) is a homeostatic process that allows the maintenance of cerebral blood flow (CBF) across a wide range of arterial blood pressures (MAP 50–150 mm Hg) (Fig. 3). In patients with impaired CA, the cerebral blood flow directly cor-

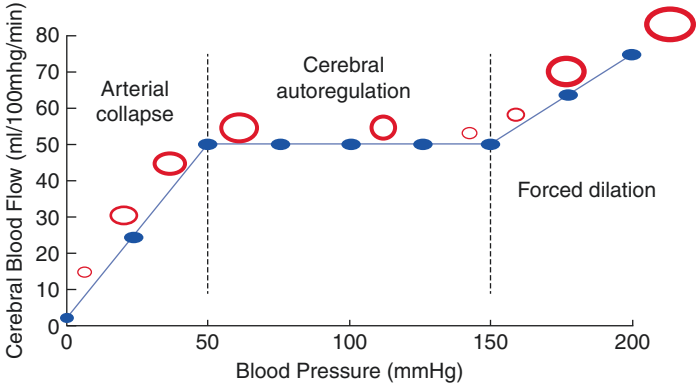

Fig. 3 Normal cerebral autoregulation curve

relates with MAP which may result in hypo or hyper-perfusion leading to secondary brain injury.

Loss of CA is commonly seen in patients with acute brain injury including TBI, SAH, ischemic stroke, hypoxic ischemic injury and inflammatory brain diseases. Impairment of CA can lead to poor functional outcome and mortality in TBI [16], higher risk of delayed cerebral ischemia in SAH [17] and larger infarct size in ischemic stroke patients [18].

Monitoring of autoregulation can be useful in guiding management of cerebral perfusion pressure and prognostication in acute brain injury (Weak recommendation, moderate quality of evidence) [19]. Continuous bedside monitoring of CA can be helpful to determine optimal CPP levels in patients with acute brain injury.

Cerebral autoregulation can be assessed by measuring relative blood flow changes (change in mFV in MCA as a result of constriction or dilation of distal cerebrovascular bed) in response to a change in CPP (static method) or by measuring the rate at which such adaptive changes occur in the event of a sudden fluctuation of CPP (dynamic method).

Methods for assessing Static and Dynamic Cerebral Autoregulation:

- **Static autoregulation:** Vasoactive agent is given to increase CPP by >20 mm Hg.

Thereafter, static autoregulatory index (sARI) is calculated as follows:

$$sARI = \%\Delta eCVR / \%\Delta CPP$$

where, estimated cerebrovascular reserve (eCVR) = MAP/mFVmca

mFVmca indicates mean flow velocity in the middle cerebral artery

When sARI is 0, cerebral autoregulation is exhausted and CBF changes linearly with CPP. Values ≤ 0.39 are considered impaired and ≥ 0.4 are normal.

Static autoregulation can also be calculated using Mx (correlation between mean flow velocity and mean CPP) where correlation coefficient between CPP and mFV are evaluated. Autoregulation is impaired when Mx <0.3 and intact when ≥0.3.

Other invasive (CPP based) and non-invasive (MAP based) ways of static CA assessment using TCD flow velocities have been described in the literature as follows:

- Sx – correlation between FVs and mean CPP
- Dx – correlation between FVd and mean CPP

The terms Mxa, Sxa and Dxa are used when CA is assessed using MAP instead of CPP.

- **Dynamic autoregulation:** Assessed by inflating BP cuff on the thigh for 3 mins (20 mm Hg above systolic pressure) followed by sudden deflation to measure mFV in MCA.

The dynamic autoregulatory index (dARI) can be calculated by comparing pre and post-deflation MCA velocities by using the following formula:

$$\text{dARI} = \left(\Delta\text{eCVR} / \Delta T\right) / \text{MAP}$$

where eCVR = MAP/MFV_{mca} and ΔT = time (seconds)

While some studies have found a correlation between indices based on MAP and CPP [20], CPP based indices have been shown to perform better in outcome and mortality prediction [21]. In addition, comparative studies have shown that Mx correlates better with laser doppler flowmetry changes suggesting its correlation with small vessel and microcirculatory dynamics [22].

Assessment of Vasomotor Reactivity (VMR):
VMR is defined as the percentage change in mean flow velocity (measured in MCAs) after stimulus application (CO_2 or acetazolamide) compared to flow velocity at rest. The CO_2 stimulus can be provided either by 30 seconds of breath holding or by infusion of 5% CO_2 through the ETT in intubated patients. Since most

patients in the NCCU with acute brain injury are intubated, infusion of the 5% CO_2 is a reasonable approach.

VMR can be calculated using the following formula:

$$\text{VMR} = \frac{\left(mFVmax - mFVmin\right)}{mFVbaseline} \times 100$$

Procedure is performed by measuring mFVbaseline in a normocarbic state (pCO_2 35–45 mm Hg). The 5% inhaled CO_2 is then administered and mFVmax is measured after achieving $ETCO_2$ increase by 10 mm Hg. The patient is then hyperventilated until $ETCO_2$ decreases by 10 mm Hg from baseline normocarbic state and mFVmin is measured.

Normal response is increase in MCA velocity by 2–4% per mm Hg increase in $PaCO_2$.

Interpretation:

- VMR <15%-exhausted
- VMR 16–38%- severely decreased
- VMR 39–69%- moderately decreased
- VMR ≥70%- normal

Acetazolamide (1 g injection) can also be used for CA assessment. Acetazolamide prevents conversion of carbonic acid (H_2CO_3) to CO_2 and H_20 thereby decreasing pH, which leads to vasodilation. In individuals with intact autoregulation, CBF increases by 30–60% using this method.

4. **Patency of Cerebrovascular Bypass and Quality of Blood Flow**

   In patients with high flow bypass (radial artery or saphenous vein graft) blood flow rates range between 65–200 ml/min with mean flow velocity of 130 ml/min. Rates <65 ml/min or >200 ml/min are associated with ischemia and hyperemia respectively. Low flow bypass (superficial temporal artery) has a flow rate <65 ml/min. In low flow bypasses, peak velocities are used due to difficulty in accurate assessment of the narrow vascular lumen. A focal increase in peak velocity or slow systolic upstroke suggests stenosis.

5. **Microemboli Detection**

   TCD can be used for detection of microemboli in patients with stroke (cryptogenic, atheroembolic, post aneurysm coiling or intracranial stent etc). Detection of microemboli and assessment of embolic burden can be helpful in guiding management in high-risk stroke patients.

6. **Assessment of Cerebral Artery Revascularization or Re-occlusion**

   TCD can also be used to assess revascularization post thrombolysis or to assess re-occlusion of a proximal intracranial vessel. Demchuck et al. evaluated a TCD based score 'thrombolysis in brain ischemia score (TIBI)' in 109 patients with IV thrombolysis and successfully demonstrated imaging correlation with initial stroke severity, clinical recovery, and mortality [23]. The TIBI score ranges from grade 0 to 5 with grade 0 indicating absence of pulsatile flow and grade 5 corresponding to normal flow. In comparison to DSA, TCD is more than 85% sensitive and specific in detecting supraclinoid ICA or proximal MCA segment lesions. The use of contrast-enhanced color-coded duplex sonography can be especially useful in this context to identify the insonated vessel.

7. **Ancillary Test for Brain Death determination**

   TCD is commonly used as an ancillary test for brain death determination as it provides a convenient bedside assessment of intracranial flow. Catastrophic brain injuries cause significant increase in ICP which progressively diminishes cerebral perfusion pressure leading to cerebral circulatory arrest. The dynamic changes in the intracranial flow related to rising ICP is reflected in the TCD. A meta-analysis by Chang et al. evaluated TCD in brain death determination and suggested sensitivity and specificity of 0.90 (95% CI, 0.87–0.92) and 0.98 (95% CI, 0.96–0.99) respectively [24]. In the right clinical context, TCD findings can confirm the determination of brain death. To reduce the chance of false positives, complete evaluation of the intracranial circulation is important. TCD findings should include a lack of diastolic flow or reverberating flow, small systolic peaks in early systole or a complete lack of flow found by the operator who previously demonstrated adequate for-

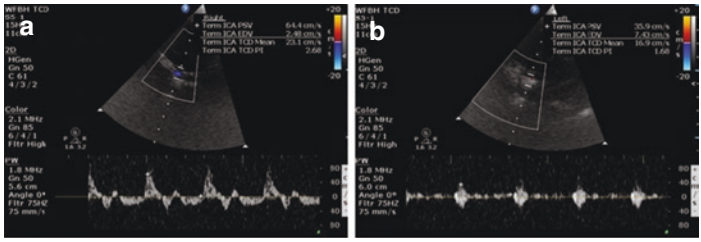

Fig. 4 (**a**) The oscillating flow pattern is defined as forward and reverse flow in one cardiac cycle with almost the same area under the envelop of the waveform. (**b**) Systolic spikes are sharp unidirectional signals in early systole, <200 ms duration, <50 cm/s peak systolic velocity, and without a flow signal during the remaining cardiac cycle

ward flow. The oscillating flow pattern is defined as forward and reverse flow in one cardiac cycle with almost the same area under the envelope of the waveform (Fig. 4a). Systolic spikes are sharp unidirectional signals in early systole, <200 ms duration, <50 cm/s peak systolic velocity, and without a flow signal during the remaining cardiac cycle (Fig. 4b). It is important to realize the limitation that TCD is helpful in measuring intracranial blood flow, but not the function of the brainstem.

Transcranial Color-Coded Ultrasound

Transcranial color-coded ultrasound (TCCS) allows visualization of intracranial structures including ventricular system and hematomas, in addition to visualization of the proximal vessels and the circle of Willis. It has multiple potential bedside applications in the NCCU, some of which are discussed below.

1. **Midline Shift**

   TCCD can be used to detect and follow brain midline shift (MLS) using a 2–5 MHz probe over the temporal window. The third ventricle is identified as a double hyperechogenic image over the midbrain. The distance from the skin (temporal win-

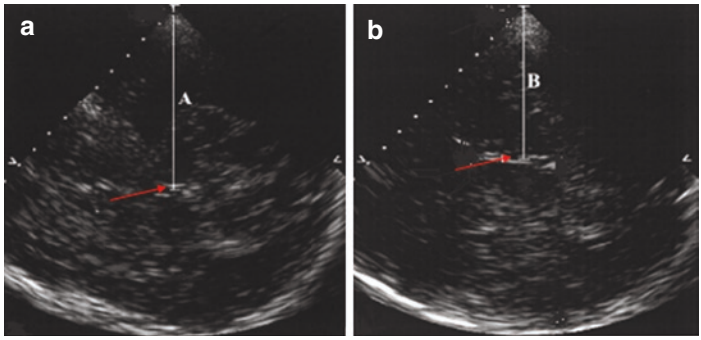

Fig. 5 **a** = measurement from right temporal window. **b** = measurement from L temporal window. Midline shift = A–B/2. The red arrow indicates 3rd ventricle

dow) to the middle of the third ventricle from each side [left and right] is measured. The midline shift will equal "long distance minus short distance/2 [25] (Fig. 5).

$$\text{i.e MLS} = \frac{A - B}{2}$$

This method was first described by Seidel et al. in 1996 [26]. Using a cutoff of 0.35 this method has 84.6% sensitivity, 84% specificity and 0.86 AUC when compared to computed tomography (CT) scans [27]. Other reports also confirmed good correlation in the setting of intracranial hemorrhage [28].

2. **Hematoma Volume**

   Supratentorial and infratentorial hematomas can be identified by TCCD in patients with adequate bone windows, making hematoma volume measurement and expansion monitoring feasible at the bedside (Fig. 6). Excellent correlation with CT measurements was reported for both hematoma volume [28] and growth [29].
3. **Hydrocephalus**

   The TCCD can be used to evaluate hydrocephalus in the NCCU as cerebrospinal fluid (CSF) appears anechoic com-

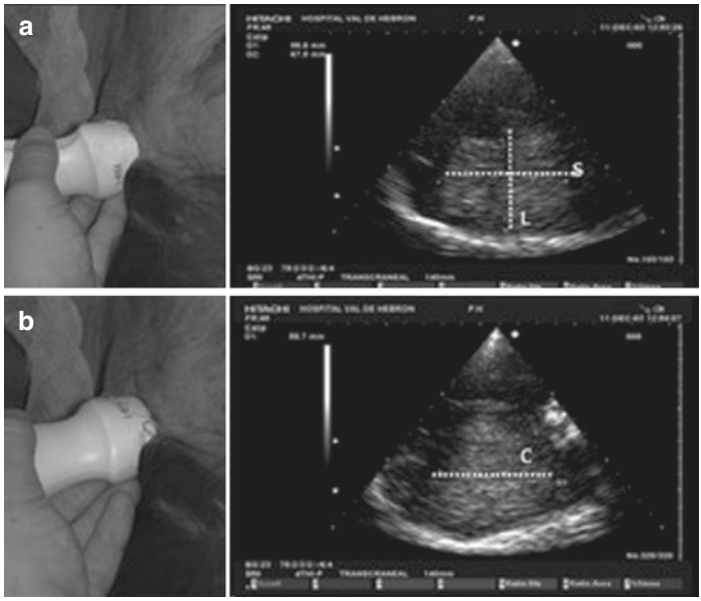

Fig. 6 Figure demonstrates measurement of intracranial hemorrhage volume using axial (**a**) and coronal (**b**) planes. Volume = LxSXC/2

pared to ependymal cells lining the cerebral ventricles that are hyperechoic. The 3rd and lateral ventricles appear as double hyperechogenic lines containing the anechoic CSF. Excellent correlation has been shown between TCCD and CT measurements of width of the 3rd ventricle, bifrontal horns and middle part of the lateral ventricles [30, 31] (Fig. 7).

Future Perspectives

Traditionally, TCD monitoring is a labor-intensive technique, with limited ability to obtain only intermittent and short duration recordings, typically ranging from 30 min to 1-h duration. Furthermore, application of TCD in the NCCU setting for long durations has been limited given the complexity of care, regular

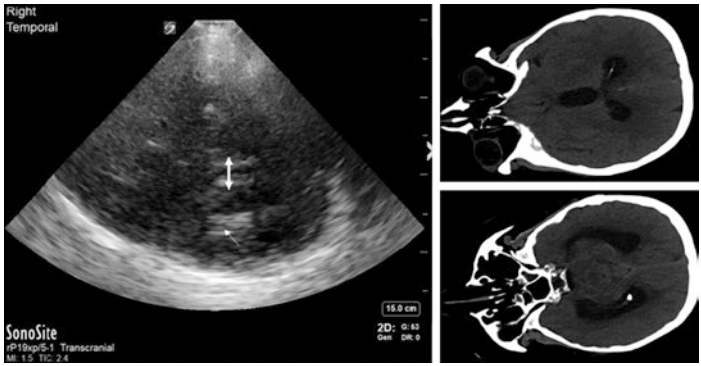

Fig. 7 Figure represents ultrasound measurement of hydrocephalus. The thick arrow measures dilation of the 3rd ventricle. The thin arrow represents incidental finding of hyperechoic choroid plexus in the temporal horn

bedside nursing care, patient manipulations, and presence of various other monitoring modalities. This limits the ability to extract important variables continuously, such as cerebral autoregulation and continuous assessment of intracranial pressure noninvasively. State-of-the-art advances in robotics have led to the development of robotically driven TCD probes, integrated with automated detection and optimization of FV signals. Given the novelty of these devices, they have not been readily applied to the NCCU setting. However, given this advancement, they provide the potential to improve dramatically the ability to obtain longer, uninterrupted, and eventually continuous TCD recordings, particularly in the moderate and severe TBI patient population.

Conclusion and Recommendations

TCD is a neuromonitoring tool that is noninvasive, portable, safe and cost-effective and has a wide range of utility in guiding day to day management in the NCCU. It is useful to incorporate TCD in the NCCU as part of a multimodal monitoring strategy. Although properly obtained TCD measures provide valuable clinical insight in patients with acute brain injury, it is important to be mindful of

its limitations and use alternate strategies of neuromonitoring when/where needed.

Acknowledgements The authors would like to thank Aarti Sarwal MD and Christy Cornwell BS, RVT, NVS for providing necessary images for this chapter.

References

1. Lysakowski C, Walder B, Costanza MC, Tramèr MR. Transcranial Doppler versus angiography in patients with vasospasm due to a ruptured cerebral aneurysm: a systematic review. Stroke. 2001;32:2292–8.
2. Sviri GE, Ghodke B, Britz GW, Douville CM, Haynor DR, Mesiwala AH, Lam AM, Newell DW. Transcranial Doppler grading criteria for basilar artery vasospasm. Neurosurgery. 2006;59:360–6; discussion 360-6.
3. Perrein A, Petry L, Reis A, Baumann A, Mertes P, Audibert G. Cerebral vasospasm after traumatic brain injury: an update. Minerva Anestesiol. 2015;81:1219–28.
4. Lindegaard KF, Nornes H, Bakke SJ, Sorteberg W, Nakstad P. Cerebral vasospasm diagnosis by means of angiography and blood velocity measurements. Acta Neurochir. 1989;100:12–24.
5. Kumar G, Alexandrov AV. Vasospasm surveillance with transcranial Doppler sonography in subarachnoid hemorrhage. J Ultrasound Med. 2015;34:1345–50.
6. Wakerley BR, Kusuma Y, Yeo LL, Liang S, Kumar K, Sharma AK, Sharma VK. Usefulness of transcranial Doppler-derived cerebral hemodynamic parameters in the noninvasive assessment of intracranial pressure. J Neuroimaging. 2015;25:111–6.
7. Cardim D, Schmidt B, Robba C, Donnelly J, Puppo C, Czosnyka M, Smielewski P. Transcranial Doppler monitoring of intracranial pressure plateau waves. Neurocrit Care. 2017;26:330–8.
8. Cardim D, Robba C, Donnelly J, Bohdanowicz M, Schmidt B, Damian M, Varsos GV, Liu X, Cabeleira M, Frigieri G, Cabella B, Smielewski P, Mascarenhas S, Czosnyka M. Prospective study on noninvasive assessment of intracranial pressure in traumatic brain-injured patients: comparison of four methods. J Neurotrauma. 2016;33:792–802.
9. Czosnyka M, Matta BF, Smielewski P, Kirkpatrick PJ, Pickard JD. Cerebral perfusion pressure in head-injured patients: a noninvasive assessment using transcranial Doppler ultrasonography. J Neurosurg. 1998;88(5):802–8.

10. Schmidt EA, Czosnyka M, Gooskens I, Piechnik SK, Matta BF, Whitfield PC, Pickard JD. Preliminary experience of the estimation of cerebral perfusion pressure using transcranial Doppler ultrasonography. J Neurol Neurosurg Psychiatry. 2001;70:198–204.
11. Bershad EM, Anand A, DeSantis SM, Yang M, Tang RA, Calvillo E, Malkin-Gosdin L, Foroozan R, Damani R, Maldonado N, Gupta P, Tan B, Venkatasubba Rao CP, Suarez JI, Clark JB, Sutton JP, Donoviel DB. Clinical validation of a transcranial Doppler-based noninvasive intracranial pressure meter: a prospective cross-sectional study. World Neurosurg. 2016;89:647–653.e1.
12. Ragauskas A, Bartusis L, Piper I, Zakelis R, Matijosaitis V, Petrikonis K, Rastenyte D. Improved diagnostic value of a TCD-based non-invasive ICP measurement method compared with the sonographic ONSD method for detecting elevated intracranial pressure. Neurol Res. 2014;36:607–14.
13. Robba C, Cardim D, Tajsic T, Pietersen J, Bulman M, Donnelly J, Lavinio A, Gupta A, Menon DK, Hutchinson PJA, Czosnyka M. Ultrasound non-invasive measurement of intracranial pressure in neurointensive care: a prospective observational study. PLoS Med. 2017;14:e1002356.
14. Martin M, Lobo D, Bitot V, Couffin S, Escalard S, Mounier R, Cook F. Prediction of early intracranial hypertension after severe traumatic brain injury: a prospective study. World Neurosurg. 2019;127:e1242–8.
15. Kimberly HH, Shah S, Marill K, Noble V. Correlation of optic nerve sheath diameter with direct measurement of intracranial pressure. Acad Emerg Med. 2008;15:201–4.
16. Sorrentino E, Budohoski KP, Kasprowicz M, Smielewski P, Matta B, Pickard JD, Czosnyka M. Critical thresholds for transcranial Doppler indices of cerebral autoregulation in traumatic brain injury. Neurocrit Care. 2011;14:188–93.
17. Budohoski KP, Czosnyka M, Smielewski P, Kasprowicz M, Helmy A, Bulters D, Pickard JD, Kirkpatrick PJ. Impairment of cerebral autoregulation predicts delayed cerebral ischemia after subarachnoid hemorrhage: a prospective observational study. Stroke. 2012;43:3230–7.
18. Reinhard M, Rutsch S, Lambeck J, Wihler C, Czosnyka M, Weiller C, Hetzel A. Dynamic cerebral autoregulation associates with infarct size and outcome after ischemic stroke. Acta Neurol Scand. 2012;125:156–62.
19. Czosnyka M, Miller C. Monitoring of cerebral autoregulation. Neurocrit Care. 2014;21(Suppl 2):S95–102.
20. Lavinio A, Schmidt EA, Haubrich C, Smielewski P, Pickard JD, Czosnyka M. Noninvasive evaluation of dynamic cerebrovascular autoregulation using Finapres plethysmograph and transcranial Doppler. Stroke. 2007;38:402–4.
21. Rivera-Lara L, Zorrilla-Vaca A, Geocadin R, Ziai W, Healy R, Thompson R, Smielewski P, Czosnyka M, Hogue CW. Predictors of outcome with

cerebral autoregulation monitoring: a systematic review and meta-analysis. Crit Care Med. 2017;45:695–704.
22. Zeiler FA, Donnelly J, Cardim D, Menon DK, Smielewski P, Czosnyka M. ICP versus laser Doppler cerebrovascular reactivity indices to assess brain autoregulatory capacity. Neurocrit Care. 2018;28:194–202.
23. Demchuk AM, Burgin WS, Christou I, Felberg RA, Barber PA, Hill MD, Alexandrov AV. Thrombolysis in brain ischemia (TIBI) transcranial Doppler flow grades predict clinical severity, early recovery, and mortality in patients treated with intravenous tissue plasminogen activator. Stroke. 2001;32:89–93.
24. Chang JJ, Tsivgoulis G, Katsanos AH, Malkoff MD, Alexandrov AV. Diagnostic accuracy of transcranial Doppler for brain death confirmation: systematic review and meta-analysis. AJNR Am J Neuroradiol. 2016;37:408–14.
25. Gerriets T, Stolz E, König S, Babacan S, Fiss I, Jauss M, Kaps M. Sonographic monitoring of midline shift in space-occupying stroke: an early outcome predictor. Stroke. 2001;32:442–7.
26. Seidel G, Gerriets T, Kaps M, Missler U. Dislocation of the third ventricle due to space-occupying stroke evaluated by transcranial duplex sonography. J Neuroimaging. 1996;6:227–30.
27. Motuel J, Biette I, Srairi M, Mrozek S, Kurrek MM, Chaynes P, Cognard C, Fourcade O, Geeraerts T. Assessment of brain midline shift using sonography in neurosurgical ICU patients. Crit Care. 2014;18:676.
28. Kukulska-Pawluczuk B, Książkiewicz B, Nowaczewska M. Imaging of spontaneous intracerebral hemorrhages by means of transcranial color-coded sonography. Eur J Radiol. 2012;81:1253–8.
29. Pérez ES, Delgado-Mederos R, Rubiera M, Delgado P, Ribó M, Maisterra O, Ortega G, Alvarez-Sabin J, Molina CA. Transcranial duplex sonography for monitoring hyperacute intracerebral hemorrhage. Stroke. 2009;40:987–90.
30. Becker G, Bogdahn U, Strassburg HM, Lindner A, Hassel W, Meixensberger J, Hofmann E. Identification of ventricular enlargement and estimation of intracranial pressure by transcranial color-coded real-time sonography. J Neuroimaging. 1994;4:17–22.
31. Seidel G, Kaps M, Gerriets T, Hutzelmann A. Evaluation of the ventricular system in adults by transcranial duplex sonography. J Neuroimaging. 1995;5:105–8.

Transcranial Doppler in Subarachnoid Hemorrhage

Jan Bittar and Yousef Hannawi

Introduction to Subarachnoid Hemorrhage

Subarachnoid hemorrhage (SAH) is a life-threatening emergency that occurs due to bleeding into the subarachnoid space between the arachnoid membrane and the pia matter [1]. The annual incidence of SAH in the United States is between 10–14 cases per 100,000 [2]. Clinically, SAH presents with acute onset of severe headache that is often described as the "worst headache of life", nausea, vomiting, photophobia, neck pain and loss of consciousness [3]. Risk factors for SAH can be divided into modifiable factors such as hypertension, smoking, heavy alcohol use and sympathomimetic drug use like cocaine and non-modifiable factors including advanced age, female sex, specific ethnicities, prior personal or familial history of SAH, type IV Ehlers-Danlos syndrome or enlarged aneurysmal diameter [2, 3]. While women have overall higher rates of aSAH than men, one study showed this may start to occur in women at the age of late thirties [4]. The overall outcomes are similar between men and women [5].

J. Bittar · Y. Hannawi (✉)
Division of Cerebrovascular Diseases and Neurocritical Care, Department of Neurology, The Ohio State University, Columbus, OH, USA

W. C. Ziai, C. L. Cornwell (eds.), *Neurovascular Sonography*,
https://doi.org/10.1007/978-3-030-96893-9_5

The etiology of SAH include aneurysmal rupture, arteriovenous malformation, trauma and secondary to other etiologies such as anticoagulation or other types of brain injuries [3]. Common forms of subarachnoid hemorrhage include spontaneous aneurysmal rupture that has a prevalence of 85% of the cases while perimesencephalic SAH constitutes about 5% of the cases. Trauma contributes to variable rates of SAH ranging between 25–53% of traumatic brain injury patients [6–8]. The location of brain aneurysm in cases of aneurysmal SAH (aSAH) are typically found in the anterior circulation ranging between 80–90% of the cases. The anterior communicating artery (ACOM) constitutes the most common site (35%), followed by internal carotid artery (ICA) in 30% (main ICA, posterior communicating artery (PCOM) and the ophthalmic artery), and middle cerebral artery (MCA) in 22% of the cases [9, 10]. The posterior circulation accounts for only 10–20% of cerebral aneurysms location with the most common site being the tip of the basilar artery [9, 10]. Cerebral angiogram remains the gold standard test to detect aneurysms in aSAH [11]. In cases of SAH that are suggestive of aneurysmal etiology, repeating cerebral angiography is recommended if the initial test was normal or equivocal for the presence of aneurysm which reduces the overall negative rate to 15.6% [12].

Aneurysmal subarachnoid hemorrhage constitutes the most severe form of SAH. Typical complications include re-bleeding, hydrocephalus, delayed cerebral ischemia (DCI), cerebral vasospasm, seizures, chemical meningitis and bacterial meningitis in addition to other medical complications [9]. The morbidity and mortality of aSAH are related to these neurological complications as well as other medical complications such as pneumonia [13]. Several scales have been created to grade the severity of aSAH which reflects mortality or poor functional outcome. In particular, the Hunt & Hess score is a clinical score that ranges between 1–5 based on the severity of the clinical symptoms at presentation where grade 1 is considered asymptomatic or with minimal headache while patients with grade 5 are in deep coma [14]. The modified fisher scale is another scale for predicting the risk of cerebral

vasospasm and severity of aSAH based on the amount and distribution blood in the subarachnoid space and the ventricles [15]. We will discuss in the following section cerebral vasospasm in further details since it is the main neurological complication following aSAH in addition to the significant role of TCD in the management of it.

Cerebral Vasospasm in SAH

The complications after subarachnoid hemorrhage can be divided into three phases based on the timing of their occurrence after SAH including the acute phase (day 0 – day 3), subacute phase (day 3 – day 30) and late phase (after day 30) [16]. Cerebral vasospasm is defined as a narrowing of the large and medium-sized intracranial arteries that typically occurs in the subacute phase (Day 3 to day 30) with a peak incidence between (7–10) days from aSAH [16, 17]. It is considered a serious complication after aSAH that is associated with regional cerebral hypoperfusion and delayed cerebral ischemia (DCI). The exact underlying pathophysiological mechanisms of cerebral vasospasm and DCI remain unknown. However, endothelial dysfunction with reduced production of endothelial nitric oxide and activation of endothelin-1 receptor on vascular smooth muscles resulting in vasoconstrictions have been implicated. In addition, oxidative stress from activation of inflammatory cascades with subsequent release of oxygen free radicals will add further injury to the vascular smooth muscle cells with subsequent vasoconstriction. The breakdown of erythrocytes in the subarachnoid space could be implicated in the initiation of these pathophysiological cascades [17, 18]. While cerebral vasospasm is typically seen following aSAH, it still can be seen following traumatic SAH and the incidence varies between 19% to 68% [19]. Interestingly, the incidence of vasospasm detected by TCD was higher in cases of traumatic epidural and subdural hematomas than intracerebral or intraventricular hemorrhage [20].

Detection of Cerebral Vasospasm

Several imaging modalities have been utilized in the detection of cerebral vasospasm and associated delayed cerebral ischemia in patients with aSAH in the neurocritical care units with variable degrees of success. Some modalities focus on the vessel directly such as TCD, CT angiography (CTA) and digital subtraction angiography (DSA). Others utilize changes in the brain function or perfusion as indirect surrogates for this phenomenon such as brain tissue oxygenation monitoring (BTO), microdialysis, CT perfusion (CTP), continuous electroencephalogram (cEEG), thermal diffusion monitoring, jugular bulb oximetry and near infrared spectroscopy (NIRS) [21]. The ideal diagnostic modality would provide an early recognition of cerebral vasospasm before the clinical symptoms occur in order to prevent the consequences of vasospasm. Additional considerations include the non-invasive nature of the technology and cost effectiveness. Digital subtraction angiography (DSA) remains the gold standard test to diagnose cerebral vasospasm. However, it is an invasive procedure that may carry risk of arterial dissection or induce thrombosis [11]. Transcranial Doppler (TCD) technology is frequently used in the neurocritical care setting as a non-invasive modality for bedside surveillance and early detection of cerebral vasospasm.

The Role of TCD in Cerebral Vasospasm Detection and Management Following SAH

Transcranial Doppler measures cerebral blood flow velocity (CBFV) in the arteries. In case of arterial diameter reduction, as seen in cerebral vasospasm, CBFV will be increased. The magnitude of increase in CBFV will serve as an indirect indicator of the severity of cerebral vasospasm [22]. Indeed, in a meta-analysis by *Kumar* et al., cerebral vasospasm detection by TCD accurately predicted DCI with high sensitivity, high negative predictive value and fair specificity [23]. However, evidence for the impact of TCD in cases of SAH on mortality and functional outcome remains lacking [23]. It is important to note though that there are several

factors that may influence CBFV in addition to cerebral vasospasm (Table 1). Hence, understanding of these factors is critical for accurate TCD interpretation [24]. These factors include:

1. *Age:*

Previous studies have shown a decline in the total cerebral blood flow with aging which has been estimated to be around 2.6 mL/min per year [25]. In association, CBFV demonstrates a decrease with aging, in particular in people older than 60 years of age. This has clinical significance as significant clinical vasospasm can be seen at lower velocities compared to younger individuals. Table 2 below lists normal reference values for CBFV across age.

Table 1 Factors influencing cerebral blood flow velocity

Factor	Change in CBFV
Age	Increase up 6–10 years then decrease
Sex	Women > men
Pregnancy	Decrement in the third trimester
Hematocrit	Increase with decreasing hematocrit
PCO2	Increase with increasing PCO2
MAP	Increase with increasing MAP

MAP main arterial pressure; *PCO2* pressure of carbon dioxide; *CBFV* cerebral blood flow velocity

Table 2 Mean cerebral blood flow velocity (cm/s) related to age

Artery	Age 20–40 years	Age 40–60 years	Age >60 years
ACA	56–60	53–61	44–51
MCA	74–81	72–73	58–59
PCA			
P1	48–57	41–56	37–47
P2	43–51	40–57	37–47
Vertebral artery	37–51	29–50	30–37
Basilar artery	39–58	27–56	29–47

ACA anterior cerebral artery; *MCA* middle cerebral artery; *PCA* posterior cerebral artery
Adopted with permission from D'Andrea A et al. [24]

2. *Sex and pregnancy status:*

Women are known to have higher CBF values compared to men [26]. This is attributed to several hormonal factors involving the lower blood viscosity in women [27], effect on estrogen on the brain leading to higher cerebral glucose metabolism [28], the lower brain weight in women [28] and the higher systemic blood flow in females due to higher cardiac index and lower peripheral vascular resistance [29]. In addition, CBF tends to increase further throughout pregnancy reaching a maximum increase of 20% above the non-pregnant value along with decreased cerebrovascular resistance [30].

3. *Fever:*

Cerebral blood flow changes in response to changes in the cerebral metabolism due to temperature variations [31]. Hyperthermia increases metabolic rate and cerebral blood flow, whereas hypothermia does the opposite leading to decrease in intracerebral volume and intracranial pressure [32, 33]. Patients with SAH and cerebral vasospasm are often febrile and fluctuations of CBFV in these patients could be related to body temperature variations.

4. *Intravascular volume and hemodynamic factors*:

Cerebral blood flow is augmented by increasing the intravascular volume as in the cases of severe anemia and insufficient delivery of oxygen to the brain in these patients [34]. Additional medications that are used in the treatment of cerebral vasospasm in the setting of SAH may further complicate the interpretation of TCD in these cases. For example, vasodilators and their intra-arterial administration such as milrinone, verapamil, nicardipine or nimodipine are all used in the treatment of cerebral vasospasm. They do not only increase CBF but also improve mean transient

time (MTT) in ischemic regions in patients with aSAH induced vasospasm [35]. Additionally, vasoactive medications are administered for the majority of SAH patients with cerebral vasospasm to augment the cerebral perfusion and that may further increase CBFV on TCDs by inducing further vasoconstriction of the brain vessels. These therapeutic interventions in patients with cerebral vasospasm may further complicate the interpretation of the TCD findings [36].

Timing of TCD surveillance in patients with aSAH:
Studies have shown that TCD examination in the first 4 to 10 days following aSAH can detect rapid increases in CBFV which helps in identifying patients at risk for developing delayed cerebral ischemia and neurological deficits [37]. Earlier application of TCD in the first 2–5 days following SAH can also help in detecting radiographic cerebral vasospasm before it becomes clinically apparent which may help inform the treating physicians to predict the occurrence of clinically relevant cerebral vasospasm [37, 38]. The utilization of TCD examination in the next two days following SAH, (5–7) days, can also help in monitoring the progression of cerebral vasospasm towards the development of delayed cerebral ischemia which can be utilized in planning therapeutic and interventional studies [39]. *Sloan* et al. revealed that the maximum sensitivity of TCD in detecting cerebral vasospasm is at 8 days following aSAH [38]. TCD monitoring after day 12 of SAH can reveal information about the resolution of cerebral vasospasm as well as detecting late or rebound cerebral vasospasm (late 2nd or mid 3rd week following SAH) [40]. However, it is not necessary in the majority of cases.

Determining the severity of cerebral vasospasm by TCD:
The severity of cerebral vasospasm is classically graded into mild, moderate and severe based on the combination of several TCD measurements including the mean CBFV (cm/s), Lindegaard ratio (LR) and Sviri ratio.

1. Lindegaard Ratio (LR):

In 1976, *Lindegaard* et al. investigated 76 patients with known aSAH by comparing cerebral angiogram findings to TCD results for the diagnosis of cerebral vasospasm [41]. They identified elevation in the middle cerebral artery (MCA) CBFV compared to the CBFV in distal extracranial ICA on TCD when there was angiographic spasm in the MCA [41]. The term "Lindegaard index" was coined which can be calculated from the TCD by dividing mean CBFV of the MCA by the ipsilateral extracranial ICA CBFV to give information on the severity of MCA spasm [41, 42]. The LR shows correlation with elevation of CBFV in the anterior circulation. We include in Table 3 a commonly used grading scale of SAH severity based on the mean CBFV and LR values. Figures 1, 2 and 3 show examples of normal waveforms at baseline and at time of cerebral vasospasm in aSAH.

2. Sviri ratio:

Sviri ratio can be calculated from TCD by dividing the mean flow velocity of the basilar artery (BA) by the extracranial vertebral artery (VA) velocity [43]. In 2006, *Sviri* conducted a study of one hundred twenty-three patients with aSAH using TCD and cerebral arteriograms. He found the BA/VA ratio to improve the sensitivity and specificity of TCD detection of BA vasospasm.

Table 3 Grading of severity of vasospasm using transcranial doppler

Degree of middle cerebral artery vasospasm	**Mean flow velocity (cm/s)**	**Lindegaard ratio**
Mild	120–149	3–6
Moderate	150–199	3–6
Severe	>200	>6
Degree of basilar artery vasospasm	**Mean flow velocity (cm/s)**	**Sviri ratio**
Vasospasm	>70	>2
Moderate or severe vasospasm	>85	>2.5
Severe vasospasm	>85	>3

Adopted with permission from Samagh N et al. with permission [40]

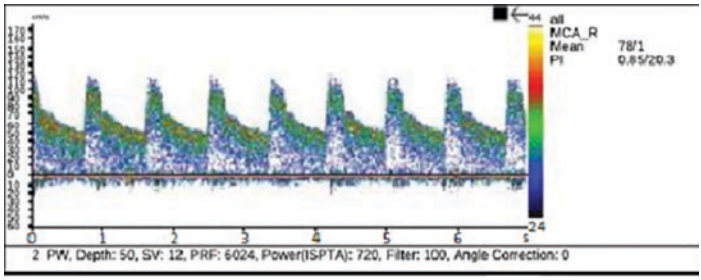

Fig. 1 Baseline TCD examination of the right middle cerebral artery acquired at 50 mm depth through the temporal window in a patient with aSAH showing mean CBFV of 78 cm/s (within normal limits)

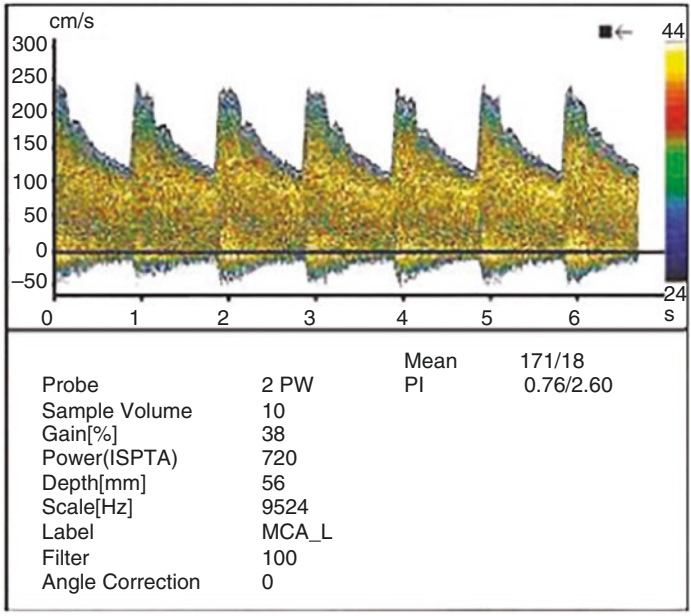

Fig. 2 TCD acquired in the left middle cerebral artery through a temporal window 56 mm depth shows development of moderate cerebral vasospasm. The mean cerebral blood flow velocity is 171 cm/s

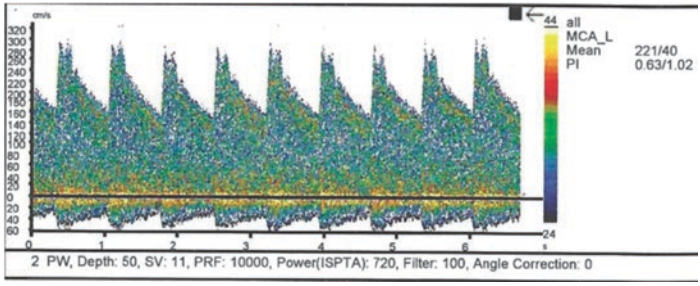

Fig. 3 TCD examination of the left middle cerebral artery at 50 mm depth through a temporal window shows severe cerebral vasospasm. The mean CBFV is now 221 cm/s

The grading of cerebral vasospasm severity according to the mean CBFV in the posterior circulation and Sviri ratio is shown Table 3.

The reliability of TCD in detecting cerebral vasospasm:
TCD technology has been extensively utilized in the screening and detection of cerebral vasospasm. However, questions have been raised regarding the specificity of this study, in particular, predicting the conversion of radiographic vasospasm to clinically relevant vasospasm. In this section, we will present the reliability of TCD in diagnosing cerebral vasospasm according to the most commonly assessed intracranial vessels.

1. *Anterior circulation:*

In a meta-analysis of five studies involving 198 patients and 317 TCD examination comparing TCD findings to angiographic cerebral vasospasm as a screening tool for MCA vasospasm, Lysakowski et al. found TCD sensitivity to be 67% (95% CI 48% to 87%), specificity of 99% (98% to 100%), positive predictive value (PPV) of 97% (95% to 98%), and negative predictive value (NPV) of 78% (65% to 91%) [44]. These data also suggested that most patients who were predicted to have vasospasm on TCD did actually have vasospasm on cerebral angiogram (high PPV) [44]. However, this study did not take into consideration the severity of

the cerebral vasospasm on the TCD or its clinical correlates. In summary, TCD has high predictability for MCA spasm in patients who have a suspicion for it.

In anterior cerebral artery vasospasm, a similar meta-analysis of 3 studies including 108 patients and 171 tests identified sensitivity of 42% (11% to 72%), specificity of 76% (53% to 100%), PPV of 56% (27% to 84%), and NPV of 69% (43% to 95%) for TCD in comparison to diagnostic angiogram [44]. This suggests that TCD has lower sensitivity and specificity in detecting cerebral vasospasm in the ACA compared to the MCA.

2. *Posterior circulation:*

In a study of 47 patients that included 84 TCD examinations of the PCAs during the cerebral vasospasm risk period in comparison to cerebral angiography within 24 hours of the test, TCD had sensitivity of 48%, specificity of 69%, PPV of 37%, and NPV of 78% [45]. The main false positive findings included occlusion of the vessel which was attributed to either anatomical factors or operator error. In another study that evaluated the reliability of TCD in the vertebrobasilary system for the detection of cerebral vasospasm in comparison to cerebral angiogram, TCD had sensitivity of 76.9%, specificity of 79%, PPV of 63%, and NPV of 88% [46]. They also found sensitivity of 43.8%, specificity of 88%, PPV of 54%, and NPV of 82% for detection of vertebral artery vasospasm by TCD [46]. This study was conducted in 64 vertebral arteries and 42 basilar arteries.

TCD and Cerebral Autoregulation in SAH

Cerebral autoregulation has been known since 1959 as the tendency of cerebral blood flow (CBF) to remain approximately constant in response to changes of mean arterial pressure (MAP) [47]. The CBF range through which autoregulation operates is typically between a MAP of 60 to 150 mmHg [48]. The assessment of cerebral autoregulation is made by measuring the relative blood

flow changes in response to slow changes in blood pressure which is known as *static autoregulation* and by measuring the rapid cerebral flow blood flow changes with blood pressure which is known as *dynamic autoregulation* [49]. While there are currently several tools that are utilized for determining cerebral autoregulation, TCD is considered an excellent non-invasive tool for this aim. There are several parameters that can be derived from TCD signals which reflect the function of cerebrovascular reactivity and autoregulation. These include analysis of CBFV waveforms, their characteristics and relative changes in comparison to changes of the systemic blood pressure [49, 50]. Additional maneuvers can be applied for measuring the cerebrovascular reactivity such as CO2 challenge [51], or the early transient hyperemic response test through brief compression of the carotid and measuring the subsequent hyperemic response of the unilateral CBFV [52]. The full extent of cerebral autoregulation assessment by TCD is beyond the scope of this chapter. We refer to previous excellent papers in this area [49, 53]. The significance of assessment of cerebral autoregulation by TCD in subarachnoid hemorrhage has been found in recent studies. For example, impaired early transient hyperemic response measurement in aSAH predicted poor outcome in one study [52]. Another study showed that impaired cerebral autoregulation early in aSAH predicts the occurrence of delayed cerebral ischemia [54]. The role of autoregulation assessment by TCD in SAH is an area of future research for the utility of TCD and advanced intracranial monitoring in the neurocritical care unit.

A simple commonly used measure by TCD which reflects CBF waveform characteristics is the pulsatility index (PI). This can also be an indirect measure of the impairment of autoregulation and it is defined as: (MCA peak systolic velocity – MCA end diastolic velocity)/MCA mean CBFV [49]. Therefore, the greater decrease in diastolic velocities relative to systolic ones, the more increase in PI [49]. The principle reason for the increase in PI is due to an increase in CBFV pulsation just before complete loss of autoregulation. A strong correlation is found between PI and intracranial pressure (ICP). In a study of 81 patients with a variety of intracranial disorders that required intraventricular catheter

placement (46 SAH, 21 closed head injury, 14 with other neurological disorders), a total of 658 TCD measurements were made in parallel with ICP registrations. The study identified a strong correlation between ICP and PI of 93.8% (correlation coefficient). In addition, a negative moderate correlation between cerebral perfusion pressure (CPP) and PI was also identified (correlation coefficient of −0.493) [55]. In SAH, these could constitute signs of decreased cerebral compliance, increased cerebral edema or development of hydrocephalus and the need for placement of intraventricular catheter for cerebrospinal fluid placement.

TCD and Emboli Detection

TCD is a considered as a sensitive technique to detect microembolic signals (MESs) which help to identify patients at high risk for cerebrovascular ischemic events. These signals are characterized by unidirectional high intensity increase, short duration, random occurrence, and a "whistling" sound on TCD [56]. Microembolic signals have been detected in a variety of cerebrovascular diseases that are associated with ischemic events including carotid artery stenosis, aortic arch plaques, atrial fibrillation, myocardial infarction, prosthetic heart valves, patent foramen ovale (PFO), valvular stenosis, during invasive procedures (angioplasty, percutaneous transluminal angioplasty) and surgery (carotid, cardiopulmonary bypass) [56]. The preferred time duration of monitoring for these MESs using the TCD varies based on the clinical scenario. For example, monitoring for 30 minutes in patients with implanted artificial heart valves in whom MESs can be detected, in the vast majority of patients is enough. Extended monitoring for patients with atrial fibrillation or carotid arterial stenosis for more than an hour is required given the low frequency of embolic signals [57]. A few small studies have evaluated MESs in patients with SAH [58–60]. In these studies, MESs were detected in up to 70% of SAH patients. These studies did not associate the presence of MESs with the development of cerebral vasospasm. However, in one of these studies, MESs were independently associated with the development of ischemic

symptoms in SAH [58]. It is important to note, however, that these previous studies had small sample sizes and future larger studies are needed to confirm the relevance of MEs in patients with SAH.

Conclusions

TCD offers a non-invasive methodology for assessment of patients with SAH. It has been particularly useful in the treatment of aSAH for the assessment of development and management of cerebral vasospasm and it is currently considered an important neurocritical care unit management tool in the United States. TCD offers an additional promising technology for advanced intracranial monitoring of cerebral autoregulation in patients with SAH that will need to be further assessed in future clinical studies.

References

1. Abraham MK, Chang WW. Subarachnoid hemorrhage. Emerg Med Clin North Am. 2016;34(4):901–16.
2. Ziu E, Mesfin FB. Subarachnoid hemorrhage. Treasure Island (FL): StatPearls; 2021.
3. Muehlschlegel S. Subarachnoid hemorrhage. Continuum (Minneap Minn). 2018;24(6):1623–57.
4. Wang YX, He J, Zhang L, Li Y, Zhao L, Liu H, et al. A higher aneurysmal subarachnoid hemorrhage incidence in women prior to menopause: a retrospective analysis of 4,895 cases from eight hospitals in China. Quant Imaging Med Surg. 2016;6(2):151–6.
5. Hamdan A, Barnes J, Mitchell P. Subarachnoid hemorrhage and the female sex: analysis of risk factors, aneurysm characteristics, and outcomes. J Neurosurg. 2014;121(6):1367–73.
6. Kundra S, Mahendru V, Gupta V, Choudhary AK. Principles of neuroanesthesia in aneurysmal subarachnoid hemorrhage. J Anaesthesiol Clin Pharmacol. 2014;30(3):328–37.
7. Hartings JA, Vidgeon S, Strong AJ, Zacko C, Vagal A, Andaluz N, et al. Surgical management of traumatic brain injury: a comparative-effectiveness study of 2 centers. J Neurosurg. 2014;120(2):434–46.

8. Flaherty ML, Haverbusch M, Kissela B, Kleindorfer D, Schneider A, Sekar P, et al. Perimesencephalic subarachnoid hemorrhage: incidence, risk factors, and outcome. J Stroke Cerebrovasc Dis. 2005;14(6):267–71.
9. Petridis AK, Kamp MA, Cornelius JF, Beez T, Beseoglu K, Turowski B, et al. Aneurysmal subarachnoid hemorrhage. Dtsch Arztebl Int. 2017;114(13):226–36.
10. Keedy A. An overview of intracranial aneurysms. Mcgill J Med. 2006;9(2):141–6.
11. Mascia L, Del Sorbo L. Diagnosis and management of vasospasm. F1000 Med Rep. 2009;1:33.
12. Pathirana N, Refsum SE, McKinstry CS, Bell KE. The value of repeat cerebral angiography in subarachnoid haemorrhage. Br J Neurosurg. 1994;8(2):141–6.
13. Rosengart AJ, Schultheiss KE, Tolentino J, Macdonald RL. Prognostic factors for outcome in patients with aneurysmal subarachnoid hemorrhage. Stroke. 2007;38(8):2315–21.
14. Hunt WE, Hess RM. Surgical risk as related to time of intervention in the repair of intracranial aneurysms. J Neurosurg. 1968;28(1):14–20.
15. Frontera JA, Claassen J, Schmidt JM, Wartenberg KE, Temes R, Connolly ES Jr, et al. Prediction of symptomatic vasospasm after subarachnoid hemorrhage: the modified fisher scale. Neurosurgery. 2006;59(1):21-7; discussion -7.
16. Daniere F, Gascou G, Menjot de Champfleur N, Machi P, Leboucq N, Riquelme C, et al. Complications and follow up of subarachnoid hemorrhages. Diagn Interv Imaging. 2015;96(7–8):677–86.
17. Daou BJ, Koduri S, Thompson BG, Chaudhary N, Pandey AS. Clinical and experimental aspects of aneurysmal subarachnoid hemorrhage. CNS Neurosci Ther. 2019;25(10):1096–112.
18. Ciurea AV, Palade C, Voinescu D, Nica DA. Subarachnoid hemorrhage and cerebral vasospasm - literature review. J Med Life. 2013;6(2):120–5.
19. Modi NJ, Agrawal M, Sinha VD. Post-traumatic subarachnoid hemorrhage: a review. Neurol India. 2016;64(Suppl):S8–S13.
20. Zubkov AY, Lewis AI, Raila FA, Zhang J, Parent AD. Risk factors for the development of post-traumatic cerebral vasospasm. Surg Neurol. 2000;53(2):126–30.
21. Kistka H, Dewan MC, Mocco J. Evidence-based cerebral vasospasm surveillance. Neurol Res Int. 2013;2013:256713.
22. Nicoletto HA, Burkman MH. Transcranial Doppler series part II: performing a transcranial Doppler. Am J Electroneurodiagnostic Technol. 2009;49(1):14–27.
23. Kumar G, Shahripour RB, Harrigan MR. Vasospasm on transcranial Doppler is predictive of delayed cerebral ischemia in aneurysmal subarachnoid hemorrhage: a systematic review and meta-analysis. J Neurosurg. 2016;124(5):1257–64.

24. D'Andrea A, Conte M, Scarafile R, Riegler L, Cocchia R, Pezzullo E, et al. Transcranial Doppler ultrasound: physical principles and principal applications in neurocritical care unit. J Cardiovasc Echogr. 2016;26(2):28–41.
25. Amin-Hanjani S, Du X, Pandey DK, Thulborn KR, Charbel FT. Effect of age and vascular anatomy on blood flow in major cerebral vessels. J Cereb Blood Flow Metab. 2015;35(2):312–8.
26. Rodriguez G, Warkentin S, Risberg J, Rosadini G. Sex differences in regional cerebral blood flow. J Cereb Blood Flow Metab. 1988;8(6):783–9.
27. Shaw TG, Mortel KF, Meyer JS, Rogers RL, Hardenberg J, Cutaia MM. Cerebral blood flow changes in benign aging and cerebrovascular disease. Neurology. 1984;34(7):855–62.
28. Baxter LR Jr, Mazziotta JC, Phelps ME, Selin CE, Guze BH, Fairbanks L. Cerebral glucose metabolic rates in normal human females versus normal males. Psychiatry Res. 1987;21(3):237–45.
29. Messerli FH, Garavaglia GE, Schmieder RE, Sundgaard-Riise K, Nunez BD, Amodeo C. Disparate cardiovascular findings in men and women with essential hypertension. Ann Intern Med. 1987;107(2):158–61.
30. Nevo O, Soustiel JF, Thaler I. Maternal cerebral blood flow during normal pregnancy: a cross-sectional study. Am J Obstet Gynecol. 2010;203(5):475 e1–6.
31. Sahuquillo J, Vilalta A. Cooling the injured brain: how does moderate hypothermia influence the pathophysiology of traumatic brain injury. Curr Pharm Des. 2007;13(22):2310–22.
32. Bisschops LL, Hoedemaekers CW, Simons KS, van der Hoeven JG. Preserved metabolic coupling and cerebrovascular reactivity during mild hypothermia after cardiac arrest. Crit Care Med. 2010;38(7):1542–7.
33. Clifton GL, Miller ER, Choi SC, Levin HS, McCauley S, Smith KR Jr, et al. Lack of effect of induction of hypothermia after acute brain injury. N Engl J Med. 2001;344(8):556–63.
34. Kuwabara Y, Sasaki M, Hirakata H, Koga H, Nakagawa M, Chen T, et al. Cerebral blood flow and vasodilatory capacity in anemia secondary to chronic renal failure. Kidney Int. 2002;61(2):564–9.
35. Nogueira RG, Lev MH, Roccatagliata L, Hirsch JA, Gonzalez RG, Ogilvy CS, et al. Intra-arterial nicardipine infusion improves CT perfusion-measured cerebral blood flow in patients with subarachnoid hemorrhage-induced vasospasm. AJNR Am J Neuroradiol. 2009;30(1):160–4.
36. Manno EM, Gress DR, Schwamm LH, Diringer MN, Ogilvy CS. Effects of induced hypertension on transcranial Doppler ultrasound velocities in patients after subarachnoid hemorrhage. Stroke. 1998;29(2):422–8.

37. Babikian VL, Feldmann E, Wechsler LR, Newell DW, Gomez CR, Bogdahn U, et al. Transcranial Doppler ultrasonography: year 2000 update. J Neuroimaging. 2000;10(2):101–15.
38. Sloan MA, Alexandrov AV, Tegeler CH, Spencer MP, Caplan LR, Feldmann E, et al. Assessment: transcranial Doppler ultrasonography: report of the Therapeutics and Technology Assessment Subcommittee of the American Academy of Neurology. Neurology. 2004;62(9):1468–81.
39. Alexandrov AV, Sloan MA, Tegeler CH, Newell DN, Lumsden A, Garami Z, et al. Practice standards for transcranial Doppler (TCD) ultrasound. Part II. Clinical indications and expected outcomes. J Neuroimaging. 2012;22(3):215–24.
40. Samagh N, Bhagat H, Jangra K. Monitoring cerebral vasospasm: how much can we rely on transcranial Doppler. J Anaesthesiol Clin Pharmacol. 2019;35(1):12–8.
41. Lindegaard KF, Nornes H, Bakke SJ, Sorteberg W, Nakstad P. Cerebral vasospasm diagnosis by means of angiography and blood velocity measurements. Acta Neurochir. 1989;100(1–2):12–24.
42. Aaslid R, Huber P, Nornes H. Evaluation of cerebrovascular spasm with transcranial Doppler ultrasound. J Neurosurg. 1984;60(1):37–41.
43. Sviri GE, Ghodke B, Britz GW, Douville CM, Haynor DR, Mesiwala AH, et al. Transcranial Doppler grading criteria for basilar artery vasospasm. Neurosurgery. 2006;59(2):360–6; discussion -6.
44. Lysakowski C, Walder B, Costanza MC, Tramer MR. Transcranial Doppler versus angiography in patients with vasospasm due to a ruptured cerebral aneurysm: a systematic review. Stroke. 2001;32(10):2292–8.
45. Wozniak MA, Sloan MA, Rothman MI, Burch CM, Rigamonti D, Permutt T, et al. Detection of vasospasm by transcranial Doppler sonography. The challenges of the anterior and posterior cerebral arteries. J Neuroimaging. 1996;6(2):87–93.
46. Sloan MA, Burch CM, Wozniak MA, Rothman MI, Rigamonti D, Permutt T, et al. Transcranial Doppler detection of vertebrobasilar vasospasm following subarachnoid hemorrhage. Stroke. 1994;25(11):2187–97.
47. Claassen JA, Meel-van den Abeelen AS, Simpson DM, Panerai RB. International Cerebral Autoregulation Research N. Transfer function analysis of dynamic cerebral autoregulation: a white paper from the International Cerebral Autoregulation Research Network. J Cereb Blood Flow Metab. 2016;36(4):665–80.
48. Paulson OB, Strandgaard S, Edvinsson L. Cerebral autoregulation. Cerebrovasc Brain Metab Rev. 1990;2(2):161–92.
49. Bellapart J, Fraser JF. Transcranial Doppler assessment of cerebral autoregulation. Ultrasound Med Biol. 2009;35(6):883–93.
50. Zeiler FA, Smielewski P, Stevens A, Czosnyka M, Menon DK, Ercole A. Non-invasive pressure reactivity index using Doppler systolic flow parameters: a pilot analysis. J Neurotrauma. 2019;36(5):713–20.

51. Fierstra J, Sobczyk O, Battisti-Charbonney A, Mandell DM, Poublanc J, Crawley AP, et al. Measuring cerebrovascular reactivity: what stimulus to use? J Physiol. 2013;591(23):5809–21.
52. Rynkowski CB, de Oliveira Manoel AL, Dos Reis MM, Puppo C, Worm PV, Zambonin D, et al. Early transcranial Doppler evaluation of cerebral autoregulation independently predicts functional outcome after aneurysmal subarachnoid hemorrhage. Neurocrit Care. 2019;31(2):253–62.
53. Panerai RB. Transcranial Doppler for evaluation of cerebral autoregulation. Clin Auton Res. 2009;19(4):197–211.
54. Budohoski KP, Czosnyka M, Smielewski P, Kasprowicz M, Helmy A, Bulters D, et al. Impairment of cerebral autoregulation predicts delayed cerebral ischemia after subarachnoid hemorrhage: a prospective observational study. Stroke. 2012;43(12):3230–7.
55. Bellner J, Romner B, Reinstrup P, Kristiansson KA, Ryding E, Brandt L. Transcranial Doppler sonography pulsatility index (PI) reflects intracranial pressure (ICP). Surg Neurol. 2004;62(1):45–51. discussion
56. Vukovic-Cvetkovic V. Microembolus detection by transcranial Doppler sonography: review of the literature. Stroke Res Treat. 2012;2012:382361.
57. Hudorovic N. Clinical significance of microembolus detection by transcranial Doppler sonography in cardiovascular clinical conditions. Int J Surg. 2006;4(4):232–41.
58. Romano JG, Rabinstein AA, Arheart KL, Nathan S, Campo-Bustillo I, Koch S, et al. Microemboli in aneurysmal subarachnoid hemorrhage. J Neuroimaging. 2008;18(4):396–401.
59. Azarpazhooh MR, Velayati A, Chambers BR, Nejad HM, Nejad PS. Microembolic signals in subarachnoid hemorrhage. J Clin Neurosci. 2009;16(3):390–3.
60. Romano JG, Forteza AM, Concha M, Koch S, Heros RC, Morcos JJ, et al. Detection of microemboli by transcranial Doppler ultrasonography in aneurysmal subarachnoid hemorrhage. Neurosurgery. 2002;50(5):1026–30. discussion 30-1

Reversible Cerebral Vasoconstriction Syndrome (RCVS) and Vasculitis

Tamara Strohm

Introduction

Reversible cerebral vasoconstriction syndrome (RCVS) and central nervous system (CNS) vasculitis both present with focal or diffuse vasculopathy and intracranial stenosis. Distinguishing features include signs and symptoms, gender predilection, etiology, MRI findings, treatment, and disease course. Daily transcranial Doppler (TCD) is well validated in the subarachnoid hemorrhage (SAH) population to assess proximal vessel vasospasm. In particular, MCA mean flow velocity (MFV) > 200 cm/s and basilar MFV > 100 cm/s represent severe spasm. Pulsatility index (PI) levels >1.19 may also signify distal stenosis. Thus, TCD represents a cost-effective, mobile, and non-invasive tool for repeated assessment of intracranial vasculopathy. Here we describe TCD application to RCVS and vasculitis: for diagnosis, monitoring during therapy, and ultimately for prognostication.

T. Strohm (✉)
Neurology, The Ohio State University Wexner Medical Center, Columbus, OH, USA

W. C. Ziai, C. L. Cornwell (eds.), *Neurovascular Sonography*,
https://doi.org/10.1007/978-3-030-96893-9_6

Literature Review

TCD to Detect Stenosis and Occlusion

Anterior Circulation

TCD can reliably detect stenosis in the anterior circulation including the middle cerebral artery M1 segment and the internal carotid siphon in both the stroke and SAH populations (Table 1). Compared to angiography, TCD has an approximate sensitivity in the MCA of 80% to 90%, specificity of 90% to 95%, positive predictive value of 85%, and negative predictive value of 98% [1, 2]. It is less reliable for the anterior cerebral arteries because of collateral flow patterns and shunting to the ACA contralateral to the spastic segment [3]. In the ACAs, sensitivity is approximately 13% to 18% and specificity is 100%.

Posterior Circulation

As compared to angiography, several studies have shown that TCD can detect stenosis and occlusion in the posterior circulation including the intracranial vertebral, and proximal basilar with an approximate sensitivity of 80% and specificity of 75% to 80% [1, 2]. The BA/VA ratio may improve the sensitivity for basilar vasospasm [4]. Given collateral flow, the sensitivity for PCA territories is poor with close to 100% specificity [3].

Table 1 TCD Criteria for Vasospasm Diagnosis

Anterior circulation		
Mild VSP	100–139 cm/s	LR < 3
Moderate VSP	140–200 cm/s	LR 3-6
Severe VSP	>200 cm/s	LR > 6
Posterior circulation		
Mild VSP	60–80 cm/s	
Moderate VSP	80–100 cm/s	
Severe VSP	>100 cm/s	

Vasospasm and SAH

TCD is much more sensitive in detecting proximal versus distal vasospasm [5]. Proximal vasospasm results in segmental or diffuse elevations in mean flow velocities without flow velocity increase in the extracranial vessels.

Daily TCD examinations help identify SAH patients at risk of delayed cerebral ischemia. Literature in the SAH population has shown that mean MCA flow velocity values greater than 120 cm/s or greater than 200 cm/s reliably predict the presence of clinically significant vasospasm [1, 5–7]. For the basilar artery, mean flow velocity >85 cm/s or >100 cm/s predicts severe vasospasm. These values are affected by factors such as age, intracranial pressure (ICP), mean arterial blood pressure, hematocrit, arterial C02 content, and collateral flow patterns. As above, TCD is most reliable for detecting vasospasm in the MCA and ICA territories, and less so for the ACA territories and vertically oriented branches of the intracranial arteries distal to the basal cisterns. TCD is well validated for the detection of cerebral vasospasm (class II, level of evidence B) [1]. Transcranial color-coded sonography is another non-invasive tool that may be utilized as well [8–10]. It combines pulsed wave Doppler ultrasound with a cross sectional view, allowing identification of arteries, velocities, and direction of flow.

As discussed in Chapter "Transcranial Doppler in Subarachnoid Hemorrhage", the ratio between the intracranial MCA and the extracranial carotid or the Lindegaard ratio (Vintracranial MCA/VeICA) helps to avoid reading hyperemia as vasospasm and is well validated when compared to angiography [11]. Hyperemia results in flow elevations in MCA and ICA with LR < 3 while vasospasm results in elevated MCA over ICA flow with LR > 6. Increased pulsatility index indicates increased resistance distal to the site of insonation, and is a surrogate marker of distal vasospasm. A similar ratio (Vbasilar artery/Vextracranial vertebral artery) exists for basilar vasospasm [4].

Gosling's pulsatility index ((PSV-EDV)/MFV) may reflect vascular resistance, with proximal stenosis lowering the PI due to distal arterial dilatation, and distal stenosis increasing the PI (normal range 0.5–1.19) [12]. Notably, the PI is not a direct reflection of vascular resistance, but reflects the interplay between CPP, arterial pulse amplitude, compliance and other factors [13].

Additionally, diagnosis of >50% stenosis using TCD is based on the following criteria: (1) increased velocity through the stenotic segment; (2) decrease in velocity distally (post-stenotic dilation); (3) left versus right side differences in velocity; and (4) disturbances in flow such as turbulence and murmurs [14, 15]. Absent flow at a normal position and depth, and increased flow in collateral vessels may signal vessel occlusion. Examples of collateral flow include flow reversal in ACA or MCA, flow reversal in the ophthalmic artery, and prominent Acomm or Pcomm flow.

The Stroke Prevention Trial in Sickle Cell Disease (STOP) trial utilized TCD to detect intracranial stenosis and stroke risk in children with SCD [16]. Children with Vmean >200 mc/s in the ICA or MCA territory were randomly assigned to standard care or periodic blood transfusion, with a 92% stroke risk reduction in the transfusion group. This study validated the use of TCD for SCD-related intracranial stenosis in children.

TCD is well-validated in vasospasm secondary to subarachnoid hemorrhage [6]. In this population, serial TCD is utilized to diagnose vasospasm, guide need for endovascular intervention, and monitor response to therapy.

Hemodynamic Effects in Vasospasm

In the SAH population, vasospasm induces a decrease in vessel lumen diameter, which causes an increase in flow resistance. Mild narrowing may not cause a sufficient change to influence flow, and cerebral autoregulation may induce elevated arterial blood pressure to compensate. In moderate narrowing, the flow velocity will increase inversely to the change in lumen area with good correlation to angiography. In severe narrowing, this relationship is more complicated [3]. Figure 1 shows a reliable relationship

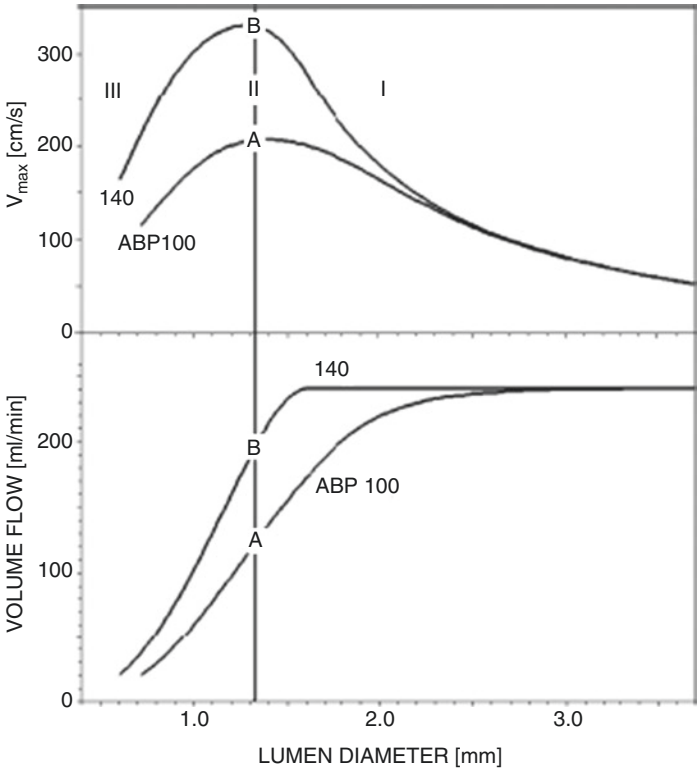

Fig. 1 Aaslid R. Transcranial Doppler assessment of cerebral vasospasm. European journal of ultrasound. 2002 Nov 1;16(1–2):3–10

between diameter and velocity in mild or moderate spasm (I, 'forward side'). II shows the 'plateau' where flow is reduced while velocity remains relatively independent of diameter. III, the 'backside' shows lower velocities with additional diameter reduction with loss of cerebral autoregulation with severe narrowing. Given these changes, TCD velocities need to be correlated to angiography and clinical findings.

Cerebral autoregulation is the ability to maintain cerebral blood flow over a range of mean arterial pressures. Cerebral autoregulation may be static or dynamic depending on the variability in blood pressure.

As discussed in other chapters, the pulsatility index may be a surrogate marker for cerebral autoregulation. It is also related to ICP, with a correlation coefficient of 0.938 ($p < 0.0001$) [17]. PI = (MCA peak systolic velocity – MCA end diastolic velocity)/MCA mean flow velocity.

RCVS

RCVS is characterized by reversible cerebral vasoconstriction of acute onset, often with severe "thunderclap" headache [18–21]. It has a female predilection with a ratio of 2-3 to 1. RCVS is often associated with vasoactive medications including sympathomimetic and serotonergic drugs, and illicit substances such as cocaine and methamphetamine. Endocrine and hormonal factors may play a role as well. Treatment is often calcium channel blockers such as nimodipine or verapamil.

Cortical SAH, ICH, seizures, and reversible posterior leukoencephalopathy often occur within the first week with ischemic complications (stroke and TIA) within the second week [22]. By definition, stenosis improves within 4–12 weeks (Fig. 2).

Cerebral angiography may show single or multi-vessel narrowing and dilation ("string and beads") with improvement following intra-arterial calcium channel blockers. As compared to vasculitis, RCVS has a relatively normal CSF profile. While the gold standard for diagnosis is angiography, TCD has been used successfully to show improvement in the blood flow velocities over time, but may underestimate changes in vessel diameter in the acute phase [18, 23–25].

Ducros et all looked at TCD in 64 patients with RCVS with 44 (69%) having increased arterial velocities with a mean of 163 ± 27 cm/s in middle cerebral arteries and 148 ± 20 cm/s in carotid siphons. Angiography confirmed multifocal segmental arterial constriction. Twelve patients had serial TCD with a moderate increase in velocities on first TCD (mean 6.8 days) but marked on the second TCD (mean 22.5 days), long after the headache had subsided [22]. Levin et al. also found that TCD flow velocities in the MCA (VMCA) reached a mean peak three to four weeks after

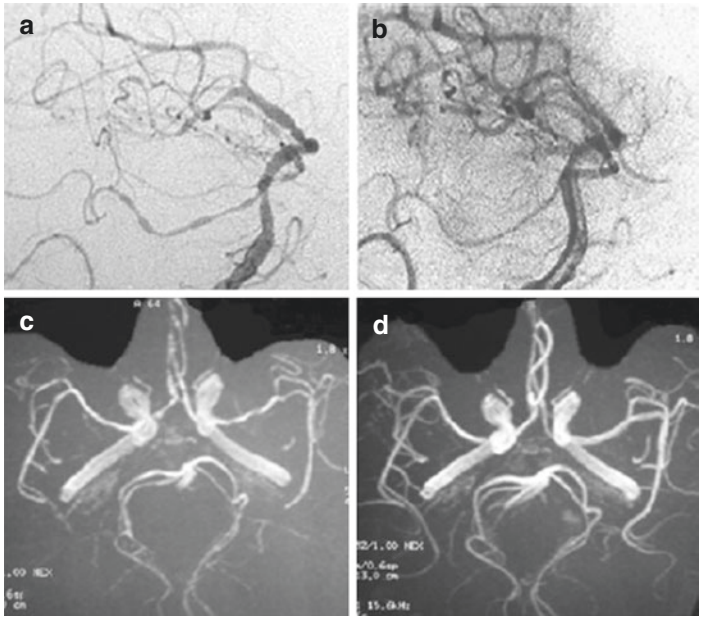

Fig. 2 (**a**) Catheter angiography at disease onset: multiple narrowing and dilatations, (**b**) Control catheter angiography at 3 months, (**c**) MRA at disease onset and (**d**) Control MRA [22]

headache onset [26]. Another case series reported bimodal peaks with increased velocities at days 15 and 17 [27]. Marsh et al. demonstrated improvement in velocities in seven patients with RCVS, which correlated to initiation of a calcium channel blocker [24].

Chen et al. utilized transcranial color-coded sonography (TCSS) to investigate hemodynamic changes in patients with RCVS [28]. They analyzed the mean flow velocity of MCA (VMCA), Lindegaard Index (LI), and maximum values every 10 days over the first month and every 20 days thereafter (average 3.9 studies per patient). They utilized vasospasm criteria for SAH patients with mild vasospasm as VMCA >120 cm/sec; and moderate-to-severe with VMCA > 200 cm/sec. Patients with VMCA > 120 cm/sec and LI > 3, had a greater risk of posterior leukoencephalopathy and ischemic strokes.

Topcuoglu et al. described impaired vasomotor reactivity in seven of eight patients with RCVS, which highlights the impaired autoregulation through vasodilation in this disease [29]. Vasomotor reactivity may be considered as an ancillary study, but the significance of abnormal findings remains unknown.

Thus, TCD remains a cost-effective, mobile, and noninvasive technology with utility for both diagnosis and therapeutic monitoring in RCVS. We still recommend the gold standard for initial diagnosis (cerebral angiography, CTA, MRA), and to determine disease extension and disease progression, particularly in small vessel vasculitides [10].

TCD offers real-time monitoring of blood flow in an intracranial artery. Therefore, it represents an important, non-invasive and non-nephrotoxic tool to monitor intracranial stenosis associated with RCVS and vasculitis over extended periods. Additionally, assessment of stenosis over time can assist with prognostication.

RCVS v Vasculitis

As compared to RCVS, CNS vasculitis (aka primary angiitis of the central nervous system [PACNS]) does not have a gender predilection, is often subacute, and CSF profile is typically abnormal [18]. MRI is abnormal in 90%, and often shows ischemic infarcts in multiple vascular territories of varying ages. Cerebral angiography may be similar but does not show reversibility with administration of intra-arterial calcium channel blockers. Other authors have reported angiographic findings of "sausage on a string" in RCVS versus "irregular notched" appearance in vasculitis [30]. Findings do not typically reverse spontaneously, and treatment includes high-dose steroids and immunotherapy. Clinical outcomes are typically better in RCVS. Singhal et al. described a 90% discharge mRS of 0-3 in patients with RCVS as compared to 75% with vasculitis [30]. A significantly greater number of RVCS patients had mRS 0-1.

Krasnianski et al. described three patients with RCVS (migraine, eclampsia, toxic encephalopathy), and three patients with vasculitis (2 with PACNS and 1 with Crohn's disease associated vasculi-

tis). They found that TCD (elevated velocities) correlated to MRA and cerebral angiography and clinical disease course [31].

Vasculitis

CNS vasculitis (primary angiitis of the CNS) refers to inflammation of the blood vessels of the brain, spinal cord and meninges [32]. Secondary causes of CNS vasculitis include infectious causes such as varicella zoster, large, medium and small vessel vasculitides, malignancy, and autoimmune diseases such as systemic lupus erythematosus and sarcoidosis. It is a rare disease, predominantly affecting males around 50 years old, and presenting in an indolent or subacute way. MRI findings include ischemic and hemorrhagic strokes, often in multiple vascular territories and of varying age, subarachnoid hemorrhage, and leptomeningeal enhancement.

Calabrese et al. proposed diagnostic criteria for primary CNS vasculitis in 1988 including: 1) new neurological or psychiatric deficit; 2) angiographic or histopathological features of CNS arteriopathy; and (3) no evidence of systemic vasculitis or other mimics [33]. Angiography reveals "beading" and multifocal vascular stenosis. The gold standard in diagnosis is pathology.

Lowe et al. performed serial TCD in two children with PACNS and one child with West Nile vasculitis [34]. All three girls had MCA infarcts, and abnormal findings on TCD (elevated peak systolic velocities over multiple examinations) which correlated with abnormalities in both MRA and cerebral angiography.

TCD Findings in Vasculitis

Several studies have validated use of TCD in cerebral vasculitis (particularly for proximal cerebral vessels) for both diagnosis and disease course as compared to cerebral angiography [10, 35–37].

Gonzalez-Suarez et al. reported TCD findings in inactive Antineutrophil Cytoplasmic Antibody (ANCA)-associated vasculitis. They found that lower mean flow velocity and lower middle

cerebral artery pulsatility index was related to altered SPECT perfusion, lower Montreal cognitive assessment test scores, and younger age [38].

Cantu et al. evaluated 21 patients with Takayasu arteritis, a large-vessel arteriopathy [36]. They compared MRA, color Doppler flow imaging, and TCD with angiography. For TCD, temporal windows were used to evaluate the MCA, ACA, and PCA. The transorbital approach was used for the intracranial ICA, and the transoccipital approach was used for the basilar artery and distal vertebral arteries. Extracranial obstruction was suggested by dampened or blunted waveforms, slow acceleration, and decreased pulsatility in the MCA and basilar artery. They found that non-invasive techniques showed at least one abnormality in 20 (95%) patients. In addition, MRA and color Doppler flow imaging highly correlated to angiography for detection of vessel occlusion. Interestingly, high resolution ultrasound detected common carotid wall thickening in vessels that were normal on other imaging studies.

Ameriso et al. also found that the systolic/diastolic ratios and pulsatility indexes were extremely low in a patient with Takayasu arteritis [37]. They also noted damping in every flow waveform recorded, consistent with pulseless flow in the intracranial circulation.

Others have validated use of ultrasound in vasculitis as compared to cerebral angiography and MRA (Figs. 3 and 4) [10, 39, 40]. Ultrasound may show inflammatory wall thickening. In the case of temporal arteritis, color Doppler ultrasound shows a concentric, hypoechoic dark wall swelling secondary to edema; increased flow velocity due to stenosis (particularly with increased velocities proximally, turbulent waveforms with several colors present, and reduced velocities behind the area of stenosis [14]. They noted that these findings improve with corticosteroids, which highlights the benefit of non-invasive techniques such as ultrasound or transcranial Doppler for real-time monitoring of treatment effect. Ultimately, improvement of stenosis with treatment over time can assist in prognostication.

Fig. 3 Imaging studies of a 37-year-old man with newly diagnosed and untreated active Wegener's granulomatosis with involvement of the carotid bifurcation and the internal carotid artery. (**a**) Angiography of the left carotid artery shows narrowing of the proximal internal carotid artery. Kinking and coiling of the artery occurs further distally. (**b**) The T1-weighted magnetic resonance image of the left carotid bifurcation shows a perivascular infiltrate. The ultrasound image in a longitudinal (**c**) and transverse view (**d**) delineates narrowing of the artery, hyperechoic (bright) wall thickening, and a perivascular infiltrate [10]

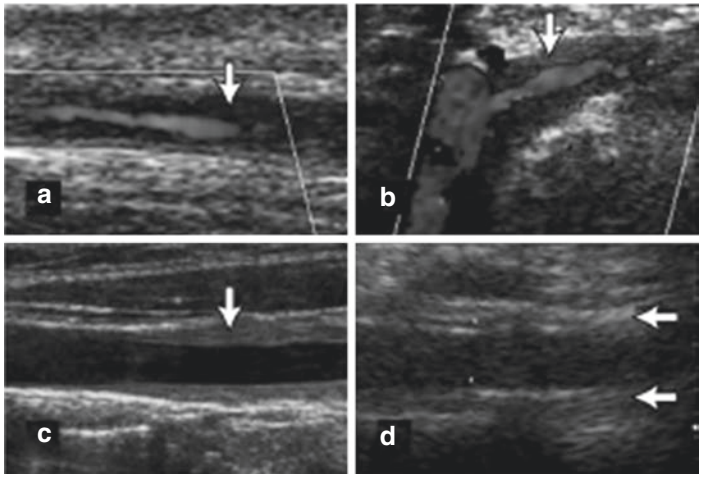

Fig. 4 Ultrasound images of vasculitis. The arrows indicate inflammatory wall thickening. The scans are longitudinal to the course of the vessels. (**a**) Left parietal ramus in acute temporal arteritis. (**b**) Left subclavian artery in acute large-vessel giant cell arteritis. (**c**) Left common carotid artery in Takayasu's arteritis. The right side of the image delineates a thickened artery wall. The distal common carotid artery (left side) is normal. (**d**) Isolated abdominal aortitis

Suggested Protocol

Obtain a complete standard TCD, including extracranial ICA flow velocities to calculate the Lindegaard ratio, to establish a baseline after diagnosis (see Chapter "Transcranial Doppler in Subarachnoid Hemorrhage": SAH and vasospasm). Repeat TCD studies daily, following additional treatment, or with a change in clinical examination.

Technical Considerations

The examination is often done in the neurocritical care unit under less than optimal conditions. Audible signals from narrowed ves-

sels are weak and a good quality headset is recommended. All studies should be conducted with the patients at rest with steady state ventilator settings (arterial CO2 content causing large artery dilation and arteriolar constriction), ICP, hematocrit, temperature, blood pressure, and mental or motor activity (neurovascular coupling).

The evaluation of RCVS or vasculitis should be similar to the routine TCD performed for vasospasm, utilizing classic acoustic windows with a 2 MHz frequency ultrasound probe at previously recommended depths.

We recommend the highest possible PRF setting to reduce the risk of PRFs aliasing [3]. Musical murmurs and bruits in distal segments can guide the sample volume toward the highest velocities.

Distal vessels such as M2 should be scanned for elevated velocities. Given the fluctuation in flow velocities, we recommend at least daily assessment over a sufficient amount of time.

Obtain extracranial Doppler for a reference velocity from the internal carotid artery (eICA) as close as possible to the base of the skull. Aim the probe inferiorly or slightly posteriorly to the angle of the jaw, with the depth set to 40 to 50 mm.

References

1. Babikian VL, Feldmann E, Wechsler LR, Newell DW, Gomez CR, Bogdahn U, Caplan LR, Spencer MP, Tegeler C, Ringelstein EB, Alexandrov AV. Transcranial Doppler ultrasonography: year 2000 update. J Neuroimaging. 2000;10(2):101–15.
2. Zanette EM, Fieschi C, Bozzao L, Roberti C, Toni D, Argentino C, Lenzi GL. Comparison of cerebral angiography and transcranial Doppler sonography in acute stroke. Stroke. 1989;20(7):899–903.
3. Aaslid R. Transcranial Doppler assessment of cerebral vasospasm. Eur J Ultrasound. 2002;16(1-2):3–10.
4. Sviri GE, Ghodke B, Britz GW, Douville CM, Haynor DR, Mesiwala AH, Lam AM, Newell DW. Transcranial Doppler grading criteria for basilar artery vasospasm. Neurosurgery. 2006;59(2):360–6.
5. Lysakowski C, Walder B, Costanza MC, Tramèr MR. Transcranial Doppler versus angiography in patients with vasospasm due to a ruptured cerebral aneurysm: a systematic review. Stroke. 2001;32(10):2292–8.

6. Sloan MA, Haley EC, Kassell NF, Henry ML, Stewart SR, Beskin RR, Sevilla EA, Tomer JC. Sensitivity and specificity of transcranial Doppler ultrasonography in the diagnosis of vasospasm following subarachnoid hemorrhage. Neurology. 1989;39(11):1514.
7. Harders AG, Gilsbach JM. Time course of blood velocity changes related to vasospasm in the circle of Willis measured by transcranial Doppler ultrasound. J Neurosurg. 1987;66(5):718–28.
8. Proust F, Callonec F, Clavier E, Lestrat JP, Hannequin D, Thiebot J, Freger P. Usefulness of transcranial color-coded sonography in the diagnosis of cerebral vasospasm. Stroke. 1999;30(5):1091–8.
9. Kubo S, Nakata H, Tatsumi T, Yoshimine T. Headache associated with postpartum cerebral angiopathy: monitoring with transcranial color-coded sonography. Headache J Head Face Pain. 2002;42(4):297–300.
10. Schmidt WA. Use of imaging studies in the diagnosis of vasculitis. Curr Rheumatol Rep. 2004;6(3):203–11.
11. Lindegaard KF, Nornes H, Bakke SJ, Sorteberg W, Nakstad P. Cerebral vasospasm diagnosis by means of angiography and blood velocity measurements. Acta Neurochir. 1989;100(1):12–24.
12. Gosling RG, King DH. The role of measurement in peripheral vascular surgery: arterial assessment by Doppler-shift ultrasound.
13. de Riva N, Budohoski KP, Smielewski P, Kasprowicz M, Zweifel C, Steiner LA, Reinhard M, Fábregas N, Pickard JD, Czosnyka M. Transcranial Doppler pulsatility index: what it is and what it isn't. Neurocrit Care. 2012;17(1):58–66.
14. Schmidt WA, Gromnica-Ihle E. Incidence of temporal arteritis in patients with polymyalgia rheumatica: a prospective study using colour Doppler ultrasonography of the temporal arteries. Rheumatology. 2002;41(1):46–52.
15. Rasulo FA, De Peri E, Lavinio A. Transcranial Doppler ultrasonography in intensive care. Eur J Anaesthesiol (EJA). 2008;25:167–73.
16. Fullerton HJ, Adams RJ, Zhao S, Johnston SC. Declining stroke rates in Californian children with sickle cell disease. Blood. 2004;104(2):336–9.
17. Bellner J, Romner B, Reinstrup P, Kristiansson KA, Ryding E, Brandt L. Transcranial Doppler sonography pulsatility index (PI) reflects intracranial pressure (ICP). Surg Neurol. 2004;62(1):45–51.
18. Calabrese LH, Dodick DW, Schwedt TJ, Singhal AB. Narrative review: reversible cerebral vasoconstriction syndromes. Ann Intern Med. 2007;146(1):34–44.
19. Call GK, Fleming MC, Sealfon S, Levine H, Kistler JP, Fisher CM. Reversible cerebral segmental vasoconstriction. Stroke. 1988;19(9):1159–70.
20. Singhal AB, Hajj-Ali RA, Topcuoglu MA, Fok J, Bena J, Yang D, Calabrese LH. Reversible cerebral vasoconstriction syndromes: analysis of 139 cases. Arch Neurol. 2011;68(8):1005–12.

21. Rocha EA, Topcuoglu MA, Silva GS, Singhal AB. RCVS2 score and diagnostic approach for reversible cerebral vasoconstriction syndrome. Neurology. 2019;92(7):e639–47.
22. Ducros A, Boukobza M, Porcher R, Sarov M, Valade D, Bousser MG. The clinical and radiological spectrum of reversible cerebral vasoconstriction syndrome. A prospective series of 67 patients. Brain. 2007;130(12):3091–101.
23. Bogousslavsky J, Despland PA, Regli F, Dubuis PY. Postpartum cerebral angiopathy: reversible vasoconstriction assessed by transcranial Doppler ultrasounds. Eur Neurol. 1989;29(2):102–5.
24. Marsh EB, Ziai WC, Llinas RH. The need for a rational approach to vasoconstrictive syndromes: transcranial doppler and calcium channel blockade in reversible cerebral vasoconstriction syndrome. Case Rep Neurol. 2016;8(2):161–71.
25. Razumovsky AY, Wityk RJ, Geocadin RG, Bhardwaj A, Ulatowski JA. Cerebral vasculitis: diagnosis and follow-up with transcranial Doppler ultrasonography. J Neuroimaging. 2001;11(3):333–5.
26. Levin JH, Benavides J, Caddick C, Laurie K, Wilterdink J, Yaghi S, Silver B, Khan M. Transcranial Doppler ultrasonography as a non-invasive tool for diagnosis and monitoring of reversible cerebral vasoconstriction syndrome. R I Med J. 2016;99(9):38.
27. Terasawa Y, Arai A, Sakai K, Mitsumura H, Iguchi Y. Transcranial color-coded sonography findings of patients with reversible cerebral vasoconstriction syndromes. J Clin Neurosci. 2019;61:290–2.
28. Chen SP, Fuh JL, Chang FC, Lirng JF, Shia BC, Wang SJ. Transcranial color doppler study for reversible cerebral vasoconstriction syndromes. Ann Neurol. 2008;63(6):751–7.
29. Topcuoglu MA, Chan ST, Silva GS, Smith EE, Kwong KK, Singhal AB. Cerebral vasomotor reactivity in reversible cerebral vasoconstriction syndrome. Cephalalgia. 2017;37(6):541–7.
30. Singhal AB, Topcuoglu MA, Fok JW, Kursun O, Nogueira RG, Frosch MP, Caviness VS Jr. Reversible cerebral vasoconstriction syndromes and primary angiitis of the central nervous system: clinical, imaging, and angiographic comparison. Ann Neurol. 2016;79(6):882–94.
31. Krasnianski M, Schluter A, Neudecker S, Spielmann RP, Stock K. Serial magnet resonance angiography in patients with vasculitis and vasculitis-like angiopathy of the central nervous system. Eur J Med Res. 2004;9:247–55.
32. Hajj-Ali RA, Calabrese LH. Diagnosis and classification of central nervous system vasculitis. J Autoimmun. 2014;48:149–52.
33. Calabrese LH, Mallek JA. Primary angiitis of the central nervous system. Report of 8 new cases, review of the literature, and proposal for diagnostic criteria. Medicine. 1988;67(1):20–39.

34. Lowe LH, Morello FP, Jackson MA, Lasky A. Application of transcranial Doppler sonography in children with acute neurologic events due to primary cerebral and West Nile vasculitis. Am J Neuroradiol. 2005;26(7):1698–701.
35. Morgenlander JC, McCallum RM, Devlin T, Moore MS, Gray L, Alberts MJ. Transcranial doppler sonography to monitor cerebral vasculitis. J Rheumatol. 1996;23(3):561–3.
36. Cantú C, Pineda C, Barinagarrementeria F, Salgado P, Gurza A, de Pablo P, Espinosa R, Martínez-Lavín M. Noninvasive cerebrovascular assessment of Takayasu arteritis. Stroke. 2000;31(9):2197–202.
37. Ameriso S, Bernard JT, Fisher M, Weaver F. "Pulseless" transcranial Doppler findings in Takayasu's arteritis. J Clin Ultrasound. 1990;18(7):592–6.
38. González-Suárez I, Arpa J, Ríos-Blanco JJ. Brain microvasculature involvement in ANCA positive vasculitis. Cerebrovasc Dis. 2016;41(5-6):313–21.
39. Ritter MA, Dziewas R, Papke K, Lüdemann P. Follow-up examinations by transcranial Doppler ultrasound in primary angiitis of the central nervous system. Cerebrovasc Dis. 2002;14(2):139–42.
40. Duna GF, Calabrese LH. Limitations of invasive modalities in the diagnosis of primary angiitis of the central nervous system. J Rheumatol. 1995;22(4):662–7.

Monitoring for Emboli Detection (Without and With Microbubbles)

Alexander Razumovsky

Monitoring for Emboli Detection (Without Micro-Bubbles Injection)

Cardioembolic stroke accounts for 14–30% of ischemic strokes [1, 2]; patients with cardioembolic infarction are prone to early and long-term stroke recurrence, although recurrences may be preventable by appropriate treatment during the acute phase and strict control at follow-up [3, 4]. Cardioembolic stroke occurs when the heart pumps unwanted materials into the brain circulation, resulting in occlusion of brain vessels and brain tissue infarction. TCD ultrasonography is the only available modality for detecting microembolic material in gaseous and solid states in real-time, within the intracranial cerebral arteries. These microembolic signals (MES) or high-intensity transient signals (HITS) have distinct acoustic impedance properties when compared to erythrocytes that flow simultaneously and early experimental studies demonstrated the high sensitivity of Doppler ultrasound in detecting arterial emboli [5, 6]. The ultrasound signals reflect off emboli prior to flowing erythrocytes in blood and due to this

A. Razumovsky (✉)
TCD Global, Inc., York, PA, USA

TCD Consultant, SpecialtyCare, Inc., Brentwood, TN, USA
e-mail: alexander.razumovsky@specialtycare.net

W. C. Ziai, C. L. Cornwell (eds.), *Neurovascular Sonography*,
https://doi.org/10.1007/978-3-030-96893-9_7

phenomenon, the reflected Doppler signal has a higher intensity signal visible within the Doppler spectrum [7]. Emboli have been detected in a number of clinical conditions: carotid artery stenosis, aortic arch plaques, atrial fibrillation, myocardial infarction, prosthetic heart valves, patent foramen ovale, valvular stenosis, during carotid surgery, open-heart surgery, stent implantation, percutaneous transluminal angioplasty, angiography and other procedures (Table 1). The 1995 Consensus Committee of the Ninth International Cerebral Hemodynamics Symposium identified embolic signals according to their defined features: short duration (lasting 0.01–0.1 second), unidirectional, high-intensity signals visible in the Doppler spectrum, occurring randomly within the cardiac cycle, accompanied by a characteristic "chirping" or "clicking" sound, and without any possible source of artifact at the same time [8] (Fig. 1). It should be noted, however, that embolic signals may occasionally produce bidirectional signals, particularly if gaseous in composition or with inadequate instrumentation settings [9]. In 1998 the International Consensus Group on microembolus detection suggested guidelines for the most important technical parameters for proper use of TCD identification of emboli in clinical practice, as well as in scientific investigations [9]. These parameters are the following:

(i) The relative intensity increase: the ratio of the acoustic power backscattered from the embolus to that of the moving blood surrounding the embolus (measured in dB).
(ii) Detection threshold: decibel thresholds ranging from 3 to 9 dB have been recommended for discriminating MES from the background noise and from spontaneous fluctuations of physiological Doppler flow signals.
(iii) The axial length of the sample volume affects the relative intensity increase and can be manipulated. Most investigators use a sample volume length $\geq$3 and $\leq$10 mm.
(iv) Frequency and temporal resolution: The data length analyzed should usually not exceed 5–10 ms to achieve a spectral resolution of the FFT of 100–200 Hz (lower FFT frequency resolution is preferred).

Table 1 Conditions in which Microembolic signals can be detected

Asymptomatic high-grade internal carotid stenosis (ACS)
Symptomatic high-grade internal carotid stenosis
Prosthetic cardiac valves
Myocardial infarction
Atrial fibrillation
Aortic arch atheroma
Fat embolization syndrome
Cerebral vascular disease
Coronary artery catheterization
Coronary angioplasty
Direct current cardioversion
Cerebral angiography
Carotid endarterectomy (CEA)
Carotid angioplasty
Cardiopulmonary bypass
Brain aneurysm
Hughes-Stovin syndrome
Marantic endocarditis
Deep vein thrombosis
Mitral valve prolapse
Polyarteritis nodosa
Pelvic vein thrombosis
IV catheter infection
Renal vein thrombosis
Idiopathic dilated cardiomyopathy
Renal vein thrombosis
Dilated cardiomyopathy
Aortic aneurysm, abdominal
Endocarditis
Atrial myxoma
Ventricular aneurysm
Surgery complication
Cholesterol embolism

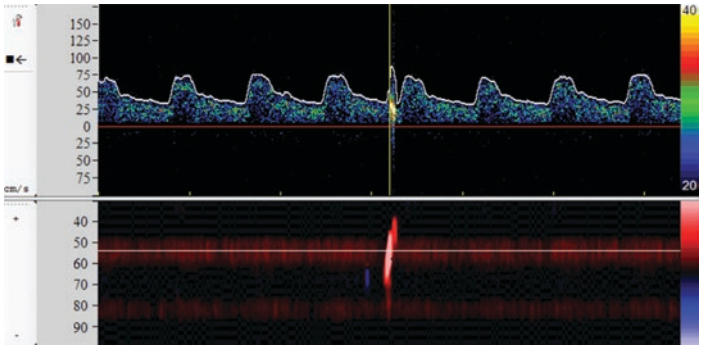

Fig. 1 Single MES reflection in regular Doppler spectrum (upper part of display) and in M-Mode (lower part of display). (This illustration is courtesy of DWL, Germany)

(v) Temporal overlap: An FFT overlap of at least 50% is important to avoid missing individual microembolic signals.
(vi) Minimizing the background signal by using a low power and low gain is recommended to allow strong embolic signals to be completely displayed within the dynamic range of the instrument.
(vii) Ultrasound frequency: The most frequently used frequency is 2 MHz because sensitivity is lower with higher frequencies.
(viii) High and low pass filter settings should be kept constant.
(ix) A recording time of at least 1 hour is recommended for patients with carotid stenosis or atrial fibrillation, but shorter times (30-minutes) may suffice in patients with mechanical heart valves.

Carotid stenosis is an important cause of ischemic stroke, with artery-to-artery embolism being the most common mechanism. In 1991, the European Carotid Surgery Trial [10] and North American Symptomatic Carotid Endarterectomy Trial [11] reported a beneficial effect in favor of CEA in recently symptomatic patients with high-grade carotid artery stenosis. In these clinical trials, the reduction in stroke risk is attributed to removal of the cerebral embolic source, carotid plaque in most cases.

Stork et al. confirmed that MES are more likely to be detected among symptomatic patients with high grade carotid stenosis compared with asymptomatic patients and that higher numbers of MES are more common among symptomatic vs. asymptomatic patients [12]. Most MES are asymptomatic, but are still believed to be a marker of risk for cerebral ischemia [13]. To define patients with ACS who will benefit from medical, surgical or endovascular intervention TCD emboli monitoring can be helpful. Molloy and Markus observed that TCD based identification of asymptomatic embolization in patients with >60% carotid artery stenosis was an independent predictor of future stroke risk in both symptomatic and asymptomatic patients [14]. Another prospective study suggested that cerebral microembolism detected with TCD sonography may define a high-risk subgroup among patients with high-grade ACS [15]. The Asymptomatic Carotid Emboli Study was a prospective observational study in patients with ACS of at least 70% from 26 centers worldwide. To detect the presence of embolic signals, patients had 1-hour TCD recordings from the ipsilateral middle cerebral artery (MCA) at baseline and at 6, 12, and 18 months. This study reported an absolute annual risk of ipsilateral stroke or TIA at 2 years of 7.13% in patients with embolic signals and 3.04% in those without, and for ipsilateral stroke, 3.62% in patients with embolic signals and 0.70% in those without [16]. Thus, the presence of emboli on TCD distal to a high-grade asymptomatic ICA stenosis identifies patients at higher risk of first-ever stroke [16]. Sometimes the presence of emboli can be the only sign of a proximal or distal arterial dissection, partially occlusive thrombus, artery-to-artery embolism or unrecognized cardiac source of embolism. Patients with ACS should not be offered surgical or endovascular intervention without first being identified as high risk as percent stenosis itself can be misleading. One way to improve the risk to benefit ratio for intervention is with TCD emboli monitoring [17]. Finally, a systematic review and meta-analysis found that TCD emboli monitoring provides clinically useful information about stroke risk for patients with carotid disease and is technically feasible in most patients [18].

Emboli detection can also be used to assess the effect of antithrombotic drugs. Antithrombotic therapy is usually prescribed to patients after initial presentation with stroke. MES are affected by antithrombotic agents [19]. Goertler et al. utilized TCD emboli monitoring to localize an embolic source and to monitor the effects of antithrombotic treatment in 81 patients with atherosclerotic CVD [20]. The CARESS trial was the first multicenter study to use MES detection with TCD monitoring as a surrogate end point to evaluate antiplatelet efficacy and showed that using MES as an outcome parameter with appropriate quality control measures is feasible [21]. Spence et al. showed that cardiovascular events and MES on TCD significantly declined with more intensive medical therapy [22]. They concluded that fewer than 5% of patients with ACS likely benefit from revascularization, and that ACS patients should receive intensive medical therapy with consideration of revascularization only if MES are observed on TCD [22]. A subsequent review of the role of TCD emboli monitoring in patients with multi-territory acute embolic strokes showed that presence of MES, especially in multiple intracranial arteries, is associated with increased risk of symptomatic, recurrent embolization [23]. This finding may justify a more aggressive treatment approach (clopidogrel load followed by dual antiplatelet therapy or alternatively therapeutic dose of low-molecular-weight heparin).

Several technical issues associated with TCD emboli monitoring warrant discussion, including validity of automatic software for emboli detection, total time for MES monitoring, and best time for MES monitoring during the natural day (24 hours). Kouame et al. suggested an approach for detection of small MES, called the neuro-fuzzy technique. In the field of artificial intelligence, neuro-fuzzy refers to combinations of artificial neural networks and fuzzy logic in which MES detection is performed using only one gate instead of multiple-gate TCD instruments [24]. Another study suggests that using only single-channel, single-frequency Doppler ultrasound, the HITS detection and character-

ization method using a weighted-frequency Fourier linear combiner that estimates baseline Doppler signal power allows more accurate and sensitive detection and segmentation of embolic signatures compared to commercial TCD emboli-detection software [25]. Abbott et al. demonstrated that embolism associated with ACS shows circadian variation with highest rates 4–6 hours before midday [26]. This corresponds with peak circadian incidence of stroke and other vascular complications. Accurate and reliable characterization of embolus size and composition is still not possible with current technology. An optimum recording protocol is not defined. One hour probably is required [27–29] but this finding has not been validated by a prospective study. In patients with mechanical heart valves, a 30-minute recording time may be sufficient.

Patients with acute and sub-acute ischemic strokes and TIAs can also undergo TCD emboli monitoring to detect, localize, and quantify cerebral embolization [30]. This information is helpful to establish the mechanism of stroke and potentially change management strategy, especially if emboli are found suggesting artery-to-artery embolization or continuing embolization despite treatment both in patients with symptomatic and asymptomatic extracranial or intracranial large artery disease [31].

TCD emboli monitoring may also be useful during surgeries, like CEA and cardiothoracic surgeries due to relatively high frequency of stroke as a complication. One study of 500 patients who underwent CEA with TCD monitoring of the ipsilateral MCA during various phases of CEA concluded that embolism (54%) is the primary cause of cerebrovascular complications from CEA [32]. TCD monitoring during CEA provides clinically useful information about embolic phenomena and flow patterns in the cerebral vasculature that may prompt appropriate measures at several stages of CEA to reduce the risk of perioperative stroke [32–34]. TCD emboli monitoring is therefore considered possibly useful during cardiac surgery, but remains investigational [35–39].

Monitoring for Emboli with Micro-Bubble Injection

Patent foramen ovale (PFO) has been associated with cryptogenic stroke allowing paradoxical embolism from the veins to the brain through an RLS [40]. PFO is a permanent opening through the interatrial septum or a hole between the upper chambers of the heart that fails to close after birth and often persists into adulthood. Blood flows back and forth through the defect depending on the pressure gradient between the atria. For the vast majority a PFO is well-tolerated. PFO is found in 34% of adults in the first three decades of life declining to 20% in the ninth and tenth decades and ranging from 1 to 19 mm in diameter [41].

Problems arise when a blood clot crosses the PFO and enters the cerebral circulation causing an ischemic stroke. This paradoxical embolism may occur more often than suspected.

Initially, PFO is considered when stroke occurs in a young person. One study reported an incidence of abnormal cardiac RLS – i.e. PFO or atrium septum defect in 40% of ischemic stroke patients compared with 10% of a control group [42]. Thus cardiac RLS is considered a risk factor in cryptogenic stroke, particularly in young patients with no additional risk factors. The frequency of PFO is even higher (55%) in patients with cerebral infarct of unknown etiology or so-called cryptogenic infarct [43], especially in the younger age group [44, 45]. Nevertheless, a recent systematic review and meta-analysis showed the association of RLS with cryptogenic events remained at older ages and overall the population burden of PFO-associated events is substantial [46]. In addition, migraine patients with aura have 3–1 odds of having a PFO compared to a non-migraine group [47]. Given that the conditions for venous thrombosis and pulmonary embolism are also common in the general population, the risk for paradoxical embolism is prevalent at all ages.

The motivation to diagnose PFO is driven by the manufacture of safe transcatheter closure devices and the popularity of contrast-TCD (c-TCD) over invasive contrast transesophageal echocardiography (c-TEE) or contrast transthoracic echocardiography

(c-TTE). Using intravenous injections of agitated saline (Fig. 2), the suspended bubbles pass through the PFO from the right to the left atrium and are easily detected by TCD as audible chirps and microembolic spectra in the cerebral arteries. A Valsalva Maneuver (VM) facilitates passage of the microbubbles through the PFO by

Fig. 2 Example of set-up for intravenous injection of agitated saline

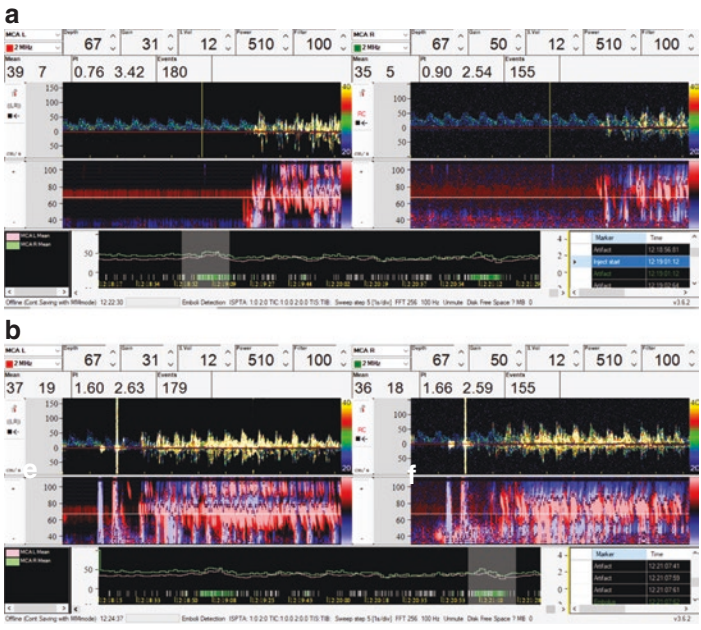

Fig. 3 C-TCD at rest (**a**) and at Valsalva maneuver demonstrating "curtain" of emboli (**b**)

raising the pressure in the right atrium over that of the left atrium (Fig. 3). Agitated saline contrast agent has been used safely for many years in echocardiography and TCD.

C-TEE until recently was considered the gold standard for PFO detection and diagnostic yield is enhanced using contrast agents. However, the c-TEE examination may lack sufficient sensitivity if sedation is required, as the sedated patient is often not capable of performing VM or forced expiratory effort adequately, which is frequently an indispensable prerequisite to elicit a RLS. Although c-TTE allows the diagnosis of RLS by means of color Doppler, the flow that is inverted intermittently may not be detected, and thus c-TTE may not be sensitive enough to diagnose RLS [48]. TCD monitoring with contrast injection has turned out to be a reliable method to diagnose PFO [49, 50] and has

demonstrated high accuracy in ruling in and ruling out PFO when compared to the gold standard c-TEE [47, 51–54]. Belvis et al. [53] showed almost perfect concordance between simultaneous c-TCD and c-TEE in the quantification of RLS. Moreover, c-TCD appears to be more sensitive and specific for PFO detection than c-TEE or c-TTE [55, 56]. c-TCD is sensitive to detect RLS, even in patients with negative TTE or TTE [58].

The 2000 International Consensus Meeting determined a four-level categorization according to emboli appearance in the TCD spectrum as category 1: up to 10 MES; category 2: 11–20 MES; category 3: more than 20 MES; category 4: "curtain-like" pattern, quantification is not possible because the MES signals fills the entire spectrum [57]. In addition, main advantages of contrast TCD as compared to TEE in the detection of RLS are: (1) the VM can more comfortably be applied during TCD than during TEE and (2) size and functional relevance of RLS can more easily be assessed using contrast TCD than using TEE. Spencer et al. [58] also suggested a PFO grading scale using a 6-level logarithmic scale: no MES – grade 0; 1–10 MES grade I; 11–30 MES grade II; 31–100 MES grade III; 101–300 MES grade IV; and above 300 MES – grade V (Table 2). Examples of c-TCD test at rest and with VM are shown in Fig. 3.

Power m-mode TCD (pmTCD) detects more bubble microemboli than traditional single gate conventional TCD [59]. If pmTCD testing is positive, TEE may be indicated to confirm the type and

Table 2 Spencer grading scale for reporting MES on TCD using power m-mode [58]

	Unilateral test	Bilateral test
Grade 0	0	0
Grade 1	1–5	1–10
Grade 2	6–15	11–30
Grade 3	16–50	31–100
Grade 4	51–150	101–300
Grade 5	>150	>300
Grade 5+	Uncountable, curtain	Uncountable, curtain

MES counted at rest and during Valsalva release

location of the shunt and to detect other potential cardiac abnormalities including an atrial septal aneurysm. If pmTCD is negative, there is no need to search further for a RLS as a cause of cryptogenic stroke. pmTCD provides greater sensitivity to contrast bubble emboli that does single-gate TCD and among candidates for transcatheter closure, pmTCD therefore offers an improved noninvasive method for diagnosing PFO and evaluating effect of transcatheter closure [48, 60–62].

Optimal patient setup and protocol for c-TCD are still to be perfected. Patient positioning while performing c-TCD is a matter of ongoing discussion. Some authors suggest raising the patient's position from supine to sitting to improve the sensitivity of c-TCD in the detection of PFO in the case of a first negative test [63, 64]. Some publications suggest using a small sample of the patient's own blood to obtain an agitated saline solution as a means of increasing the number of microbubbles generated [65, 66]. Other authors discuss the importance of the time interval between injection in the antecubital vein and detection of microbubbles in the MCA and concluded that observation of >10 microbubbles of agitated saline at less than 10 seconds on TCD (with VM) is highly sensitive and specific for the diagnosis of RLS [67]. They also found that use of a plasma volume expander, oxypolygelatine, caused a significantly higher number of microbubbles compared with saline as contrast media. Similarly, Droste et al. showed that c-TCD yielded 100% sensitivity to identify TEE–proven cardiac RLS [51]. Patients in this study were asked to perform VM 5 seconds after administration of contrast. Schwarze et al. suggested that 10 mL of contrast medium should be injected with the patient in the supine position and that VM be performed 5 seconds after the start of the injection [68]. A strong relationship is reported between the size of the PFO on TEE and the number of MES on c-TCD ($P < 0.0001$) [69]. A consensus statement established a standardization of the c-TCD technique protocol and its interpretation [46]. Among these recommendations: (a) Always quantify the MES at rest and during provocative maneuvers; report numbers of MES separately; (b) Perform the examination three times at rest, and afterwards three times under provocative maneuvers. Consider the examination

completed if the "curtain-like" pattern is observed at rest; (c) Explain the Valsalva maneuver to the patient and have them practice it prior to beginning the test in order to check that the provocative test has a reliable response; (d) Consider a positive result the detection of at least one MES with spectral visualization and coincident signal on M-mode, as well as the typical sound pattern. Consider it a non-significant positive result if fewer than 10 MES are detected only during the provocative maneuver; (e) Report the findings according to four categorization levels [57]; (f) For bilateral tests, use the highest number obtained in each channel and do not sum the number of MES detected in the right and left MCA; g) Document results for "at rest" and VM separately.

Conclusion

C-TCD monitoring with contract injection has established value for evaluation of patients with unknown cause of stroke and suspected RLS. Although c-TCD itself is sufficient for diagnostic screening of RLS with high sensitivity (97%) and specificity (93%) – class IIA, its use alone is not recommended [35]. The direct evaluation of RLS and anatomical observation of the atrial septum remains important, especially if PFO closure is to be considered.

References

1. Arboix A, Alio J. Acute cardioembolic cerebral infarction: answers to clinical questions. Curr Cardiol Rev. 2012;8(1):54–67.
2. Benjamin EJ, Muntner P, Alonso A, et al. Heart disease and stroke statistics—2019 update: summary. A report from the American Heart Association. Circulation. 2019;139(10):e56–e528.
3. Rabinstein AA. Treatment of acute ischemic stroke. Continuum (Minneap Minn). 2017;23(1, Cerebrovascular Disease):62–81.
4. Easton JD, Lopes RD, Bahit MC, Wojdyla DM, Granger CB, Wallentin L, et al. Apixaban compared with warfarin in patients with atrial fibrillation and previous stroke or transient ischaemic attack: a subgroup analysis of the ARISTOTLE trial. Lancet Neurol. 2012;11(6):503–11.

5. Spencer MP, Campbell SD, Sealey JL, Henry FC, Lindbergh J. Experiments on decompression bubbles in the circulation using ultrasonic and electromagnetic flowmeters. J Occup Med. 1969;11(5):238–44.
6. Russell D, Madden KP, Clark WM, Sandset PM, Zivin JA. Detection of arterial emboli using Doppler ultrasound in rabbits. Stroke. 1991;22(2):253–8.
7. Russel D. The detection of cerebral emboli using Doppler ultrasound. In: Newel DW, Aaslid R, editors. Transcranial Doppler. New York: Raven Press; 1992. p. 207–13.
8. Basic identification criteria of Doppler microembolic signals. Consensus Committee of the Ninth International Cerebral Hemodynamics Symposium. Stroke. 1995;26(6):1123.
9. Ringelstein EB, Droste DW, Babikian VL, Evans DH, Grosset DG, Kaps M, et al. Consensus on microembolus detection by TCD. International Consensus Group on Microembolus Detection. Stroke. 1998;29(3):725–9.
10. European Carotid Surgery Trialists' (ECST) Collaborative Group. MRC European Carotid Surgery Trial: interim results for symptomatic patients with severe (70–99%) or with mild (0–29%) carotid stenosis. Lancet. 1991;337(8752):1235–43.
11. Barnett HJM, Taylor DW, Haynes RB, Sackett DL, Peerless SJ, Ferguson GG, et al. North American Symptomatic Carotid Endarterectomy Trial (NASCET) Collaborators. Beneficial effect of carotid endarterectomy in symptomatic patients with high-grade carotid stenosis. N Engl J Med. 1991;325(7):445–53.
12. Stork JL, Kimura K, Levi CR, Chambers BR, Abbott AL, Donnan GA. Source of microembolic signals in patients with high-grade carotid stenosis. Stroke. 2002;33(8):2014–8.
13. Siebler M, Sitzer M, Steinmetz H. Detection of intracranial emboli in patients with symptomatic extracranial carotid artery disease. Stroke. 1992;23(11):1652–4.
14. Molloy J, Markus HS. Asymptomatic embolization predicts stroke and TIA risk in patients with carotid artery stenosis. Stroke. 1999;30(7):1440–3.
15. Siebler M, Nachtmann A, Sitzer M, Rose G, Kleinschmidt A, Rademacher J, et al. Cerebral microembolism and the risk of ischemia in asymptomatic high-grade internal carotid artery stenosis. Stroke. 1995;26(11):2184–6.
16. Markus HS, King A, Shipley M, Topakian R, Cullinane M, Reihill S, et al. Asymptomatic embolisation for prediction of stroke in the Asymptomatic Carotid Emboli Study (ACES): a prospective observational study. Lancet Neurol. 2010;9(7):663–71.
17. Spence JD. Transcranial Doppler monitoring for microemboli: a marker of a high-risk carotid plaque. Semin Vasc Surg. 2017;30(1):62–6.
18. Best LM, Webb AC, Gurusamy KS, Cheng SF, Richards T. Transcranial Doppler ultrasound detection of microemboli as a predictor of cerebral events in patients with symptomatic and asymptomatic carotid disease: a

systematic review and meta-analysis. Eur J Vasc Endovasc Surg. 2016;52(5):565–80.
19. Siebler M, Nachtmann A, Sitzer M, Steinmetz H. Anticoagulation monitoring and cerebral microemboli detection. Lancet. 1994;344(8921):555.
20. Goertler M, Blaser T, Krueger S, Hofmann K, Baeumer M, Wallesch CW. Cessation of embolic signals after antithrombotic prevention is related to reduced risk of recurrent arterioembolic transient ischaemic attack and stroke. J Neurol Neurosurg Psychiatry. 2002;72(3):338–42.
21. Dittrich R, Ritter MA, Kaps M, Siebler M, Lees K, Larrue V, et al. The use of embolic signal detection in multicenter trials to evaluate antiplatelet efficacy: signal analysis and quality control mechanisms in the CARESS (Clopidogrel and Aspirin for Reduction of Emboli in Symptomatic carotid stenosis) trial. Stroke. 2006;37(4):1065–9.
22. Spence DJ, Coates V, Li H, Tamayo A, Muñoz C, Hackam DG, et al. Effects of intensive medical therapy on microemboli and cardiovascular risk in asymptomatic carotid stenosis. Arch Neurol. 2010;67(2):180–6.
23. Kargiotis O, Psychogios K, Safouris A, Magoufis G, Zervas PD, Stamboulis E, et al. The role of transcranial Doppler monitoring in patients with multi-territory acute embolic strokes: a review. J Neuroimaging. 2019;29(3):309–22.
24. Kouamé D, Biard M, Girault JM, Bleuzen A. Adaptive AR and neuro-fuzzy approaches: access to cerebral particle signatures. IEEE Trans Inf Technol Biomed. 2006;10(3):559–66.
25. Imaduddin SM, LaRovere KL, Kussman BD, Heldt T. A time-frequency approach for cerebral embolic load monitoring. IEEE Trans Biomed Eng. 2020;67(4):1007–18.
26. Abbott AL, Merican J, Pearce DC, Juric A, Worsnop C, Foster E, et al. Asymptomatic carotid stenosis is associated with circadian and other variability in embolus detection. Front Neurol. 2019;10:322.
27. Abbott AL, Chambers BR, Stork JL, Levi CR, Bladin CF, Donnan GA. Embolic signals and prediction of ipsilateral stroke or transient ischemic attack in asymptomatic carotid stenosis: a multicenter prospective cohort study. Stroke. 2005;36(6):1128–33.
28. Molloy J, Khan N, Markus HS. Temporal variability of asymptomatic embolization in carotid artery stenosis and optimal recording protocols. Stroke. 1998;29(6):1129–32.
29. Blaser T, Glanz W, Krueger S, Wallesch CW, Kropf S, Goertler M. Time period required for transcranial Doppler monitoring of embolic signals to predict recurrent risk of embolic transient ischemic attack and stroke from arterial stenosis. Stroke. 2004;35(9):2155–9.
30. Alexandrov AV, Sloan MA, Tegeler CH, Newell DN, Lumsden A, Garami Z, et al. Practice standards for transcranial Doppler (TCD) ultrasound. Part II. Clinical indications and expected outcomes. J Neuroimaging. 2012;22(3):215–24.

31. King A, Markus HS. Doppler embolic signals in cerebrovascular disease and prediction of stroke risk: a systematic review and meta-analysis. Stroke. 2009;40(12):3711–7.
32. Spencer MP. Transcranial Doppler monitoring and causes of stroke from carotid endarterectomy. Stroke. 1997;28(4):685–91.
33. Ackerstaff RGA, Vos JA. TCD-detected cerebral embolism in carotid endarterectomy versus angioplasty and stenting of the carotid bifurcation. Acta Chir Belg. 2004;104(1):55–9.
34. Naylor AR, Sayers RD, McCarthy MJ, Bown MJ, Nasim A, Dennis MJ. Closing the loop: a 21-year audit of strategies for preventing stroke and death following carotid endarterectomy. Eur J Vasc Endovasc Surg. 2013;46(2):161–70.
35. Edmonds H, Isley MR, Sloan TB, Alexandrov AV, Razumovsky A. American Society of Neurophysiologic Monitoring (ASNM) and American Society of Neuroimaging (ASN) joint guidelines for transcranial Doppler (TCD) ultrasonic monitoring. J Neuroimaging. 2011;21(2):177–83.
36. Halkos ME, Anderson A, Binongo JNG, Stringer A, Lasanajak Y, Thourani VH, et al. Operative strategies to reduce cerebral embolic events during on- and off-pump coronary artery bypass surgery: a stratified, prospective randomized trial. J Thorac Cardiovasc Surg. 2017;154(4):1278–85.
37. Sloan MA, Alexandrov AV, Tegeler CH, Spencer MP, Caplan LR, Feldmann E, et al. Assessment: transcranial Doppler ultrasonography: report of the therapeutics and technology assessment subcommittee of the American Academy of Neurology. Neurology. 2004;62(9):1468–81.
38. Mas JL, Arquizan C, Lamy C, Zuber M, Cabanes L, Derumeaux G, et al. Recurrent cerebrovascular events associated with patent foramen ovale, atrial septal aneurysm, or both. N Engl J Med. 2001;345(24):1740–6.
39. Hagen PT, Scholz DG, Edwards WD. Incidence and size of patent foramen ovale during the first 10 decades of life: an autopsy study of 965 normal hearts. Mayo Clin Proc. 1984;59(1):17–20.
40. Lechat P, Mas JL, Lascault G, Loron P, Theard M, Klimczac M, et al. Prevalence of patent foramen ovale in patients with stroke. N Engl J Med. 1988;318(8):1148–52.
41. Adams HP, Bendixen BH, Kappelle LJ, et al. Classification of subtype of acute ischemic stroke. Definitions for use in a multicenter clinical trial. TOAST. Trial of Org 10172 in Acute Stroke Treatment. Stroke. 1993;24(1):35–41.
42. Serena J, Segura T, Perez-Ayuso MJ, Bassaganyas J, Molins A, Davalos A. The need to quantify right-to-left shunt in acute ischemic stroke: a case-control study. Stroke. 1998;29(7):1322–8.
43. Job FP, Ringelstein EB, Grafen Y, Flachskampf FA, Doherty C, Stockmanns A, et al. Comparison of transcranial contrast Doppler sonography and transesophageal contrast echocardiography for the detection of patent foramen ovale in young stroke patients. Am J Cardiol. 1994;74(4):381–4.

44. Mazzucco S, Li L, Binney L, Rothwell PM. Prevalence of patent foramen ovale in cryptogenic transient ischaemic attack and non-disabling stroke at older ages: a population-based study, systematic review, and meta-analysis. Lancet Neurol. 2018;17(7):609–17.
45. Anzola GP, Magoni M, Guindani M, Rozzini L, Dalla Volta G. Potential source of cerebral embolism in migraine with aura: a transcranial Doppler study. Neurology. 1999;52(8):1622–5.
46. Zetola V, Lange MC, Scavasine VC, Bazan R, Braga GP, Celestino AC, et al. Latin American Consensus Statement for the use of contrast-enhanced transcranial ultrasound as a diagnostic test for detection of right-to-left shunt. Cerebrovasc Dis. 2019;48(3–6):99–108.
47. Klotzsch C, Janssen G, Berlit P. Transesophageal echocardiography and contrast-TCD in the detection of a patent foramen ovale: experiences with 111 patients. Neurology. 1994;44(9):1603–6.
48. Anzola GP, Renaldini E, Magoni M, Costa A, Cobelli M, Guindani M. Validation of transcranial Doppler sonography in the assessment of patent foramen ovale. Cerebrovasc Dis. 1995;5:194–8.
49. Teague S, Sharma MK. Detection of paradoxical cerebral echo contrast embolization by transcranial Doppler ultrasound. Stroke. 1991;22(6):7–10.
50. Jauss M, Kaps M, Keberle M, Haberbosch W, Dorndorf W. A comparison of transesophageal echocardiography and transcranial Doppler sonography with contrast medium for detection of patent foramen ovale. Stroke. 1994;25(6):1265–7.
51. Droste DW, Kriete JU, Stypmann J, Castrucci M, Wichter T, Tietje R, et al. Contrast transcranial Doppler ultrasound in the detection of right-to-left shunts: comparison of different procedures and different contrast agents. Stroke. 1999;30(9):1827–32.
52. Devuyst G, Despland PA, Bogousslavsky J, Jeanrenaud X. Complementarity of contrast transcranial Doppler and contrast transesophageal echocardiography for the detection of patent foramen ovale in stroke patients. Eur Neurol. 1997;38(1):21–5.
53. Belvís R, Leta RG, Martí-Fàbregas J, Cocho D, Carreras F, Pons-Lladó G, et al. Almost perfect concordance between simultaneous transcranial Doppler and transesophageal echocardiography in the quantification of right-to-left shunts. J Neuroimaging. 2006;16(2):133–8.
54. Van H, Poommipanit P, Shalaby M, Gevorgyan R, Tseng CH, Tobis J. Sensitivity of transcranial Doppler versus intracardiac echocardiography in the detection of right-to-left shunt. JACC Cardiovasc Imaging. 2010;3(4):343–8.
55. Komar M, Olszowska M, Przewłocki T, Podolec J, Stępniewski J, Sobień B, et al. Transcranial Doppler ultrasonography should it be the first choice for persistent foramen ovale screening? Cardiovasc Ultrasound. 2014;12:16.
56. Maillet A, Pavero A, Salaun P, Pibourdin A, Skopinski S, Thambo JB, et al. Transcranial Doppler to detect right to left communication: evaluation versus transesophageal echocardiography in real life. Angiology. 2018;69(1):79–82.

57. Jauss M, Zanette E for the Consensus Conference. Detection of right-to-left shunt with ultrasound contrast agent and transcranial Doppler sonography. Cerebrovasc Dis. 2000;10(6):490–6.
58. Spencer MP, Moehring MA, Jesurum J, Gray WA, Olsen JV, Reisman M. Power M-mode transcranial Doppler for diagnosis of patent foramen ovale and assessing transcatheter closure. J Neuroimaging. 2004;14(4):342–9.
59. Moehring MA, Spencer MP. Power M-Mode Doppler (PMD) for observing cerebral blood flow and tracking emboli. Ultrasound Med Biol. 2002;28(1):49–57.
60. Tobe J, Bogiatzi C, Munoz C, Tamayo A, Spence JD. Transcranial Doppler is complementary to echocardiography for detection and risk stratification of patent foramen ovale. Can J Cardiol. 2016;32(8):986.e9–16.
61. Palazzo P, Ingrand P, Agius P, Belhadj Chaidi R, Neau JP. Transcranial Doppler to detect right-to-left shunt in cryptogenic acute ischemic stroke. Brain Behav. 2019;9(1):e01091.
62. Mojadidi MK, Roberts SC, Winoker JS, Romero J, Goodman-Meza D, Gevorgyan R, et al. Accuracy of transcranial Doppler for the diagnosis of intracardiac right-to-left shunt: a bivariate meta-analysis of prospective studies. JACC Cardiovasc Imaging. 2014;7(3):236–50.
63. Telman G, Kouperberg E, Sprecher E, Yarnitsky D. The positions of the patients in the diagnosis of patent foramen ovale by transcranial Doppler. J Neuroimaging. 2003;13(4):356–8.
64. Lao AY, Sharma VK, Tsivgoulis G, Malkoff MD, Alexandrov AV, Frey JL. Effect of body positioning during transcranial Doppler detection of right-to-left shunts. Eur J Neurol. 2007;14(9):1035–9.
65. Sastry S, Daly K, Chengodu T, McCollum C. Is transcranial Doppler for the detection of venous-to-arterial circulation shunts reproducible? Cerebrovasc Dis. 2007;23(5–6):424–9.
66. Lange MC, Zétola VF, Piovesan ÉJ, Werneck LC. Saline versus saline with blood as a contrast agent for right-to-left shunt diagnosis by transcranial Doppler: is there a significant difference? J Neuroimaging. 2012;22(1):17–20.
67. Albert A, Müller HR, Hetzel A. Optimized transcranial Doppler technique for the diagnosis of cardiac right-to-left shunts. J Neuroimaging. 1997;7(3):159–63.
68. Schwarze JJ, Sander D, Kukla C, Wittich I, Babikian VL, Klingelhofer J. Methodological parameters influence the detection of right-to-left shunts by contrast transcranial Doppler ultrasonography. Stroke. 1999;30(6):1234–9.
69. Telman G, Yalonetsky S, Kouperberg E, Sprecher E, Lorber A, Yarnitsky D. Size of PFO and amount of microembolic signals in patients with ischaemic stroke or TIA. Eur J Neurol. 2008;15(9):969–72.

Evaluation of Cerebral Circulatory Arrest

Armando Mario Cacciatori Castro

Development

TCD has become a valuable multimodal neuromonitoring (MNM) tool applicable in ICUs that treat neurocritically ill patients. It allows monitoring of a wide range of neurological pathologies, with the advantages of being a method that can be practiced next to the patient's bed, in a serial manner at low cost. Aaslid et al. published in 1982 the first results regarding the study of cerebral arteries, using a low frequency pulsed Doppler and demonstrating specific patterns thereof as distinctive of CCA [1]. TCD has constituted a significant step forward in the diagnosis of CCA. The normal sonographic appearance of extracerebral intracranial arteries that form the circle of Willis (CoW) is of continuous flow, with average rates that vary in accordance with each other (Fig. 1). The alterations observed on TCD of a patient with brain injury, on its way to CCA, are due to an increase in intracranial pressure (ICP) [2]. In 1998, TCD diagnostic criteria for BD were published by a task force of the World Federation of Neurology (WFN) [3]. CCA develops in four steps according to the WFN:

A. M. C. Castro (✉)
National Institute of Donations and Transplants, Clinic Hospital, Montevideo, Uruguay

W. C. Ziai, C. L. Cornwell (eds.), *Neurovascular Sonography*,
https://doi.org/10.1007/978-3-030-96893-9_8

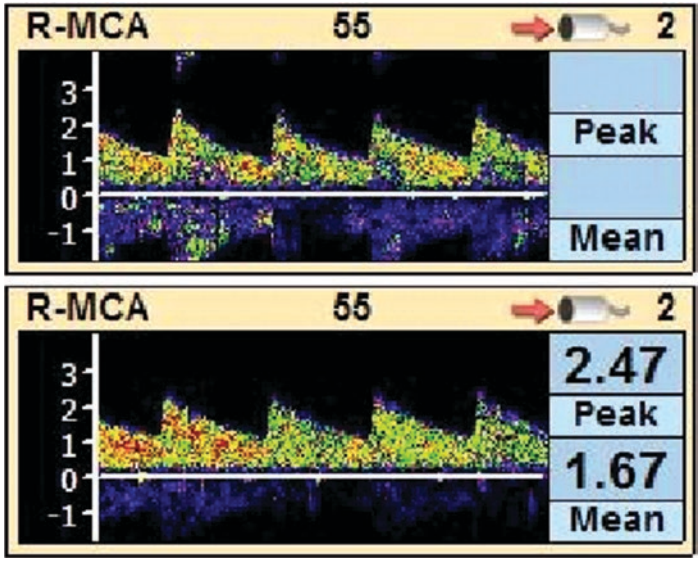

Fig. 1 Normal TCD study of right middle cerebral artery (R- MCA), near the bifurcation of the internal carotid artery (ICA). Male, 24 years old

1. Increasing pulsatility index with decreasing diastole until the cerebral blood flow velocity at the end of diastole equals zero. This occurs when the ICP reaches the diastolic blood pressure (DBP). Extensive TCD monitoring studies in patients with traumatic brain injury (TBI) have provided information regarding the relationship between ICP and TCD. The diastolic flow rate is influenced by the cerebral vascular resistance, mostly determined by the ICP and the vessel diameter. TCD images show that the diastolic flow rate becomes zero when the ICP equals DBP [4]. Since forward flow persists in systole, this stage does not correspond to CCA. This is a warning signal, at which point the TCD diastolic waveforms are comparable with the DBP (instead of the systolic or mean pressure) [5].
2. Biphasic or oscillating flow (Fig. 2). When the ICP is equal to or higher than the systolic blood pressure (SBP), cessation of cerebral perfusion occurs and "positive and reverse" flow

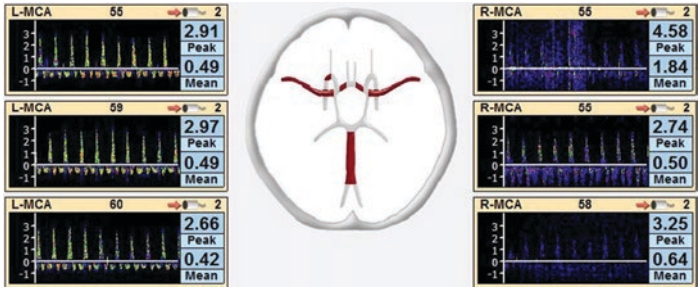

Fig. 2 TCD study that shows reverse/oscillating /reverberant diastolic flow pattern registered in both MCAs. Male, 26 years old. TBI due to firearm injury

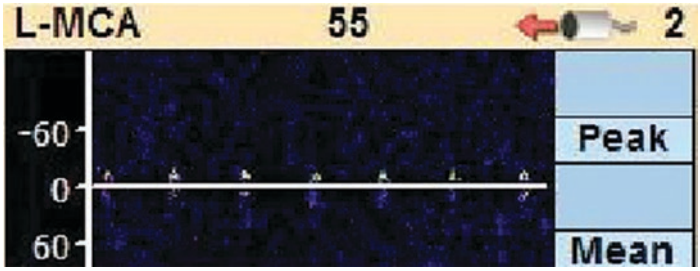

Fig. 3 TCD study that shows systolic spikes pattern in L- MCA. Male, 31 years old. Subarachnoid hemorrhage, DC and evolution into CCA

waveforms are almost alike, with a zero net flow. This correlates with circulatory arrest on the cerebral arteriogram.

3. Systolic spikes (Fig. 3). This pattern is highly distinctive of CCA. With further reduction in blood flow, only a small peak of systolic velocity can be seen. At this stage, we can assume that the slowness of the reverse flow component could be hidden by the filters. Every TCD machine uses high pass filters in order to remove signals that come from vessel wall motion. For CCA diagnosis this filter should be set at its lowest levels (for example, 50 Hz).
4. There is no flow signal. If ICP continues to increase, obstruction of flow occurs more proximally in the CoW and no flow

signal is detected distally. The failure of signal detection may be due to problems in the transmission of sound (bad sonic window); in these cases, it is paramount to examine the extracranial carotid and the vertebral arteries, since they represent important diagnostic criteria [3]. It is a major concern whether the absence of signal corresponds to CCA or to the absence of a sonic window. In order to accept this finding as a criterion for CCA, the TCD should be conducted under the same clinical conditions and by the same expert examiner who previously found flow in the patient [6]. Recall that the TCD probe may penetrate through the skull barrier, in areas where the bone is thinner; these areas of greatest transparency are called windows, and three of them are used: temporal, orbital and suboccipital or transforaminal. Cervical Color Doppler (CCD) sonography may be considered a valid and accurate diagnostic tool for detecting CCA, with a general sensitivity of 78% in comparison to other ancillary tests. Pedicelli et al. have demonstrated in their study that in a subgroup of patients with appropriate bone windows on TCD, the CCD sensitivity was around 80%, showing the same flow patterns as TCD and implying that in most cases CCD may document the same CCA pattern detected by TCD [7].

In certain jurisdictions (ex. the Spanish legislation, Royal Decree 1723/2012) [8], the documentation of these criteria which signify the existence of CCA allows a BD diagnosis to be confirmed without prolonging the observation period. In order to complete the diagnosis, it would be advisable to carry out some instrumental test [8]. However, on account of the description in the literature, of some isolated cases in which cerebral blood flow (CBF) was only temporarily interrupted (generally patients with subarachnoid hemorrhage (SAH) in which the TCD study coincided with a sudden increase in ICP due to rebleeding), some societies (ex. the Spanish Society of Neurosonology) recommend to confirm the CCA through a second study of flow velocities after at least 30 minutes [9]. It is interesting to highlight that a systolic-diastolic separation pattern can show up before biphasic or oscillating flow. This pattern is characterized by the presence of

an anterograde flow systolic wave in the sonogram (also called "systolic peak" by some authors) associated with another flow wave, also anterograde, of short duration during the mesodiastolic (middle of diastole) period. In protodiastole (period in the cardiac cycle between the end of systole and closure of the aortic valve marking the start of diastole) and telediastole (towards the end of ventricular diastole) the flow equals zero [10]. According to Domínguez Roldán et al., it is the pattern with the lowest frequency, given that it has a short time of existence [10]. We believe it is important to note that, when such a pattern is observed, the TCD should be repeated within the following 12 hours. We also emphasize that, when the systolic-diastolic separation pattern is seen, the clinical neurological examination should simultaneously be performed [11]. In a previous study of 9 cases with this TCD pattern, we reported in one case, a 22-year-old male with severe TBI, persistence of cough reflex and spontaneous breathing (Fig. 4) [11]. Based on these concepts, the following questions emerge:

1. Is CCA associated with BD?
2. Does interruption of brain circulation cause neuronal death?

The neuron is a remarkably hypoxia-ischemia-sensitive cell. The global brain ischemic threshold with the production of irreversible lesions is around 5 minutes [12]. Therefore, every such

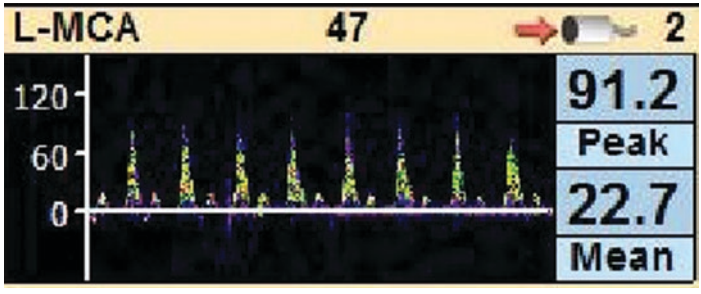

Fig. 4 Systolic-diastolic separation image registered in the left middle cerebral artery (L-MCA). Male, 22 years old. Severe TBI due to traffic accident

situation that modifies the normal brain circulation may provoke changes in neuron function and structure. The neuron is nourished via telediastole (the interval in which neurotransmitters are released), which means that if in that phase a deficit in the circulation occurs and, hence, in the supply of oxygen and glucose, the neuron will suffer injuries of variable severity. The neuron has practically no capacity for anaerobic metabolism. Flow drops below 10 ml/min/100 g cause irreversible neuronal injury [13]. In structural SBI of different types (traumatic, vascular, tumoral, anoxic-ischemic, infectious) it may be an increase of the brain volume (cerebral edema) which provokes intracranial hypertension (ICH), which has a negative impact on cerebral blood flow (CBF), causing decreases to critical levels. The CBF measurement with TCD shows a good correlation with other direct measurements thereof, such as the xenon method [14]. Moreover, the waveform morphology in the diastolic phase may earlier or later indicate signs of ICH, with subsequent mitigation of diastolic cerebral flow [14]. The interplay of pressures inside the cranial cavity affects the equation: cerebral perfusion pressure (CPP) = mean blood pressure (MBP) – ICP, and, in accordance with its values, will be translated into changes in the morphology of the velocity waveform. The attenuation of the waveform's diastolic phase, a sign of ICH with a subsequent decrease in cerebral perfusion, is associated with a decrease in the blood supply to the neuron. When ICP surpasses DBP initially, and then SBP, CBF decreases to zero and there is no forward flow in the arterial circulation. At this time, the TCD will show patterns suggesting CCA. This phenomenon, which is a result of cerebral herniation, does not allow neuronal telediastolic nutrition, leading to its functional and structural damage, culminating, after a short period, in neuronal death. This is the reason why CCA can be correlated to neuronal death and, hence, to BD, although it is worth emphasizing that these are not synchronous phenomena, but can be separated by a short period. There are, however, cases of complete and irrecoverable absence of brain function, even in the presence of continued CBF [15]. An example is reperfusion in patients after cardiac arrest. Under these circumstances, the patient's brain is irreversibly damaged due to global ischemia. Nevertheless, CBF

is reestablished and persists for a while, so the discovery of flow does not rule out BD [16]. If cardiorespiratory function in this patient is artificially maintained, however, dead brain cells cause edema and intracranial hypertension, which finally leads to a decrease in the CPP and the absence of flow. If the ultrasound study is repeated, it will eventually show the CCA pattern [15]. The TCD as ancillary test for BD is highly sensitive and specific, with rates of 89% and 98%, respectively [17]. In order to establish a CCA diagnosis that accompanies BD, the anterior and posterior territories of the Circle of Willis must be insonated, while the CCA findings must be sustained for a period of 30 minutes. This process entails the insonation of the middle cerebral arteries (MCA), on a bilateral basis, through the temporal window and following the blood vessel track as much as possible, as well as the basilar artery (BA), through the suboccipital or transforaminal window. There are reports of infratentorial injuries associated with CCA in which the anterior cerebral circulation may be preserved by means of the internal carotid artery circulation [18]. In one of my latter investigations, two cases of patients with brain stem (BS) infarcts had TCD studies that observed continuous flow in both MCAs and an arrest pattern in the BA. In both cases, the neurological examination confirmed BD. For this reason, the TCD may not be a reliable ancillary method for CCA in infratentorial processes, since it cannot confirm CCA in all the CoW vessels [19]. The clinical neurological examination remains the primary method of BD determination in most situations. The use of TCD as an ancillary test for making a diagnosis of BD has long sparked the interest of researchers. One of the questions posed by the American Academy of Neurology (AAN) Quality Standards Subcommittee is whether there are ancillary tests that accurately identify those patients with BD, giving the greatest importance to the clinical examination. Within the recommendations published in this document, there is insufficient evidence to determine whether the complementary tests accurately confirm the cessation of function of the whole brain (Level U) [20]. In the AAN evidence-based guideline, TCD is useful only if a reliable signal is found, and accepted abnormalities can only include either reverberating flow or small systolic peaks in early systole. Com-

plete absence of flow is not reliable due to possibility of inadequate transtemporal windows for insonation. The other requirement is bilateral insonation and both anterior and posterior circulation insonation [20].

In some practical guides for the determination of BD, TCD is included in the ancillary tests used in adults. Its application would be in those situations that do not allow a complete neurological examination, including the apnea test. This requires expertise of the specialist to interpret the results, and that physicians be aware of the possibility of false positive results [20]. An important fact is that in patients with an aborted apnea test, the time of death is when the ancillary test has been officially interpreted [20]. In a TCD study observing CCA, many patterns that express the same findings may concur, as we have demonstrated in our series of investigative articles [10]. In the first series, CCA patterns most frequently found were: reverse, oscillating, reverberant diastolic flow in 66 studies (75%); systolic spikes in 48 (54.5%), and absence of flow in only 2 cases (2.3%) [11]. In the second, CCA patterns most frequently found were: reverse-oscillating diastolic flow (77%), followed by systolic spikes (55%) (Figs. 3 and 4). This finding reflects a chronological progress in the patterns of CCA, linked to an increase of ICP. The same study noted the frequency distribution of the insonated arteries, corresponding to the insonation of the MCAs and BA in 30% of studies [21]. Also important to consider when using TCD to asses CCA is the chance of false negative and false positive results. False negatives correspond to individuals with clinical BD and continuous CBF. These can appear in situations in which the cranial cavity is not closed: decompressive craniectomy (DC), ventriculostomy, open fractures, open fontanelles (in the case of children). Decompressive craniectomy (DC) is an increasingly popular therapeutic alternative for managing ICH and cerebral edema in SBI. The procedure results in a loss of cranial impenetrability with the aim of alleviating ICP. When DC is performed, CBF is maintained [22]. TCD

performed after DC (compared to pre-operatively) shows a substantial increase in CBFVs, not only on the side of the procedure, but also in the contralateral hemisphere [23]. It may be necessary to repeat the study [22].

A false positive corresponds to individuals with a CCA pattern and negative apnea test or other findings for the BD diagnosis. The occurrence of CCA and BD may not be synchronous and the false positive can appear during a short period of minimum brainstem activity after CCA (persistence of a BS reflex) [22]. In the same way as for making a clinical diagnosis of BD, a series of clinical conditions or previous requirements must be met, for the performance of TCD in diagnosing CCA. The patient's hemodynamic and blood gas status must be stable during the course of the study, with a MAP ≥70 mmHg (SBP and DBP not <90/50 mmHg) and a $PaCO_2$ between 35 and 45 mmHg [9]. Furthermore, it is recommended that before performing a TCD for evaluation of CCA, the neurological examination be performed. Finally, there are several limitations of TCD as pertains to confirming BD:

- TCD has lower sensitivity in comparison with the clinical examination.
- Sensitivity of TCD is associated with the mechanism of neurological injury.
- The impossibility of preventing false-positive results [17].

With reference to the neurological injury mechanism, there are situations in which, due to supratentorial unilateral injuries, a large vessel can show a CCA pattern, without this occurring in the contralateral vessel [24]. This was reported in a 20-year-old male patient, who suffered a structural SBI due to a penetrating cranial wound, involving injury to the M1 segment of the MCA. This resulted in deformation of the vascular architecture of the CoW, preventing a complete sonographic examination in order to diagnose CCA. BD was confirmed by clinical examination (Fig. 5).

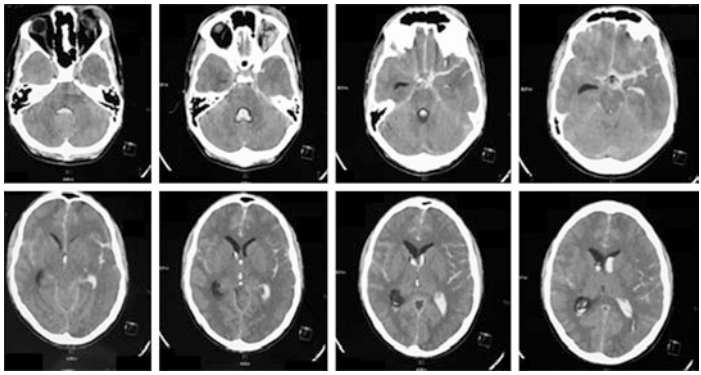

Fig. 5 Tomographic study that reveals penetrating head injury with wound in M1 segment of the L- MCA. Male, 20 years old. BD diagnosed by clinical examination

Conclusions

Cerebral circulatory arrest (CCA) derives from cerebral tamponade or herniation, as the final stage of SBI and which in quasi-real time accompanies BD. There exist specific patterns thereof that can be identified by TCD which can be performed serially and economically at the bedside. It has a sensitivity of 89% and a specificity of 98% [15], taking into account situations that may cause both false negatives and positives.

Personal Perspectives

In many jurisdictions, TCD for evaluation of CCA is an accepted ancillary test to accompany the diagnosis of BD, notably in situations in which the clinical preconditions for a complete neurological examination for BD are not met. The addition of TCD to the BD diagnostic process is considered a major milestone in the procurement of organs, since it may enable the recruitment of individuals with BD who may be otherwise lost to the organ donation option.

References

1. Hadani M, Bruk B, Ram Z, Knoller N, Spiegelmann R, Segal E. Application of transcraneal Doppler ultrasonography for the diagnosis of brain death. Intensive Care Med. 1999;25:822–8.
2. Perez Calatayud AA, Carrillo Esper R, Díaz Carrillo A, Zepeda Mendoza AD. Doppler transcraneal y cese de la circulación cerebral en Muerte encefálica. J Mex Assoc Crit Med Intensive Care. 2016;XXX(1):59–60.
3. Ducrocq X, Hassler W, Moritake K, Newell DW, von Reutern GM, Shiogay T, et al. Consensus opinion on diagnosis of cerebral circulatory arrest using Doppler-sonography. Task Force Group on cerebral death of the Neurosonology Research Group of the World Federation of Neurology. J Neurol Sci. 1998;159:145–50.
4. Hassler WI, Steinmetz H, Gawlowski J. Transcranial Doppler ultrasonography in raised intracranial pressure and in intracranial circulatory arrest. J Neurosurg. 1988;68:745–51.
5. Sidi A, Mahla M. Noninvasive monitoring of cerebral perfusion by transcranial Doppler during fulminant hepatic failure and liver transplantation. Anesth Analg. 1995;80:194–200.
6. Escudero D, Otero J, Quindós B, Viña L. Doppler transcraneal en el diagnóstico de la muerte encefálica. ¿Es útil o retrasa el diagnóstico? Intensive Med. 2015;39(4):244–50. https://doi.org/10.1016/j.medin.2014.11.005.
7. Pedicelli A, Bartocci M, Lozupone E, D'Argento F, Alexandre A, Garignano G, et al. The role of cervical color Doppler ultrasound in the diagnosis of brain death. Neuroradiology. 2019;61:137–45. https://doi.org/10.1007/s00234-018-2111-4.
8. Royal Decree 1723/2012, 28th of December, by which the activities of obtaining, clinical use and territorial coordination of human organs destined for transplantation are regulated and quality and safety requirements are established. Health, Social Services and Equality Ministry. "BOE" number 313, 29th of December of 2012. Reference: BOE-A-2012-15715.
9. Calleja S, Tembl JL, Segura T. Recomendaciones sobre el uso del Doppler transcraneal para determinar la existencia de paro circulatorio cerebral como apoyo diagnóstico de la muerte encefálica. Neurology. 2007;22(7):441–7.
10. Dominguez Roldán JM, Barrera Chacón JM, Rivera Fernández MV, García Alfaro C. Sonografía Doppler transcraneal: su utilidad en el diagnóstico de las parada circulatoria cerebral que acompaña a la muerte encefálica. Intensive Med. 2000;24:151–60.
11. Cacciatori A, Godino M, Mizraji R. Systodiastolic separation expresses circulatory cerebral arrest? Transplant Proc. 2018;50:412–5.
12. Roig C. Chap. 19: Muerte Encefálica causada por anoxia encefálica. In: López-Navidad A, Kulisovsky J, Caballero F, editors. El donante de órganos y tejidos. Evaluación y manejo. Barcelona: Springer –Verlag Ibérica; 1997. p. 202–9.

13. Jimenez OC, Guerrero Peral AL. Chap. 3: Fisiología de la circulación cerebral. In: Castillo Sánchez J, Alvarez Sabín J, Martí-Vilalta JL, Martínez Vila E, et al., editors. Manual de enfermedades vasculares cerebrales. Barcelona: J. R. Prous, S.A; 1995. p. 20–5.
14. Raghavan M, Marik P. Therapy of intracranial hypertension in patients with fulminant hepatic failure. Neurocrit Care. 2006;04:179–89.
15. Consensus Group on Transcranial Doppler in the Diagnosis of Brain Death. Latin American Consensus on the use of transcranial Doppler in the diagnosis of brain death. Braz J Intensive Ther. 2014;26(3):240–52.
16. Flowers WM Jr, Patel BR. Persistence of cerebral blood flow after brain death. South Med J. 2000;93(4):364–70.
17. Chang JJ, Tsivgoulis G, Katsanos AH, Malkoff MD, Alexandrov AV. Diagnostic accuracy of transcraneal Doppler for brain death confirmation: systematic review and meta-analysis. AJNR Am J Neuroradiol. 2016;37:408–14. www.ajnr.org.
18. Escudero D. Diagnóstico de muerte encefálica. Intensive Med. 2009;33(4):185–95.
19. Cacciatori A, Godino M, Mizraji R, Domínguez Roldán JM. Diagnosis of brain death in infratentorial neurological pathology how to approach it in the Intensive Care Unit? Case reports. Transplant Proc. 2020;52:1042–8.
20. Wijdicks Eelco FM, Varelas PN, Gronseth GS, Greer DM. Evidence – based guideline update: determining brain death in adults. Report of the Quality Standards Subcommittee of the American Academy of Neurology. Neurology. 2010;74:1911–8.
21. Cacciatori A, Godino M, Mizraji R. Utility of transcranial Doppler in the coordination of transplants. 10 years of experience. Transplant Proc. 2018;50:408–11.
22. Correa H, Puppo C, Biestro A, Mizraji R, Cancela M, Grille P, et al. Actualización de Consenso de Muerte Encefálica en adultos. 5th edn. National Institute of Donations and Transplants of Cells, Tissues and Organs of the Republic of Uruguay. Ministry of Public Health – School of Medicine, University of the Republic; 2016. p. 1–18.
23. Bon-Seng-Shu E, Jacobsen Teixeira M, Hirsch R, Ferreira de Andrade A, Marino R Jr. Transcranial Doppler sonography in two patients who underwent decompressive craniectomy for traumatic brain swelling: report of two cases. Neuropsychiatric Arch. 2004;62:715–21.
24. Paolin A, Manuali A, Di Paola F, et al. Reliability in diagnosis of brain death. Intensive Care Med. 1995;21:657–62. CrossRef Medline.

Intracranial Stenosis

Mark N. Rubin and Andrei V. Alexandrov

Definition

"Intracranial stenosis" is pathological narrowing of an intracranial blood vessel.

Etiology

The predominant mechanism of intracranial stenosis is atherosclerotic plaque formation commonly affecting Asians and African Americans. However, it is also increasingly found in Hispanics and Caucasians. Sickle cell anemia, endothelial proliferation, smooth muscle spasm, arterial dissection and non-occlusive thrombosis can also cause pathological narrowing of intracranial vessels. However, using the term stenosis implies atheromatous etiology rather than other conditions.

M. N. Rubin (✉)
Neurology, University of Tennessee Health Science Center, Memphis, TN, USA
e-mail: mrubin3@uthsc.edu

A. V. Alexandrov
Department of Neurology, University of Tennessee Health Science Center, Memphis, TN, USA

W. C. Ziai, C. L. Cornwell (eds.), *Neurovascular Sonography*,
https://doi.org/10.1007/978-3-030-96893-9_9

Complications

Intracranial stenosis can cause "downstream" ischemic injury by hemodynamic compromise, athero-thrombosis, or artery-to-artery embolism. Atherosclerotic changes are common in the intracranial vasculature with increasing incidence with age across all demographics. Modifiable risk factors include tobacco use, hypertension, dyslipidemia and hyperglycemia.

Differential Diagnosis

The main differential diagnosis to be considered with evidence of narrowing of a vessel is congenital physiological atresia as a normal variant. There are many variants of normal and hypoplastic segments within the circle of Willis, such that a "complete" and symmetric circle of Willis is found in only a minority of patients. The length of the narrowed vessel (longer favoring atresia, short segment stenosis favoring pathology) and the presence or absence of compensatory velocity or vasculature changes on imaging serve as clues to help differentiate pathological stenosis *versus* atresia.

Transcranial Doppler Results

Transcranial Doppler [1] (TCD) measures a shift in frequency when echoes are reflected off of moving red blood cells, and from these shifts the velocity of the flowing blood is calculated. There are published normative data [2] that suggest a broad range of normal across primarily age strata and to a lesser degree gender.

First, to best understand TCD results, one must recall the key physical principles of:

- The assumed zero angle of insonation
- Flow dynamics, namely the Bernoulli and Hagen-Poiseuille principles
- The Spencer curve [3]

Handheld, non-imaging TCD instruments are generally calibrated to measure echoes at a 0° or 180° angle, and sampling a vessel at an unknown angle of intercept will give a fraction of the "true" velocity; the practical implication is that one can insonate only the most proximal segments of the basal intracranial vessels because of the limitation of traditional windows of insonation and typical vascular neuroanatomy to make a diagnosis of intracranial stenosis.

The purpose of brain vasculature is to maintain continuous flow in systolic and diastolic phases of the cardiac cycle to ensure uninterrupted supply of blood with oxygen and glucose to neurons. Blood flow to the brain depends on the cerebral vasculature being a low-pressure "sink" such that it is a path of least resistance. The pressure gradient (ΔP) is – in a simplified way – quantified by the Hagen-Poiseuille as $8\mu LQ/\pi r^4$ where μ is the viscosity, L is the length of the vessel, Q is the volume flow rate, and r is the vessel radius. The expression $8\mu L/\pi r^4$ can be thought of more broadly as "resistance to flow" and given the label R. The formula can be rearranged, then, to $Q = \Delta P/R$; in words, the volume flow rate is directly related to the pressure gradient and indirectly related to the resistance to flow. By these expressions, a progressively shrinking vessel radius will lead to an increase in resistance to flow, necessitating a corresponding drop in pressure gradient to maintain volume flow rate.

The Bernoulli principle states, as an extension of conservation of energy, that any change in potential (hydrostatic or pressure) energy must be met with a corresponding change in kinetic (velocity) energy such that total energy is equal at all points along a streamline. Therefore, in our example of a dropping pressure gradient due to increased resistance to flow, the drop in pressure (potential energy) theoretically necessitates an increase in kinetic energy, or velocity, which is exactly what we observe clinically when diagnosing intracranial stenosis with flow velocity increase across short and focal stenosis.

From the Hagen-Poiseuille and Bernoulli principles, Drs. Merrill Spencer and John Reid published a theoretical model [3] of flow velocity changes in the setting of an idealized stenosis – focal, axis-symmetric – which yielded a complex curve with

exponentially increasing velocity with decreasing lumen diameter up to approximately 80% stenosis, where beyond that critical level of stenosis velocity begins to exponentially decrease until it reaches zero with complete occlusion. This model, now referred to as "The Spencer Curve," although idealized and conceptualized for cervical carotid stenosis, has since become recognized as a foundational concept for developing diagnostic criteria for cerebrovascular hemodynamics, including intracranial vessels [4]. See Fig. 1.

Complementary to the observation of very elevated or very diminished mean flow velocity in the setting of intracranial steno-

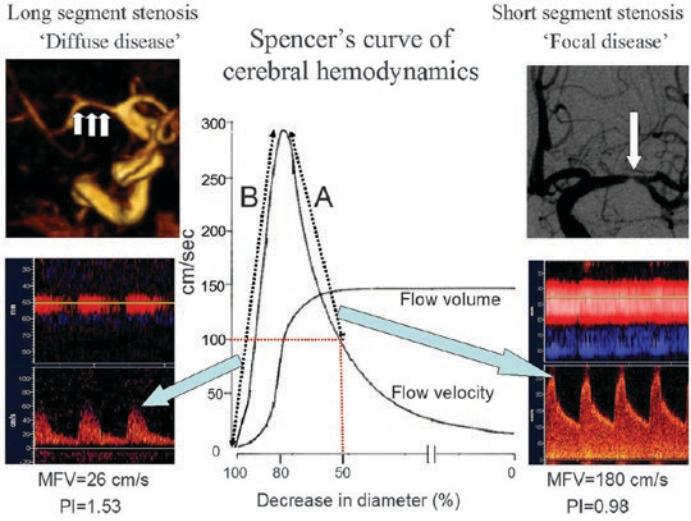

Fig. 1 Spencer's curve of cerebral hemodynamics [21]. Blood flow patterns in the intracranial arteries due to stenosis are predicted by their position on the Spencer's curve of cerebral hemodynamics. Dotted line A corresponds to abnormally elevated flow velocity on the "up slope" of the curve caused by short, focal stenoses of ≥50%, as is depicted in the DSA (upper right) with corresponding elevated TCD velocity (lower right). Dotted line B shows the "down slope" of the Spencer's curve when the velocities decrease due to increasing resistance to flow with the most severe and/or elongated lesions. The CTA image (top left) shows an elongated (>1 cm) stenosis with low mean velocity and high pulsatility on TCD (bottom left)

sis, the Thrombolysis in Brain Ischemia (TIBI) grading scale was introduced by Demchuk, et al. [5] This scale (see Fig. 2) essentially enumerated "where on the Spencer curve" – the accelerating slope on the right half or the decelerating slope on the left – the waveform profile associated with intracranial steno-occlusive disease happens to be and associated those strata with increasingly worse response to systemic thrombolysis and overall outcome with decreasing TIBI score. Increasing TIBI scores reflect the recanalization process, or "climbing back out to the other side" of the Spencer's Curve. See Fig. 2.

Given the individually unique complex nature of neurovascular anatomy, the typically axis-asymmetric nature of the pathological processes that cause intracranial stenosis, variability in operator technique and differences in ultrasound hardware, there are no discrete mean flow velocity cut-points that reliably identify significant intracranial stenosis with perfect granularity in all patients. Akin to best practices with carotid ultrasonography [6],

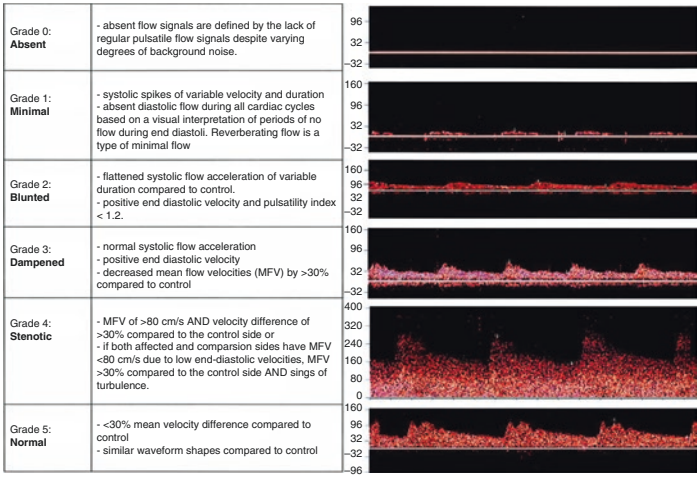

Fig. 2 Thrombolysis in brain ischemia (TIBI) flow grades. The TIBI grading scale. Lower scores are associated with worse response to systemic tPA and outcome. Grades 3–0 reflect progressive descent down the "left half" of the Spencer Curve

specific velocity values and corresponding degree of stenosis must be internally derived as a matter of routine quality assurance. That said, published clinical investigations have established reasonable starting points for new neurovascular laboratories. See Table 1. When following standard technique, TCD can be sensitive, specific and accurate for the diagnosis of intracranial stenosis or occlusion in patients with acute ischemic stroke [7].

TCD monitoring techniques also have a role in the diagnosis and management of intracranial stenosis. More specifically, longitudinal non-invasive surveillance can determine if the stenosis is stable, progresses or regresses after risk factor modification and best medical therapy that could be motivational to the patient. TCD also can assess vasomotor reactivity (VMR) and microembolic signal (MES) monitoring that further refine diagnosis, prognosis and management of intracranial stenosis. Vasomotor reactivity testing has been done primarily in the setting of cervical carotid artery stenosis, but there are series focusing on intracranial stenosis that have demonstrated findings similar to that which is published in the setting of cervical internal carotid artery stenosis, namely that impaired vasomotor reactivity "downstream" from an intracranial stenosis is associated with current ischemic stroke, history of stroke, and poorer prognosis as compared to a normal

Table 1 Published "starter" mean flow velocity cut points of intracranial artery stenosis [13, 19, 20]

Vessel	≥50%	≥80%
MCA	100 cm/s	240 cm/s
ICA	90 cm/s	120 cm/s
ACA	80 cm/s	–
PCA	80 cm/s	–
VA	90 cm/s	110 cm/s
BA	90 cm/s	130 cm/s

Legend: *MCA* middle cerebral artery, *ICA* internal carotid artery, *ACA* anterior cerebral artery, *PCA* posterior cerebral artery, *VA* vertebral artery, *BA* basilar artery, *cm/s* centimeters per second

vessel with normal VMR [8–10]. A series of MES monitoring of middle cerebral artery stenosis demonstrated that MES are common with stenosis (22%) and independently predicted ipsilateral stroke within 1 year [11].

Other Procedures

Both invasive and non-invasive angiography can be used to glean similar and complementary information as compared to TCD. Direct subtraction angiography (DSA), or "conventional" angiography, remains the "gold standard" for evaluating vessel lumen due to extremely high spatial and temporal resolution. CT and MR angiography (CTA or MRA, respectively) are non-invasive means of imaging intracranial vessel lumen with high (but not as high as DSA) spatial resolution but represent a "snapshot in time" such that there is no objective hemodynamic data other than opacification of a vessel. A seminal prospective comparison of DSA to TCD (as well as MRA) came in a subset of the WASID trial [12] called the Stroke Outcomes and Neuroimaging of Intracranial Atherosclerosis (SONIA) trial [13]. In brief, this study demonstrated substantial negative predictive value of 50–99% stenosis, 86% across all vessels, of TCD as compared to DSA. Positive predictive value was low at 36%. The trial method and findings established that a normal TCD can reliably exclude intracranial stenosis, however, since no TCD standardization has been performed across participating centers, positive predictive values were less than optimal. An international multi-center group that validated TCD scanning protocols and adopted same diagnostic criteria showed that WASID-SONIA criteria perform reliably with high sensitivity and specificity [14]. Furthermore, TCD provides additional complementary information such as embolization, collateralization and steal that are not obtained by CTA. See Fig. 3 [15].

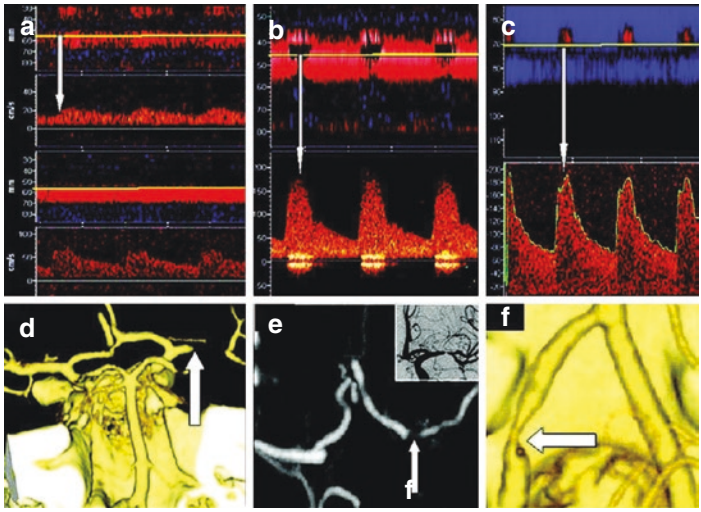

Fig. 3 CTA and TCD correlation [15]. (**a**) Power-motion TCD showing left M1-MCA occlusion with blunted signals at 54 mm and normal contralateral MCA below; (**b**) left M1-MCA stenosis with elevated velocities and systolic bruit at 48 mm; (**c**) right terminal VA stenosis with MFV of 113 cm/s at 70 mm. TCD findings (**a** through **c**) were confirmed by CTA (**d** through **f**, respectively). Insert in (**e**) represents urgent DSA image in the patient with M1-MCA stenosis

Treatment

The treatment of intracranial stenosis depends on the mechanism – again, most commonly atherosclerosis – and whether or not the patient is experiencing symptoms in association with the stenosis. Asymptomatic intracranial atherosclerotic stenosis is incidentally diagnosed and does not necessarily require directed medical or surgical therapy outside of maximizing control of common health concerns such as hypertension, dyslipidemia and hyperglycemia. Symptomatic intracranial atherosclerotic stenosis – whether it manifests as stroke or transient ischemic attack – bears high risk of stroke recurrence directly proportionate to the number of vessels affected and increases with increasingly severe

degree of stenosis. It is treated with antiplatelet medications, thoughtful blood pressure control (to avoid both hypotension or persistently elevated pressure) and high intensity statin therapy in addition to maximal control of the aforementioned common health concerns. The use of two antiplatelet agents is common for 90 days after a cerebral ischemic event suggestive of symptomatic intracranial stenosis. TCD is particularly helpful in diagnosing MES distal to an intracranial stenosis, which are a predictor of ipsilateral stroke [11, 16] and informs treatment, namely necessitating dual antiplatelet [17, 18] and occasionally anticoagulation if refractory.

Stenosis caused by other, less common conditions such as sickle cell anemia, endothelial proliferation ("vasospasm"), dissection, arterial smooth-muscle spasm or non-occlusive thrombus require different means of evaluation and management. For example, most spasmodic disease – vasospasm of aneurysmal subarachnoid hemorrhage or that of Call- Fleming syndrome (reversible cerebral vasoconstriction syndrome) calls for calcium channel blockade and supportive care of what is usually a time-limited pathology that resolves within 3 weeks to 3 months, but antithrombotic medications are not indicated. Arterial dissection and non-occlusive thrombosis, on the other hand, calls for lifelong antiplatelet medication and occasionally anticoagulation because of transitory (but at least weeks) to permanent alteration in a vessel lumen causing disturbance of laminar flow of arterial blood.

TCD is perhaps best known and most widely used to screen for the occurrence and to monitor the dynamic nature of vasospasm after subarachnoid hemorrhage. Serial studies can help guide treatment as severe cases often necessitate endovascular reperfusion therapies such as angioplasty and/or local calcium channel blocker injection to avoid ischemic injury. As seen in Fig. 4 there can also be thrombotic complications of the intravascular hardware needed to coil an aneurysm, such that this TCD recording indicated the need for both antiplatelet medication and intra-arterial therapy, neither of which would have been indicated without TCD diagnosis of a MES and mean velocity elevation in the range of severe vasospasm, respectively.

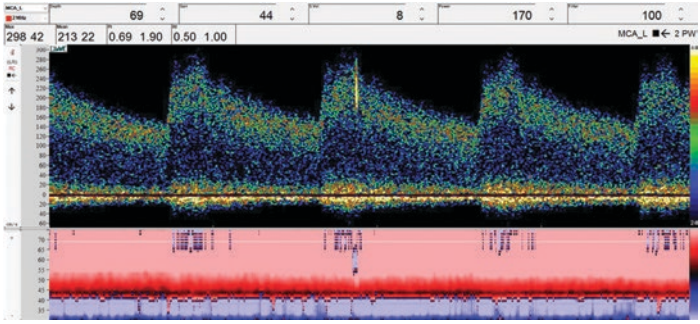

Fig. 4 TCD to diagnose complications of aneurysmal subarachnoid hemorrhage. Bedside TCD of the left MCA after left terminal ICA aneurysm coiling. Mean flow velocity is elevated into a range concerning for moderate to severe vasospasm and there was a spontaneous microembolic signal, seen as a bright "streak" in the single gate and a "backslash" in the multigate window

Conclusions

Intracranial stenosis, caused by various mechanisms, is an unfortunately common and morbid if not mortal condition, and the ability to diagnose the presence or absence of it is essential to not only stroke care but general wellness. TCD can reliably rule out hemodynamically significant stenoses in the intracranial vasculature and, in the hands of trained experts, can accurately diagnose and localize treatable lesions in concordance with both DSA and non-invasive angiography as well as provide complementary real-time flow related and embolic data that only ultrasound can provide.

Personal Perspectives

TCD is a necessity of daily stroke practice at our institution. We listen to intracranial stenoses on a serial basis – much like one would listen to a patient's lungs when dealing with and recovering from pneumonia – to ascertain whether or not our treatments have been effective in reducing the degree of stenosis or otherwise

restoring cerebral perfusion to an afflicted hemisphere. That it can be deployed rapidly, safely and noninvasively affords us the opportunity to rapidly diagnose and accurately manage acute neurological decline in the hospital setting, where it is imperative for the patient that we rapidly and reliably rule in or out the presence of intracranial steno-occlusive disease. VMR and MES monitoring can differentiate asymptomatic from concerning, hemodynamically significant stenoses that require further blood pressure and/or antithrombotic therapy. TCD is a reliable bedside diagnostic for the practicing vascular neurologist.

References

1. Aaslid R, Markwalder TM, Nornes H. Noninvasive transcranial Doppler ultrasound recording of flow velocity in basal cerebral arteries. J Neurosurg. 1982;57(6):769–74.
2. Tegeler CH, Crutchfield K, Katsnelson M, Kim J, Tang R, Passmore Griffin L, et al. Transcranial Doppler velocities in a large, healthy population. J Neuroimaging. 2013;23(3):466–72.
3. Spencer MP, Reid JM. Quantitation of carotid stenosis with continuous-wave (C-W) Doppler ultrasound. Stroke. 1979;10(3):326–30.
4. Alexandrov AV. The Spencer's curve: clinical implications of a classic hemodynamic model. J Neuroimaging. 2007;17(1):6–10.
5. Demchuk AM, Burgin WS, Christou I, Felberg RA, Barber PA, Hill MD, et al. Thrombolysis in brain ischemia (TIBI) transcranial Doppler flow grades predict clinical severity, early recovery, and mortality in patients treated with intravenous tissue plasminogen activator. Stroke. 2001;32(1):89–93.
6. Grant EG, Benson CB, Moneta GL, Alexandrov AV, Baker JD, Bluth EI, et al. Carotid artery stenosis: gray-scale and Doppler US diagnosis—Society of Radiologists in Ultrasound Consensus Conference. Radiology. 2003;229(2):340–6.
7. Mattioni A, Cenciarelli S, Eusebi P, Brazzelli M, Mazzoli T, Del Sette M, et al. Transcranial Doppler sonography for detecting stenosis or occlusion of intracranial arteries in people with acute ischaemic stroke. Cochrane Stroke Group, editor. Cochrane Database Syst Rev [Internet]. 2020 [cited 2020 Sep 23]. Available from: http://doi.wiley.com/10.1002/14651858.CD010722.pub2.
8. Lee J-Y, Lee Y-S. Vasomotor reactivity in middle cerebral artery stenosis. J Neurol Sci. 2011;301(1–2):35–7.

9. Sharma VK, Tsivgoulis G, Ning C, Teoh HL, Bairaktaris C, Chong VF, et al. Role of multimodal evaluation of cerebral hemodynamics in selecting patients with symptomatic carotid or middle cerebral artery stenoocclusive disease for revascularization. J Vasc Interv Neurol. 2008;1(4):96–101.
10. Uzunca I, Asil T, Balci K, Utku U. Evaluation of vasomotor reactivity by transcranial Doppler sonography in patients with acute stroke who have symptomatic intracranial and extracranial stenosis. J Ultrasound Med. 2007;26(2):179–85.
11. Gao S, Wong KS, Hansberg T, Lam WWM, Droste DW, Ringelstein EB. Microembolic signal predicts recurrent cerebral ischemic events in acute stroke patients with middle cerebral artery stenosis. Stroke. 2004;35(12):2832–6.
12. Chimowitz MI, Lynn MJ, Howlett-Smith H, Stern BJ, Hertzberg VS, Frankel MR, et al. Comparison of warfarin and aspirin for symptomatic intracranial arterial stenosis. N Engl J Med. 2005;352(13):1305–16.
13. Feldmann E, Wilterdink JL, Kosinski A, Lynn M, Chimowitz MI, Sarafin J, et al. The stroke outcomes and neuroimaging of intracranial atherosclerosis (SONIA) trial. Neurology. 2007;68(24):2099–106.
14. Zhao L, Barlinn K, Sharma VK, Tsivgoulis G, Cava LF, Vasdekis SN, et al. Velocity criteria for intracranial stenosis revisited: an international multicenter study of transcranial Doppler and digital subtraction angiography. Stroke. 2011;42(12):3429–34.
15. Tsivgoulis G, Sharma VK, Lao AY, Malkoff MD, Alexandrov AV. Validation of transcranial Doppler with computed tomography angiography in acute cerebral ischemia. Stroke. 2007;38(4):1245–9.
16. Ritter MA, Dittrich R, Thoenissen N, Ringelstein EB, Nabavi DG. Prevalence and prognostic impact of microembolic signals in arterial sources of embolism: a systematic review of the literature. J Neurol. 2008;255(7):953–61.
17. Wong KSL, Chen C, Fu J, Chang HM, Suwanwela NC, Huang YN, et al. Clopidogrel plus aspirin versus aspirin alone for reducing embolisation in patients with acute symptomatic cerebral or carotid artery stenosis (CLAIR study): a randomised, open-label, blinded-endpoint trial. Lancet Neurol. 2010;9(5):489–97.
18. Markus HS, Droste DW, Kaps M, Larrue V, Lees KR, Siebler M, et al. Dual antiplatelet therapy with clopidogrel and aspirin in symptomatic carotid stenosis evaluated using Doppler embolic signal detection: the clopidogrel and aspirin for reduction of emboli in symptomatic carotid stenosis (CARESS) trial. Circulation. 2005;111(17):2233–40.

19. Felberg RA, Christou I, Demchuk AM, Malkoff M, Alexandrov AV. Screening for intracranial stenosis with transcranial Doppler: the accuracy of mean flow velocity thresholds. J Neuroimaging. 2002;12(1):9–14.
20. Lindegaard KF, Bakke SJ, Aaslid R, Nornes H. Doppler diagnosis of intracranial artery occlusive disorders. J Neurol Neurosurg Psychiatry. 1986;49(5):510–8.
21. Alexandrov AV, editor. Cerebrovascular ultrasound in stroke prevention and treatment. 2nd ed. Chichester: Wiley-Blackwell; 2011. 280 p.

Therapeutic TCD for Patients with Acute Cerebral Ischemia

Mark N. Rubin and Andrei V. Alexandrov

There is a body of evidence that suggests ultrasound, specifically 2 MHz transcranial Doppler, may have therapeutic effects through potentiation of thrombolysis for acute ischemic stroke [1, 2]. Experimental models demonstrate facilitation of thrombolytics through improved drug delivery, modification of fibrin structure and enhanced binding of a thrombolytic to fibrin [3–9]. A study of thrombolysis monitoring [10, 11] – namely the continuous monitoring of MCA waveforms representing residual flow with 2 MHz pulsed wave Doppler during provision of tPA in the setting of acute cerebral ischemia – demonstrated a rate of dramatic and early neurological recovery (>10 points on National Institutes of Health Stroke Scale (NIHSS) in 40%, >4 points in 62.5%) much higher than those seen in the pivotal trial that established thrombolysis for acute ischemic stroke as the worldwide standard of care for stroke (>10 points in 27%, >4 points in 40%, see Fig. 1). This led to a phase I [12] and then phase II trial [1] of Ultrasound

M. N. Rubin (✉)
Neurology, University of Tennessee Health Science Center, Memphis, TN, USA
e-mail: mrubin3@uthsc.edu

A. V. Alexandrov
Department of Neurology, University of Tennessee Health Science Center, Memphis, TN, USA

W. C. Ziai, C. L. Cornwell (eds.), *Neurovascular Sonography*,
https://doi.org/10.1007/978-3-030-96893-9_10

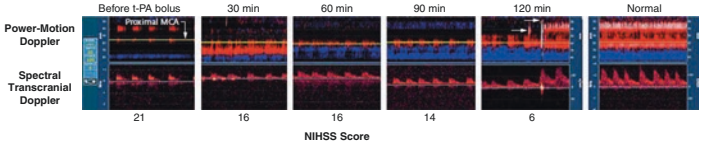

Complete Recanalization with the Use of Power-Motion Transcranial Doppler Ultrasonography.

Spectral wave forms from the proximal middle cerebral artery (MCA) were obtained at a depth of 58 to 60 mm (left-hand image, arrow) from the left transtemporal window. A minimal, grade 1, signal as measured on the TIBI scale, with absent diastolic flow is seen on power-motion Doppler images (top) and spectral-transcranial Doppler images (bottom) obtained before the administration of a t-PA bolus. Thirty minutes after the t-PA was given, TIBI grade 3 dampened signals (i.e, cycle with positive end-diastolic flow) indicate the beginning of the recanalization of the proximal middle cerebral artery. TIBI grade 3 signals remain at 60 and 90 minutes. At 120 minutes, embolic tracks are shown by power-motion Doppler display (top, arrows), followed by restoration of low-resistance normal flow in both proximal and distal parts of the middle cerebral artery. Normal flow through the unaffected middle cerebral artery is shown in the far right-hand image for comparison. Corresponding National Institutes of Health Stroke Scale (NIHSS) score are provided below each frame. (In general population with stroke, scores range from 0 to 34, with higher scores indicating greater neurologic deficits.) At 24 hours, this patients had an NIHSS score of 4. At three months, he had no residual neurologic deficits, and his modified Rankin score was 0.

Fig. 1 Real-time monitoring of MCA recanalization via sonothrombolysis [1]

Enhanced Thrombolysis – or sonothrombolysis – which established that patients undergoing continuous 2 MHz pulsed wave TCD during tPA infusion were more likely to completely recanalize or show dramatic improvement within 2 hours of tPA infusion (31/63, 49%) as compared to controls (19/63, 30%; $p = 0.03$) and a trend toward better chance of recovery to modified Rankin scale (mRS) of 0–1 at 3 months (22/53, 42% sonothrombolysis group vs 14/49, 29% controls, $p = 0.2$). See Fig. 2.

Building on the finding of enhanced recanalization with TCD, investigators began trialing gaseous microspheres, commonly used as contrast agents for ultrasound-based imaging studies, to further enhance sonothrombolysis. These microspheres expand, oscillate or collapse when exposed to ultrasound, producing stable cavitation and strongly reflected echoes [13]. The mechanical energy generated by agitating the microbubbles avidly enhances clot lysis in a swine model [14] and the first published trial in people with acute ischemic stroke was by Molina, et al. in 2006 [15]. Two-hour recanalization was seen in 14 (39%), 25 (68%), and 27 patients (71%) in the tPA, tPA/US, and tPA/US/microbubble groups, respectively (P = 0.004). Two-hour complete recanalization rate was significantly (P = 0.038) higher in the tPA/US/microbubble group (54.5%) compared with tPA/US (40.8%) and tPA (23.9%) groups. A subsequent pilot [16] showed similarly encouraging results: as compared to the tPA (control) arm in CLOTBUST [1], they demonstrated complete recanalization in 50% vs. 18%, partial 33% vs. 33%, none 17% vs. 49% ($p = 0.028$).

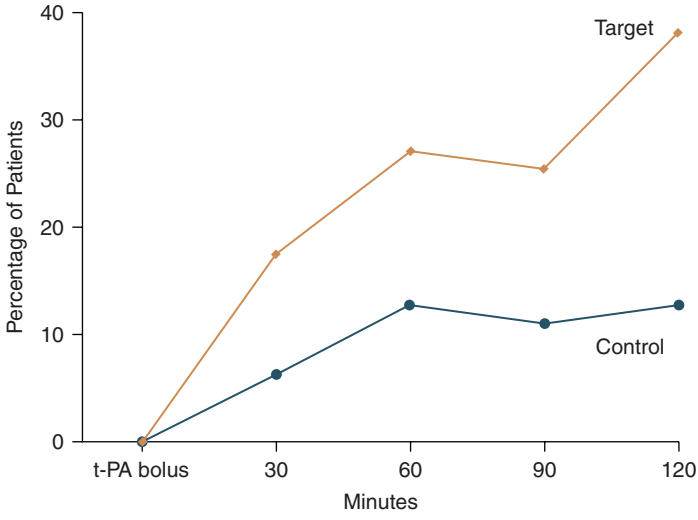

Rate of Sustained Complete Recanalization within Two Hours after Administration of a t-PA Bolus.

A trend toward the achievement of complete recanalization was observed over time with active treatment with the use of transcranial Doppler ultrasonography. Complete recanalization had occurred at 30 minutes after the t-PA bolus in 4 patients in the control group (6 percent; 95 percent confidence interval, 1.8 to 15.5) and in 11 patients in the target group (18 percent; 95 percent confidence interval, 9.0 to 29.1). At 60 minutes, 8 patients in the control group (13 percent; 95 percent confidence interval, 5.6 to 23.5) and 17 in the target group (27 percent; 95 percent confidence interval, 16.6 to 39.7) had completed recanalization. At 90 minutes, 7 patients in the control group (11 percent; 95 percent confidence interval, 4.6 to 21.6) and 16 in the target group (25 percent; 95 percent confidence interval, 15.3 to 27.9) had complete recanalization. At 120 minutes, 8 patients in the control group (13 percent; 95 percent confidence interval, 5.6 to 23.5) and 24 in the target group (38 percent; 95 percent confidence interval, 26.1 to 51.2) had complete recanalization. All 63 patients per group were accounted for at each time point.

Fig. 2 MCA recanalization in CLOTBUST [1]

At 2 hours, sustained complete recanalization was noted in 42% vs. 13%, ($p = 0.003$), and NIHSS scores 0 to 3 were reached by 17% vs. 8%, ($p = 0.456$). These investigators combined efforts for a phase II (TUCSON [17]) randomized investigation of microbubble-enhanced sonothrombolysis, further demonstrating promising therapeutic results with acceptable safety, albeit in a

small cohort and with the lowest dose of microbubbles tested. The largest, phase III trial of microbubble-enhanced sonothrombolysis was conducted in Norway (NOR-SASS) and was a "practical" study of all patients receiving systemic thrombolysis for acute ischemic stroke. In light of the absence of data at the time on microbubble-enhanced sonothrombolysis without visible occlusion on vascular imaging, which was an inclusion criterion for previous studies, this trial demonstrated the safety of microbubble-enhanced sonothrombolysis in an unselected population but did not show clinical benefit and the trial was halted prematurely [18].

The largest, phase III trial of sonothrombolysis without microbubbles, CLOTBUST-ER [2] included severe (NIHSS >10 points) patients with acute ischemic stroke eligible for tPA – with or without angiographically confirmed occlusion – to test a novel, operator-independent headframe with 2 MHz pulse wave Doppler sequentially delivered through the bilateral transtemporal and the suboccipital windows so that the beams would cover all possible proximal intracranial occlusion locations but would not overlap in time to avoid summation of energy. The study was terminated early for lack of efficacy and, running alongside the multiple strongly positive mechanical thrombectomy trials published in 2015, a shift in clinical equipoise in favor of thrombectomy further affected the results [19]. In a post-hoc analysis controlling for perceived shift in equipoise, sonothrombolysis groups showed a signal of efficacy in improving 3 month outcomes over standard thrombolytic treatment.

Although most studies demonstrated acceptable safety of sonothrombolysis with or without microbubbles, there are some notable exceptions [20–24]. The most stark safety issue led to termination of a phase II trial, called TRUMBI [22], of low frequency (300 KHz) ultrasound for sonothrombolysis compared to tPA alone. The trial was halted prematurely after only enrolling 26 patients because 13 of 14 patients treated with tPA with low frequency ultrasound showed signs of bleeding as compared to 5 of 12 patients without ultrasound, and 5 of the 14 patients exposed to ultrasound experienced symptomatic hemorrhage. The two reported trials of microbubble-enhanced sonothrombolysis using 2 MHz transcranial duplex [20, 21] also demonstrated relatively high rates of hemorrhage in their small cohorts, with 78% of

patients with sonothrombolysis experiencing asymptomatic hemorrhage (0% symptomatic) in one [21] of the studies and 9% symptomatic hemorrhage rate in the other [20]. The common thread and proposed basis for increased hemorrhage in the setting of sonothrombolysis is the field of exposure as compared to standard 2 MHz diagnostic Doppler ultrasound devices which were used in the original studies of sonothrombolysis. Duplex devices and low frequency ultrasound expose more tissue to the mechanical and thermal bioeffects of ultrasound thus, in the setting of acute ischemic stroke and systemic thrombolysis, increasing the risk of hemorrhage near and remote to the site of infarction.

Sonothrombolysis remains an active area of research [25, 26], particularly in the era of expanding indication and availability of mechanical thrombectomy [19]. See Table 1 for a summary table of sonothrombolysis evidence. Sonothrombolysis may prove use-

Table 1 Summary table of sonothrombolysis evidence

Reference	Patients	Intervention	Efficacy	% sICH
Demchuk et al. [10]	1	TCD + tPA	–	0
Alexandrov et al. [11]	40	TCD + tPA	Complete recanalization 30%, partial recanalization 40%; improvement by ≥4 NIHSS @ 24 = 62.5%	7.5
Eggers et al. [23]	25	TCCD + tPA vs tPA	Complete recanalization 1 h after tPA: 27% vs 21%; partial recanalization 1 h after tPA 18% vs 0%	18 vs 0
Alexandrov et al. [12]	55	TCD + tPA	Complete recanalization 36%	6
Alexandrov et al. [1]	126	TCD + tPA vs tPA	Complete recanalization 38% vs 13%	5 vs 5

(continued)

Table 1 (continued)

Reference	Patients	Intervention	Efficacy	% sICH
Daffertshofer et al. [22]	26	kHz US + tPA vs tPA	Any recanalization 29% vs 50%	36 vs 0
Molina et al. [15]	111	TCD + tPA + μB vs TCD + tPA vs tPA	Complete recanalization 55% vs 40% vs 22%	3 vs 3 vs 6
Larrue et al. [21]	20	TCCD + tPA + μB vs tPA	Complete recanalization 50% vs 50%	0 vs 0
Eggers et al. [24]	12	TCCD + tPA vs tPA	Complete recanalization 0% vs 0%, partial recanalization 57% vs 40%	14 vs 0
Alexandrov et al. 2008 [16]	15	TCD + tPA + μB vs TCD + tPA	Complete recanalization 50% vs 0%, partial recanalization 33% vs 66%	0 vs 0
Perren et al. [20]	26	TCCD + tPA + μB vs TCCD + tPA	Complete recanalization 64% vs 53%	9% vs 7%
Molina et al. [17]	35	TCD + tPA + μB vs TCD + tPA	Complete recanalization 57% vs 33%, partial recanalization 9% vs 25%	13% vs 0
Barreto et al. [34]	20	TCD + tPA	Complete recanalization 40%, partial recanalization 10%	0
Nacu et al. [18]	183	TCD + tPA + μB vs sham TCD + sham μB + tPA	No difference in early improvement or 90d mRS	6% vs 9%
Alexandrov et al. [2]	676	TCD + tPA vs sham TCD + tPA	No difference in 90d mRS	3% vs 2%

Legend: *TCD* transcranial Doppler, *tPA* tissue plasminogen activator, *sICH* symptomatic intracranial hemorrhage, *NIHSS* National Institute of Health Stroke Scale, *TCCD* transcranial Color Coded Duplex, *μB* microbubble

ful at hospitals and countries where thrombectomy is still not available and in a drip-and-ship paradigm when patients with large vessel occlusions (LVO) receive tPA if eligible but could not be immediately taken for thrombectomy. Often unavoidable delays in transfer between facilities open an opportunity for sonothrombolysis to aid early reperfusion and show feasibility to test sonothrombolysis in the next phase 3 trial. Although more definitive clinical evidence is needed to support the use sonothrombolysis in routine acute stroke practice, thrombolysis monitoring can still be considered routinely in light of the diagnostic data – namely clot localization, recanalization, re-occlusion and hyperemic reperfusion – that can change management and inform prognosis [27].

Procedure Thrombolysis monitoring/sonothrombolysis.

Purpose To monitor in real-time the effect of tPA, the presence or absence of vessel stenosis or occlusion, and augment the effect of thrombolysis.

Indications Acute ischemic stroke, particularly if due to suspected LVOs (M1 or proximal M2 MCA, ICA & vertebrobasilar occlusions).

Limitations Cranial windows, operator-dependency.

Equipment Transcranial Doppler instrument (standard retail), headframe and two 2 MHz pulsed-wave headframe-mountable transducers (ideal) or at least one 2 MHz pulsed wave transducer for manual monitoring, specialized software for recording and analyzing signal during monitoring (vendor-dependent).

Supplies Ultrasound gel, linens, transducer sanitation, personal protective equipment.

Equipment Quality and Control Equipment must be in standard operating condition.

Patient Assessment and Communication The benefits, risks and alternatives to doing the study are discussed with the patient and/or family as available, as is the technical nature of the diagnostic, so as to know what to expect.

Technique A patient is usually lying supine in an emergency department gurney. Care is taken to be sure that the patient's emergent needs such as airway, blood pressure management, and stroke treatment candidacy are addressed in parallel and in no way hindered by deployment of thrombolysis monitoring. Assuming the patient does not need to be ventilated, which is the case with most acute ischemic stroke patients, the sonographer and equipment should be near, and ideally behind the head of the bed. The ultrasound device should be turned on, and at least one waveform of the non-affected homologous segment (e.g., "the good side") should be documented with a handheld probe. This is to compare the residual flow signals of the affected vessel to "the good side." Technically proficient and experienced operators can consider a fast track insonation protocol [28], which will provide diagnostic information and will not delay emergent elements of acute stroke care. With this examination an experienced sonographer can often localize the acute occlusion, if clear windows are present, within 2–5 min. Once the presence (or absence) of windows – transtemporal in particular – and localization of the occlusion is determined, the handheld probe for the fast-track study is put away and the patient is prepared for headframe probe mounting. Apply the probe mounting headframe as directed by the manufacturer, and attach probes in the region where windows were previously discovered during the fast-track examination. This is usually over the transtemporal windows but some headframes support suboccipital window mounting. If a headframe is not available then "mounting" can always be attempted by a sonographer with good endurance and a steady hand.

If a headframe is applied it is important to:

1. Place the frame below the occipital protuberance and under the hair in the back of the head for vertebrobasilar monitoring
2. Place the frame well above temporal windows to allow sufficient range of transducer application

3. Localize the window and the worst residual flow signal in the affected vessel
4. Tighten knobs fixating transducer position over temporal window and angulation towards the target vessel
5. Tighten the headband as much as is tolerated – at the borderline between snug and too tight – so as to have close contact between the probe and skin
6. Once headband is tightened, slightly readjust transducer position/knobs to secure the best quality residual flow signal.

The tighter the fixation, the more ultrasound is transmitted. See Fig. 3. The depth of the sample window for thrombolysis monitoring/sonothrombolysis should be determined by scanning the affected vessel from its proximal to distal portion, and the last depth before the residual flow signals completely disappear usually corresponds to an acute occlusion location where the blood flow is impacted most severely.

If using two probes for monitoring of homologous segments, one will often notice after orienting the first probe, it can be difficult to adjust the contralateral probe without disturbing the signal of the first probe applied, and a "back and forth" adjusting of the two probes is often necessary. In this case, fix the headframe tightly first so that transducer adjustments are not displacing the headframe.

Once probes are oriented as desired and "locked" in place according to manufacturer design, the recording function of the instrument's software should be engaged. The thrombolysis monitoring study should run at least through the 60 min period of tPA infusion but ideally up to 2 hours as performed in the observational studies and clinical trials. Recanalization is likely to occur during tPA infusion whereas re-occlusion is common after tPA is stopped due to its short half-life. Most valuable information is obtained in real time and the sonographer should know typical changes with recanalization, re-occlusion and hyperemic reperfusion [29–33] and alert treating physician immediately. The interpreting physician should be alerted if the treating physician is un-familiar with ultrasound. Ideally, a protocol should be in place where the sonographer is encouraged to disclose technical findings to the treating physician to act upon this, if appropriate. At

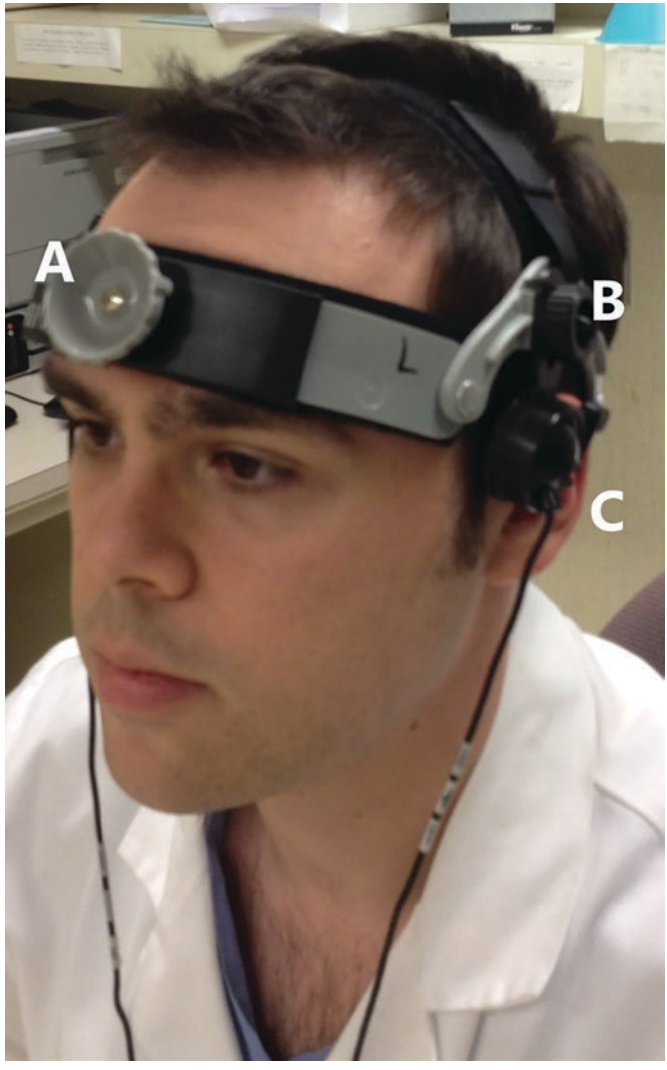

Fig. 3 Sonothrombolysis setup. This figure depicts a headframe and TCD monitoring probes over each transtemporal window. It is important to tighten the headband (A) to ensure adequate contact for ultrasound transmission. It takes patience and skill to adjust the location (B) and the angulation (C) of the probes so as to have optimal thrombolysis monitoring/sonothrombolysis

the end of the study the study data should be saved and prepared for reporting, probes and headframe should be disengaged, cleaned and disinfected according to manufacturer and institutional protocols, and the patient cleaned as this study often requires copious amounts of ultrasound gel for optimal signals.

Criteria and References

Report Generation All reports should conform to the Intersocietal Accreditation Commission (IAC) Vascular Testing Standards.

See https://www.intersocietal.org/vascular/seeking/vascular_standards.htm

Review of Diagnostic Findings The sonographer should identify and adequately capture any abnormalities of mean flow velocity, direction of flow or high intensity transient signals noted. The treating physician reviewing the technical findings should discuss the clinical relevance of these findings with the interpreting physician and, in the case of thrombolysis monitoring, specifically comment on the persistence of occlusion, recanalization, hyperemic reperfusion, reocclusion, continuing embolization, or the presence of an intracranial arterial steal.

Conclusions

Therapeutic TCD, "sonothrombolysis," for acute ischemic stroke is rooted in biological plausibility of a mechanical pressure wave to augment enzymatic activity of tPA and had promising results in the original clinical trials but whether or not it can have a role in routine clinical practice is being actively researched. Thrombolysis monitoring – the technique on which sonothrombolysis is based – is safe and useful in diagnosis of aforementioned conditions and stroke prognostication.

Personal Perspectives

Sonothrombolysis for acute ischemic stroke is likely to be most effective only in those vessels in which we can be close to a 0° or 180° sampling – namely the M1 MCA and basilar arteries, and has potential to be of therapeutic benefit to patients who cannot undergo rapid mechanical thrombectomy for clinical or logistical reasons. Thrombolysis monitoring is part of our routine clinical practice because it enables us to diagnose re-occlusion that could prompt thrombectomy if a patient was not initially deemed appropriate, change blood pressure management if hypo- or hyperperfusion is found, and discuss prognosis based on persistent occlusion or recanalization. TCD information allows us to more effectively counsel the patient and their loved ones during a difficult time when all involved are wondering "will they be ok?"

References

1. Alexandrov AV, Molina CA, Grotta JC, Garami Z, Ford SR, Alvarez-Sabin J, et al. Ultrasound-enhanced systemic thrombolysis for acute ischemic stroke. N Engl J Med. 2004;351(21):2170–8.
2. Alexandrov AV, Köhrmann M, Soinne L, Tsivgoulis G, Barreto AD, Demchuk AM, et al. Safety and efficacy of sonothrombolysis for acute ischaemic stroke: a multicentre, double-blind, phase 3, randomised controlled trial. Lancet Neurol. 2019;18(4):338–47.
3. Lauer CG, Burge R, Tang DB, Bass BG, Gomez ER, Alving BM. Effect of ultrasound on tissue-type plasminogen activator-induced thrombolysis. Circulation. 1992;86(4):1257–64.
4. Kimura M, Iijima S, Kobayashi K, Furuhata H. Evaluation of the thrombolytic effect of tissue-type plasminogen activator with ultrasonic irradiation: in vitro experiment involving assay of the fibrin degradation products from the clot. Biol Pharm Bull. 1994;17(1):126–30.
5. Blinc A, Kennedy SD, Bryant RG, Marder VJ, Francis CW. Flow through clots determines the rate and pattern of fibrinolysis. Thromb Haemost. 1994;71(2):230–5.
6. Trübestein G, Engel C, Etzel F, Sobbe A, Cremer H, Stumpff U. Thrombolysis by ultrasound. Clin Sci Mol Med Suppl. 1976;3:697s–8s.

7. Tachibana S. Ultrasonic vibration for boosting fibrinolytic effect of urokinase. Thromb Haemost. 1981;46(1):665.
8. Francis CW. Ultrasound-enhanced thrombolysis. Echocardiography. 2001;18(3):239–46.
9. Francis CW, Blinc A, Lee S, Cox C. Ultrasound accelerates transport of recombinant tissue plasminogen activator into clots. Ultrasound Med Biol. 1995;21(3):419–24.
10. Demchuk AM, Felburg RA, Alexandrov AV. Clinical recovery from acute ischemic stroke after early reperfusion of the brain with intravenous thrombolysis. N Engl J Med. 1999;340(11):894–5.
11. Alexandrov AV, Demchuk AM, Felberg RA, Christou I, Barber PA, Burgin WS, et al. High rate of complete recanalization and dramatic clinical recovery during tPA infusion when continuously monitored with 2-MHz transcranial doppler monitoring. Stroke. 2000;31(3):610–4.
12. Alexandrov AV, Demchuk AM, Burgin WS, Robinson DJ, Grotta JC, CLOTBUST Investigators. Ultrasound-enhanced thrombolysis for acute ischemic stroke: phase I. Findings of the CLOTBUST trial. J Neuroimaging. 2004;14(2):113–7.
13. Meairs S. Contrast-enhanced ultrasound perfusion imaging in acute stroke patients. Eur Neurol. 2008;59(1):17–26.
14. Culp WC, Porter TR, Lowery J, Xie F, Roberson PK, Marky L. Intracranial clot lysis with intravenous microbubbles and transcranial ultrasound in swine. Stroke. 2004;35(10):2407–11.
15. Molina CA, Ribo M, Rubiera M, Montaner J, Santamarina E, Delgado-Mederos R, et al. Microbubble administration accelerates clot lysis during continuous 2-MHz ultrasound monitoring in stroke patients treated with intravenous tissue plasminogen activator. Stroke. 2006;37(2):425–9.
16. Alexandrov AV, Mikulik R, Ribo M, Sharma VK, Lao AY, Tsivgoulis G, et al. A pilot randomized clinical safety study of sonothrombolysis augmentation with ultrasound-activated perflutren-lipid microspheres for acute ischemic stroke. Stroke. 2008;39(5):1464–9.
17. Molina CA, Barreto AD, Tsivgoulis G, Sierzenski P, Malkoff MD, Rubiera M, et al. Transcranial ultrasound in clinical sonothrombolysis (TUCSON) trial. Ann Neurol. 2009;66(1):28–38.
18. Nacu A, Kvistad CE, Naess H, Øygarden H, Logallo N, Assmus J, et al. NOR-SASS (Norwegian Sonothrombolysis in Acute Stroke Study): randomized controlled contrast-enhanced sonothrombolysis in an unselected acute ischemic stroke population. Stroke. 2017;48(2):335–41.
19. Alexandrov AV, Tsivgoulis G, Köhrmann M, Katsanos AH, Soinne L, Barreto AD, et al. Endovascular equipoise shift in a phase III randomized clinical trial of sonothrombolysis for acute ischemic stroke. Ther Adv Neurol Disord. 2019;12:1756286419860652.

20. Perren F, Loulidi J, Poglia D, Landis T, Sztajzel R. Microbubble potentiated transcranial duplex ultrasound enhances IV thrombolysis in acute stroke. J Thromb Thrombolysis. 2008;25(2):219–23.
21. Larrue V, Viguier A, Arnaud C, et al. #82 Trancranial ultrasound combined with intravenous microbubbles and_tissue plasminogen activator for acute ischemic stroke: a randomized controlled study. Abstracts from the 2007 International Stroke Conference. Stroke. 2007;38(2):472.
22. Daffertshofer M, Gass A, Ringleb P, Sitzer M, Sliwka U, Els T, et al. Transcranial low-frequency ultrasound-mediated thrombolysis in brain ischemia: increased risk of hemorrhage with combined ultrasound and tissue plasminogen activator: results of a phase II clinical trial. Stroke. 2005;36(7):1441–6.
23. Eggers J, Koch B, Meyer K, König I, Seidel G. Effect of ultrasound on thrombolysis of middle cerebral artery occlusion. Ann Neurol. 2003;53(6):797–800.
24. Eggers J, König IR, Koch B, Händler G, Seidel G. Sonothrombolysis with transcranial color-coded sonography and recombinant tissue-type plasminogen activator in acute middle cerebral artery main stem occlusion: results from a randomized study. Stroke. 2008;39(5):1470–5.
25. Alexandrov AV. ClinicalTrials.gov [Internet]. Bethesda: National Library of Medicine (US). Identifier: NCT03519737. Aureva transcranial ultrasound device with tPA in patients with acute ischemic stroke (TRUST) [Internet]. 2018 [cited 2020 Jan 12]. Available from: https://clinicaltrials.gov/ct2/show/record/NCT03519737?view=record.
26. Saqqur M, Tsivgoulis G, Nicoli F, Skoloudik D, Sharma VK, Larrue V, et al. The role of sonolysis and sonothrombolysis in acute ischemic stroke: a systematic review and meta-analysis of randomized controlled trials and case-control studies: a meta-analysis of the role of sonothrombolysis in acute ischemic stroke. J Neuroimaging. 2014;24(3):209–20.
27. Saqqur M, Uchino K, Demchuk AM, Molina CA, Garami Z, Calleja S, et al. Site of arterial occlusion identified by transcranial Doppler predicts the response to intravenous thrombolysis for stroke. Stroke. 2007;38(3):948–54.
28. Alexandrov AV, Demchuk AM, Wein TH, Grotta JC. Yield of transcranial Doppler in acute cerebral ischemia. Stroke. 1999;30(8):1604–9.
29. Demchuk AM, Christou I, Wein TH, Felberg RA, Malkoff M, Grotta JC, et al. Specific transcranial Doppler flow findings related to the presence and site of arterial occlusion. Stroke. 2000;31(1):140–6.
30. Demchuk AM, Burgin WS, Christou I, Felberg RA, Barber PA, Hill MD, et al. Thrombolysis in brain ischemia (TIBI) transcranial Doppler flow grades predict clinical severity, early recovery, and mortality in patients treated with intravenous tissue plasminogen activator. Stroke. 2001;32(1):89–93.
31. Tsivgoulis G, Ribo M, Rubiera M, Vasdekis SN, Barlinn K, Athanasiadis D, et al. Real-time validation of transcranial Doppler criteria in assessing

recanalization during intra-arterial procedures for acute ischemic stroke an international, multicenter study. Stroke. 2013;44(2):394–400.
32. Baracchini C, Farina F, Palmieri A, Kulyk C, Pieroni A, Viaro F, et al. Early hemodynamic predictors of good outcome and reperfusion injury after endovascular treatment. Neurology. 2019;92(24):e2774–83.
33. He Y-B, Su Y-Y, Rajah GB, Zhang Y-B, Fan L-L, Liu G, et al. Transcranial Doppler predicts early neurologic deterioration in anterior circulation ischemic stroke after successful endovascular treatment. Chin Med J (Engl) [Internet]. 2020 [cited 2020 Sep 14]; Publish Ahead of Print. Available from: https://journals.lww.com/10.1097/CM9.0000000000000881.
34. Barreto AD, Alexandrov AV, Shen L, Sisson A, Bursaw AW, Sahota P, et al. CLOTBUST-hands free: pilot safety study of a novel operator-independent ultrasound device in patients with acute ischemic stroke. Stroke. 2013;44(12):3376–81.

Clinical Application of Cerebrovascular Physiology

William K. Cornwell III

Introduction

Normal brain function depends on the ability of the cerebral vasculature to regulate cerebral blood flow (CBF). Under normal circumstances, resting and exertional CBF is maintained despite fluctuations in blood pressure and arterial perfusion pressure – which may be quite dramatic, such as when exercising, or when rising from a supine to standing position. The mechanisms by which CBF is maintained are complex and multifactorial. A breakdown of these processes, such as may occur in different clinical settings such as traumatic brain injury, intracerebral hemorrhage, or subarachnoid hemorrhage, are often associated with poor neurological outcomes [1–8].

In this chapter, an overview of cerebrovascular anatomy and clinically relevant physiology is provided, and factors contributing to regulation of CBF in health and disease are reviewed. The

W. K. Cornwell III (✉)
Medicine-Cardiology, Advanced Heart Failure, LVAD and Cardiac Transplant, Wilderness and Environmental Medicine, University of Colorado Anschutz Medical Campus, Aurora, CO, USA
e-mail: william.cornwell@ucdenver.edu

W. C. Ziai, C. L. Cornwell (eds.), *Neurovascular Sonography*,
https://doi.org/10.1007/978-3-030-96893-9_11

effects of fluctuations in blood pressure and carbon dioxide (CO_2) on autoregulatory processes are described, with an emphasis clinically relevant considerations when managing patients suffering from neurologic injury.

Cerebrovascular Anatomy and Physiology: An Overview

Cerebral arterial perfusion is provided through anterior and posterior systems. The anterior system consists of the internal carotid arteries, while the posterior system is comprised of the vertebrobasilar system. The anterior and posterior systems merge at the circle of Willis. The unique vascular design of the circle of Willis is particularly advantageous in the setting of acute and chronic disease, since the multiple anastomotic connections provide a wealth of collateral flow, which may protect against, or at least mitigate, areas of ischemia. While the majority of individuals have a complete circle, anatomic variations do occur on a population level and in up to 20–50% of individuals the circle is incomplete. One of the most common anomalies involves a fetal posterior cerebral artery, which involves a hypoplastic/underdeveloped portion of the proximal posterior cerebral artery, resulting in an enlarged ipsilateral posterior communicating artery.

Under normal resting conditions, CBF consumes about 15% of total cardiac output, at a flow rate of approximately 50 ml/100 g/min. Thus, despite only contributing to ~2% of total body weight, the body delivers a disproportionately large supply of oxygenated blood to the brain to support its very high metabolic demand.

Cerebral Blood Flow and Autoregulation

Cerebral autoregulatory processes ensure that brain blood flow is maintained within a normal level despite fluctuations in arterial perfusion pressure [9–13]. The concept of autoregulation was first described by Lassen in 1959 [14], and is heavily relied upon to guide blood pressure management in a variety of clinical

settings. Cerebral autoregulation is generally depicted by plotting the relationship of cerebral blood flow (CBF) against mean arterial pressure (MAP) or cerebral perfusion pressure (Fig. 1a). Three critical relationships in the autoregulatory curve are worthy of mention: (1) the lower limit, (2) the autoregulatory plateau; and (3) the upper limit. The lower and upper limits represent the boundaries of the autoregulatory plateau and beyond these limits, autoregulatory processes give way to passive flow that is highly dependent on pressure. That said, autoregulatory processes still occur, but have a diminishing impact on CBF the further away pressure is from the lower and upper limits [15]. It is at the severe extremes where the relationship between pressure and flow becomes linear [15]. Operating within the plateau, autoregulatory processes ensure that CBF is relatively insensitive to fluctuations in pressure and that CBF is held within a margin that maintains normal cerebral function. However, it is important to note that the plateau is not "flat". Rather, the plateau is a gentle slope [9, 12, 15, 16]. Regarding the limits of the plateau, the most often quoted values for the lower and upper limits are a CPP of 60 mmHg and 150 mmHg,

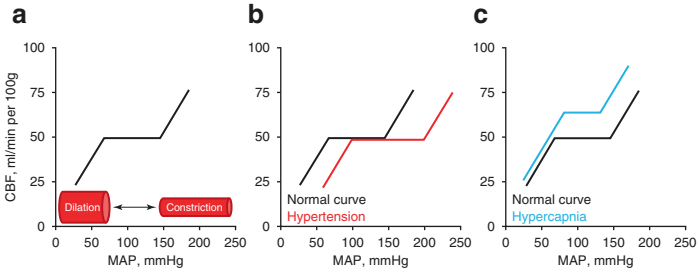

Fig. 1 Cerebral autoregulation under normal conditions (**a**) demonstrating vascular dilation at the lower end of the curve, as well as vascular constriction at the upper end. Under conditions of hypertension (**b**), the lower and upper ends of the autoregulatory plateau may be rightward shifted by as much as 30 mmHg and 50 mmHg, respectively. Hypercapnia (**c**), causes an up- and rightward shift in the lower limit of the autoregulatory curve, and a leftward shift in the upper limit of the curve. The net result is a shortening of the autoregulatory plateau. CBF cerebral bloodflow; MAP mean arterial pressure

respectively [17, 18]. Similarly, within the autoregulatory plateau, CBF is most often cited to be 50 ml/min per 100 g [17, 18]. However, it must be pointed out that these numbers represent average values derived from different patient groups and for any individual, may under- or overestimate the actual values [19].

Autoregulatory mechanisms are multifactorial and consist of both a vascular component and a neurogenic component [20]. The vascular arm of cerebral autoregulation involves constriction and dilatation of vascular smooth muscle cells, which occur in response to alterations in intraluminal pressure [21]. In addition, vasoactive substances (nitric oxide, endothelin-1) are released from endothelial cells which act to buffer changes in arterial pressure [20]. The neurogenic component involves the very rich supply of sympathetic nerve fibers that innervate the cerebral vasculature and mediate changes in vessel diameter in response to alterations in cerebral perfusion pressure [9].

Cerebral autoregulation may be referred to either in terms of "static" or "dynamic" responses [22]. Static measurements of cerebral autoregulation determine the overall efficiency of autoregulatory processes, meaning the degree to which changes in MAP elicit changes in cerebrovascular resistance to regulate CBF. However, static measurements do not provide information on the temporal relationship – ie, the time required for changes in cerebrovascular resistance to occur, in response to fluctuations in MAP. Animal models [10] and human studies [11, 12] alike have shown that autoregulatory processes operate very quickly over a period of several seconds. Dynamic measurements characterize this time course, or the "latency" of changes in cerebrovascular resistance that occur in response to fluctuations in MAP, which ultimately maintain CBF within normal values [22].

Effect of Blood Pressure on Autoregulation

Changes in arterial perfusion pressure – whether acute or chronic, have a profound effect on the autoregulatory curve (Fig. 1b). Chronic hypertension, for example, leads to two major changes in the autoregulatory curve. First, there is a rightward shift in the autoregulatory plateau by as much as 30 mmHg at the lower end

of the curve, and 50 mmHg at the upper end of the curve [9, 23]. This shift occurs as a result of arteriolar constriction and hypertrophy (according to the law of Laplace) in response to chronically elevated intraluminal pressures [23]. This rightward shift exerts a protective effect on the blood-brain barrier and prevents overdistension of the cerebral vasculature in the setting of elevated blood pressures [23, 24]. As a result, CBF remains stable despite elevated levels of blood pressure, that would otherwise result in passive vasodilatation [25]. At the lower end of the autoregulatory curve, reductions in CBF occur at increasing levels of arterial pressure because of impairments in cerebral vasodilatation in the setting of cerebral hypertrophy [23, 25]. The second major effect of hypertension on cerebral autoregulation is a reduction in maximal vasodilatory capacity of the cerebral vasculature [23, 26]. Animal models have demonstrated that cerebrovascular resistance is greater among hypertensive as compared to normotensive animals during iatrogenic seizures that cause vessels to maximally dilate, which modulates increases in CBF that would otherwise occur [25, 26]. The mechanism accounting for this increase in cerebrovascular resistance is related – at least in part, to hypertrophy of the cerebral vasculature [25, 27].

Carbon Dioxide and Autoregulation

CO_2 levels exert a powerful effect on the cerebral vasculature and CBF (Fig. 1c). Hypercapnia exerts a vasodilatory effect on cerebral vessels that leads an increase in CBF [17]. Animal models suggest that the lower limit of the autoregulatory curve is right- and upward shifted in settings of acute hypercapnia and eventually is abolished in a dose-response fashion as the partial pressure of CO_2 increases to severely elevated levels, with a near-linear relationship between MAP and CBF [28–30]. At the upper limit of the autoregulatory curve, hypercapnia may cause a leftward shift in the inflection point of the curve [17, 31, 32]. The net consequence of hypercapnia on the autoregulatory curve is an upward shift of the autoregulatory plateau, as well as a shortening of the plateau. The degree to which these changes occur from baseline depends on the severity of the hypercapnia. In cases of severe

hypercapnia, cerebral vessels become maximally dilated, autoregulation becomes nonexistent and a linear relationship develops between pressure and flow.

Autoregulatory Processes During Acute Stroke

An ischemic stroke occurs when perfusion pressure remains insufficient for a long enough period of time to cause cell death [13]. In the setting of an acute stroke, the integrity of cerebral autoregulation is of vital importance insomuch as preservation of flow to the affected (and surrounding) territories determines tissue survival [13]. While it has been postulated that acute ischemia may predispose to either local or global impairments in cerebral autoregulation [13, 33–35], it is not clear that this is the rule. For example, in humans, pharmacologic reductions in MAP during an ischemic stroke did not reduce CBF as measured by single-photon emission computed tomography, or reduce internal carotid arterial flow, or middle cerebral arterial velocities as measured by transcranial Doppler [36, 37]. Other studies measuring CBF by positron emission tomography found that cerebral autoregulation was preserved in the core, penumbra, and other regions of the ipsilateral hemisphere [38, 39]. However, among patients with large infarcts involving the middle cerebral artery distribution, transcranial Doppler studies have demonstrated that autoregulatory processes are impaired in response to even small oscillations in blood pressure when reperfusion is unsuccessful [40].

Subarachnoid Hemorrhage and Cerebral Autoregulation

Cerebral autoregulation is frequently impaired in the first several days following a subarachnoid hemorrhage [4–8]. Importantly, impairments in autoregulation may precede clinical and/or radiologic evidence of further neurologic deterioration [41]. Early in the clinical course of subarachnoid hemorrhage, the breakdown of autoregulatory processes means that there is minimal dampening of fluctuations in MAP, and these fluctuations may very quickly

lead to large changes in CBF [41]. As a consequence, this impairment predisposes to a number of consequences including vasospasm, delayed cerebral ischemia, and overall poor clinical outcomes [5, 6, 41]. Indeed, it has been shown that vasospasm is preceded by a breakdown in cerebral autoregulation [7], but that the preservation of autoregulatory processes following subarachnoid hemorrhage is associated with marked reductions in risk of vasospasm and delayed cerebral ischemia, regardless of the absolute level of cerebral blood flow velocity [6, 41–43].

Conclusion

Normal brain function depends on tight regulation of CBF. Cerebral autoregulation is responsible for maintaining CBF within a healthy range, and these autoregulatory forces work very quickly – over a period of several seconds, to buffer fluctuations in pressure and control flow. Factors such as MAP and CO_2 elicit a profound effect on the autoregulatory curve and are important to consider when providing clinical care to patients suffering from neurologic injury. When autoregulatory forces are impaired, such as occurs in the setting of subarachnoid hemorrhage, prognosis is poor and overall outcomes may be compromised.

Sources of Funding/Disclosures Dr. Cornwell has received funding by an NIH/NHLBI Mentored Patient-Oriented Research Career Development Award (#1K23HLI32048-01), as well as the NIH/NCATS (#UL1TR002535), Susie and Kurt Lochmiller Distinguished Heart Transplant Fund, the Clinical Translational Science Institute at the University of Colorado Anschutz Medical Campus, and Medtronic Inc.

References

1. Hlatky MA, Furuya Y, Valadka AB, Gonzalez J, Chacko A, Mizutani Y, et al. Dynamic autoregulatory response after severe head injury. J Neurosurg. 2002;97(5):1054–61.
2. Jaeger M, Schuhmann MU, Soehle M, Meixensberger J. Continuous assessment of cerebrovascular autoregulation after traumatic brain injury using brain tissue oxygen pressure reactivity. Crit Care Med. 2006;34:1783–8.

3. Dohmen C, Bosche B, Graf R, Reithmeier T, Ernestus RI, Brinker G, et al. Identification and clinical impact of impaired cerebrovascular autoregulation in patients with malignant middle cerebral artery infarction. Stroke. 2007;38(1):56–61.
4. Fontana J, Moratin J, Ehrlich G, Scharf J, Weiss C, Schmieder K, et al. Dynamic autoregulatory response after aneurysmal subarachnoid hemorrhage and its relation to angiographic vasospasm and clinical outcome. Neurocrit Care. 2015;23(3):355–63.
5. Jaeger M, Schuhmann MU, Soehle M, Nagel C, Meixensberger J. Continuous monitoring of cerebrovascular autoregulation after subarachnoid hemorrhage by brain tissue oxygen pressure reactivity and its relation to delayed cerebral infarction. Stroke. 2007;38(3):981–6.
6. Lam JMK, Smielewski P, Czosnyka M, Pickard JD, Kirkpatrick PJ. Predicting delayed Ishcemic deficits after aneurysmal subarachnoid hemorrhage using a transient hyperemic response test of cerebral auroregulation. Neurosurgery. 2000;47(4):819–26.
7. Lang EW, DIehl RR, Mehdorn M. Cerebral autoregulation testing after aneurysmal subarachnoid hemorrhage: the phase relationship between arterial blood pressure and cerebral blood flow velocity. Crit Care Med. 2001;2001(29):1.
8. Budohoski KP, Czosnyka M, Smielewski P, Varsos GV, Kasprowicz M, Brady KM, et al. Cerebral autoregulation after subarachnoid hemorrhage: comparison of three methods. J Cereb Blood Flow Metab. 2013;33(3):449–56.
9. Cornwell WK III, Ambardekar AV, Tran T, Pal J, Cava L, Lawley J, et al. Stroke incidence and impact of continuous-flow left ventricular assist devices on cerebrovascular physiology. Stroke. 2019;50:542–8.
10. Symon L, Held K, Dorsch NWC. A study of regional autoregulation in the cerebra circulation to increased perfusion pressure in normocapnia and hypercapnia. Stroke. 1973;4:139–47.
11. Aaslid R, Lindegaard KF, Sorteberg W, Nornes H. Cerebral autoregulation dynamics in humans. Hypertension. 1989;20:45–52.
12. Cornwell WK 3rd, Tarumi T, Aengevaeren VL, Ayers C, Divanji P, Fu Q, et al. Effect of pulsatile and nonpulsatile flow on cerebral perfusion in patients with left ventricular assist devices. J Heart Lung Transplant. 2014;33(12):1295–303.
13. Jordan JD, Powers WJ. Cerebral autoregulation and acute ischemic stroke. Am J Hypertens. 2012;25(9):946–50.
14. Lassen N. Cerebral blood flow and oxygen consumption in man. Physiol Rev. 1959;39(2):183–238.
15. Rosenblum W. Cerebral dynamics of autoregulation and hypoperfusion. Stroke. 2000;31(3):791–9.
16. Zaharchuk G, Mandeville JB, Bogdanov AA, Weissleder R, Rosen BR, Marota JJA. Cerebrovascular dynamics of autoregulation and hypoperfusion. An MRI study of CBF and changes in total and microvascular cerebral blood volume during hemorrhagic hypotension. Stroke. 1999;30: 2197–205.

17. Meng L, Gelb AW. Regulation of cerebral autoregulation by carbon dioxide. Anesthesiology. 2015;122(1):196–205.
18. Paulson OB, Strandgaard S, Edvinsson L. Cerebral autoregulation. Cerebrovasc Brain Metab Rev. 1990;2(2):161–92.
19. Drummond JC. The lower limit of autoregulation: time to revise our thinking? Anesthesiology. 1997;86:1431–3.
20. Edvinsson L, Krause DN. Cerebral blood flow and metabolism. 2nd ed. Lippincott Williams & Wilkins; 2002.
21. Folklow B. Description of the myogenic hypothesis. Circ Res. 1964;15:279–87.
22. Tiecks FP, Lam AM, Aaslid R, Newell DW. Comparison of static and dynamic cerebral autoregulation measurements. Stroke. 1995;26:1014–9.
23. Harper SL, Bohlen HG. Microvascular adaptation in the cerebral cortex of adult spontaneously hypertensive rats. Hypertension. 1984;6:408–19.
24. Hart MN, Heistad DD, Brody MJ. Effect of chronic hypertension and sympathetic denervation on wall:lumen ratio of cerebral vessels. Hypertension. 1980;2:419–23.
25. Faraci FM, Baumbach GL, DD. H. Cerebral circulation: humoral regulation and effects of chronic hypertension. J Am Soc Nephrol. 1990;1:53–7.
26. Sadoshima S, Bisija DW, Heistad DD. Mechanisms of protection against stroke in stroke-prone spontaneously hypertensive rats. Am J Physiol. 1983;244(3):H406–H12.
27. Johansson BB, Nilsson B. Cerebral vasomotor reactivity in normotensive and spontaneously hypertensive rats. Stroke. 1979;10(5):572–6.
28. harper AM. Autoregulation of cerebral blood flow - influence of the arterial blood pressure on the blood flow through the cerebral cortex. J Neurol Neurosurg Psychiatry. 1966;29:398–403.
29. Haggendal E, Johansson B. Effects of arterial carbon dioxide tension and oxygen saturation on cerebral blood flow autoregulation in dogs. Acta Physiol Scand Suppl. 1965;258:27–53.
30. Raichle ME, Stone HL. Cerebral blood flow autoregulation and graded hypercapnia. Eur Neurol. 1971;6:1–5.
31. Ekstrom-jodal B, Haggendal E, Linder LE, Nilsson NJ. Cerebral blood flow autoregulation at high arterial pressures and different levels of carbon dioxide tension in dogs. Eur Neurol. 1971;6:6–10.
32. McCulloch TJ, Visco E, Lam AM. Graded hypercapnia and cerebral autoregulation during sevoflurane or propofol anesthesia. Anesthesiology. 2000;93:1205–9.
33. Cupini LM, Diomedi M, Placidi F, Silvestrini M, Giacomini P. Cerebrovascular reactivity and subcortical infarctions. Arch Neurol. 2001;58(4):577–81.
34. Dawson SL, Blake MJ, Panerai RB, Potter JF. Dynamic but not static cerebral autoregulation is impaired in acute ischaemic stroke. Cerebrovasc Dis. 2000;10(2):126–32.

35. Dawson SL, Panerai RB, Potter JF. Serial changes in static and dynamic cerebral autoregulation after acute ischaemic stroke. Cerebrovasc Dis. 2003;16:69–75.
36. Nazir F, Overell J, Bolster A, Hilditch T, Reid JL, Lees K. The effect of losartan on global and focal cerebral perfusion and on renal function in hypertensives in mild early ischaemic stroke. J Hypertens. 2004;22(5):989–95.
37. Nazir FS, Overell JR, Bolster A, Hilditch TE, Lees KR. Effect of perindopril on cerebral and renal perfusion in normotensives in mild early ischaemic stroke: a randomized controlled trial. Cerebrovasc Dis. 2005;19:77–83.
38. Hakim AM, Evans AC, Berger L, Kuwaabara H, Worsley K, Marchal G, et al. The effect of Nimodipine on the evolution of human cerebral infarction studied by PET. J Cereb Blood Flow Metab. 1989;9:523–34.
39. Powers WJ, Videen TO, Diringer MN, Aiyagari V, Zazulia A. Autoregulation after ischaemic stroke. J Hypertens. 2009;22(11):2218–22.
40. Reinhard MCW, Roth M, Harloff A, Niesen WD, Timmer J, et al. Cerebral autoregulation dynamics in acute ischemic stroke after rtPA thrombolysis. Cerebrovasc Dis. 2008;26:147–55.
41. Otite F, Mink S, Tan CO, Puri A, Zamani AA, Mehregan A, et al. Impaired cerebral autoregulation is associated with vasospasm and delayed cerebral ischemia in subarachnoid hemorrhage. Stroke. 2014;45(3):677–82.
42. Ratsep T, Asser T. Cerebral hemodynamic impairment after aneurysmal subarachnoid hemorrhage as evaluated using transcranial Doppler ultrasonography: relationship to delayed cerebral ischemia and clinical outcome. J Neurosurg. 2001;95(3):393–401.
43. Soehle M, Czosnyka M, Pickard JD, Kirkpatrick PJ. Continuous assessment of cerebral autoregulation in subarachnoid hemorrhage. Anesth Analg. 2004;98(4):1133–9. table of contents

Adult Traumatic Brain Injury

Creagh Boulger and Varun Shah

Introduction

Epidemiology

Traumatic brain injury (TBI) is defined by the Centers for Disease Control (CDC) as any shearing, blunt or penetrating injury to the head that alters normal function [1, 2]. According to the CDC there has been a 53% rise in TBI visits and deaths from 2006 to 2014 with 2.87 million affected in 2014 [1, 3]. This is likely an underestimate as nearly 25% of the population has had self-reported head injury and many do not seek medical care [4]. TBI are typically graded mild to severe. All grades of TBI can have lasting effects on patients and their families. Long term consequences can include memory loss, chronic headaches, neurologic deficits, anxiety, depression, post-traumatic stress disorder and cognitive delays [5–9]. In 2005 3.17 million Americans were living with TBI related disability [10]. Patients

C. Boulger (✉)
Department of Emergency Medicine, The Ohio State University Wexner Medical Center, Columbus, OH, USA
e-mail: Creagh.boulger@osumc.edu

V. Shah
College of Medicine, The Ohio State University Wexner Medical Center, Columbus, OH, USA

W. C. Ziai, C. L. Cornwell (eds.), *Neurovascular Sonography*,
https://doi.org/10.1007/978-3-030-96893-9_12

and families also have significant financial and social impact from TBI. Unfortunately, statistics suggest an upward trend in rates of TBI and TBI related death. TBI related deaths account for 155 deaths per day [1]. The population most likely to suffer a lethal TBI is those 75 years and older [1].

TBIs have a variety of etiologies with most common varying by age group. However, falls account for 48% of TBI related ED visits, being struck by or against an object are 2nd accounting for 17% [1]. Falls are more likely than other etiologies to lead to hospitalization with motor vehicle collision in a distant second [1]. Self-harm related TBI accounts for nearly a third of TBI related deaths despite not being in the top 3 etiologies of TBI; this is likely secondary to the lethality and intent associated with these injuries. This population has also, unfortunately, seen the largest rise in occurrence from 2006 to 2014, rising by 60% [1].

Pathophysiology

Traumatic brain injury can be broken up into two components, primary and secondary brain injury. Primary brain injury is a result of the direct forces and acceleration and deceleration [10–13]. Following this initial trauma secondary brain injury occurs. This is the more complicated and less understood process that is believed to contribute many of the long-term complications and variability in patient symptoms and outcomes [10–14]. Secondary injury involves activation of inflammatory cascades, increased metabolic demand, ischemia, and edema. Secondary injury is a frequent cause of morbidity and mortality in TBI patients. Fatima et al. describes the alterations in cerebral blood flow during secondary injury. Day 0 presents with hypoperfusion followed over days 1–3 with hyperemia and then the remainder of the first 2 weeks the patient is at risk for vasospasm. Risk of elevated intracranial pressure (ICP) is also most prevalent during this time [11, 12].

Defining the Disease

GCS the Glasgow Coma Scale is a commonly utilized neurologic assessment in trauma patients. It is utilized by nursing, prehospital providers, and physicians to communicate the global neurologic state of the patient.

The components of the GCS are motor, verbal, and eye opening. The scoring is demonstrated in Table 1. Patients can get a minimum score of 3 and a maximum score of 15. Score is made based on best effort, even if unilateral. Traditionally ranges of GCS have been used to grade TBI [13, 14]. However, recent literature proposes that this may not be sufficient [15–21].

Mild – Moderate TBI

Mild and moderate TBI account for at least 80% of traumatic injuries that present to the ED [1, 22, 23]. Mild TBI is GCS 14-15. Moderate TBI is GCS 9-13 [18, 24, 25].

Severe TBI

Severe TBI is diagnosed by GCS < 9 [18, 24–26].

Table 1 Glasgow Coma Scale

Eyes	Verbal	Motor
1 = will not open eyes	1 = Nonverbal	1 = No response
2 = opens to painful stimuli	2 = Incomprehensible sound	2 = Decerebrate Posturing
3 = opens to voice	3 = Inappropriate words	3 = Decorticate Posturing
4 = spontaneously opens eyes	4 = Confused	4 = Withdraws from pain
	5 = Oriented	5 = Localizes Pain
		6 = Follows commands

Signs and Symptoms

The signs and symptoms of TBI vary greatly depending on the severity of the injury. Patients may present with headache, confusion, nausea and vomiting with mild TB. Patients with more severe TBI may have focal neurologic deficits, and decreased level of consciousness. The most severe TBIs will present unresponsive and may even display signs of herniation such as a fixed dilated pupil, Cheyne stokes respirations, and decorticate or decerebrate posturing.

Complications

Given the wide range of severity of TBI, complications too can vary significantly. Short term complications of TBI can include difficulty concentrating, aspiration, neurologic deficits, airway compromise, elevated intracranial pressure, cerebral and cerebellar herniation. Long term complications can include memory loss, short and long term, mood disturbances, cognitive delay, chronic headaches, pituitary dysfunction, sleep dysfunction, permanent neurologic deficits and death [5, 27–30].

Differential Diagnosis

Altered level of consciousness and headache are common presentations of TBI. These two presentations can have a broad spectrum of differential diagnoses .

TCD Findings

Transcranial Doppler allows for in-vivo monitoring of ICP and cerebral perfusion pressure (CPP) in patients with TBI. Often these patients are critically ill and are not optimal candidates to be transported to and from other imaging modalities [12, 31]. TCD

monitors cerebral blood flow via mean blood flow velocity (MFV) and ICP via pulsatility index of the MCA and other vessels. It also allows for monitoring of vasospasm. All of this can be done on serial exams, and is a non-invasive, low cost, low risk, bedside available imaging modality for real time assessment [31].

TCD has been proposed as a useful tool for predicting neurologic outcomes with all grades of TBI, see Table 2 [23, 32–34]. Neurologic outcomes after TBI are dependent on a number of variables including initial injury severity, concomitant injuries, comorbidities, associated organ dysfunction and extent of secondary brain injury [22, 23, 34].

TCD has been shown to be a good screening tool for secondary neurologic deterioration in patients with initial head CT that does not show signs of severe injury [22].

In one study by Bouzat et al. they found that the two most predictive factors for secondary neurologic deterioration (SND) were mean diastolic blood flow velocity of <25 cm/s and pulsatility index >= 1.25 in the MCA [22, 23].

In Mild TBI these findings had a sensitivity of 91%, and a specificity of 80%, 100% NPV, 15.6% PPV for neurologic decline. In moderate TBI the aforementioned measurements had a sensitivity of 67%, specificity of 74%, 94% NPV, and 26% PPV for neurologic decline [23]. These numbers suggest that a normal TCD should be reassuring for likely neurologic stability. An abnormal TCD measurement is more useful in mild TBI for predicting neurologic decline [23].

Another study by Fatima et al. found several measures that were associated with poor neurologic outcomes. These measures

Table 2 Grades of TBI

Grade of TBI	GCS	Altered LOC Duration	Post Trauma Amnesia	Mortality
Mild	13–15	<30 minutes	<24 hours	0.1%
Moderate	9–12	30 minutes-24 hours	1–7 days	10%
Severe	<9	>24 hours	>7 days	40%

include MCA MFV <35 cm/s within 72 hours of head injury, moderate basilar artery vasospasm (MFV >60 cm/s), and severe basilar artery vasospasm (MFV > 85 cm/s) which were all associated with poor neurologic outcomes. In addition, this study also found that MCA PI >= 1.56 was associated with 83% rate of poor outcome whereas PI <=1 was associated with 71% rate of good neurologic outcome at 6 months [12].

TCD also has a role in severe TBI. In the first 24 hours, low CBF (MFV < 40 cm/s) can be a surrogate marker of ischemia and can be acted upon to minimize secondary brain injury. This measurement becomes less reliable after the first 24 hours [35]. Ract et al. evaluated resuscitation of TBI patients guided by TCD. Early TCD to screen severe TBI patients with signs of decreased CPP or increased ICP was beneficial. Patients with these abnormal TCDs were given treatment to increase cerebral blood flow early. In response, they saw that ICP was still higher at the time of pressure monitoring but CPP and jugular venous oxygen saturation were the same as in the normal TCD group. From these findings they concluded that early TCD in those with compromised CPP could possibly decrease in secondary brain injury [36]. In their study Vd < 20 cm/s and PI > 1.4 were the best predictors of decreased CPP.

In severe TBI patients serial TCD in conjunction with ICP monitoring is useful in TBI patients after decompressive hemicraniectomy to monitor for decreased CPP or increase in ICP using FVd, MFV, and PI. Those with more regular monitoring and early detection of these changes had more favorable outcomes at 6 months than the traditional ICP only monitoring group [37].

Severe TBI is often associated with high morbidity and mortality. However, one study showed that 80% of patients with normal TCD measurements can expect good outcomes, those with hypoperfusion have a 90% chance of brain death and 98.6% chance of overall mortality. However, 14% of those with normal TCD expired prior to discharge, 4 from brain death [38]. While this was a single study, one could take away that normal TCDs are reassuring of better outcomes but prognosis should still be guarded as a significant percent of those with initially normal TCDs died.

Table 3 TCD Findings Associated with Poor Neurologic outcome

Vd < 20 cm/s
PI > 1.4
MFV < 40 cm/s @ 24 hours
MCA MFV < 35 cm/s @ 72 hours
Basilar Artery MFV > 60 cm /s
MCA PI > 1.56

Table 3 summarizes the various measurements from the aforementioned studies that are associated with poor neurologic outcomes.

Other Imaging

As mentioned earlier in this chapter just as GCS is not an adequate tool in isolation neither is TCD for diagnosis, management and prognosis of TBI patients. CT, MRI and EEG all have a role in monitoring and guidance of care of these patients.

Computed Tomography (CT)

CT is often the initial imaging modality in the developed world for moderate and severe TBI. It is readily available and more affordable than MRI. However, CT does have some associated risks such as radiation, and typically requires transport out of the critical care unit. According to CDC guidelines, CT imaging is indicated under conditions of: GCS < 15, polytrauma, neurologic deficit, coagulopathy, severe headache, age > 65 years, dangerous mechanism, or signs of basilar skull fracture [39–44].

Magnetic Resonance Imaging (MRI)

MRI has sensitivities approaching 100% for intracranial injury [44]. In addition, MRI unlike CT has no radiation. However, MRI is more costly and has limited availability. In addition MRI takes significantly more time than CT requiring potentially ill patients to be off the critical care unit and unable to receive certain treatments and intensive monitoring [44]. MRI also has better ability to assess the skull base and brainstem. Additionally, MRI has the capability to assess perfusion, diffusion, and proton spectroscopy which further enhance its sensitivity.

Positron Emission Tomography (PET)

PET scan is an even more highly limited imaging modality. It evaluates tissue metabolism. PET can detect non anatomic lesions and areas with potentially reversible insults that were not detected on CT, MRI, or EEG [44].

Electroencephalography (EEG)

EEG is one of the oldest modalities used in monitoring of TBI patients however in the past 2 decades has been surpassed by other modalities. However, new research is looking into the value of EEG in determining prognosis in TBI patients.

Treatment

Treatments for TBI are constantly evolving as the pathophysiology of the secondary injury is being revealed. Several treatments exist with varying levels of evidence. These include decompressive craniotomy/craniectomy, targeted temperature management, steroids, glucose, hypertonic saline, amphetamines, bone marrow transplants, mannitol.

Summary

Traumatic Brain Injury is a prevalent disease in the United States and across the world. Patients with even minor TBI are prone to long term sequelae including but not limited to cognitive delay, emotional disturbances, interpersonal and professional challenges. The more severe TBIs face the aforementioned sequelae in addition to the potential for neurologic deficits. TCD has a significant role in screening TBI patients and aiding in management and prognostication. In these patients TCD is best if used in conjunction with other modalities such as invasive monitoring, physical exam findings, EEG, and neuroimaging.

References

1. of Health D, Services H, for Disease Control C. Centers for Disease Control and Prevention Prevention and Control SURVEILLANCE REPORT Surveillance Report of Traumatic Brain Injury-related Emergency Department Visits, Hospitalizations, and Deaths TBI: SURVEILLANCE REPORT ACKNOWLEDGEMENTS [Internet]. [cited 2020 Jan 18]. Available from: www.cdc.gov/TraumaticBrainInjury
2. Menon DK, Schwab K, Wright DW, Maas AI. Position statement: definition of traumatic brain injury. Arch Phys Med Rehabil. 2010;91:1637.
3. Summers CR, Ivins B, Schwab KA. Traumatic brain injury in the United States: an epidemiologic overview. Mount Sinai J Med J Transl Personal Med [Internet]. 2009 Apr [cited 2020 Jan 18];76(2):105–10. Available from: http://doi.wiley.com/10.1002/msj.20100.
4. Corrigan JD, Selassie AW, Orman JA. The epidemiology of traumatic brain injury. J Head Trauma Rehabil. 2010;25:72–80.
5. Mollayeva T, Kendzerska T, Colantonio A. Self-report instruments for assessing sleep dysfunction in an adult traumatic brain injury population: a systematic review. Sleep Med Rev. 2013;17:411.
6. Williams BR, Lazic SE, Ogilvie RD. Polysomnographic and quantitative EEG analysis of subjects with long-term insomnia complaints associated with mild traumatic brain injury. Clin Neurophysiol. 2008;119(2):429–38.
7. Bushnik T, Englander J, Katznelson L. Fatigue after TBI: association with neuroendocrine abnormalities. Brain Inj. 2007;21(6):559–66.
8. Tulsky DS, Kisala PA. An overview of the Traumatic Brain Injury-Quality of Life (TBI-QOL) measurement system. J Head Trauma Rehabil Lippincott Williams and Wilkins. 2019;34:281–8.

9. Ashman TA, Cantor JB, Gordon WA, Sacks A, Spielman L, Egan M, et al. A comparison of cognitive functioning in older adults with and without traumatic brain injury. J Head Trauma Rehabil [Internet]. 2008 May [cited 2020 Jan 18];23(3):139–48. Available from: https://insights.ovid.com/crossref?an=00001199-200805000-00002.
10. Huebner RA, Johnson K, Bennett CM, Schneck C. Community participation and quality of life outcomes after adult traumatic brain injury. Am J Occup Ther. 2003;57(2):177–85.
11. Kramer DR, Winer JL, Pease BAM, Amar AP, Mack WJ. Cerebral vasospasm in traumatic brain injury. Neurol Res Int [Internet]. 2013 [cited 2020 Jan 18];2013. Available from: http://dx.
12. Fatima N, Shuaib A, Chughtai T, Ayyad A, Saqqur M. The role of transcranial doppler in traumatic brain injury: a systematic review and meta-analysis. Asian J Neurosurg. 2019;14(3):626.
13. Teasdale G, Jennett B. Assessment of coma and impaired consciousness. A practical scale. Lancet. 1974;304(7872):81–4.
14. Jennett B, Teasdale G, Braakman R, Minderhoud J, Knill-Jones R. Predicting outcome in individual patients after severe head injury. Lancet. 1976;307(7968):1031–4.
15. Grote S, Böcker W, Mutschler W, Bouillon B, Lefering R. Diagnostic value of the Glasgow coma scale for traumatic brain injury in 18,002 patients with severe multiple injuries. J Neurotrauma. 2011;28(4):527–34.
16. Stahel PF. Pupil evaluation in addition to Glasgow Coma Scale components in prediction of traumatic brain injury and mortality (Br J Surg 2012; 99(Suppl 1): 122-130). Br J Surg. 2012;99:131.
17. Majdan M, Steyerberg EW, Nieboer D, Mauritz W, Rusnak M, Lingsma HF. Glasgow coma scale motor score and pupillary reaction to predict six-month mortality in patients with traumatic brain injury: comparison of field and admission assessment. J Neurotrauma. 2015;32(2):101–8.
18. Chieregato A, Martino C, Pransani V, Nori G, Russo E, Noto A, et al. Classification of a traumatic brain injury: the Glasgow Coma scale is not enough. Acta Anaesthesiologica Scandinavica [Internet] 2010 [cited 2020 Jan 18];54(6):696–702. Available from: http://doi.wiley.com/10.1111/j.1399-6576.2010.02234.x.
19. Emami P, Czorlich P, Fritzsche FS, Westphal M, Rueger JM, Lefering R, et al. Impact of Glasgow coma scale score and pupil parameters on mortality rate and outcome in pediatric and adult severe traumatic brain injury: a retrospective, multicenter cohort study. J Neurosurg. 2017;126(3):760–7.
20. Marmarou A, Lu J, Butcher I, McHugh GS, Murray GD, Steyerberg EW, et al. Prognostic value of the Glasgow Coma Scale and pupil reactivity in traumatic brain injury assessed pre-hospital and on enrollment: an IMPACT analysis. J Neurotrauma. 2007;24(2):270–80.

21. Hudak AM, Caesar RR, Frol AB, Krueger K, Harper CR, Temkin NR, et al. Functional outcome scales in traumatic brain injury: a comparison of the Glasgow Outcome Scale (extended) and the functional status examination. J Neurotrauma. 2005;22(11):1319–26.
22. Bouzat P, Francony G, Declety P, Genty C, Kaddour A, Bessou P, et al. Transcranial doppler to screen on admission patients with mild to moderate traumatic brain injury. Neurosurgery. 2011;68(6):1603–9.
23. Bouzat P, Almeras L, Manhes P, Sanders L, Levrat A, David JS, et al. Transcranial doppler to predict neurologic outcome after mild to moderate traumatic brain injury. Anesthesiology. 2016;125(2):346–54.
24. Scale TGJB. Assessment of coma and impaired consciousness. A practical scale. Lancet II. 1974;1974:81–4.
25. Maas AIR, Marmarou A, Murray GD, Teasdale GM, Steyerberg EW. Prognosis and clinical trial design in traumatic brain injury: the IMPACT study. J Neurotrauma. 2007;24:232–8.
26. Saatman KE, Duhaime AC, Bullock R, Maas AIR, Valadka A, Manley GT, et al. Classification of traumatic brain injury for targeted therapies. J Neurotrauma. 2008;25:719–38.
27. Self-report instruments for assessing sleep dysfunction in an adult traumatic brain injury population: a systematic review - ScienceDirect [Internet]. [cited 2020 Jan 18]. Available from: https://www.sciencedirect.com/science/article/pii/S1087079213000245
28. Jullienne A, Obenaus A, Ichkova A, Savona-Baron C, Pearce WJ, Badaut J. Chronic cerebrovascular dysfunction after traumatic brain injury. J Neurosci Res. John Wiley and Sons Inc. 2016;94:609–22.
29. Schneider HJ, Kreitschmann-Andermahr I, Ghigo E, Stalla GK, Agha A. Hypothalamopituitary dysfunction following traumatic brain injury and aneurysmal subarachnoid hemorrhage: a systematic review. J Am Med Assoc. 2007;298:1429–38.
30. Kelly DF, Chaloner C, Evans D, Mathews A, Cohan P, Wang C, et al. Prevalence of pituitary hormone dysfunction, metabolic syndrome, and impaired quality of life in retired professional football players: a prospective study. J Neurotrauma Mary Ann Liebert Inc. 2014;31:1161–71.
31. D'andrea A, Conte M, Scarafile R, Riegler L, Cocchia R, Pezzullo E, et al. Transcranial Doppler ultrasound: physical principles and principal applications in Neurocritical care unit. J Cardiovasc Echograph Medknow Publications. 2016;26:28–41.
32. Bouzat P, Almeras L, Manhes P, Sanders L, Levrat A, David JS, et al. Transcranial doppler to predict neurologic outcome after mild to moderate traumatic brain injury. Anesthesiology. 2016;125(2):346–54.
33. Chastain CA, Oyoyo UE, Zipperman M, Joo E, Ashwal S, Shutter LA, et al. Predicting outcomes of traumatic brain injury by imaging modality and injury distribution. J Neurotrauma. 2009;26(8):1183–96.
34. Baum J, Entezami P, Shah K, Medhkour A. Predictors of outcomes in traumatic brain injury. World Neurosurg. 2016;90:525.

35. Sokoloff C, Williamson D, Serri K, Albert M, Odier C, Charbonney E, et al. Clinical usefulness of transcranial Doppler as a screening tool for early cerebral hypoxic episodes in patients with moderate and severe traumatic brain injury. Neurocrit Care. 2019;32:486.
36. Ract C, le Moigno S, Bruder N, Vigué B. Transcranial Doppler ultrasound goal-directed therapy for the early management of severe traumatic brain injury. Intensive Care Med. 2007;33(4):645–51.
37. Chang T, Li L, Yang Y, Li M, Qu Y, Gao L. Transcranial Doppler ultrasonography for the management of severe traumatic brain injury after decompressive craniectomy. World Neurosurg. 2019;126:e116.
38. Ziegler D, Cravens G, Poche G, Gandhi R, Tellez M. Use of transcranial Doppler in patients with severe traumatic brain injuries. J Neurotrauma [Internet]. 2017 [cited 2020 Jan 19];34(1):121–7. Available from: http://www.liebertpub.com/doi/10.1089/neu.2015.3967
39. CDC, Acep. Updated mild traumatic brain injury guideline for adults [Internet]. [cited 2020 Jan 19]. Available from: www.cdc.gov/TraumaticBrainInjury
40. McAllister TW, Sparling MB, Flashman LA, al. et. Neuroimaging findings in mild traumatic brain injury. J Clin Exp Neuropsychol. 2001;23:775–91.
41. Vos PE, de la Plata CM, Diaz-Arrastia R. Neuroimaging in traumatic brain injury. In: Traumatic brain injury [Internet]. Chichester, UK: Wiley; 2014. [cited 2020 Jan 18]. p. 13–42. Available from: http://doi.wiley.com/10.1002/9781118656303.ch2.
42. Wintermark M, Sanelli PC, Anzai Y, Tsiouris AJ, Whitlow CT. Imaging evidence and recommendations for traumatic brain injury: conventional neuroimaging techniques. J Am Coll Radiol. 2015;12(2):e1–14.
43. Amyot F, Arciniegas DB, Brazaitis MP, et al. A review of the effectiveness of neuroimaging modalities for the detection of traumatic brain injury. J Neurotrauma [Internet]. 2015;32(22):1693–721. Available from: https://www.ncbi.nlm.nih.gov/pmc/articles/PMC4651019/
44. Lee B, Newberg A. Neuroimaging in traumatic brain imaging. NeuroRx. 2005;2(2):372–83.

Traumatic Brain Injury – Pediatric

Francisco Abecasis

Traumatic brain injury (TBI) is the leading cause of trauma-related death and permanent disability in children. Worldwide, it affects more than three million children annually [1] and in the United States alone, TBI contributes to the death of more than 1000 children every year [2].

When a child is admitted to the hospital after a moderate or severe TBI, management is targeted at avoiding secondary damage to the injured brain. In order to achieve this goal, maintaining an adequate cerebral blood flow (CBF) is crucial. Guidelines have traditionally used intracranial pressure (ICP) monitoring and treatment of increased ICP as the main objective to improve outcome following TBI. In children, adequate randomized controlled studies to evaluate the role of ICP monitoring and treatment have not been performed and the strength of recommendation of the latest guidelines on ICP monitoring and ICP treatment thresholds is weak (Level III) [3].

Cerebral perfusion pressure (CPP) is defined as the difference between mean arterial blood pressure (ABP) and mean ICP, and it is the pressure gradient driving cerebral blood flow. In normal

F. Abecasis (✉)
Pediatric Intensive Care Unit, Centro Hospitalar Universitário Lisboa Norte, Hospital de Santa Maria, Lisbon, Portugal
e-mail: francisco@abecasis.name

W. C. Ziai, C. L. Cornwell (eds.), *Neurovascular Sonography*,
https://doi.org/10.1007/978-3-030-96893-9_13

conditions, CBF is autoregulated to maintain an adequate oxygen and glucose delivery to the brain across physiological range of CPP. After TBI, cerebral autoregulation might be impaired and decreases in CPP could lead to cerebral ischemia. Thresholds for adequate CPP in children with TBI have recently been published suggesting that CPP targets should be age-specific: above 40 mmHg in children under 6 years-old and above 50 mmHg in children from 6 to 17 years-old [4]. If CPP is the driving pressure of CBF, it is logical that treatment protocols should focus on CPP, rather then on ICP. CPP by definition can be manipulated by changing ICP or ABP.

Traditionally, an ICP bolt and an arterial line are used to monitor ICP and CPP invasively. In children, invasive ICP-CPP monitoring is reserved for patients in whom the severity of the clinical conditions demand ICP-CPP guided treatment. Otherwise, the risks associated with invasive neuromonitoring, such as bleeding and infection, may not represent a beneficial intervention. In these cases, non-invasive methods, like transcranial Doppler ultrasonography (TCD), for assessment of these parameters could offer an alternative for treatment or a screening tool to determine the need for invasive monitoring.

Role of transcranial Doppler ultrasonography on Pediatric TBI:

Non-invasive Estimate of ICP

One of the most studied roles of TCD in TBI is the ability to estimate or predict ICP non-invasively.

There are two indices commonly used to estimate ICP with TCD:

- Resistance index (Pourcelot) [5]:
  - (peak systolic velocity – end diastolic velocity)/peak systolic velocity
- Pulsatility index (Gosling) [6]:
  - (peak systolic velocity – end diastolic velocity)/mean velocity

Although the accuracy of TCD to estimate ICP in adult patients with TBI has been studied over the years with generally good results [7], there is less evidence in children and results are conflicting. Some authors state that transcranial Doppler pulsatility index is not a reliable indicator of intracranial pressure in children with severe traumatic brain injury, based in data from 34 children and 275 examinations [8]. A threshold PI of 1 was used to detect ICP 20 mm Hg or higher and the sensitivity and specificity was 25% and 88%, respectively. But if the PI threshold was increased to 1.2 the specificity would be 100%. This is in line with our experience that a high PI, in face of a normal arterial pressure and normal pCO2, implies a high ICP. There are also studies with good results in children [9–11]. The largest study, included 117 children with severe TBI and PI >1.31 had a sensitivity of 94% and a specificity of 41% to identify patients with ICP >20 mmHg. The authors conclude that TCD examination is a safe, reproducible, and reliable method to identified children at increased risk of ICH and decreased CPP after severe TBI, and its use should be encouraged in PICU [11]. In our own experience we evaluated 18 children with severe TBI with TCD and invasive ICP. Sixteen patients had ICP values above 20 mmHg, with a mean highest value of 35.7 ± 11.2 mmHg. The first measurement of PI had a mean of 1.12 ± 0.33. There was a significant correlation between the first PI determination and the corresponding ICP value (Pearson correlation coefficient $r = 0.755$, $p < 0.0001$) [10].

Other studies on mathematical models for continuous non-invasive ICP prediction using simultaneous measurements of systemic arterial blood pressure and transcranial Doppler flow velocity waveforms have shown better ability of TCD to estimate and track ICP changes [12–14].

In summary, TCD can accurately predict a raised ICP in pediatric TBI, especially if a higher cut-off value for PI is used. In our clinical practice we use a threshold of 1.4 using the Gosling PI. We have to take into consideration arterial blood pressure and pCO2 as these parameters can change PI and give false negatives, in case of arterial hypertension, and false positives, in case of hypotension or hyperventilation. This non-invasive technique can be extremely useful at admission to help determine the level of

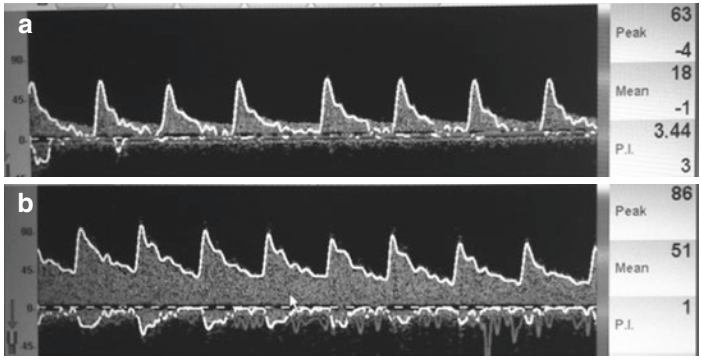

Fig. 1 TCD examinations in a 17-year-old girl with severe TBI revealing severe compromise of blood flow in the left middle cerebral artery (**a**). After draining a large subdural hematoma, TCD showed normal velocities and PI (**b**)

care and prioritize actions to take in children who suffered a TBI [15]. This is best exemplified by the case of a patient where TCD at admission revealed a very high PI and prompted an emergent surgery instead of invasive ICP monitoring in the PICU (Fig. 1).

Non-invasive Estimate of CPP

Among the several non-invasive methods reported for CPP assessment (nCPP) [7, 16, 17], ultrasound-based alternatives are of special interest since these techniques are low-cost and widely available in the neurocritical care settings. TCD has been one of the most used methods for determination of nCPP in TBI [7]. Several studies have tested the feasibility of TCD for these purposes in children [8, 11, 18]. Although Figaji et al. concluded that PI was not a reliable indicator of ICP, they found that the correlation of PI with CPP was much better and significantly related ($p = 0.001$) [8]. These data were corroborated in more recent stud-

ies that found a sensitivity of 80% of PI to detect a CPP of less than 50 mmHg [11] and in another study where a novel estimator of CPP was calculated using TCD-spectral accounting method that showed a good correlation of nCPP and CPP (Spearman correlation coefficient, $R = 0.67$ ($p < 0.0001$) and the ability of nCPP to predict values of CPP below 70 mmHg was excellent as demonstrated by an area under the curve of 0.91 (95% CI = 0.83–0.98) using a receiver operating curve analysis [18].

It is not a surprise that PI correlates better with CPP than with ICP. It has been elegantly demonstrated by de Riva et al. that PI is not dependent solely on cerebrovascular resistance but it is a product of the interplay between CPP, pulse amplitude of arterial pressure, cerebrovascular resistance and compliance of the cerebral arterial bed as well as the heart rate. Therefore, PI is not an accurate estimator of ICP and it describes CPP in a more accurate manner [19]. This is consistent with our practice where we have found cases of pediatric TBI with high PI and normal ICP in patients with low arterial blood pressure (Fig. 2) [15].

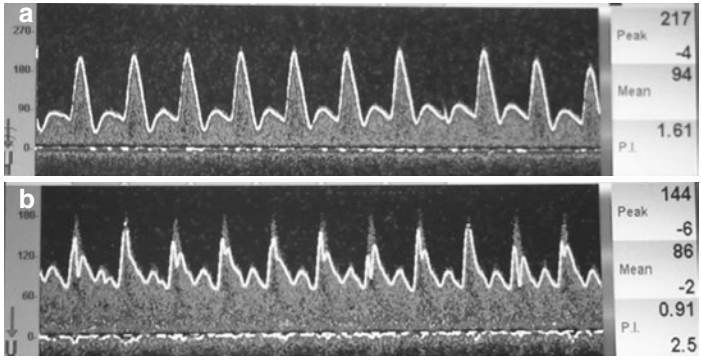

Fig. 2 TCD of a 16-year-old girl with severe TBI with normal ICP and raised PI due to hypovolemic shock and decreased CPP (**a**). PI and CPP improved after fluid boluses in order to optimize cerebral blood flow (**b**)

Autoregulation and Continuous Monitoring of TCD Signals

Cerebrovascular autoregulation is a hemodynamic mechanism that allows cerebral blood flow to remain constant with changes of CPP. This is fundamental to protect the brain against inappropriate CBF. If cerebrovascular autoregulation is impaired, CBF becomes dependent on CPP and any changes in arterial blood pressure will reflect directly on CBF. It has been shown that after a TBI, impaired autoregulation is independently associated with a worse outcome and mortality [20–22].

The requirements to measure and monitor dynamic autoregulation over time are:

- Continuous arterial blood pressure monitoring (invasive or non-invasive)
- A surrogate for CBF:
  - Non-invasive (TCD, Near-infrared spectroscopy – NIRS)
  - Invasive (PbtO2, ICP, Laser Doppler Flow)
- A mathematical model to quantificate the relationship between ABP and CBF
  - Time domain analysis (PRx, COx, Mx, Lx, ORx)
  - Frequency domain analysis (coherence, gain of transfer, phase shift)

In the case of TCD, autoregulation monitoring uses the signals of ABP, ICP and cerebral blood flow velocities to calculate indices of autoregulation [23]:

- Mx index is the correlation coefficient between mean flow velocity and CPP
- Sx index is the correlation coefficient between systolic flow velocity and CPP

If Mx and Sx are positive it means autoregulation is impaired and this is associated with a bad outcome after TBI. In the example below, we can see a patient with adequate autoregulation and a negative Mx (Fig. 3).

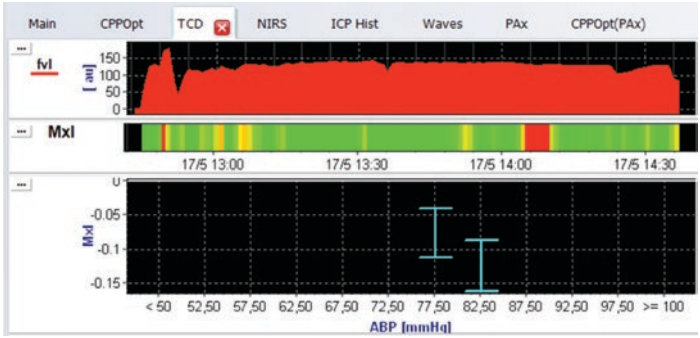

Fig. 3 Monitoring of blood flow velocity in the left mean cerebral artery for a period of 2 h using TCD. Mx is almost always negative indicating a preserved cerebrovascular autoregulation

One of the major challenges in using TCD signals to evaluate autoregulation is the necessity to be able to record flow velocities for a long period of time. This can be accomplished with probe holders, but the signal can be lost with positioning of the patient or spontaneous movement. Children represent an additional challenge because of different head sizes and some holders are difficult to use in small children. More recently, new devices using robotic probes allow for continuous monitoring over extended time periods with good results for at least 4 hours of monitoring [24].

In summary, dynamic cerebrovascular autoregulation monitoring can be done non-invasively with TCD but it is difficult to accomplish due to the necessity of long-term acquisition of the TCD signals. New technological advances in this area will make it more usable in clinical practice.

Detect Regional Variations on Cerebral Hemodynamics

One of the challenges in studying the injured brain is that many devices only allow for measurements in one particular area of the brain. This is the case with ICP bolts or PbtO2 probes. TCD has

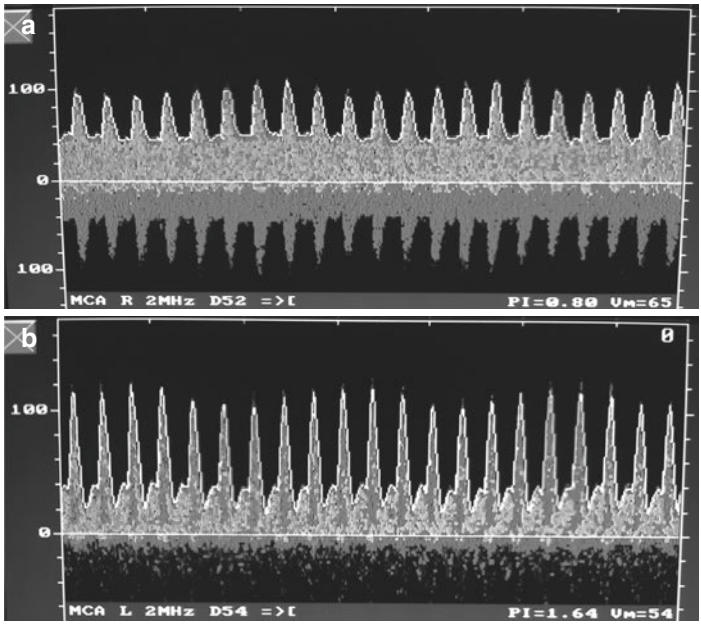

Fig. 4 TCD at admission of an eight-year-old boy with severe TBI after a road traffic accident. (**a**) Right middle cerebral artery with normal flow velocities and PI of 0.80. (**b**) Left middle cerebral artery with low diastolic flow velocity and PI of 1.64, compatible with raised ICP/low CPP

the major advantage of allowing insonation of different territories. This is particularly important in pathologies like TBI that can have focal lesions. Although a raised ICP, especially if severe, will ultimately be transmitted to the whole brain, we have found cases with important asymmetries at an initial phase (Fig. 4).

Diagnosis of Brain Death

Use of TCD as a tool to aid in the diagnosis of brain death is beyond the scope of this chapter. Nonetheless, TBI is one of the major indications for organ donation and TCD can identify cerebral circulatory arrest and can be extremely useful in determined circumstances. Although TCD is not accepted in all countries for

the diagnosis of brain death, it is commonly used in others. The indications for using an ancillary test of no cerebral blood flow are:

- Impossibility to complete components of the examination or the apnea test
- Uncertainties about the results of the neurological examination
- If a medication effect may be present
- To allow a shorter period of time between the two examinations (in children an interval of 12 h is necessary if no ancillary test is used)

In our practice we use TCD in every patient that is considered for organ donation. We find it reassuring for both family members and staff.

Conclusions

An experienced operator only needs a few minutes to understand if CBF is normal or compromised when performing a TCD. PI is calculated instantaneously and, as previously described, it will be high in cases with decreased CPP. This can be extremely useful for point of care decisions at the bedside in cases of pediatric TBI.

Although TCD can and has been used for cerebrovascular autoregulation monitoring this is more difficult to accomplish in clinical practice and is often performed in investigation settings. New technological advances will make this tool easier to use and help guide patient management.

References

1. Dewan MC, Mummareddy N, Wellons JC, Bonfield CM. Epidemiology of global pediatric traumatic brain injury: qualitative review. World Neurosurg. 2016;91:497–509.e1. https://doi.org/10.1016/j.wneu.2016.03.045.
2. Taylor CA, Bell JM, Breiding MJ, Xu L. Traumatic brain injury–related emergency department visits, hospitalizations, and deaths — United

States, 2007 and 2013. MMWR Surveill Summ. 2017;66:1–16. https://doi.org/10.15585/mmwr.ss6609a1.
3. Kochanek PM, Tasker RC, Carney N, et al. Guidelines for the management of pediatric severe traumatic brain injury, third edition. Pediatr Crit Care Med. 2019;20:S1–S82. https://doi.org/10.1097/PCC.0000000000001735.
4. Allen BB, Chiu Y, Gerber LM, et al. Age-specific cerebral perfusion pressure thresholds and survival in children and adolescents with severe traumatic brain injury. Pediatr Crit Care Med. 2014;15:62–70. https://doi.org/10.1097/PCC.0b013e3182a556ea.
5. Planiol T, Pourcelot L, Pottier JM, Degiovanni E. [Study of carotid circulation by means of ultrasonic methods and thermography]. Rev Neurol (Paris). 1972;126:127–41.
6. Gosling R, King D. Arterial assessment by Doppler-shift ultrasound. Proc Roy Soc Med. 1974;67:447–9.
7. Cardim D, Robba C, Bohdanowicz M, et al. Non-invasive monitoring of intracranial pressure using transcranial Doppler ultrasonography: is it possible? Neurocrit Care. 2016;25:473–91. https://doi.org/10.1007/s12028-016-0258-6.
8. Figaji AA, Zwane E, Fieggen AG, et al. Transcranial Doppler pulsatility index is not a reliable indicator of intracranial pressure in children with severe traumatic brain injury. Surg Neurol. 2009;72:389–94. https://doi.org/10.1016/j.surneu.2009.02.012.
9. O'Brien NF, Maa T, Reuter-Rice K. Noninvasive screening for intracranial hypertension in children with acute, severe traumatic brain injury. J Neurosurg Pediatr. 2015;16:420–5. https://doi.org/10.3171/2015.3.PEDS14521.
10. Vieira F, Cardoso K, Abecasis F, et al. Doppler transcraniano na monitorização do traumatismo craniencefálico grave em pediatria. Acta Pediátrica Port. 2012;43:239–45.
11. Melo JRT, Di Rocco F, Blanot S, et al. Transcranial Doppler can predict intracranial hypertension in children with severe traumatic brain injuries. Childs Nerv Syst. 2011;27:979–84. https://doi.org/10.1007/s00381-010-1367-8.
12. Schmidt B, Czosnyka M, Raabe A, et al. Adaptive noninvasive assessment of intracranial pressure and cerebral autoregulation. Stroke. 2003;34:84–9. https://doi.org/10.1161/01.STR.0000047849.01376.AE.
13. Kashif FM, Verghese GC, Novak V, et al. Model-based noninvasive estimation of intracranial pressure from cerebral blood flow velocity and arterial pressure. Sci Transl Med. 2012;4:129ra44-129ra44. https://doi.org/10.1126/scitranslmed.3003249.
14. Cardim D, Schmidt B, Robba C, et al. Transcranial Doppler monitoring of intracranial pressure plateau waves. Neurocrit Care. 2016;1–9 https://doi.org/10.1007/s12028-016-0356-5.

15. Abecasis F, Oliveira V, Robba C, Czosnyka M. Transcranial Doppler in pediatric emergency and intensive care unit: a case series and literature review. Childs Nerv Syst. 2018;34:1465–70. https://doi.org/10.1007/s00381-018-3877-8.
16. Robba C, Bacigaluppi S, Cardim D, et al. Non-invasive assessment of intracranial pressure. Acta Neurol Scand. 2015; https://doi.org/10.1111/ane.12527.
17. Zhang X, Medow JE, Iskandar BJ, et al. Invasive and noninvasive means of measuring intracranial pressure: a review. Physiol Meas. 2017;38:R143–82.
18. Abecasis F, Cardim D, Czosnyka M, et al. Transcranial Doppler as a non-invasive method to estimate cerebral perfusion pressure in children with severe traumatic brain injury. Childs Nerv Syst. 2020;36:125–31. https://doi.org/10.1007/s00381-019-04273-2.
19. de Riva N, Budohoski KP, Smielewski P, et al. Transcranial Doppler pulsatility index: what it is and what it isn't. Neurocrit Care. 2012;17:58–66. https://doi.org/10.1007/s12028-012-9672-6.
20. Jaeger M, Schuhmann MU, Soehle M, Meixensberger J. Continuous assessment of cerebrovascular autoregulation after traumatic brain injury using brain tissue oxygen pressure reactivity. Crit Care Med. 2006;34:1783–8. https://doi.org/10.1097/01.CCM.0000218413.51546.9E.
21. Radolovich DK, Aries MJH, Castellani G, et al. Pulsatile intracranial pressure and cerebral autoregulation after traumatic brain injury. Neurocrit Care. 2011;15:379–86. https://doi.org/10.1007/s12028-011-9553-4.
22. Chaiwat O, Sharma D, Udomphorn Y, et al. Cerebral hemodynamic predictors of poor 6-month Glasgow outcome score in severe pediatric traumatic brain injury. J Neurotrauma. 2009;26:657–63. https://doi.org/10.1089/neu.2008.0770.
23. Czosnyka M, Smielewski P, Kirkpatrick P, et al. Monitoring of cerebral autoregulation in head-injured patients. Stroke. 1996;27:1829–34. https://doi.org/10.1161/01.STR.27.10.1829.
24. Zeiler FA, Smielewski P. Application of robotic transcranial Doppler for extended duration recording in moderate/severe traumatic brain injury: first experiences. Crit Ultrasound J. 2018;10:16. https://doi.org/10.1186/s13089-018-0097-0.

Cerebrovascular Reactivity Assessments in Traumatic Brain Injury

Alwyn Gomez and Frederick A. Zeiler

Introduction

Cerebral autoregulation (CA) refers to the innate ability of the cerebral vasculature to maintain a relatively constant cerebral blood flow (CBF), in response to fluctuations in systemic mean arterial pressure (MAP) or cerebral perfusion pressure (CPP) [1, 2]. This CBF regulation is dictated by small-to-medium sized vessels, measuring up to a few hundred microns in diameter [3–6]. To date, validated continuous measures of CA in humans have been lacking. The term cerebrovascular reactivity, sometimes used in

A. Gomez
Section of Neurosurgery, Department of Surgery, Rady Faculty of Health Sciences, University of Manitoba, Winnipeg, MB, Canada

F. A. Zeiler (✉)
Section of Neurosurgery, Department of Surgery, Rady Faculty of Health Sciences, University of Manitoba, Winnipeg, MB, Canada

Department of Human Anatomy and Cell Science, Rady Faculty of Health Sciences, University of Manitoba, Winnipeg, MB, Canada

Biomedical Engineering, Faculty of Engineering, University of Manitoba, Winnipeg, MB, Canada

Division of Anaesthesia, Department of Medicine, Addenbrooke's Hospital, University of Cambridge, Cambridge, UK
e-mail: Frederick.Zeiler@umanitoba.ca

W. C. Ziai, C. L. Cornwell (eds.), *Neurovascular Sonography*,
https://doi.org/10.1007/978-3-030-96893-9_14

place of CA, describes the cerebrovascular response as measured through either dynamic or static means. When intact, the brain is able to maintain a consistent and sufficient cerebral blood flow during fluctuations in CPP over a given range. This is one of the major mechanisms by which the brain protects itself in situations where CPP may become unstable [7]. Static CA describes the extent to which the cerebral vasculature can accommodate variations in CPP varies and dynamic CA describes the rate at which such changes occur. It has been known for some time now that CA can be disrupted in a number of situations including chronic hypertension [8], ischemic stroke [9], subarachnoid hemorrhage [10, 11], infection [12], and traumatic brain injury (TBI) [13–15].

The past two decades have seen a marked increase in the examination of cerebrovascular reactivity following TBI. This stems from advances in bedside biomedical signal acquisition and processing techniques, designed to provide continuous uninterrupted metrics of cerebrovascular reactivity derived from various multimodal cerebral physiologic monitoring devices. Extensive literature has emerged documenting the strong association between impaired cerebrovascular reactivity and poor global outcome in adult TBI [16–19]. Furthermore, recent multi-centre prospective data supports the independent prognostic significance of cerebrovascular reactivity monitoring, above and beyond ICP monitoring, in TBI [20–22].

Current Standard Monitoring of Cerebrovascular Reactivity in TBI

Various indices for continuously examining cerebrovascular reactivity status have been described based on different invasive/non-invasive cerebral physiologic monitoring devices. Such indices are derived through evaluating the correlation between slow-wave vasogenic fluctuations in a surrogate measure of pulsatile cerebral blood volume/CBF, and a driving pressure for flow, such as MAP or CPP [23, 24]. Arguably the current favoured continuous index is the pressure reactivity index (PRx), which is the correlation between slow-wave vasogenic fluctuations in intracranial pressure (ICP) and mean arterial pressure (MAP) [25]. PRx requires insertion of an invasive ICP monitor and continuous blood pres-

sure monitoring. It is calculated as a Pearson correlation coefficient between 10-second averaged signals of ICP and MAP over a 5-minute window. This index has been extensively studied and demonstrates a strong association with patient outcomes following TBI, with negative values believed to denote 'intact' cerebrovascular reactivity, and positive values believed to represent 'impaired' reactivity [26]. PRx has received some experimental validation as a measure of the lower limit of autoregulation in animal models of arterial hypotension and intra-cranial hypertension [27–29]. There has also been recent work that has identified clinically relevant thresholds for morbidity and mortality at 6 months post-TBI [19]. Additionally, there is evidence to support the association of PRx-derived personalized CPP targets (referred to as CPP optimum or CPPopt) [30], and ICP targets (termed individual ICP threshold (iICP)) [31], and global outcomes. In the future this may drive targeted therapy following TBI, however, further prospective studies are still required.

While there is much promise in PRx guided therapy, its invasive nature and requirement for intracranial placement of a monitoring device limits it's utility to examining cerebrovascular reactivity in the acute setting where ICP monitoring is indicated. Additionally, PRx utilizes fluctuations in ICP as a surrogate for fluctuations in total cerebral blood volume and therefore its reliability post-hemicraniectomy is questionable as the pressure-volume relationship is altered [32]. These limitations have expanded the search for alternative methods of monitoring cerebrovascular reactivity in TBI. Examination into indices that correlate tissue oxygenation with MAP have been developed in both invasive and non-invasive forms but are subject to interference from systemic factors that can alter tissue oxygenation (FiO_2, cardiovascular status, pulmonary gas exchange, hemoglobin level etc.) [17, 33, 34].

Application of TCD for Cerebrovascular Reactivity Monitoring in TBI

Transcranial Doppler (TCD) ultrasonography provides a relatively inexpensive and non-invasive real-time measurement of blood flow metrics in the cerebral vasculature. Ultrasound waves from the Doppler probe are transmitted through the calvarium and

reflected by moving red blood cells within the cerebral vessels. The resultant shift in frequency from the transmitted signal to the reflected signal is proportional to the blood flow velocity. This non-invasive method of determining blood flow velocities, usually through the middle cerebral artery (MCA), can be utilized to monitor cerebrovascular reactivity by utilizing flow velocities (FV) as a surrogate for cerebral blood flow. This assumption is true so long as the caliber of the MCA remains relatively constant [35]. By comparing vasogenic slow-wave fluctuations in FV in response to fluctuations in arterial pressure, information can be gleaned about the state of cerebrovascular reactivity.

TCD derived assessment of cerebrovascular reactivity in TBI can be performed in an intermittent or continuous fashion. While both take advantage of the time resolution of TCD to provide information about dynamic vascular reactivity, the methods by which they gather this information is different. Intermittent TCD techniques generally require observing the dynamic changes in cerebrovascular reactivity following an initiated perturbance in systemic blood pressure over a short period of time and give a single 'snap-shot' measure. Continuous methods allow the assessment of autoregulation following spontaneous changes in systemic blood pressure and provide a regularly updating index of cerebrovascular reactivity status, and a more attractive method for bedside monitoring in TBI. The following sub-sections outline briefly the intermittent and continuous cerebrovascular reactivity techniques, with the main focus on continuous methodology.

Intermittent Methodologies

Various intermittent techniques utilizing TCD to assess cerebrovascular reactivity exist, including: rate of regulation (RoR), thigh cuff deflation technique (TCDT), transient hyperemic response testing (THRT), orthostatic response testing (ORT), and autoregulation index (ARI) derivation. We only mention exemplar techniques below, and refer the reader to recently published reviews on the topic for more details [36]. Table 1 provides a list of the intermittent TCD based techniques, advantages and disadvantages.

Table 1 TCD-based intermittent cerebrovascular reactivity measurement techniques

Technique	Advantages	Disadvantages
Thigh Cuff Deflation Technique based Autoregulatory Index (TCDT-ARI)	Predefined normal/abnormal range	Not suitable for those with cardiac preload dependence Requires specialized set-up for cuffs, and second order differential equation modelling
Transient Hyperemic Response Testing (THRT)	Validated threshold for intact autoregulation	Majority of literature only assesses concordance with other measures of autoregulation
Orthostatic Response Testing (ORT)		Difficult to perform in the ICU setting, and requires specialized set-up Small body of literature evaluating accuracy
TCD based Mean Flow Index (Mx)	Previously identified thresholds (+0.05 and + 0.30) for increased mortality and poor outcomes [37]. Literature showing strong association with patient outcomes	Requires invasive ICP monitoring Data mainly generated from single institution
Transfer Function Autoregulatory Index (TF-ARI)	TF-ARI associated with GOS at 6–12 months post-TBI	Technically complex and requires specialized expertise Data mainly generated from single institution

ARI transfer function autoregulatory index, *ICP* intracranial pressure, *ICU* intensive care unit, *GOS* Glasgow Outcome Scale, *Mx* mean flow index (correlation between slow-waves of mean TCD flow velocity (FVm) and cerebral perfusion pressure (CPP); considered a 'semi-intermittent' technique given typical short duration recording related to technique limitations), *ORT* orthostatic response testing, *TCD* transcranial Doppler, *TCDT* thigh cuff deflation technique, *THRT* transient hyperemic response testing

One of the earliest studied intermittent TCD derived assessments of CA is the Thigh Cuff Deflation Technique (TCDT) first described in 1989 [38]. This method involves the use of bilateral thigh cuffs inflated for 2–3 minutes above SBP, producing a vasodilatory state given the reduction in cardiac preload. Rapid deflation of the cuffs results in a dramatic drop in the MAP. This is usually sustained for a period of up to 30 seconds with an adequate test defined as at least a 15–20 mm Hg drop in pressure from baseline. This sudden decrease in BP is subsequently followed by a reflex cerebral vascular response to correct for the change in blood pressure. TCD is utilized to measure the cerebral blood flow velocity (CBFV) within the MCA and cerebrovascular resistance (CVRes) estimated by dividing ABP by CBFV (Eq. 1).

$$\text{CVRes} = \frac{\text{ABP}}{\text{CBFV}} \tag{1}$$

$$\text{RoR} = \frac{\text{CVRes}}{\text{T}} \div \text{ABP} \tag{2}$$

Two metrics have been derived from the TCDT that are utilized to describe the state of CA. The first was the rate of regulation (RoR) which can be understood as the change of CVRes over change in time (T) per change in ABP (Eq. 2) and with value of 0.2/second being considered normal [38]. The second was introduced by Tiecks et al. in 1995 and is known as autoregulation index (ARI). This method uses a second order differential model of CA to construct a grading of overall level of autoregulation on the scale of 0 (complete loss of autoregulation) to 9 (hyperactive regulatory response) with normal CA defined as an ARI of 4–7, and abnormal as 3 and below. The ARI is obtained by normalizing the TCD based CBFV changes recorded during the step change in MAP. The resultant plot is then compared to the model generated responses corresponding to the 10 grades. The model that represents the best fit constitutes the ARI. The mathematics behind this complex index is far beyond the scope of this chapter but the authors direct any interested reader to the original article for full details of this calculation [39].

Continuous Methodologies

By evaluating the relationship between spontaneous vasogenic slow-wave fluctuations in TCD based cerebral blood flow velocity (CBFV), and MAP or CPP, one can provide a continuous assessment of cerebrovascular reactivity. Utilizing various components of the CBFV waveform, such as the mean FV (FVm), systolic FV (FVs) or diastolic FV (FVd), different metrics of cerebrovascular reactivity may be derived. Table 2 provides a summary of the TCD derived indices of cerebrovascular reactivity.

Table 2 Continuous besides TCD-based cerebrovascular reactivity measures

Index	Correlation variables	Advantages	Disadvantages
Mx	FVm, CPP	Most extensively examined index Defined thresholds for morbidity and mortality [37] Provides surrogate assessment of cortical pial cerebrovascular reactivity [40]	Requires invasive ICP monitoring
Sx	FVs, CPP	Strong Association with outcomes [41, 42] Strong Association with PRx [34, 41–44] Defined thresholds for morbidity and mortality [42]	Requires invasive ICP monitoring
Dx	FVd, CPP		Requires invasive ICP monitoring Poor association with global outcome and other TCD and non-TCD continuous metrics Poorly defined thresholds Performs poorly during elevated ICP

(continued)

Table 2 (continued)

Index	Correlation variables	Advantages	Disadvantages
Mx-a	FVm, MAP	Does not require invasive ICP monitoring Thresholds defined for morbidity and mortality [37]	Weaker outcome association compared to Mx
Sx-a	FVs, MAP	Does not require invasive ICP monitoring Strong association with outcomes Strong association with PRx [43, 44] Defined thresholds for morbidity and mortality [42]	Weaker outcome association compared to Sx
Dx-a	FVd, MAP	Does not require invasive ICP monitoring	Poor outcome association Poorly defined thresholds for morbidity and mortality Performs poorly during elevated ICP

CPP Cerebral perfusion pressure, *MAP* Mean arterial pressure, *FVm* Mean flow velocity, *FVs* Systolic flow velocity, *FVd* Diastolic flow velocity

The most commonly described TCD based cerebrovascular reactivity index in TBI is mean flow index (Mx), derived from the correlation between slow-wave fluctuations in FVm and CPP. Conceptually, the response of FVm, a surrogate measure of pulsatile CBF, to slow-waves in CPP, a driving pressure for flow, are believed to be determined by cerebrovascular reactivity capacity. Like PRx, continuous recording of MAP and ICP are required for determination of CPP (based on: CPP = MAP – ICP). Additionally, TCD ultrasound is used to capture the middle cerebral artery (MCA) velocity. The signals are recorded and stored, with the option of both off-line and real-time calculation.

Specifically, the TCD based Mx is calculated by replacing original FVm and CPP by times series composed of their non-overlapping 10s averages (i.e. FVm and CPP are processed via a 10-second moving average filter and sampling frequency decimated to 0.1 Hz). The correlation coefficient (Mx) is then calculated based on 30 consecutive readings of those 10-second mean values (i.e. 5 minutes), with the coefficient updated every 10 seconds or 60 seconds, depending on recording durations. Ideally, Mx is typically averaged on a minimum period of 30 minutes to reduce its inherent variance. Again, negative values are believed to represent 'intact' reactivity, while positive values represent 'impaired' reactivity. Of note, to date there are no experimental studies validating these measures as metrics of CA capacity.

Some variations in TCD derived indices of CA have been described. These include Sx and Dx which are similar to Mx except they substitute FVm with FVs or FVd respectively. Another permutation of these indices eliminates the need for ICP monitoring by substituting CPP for simply MAP. Denoted as Mx-a, Sx-a or Dx-a, they still utilize the TCD derived signals FVm, FVs, or FVd respectively. Recent work employing semi-automatic machine learning methodologies appears to suggest these indices provide different information regarding cerebrovascular reactivity in TBI. Measures based on FVm appear to be more representative of cortical pial microcirculatory cerebrovascular reactivity and CBF-based measures [40]. Systolic/diastolic based metrics appear to be more closely related to invasively derived and near infrared based measures, suggesting they represent pulsatile CBV based reactivity [34, 40, 42]. Derivation method of diastolic and systolic indices, as well as the MAP-based alternatives, are outlined in Table 2. Finally, if bilateral MCA insonation is conducted, hemispheric based cerebrovascular reactivity metrics may be derived [45, 46]. Figure 1 provides an example of the raw recorded physiology and derived indices utilizing bedside third party software.

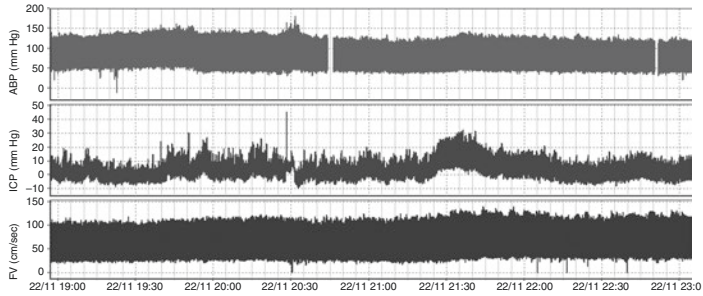

Fig. 1 Raw ABP, ICP and TCD Flow Velocity Signals. ABP arterial blood pressure, ICP intra-cranial pressure, FV flow velocity, mmHg millimetres of Mercury, TCD transcranial Doppler. (*Note: Image adapted from Zeiler et al. (with permission from corresponding author) [47])

Recent Advances in Continuous Cerebrovascular Reactivity Monitoring

A limitation in utilization of TCD in the derivation of continuous cerebrovascular reactivity indices is the labor-intensive nature of the bedside techniques, and interrupted nature of CBFV signal acquisition. Typical requirements of an operator are to make adjustments to maintain a good quality signal of FV. This practically limits current methodologies to 60-minute recording periods and is therefore more of a "semi-intermittent" technique in TBI monitoring. Recent advances in robotic technology have led to robotic TCD (rTCD) devices which allow for extended duration CBFV recordings, and have been employed in critically ill TBI patients for cerebrovascular reactivity monitoring [43, 47, 48]. Figure 2 demonstrates one of these currently available rTCD devices. These robotically driven TCD examination probes are integrated with automated algorithms for MCA CBFV detection as well as optimization of recorded signal intensity. Recent work published by the senior author has demonstrated continuous signal acquisition utilizing rTCD in excess of 4 hours [48]. Follow up work has demonstrated the utility of deriving personalized CA metrics such an optimal CPP (CPPopt) utilizing rTCD [47].

Fig. 2 Robotic TCD Device Example. TCD transcranial Doppler. (Panel **a**) Displays robotic TCD headframe with two robotic drives mounted to a ratcheting headband system. (Panel **b**) displays close up imagine of TCD probe encased in robotic drive. (Panel **c**) example of set up for multi-modal monitoring with left frontal triple bolt, (Panel **d**) Delica EMS 9D TCD program display, showing automatic flow velocity sampling algorithm, producing a square grid of sampled insonation positions. The system insonates at multiple sites, finding the area with superior signal quality). (*Figure is a color adaptation from Zeiler et al. (with permission from corresponding author) [47])

TCD Derived Indices in Adult TBI

Association with Global Outcome

Of all the variations in TCD based indices Mx has been the most extensively examined with one recent review identifying 17 studies with 50 or more patients documenting an association with patient outcome [26]. Mx has been found to be negatively correlated with mortality and morbidity at 6 months ($r = -0.34$, $p < 0.0025$; $r = 0.41$, $p < 0.0002$) [49]. From a clinical stand point, thresholds of +0.05 and +0.3 for Mx have been found to be associated with morbidity and mortality respectively [37]. As previously noted, Mx requires the measurement of CPP which is defined as the difference between ABP and ICP. Clinically, ICP is measured utilizing invasive intracranial probes or catheters. In recent years, there has been an increase in interest in the Mx-a as it does not require invasive intracranial monitoring as it relies on MAP and not CPP. A study was performed by Lang et al. in 2003 on 37 TBI patients in which impaired CA as indicated by both Mx and Mx-a was correlated with poor outcomes ($r = -0.56$, $p < 0.01$; $r = -0.42$, $p < 0.05$) [50]. These results were further supported in a larger study performed by Lui et al. in 2014 on 288 TBI patients which found that both Mx and Mx-a were significantly correlated with patient outcomes ($r = -0.404$, $p < 0.01$; $r = -0.38$, $p < 0.01$). It should be noted, however, that Mx was found to have a stronger association [51].

Which Component of TCD Flow Velocity Is Best?

As mentioned earlier some groups feel that more information about CA status can be gleaned from analysis of the waveform of the FV. In particular, assessing the correlation between FVs or FVd with CPP or MAP. In 2012 Budohoski et al. published a study on 300 TBI patients investigating the association between multiple TCD based indices (Mx, Mx-a, Sx, Sx-a, Dx, and Dx-a) and dichotomized 6-month outcomes. Somewhat surprisingly systolic

flow indices (Sx and Sx-a) were found to have a stronger association with outcome than the mean flow indices (Mx and Mx-a). This was irrespective of whether CPP or MAP was used for calculation [41]. Follow up work published by the senior author of this chapter in 2018 analyzed recordings from 347 TBI patients in order to explore relationships between TCD indices of CA and those derived from ICP. They were able to confirm a co-variance of Sx/Sx-a with PRx. Additionally, they were able to identify threshold values for unfavorable outcomes and mortality in Sx and Sx-a. Their most interesting finding was that TCD systolic indices (Sx and Sx-a) were the most closely associated with ICP indices and likely provide better approximation of ICP indices when compared to TCD diastolic and mean indices. This work identified TCD systolic indices as possibly the most promising TCD based index clinically [42].

Future for Entirely Non-invasive Means of Continuous Cerebrovascular Reactivity Monitoring

Given the body of research that points to the association of TCD based indices with morbidity and mortality and the co-variance they have with the gold standard PRx index there is now work being started on examining TCD based indices as a non-invasive alternative to PRx. In 2019 the senior author of this chapter was able to show in a small cohort of ten patients that it is possible to predict PRx using non-invasive TCD measures. That is to say, without any invasive intracranial monitoring. This was made possible by obtaining continuous extended duration time series recordings of MCA FV utilizing rTCD [43]. Given advances in continuous non-invasive blood pressure monitoring such as the Finapres NOVA and the growing evidence supporting the utility of TCD based indices of CA it may not be long before entirely non-invasive monitoring of CA may be possible. Figure 3 displays this non-invasive continuous full waveform ABP device.

Fig. 3 Non-Invasive Continuous Full Waveform ABP Monitoring Device. ABP arterial blood pressure. (Panel **a**) Photo of the Finapres NOVA non-invasive ABP monitor, (Panel **b**) Photo of analogue output ports on Finapres NOVA system, allowing full integration with other bedside monitoring and data acquisition platforms, (Panel **c**) Examples of wrist mounted and finger-tip based ABP monitoring system, (Panel **d**) example of continuous full waveform non-invasive ABP monitoring

While the possible benefits to patient safety are evident, perhaps the more intriguing prospect is that total non-invasive monitoring provides the ability to examine the progression of CA dysfunction past the acute phase of TBI and into the sub-acute and chronic phases. While there is still much work that needs to be done the insights it may review about CA could profoundly impact the way in which TBI is managed.

Conclusions

There is a growing body of evidence that is supporting the clinical utility of following cerebrovascular reactivity in patients following severe TBI. While there are numerous described surrogates for cerebral autoregulation methods, utilizing indices derived from TCD measurements are gaining favor given their relatively non-invasive nature, utility for prolonged assessment and mounting evidence of their correlation with outcomes. The future may find us targeting therapies following TBI based on TCD derived fully non-invasive metrics of cerebral autoregulation.

References

1. Lassen NA. Cerebral blood flow and oxygen consumption in man. Physiol Rev. 1959;39(2):183–238.
2. Fog M. The relationship between the blood pressure and the tonic regulation of the PIAL arteries. J Neurol Psychiatry. 1938;1(3):187–97.
3. Mchedlishvili G. Physiological mechanisms controlling cerebral blood flow. Stroke. 1980;11(3):240–8.
4. Hundley WG, Renaldo GJ, Levasseur JE, Kontos HA. Vasomotion in cerebral microcirculation of awake rabbits. Am J Phys. 1988;254(1 Pt 2):H67–71.
5. Halpern W, Osol G. Influence of transmural pressure of myogenic responses of isolated cerebral arteries of the rat. Ann Biomed Eng. 1985;13(3–4):287–93.
6. Auer LM, Ishiyama N, Pucher R. Cerebrovascular response to intracranial hypertension. Acta Neurochir. 1987;84(3–4):124–8.
7. Paulson OB, Strandgaard S, Edvinsson L. Cerebral autoregulation. Cerebrovasc Brain Metab Rev. 1990;2(2):161–92.
8. Shekhar S, Liu R, Travis OK, Roman RJ, Fan F. Cerebral autoregulation in hypertension and ischemic stroke: a mini review. J Pharm Sci Exp Pharmacol. 2017/10/27 ed. 2017, 2017;(1):21–7.
9. Aries MJH, Elting JW, De Keyser J, Kremer BPH, Vroomen PCAJ. Cerebral autoregulation in stroke: a review of transcranial Doppler studies. Stroke. 2010;41(11):2697–704.
10. Lam JM, Smielewski P, Czosnyka M, Pickard JD, Kirkpatrick PJ. Predicting delayed ischemic deficits after aneurysmal subarachnoid hemorrhage using a transient hyperemic response test of cerebral autoregulation. Neurosurgery. 2000;47(4):816–9.

11. Jaeger M, Soehle M, Schuhmann MU, Meixensberger J. Clinical significance of impaired cerebrovascular autoregulation after severe aneurysmal subarachnoid hemorrhage. Stroke. 2012;43(8):2097–101.
12. Schramm P, Klein KU, Falkenberg L, Berres M, Closhen D, Werhahn KJ, et al. Impaired cerebrovascular autoregulation in patients with severe sepsis and sepsis-associated delirium. Crit Care (London, England). 2012;16(5):R181.
13. Cold GE, Jensen FT. Cerebral blood flow in the acute phase after head injury. Part 1: correlation to age of the patients, clinical outcome and localisation of the injured region. Acta Anaesthesiol Scand. 1980;24(3):245–51.
14. Cold GE, Jensen FT. Cerebral autoregulation in unconscious patients with brain injury. Acta Anaesthesiol Scand. 1978;22(3):270–80.
15. Bruce DA, Langfitt TW, Miller JD, Schutz H, Vapalahti MP, Stanek A, et al. Regional cerebral blood flow, intracranial pressure, and brain metabolism in comatose patients. J Neurosurg. 1973;38(2):131–44.
16. Lam JM, Hsiang JN, Poon WS. Monitoring of autoregulation using laser Doppler flowmetry in patients with head injury. J Neurosurg. 1997;86(3):438–45.
17. Jaeger M, Schuhmann MU, Soehle M, Meixensberger J. Continuous assessment of cerebrovascular autoregulation after traumatic brain injury using brain tissue oxygen pressure reactivity. Crit Care Med. 2006;34(6):1783–8.
18. Radolovich DK, Aries MJH, Castellani G, Corona A, Lavinio A, Smielewski P, et al. Pulsatile intracranial pressure and cerebral autoregulation after traumatic brain injury. Neurocrit Care. 2011;15(3):379–86.
19. Sorrentino E, Diedler J, Kasprowicz M, Budohoski KP, Haubrich C, Smielewski P, et al. Critical thresholds for cerebrovascular reactivity after traumatic brain injury. Neurocrit Care. 2012;16(2):258–66.
20. Czosnyka M, Miller C. Monitoring of cerebral autoregulation. Neurocrit Care. 2014;21 Suppl 2:S95–102.
21. Zeiler FA, Ercole A, Beqiri E, Cabeleira M, Thelin EP, Stocchetti N, et al. Association between cerebrovascular reactivity monitoring and mortality is preserved when adjusting for baseline admission characteristics in adult TBI: a CENTER-TBI study. J Neurotrauma. 2019;
22. Zeiler FA, Ercole A, Cabeleira M, Zoerle T, Stocchetti N, Menon DK, et al. Univariate comparison of performance of different cerebrovascular reactivity indices for outcome association in adult TBI: a CENTER-TBI study. Acta Neurochir. 2019;161(6):1217–27.
23. Fraser CD, Brady KM, Rhee CJ, Easley RB, Kibler K, Smielewski P, et al. The frequency response of cerebral autoregulation. J Appl Physiol. 2013;115(1):52–6.

24. Howells T, Johnson U, McKelvey T, Enblad P. An optimal frequency range for assessing the pressure reactivity index in patients with traumatic brain injury. J Clin Monit Comput. 2015;29(1):97–105.
25. Czosnyka M, Smielewski P, Kirkpatrick P, Laing RJ, Menon D, Pickard JD. Continuous assessment of the cerebral vasomotor reactivity in head injury. Neurosurgery. 1997;41(1):11–9.
26. Calviello LA, Donnelly J, Zeiler FA, Thelin EP, Smielewski P, Czosnyka M. Cerebral autoregulation monitoring in acute traumatic brain injury: what's the evidence? Minerva Anestesiol. 2017;83(8):844–57.
27. Zeiler FA, Lee JK, Smielewski P, Czosnyka M, Brady K. Validation of intracranial pressure-derived cerebrovascular reactivity indices against the lower limit of autoregulation, part II: experimental model of arterial hypotension. J Neurotrauma. 2018;35(23):2812–9.
28. Zeiler FA, Donnelly J, Calviello L, Lee JK, Smielewski P, Brady K, et al. Validation of pressure reactivity and pulse amplitude indices against the lower limit of autoregulation, part I: experimental intracranial hypertension. J Neurotrauma. 2018;35(23):2803–11.
29. Brady KM, Lee JK, Kibler KK, Easley RB, Koehler RC, Shaffner DH. Continuous measurement of autoregulation by spontaneous fluctuations in cerebral perfusion pressure: comparison of 3 methods. Stroke. 2008;39(9):2531–7.
30. Needham E, McFadyen C, Newcombe V, Synnot AJ, Czosnyka M, Menon D. Cerebral perfusion pressure targets individualized to pressure-reactivity index in moderate to severe traumatic brain injury: a systematic review. J Neurotrauma. 2017;34(5):963–70.
31. Lazaridis C, DeSantis SM, Smielewski P, Menon DK, Hutchinson P, Pickard JD, et al. Patient-specific thresholds of intracranial pressure in severe traumatic brain injury. J Neurosurg. 2014;120(4):893–900.
32. Timofeev I, Czosnyka M, Nortje J, Smielewski P, Kirkpatrick P, Gupta A, et al. Effect of decompressive craniectomy on intracranial pressure and cerebrospinal compensation following traumatic brain injury. J Neurosurg. 2008;108(1):66–73.
33. Zweifel C, Castellani G, Czosnyka M, Carrera E, Brady KM, Kirkpatrick PJ, et al. Continuous assessment of cerebral autoregulation with near-infrared spectroscopy in adults after subarachnoid hemorrhage. Stroke. 2010;41(9):1963–8.
34. Zeiler FA, Donnelly J, Menon DK, Smielewski P, Zweifel C, Brady K, et al. Continuous autoregulatory indices derived from multi-modal monitoring: each one is not like the other. J Neurotrauma. 2017;34(22):3070–80.
35. Lindegaard KF, Lundar T, Wiberg J, Sjoberg D, Aaslid R, Nornes H. Variations in middle cerebral artery blood flow investigated with non-invasive transcranial blood velocity measurements. Stroke. 1987;18(6):1025–30.

36. Zeiler FA, Donnelly J, Calviello L, Menon DK, Smielewski P, Czosnyka M. Pressure autoregulation measurement techniques in adult traumatic brain injury, part I: a scoping review of intermittent/semi-intermittent methods. J Neurotrauma. 2017;34(23):3207–23.
37. Sorrentino E, Budohoski KP, Kasprowicz M, Smielewski P, Matta B, Pickard JD, et al. Critical thresholds for transcranial Doppler indices of cerebral autoregulation in traumatic brain injury. Neurocrit Care. 2011;14(2):188–93.
38. Aaslid R, Lindegaard KF, Sorteberg W, Nornes H. Cerebral autoregulation dynamics in humans. Stroke. 1989;20(1):45–52.
39. Tiecks FP, Lam AM, Aaslid R, Newell DW. Comparison of static and dynamic cerebral autoregulation measurements. Stroke. 1995;26(6):1014–9.
40. Zeiler FA, Donnelly J, Cardim D, Menon DK, Smielewski P, Czosnyka M. ICP versus laser Doppler cerebrovascular reactivity indices to assess brain autoregulatory capacity. Neurocrit Care. 2018;28(2):194–202.
41. Budohoski KP, Reinhard M, Aries MJH, Czosnyka Z, Smielewski P, Pickard JD, et al. Monitoring cerebral autoregulation after head injury. Which component of transcranial Doppler flow velocity is optimal? Neurocrit Care. 2012;17(2):211–8.
42. Zeiler FA, Cardim D, Donnelly J, Menon DK, Czosnyka M, Smielewski P. Transcranial doppler systolic flow index and ICP-derived cerebrovascular reactivity indices in traumatic brain injury. J Neurotrauma. 2018;35(2):314–22.
43. Zeiler FA, Smielewski P, Stevens A, Czosnyka M, Menon DK, Ercole A. Non-invasive pressure reactivity index using doppler systolic flow parameters: a pilot analysis. J Neurotrauma. 2019;36(5):713–20.
44. Zeiler FA, Smielewski P, Donnelly J, Czosnyka M, Menon DK, Ercole A. Estimating pressure reactivity using noninvasive doppler-based systolic flow index. J Neurotrauma. 2018;35(14):1559–68.
45. Schmidt EA, Czosnyka M, Steiner LA, Balestreri M, Smielewski P, Piechnik SK, et al. Asymmetry of pressure autoregulation after traumatic brain injury. J Neurosurg. 2003;99(6):991–8.
46. Kumar A, Schmidt EA, Hiler M, Smielewski P, Pickard JD, Czosnyka M. Asymmetry of critical closing pressure following head injury. J Neurol Neurosurg Psychiatry. 2005;76(11):1570–3.
47. Zeiler FA, Czosnyka M, Smielewski P. Optimal cerebral perfusion pressure via transcranial Doppler in TBI: application of robotic technology. Acta Neurochir. 2018;160(11):2149–57.
48. Zeiler FA, Smielewski P. Application of robotic transcranial Doppler for extended duration recording in moderate/severe traumatic brain injury: first experiences. Crit Ultrasound J. 2018;10(1):16.

49. Czosnyka M, Smielewski P, Kirkpatrick P, Menon DK, Pickard JD. Monitoring of cerebral autoregulation in head-injured patients. Stroke. 1996;27(10):1829–34.
50. Lang EW, Lagopoulos J, Griffith J, Yip K, Mudaliar Y, Mehdorn HM, et al. Noninvasive cerebrovascular autoregulation assessment in traumatic brain injury: validation and utility. J Neurotrauma. 2003;20(1):69–75.
51. Liu X, Czosnyka M, Donnelly J, Budohoski KP, Varsos GV, Nasr N, et al. Comparison of frequency and time domain methods of assessment of cerebral autoregulation in traumatic brain injury. J Cerebral Blood Flow Metabol. 2015;35(2):248–56.

Transcranial Doppler Protocols and Procedures: Vasomotor Reactivity

Brenda Rinsky

Introduction

Evaluating cerebral vasomotor reactivity (VMR) using TCD provides information about cerebrovascular capacity and has utility in assessing stroke risk. It is relatively easy to perform, reliable, safe, inexpensive, and well-tolerated. While there is no significant change in the large vessel diameter with increased PCO2, the arterioles dilate or contract as needed to maintain constant brain blood flow. CO2 inhalation or breath-holding are used to evaluate the arteriolar function and provide a "stress" test for the collateral circulation during carotid high-grade stenosis or occlusion. Various methods are available to monitor intracranial hemodynamics using vasomotor reactivity. This protocol will describe the two most widely used VMR measurement techniques:

1. CO2 challenge – This study requires inhalation of 5% medical grade CO2, 95% O2 gas mixture and a dedicated gas delivery system.
2. Breath-holding – This study requires the patient to hold their own breath for 30 seconds.

B. Rinsky (✉)
Neurovascular Ultrasound Laboratory, Department of Neurology, Cedars-Sinai Medical Center, Los Angeles, CA, USA
e-mail: Brenda.rinsky@cshs.org

W. C. Ziai, C. L. Cornwell (eds.), *Neurovascular Sonography*,
https://doi.org/10.1007/978-3-030-96893-9_15

Indications for Vasomotor Reactivity and Breath-Holding [1, 2, 3]

1. Evaluate the adequacy of collateral flow pathways due to carotid artery high-grade stenosis or occlusions
2. Assess hemodynamic insufficiency in patients who may benefit from cerebral re-vascularization
3. Pre-operative assessment of hemodynamic risk from carotid stenosis or occlusion prior to:
   (a) Carotid Endarterectomy (CEA)
   (b) Coronary Bypass Grafts (CABG)
   (c) Cardiothoracic surgeries such as TEVAR, circulatory arrest, carotid bypass, aortic replacement/repair

The CO2 inhalation method is performed using dedicated non-imaging TCD equipment with dual-channel capabilities. Many of the equipment manufacturers now have vasomotor reactivity software programs with calculation packages for both CO2 and breath-holding. The programs demonstrate velocity and pulsatility index trends and can accommodate the inclusion of PCO2 and blood pressure readings for proof of change over time. Capnometry will serve to display changes in end tidal PCO2 throughout the procedure.

The equipment requirements are a source for medical grade 5% CO2, 95% O2 carbogen mixture [1], a storage tank, and a dedicated delivery system that is effective and patient friendly. Compared to breath-holding there are increased costs involved in putting together the initial system. The gas tanks can be rented or owned. The small, portable "E" tank can provide gas for between 5 and 10 studies before needing to be refilled. The larger capacity "H" tank will need to be secured to the wall and is not portable. Gas refills are relatively inexpensive, and obtaining the gas, tank, and regulators can be arranged through "Cylinder Management" in most hospital settings. Independent companies like Air West, Inc. and Praxair, Inc. are located across the United States and can provide gas, tanks, regulators, and flow meters. The delivery system is semi-disposable, but mouth and nose pieces should be disposed of after each use. The advantage of using a delivery system is that it provides a quantifiable result that is not dependent on the patient's

ability to breath-hold. Both hypercapnia and hypocapnia can be demonstrated in the same trending program allowing for visual documentation of both hyper, and hypocapnia. With the assistance of respiratory therapy, even ventilated patients can be safely tested. The CO2 inhalation method demonstrates velocity trending over time and produces reliable, reproducible results. The patient can breathe and participate throughout the entire study.

CO2 Delivery System Set Up: (Courtesy of Cedars-Sinai Medical Center)

(a) Universal or multi-airway adapters (small and large)
(b) (1) each male/female one-way valve or aerosol "TEE" with built-in one-way valves
(c) (1) Aerosol "Tee" adapter (top load or side load depending on capnometry)
(d) Disposable mouthpiece and nose clip, or full-face mask if tolerated
(e) Corrugated tubing – ≤1 ft.
(f) Large air mix bag with "Y" adapter
(g) Small bore oxygen tubing that fits flow meter and "Y" adapter
(h) Nipple- connects the oxygen tubing to the air mix bag
(i) 22-micron filter
(j) Flow meter
(k) Christmas tree adaptor – connects the small-bore tubing from the tank to the nipple
(l) Regulator – Specific for carbogen gas mixture

Starting with the tank: Attach the regulator and flow meter onto the tank. Connect one side of the small-bore tubing to the Christmas tree adaptor on the flow meter and connect the other side to the nipple attached to one side of the "Y" in the air bag. Connect the corrugated tubing to the other port in the "Y". This system is comprised of small parts that can be purchased through the hospital purchasing dept., respiratory therapy group, or directly through the vendors. There is a filter in the bag that allows room air to mix with the CO2 and O2 gas mixture. Now connect the corrugated tubing into the male one-way valve and then fit the male one-way

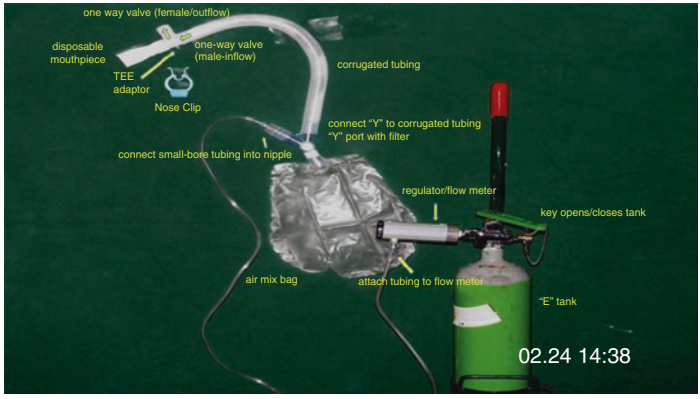

Fig. 1 CO2 delivery system without capnometry in place – Original delivery system developed by Brenda Rinsky, RDMS, RVT, NVS

valve into one end of the aerosol TEE adaptor. The female one-way valve will fit onto the opened top of the TEE adaptor. This keeps the patient from re-breathing. It may be possible to purchase a TEE adaptor that has built-in male and female valves for ease of use and reduced costs. If using a top loading capnometer, attach into the end of the aerosol TEE adaptor on the side of the patient's mouth. Universal adaptors can be used if the diameter of the TEE adaptor, micron filter, or mouthpieces are different. If using a side-loading capnometer, choose a side-load TEE adaptor. Attach the mouthpiece into the open end of the TEE adaptor. The delivery system is now in place (Fig. 1).

Procedure

Performance of a complete TCD prior to VMR testing can be an important way to Identify collateral flow pathways and to determine if the bone windows will be acoustically sufficient. Place the stationary headband around the patient's head making sure to slide the back of the band down around the back of the neck. Tighten the headband so that it is snug, but not painful. Add a generous amount of gel and attach each transducer. Avoid bi-directional flow from the bifurcation by setting the depth between

45 and 55 mm in the bilateral M1 portion of the Middle Cerebral Arteries (MCA). Adjust the power and gain settings to obtain a quality Doppler signal and maintain that the envelop fits well around the spectral waveform. Adjust the transducer angle to obtain the highest velocity. A weak waveform can be monitored, but the transducer may need constant adjustment during the procedure. Adjust the scale so the systolic peak is clear of the top of the screen. This can be achieved by lowering the zero line toward the bottom of the screen or increasing the scale to avoid aliasing of the peak systolic velocity during hypercapnia. Be sure the bilateral scale and choice of sampling depth are symmetric for a true side-to-side comparison.

To begin the study, power up and calibrate the capnograph. Place the disposable mouthpiece into the patient's mouth and place the nose clip over the nostrils to eliminate breathing through the nose during the study. Attach the capnograph into either the side port, or top port near the mouthpiece. Trend the velocities for 1–3 minutes, allowing the patient to relax and calm down, waiting for the velocities to become stable. Do not connect in the delivery system until after a baseline waveform has been saved or marked if trending (Fig. 2). Normal entidal CO2 is between 35 and 40

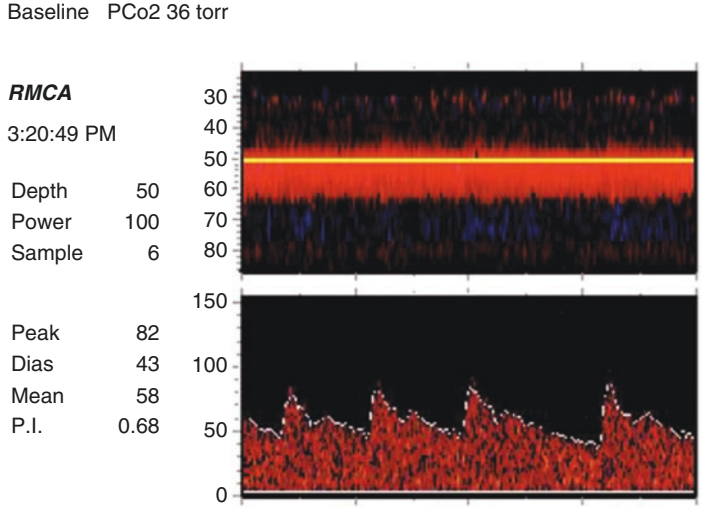

Fig. 2 Baseline velocity and end-tidal PCO2

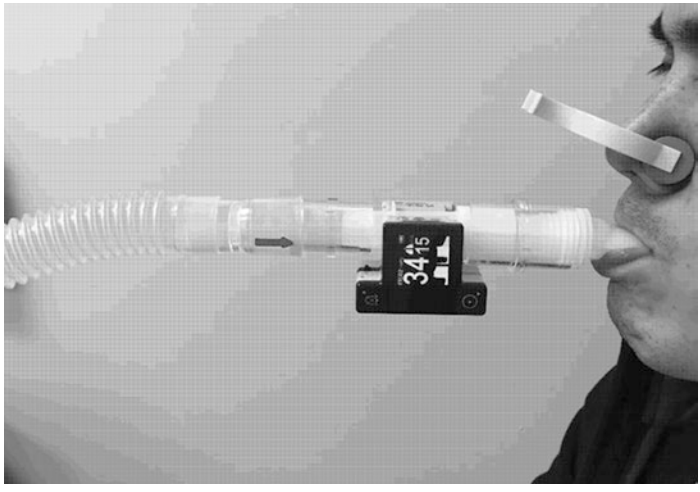

Fig. 3 Aerosol TEE connected to the corrugated tubing and capnometry. Female one-way valve is not in view

mmhg. Note the patient's baseline end-tidal CO2. At this point, attach the nose clip and delivery system consisting of the inflow aerosol TEE adaptor that has been previously fitted with the one-way valves and corrugated tubing to the patient's mouthpiece (Fig. 3).

After the baseline velocity has been established, open the valve on the CO2 tank and set the flow meter to between 8 and 12 liters to begin CO2 inhalation. The flow meter can be adjusted according to how deeply the patient inhales. The gas mixture bag should collapse almost completely during inhalation and then refill again during exhalation. Have the patient take in deep, slow breaths through the mouthpiece into their upper chest. The CO2 gas will begin to build up in the lungs and in normal circumstances, the velocities will increase as the arterioles begin to dilate producing an increase in cerebral blood flow. The diastolic component of the waveform will also increase as the pulsatility indices will decrease. This portion of the study will take up to 3 minutes to perform. Keep the patient calm and try to slow their breathing. As the CO2 increases, the patient's respiratory drive will engage, forcing the

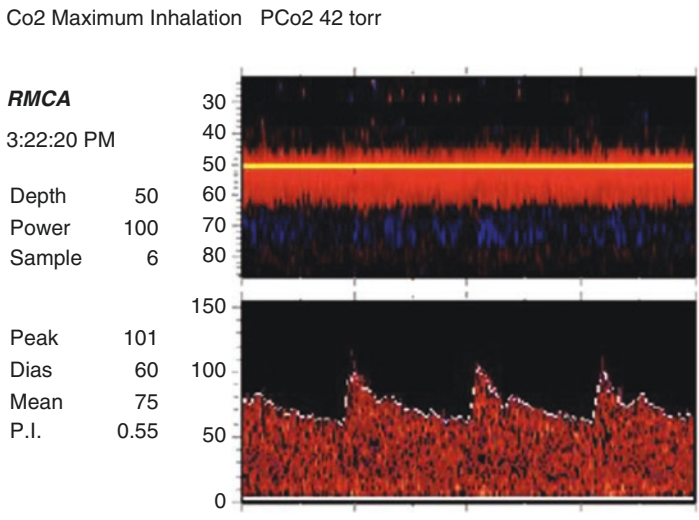

Fig. 4 CO2 inhalation causes arteriolar dilatation, increasing the velocity and decreasing the pulsatility indices

patient to breathe rapidly to eliminate the excess CO2. Maximum velocity is achieved when the velocities become stable and no longer increase. Save the waveforms or mark the event and note the end-tidal CO2 (Fig. 4). The objective is to increase the PCO2 approximately 20% from the baseline Torr. Turn the CO2 gas off at the regulator and tank. Remove the gas delivery apparatus to allow the CO2 to normalize while the patient breaths room air. The nose clip can be left in place. Make sure the end-tidal reading from the capnometer returns to baseline for at least 30 seconds before proceeding with the next step.

Hypocapnia starts with the patient breathing rapidly and consistently through the mouth. Demonstrating how to hyperventilate in a controlled fashion will enhance the patient's ability to perform this part of the testing. Have the patient breathe rhythmically with the objective of decreasing the end-tidal CO2 to approximately 20% of baseline Torr. The velocities will decrease as the arterioles constrict, decreasing cerebral blood flow. The pulsatility

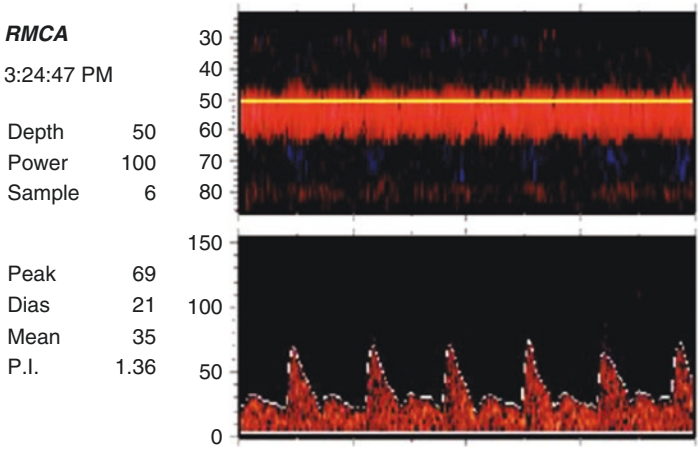

Fig. 5 Hyperventilation constricts the arterioles causing decreased velocity and increased pulsatility indices

indices will increase significantly. Save the waveforms once again and note the final end-tidal CO2 (Fig. 5). Remove the nose clip. Allow the end-tidal CO2 to go back to baseline once again before allowing the patient to sit up. The study is now complete.

Alternate Procedure Without Capnometry

Allow 1–3 minutes for the patient to relax and become calm. Acquire the MCA velocities making sure to keep the envelop on for monitoring both the velocities and Pulsatility indices. Adjust the scale and sample depth to avoid aliasing. Capture the baseline velocities. Follow the CO2 inhalation and hyperventilation directions as described above. Without capnometry to gage whether the end-tidal PCO2 has effectively increased or decreased, it will be very important to monitor the waveforms closely. Once the velocities are stable

and no longer changing, then save the maximum velocity for hypercapnia, and the minimum velocity for hypocapnia.

Although highly unlikely, should the patient experience neurologic change or respiratory distress, immediately turn off the gas, remove the mouthpiece and nose clip, and allow the patient to breathe room air. Evaluate the patient when they return to their baseline CO2. The gas will exit the lungs very quickly, and the patient should recover back to their normal state. If the symptoms persist, get immediate medical assistance.

Several of the TCD equipment manufacturers now have automated VMR and breath holding calculation programs. Although the procedure is the same, the equipment will automatically calculate the vasomotor reactivity.

Calculations [3]

$$1.\ \%\text{Change in } PCO2 = \frac{PCO2 \text{ at Maximum } (C02 \text{ inhalation}) - PCO2 \text{ at Minimum } (HVT)}{PCO2 \text{ at Baseline}} \times 100$$

$$2.\ \%\text{Change in } VMR = \frac{(CO2 \text{ inhalation}) \text{ Maximum Velocity} - (HVT) \text{ Minimum Velocity}}{\text{Baseline Velocity}} \times 100$$

Results

=/<15%	Exhausted VMR
16–38%	Severely reduced VMR
39–69%	Mild to moderately reduced VMR
>70%	Normal VMR
Paradoxical Effect	Velocities drop during hypercapnia and increase during hyperventilation. This is consistent with exhausted VMR and the steal effect is reported in the interpretation

Breath-Holding Method

Breath holding is used to establish a state of hypercapnia. Like the CO2 challenge, it is used to evaluate the effects of carotid stenosis or occlusion on the cerebral circulation. By having the patient hold their own breath, the buildup of natural CO2 in the lungs replaces the need for inhalation of additional CO2. Storing CO2 gas is not required reducing overall costs, and eliminating the need for a gas delivery system. Unfortunately, this technique is also very dependent upon the patient's ability to follow instructions and cooperate fully. Results may be limited depending on the patient's mental status, respiratory status, and breath-holding capabilities.

Generally, breath-holding is performed using dedicated non-imaging TCD equipment with dual-channel capabilities. Once the initial TCD is completed, set the stationary head gear up for unilateral or bilateral monitoring as previously described in the CO2 inhalation section. Because this study requires accurate timing, be sure to have access to a stopwatch or clock with a second hand.

Procedure [2]

1. The patient should begin the study in a state of normal breathing. Record or save the MCA baseline velocity(s) once they are stable
2. Begin hyperventilation and continue for 2 minutes, record or save the MCA velocity(s) at 2 minutes
3. Let the patient return to normal breathing for 4 minutes
4. Start breath-holding after normal respiration. The patient should avoid taking in a deep breath before they stop breathing. The established time to breath-hold is for 30 seconds. After 30 seconds, allow the patient to breath and then wait 4 seconds before saving the final velocity (s)
5. The patient can breathe normally, the testing is now complete
6. Record the time that the breath was held and calculate the results

Calculations [2]

1. $$\text{BHI} = \frac{\text{MFV end} - \text{MFV baseline}}{\text{MFV baseline}} \times \frac{100}{\text{Seconds of breath} - \text{holding}}$$

2. $\Delta V_{MCA/t}\Delta$ = increase in V_{MCA} during breath-holding/t = Time of breath-holding

Results

>0.6:	Normal VMR
0.02–0.6:	Impaired VMR
<0.02:	Severely impaired VMR

References

1. Kleiser B, Widder B. Course of carotid artery occlusions with impaired cerebrovascular reactivity. Stroke. 1992;23(2):171–4. https://doi.org/10.1161/01.str.23.2.171.
2. Markus HS, Harrison MJ. Estimation of cerebrovascular reactivity using transcranial Doppler, including the use of breath-holding as the vasodilatory stimulus. Stroke. 1992;23(5):668–73. https://doi.org/10.1161/01.str.23.5.668.
3. Ringelstein EB, Sievers C, Ecker S, Schneider PA. Noninvasive assessment of CO2-induced cerebral vasomotor response in normal individuals and patients with internal carotid artery occlusions. Stroke. 1988;19(8):963–9. https://doi.org/10.1161/01.str.19.8.963.

Continuous Cerebral Autoregulation Monitoring Using TCD

Lucia Rivera-Lara and Frederick A. Zeiler

Background

Monitoring cerebral blood flow velocity via transcranial doppler (TCD) can also be applied to measure the brain's vasculature reactivity. Cerebral autoregulation (CA) is the ability of the brain's blood vessels to constrict or dilate to adapt to variations in mean arterial blood pressure (MAP) to maintain a stable cerebral perfusion pressure.

L. Rivera-Lara (✉)
Division of Neurosciences Critical Care, Department of Neurology and Neurosurgery, Anesthesia and Critical Care Medicine, Johns Hopkins University School of Medicine, Baltimore, MD, USA
e-mail: riveral@stanford.edu

F. A. Zeiler
Section of Neurosurgery, Department of Surgery, Rady Faculty of Health Sciences, University of Manitoba, Winnipeg, MB, Canada

Department of Human Anatomy and Cell Science, Rady Faculty of Health Sciences, University of Manitoba, Winnipeg, MB, Canada

Biomedical Engineering, Faculty of Engineering, University of Manitoba, Winnipeg, MB, Canada

Division of Anaesthesia, Department of Medicine, Addenbrooke's Hospital, University of Cambridge, Cambridge, UK

W. C. Ziai, C. L. Cornwell (eds.), *Neurovascular Sonography*,
https://doi.org/10.1007/978-3-030-96893-9_16

TCD is widely used to monitor cerebral blood flow velocity and cerebral autoregulation, assuming that the monitored vessel diameter does not change (steady state) during the monitoring period. If this assumption holds true, we can apply the volumetric flow rate definition where cerebral blood flow equals cerebral blood flow velocity. TCD is able to insonate the largest intracranial arteries and the circle of Willis. The most common monitored artery in CA is the middle cerebral artery.

Continuous monitoring of CA with TCD has more advantages over static measurements as it does not require any intervention to change the MAP. It relies on spontaneous variations of slow waves to measure CA. Healthy adults exhibit slow wave oscillations of cerebral blood volume, cerebral blood flow and tissue oxygenation in the frequency of 0.004–0.05 Hz; these slow waves occur in the setting of normal physiologic functions such as breathing and variations in neuronal and cerebrovascular tone [1]. These slow waves are recorded with TCD.

Monitoring cerebral autoregulation with TCD can be helpful in prognostication for unfavorable clinical outcomes and mortality [2] in patients who suffer aneurysmal subarachnoid hemorrhage (aSAH) [3], traumatic brain injury (TBI) [4, 5], large artery vessel occlusion [6], intracerebral hemorrhage (ICH) [7], and patients undergoing cardiac bypass [8].

Cerebral autoregulation can also be applied to optimizing blood pressure management by delineating the cerebral autoregulatory curve and optimal MAP. By delineating the lower and upper limit of CA we can target the MAP or cerebral perfusion pressure to prevent hypoperfusion leading to cerebral ischemia and hyperperfusion leading to cerebral edema and worsening intracranial hypertension. This can facilitate precision medicine by individualizing blood pressure goals with the hope of preventing secondary injury, decreasing mortality and disability [9–11]. In a nested randomized controlled trial, patients undergoing cardiac bypass were monitored with TCD to determine the lower limit of CA. The group that was assigned to keep a MAP above the lower limit of CA determined by TCD during cardiac bypass had a lower incidence of postoperative delirium [12]. Individualized blood pressure management during cardiac bypass has also been shown to lead to improved cognitive function and better memory testing in a ran-

domized clinical trial [13]. The objective of these trials is to target personalized blood pressure goals to prevent mainly hypoperfusion leading to increased risk for kidney disease, cognitive impairment and stroke [8, 11, 14, 15].

Step by Step Using Analog Hemodynamic Monitors (Fig. 1)

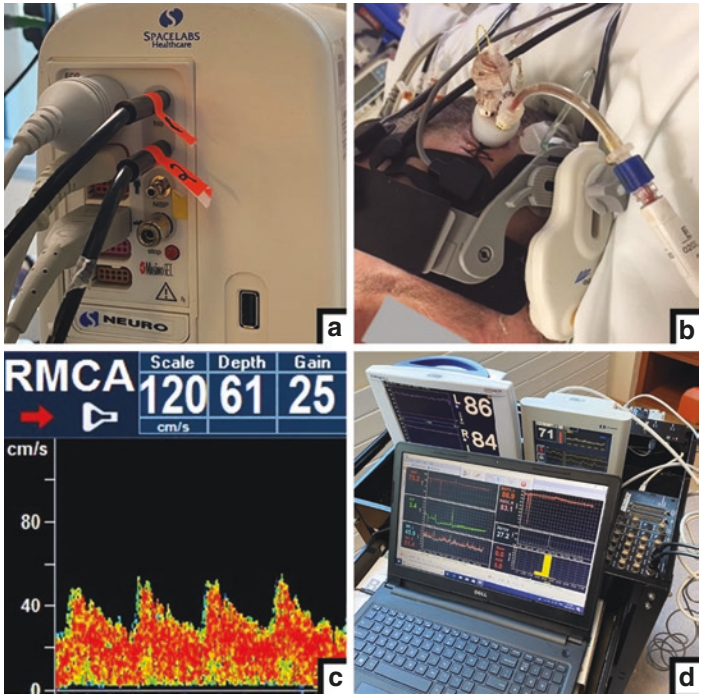

Fig. 1 Example of robotic transcranial Doppler (rTCD) bedside setup for multimodal monitoring. (Panel **a**) High level analog output (HLO) ports used to stream data from patient monitor to analog-to-digital convertor (ADC). (Panel **b**) Multimodal monitoring of a traumatic brain injury patient including rTCD probe and headband. (Panel **c**) Typical rTCD tracing of right middle cerebral artery (MCA). (Panel **d**) Laptop compiling and recording time-locked multimodal data streams. (*Figure is a color adaptation from Zeiler et al. Acta Neurochir (Wien). 2018; 160 (11): 2149–57 (with permission from corresponding author))

Equipment

- Analog hemodynamic monitor
- ADC converter (converts analog to digital signals)
- TCD machine with headset
- Laptop
- Autoregulation software
- Cables connecting hemodynamic monitor to ADC converter

Requirements

- Arterial catheter for continuous MAP monitoring

Steps

1. Connect the ADC converter to the hemodynamic monitor
2. Connect the ADC converter to laptop through USB cord
3. Connect TCD machine to laptop through USB cord
4. Turn on TCD monitor and find the bilateral MCA's signals on the monitored patient using the head-set
5. Turn on laptop
6. Open autoregulation software (software that runs automatic correlations between MAP and cerebral blood flow velocity)
   (a) Enter patient identifiers
   (b) Select autoregulation profile
   (c) Test connections, make sure the analog signals from hemodynamic monitor are connected to the correct channels on the ADC converter
   (d) Click start to begin recording
7. When finished, click "stop", and then click "save" before exiting the program.
8. Open the file and start analyzing the file. See Fig. 2 showing a monitoring period with the index of CA derived from the correlation between cerebral blood flow velocity and MAP, Mx (mean velocity index). When the index approaches 0 and is <0.45 this indicates intact autoregulation, when the index approaches 1 and is ≥ 0.45 there is impaired autoregulation.

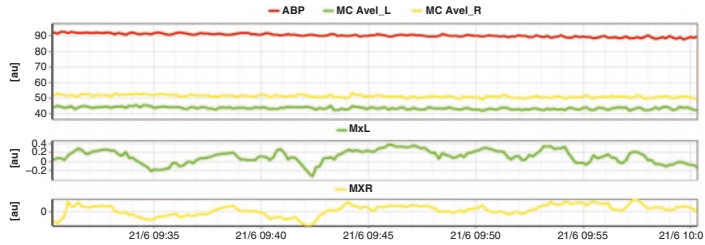

Fig. 2 Example of 30 minute recording of continuous monitoring of cerebral autoregulation monitoring with TCD. 51-year old with high grade aneurysmal subarachnoid hemorrhage who underwent CA monitoring with TCD upon admission to the neurocritical care unit. In the top panel ABP (mean arterial blood pressure) and left (L) and right (R) middle cerebral artery velocities (MCAvel) are displayed. In the two bottom panels, the CA index derived from TCD, Mx (mean velocity index) is displayed. Mx is <0.45 during the monitoring period indicating intact cerebral autoregulation

Step by Step with Digital Hemodynamic Monitors

Equipment

- Digital hemodynamic monitor
- TCD machine with headset
- Laptop
- Autoregulation software
- Cables connecting hemodynamic monitor and TCD monitor to laptop

Requirements

- Arterial catheter for continuous MAP monitoring

Steps

1. Turn on TCD monitor and find the bilateral MCA signals on the monitored patient using the headset
2. Connect TCD monitor to laptop via USB port
3. Connect hemodynamic monitor to laptop via USB port
4. Turn on laptop

5. Open autoregulation software (software that runs automatic correlations between MAP and cerebral blood flow velocity)
   (a) Enter patient identifiers
   (b) Select monitoring profile
   (c) Test connections
   (d) Click "start" to begin recording
6. When finished, click "stop", and then click "save" before exiting the program
7. Open file to start analyzing

Limitations

The assumption that the vessel caliber does not change during the monitoring period is a big limitation. If an instantaneous change occurs with a narrowing or dilation of the blood vessel, there will be a significant change in velocity which may not be proportional to the change in flow. Secondly, continuous monitoring with 2-MHz ultrasonic waves through the temporal bone (energy used for diagnostic ultrasonography) is known to be sufficient to enhance thrombolysis [16], so caution should be taken when monitoring patients with or at risk of intracranial bleeding. Lastly, movement artifact is always problematic especially in patients who are not sedated.

References

1. Lee JK, Kibler KK, Benni PB, Easley RB, Czosnyka M, Smielewski P, et al. Cerebrovascular reactivity measured by near-infrared spectroscopy. Stroke. 2009;40(5):1820–6.
2. Rivera-Lara L, Zorrilla-Vaca A, Geocadin R, Ziai W, Healy R, Thompson R, et al. Predictors of outcome with cerebral autoregulation monitoring: a systematic review and meta-analysis. Crit Care Med. 2017;45(4):695–704.
3. Barth M, Woitzik J, Weiss C, Muench E, Diepers M, Schmiedek P, et al. Correlation of clinical outcome with pressure-, oxygen-, and flow-related indices of cerebrovascular reactivity in patients following aneurysmal SAH. Neurocrit Care. 2010;12(2):234–43.

4. Czosnyka M, Smielewski P, Kirkpatrick P, Menon DK, Pickard JD. Monitoring of cerebral autoregulation in head-injured patients. Stroke. 1996;27(10):1829–34.
5. Czosnyka M, Smielewski P, Piechnik S, Schmidt EA, Seeley H, al-Rawi P, et al. Continuous assessment of cerebral autoregulation–clinical verification of the method in head injured patients. Acta Neurochir Suppl. 2000;76:483–4.
6. Reinhard M, Rutsch S, Lambeck J, Wihler C, Czosnyka M, Weiller C, et al. Dynamic cerebral autoregulation associates with infarct size and outcome after ischemic stroke. Acta Neurol Scand. 2012;125(3):156–62.
7. Reinhard M, Neunhoeffer F, Gerds TA, Niesen WD, Buttler KJ, Timmer J, et al. Secondary decline of cerebral autoregulation is associated with worse outcome after intracerebral hemorrhage. Intensive Care Med. 2010;36(2):264–71.
8. Ono M, Joshi B, Brady K, Easley RB, Zheng Y, Brown C, et al. Risks for impaired cerebral autoregulation during cardiopulmonary bypass and postoperative stroke. Br J Anaesth. 2012;109(3):391–8.
9. Rivera-Lara L, Zorrilla-Vaca A, Geocadin RG, Healy RJ, Ziai W, Mirski MA. Cerebral autoregulation-oriented therapy at the bedside: a comprehensive review. Anesthesiology. 2017;126(6):1187–99.
10. Aries MJ, Czosnyka M, Budohoski KP, Steiner LA, Lavinio A, Kolias AG, et al. Continuous determination of optimal cerebral perfusion pressure in traumatic brain injury. Crit Care Med. 2012;40(8):2456–63.
11. Ono M, Brady K, Easley RB, Brown C, Kraut M, Gottesman RF, et al. Duration and magnitude of blood pressure below cerebral autoregulation threshold during cardiopulmonary bypass is associated with major morbidity and operative mortality. J Thorac Cardiovasc Surg. 2014;147(1):483–9.
12. Brown CH, Neufeld KJ, Tian J, Probert J, LaFlam A, Max L, et al. Effect of targeting mean arterial pressure during cardiopulmonary bypass by monitoring cerebral autoregulation on postsurgical delirium among older patients: a nested randomized clinical trial. JAMA Surg. 2019;154(9):819–26.
13. Hogue CW, Brown CH, Hori D, Ono M, Nomura Y, Balmert LC, et al. Personalized blood pressure management during cardiac surgery with cerebral autoregulation monitoring: a randomized trial. Semin Thorac Cardiovasc Surg. 2021;33(2):429–38.
14. Ono M, Arnaoutakis GJ, Fine DM, Brady K, Easley RB, Zheng Y, et al. Blood pressure excursions below the cerebral autoregulation threshold during cardiac surgery are associated with acute kidney injury. Crit Care Med. 2013;41(2):464–71.
15. Ono M, Arnaoutakis G, Fine D, Brady K, Easley R, Zheng Y, et al. Blood pressure excursions below the cerebral autoregulation threshold during cardiac surgery are associated with acute kidney injury. Crit Care Med. 2012;41(2):464–71.
16. Alexandrov AV, Molina CA, Grotta JC, Garami Z, Ford SR, Alvarez-Sabin J, et al. Ultrasound-enhanced systemic thrombolysis for acute ischemic stroke. N Engl J Med. 2004;351(21):2170–8.

Optic Nerve Sheath Diameter for Increased Intracranial Pressure

Becky J. Riggs and Megan F. Hunt

Introduction

Rapid assessment of intracranial hypertension (ICH) is essential in the diagnosis and management of acute intracranial insults. With severe traumatic brain injury (TBI), the gold standard method of diagnosing and monitoring ICH is by invasive methods. However, the routine use of invasive intracranial pressure (ICP) monitors is often limited by comorbidities, complications, availability, and projected outcomes [1–6]. A recent review of the literature concluded that optic nerve sheath diameter (ONSD) and transcranial Doppler are the most superior non-invasive tools clinically proven to detect intracranial hypertension [14].

B. J. Riggs (✉)
Department of Anesthesiology and Critical Care, Division of Pediatric Anesthesiology & Critical Care Medicine, Charlotte Bloomberg Children's Center, Baltimore, MD, USA

Oregon Health Science University, Doernbecher Children's Hospital, Portland, OR, USA
e-mail: riggsbe@ohsu.edu

M. F. Hunt
School of Medicine, Johns Hopkins, Baltimore, MD, USA

W. C. Ziai, C. L. Cornwell (eds.), *Neurovascular Sonography*,
https://doi.org/10.1007/978-3-030-96893-9_17

An ideal non-invasive ICP monitor should be safe, reliable, cost effective, and readily available [7]. Bedside ultrasound measurement of the ONSD is an accurate, non-invasive, radiation-free, and widely available method of detecting ICH that can allow for rapid formulation of an individualized treatment plan in patients presenting with symptoms of ICH [8–13]. The integration of ultrasound guided noninvasive ONSD measurements can assist in determining which patients with altered mental status are experiencing ICH, tipping the scales in favor of placing an invasive monitor. At the same time, ONSD measurements could be reassuring that a patient with altered mental status is not experiencing ICH and should not have an invasive monitor placed. A recent literature review determined that ultrasound guided ONSD studies and transcranial Doppler studies are superior to all other non-invasive modalities currently in use to predict early ICH [14].

While head computed tomography (CT) and brain magnetic resonance imaging (MRI) have been validated to identify ICH, these techniques require transporting the critically ill patient to a scanner, which can be time consuming and possibly dangerous [15–18]. Interpretation and measurement of the ONSD via head CT and brain MRI is often conducted by Neuro-radiologists, which can delay results even further [15–18, 117, 118]. Point-of-care ultrasound, in the form of transcranial Doppler or ocular ultrasound, is an alternative that provides immediate results. Transcranial Doppler is a useful option but requires extensive training to yield reliable and consistent results. Ultrasound guided ONSD measurement has been proven to be reliably reproducible with high inter-rater reliability to detect and monitor changes of the ONSD in response to intracranial pressure changes [8, 9, 12, 14, 19–21]. The ONSD immediately reflects changes in ICP, whereas papilledema takes hours or days before it is often recognized in adults and can take weeks to months to recognize in children [22–25]. Ultrasound guided ONSD measurement is applicable in intensive care units, operating rooms, and emergency departments where machines are widely available. While further research is warranted to elucidate further granularity and application of the technique, clinicians should utilize ultrasound guided ONSD in

the diagnostic workup of pediatric and adult patients with suspected intracranial pathology, especially in emergency settings.

The Physiology Supporting ONSD Measurements

The mechanism that drives ONSD changes with fluctuating ICP levels is the anatomical continuity that allows cerebrospinal fluid to freely move between the intracranial and orbital subarachnoid spaces [26, 27]. As the ICP increases, cerebrospinal fluid is pushed down the path of least resistance into the orbital subarachnoid space causing the optic nerve sheath to expand, thus increasing its diameter [9]. When the ICP decreases, the orbital cerebrospinal fluid returns to the intracranial subarachnoid space causing the optic nerve sheath to decompress [28]. The fluctuation of cerebrospinal fluid between the orbital subarachnoid space and the intracranial subarachnoid space is within seconds of an acute increase in ICP [7, 30–32]. Unlike the development of papilledema that evolves and resolves over several days to months, ONSD changes are a more immediate marker of ICH [22–25, 29]. However, some studies have suggested that with chronic exposure to ICH, for example with slow growing brain tumors or pseudotumor cerebri, the optic nerve sheath might become less pliable and thus less reactive. Hence, the use of point-of-care ultrasound measurements of the ONSD is possibly more accurate and applicable when detecting acute rapid changes in ICP as opposed to chronic slow changes in ICP; however, to our knowledge, this has not been specifically studied and reported on in the literature.

Clinical Application of ONSD Measurements

Ultrasound guided ONSD measurements can be used as a non-invasive bedside tool to detect and monitor changes in ICH. Bedside ONSD measurement is indicated when a patient's clinical exam or pathology is suggestive of intracranial hyperten-

sion. In the emergency department, ONSD measurements can be rapidly utilized in a patient who is non-responsive or minimally responsive to determine if their altered mental status is due to ICH or intoxication. Within intensive care units (ICUs), ultrasound-guided ONSD measurement have been applied to the following clinical pathologies: head trauma [8, 33–35], intracranial hemorrhage [35, 36], stroke [37–39], sinus venous thrombosis [40], craniosynostosis [41, 42], meningitis/encephalitis [43, 44], posterior reversible encephalopathy [45–47], and hydrocephalus [10, 48, 49]. Significantly elevated ONSDs in conjunction with a patient's clinical exam and history might encourage the placement of an invasive ICP monitor [8, 25, 50], while normal ONSD measurements might argue against placement of an ICP monitor. Patients with ICH who also have significant comorbidities, are taking anticoagulants, are immune compromised, or have bleeding disorders are not ideal candidates for invasive ICP monitor placement [1–4]; therefore, monitoring ICH with serial measurements of ONSD might be even more beneficial. For example, research has shown that ultrasound guided ONSD measurements are being integrated into the care of patients with ICH due to liver failure [51–53], diabetic ketoacidosis [54–57], metabolic crisis, and HIV [58].

Aside from the identification and monitoring of ICH, additional applications of ultrasound guided ONSD measurements within ICUs have been suggested. ONSD measurements have been used to predict outcomes in stroke patients [38, 39] and in patients with spontaneous intracranial hemorrhages [119]. Gokcen et al. suggests that ONSD measurements can help predict which stroke patients will develop malignant middle cerebral artery syndrome [37]. In post-cardiac arrest patients, ONSD measurements have been used as a prognostic indicator of hypoxic encephalopathy [59], at predicting mortality, and predicting a favorable versus a poor clinical prognosis [60–62]. Some have used ONSD measurements to determine the effectiveness of decompressive craniotomy in patients [63].

Monitoring changes in ONSD with point-of-care ultrasound in the operating room when there is concern for fluctuations in intra-

cranial pressure is becoming more common. For example, ultrasound guided ONSD measurements have been used to assess the different effects that propofol vs. sevoflurane have on ICP during surgery [64]. When performing laparoscopic abdominal surgery in the Trendelenburg position while inducing pneumoperitoneum, the patient is at risk for increases in ICP [65, 66]; therefore, there have been several studies utilizing ultrasound guided ONSD measurements to minimize ICH during these cases [67–71]. The effects of dexmedetomidine on ICP in patients in steep Trendelenburg position during surgery has been quantified via ONSD measurements [72]. ONSD measurements have been used to optimize the neck position to reduce ICH during craniosynostosis surgery [73]. Ultrasound guided ONSD measurements are commonly used during liver transplant surgery [53, 74–76, 116] to monitor changes in ICP. Given the availability of and understanding of most anesthesiologists to use ultrasound machines in general, the authors predict the continued expansion of ultrasound guided ONSD monitoring in the operating room.

There have been some studies further expanding the use of ultrasound guided ONSD measurements beyond the emergency department, ICUs, and operating rooms. Obstetricians have used ONSD values to predict and monitor the development of preeclampsia and eclampsia [77, 78]. Neuro-ophthalmologists have trended ultrasound guided ONSD measurements in patients with idiopathic intracranial hypertension, also known as pseudotumor cerebri syndrome, in their clinics [79–81]. ONSD measurements have been used to diagnose symptomatic intracranial hypotension following lumbar punctures [82] and have been used to determine the efficacy of lumbar epidural blood patching in these patients [83]. The military and prehospital transportation units have evaluated the feasibility and applications of handheld ultrasound guided ONSD measurements to traumatic brain injury patients in the field [84–86]. And finally, given the effects of zero gravity leading to ICH, astronauts have applied the use of ultrasound guided ONSD measurements in space [87, 88].

Equipment and Supplies Needed to Obtain ONSD Measurements

Ophthalmic ultrasound can be safely performed using any point-of-care ultrasound machine that can be placed in "ophthalmic safety" mode, or where the power (<30%), mechanical index (<0.23), and thermal index (<1) can be manually decreased below safety thresholds [89–92]. High frequency (10 mHz–22 mHz) linear array probes are ideal for ocular ultrasound; however, low frequency (6 mHz–13 mHz) linear array probes often referred to as "vascular probes" are more commonly used due to their availability [93]. Contact your ultrasound vender to provide instructions on how to manually decrease the power below 30%, the mechanical index below 0.23, and the thermal index below 1. To locate the "ophthalmic safety mode," push the exam button and scroll through the exam options available. Often the "ophthalmic safety mode" is embedded within the "small parts", "ED", or "other" exam modalities. Never perform ophthalmic ultrasound if there is a concern for penetrating or direct eye trauma. Always perform bedside ophthalmic ultrasonography through a closed eyelid. Never allow the ultrasound probe to come in contact with an open eye as this can cause corneal abrasions and puts the patient at risk for ocular infection. To protect your patient's eyes, either apply a generous amount of ophthalmic safe eye gel to the ultrasound probe instead of ultrasound gel or place a Tegaderm™ over a closed eye and cover the Tegaderm™ with ultrasound gel. Two commonly used over-the-counter ophthalmic safe lubricating gels are GenTeal® eye lubricant (Novartis Pharmaceuticals Corporation, East Hanover, NJ) and Systane® eye lubricant (Alcon laboratories, Inc., Fort Worth, TX). Always securely ground the hand holding the ultrasound probe on your patient's face (forehead, cheek, nose, or orbital ridge) hold the probe delicately between your thumb and forefinger to minimize the pressure placed on the eye through the closed eyelid. If unable to ground your hand on your patient's face, place a firm pillow or rolled up towel next to their face to stabilize your hand to prevent pressure on the closed eye. For a detailed description of how to

obtain and measure point-of-care ultrasound images of the ONSD, see Chap. 31 of this book titled: "How to obtain measurements of the optic nerve sheath diameter in adults and children utilizing point-of-care ophthalmic ultrasonography."

Interpretation of ONSD Measurements for Adult Patients

Prior to interpreting ONSD measurements, it is imperative that the ONSD images are accurate. Correct axial cuts through the eye and optic nerve should include a symmetric and straight longitudinal section of the optic nerve and optic nerve sheath (Fig. 1). Accurate transection of the optic nerve, which is often an approach obtained in uncooperative pediatric patients, shows a double circle or "bulls-eye" appearance of the optic nerve and optic nerve sheath in asso-

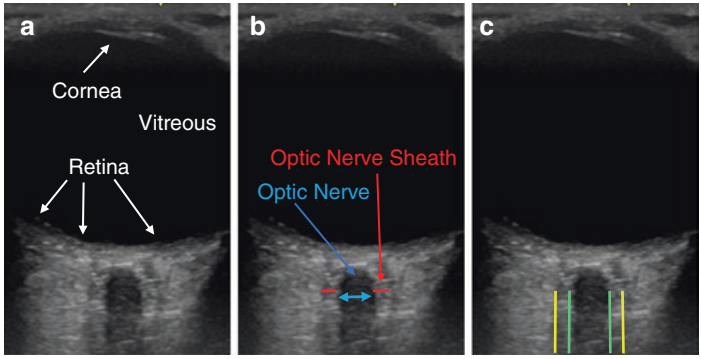

Fig. 1 Appropriately Aligned Ophthalmic Ultrasound Images. (**a**) Normal ophthalmic ultrasound images obtained in the transverse view with the anterior portion of the eye facing upwards and the optic nerve attaching posteriorly. (**b**) The same ultrasound image showing a symmetric and straight longitudinal section of the hypoechoic optic nerve (blue arrow) surrounded by a symmetric and straight hyperechoic optic nerve sheath (red lines). (**c**) The same image with straight green lines along the internal border of the optic nerve sheath and yellow lines on the external border of the optic nerve sheath reinforcing the straight and symmetric alignment of the optic nerve and nerve sheath

ciation with a symmetric straight optic nerve (Fig. 2). Examples of inaccurate optic nerve images are in Fig. 3. If inaccurate images of the optic nerve sheath are taken, the measurements will also be inaccurate. See Chap. 31 of this book titled "How to obtain measurements of the optic nerve sheath diameter in adults and children utilizing point-of-care ophthalmic ultrasonography," for a detailed description of how to accurately measure the ONSD.

Once the image is acquired and the measurement determined, the ONSD must be interpreted and used as a complementary technique combined with the clinical exam and standard neuroimaging findings to guide the care of the patient. In 2011, Dubourg et al. conducted a systematic review and meta-analysis of adult patients finding a pooled sensitivity of 0.90 (95% CI 0.8–0.95), specificity of 0.85 (95% CI 0.73–0.93), and diagnostic odds ratio of 51 (95% CI 22–121) with the area under the SROC curve of 0.94 (95% CI 0.91–0.96) [98]. However, the cutoff thresholds for

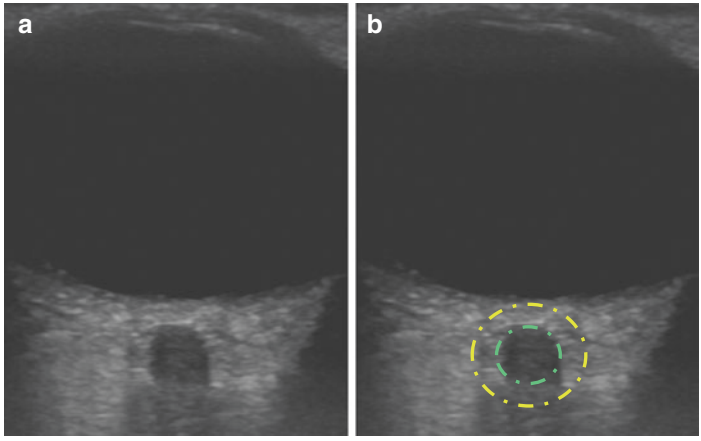

Fig. 2 Appropriate Bullseye transection of the Optic Nerve. (**a**). Normal ophthalmic ultrasound images obtained in the transverse view showing a circular cross-section of the optic nerve (dark circle) surrounded by the optic nerve sheath mimicking a bullseye. (**b**) The same image with green dotted lines outlining the outer edge of the optic nerve and yellow dotted lines outlining the outer edge of the optic nerve sheath to emphasize the appropriately aligned bullseye appearance

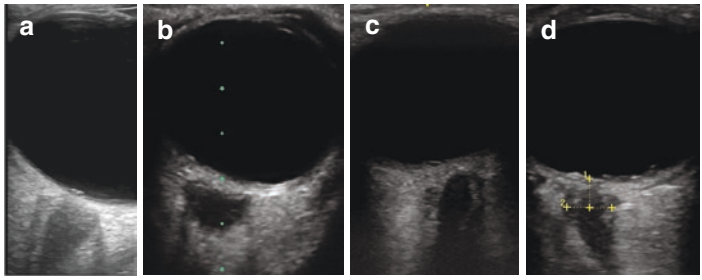

Fig. 3 Inappropriately aligned images of the Optic Nerve. (**a**–**d**) All images of poorly aligned, asymmetric, and crooked images of the hypoechoic or dark optic nerve surrounded by the hyperechoic or lighter optic nerve sheath with the outermost boarder of the optic nerve sheath appearing hypoechoic or black where the cerebral spinal fluid flows through the subarachnoid space. (**d**) Inaccurate measurement (2) of the optic nerve sheath diameter (due to poor alignment) measured 3 mm behind the orbit (1)

optimal ONSD to identify ICH from normal ICP ranged from 5.0 mm to 5.9 mm in this systematic review. Eight years later, Koziarz et al. provided an updated systematic review and meta-analysis with over ten times the studies compared to Dubourge et al. including both pediatric and adult studies. Koziarz group also separated data based on traumatic brain injury and non-traumatic brain injury, finding pooled sensitivity and specificity of ONSD ultrasonography to identify ICH in patients with traumatic brain injury to be 97% (95% CI, 92% to 99%) and 86% (CI, 74% to 93%) respectively [8]. For patients with non-traumatic brain injuries the pooled sensitivity was 92% (CI, 86% to 96%) and specificity was 86% (CI, 77% to 92%). The SROC curve of all patients showed a pooled sensitivity and specificity of 94% (CI, 91% to 96%) and 87% (CI, 82% to 91%), respectively [8]. Koziarz et al. was the first systematic review and meta-analysis to compare variable cutoff values and calculation methods to determine that 5.0 mm is the optimal cutoff to diagnose ICH in adult patients [8]. However, other studies have shown that an ONSD of 5.5 mm can be a normal finding in adults stating that a more reliable cutoff value to predict ICH is 5.7–6.0 mm showing sensitivity of 87–95% and specificity of 79–100% [92, 99–102].

Further questions exist in the global meaning of these ONSD measurements. Individual trends are trusted more than absolute numbers regarding the ONSD. We recommend averaging at least 3 measurements, as the average best accommodates for technique, anomalies in images, and anatomic differences. There also remains controversy regarding the validity of ONSD measurements in acute versus chronic changes of intracranial pressure. Acute changes have been more robustly studied, and it has been suggested that chronically elevated ICP may undergo a decrease in optic nerve sheath distensibility such that measurements will not reflect accurately the clinical context. Ensure that the duration of intracranial pathology is a consideration with interpretation of the ONSD measurements.

Interpretation of ONSD Measurements for Pediatric Patients

Despite the limited number of pediatric specific studies compared to adult studies investigating ultrasonographic measurements of ONSD in detecting intracranial hypertension, the first suggested cutoff value for children was published just over 25 years ago, suggesting a cutoff of 5.0 mm based on 39 children all over the age of 4 years old [30, 94]. Three years later, Ballantyne et al. created generalized normative pediatric ONSD based on optic nerve growth curves from 102 children ages 0–15 years proposing far lower cutoff values of 4 mm for infants <1 year old and 4.5 mm for children >1 year old [20]. These same lower cutoff values were reproduced several times over the following 10 years [10, 11, 29, 120, 121], with the addition of Moretti and Pizzi suggesting a cutoff of 4.0 mm for children ≤1 year old, 4.5 mm for children 1–4 years old, and 5.0 mm for children >4 years old [119]. However, Le et al., calculated the accuracy of the 4 mm and 4.5 mm cutoff points and found a sensitivity of 83% and specificity of 38% based on 64 pediatric patients [103]. Beare et al., published a study including 51 pediatric patients >1 year old using a cutoff value of 4.2 mm, finding the sensitivity and specificity of ONSD to diagnose ICH to be 100% and 86% respectively [12].

Young et al. was less keen on a direct cutoff that could be applied across pediatric cohorts. Instead, they indicated that <4.9 mm was unlikely to correlate with increased ICP suggesting an optimal cutoff of 6.1 mm with a sensitivity of 77%, specificity of 91%, and area under the ROC curve of 0.85 [104]; however, this was only based on 36 patients with an average age of 8 years old. Padayachy et al. reported a cutoff of 5.16 mm for children ≤1 year old and 5.75 mm for children >1 year old and an overall cutoff for their entire cohort of 5.5 mm based on 174 patients [13, 19]. Steinborn et al. has also suggested a significantly higher ONSD cutoff value be used in children to suggest ICH [105].

In the past few years, it has been argued that the optic nerve growth curve must be more heavily considered when establishing ONSD cutoff values in relation to children as their visual pathways are developing through childhood [106]. The development of the nervous system and the visual pathway has a rapid initial growth phase significantly slowing by age 4 with continued very slow development until the age of 8–10 years old [106, 107]. Therefore, it has been suggested that age stratification is essential when interpreting ONSD in children. Fontanel et al. developed an optic nerve growth curve for normal children 4–18 years of age based on 165 children, which showed progressive increase of the optic nerve up to approximately 10 years of age; therefore, they calculated cutoff values for children between 4 and 10 years and between 11 and 18 years old separately based on 29 children with ICH and 165 healthy children [22]. They reported an optimal cutoff value of 4.1 mm for the 4–10 year old subgroup and a cutoff of 4.4 mm for the 11–18 year old subgroup both cutoffs had a 100% sensitivity with specificity ranging from 83.9% to 98.8%. Fontanel et al. also evaluated a cutoff of 5.0 mm in their 29 children with ICH finding a sensitivity of 28.6% with 100% specificity [22], thus reinforcing lower cutoff values. Never before have such low cutoff thresholds been suggested. A possible limitation of Fontanel and associates is that all patients had non-traumatic chronic ICH (pseudotumor 52%, cerebral tumors 38%, and cerebral venous sinus thrombosis 10%), and ICH was defined as having an opening pressure on LP >28 cm H_2O, and no absolute or average opening pressures were reported.

To our knowledge, there are no pediatric studies that have determined optic nerve growth curves or more precise age stratification of ONSD measurements for neonates, babies, and children <4 years old. Along with the rapid growth of the optic nerve within the first year of life, it has also been suggested that having an open fontanel might affect accurate readings of ONSD measurements [19, 108]. Research has shown that patency of the anterior fontanelle can be used to help stratify patients into different ICP cutoff values [19]. With infants experiencing such profound growth of their optic nerves and closure of their fontanelles in the first year of life, it might be worthwhile to develop normative values and ONSD cutoff points with tighter age stratification cohorts such as: 0–6 months, 6–12 months, 12–24 months, 2–3 years, 3–4 years.

Specifically, with the pediatric population the recent variability in reported cutoff thresholds without consensus suggests that caution should be used when interpreting ONSD measurements in children. It is imperative that ONSD measurements are interpreted in conjunction with physical exam and other imaging modalities when making clinical decisions. It appears that the application of ONSD measurements in the pediatric population is most likely primarily utilized in research as opposed to daily clinical practice.

Limitations

There are several overall limitations to applying ultrasound guided ONSD measurements. For example, shadowing artifacts caused by the lens of the eye and the optic disc or by inexperienced operators may significantly alter measurements of the ONSD making them inaccurate [109]. Ophthalmic ultrasound cannot be performed in patients with ocular trauma or glaucoma. ONSD measurements in patients who suffer from congenital or acquired optic nerve atrophy will be grossly inaccurate. Some have suggested that ultrasound B scan technology is less reliable than A scan technology because of the "blooming effect;" if the gain setting is not optimized the edges of small objects (<0.5 mm) can become blurred. The blooming effect can make exact placement of measurement calipers' difficult due to the blurred edges of the

optic nerve sheath [110–112]. The blooming effect can be overcome with optimization of the gain function and will be less relevant as ultrasound B scan technology continues to evolve. It has been suggested that A scan technology replace B scan technology when obtaining ONSD measurements to eliminate the blooming effect [106, 113]. However, given the lack of availability of A scan technology outside of the ophthalmology specialty and the additional training needed to use the technology, we do not support this suggestion. Optimization and standardization of the gain setting and utilization of high frequency probes appears more feasible than transitioning from B scan to A scan technology.

Most published cutoff values for diagnosing ICH are based on measurements obtained from the external edge of the optic nerve sheath or the outer hyperechogenic (dark) borders of the subarachnoid space internal to the hypoechogenic (light) dura mater [21, 92, 95, 96]. The correct way to measure ONSD is the distance inside the dura mater, not the distance outside the dura mater see Fig. 4. Some studies have published data incorrectly measuring from the internal edges of the optic nerve sheath, or the distance between the outer edges of the pia mater. Measurements taken from the internal edge of the ONSD will be smaller than those taken from the external edge, which can lead to inconsistent data [21, 96]. Several studies also exist where the ONSD was incorrectly obtained by measuring the distance between the outer hypoechogenic borders of the dura mater, leading to falsely enlarged ONSD values [96, 97]. Therefore, it is important when evaluating the literature to identify exactly how the ONSD measurements were obtained. And more importantly in clinical practice, accurately measuring the ONSD is imperative to the application of this technology.

Some studies suggest that the distensibility of the ONSD is variable in individuals even who are the same age, sex, and suffer the same pathology; therefore, there is some concern about the standardization of ONSD measurement cutoff values. Many suggest that trending changes of the ONSD of a single individual might be more clinically relevant than applying universal cutoff values to all [9, 114, 115]. There is a marked variability in the size of the ONSD in healthy children of different ages calling for further research to establish tighter age stratifications for normative

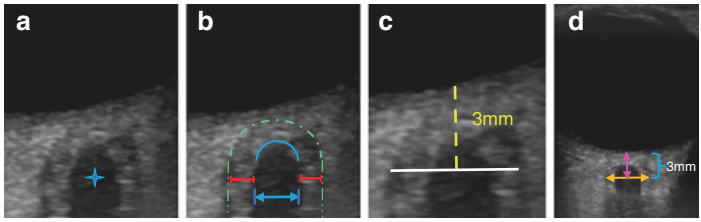

Fig. 4 Measuring the Optic Nerve Sheath. (**a**). Normal ophthalmic ultrasound image zoomed in focusing on the posterior chamber of the eye where the optic nerve (blue star) meets the orbit often referred to as the papilla. (**b**) The same ultrasound image with a blue line with arrows showing a cross-section of the optic nerve. Blue lines along the pia mater enhance the separation of the optic nerve (hypoechoic) from the internal edge of the optic nerve sheath (hyperechoic). Red lines show the distance between the internal and external edges of the optic nerve sheath. Green dashed lines along the external edge of the optic nerve sheath or the outer hyperechoic borders of the subarachnoid space internal to the hypoechoic (light) dura mater. (**c**) The same image with a yellow dashed line measuring 3 mm behind the papilla with a white line transecting the optic nerve sheath measured from the distance between the external edges of the subarachnoid space. (**d**) Pink line measuring 3 mm up the optic nerve from the papilla with orange line measuring the optic nerve sheath diameter between the external edges of the subarachnoid space

and pathologic ONSD measurements. Other factors that may bias measurements include level of magnification, frequency of linear array probes, position of the patient, and whether monocular or binocular measurements were obtained. Currently, the biggest limitation is the marked variability in ONSD values reported across studies in both healthy people and people suffering from neuropathology; therefore, further scientifically sound research is needed to better assess the usefulness and limits of ultrasound guided ONSD measurements.

Conclusion

Because this bedside tool allows for fast and safe real time assessment of conditions associated with elevated intracranial pressure, we propose routine inclusion of ONSD measurements in the mul-

timodal monitoring of patients in adult and pediatric neurocritical care. Ultrasound guided ONSD measurement should be used in conjunction with invasive ICP monitoring for patients with neurological conditions at risk for developing ICH. Ultrasound guided ONSD measurements should be used as a complementary technique for identifying and monitoring ICH but should not substitute current standard techniques of measuring ICP. The technique can also provide interval monitoring to follow responses of ICP to therapy or disease progression. Caution should be used when applying universal cutoff values to determine ICH. Though future research should address honing cutoff values and enhancing techique, optic nerve sheath diameter has proven to be a beneficial tool for clinicians to diagnose pediatric and adult patients with suspected intracranial pathology, which should be utilized in a variety of clinical settings.

References

1. Karvellas CJ, Fix OK, Battenhouse H, Durkalski V, Sanders C, Lee WM, Group USALFS. Outcomes and complications of intracranial pressure monitoring in acute liver failure: a retrospective cohort study. Crit Care Med. 2014;42:1157–67.
2. Peck M, Wendon J, Sizer E, Auzinger G, Bernal W. Intracranial pressure monitoring in acute liver failure: a review of 10 years experience. Crit Care. 2010;14:P542.
3. Vaquero J, et al. Complications and use of intracranial pressure monitoring in patients with acute liver failure and severe encephalopathy. Liver Transpl. 2005;11:1581–9.
4. Chau CYC, Craven CL, Rubiano AM, Adams H, Tulu S, Czosnyka M, Servadei F, Ercole A, Hutchinson PJ, Kolias AG. The evolution of the role of external ventricular drainage in traumatic brain injury. J Clin Med. 2019;8(9). Pii: E1422.
5. Alkhoury F, Kyriakides TC. Intracranial pressure monitoring in children with severe traumatic brain injury: National Trauma Data Bank-Based Review of outcomes. JAMA Surg. 2014;149(6):544–8.
6. Roumeliotis N, Pettersen G, Crevier L, Emeriaud G. ICP monitoring in children: why are we not adhering to guidelines? Childs Nerv Syst. 2015;31:2011–4.
7. Khan M, Shallwani H, Khan M, Shamim M. Noninvasive monitoring intracranial pressure? A review of available modalities. Surg Neurol Int. 2017;8(1):51.

8. Koziarz A, Sne N, Kegel F, Nath S, Badhiwala JH, Nassiri F, Mansouri A, Yang K, Zhou Q, Rice T, Faidi S, Passos E, Healey A, Banfield L, Mensour M, Kirkpatrick AW, Nassar A, Fehlings MG, Hawryluk GWJ, Almenawer SA. Bedside optic nerve ultrasonography for diagnosing increased intracranial pressure: a systematic review and meta-analysis. Ann Intern Med. 2019;171(12):896–905.
9. Lochner P, Czosnyka M, Naldi A, Lyros E, Pelosi P, Mathur S, Fassbender K, Robba C. Optic nerve sheath diameter: present and future perspectives for neurologists and critical care physicians. Neurol Sci. 2019;40(12):2447–57.
10. Newman WD, Hollman AS, Dutton GN, et al. Measurement of optic nerve sheath diameter by ultrasound: a means of detecting acute raised intracranial pressure in hydrocephalus. Br J Ophthalmol. 2002; 86:1109–13.
11. Malayeri AA, Bavarian S, Mehdizadeh M. Sonographic evaluation of optic nerve diameter in children with raised intracranial pressure. J Ultrasound Med. 2005;24:143–7.
12. Beare NA, Kampodeni S, Glover SJ, Molyneux E, Taylor TE, Harding SP, Molyneux ME. Detection of raised intracranial pressure by ultrasound measurement of optic nerve sheath diameter in African children. Tropical Med Int Health. 2008;13(11):1400–4.
13. Padayachy LC, Padayachy V, Galal U, Gray R, Fieggen AG. The relationship between transorbital ultrasound measurement of the optic nerve sheath diameter (ONSD) and invasively measured ICP in children: part I: repeatability, observer variability and general analysis. Childs Nerv Syst. 2016;32(10):1769–78.
14. Narayan V, Mohammed N, Savardekar AR, Patra DP, Notarianni C, Nanda A. Non-invasive intracranial pressure monitoring for severe traumatic brain injury in children: a concise update on current methods. World Neurosurg. 2018;114:293–300.
15. Raval R, Shen J, Lau D, Ferguson N, Kelly T, Daniels J, Dorotta I, Ramsingh D. Comparison of three point-of-care ultrasound views and MRI measurements for optic nerve sheath diameter: a prospective validity study. Neurocrit Care. 2020;33(1):173–81.
16. Liu M, Yang ZK, Yan YF, Shen X, Yao HB, Fei L, Wang ES. Optic nerve sheath measurements by computed tomography to predict intracranial pressure and guide surgery in patients with traumatic brain injury. World Neurosurg. 2020;134:e317–24.
17. Kang C, Min JH, Park JS, You Y, Yoo I, Cho YC, Jeong W, Ahn HJ, Ryu S, Lee J, Kim SW, Cho SU, Oh SK, Lee IH, Lee B, Lee D, Chae MK. Relationship between optic nerve sheath diameter measured by magnetic resonance imaging, intracranial pressure, and neurological outcome in cardiac arrest survivors who underwent targeted temperature management. Resuscitation. 2019;145:43–9.

18. Gospe SM 3rd, Amrhein TJ, Malinzak MD, Bhatti MT, Mettu P, El-Dairi MA. Magnetic resonance imaging abnormalities of the optic nerve sheath and intracranial internal carotid artery in giant cell arteritis. J Neuroophthalmol. 2020;41(1):54–9.
19. Padayachy LC, Padayachy V, Galal U, Pollock T, Fieggen AG. The relationship between transorbital ultrasound measurement of the optic nerve sheath diameter (ONSD) and invasively measured ICP in children. Part II: age-related ONSD cut-off values and patency of the anterior fontanelle. Childs Nerv Syst. 2016;32(10):1779–85.
20. Ballantyne J, Hollman AS, Hamilton R, Bradnam MS, Carachi R, Young DG, Dutton GN. Transorbital optic nerve sheath ultrasonography in normal children. Clin Radiol. 1999;54(11):740–2.
21. Bauerle J, Schuchardt F, Schroeder L, et al. Reproducibility and accuracy of optic nerve sheath diameter assessment using ultrasound compared to magnetic resonance imaging. BMC Neurol. 2013;13:187.
22. Fontanel L, Pensiero S, Ronfani L, Rosolen V, Barbi E. Optic nerve sheath diameter ultrasound: optic nerve growth curve and its application to detect intracranial hypertension in children. Am J Ophthalmol. 2019;208:439.
23. Cleves-Bayon C. Idiopathic intracranial hypertension in children and adolescents: an update. Headache. 2018;58:485–93.
24. Maissan IM, Dirven PJAC, Haitsma IK, et al. Ultrasonographic measured optic nerve sheath diameter as an accurate and quick monitor for changes in intracranial pressure. J Neuro-Oncol. 2015;123:743–7.
25. Soliman I, Johnson GGRJ, Gillman LM, et al. New optic nerve sonography quality criteria in the diagnostic evaluation of traumatic brain injury. Crit Care Res Pract. 2018;2018:3589762.
26. Hansen HC, Helmke K. The subarachnoid space surrounding the optic nerves: an ultrasound study of the optic nerve sheath. Surg Radiol Anat. 1996;18(4):323–8.
27. Hayreh SS. Pathogenesis of oedema of the optic disc. Doc Ophthalmol. 1968;24(2):289–411.
28. Wilson MH, Wright A, Imray CH. Intracranial pressure at altitude. High Alt Med Biol. 2014;15:123–32.
29. Hansen HC, Helmke K. Validation of the optic nerve sheath response to changing cerebrospinal fluid pressure: ultrasound findings during intrathecal infusion tests. J Neurosurg. 1997;87:34–40.
30. Helmke K, Hansen HC. Fundamentals of transorbital sonographic evaluation of optic nerve sheath expansion under intracranial hypertension II. Patient study. Pediatr Radiol. 1996;26:706–10.
31. Liu D, Li Z, Zhang X, Zhao L, Jia J, Sun F, Wang Y, Ma D, Wei W. Assessment of intracranial pressure with ultrasonographic retrobulbar optic nerve sheath diameter measurement. BMC Neurol. 2017;17:188.

32. Lee SH, Kim HS, Yun SJ. Optic nerve sheath diameter measurement for predicting raised intracranial pressure in adult patients with severe traumatic brain injury: a meta-analysis. J Crit Care. 2020;56:182–7.
33. Du J, Deng Y, Li H, Qiao S, Yu M, Xu Q, Wang C. Ratio of optic nerve sheath diameter to eyeball transverse diameter by ultrasound can predict intracranial hypertension in traumatic brain injury patients: a prospective study. Neurocrit Care. 2019;31(3):594–5.
34. Rehman Siddiqui NU, Haque A, Abbas Q, Jurair H, Salam B, Sayani R. Ultrasonographic optic nerve sheath diameter measurement for raised intracranial pressure in a Tertiary care centre of a developing country. J Ayub Med Coll Abbottabad. 2018;30(4):495–500.
35. Naldi A, et al. Ultrasonography monitoring of optic nerve sheath diameter and retinal vessels in patients with cerebral hemorrhage. J Neuroimaging. 2019;29(3):394–9.
36. Skoloudik D, et al. Distal enlargement of the optic nerve sheath in the hyperacute stage of intracerebral haemorrhage. Br J Ophthalmol. 2011;95:217–21.
37. Gokcen E, Caltekin I, Savrun A, Korkmaz H, Savrun ST, Yildirim G. Alterations in optic nerve sheath diameter according to cerebrovascular disease sub-groups. Am J Emerg Med. 2017;35:1607–11. https://doi.org/10.1016/j.ajem.2017.04.073.
38. Zhao L, Huang Q, Huang P, Zhao Q, Xie H, Wang R. Optic nerve sheath diameter and eyeball transverse diameter as a useful tool for the clinical prognosis in patients with stroke during hospitalization. Zhonghua Wei Zhong Bing Ji Jiu Yi Xue. 2019;31(10):1242–6.
39. Seyedhosseini J, Aghili M, Vahidi E, Shirani F. Association of optic nerve sheath diameter in ocular ultrasound with prognosis in patients presenting with acute stroke symptoms. Turk J Emerg Med. 2019;19(4):132–5.
40. Arthur J, Duran-Gehring P, Kumetz C, Chadwick S, McIntosh M. Cerebral venous thrombosis: an uncommon cause of papilledema on bedside ocular ultrasound. J Emerg Med. 2019;56(3):288–93.
41. Nischal KK, Smith DM, Losee JE. Discussion: nocturnal ultrasound measurements of optic nerve sheath diameter correlate with intracranial pressure in children with craniosynostosis. Plast Reconstr Surg. 2012;130(3):452e–4e.
42. Driessen C, Bannink N, Lequin M, van Veelen ML, Naus NC, Joosten KF, Mathijssen IM. Are ultrasonography measurements of optic nerve sheath diameter an alternative to funduscopy in children with syndromic craniosynostosis? J Neurosurg Pediatr. 2011;8(3):329–34.
43. Nabeta HW, Bahr NC, Rhein J, Fossland N, Kiragga AN, Meya DB, Dunlop SJ, Boulware DR. Accuracy of noninvasive intraocular pressure or optic nerve sheath diameter measurements for predicting elevated intracranial pressure in cryptococcal meningitis. Open Forum Infect Dis. 2014;1(3):ofu093.

44. Sangani SV, Parikh S. Can sonographic measurement of optic nerve sheath diameter be used to detect raised intracranial pressure in patients with tuberculous meningitis? A prospective observational study. Indian J Radiol Imaging. 2015;25(2):173–6.
45. Caputo ND, Fraser RM, Abdulkarim J. Posterior reversible encephalopathy syndrome presenting as papilledema. Am J Emerg Med. 2012;30(5):835.e5–7.
46. Lochner P, Mader C, Nardone R, Cantello R, Orioli A. Brigo F usefulness of ultrasonography in posterior reversible encephalopathy syndrome. Neurol Sci. 2014 Mar;35(3):475–7.
47. Lochner P, Nardone R, Brigo F, Tamber MS, Zuccoli G. The diagnosis of posterior reversible encephalopathy syndrome. Lancet Neurol. 2015;14(11):1074–5.
48. Brzezinska R, Schumacher R. Diagnosis of elevated intracranial pressure in children with shunt under special consideration of transglobe sonography of the optic nerve. Ultraschall Med. 2002;23(5):325–32.
49. Ertl M, Aigner R, Krost M, Karnasova Z, Muller K, Naumann M, Schlachetzki F. Measuring changes in the optic nerve sheath diameter in patients with idiopathic normal-pressure hydrocephalus: a useful diagnostic supplement to spinal tap tests. Eur J Neurol. 2017;24(3):461–7.
50. Nag DS, Sahu S, Swain A, Kant S. Intracranial pressure monitoring: Gold standard and recent innovations. World J Clin Cases. 2019;7(13):1535–53.
51. Das MC, Srivastava A, Yadav RK, Yachha SK, Poddar U. Optic nerve sheath diameter in children with acute liver failure: a prospective observational pilot study. Liver Int. 2020;40(2):428–36.
52. Rajajee V, Williamson CA, Fontana RJ, Courey AJ, Patil PG. Noninvasive intracranial pressure assessment in acute liver failure. Neurocrit Care. 2018;29(2):280–90. 76.
53. Ganschow R, Nolkemper D, Helmke K, Harps E, Commentz JC, Broering DC, Pothmann W, Rogiers X, Hellwege HH, Burdelski M. Intensive care management after pediatric liver transplantation: a single-center experience. Pediatr Transplant. 2000;4(4):273–9.
54. Cornetta P, Vitiello L, De Bernardo M, Rosa N. Optic nerve sheath diameter appraisal in children affected by diabetic ketoacidosis. J Pediatr Endocrinol Metab. 2019;32(11):1203–4.
55. Kendir OT, Yilmaz HL, Ozkaya AK, Turan I, Gokay SS, Bilen S, Yildizdas RD, Yuksel B. Determination of cerebral edema with serial measurement of optic nerve sheath diameter during treatment in children with diabetic ketoacidosis: a longitudinal study. J Pediatr Endocrinol Metab. 2019;32(9):943–9.
56. Jeziorny K, Waszczykowska A, Barańska D, Szadkowska A, Młynarski W, Zmysłowska A. Can we effectively predict the occurrence of cerebral edema in children with ketoacidosis in the course of type 1 diabetes?

-case report and literature review. J Pediatr Endocrinol Metab. 2020;33(2):319–22.
57. Jeziorny K, Niwald A, Moll A, Piasecka K, Pyziak-Skupien A, Waszczykowska A, Baranska D, Malachowska B, Szadkowska A, Mlynarski W, Zmyslowska A. Measurement of corneal thickness, optic nerve sheath diameter and retinal nerve fiber layer as potential new non-invasive methods in assessing a risk of cerebral edema in type 1 diabetes in children. Acta Diabetol. 2018;55(12):1295–301.
58. Ebisike PI, Habib SG, Hassan S, Suwaid MA, Hikima MS, Saleh MK, Jibo U, Yusuf L. Transorbital sonographic measurement of optic nerve sheath diameter among HIV-Positive patients in Northwestern Nigeria. Niger J Clin Pract. 2019;22(11):1570–5.
59. Chelly J, Deye N, Guichard JP, Vodovar D, Vong L, Jochmans S, Thieulot-Rolin N, Sy O, Serbource-Goguel J, Vinsonneau C, Megarbane B, Vivien B, Tazarourte K, Monchi M. The optic nerve sheath diameter as a useful tool for early prediction of outcome after cardiac arrest: a prospective pilot study. Resuscitation. 2016;103:7–13.
60. Chae MK, Ko E, Lee JH, Lee TR, Yoon H, Hwang SY, Cha WC, Shin TG, Sim MS, Jo IJ, Song KJ, Rhee JE, Jeong YK. Better prognostic value with combined optic nerve sheath diameter and grey-to-white matter ratio on initial brain computed tomography in post-cardiac arrest patients. Resuscitation. 2016;104:40–5.
61. Ueda T, Ishida E, Kojima Y, Yoshikawa S, Yonemoto H. Sonographic optic nerve sheath diameter: a simple and rapid tool to assess the neurologic prognosis after cardiac arrest. J Neuroimaging. 2015;25(6):927–30.
62. Ertl M, Weber S, Hammel G, Schroeder C, Krogias C. Transorbital sonography for early prognostication of hypoxic-ischemic encephalopathy after cardiac arrest. J Neuroimaging. 2018;28:542–8.
63. Wang J, Li K, Li H, Ji C, Wu Z, Chen H, Chen B. Ultrasonographic optic nerve sheath diameter correlation with ICP and accuracy as a tool for noninvasive surrogate ICP measurement in patients with decompressive craniotomy. J Neurosurg. 2019:1–7.
64. Kim Y, Choi S, Kang S, Park B. Propofol affects optic nerve sheath diameter less than sevoflurane during robotic surgery in the steep trendelenburg position. Biomed Res Int. 2019;2019:5617815.
65. Citerio G, Vascotto E, Villa F, Celotti S, Pesenti A. Induced abdominal compartment syndrome increases intracranial pressure in neurotrauma patients: a prospective study. Crit Care Med. 2001;29(7):1466–71.
66. Cooke SJ, Paterson-Brown S. Association between laparoscopic abdominal surgery and postoperative symptoms of raised intracranial pressure. Surg Endosc. 2001;15(7):723–5.
67. Kim MS, Bai SJ, Lee JR, Choi YD, Kim YJ, Choi SH. Increase in intracranial pressure during carbon dioxide pneumoperitoneum with steep

trendelenburg positioning proven by ultrasonographic measurement of optic nerve sheath diameter. J Endourol. 2014;28(7):801–6.
68. Robba C, Cardim D, Donnelly J, Bertuccio A, Bacigaluppi S, Bragazzi N, Cabella B, Liu X, Matta B, Lattuada M, Czosnyka M. Effects of pneumoperitoneum and Trendelenburg position on intracranial pressure assessed using different non-invasive methods. Br J Anaesth. 2016;117(6):783–91.
69. Kim EJ, Koo BN, Choi SH, Park K, Kim MS. Ultrasonographic optic nerve sheath diameter for predicting elevated intracranial pressure during laparoscopic surgery: a systematic review and meta-analysis. Surg Endosc. 2018;32(1):175–82.
70. Ertl M, Schierling W, Kasprzak P, Schomig B, Bruckl C, Schlachetzki F, Pfister K. Optic nerve sheath diameter measurement to identify high-risk patients for spinal ischemia after endovascular thoracoabdominal aortic aneurysm repair. J Neuroimaging. 2015;25(6):910–5.
71. Dip F, Nguyen D, Rosales A, Sasson M, Lo Menzo E, Szomstein S, Rosenthal R. Impact of controlled intraabdominal pressure on the optic nerve sheath diameter during laparoscopic procedures. Surg Endosc. 2016;30(1):44–9.
72. Yu J, Park JY, Kim DH, Koh GH, Jeong W, Kim E, Hong JH, Hwang JH, Kim YK. Dexmedetomidine attenuates the increase of ultrasonographic optic nerve sheath diameter as a surrogate for intracranial pressure in patients undergoing robot-assisted laparoscopic prostatectomy: a randomized double-blind controlled trial. Medicine (Baltimore). 2019;98(33):e16772.
73. Yoon SB, Ji SH, Jang YE, Lee JH, Kim EH, Kim JT, Kim HS. Effects of prone positioning with neck extension on intracranial pressure according to optic nerve sheath diameter measured using ultrasound in children. Childs Nerv Syst. 2020;36(5):1001–7.
74. Singh S, Nasa V, Tandon M. Perioperative monitoring in liver transplant patients. J Clin Exp Hepatol. 2012;2(3):271–8.
75. Pal A, Dhar P, Goyal N. Perioperative monitoring of intracranial pressure using optic nerve sheath diameter in paediatric liver transplantation. Indian J Anaesth. 2018;62(11):892–5.
76. Seo H, Kim YK, Shin WJ, Hwang GS. Ultrasonographic optic nerve sheath diameter is correlated with arterial carbon dioxide concentration during reperfusion in liver transplant recipients. Transplant Proc. 2013;45(6):2272–6.
77. Dubost C, Le Gouez A, Jouffroy V, Roger-Christoph S, Benhamou D, Mercier FJ, Geeraerts T. Optic nerve sheath diameter used as ultrasonographic assessment of the incidence of raised intracranial pressure in preeclampsia: a pilot study. Anesthesiology. 2012;116(5):1066–71.
78. Brzan Simenc G, Ambrozic J, Prokselj K, Tul N, Cvijic M, Mirkovic T, Lucovnik M. Ocular ultrasonography for diagnosing increased intracra-

nial pressure in patients with severe preeclampsia. Int J Obstet Anesth. 2018;36:49–55.
79. Lochner P, Nardone R, Tezzon F, Coppo L, Brigo F. Optic nerve sonography to monitor treatment efficacy in idiopathic intracranial hypertension: a case report. J Neuroimaging. 2013;23(4):533–4.
80. Lochner P, Brigo F, Zedde ML, Sanguigni S, Coppo L, Nardone R, Naldi A, Sola D, Stolz E. Feasibility and usefulness of ultrasonography in idiopathic intracranial hypertension or secondary intracranial hypertension. BMC Neurol. 2016;16:85.
81. Lochner P, et al. B-mode transorbital ultrasonography for the diagnosis of idiopathic intracranial hypertension: a systematic review and meta-analysis. Ultraschall Med. 2019;40(2):247–52.
82. Fichtner J, Ulrich CT, Fung C, Knüppel C, Veitweber M, Jilch A, Schucht P, Ertl M, Schömig B, Gralla J, Z'Graggen WJ, Bernasconi C, Mattle HP, Schlachetzki F, Raabe A, Beck J. Management of spontaneous intracranial hypotension—transorbital ultrasound as discriminator. J Neurol Neurosurg Psychiatry. 2016;87(6):650–5.
83. Dubost C, Le Gouez A, Zetlaoui PJ, Benhamou D, Mercier FJ, Geeraerts T. Increase in optic nerve sheath diameter induced by epidural blood patch: a preliminary report. Br J Anaesth. 2011;107(4):627–30.
84. Betcher J, Becker TK, Stoyanoff P, Cranford J, Theyyunni N. Military trainees can accurately measure optic nerve sheath diameter after a brief training session. Mil Med Res. 2018;5(1):42.
85. Maissan IM, Verbaan LA, van den Berg M, Houmes RJ, Stolker RJ, den Hartog D. Helicopter transportation increases intracranial pressure: a proof-of-principle study. Air Med J. 2018;37(4):249–52.
86. Houzé-Cerfon CH, Bounes V, Guemon J, Le Gourrierec T, Geeraerts T. Quality and feasibility of sonographic measurement of the optic nerve sheath diameter to estimate the risk of raised intracranial pressure after traumatic brain injury in prehospital setting. Prehosp Emerg Care. 2019;23(2):277–83.
87. Martin DS, Caine TL, Matz T, Lee SM, Stenger MB, Sargsyan AE, Platts SH. Virtual guidance as a tool to obtain diagnostic ultrasound for spaceflight and remote environments. Aviat Space Environ Med. 2012;83(10):995–1000.
88. Chiao L, Sharipov S, Sargsyan AE, Melton S, Hamilton DR, McFarlin K, Dulchavsky SA. Ocular examination for trauma; clinical ultrasound aboard the International Space Station. J Trauma. 2005;58(5):885–9.
89. Lizzi FL, Coleman DJ, Driller J, et al. Effects of pulsed ultrasound on ocular tissue. Ultrasound Med Biol. 1981;7:245–52.
90. Food and Drug Administration: Information for Manufacturers Seeking Clearance of Diagnostic Ultrasound Systems and Transducers; 2008. Available from: http://www.fda.gov/medicaldevices/deviceregulationandguidance/guidancedocuments/ucm070856.htm.

91. Section 7–discussion of the mechanical index and other exposure parameters. American Institute of Ultrasound in Medicine. J Ultrasound Med. 2000;19:143–148, 54–68.
92. Ertl M, Barinka F, Torka E, Altmann M, Pfister K, Helbig H, Bogdahn U, Gamulescu MA, Schlachetzki F. Ocular color-coded sonography - a promising tool for neurologists and intensive care physicians. Ultraschall Med. 2014;35(5):422–31.
93. Shah S, Kimberly H, Marill K, Noble V. Ultrasound techniques to measure the optic nerve sheath: is a specialized probe necessary? Med Sci Monit. 2009;15:63–8.
94. Helmke K, Hansen HC. Fundamentals of transorbital sonographic evaluation of optic nerve sheath expansion under intracranial hypertension. I Experimental study. Pediatr Radiol. 1996;26:701–5.
95. Aspide R, Bertolini G, Albini Riccioli L, Mazzatenta D, Palandri G, Biasucci DG. A proposal for a new protocol for sonographic assessment of the optic nerve sheath diameter: the CLOSED protocol. Neurocrit Care. 2020;32(1):327–32.
96. Topcuoglu M, Arsava EM, Bas DF, Kozak HH. Transorbital ultrasonographic measurement of optic nerve sheath diameter in brain death. J Neuroimaging. 2015;25(6):906–9.
97. Krogias C, Ayzenberg I, Schroeder C, Gruter T, Gold R, Yoon MS. Transorbital sonography in CIDP patients: no evidence for optic nerve hypertrophy. J Neurol Sci. 2016;362:206–8.
98. Dubourg J, Javouhey E, Geeraerts T, Messerer M, Kassai B. Ultrasonography of optic nerve sheath diameter for detection of raised intracranial pressure: a systematic review and meta-analysis. Intensive Care Med. 2011;37(7):1059–68.
99. Soldatos T, Karakitsos D, Chatzimichail K, et al. Optic nerve sonography in the diagnostic evaluation of adult brain injury. Crit Care. 2008;12:R67.
100. Geeraerts T, Launey Y, Martin L, et al. Ultrasonography of the optic nerve sheath may be useful for detecting raised intracranial pressure after severe brain injury. Intensive Care Med. 2007;33:1704–11.
101. Watanabe A, Kinouchi H, Horikoshi T, et al. Effect of intracranial pressure on the diameter of the optic nerve sheath. J Neurosurg. 2008;109:255–8.
102. Geeraerts T, Merceron S, Benhamou D, et al. Non-invasive assessment of intracranial pressure using ocular sonography in neurocritical care patients. Intensive Care Med. 2008;34:2062–7.
103. Le A, Hoehn ME, Smith ME, Spentzas T, Schlappy D, Pershad J. Bedside sonographic measurement of opticnerve sheath diameter as a predictor of increased intracranial pressure in children. Ann Emerg Med. 2009;53:785–91.58.
104. Young AMH, Guilfoyle MR, Donnelly J, Scoffings D, Fernandes H, Garnett M, et al. Correlating optic nerve sheath diameter with opening

intracranial pressure in pediatric traumatic brain injury. Pediatr Res. 2017;81(3):443–7.
105. Steinborn M, Friedmann M, Makowski C, Hahn H, Hapfelmeier A, Juenger H. High resolution transbulbar sonography in children with suspicion of increased intracranial pressure. Childs Nerv Syst. 2016;32:655–60.
106. De Bernardo M, Vitiello L, Rosa N. Optic nerve sheath diameter ultrasound: optic nerve growth curve and its application to detect intracranial hypertension in children. Am J Ophthalmol. 2019;208:438.
107. Yu DY, Cringle SJ, Balaratnasingam C, Morgan WH, Yu PK, Su EN. Retinal ganglion cells: energetics, compartmentation, axonal transport, cytoskeletons and vulnerability. Prog Retin Eye Res. 2013;36:217–46.
108. Kerscher SR, Schöni D, Hurth H, Neunhoeffer F, Haas-Lude K, Wolff M, Schuhmann MU. The relation of optic nerve sheath diameter (ONSD) and intracranial pressure (ICP) in pediatric neurosurgery practice – Part I: correlations, age-dependency and cut-off values. Childs Nerv Syst. 2020;36(1):99–106.
109. Copetti R, Cattarossi L. Optic nerve ultrasound: artifacts and real images. Intensive Care Med. 2009;35:1488–9; author reply 1490–1481.
110. Rosa N, De Bernardo M. Ultrasound assessment of optic nerve sheath diameter in healthy volunteers. J Crit Care. 2017;40:279.
111. De Bernardo M, Rosa N. Clarification on using ultrasonography to detect intracranial pressure. JAMA Ophthalmol. 2017;135:1004–5. 4.
112. Rosa N, Vitiello L, De Bernardo M. Optic nerve sheath diameter measurement in hypoxic ischaemic brain injury after cardiac arrest. Resuscitation. 2019;138:310–1.
113. De Bernardo M, Vitiello L, Capone M, Rosa N. A-scan ultrasonography and optic nerve sheath diameter evaluation in children with acute liver failure. Liver Int. 2020;40(6):1504.
114. Robba C, Santori G, Czosnyka M, Corradi F, Citerio G. Optic nerve sheath diameter: the next steps. Intensive Care Med. 2019;45(12):1842–3.
115. Hansen HC, Helmke K. Optic nerve sheath responses to pressure variations. Intensive Care Med. 2019;45(12):1840–1.
116. Krishnamoorth V, Beckmann K, Mueller M, Sharma D, Vavilala M. Perioperative estimation of the intracranial pressure using the optic nerve sheath diameter during liver transplantation. Liver Transplant. 2013;19:246–9.
117. Shofty B, Ben-Sira L, Constantini S, Freedman S. Optic nerve sheath diameter on MR imaging: establishment of norms and comparison of pediatric patients with idiopathic intracranial hypertension with healthy controls. Am J Neuroradiol. 2012;33:366–9.

118. Legrand A, et al. Estimation of optic nerve sheath diameter on an initial brain computed tomography scan can contribute prognostic information in traumatic brain injury patients. Crit Care. 2013;17:R61.
119. Moretti R, Pizzi B, Cassini F, Vivaldi N. Reliability of optic nerve ultrasound for the evaluation of patients with spontaneous intracranial hemorrhage. Neurocrit Care. 2009;11:406.
120. Körber F, Scharf M, Moritz J, Dralle D. Sonography of the optical nerve – experience in 483 children. Rofo. 2005;177(2):229–35.
121. McAuley D, Paterson A, Sweeney L. Optic nerve sheath ultrasound in the assessment of paediatric hydrocephalus. Childs Nerv Syst. 2009;25(1):87–90.

Cranial Ultrasound

Aarti Sarwal

Cranial Anatomy on B Mode Ultrasound

Transtemporal insonation of the skull allows 2-dimensional imaging of the brain parenchyma and intracranial vessels with B mode imaging, color Doppler imaging of the Circle of Willis and Pulse Wave Doppler of individual intracranial vessel segments [1–5]. Components of transcranial ultrasound imaging are known by several terms: transcranial Doppler (TCD) or non-imaging Doppler, transcranial color-coded sonography (TCCS) or duplex ultrasound or imaging Doppler and brain echography. Acquisition of B mode images to identify the midbrain is the first step before vessel insonation for all transcranial ultrasound studies [6]. Since TCD or TCCS inherently includes vessel Doppler insonation and brain parenchyma assessment only requires B mode images on ultrasound, the term "cranial ultrasound" or "brain echography" has been introduced to distinguish between these studies.

Cranial ultrasound has been performed in children for the last 50 years for germinal matrix hemorrhage detection through the patent fontanel [7]. Thickening of temporal bones with increasing

A. Sarwal (✉)
Neurology, Neurocritical Care, Wake Forest Baptist Medical Center, Winston Salem, NC, USA
e-mail: asarwal@wakehealth.edu

W. C. Ziai, C. L. Cornwell (eds.), *Neurovascular Sonography*,
https://doi.org/10.1007/978-3-030-96893-9_18

age makes insonation much more difficult in adults. About 80–90% of the population has sufficiently thin temporal bones (acoustic windows) that permit high-resolution B mode imaging of brain parenchymal structures through the temporal bone while a thick skull impedes ultrasound penetration in 10–20% of patients [5, 8–11]. Though adult applications of cranial ultrasound came forth in the 1970s, rapid availability of 24 h computed tomography (CT) and magnetic resonance imaging (MRI) in addition to lack of sensitivity and specificity of ultrasound in detecting ischemic stroke (most stroke presentations) prevented widespread adoption of this diagnostic modality. Recent increase in accessibility to high-resolution point of care ultrasound devices and increasing use of these by in-house emergency medicine and critical care medicine physicians has brought about a resurgence of ultrasound, including cranial ultrasound [12–17]. Detection of intracranial hemorrhage and assessment of midline shift are two point of care applications where screening with point of care ultrasound may have contemporary applications. This chapter lists the techniques and point of care applications of cranial ultrasound in patients where CT head may not be immediately feasible.

Technique A cranial ultrasound can be performed using a 1–2 MHz probe (echo probe or phased array probe) to obtain B mode or gray scale images of the brain. The probe is positioned with the index marker pointed to the eyes to provide axial images of the brain at the midbrain level. Tissues are characterized as hyperechoic if they reflect significant amount of sound (appearing bright and white) compared to tissues that reflect less sound allowing absorption of ultrasound (appearing gray or hypoechoic). The normal brain parenchyma has a gray appearance (hypoechoic) due to its ability to transmit ultrasound through it. Adequate depth should be adjusted to ensure the convexity of the opposite skull is visible at the bottom of the screen as a hyperechoic convexity. By convention, anterior or eyes are oriented to the left of the screen which also represents the direction of the index marker on the probe. The midbrain (shaped like a butterfly) and lateral ventricles can be visualized as distinct structures from brain

parenchyma due to their texture causing a different amount of reflection and scatter of ultrasound waves. The probe can be sweeped above and below the midbrain to visualize the supratentorial compartment. Upper part of the brainstem may be visible but lower part of brainstem and posterior fossa have significant surrounding bone to allow insonation of brain stem and cerebellar parenchyma. The transcranial Doppler preset can help visualize the brain structures and has high enough mechanical and thermal index to allow differentiation of falx cerebri and midbrain in most patients. Abdominal preset on point of care ultrasound machines can be used to provide satisfactory images with elimination of tissue harmonic imaging if a transcranial preset is not available. In patients who have undergone a hemicraniectomy, absence of skull flap facilitates imaging with much higher resolution and degree of details visible is significantly increased [14, 18] (Figs. 1 and 2).

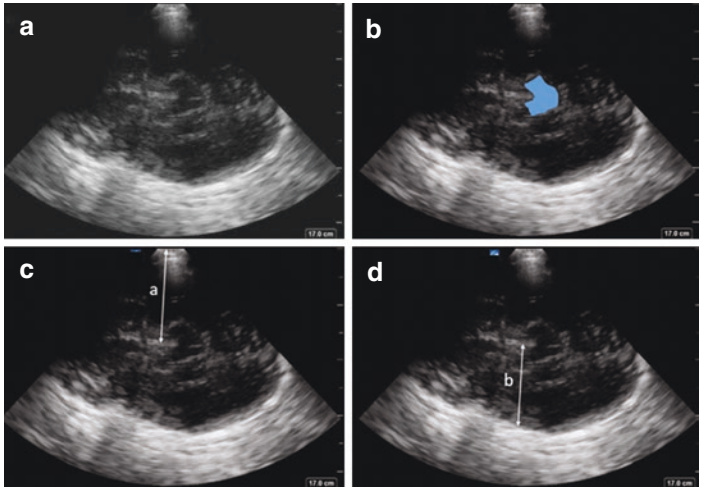

Fig. 1 Cranial ultrasound through the temporal window showing an axial section of the brain at the level of midbrain visible like a "butterfly (**a** and **b**). Third ventricle is commonly used as a midline landmark to calculate midline shift calculated from the distance between third ventricle and skull from either side (**a** and **b**) represent the technique of measuring the midline shift from the same temporal window (**c** and **d**)

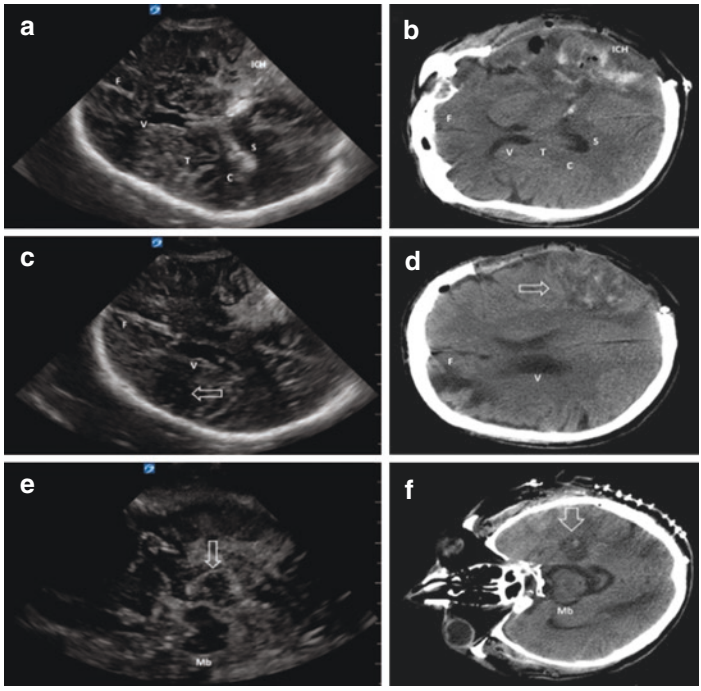

Fig. 2 Cranial ultrasound through the left transtemporal window (left column, panels **a**, **c**, **e**), with corresponding cross-sectional anatomy on a non-contrast computed tomography of brain (right column, panels **b**, **d**, **f**) in a 74-year-old male with a left hemicraniectomy. Intracranial hemorrhage (ICH) and hypodense ischemic areas are indicated by white arrows. F falx cerebri, V lateral ventricles, Mb midbrain, C choroid plexus, S splenium of corpus callosum, T thalami. (Copyright @Elder 2018 permission under Creative Commons Attribution License [14])

Brain Anatomy on Cranial Ultrasound B mode anatomy can visualize the midbrain in the axial plane visible as a "butterfly shape" with cerebral peduncles and colliculi. Figure 2a illustrates brain anatomy on ultrasound in a patient without a skull flap after undergoing hemicraniectomy for intracranial hemorrhage resection. Most patients with intact skull and adequate temporal windows will have midbrain and falx cerebri visible

as a hyperechoic structure. Rarely, lateral ventricles can be visible. Above the midbrain plane, third ventricle can be visible as a pulsating structure anterior to the thalami. Pulsations of the vessels comprising the Circle of Willis can often be seen anterior to the midbrain on B mode images and confirm insonation in the basal cistern plane. During trans-temporal insonation, opposite parenchyma is more amenable to inspection by B mode compared to ipsilateral that is obscured by bone related artifacts.

Intracranial Pathology Studies from the 1990s showed that cranial ultrasound allowed the visualization of major parenchymal structures in the adult brain and brain lesions such as tumors and bleeding from the lower brainstem up to the parietal lobe [10, 19–22]. Further studies assessed high-resolution imaging of deep brain structures and the ventricular system inciting a spurt of investigations in the use of cranial ultrasound in adults [1, 2, 5, 9, 10, 23–32]. But most of these applications have now been replaced by availability of high resolution images of computer tomography and magnetic resonance imaging and may not warrant further use.

Cranial ultrasound does not have the diagnostic ability to detect an ischemic stroke though isolated hypodense areas of ischemic brain may be visualized in hemicraniectomy patients (Figs. 2e, f and 3f). Use of cranial ultrasound in detecting supratentorial hemorrhage (intracranial, epidural or subdural hemorrhage) has seen resurgence for several reasons [33]. Point of care ultrasound may be the only diagnostic modality available in austere environments and remote areas with delayed access to emergency transport. However, in subspecialty intensive care units that do not have access to a mobile CT scanner, cranial ultrasound may offer a radiation free serial diagnostic modality to screen for bleeds in high risk patients (Table 1). Cranial ultrasound can accurately differentiate an acute supratentorial ICH (>1 cm wide in horizontal dimension) from an ischemic stroke with sensitivity of 78–95% and specificity of 95–97.4% [3, 9, 10, 14, 20, 34–40]. The hyperechogenicity

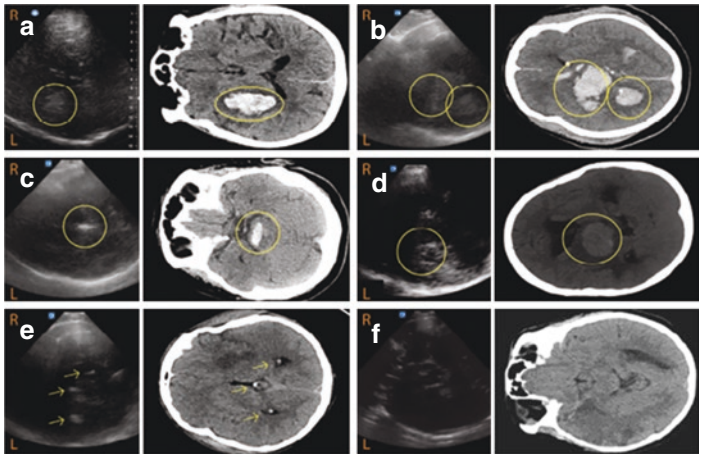

Fig. 3 **(a–e)** Marked up regions on ultrasound (left of each pair of images) corresponding to lesions seen on the computer tomography scans (right of each pair of images). (**d**) Additionally shows acoustic shadow- an ultrasound related artifact seen below the tumor. (**f**) shows the appearance of acute ischemic stroke which is indistinguishable from normal brain appearance on ultrasound

Table 1 Clinical scenarios for potential use of cranial ultrasound as a screening tool for intracranial hemorrhage

Patients on therapeutic anticoagulation or significant coagulopathy/ thrombocytopenia
Cerebral venous sinus thrombosis
Hepatic encephalopathy
Neurotoxicity related to chemotherapeutic agents
Difficult to transport patients
High ventilator settings impairing use of transport ventilators
Systemic instability due to high need of vasopressors
ExtraCorporeal Membrane Oxygenation (ECMO)
High-Frequency Oscillator mechanical ventilation (HFO)
Intra-Aortic Balloon Pump (IABP)
Continuous Renal Replacement Therapy (CRRT)

(white bright signal) of ICH compared to hypoechoic normal or ischemic brain (gray signal) allows biological plausibility of using ultrasound to diagnose ICH on ultrasound although tumors may produce similar appearance (Figs. 3 and 4). Dynamic scanning elucidates distinction of hemorrhage margins better than two dimensional snapshots. In the acute phase, ICH appears homogenous, sharply demarcated and hyperechoic, with bright white signal compared to surrounding brain that appears hypoechoic or relatively gray. After 5–10 days, the hematoma becomes hypoechoic and is surrounded by a peripheral hyperechoic halo [28]. Similar sensitivity to detect epidural and subdural hemorrhages has been described in brain injury patients both with intact skulls as well those with hemicraniectomy [32, 33, 41].

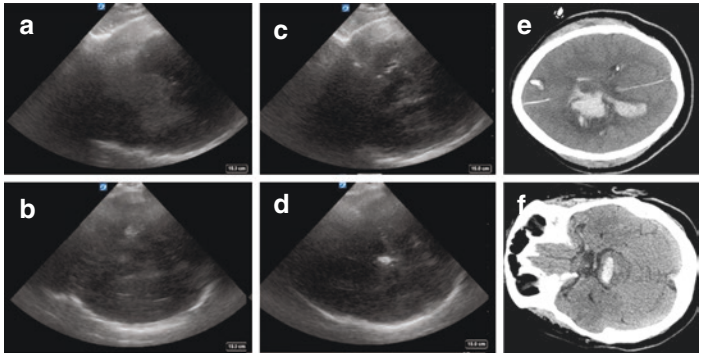

Fig. 4 Two panels show two cases of hemorrhage where the full extent of hemorrhage seen on ultrasound correlated well anatomically with computed tomography scans. Upper panel shows parenchymal (**a**) and lateral ventricular hemorrhage (**c**) corresponding to thalamic hemorrhage and intraventricular hemorrhage seen on computed tomography scan (**e**). Lower panel shows an axial section of brain with midbrain (**b**) devoid of any pathology but hyperechoic area in a plane below that (**d**) corresponding to hemorrhage at midbrain pons junction sparing upper midbrain (**f**)

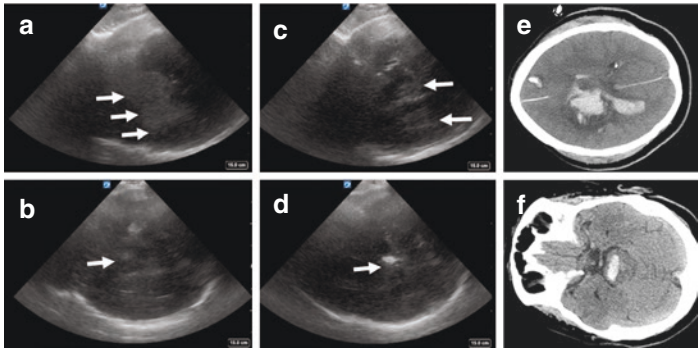

Fig. 4 (continued)

Becker et al. investigated the feasibility of visualizing ICH on cranial ultrasound comparing the hyperechoic appearance of ICH to ultrasound findings in patients with ischemic stroke diagnosed by CT brain that appeared hypoechoic [34, 36]. Seidel et al. reproduced these results and localized ICH with ultrasound in 18/23 patients (78%). They were the first to describe an alteration of the sonographic appearance of intracerebral hematomas over time with a decrease in echo intensity beginning at the center of the lesion [10]. Mäurer et al. published the largest study on transcranial B-mode ultrasound in stroke patients aiming at differentiating between ischemic and hemorrhagic stroke in 151 patients. Of these, 60 had ICH, 67 had ischemic stroke, and 24 had inconclusive CT findings showing neither bleeding nor an ischemic stroke. In the study, 8 patients (12%) had insufficient acoustic bone windows. Of the remaining 133 patients, 126 (95%) were diagnosed correctly by sonography in agreement with CT. Sonography missed 3 atypical bleedings (2 with upper parietal location). In 4 patients without bleeding, an ICH was suspected by cranial ultrasound because of increased white matter echo density due to microangiopathy [3]. Despite over 10 published studies reporting ICH diagnosis with cranial ultrasound in >350 patients, rapid accessibility to high-resolution CT scans presented a competing neuroimaging modality and wide range of false positives impairing more widespread use of ultrasound (Table 2). Several

hyperechoic signals in a physiological normal brain can simulate the ultrasound findings of hemorrhage. The calcifications of the choroid plexus and acoustic shadow of the midbrain are key signals important to recognize that may be mistaken for bleed to the untrained eye. Figure 5 details several normal and abnormal anatomical structures that can create false positive findings of intracranial hemorrhage unless well recognized.

Use of ultrasound to diagnose hydrocephalus has shown potential correlations as well and is described elsewhere in this book.

Table 2 Clinical conditions contributing to cranial ultrasound inaccuracy in detection of intracranial hemorrhage

False positives	False negatives
Tumor or hemorrhagic metastasis	Infratentorial or lower brainstem bleeds
Acoustic shadows created by midbrain and choroid plexus	High parietal or frontal bleeds
Calcified choroid plexus	Bleeds <1 cm in size
Extensive leukoaraiosis	Bleeds several days after onset

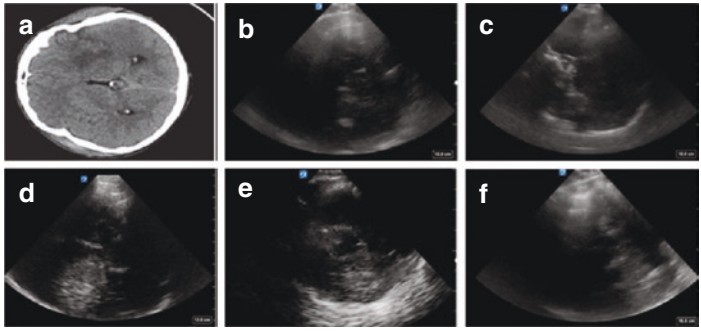

Fig. 5 Appearance of choroid plexus calcification on head computed tomography scan (**a**) compared to cranial ultrasound appearance (**b**). The bony division of anterior and middle cranial fossa created by petrous part of temporal bone and lesser wing of sphenoid can be seen as hyperechoic areas (**c**). The acoustic signals of a intracranial hemorrhage (**d**) can be mistaken with the acoustic shadow created by a midbrain (**e**). Lastly, posterior table of skull can produce linear shadows in right inferior part of the image (**f**) this serves as a useful landmark for imaging the transverse venous sinus on doppler imaging but may create false positive signals similar to intracranial hemorrhage

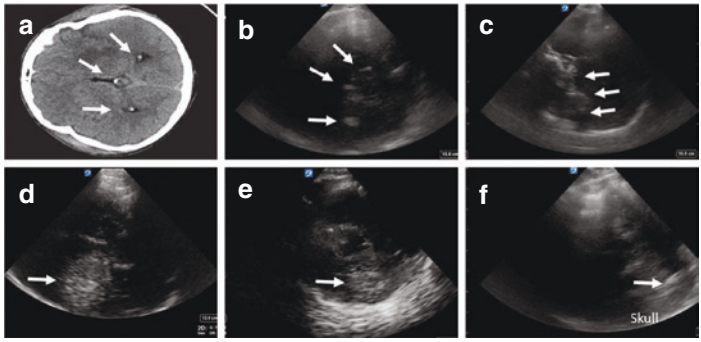

Fig. 5 (continued)

Evaluation for Midline Shift CT continues to be the standard neuroimaging for urgent evaluation of midline shift which is often used as a surrogate for cerebral edema or mass effect. When this modality is not available for high risk patients (Table 1) ultrasound assessed midline shift can be used for follow up of high-risk patients with unilateral lesions to assess evolution of cerebral edema or detect high likelihood for unilateral focal pathology in patient with newly diagnosed midline shift. Midline shift has traditionally been measured by displacement of the hyperechoic signal of third ventricle (provided it's not enlarged), septum pellucidum or the calcified pineal gland. Brain Trauma Foundation guidelines in 2006 proposed a standardized technique of measuring the midline shift at the level of Foramen of Monroe which is also the superior most point of third ventricle [42]. The guidelines recommend calculating the shift as the difference between the intracranial space at this level and shorter distance to the septum pellucidum (Fig. 6). Third ventricle is the most reproducible landmark for ultrasound and is usually recommended for measuring midline shift [43]. Reproducing the exact same plane when bilateral insonation is done on ultrasound can be challenging hence we recommend measuring the midline shift in the same place using unilateral insonation. The distance between the ultrasound probe and the third ventricle (d1) and the distance between the third ventricle and opposite skull (d2) can serve as to help calculate midline shift as $(d1 - d2)/2$ (Fig. 6).

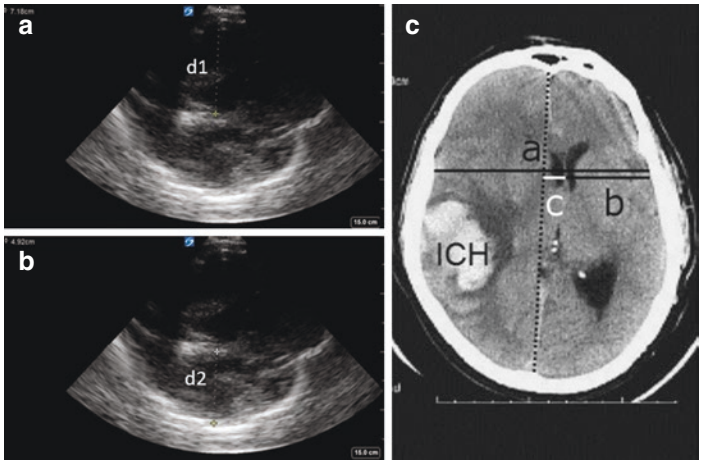

Fig. 6 Midline shift measurements using the third ventricle as a landmark using the same temporal window. Ipsilateral measurement d1 = 7.18 cm (**a**), contralateral measurement d2 = 4.92 cm (**b**). Midline shift can be calculated as (d1 − d2)/2 = 1.13 cm. Brain Trauma Foundation guidelines in 2006 suggested this standardized technique of assessing midline shift (**c**). (Copyright © 2018 Chun-Chih Liao et al. permission under the Creative Commons Attribution License [43])

Published literature has shown good correlations between midline shift measured by ultrasound and CT head with 95% confidence intervals ±1.78 mm and correlation coefficient between 0.88 and 0.93 despite most studies comparing the midline shift measured on CT head using the septum pellucidum but the third ventricle as the landmark in ultrasound studies [44–48]. One study has shown lower but good correlations even when midline shift measurements were standardized for third ventricle for both CT and ultrasound [44]. Serial assessments can be more useful for ultrasound measured midline shift with standardized acquisition technique.

While cranial ultrasound may not replace CT head in acute assessment of intracranial pathology, bedside cranial assessment can elucidate a hemorrhage in an unstable patient or reflect focal pathology by presence of significant midline shift. When combined with transcranial Doppler, B mode cranial ultrasound can be a useful tool and non-invasive surrogate for neurological assessments in a small but key subset of critically ill patients.

References

1. Walter U. Transcranial sonography of the cerebral parenchyma: update on clinically relevant applications. Pers Med. 2012;1(1):334–43.
2. Caricato A, Pitoni S, Montini L, Bocci MG, Annetta P, Antonelli M. Echography in brain imaging in intensive care unit: state of the art. World J Radiol. 2014;6(9):636–42.
3. Becker MM, Shambal S, Berg D, Woydt M, Hofmann E, Georgiadis D, et al. Differentiation between intracerebral hemorrhage and ischemic stroke by transcranial color-coded duplex-sonography. Stoke. 1998;29(12):2563–7.
4. Robba C, Goffi A, Geeraerts T, Cardim D, Via G, Czosnyka M, et al. Brain ultrasonography: methodology, basic and advanced principles and clinical applications. A narrative review. Intensive Care Med. 2019;45(7):913–27.
5. Seidel G, Cangür H, Albers T, Meyer W. Transcranial sonographic monitoring of hemorrhagic transformation in patients with acute middle cerebral artery infarction. J Neuroimaging. 2020;15(4):326–30.
6. Kaps MN, Erwin S, Tibo G, Ralf WB, Giovanni M, Guenter S, et al. Consensus recommendations for transcranial color-coded duplex sonography for the assessment of intracranial arteries in clinical trials on acute stroke. Stroke. 2009;40(10):3238–44.
7. Parodi A, Govaert P, Horsch S, Bravo MC, Ramenghi LA. Cranial ultrasound findings in preterm germinal matrix haemorrhage, sequelae and outcome. Pediatr Res. 2020;87(Suppl 1):13–24.
8. Marinoni M, Ginanneschi A, Forleo P, Amaducci L. Technical limits in transcranial Doppler recording: inadequate acoustic windows. Ultrasound Med Biol. 1997;23(8):1275–7.
9. Seidel G, Cangür H, Albers T, Burgemeister A, Meyer-Wiethe K, et al. Stroke. 2009;40(1):119–23.
10. Dorndorf GS, Kaps M. Transcranial color-coded duplex sonography of intracerebral hematomas in adults. Stroke. 1993;24(10):1519–27.
11. Lin Y-P, Fu M-H, Tan T-Y. Factors associated with no or insufficient temporal bone window using transcranial color-coded sonography. J Med Ultrasound. 2015;23(3):129–32.
12. Robba C, Citerio G, editors. Echography and doppler of the brain. Springer; 2020.
13. A S. Neurocritical Care Ultrasound. Comprehensive critical care ultrasound. 2nd ed. Society of Critical Care Medicine; 2020.
14. Sarwal A, Elder NM. Point-of-care cranial ultrasound in a hemicraniectomy patient. Clin Pract Cases Emerg Med. 2018;2(4):375–7.
15. Frankel HL, Kirkpatrick AW, Elbarbary M, Blaivas M, Desai H, Evans D, et al. Guidelines for the appropriate use of bedside general and cardiac

ultrasonography in the evaluation of critically ill patients-part I: general ultrasonography. Crit Care Med. 2015;43(11):2479–502.
16. Mayo PH, Beaulieu Y, Doelken P, Feller-Kopman D, Harrod C, Kaplan A, et al. American College of Chest Physicians/La Société de Réanimation de Langue Française statement on competence in critical care ultrasonography. Chest. 2009;135(4):1050–60.
17. Emergency ultrasound guidelines. Ann Emerg Med. 2009;53(4):550–70.
18. Srinivasan V, Smith M, Bonomo J. Bedside cranial ultrasonography in patients with hemicraniectomies: a novel window into pathology. Neurocrit Care. 2019;31(2):432–3.
19. Seidel G, Gerriets T, Kaps M, Hutzelmann A. Evaluation of the ventricular system in adults by transcranial duplex sonography. J Neuroimaging. 1995;5(2):105–8.
20. Woydt M, Greiner K, Perez J, Becker G, Krone A, Roosen K. Transcranial duplex-sonography in intracranial hemorrhage. Evaluation of transcranial duplex-sonography in the diagnosis of spontaneous and traumatic intracranial hemorrhage. Zentralblatt fur Neurochirurgie. 1996;57(3):129–35.
21. Mäurer M, Becker G, Wagner R, Woydt M, Hofmann E, Puls I, et al. Early postoperative transcranial sonography (TCS), CT, and MRI after resection of high grade glioma: evaluation of residual tumour and its influence on prognosis. Acta Neurochir. 2000;142(10):1089–97.
22. Becker G, Krone A, Koulis D, Lindner A, Hofmann E, Roggendorf W, Bogdahn U, et al. Reliability of transcranial colour-coded real-time sonography in assessment of brain tumours: correlation of ultrasound, computed tomography and biopsy findings. Neuroradiology. 1994;36(8):585–90.
23. Berg D, Godau J, Walter U. Transcranial sonography in movement disorders. Lancet Neurol. 2008;7(11):1044–55.
24. Kern R, Perren F, Kreisel S, Szabo K, Hennerici M, Meairs S. Multiplanar transcranial ultrasound imaging: standards, landmarks and correlation with magnetic resonance imaging. Ultrasound Med Biol. 2005;31(3):311–5.
25. Walter U, Kanowski M, Kaufmann J, Grossmann A, Benecke R, Niehaus L. Contemporary ultrasound systems allow high-resolution transcranial imaging of small echogenic deep intracranial structures similarly as MRI: a phantom study. NeuroImage. 2008;40(2):551–8.
26. Hambardzumyan A. Transcranial ultrasound imaging of brain tumors. Endosc Surg Armenia. 2006;2:18–23.
27. Blanco P, Abdo-Cuza A. Transcranial Doppler ultrasound in neurocritical care. J Ultrasound. 2018;21(1):1–16.
28. Blanco P, Blaivas M. Applications of transcranial color-coded sonography in the emergency department. J Ultrasound Med. 2017;36(6):1251–66.

29. Abadal JM, Llompart-Pou JA, Homar J, Pérez-Bárcena J, Ibáñez J. Applications of transcranial color-coded duplex sonography in monitoring neurocritical patients. Med Intensiva. 2007;31(9):510–7.
30. Zipper SG, Stolz E. Clinical application of transcranial colour-coded duplex sonography--a review. Eur J Neurol. 2002;9(1):1–8.
31. Becker G, Krone A, Koulis D, Lindner A, Hofmann E, Roggendorf W, et al. Reliability of transcranial colour-coded real-time sonography in assessment of brain tumours: correlation of ultrasound, computed tomography and biopsy findings. Neuroradiology. 1994;36(8):585–90.
32. Niesen WD, Rosenkranz M, Weiller C. Bedsided transcranial sonographic monitoring for expansion and progression of subdural hematoma compared to computed tomography. Front Neurol. 2018;9:374.
33. Lacerda FH, Rahhal H, Soares LJ, Ureña FDRM, Park M. Intracranial epidural hematoma follow-up using bidimensional ultrasound. Rev Bras Ter Intensiva. 2017;29(2):259–60.
34. Becker G, Winkler J, Bogdahn U. Transcranial color-coded real time sonography in adults. Part 2: cerebral hemorrhage and tumors. Ultraschall Med. 1991;12(5):211–7.
35. Puls I, Berg D, Mäurer M, Schliesser M, Hetzel G, Becker G. Transcranial sonography of the brain parenchyma: comparison of B-mode imaging and tissue harmonic imaging. Ultrasound Med Biol. 2000;26(2):189–94.
36. Becker G, Winkler J, Hofmann E, Bogdahn U. Differentiation between ischemic and hemorrhagic stroke by transcranial color-coded real-time sonography. J Neuroimaging. 1993;3(1):41–7.
37. Matsumoto N, Kimura K, Iguchi Y, Aoki J. Evaluation of cerebral hemorrhage volume using transcranial color-coded duplex sonography. J Neuroimaging. 2011;21(4):355–8.
38. Meyer-Wiethe K, Sallustio F, Kern R. Diagnosis of intracerebral hemorrhage with transcranial ultrasound. Cerebrovasc Dis. 2009;27(Suppl):2.
39. Olatunji RB, Ogbole GI, Atalabi OM, Adeyinka AO, Lagunju I, Oyinlade A, et al. Role of transcranial colour-coded duplex sonography in stroke management – review article. West Afr J Ultrasound. 2015;16(1):33–42.
40. Seidel G, Albers T, Meyer-Wiethe K. Transcranial sonographic monitoring of hemorrhagic transformation in patients with acute middle cerebral artery infarction. J Neuroimaging. 2005;15(4):326–30.
41. Caricato A, Mignani V, Sandroni C, Pietrini D. Bedside detection of acute epidural hematoma by transcranial sonography in a head-injured patient. Intensive Care Med. 2010;36(6):1091–2.
42. The Brain Trauma Foundation. The American Association of Neurological Surgeons. The Joint Section on Neurotrauma and Critical Care. Computed tomography scan features. J Neurotrauma. 2000;17(6–7):597–627.
43. Liao C-C, Chen Y-F, Xiao F. Brain midline shift measurement and its automation: a review of techniques and algorithms. Int J Biomed Imaging. 2018;2018:4303161.

44. Motuel J, Biette I, Srairi M, Mrozek S, Kurrek MM, Chaynes P, et al. Assessment of brain midline shift using sonography in neurosurgical ICU patients. Crit Care. 2014;18(6):676.
45. Stolz E, Gerriets T, Fiss I, Babacan SS, Seidel G, Kaps M. Comparison of transcranial color-coded duplex sonography and cranial CT measurements for determining third ventricle midline shift in space-occupying stroke. AJNR Am J Neuroradiol. 1999;20(8):1567–71.
46. Llompart Pou JA, Abadal Centellas JM, Palmer Sans M, Pérez Bárcena J, Casares Vivas M, Homar Ramírez J, et al. Monitoring midline shift by transcranial color-coded sonography in traumatic brain injury. A comparison with cranial computerized tomography. Intensive Care Med. 2004;30(8):1672–5.
47. Tang SC, Huang SJ, Jeng JS, Yip PK. Third ventricle midline shift due to spontaneous supratentorial intracerebral hemorrhage evaluated by transcranial color-coded sonography. J Ultrasound Med. 2006;25(2):203–9.
48. Gerriets T, Stolz E, König S, Babacan S, Fiss I, Jauss M, et al. Sonographic monitoring of midline shift in space-occupying stroke: an early outcome predictor. Stroke. 2001;32(2):442–7.

Applications of Transcranial Doppler Ultrasonography in Sickle Cell Disease, Stroke, and Critical Illness in Children

Kerri L. LaRovere and Nicole F. O'Brien

Background

Since the 1980s, TCD has remained the gold standard stroke risk prediction tool in children with sickle cell disease (SCD) by identifying those who benefit from blood transfusion [1–5]. The rigor of this prior research and impact of TCD on the health of children with SCD has remained unmatched to date in other pediatric populations. Results largely from single center, small pediatric studies, and precedent from adult neurocritical care, however, suggest that use of TCD in critically ill children may have promise. According to a survey of 27 centers in the United States with an expert interest in pediatric neurocritical care (PNCC), TCD was

K. L. LaRovere
Department of Neurology, Boston Children's Hospital and Harvard Medical School, Boston, MA, USA
e-mail: kerri.larovere@childrens.harvard.edu

N. F. O'Brien (✉)
Department of Pediatrics, The Ohio State University/Nationwide Children's Hospital, Columbus, OH, USA
e-mail: Nicole.obrien@nationwidechildrens.org

W. C. Ziai, C. L. Cornwell (eds.), *Neurovascular Sonography*,
https://doi.org/10.1007/978-3-030-96893-9_19

being applied in the PICU for a variety of conditions including: traumatic brain injury (TBI), hypoxic-ischemic encephalopathy (HIE) following cardiac arrest, arterial ischemic stroke, subarachnoid hemorrhage, cerebral vascular malformation, hepatic encephalopathy, sepsis, and diabetic ketoacidosis (DKA). Importantly, TCD seemed to direct clinical care in 75% of the contributing PICUs in this survey [6]. In acute care settings like the PICU and pediatric emergency department (ED), TCD has several potential roles: as a point of care ultrasound (POCUS) study to rapidly diagnose disorders of cerebral perfusion and incorporate findings into clinical decisions in an aim to improve clinical care and outcomes; and as a continuous non-invasive neuromonitoring tool alone or integrated with multi-modal monitoring systems.

There are a number of barriers that must be overcome, however, before TCD can be used in a safe, meaningful, and effective way in pediatric acute care. First and foremost, normal values with a clear understanding of variability due to age, gender, type of critical illness, and associated therapies are needed [7, 8]. Although there is a reasonable starting point for normative values in healthy children and in those sedated and mechanically ventilated, the main limitation of these prior studies is the small sample size for each age category [8, 9]. Normative data for healthy children are available in Table 1 [8]. In the absence of reliable normative data, abnormal TCD findings in critically ill children should be treated as hypothesis-generating. Secondly, large cohort studies are needed to validate TCD findings in children against an acceptable gold standard (e.g. imaging studies, measurements of absolute intracranial pressure [ICP] from invasive ICP monitors), to determine the appropriate clinical indications for the performance of TCD, and to quantify the impact of TCD findings on clinical care and outcomes. Finally, there are several technical challenges to overcome in order to achieve consistent results in children including: properly fitting, safe, and comfortable headgear for uninterrupted signal acquisition; standardized performance of the TCD examination in the PICU for reproducible and verifiable waveforms; and examiner expertise in the care of criti-

Table 1 Normative transcranial doppler ultrasound values by age (mean (SD) [8]

Age	MCA	ICA	ACA	PCA	BA
Systolic peak velocity:					
0–10 days	*46 (10)*	47 (9)	35 (8)	–	–
11–90 days	*75 (15)*	77 (19)	58 (15)	–	–
3–11.9 months	*114 (20)*	104 (12)	77 (15)	–	–
1–2.9 years	*124 (10)*	118 (24)	81 (19)	69 (9)	71 (6)
3–5.9 years	*147 (17)*	144 (19)	104 (22)	81 (16)	88 (9)
6–9.9 years	*143 (13)*	140 (14)	100 (20)	75 (10)	85 (17)
10–18 years	*129 (17)*	125 (18)	92 (19)	66 (10)	68 (11)
Mean flow velocity[a]:					
0–10 days	*24 (7)*	25 (6)	19 (6)	–	–
11–90 days	*42 (10)*	43 (12)	33 (11)	–	–
3–11.9 months	*74 (14)*	67 (10)	50 (11)	–	–
1–2.9 years	*85 (10)*	81 (8)	55 (13)	50 (12)	51 (6)
3–5.9 years	*94 (10)*	93 (9)	71 (15)	48 (11)	58 (6)
6–9.9 years	*97 (9)*	93 (9)	65 (13)	51 (9)	58 (9)
10–18 years	*81 (11)*	79 (12)	56 (14)	45 (9)	46 (8)
End diastolic peak velocity:					
0–10 days	*12 (7)*	12 (6)	10 (6)	–	–
11–90 days	*24 (8)*	24 (8)	19 (9)	–	–
3–11.9 months	*46 (9)*	40 (8)	33 (7)	–	–
1–2.9 years	*65 (11)*	58 (5)	40 (11)	35 (7)	35 (6)
3–5.9 years	*65 (9)*	66 (8)	48 (9)	35 (9)	41 (5)
6–9.9 years	*72 (9)*	68 (10)	51 (10)	38 (7)	44 (8)
10–18 years	*60 (8)*	59 (9)	46 (11)	33 (7)	36 (7)

MCA Middle Cerebral Artery, *ICA* Internal Carotid Artery, *ACA* Anterior Cerebral Artery, *PCA* Posterior Cerebral Artery, *BA* Basilar Artery
[a]Mean Flow Velocity = time mean of the maximal velocity envelope curve

cally ill children for appropriate interpretation and integration of the waveforms into clinical decision making.

In this chapter we will review some potential emerging clinical applications for TCD in children recognizing that these limitations must be resolved before TCD can be put into clinical practice. We will focus on: first, childhood stroke and arteriopathies; and

second, those applications that may be well suited for children in the critical care setting including traumatic brain injury (TBI), cerebral vasospasm, monitoring during extracorporeal membrane oxygenation (ECMO), and brain death. The content of this chapter is relevant not only for providers in PNCC (e.g. intensivists, neurologists, anesthesiologists), but also for radiologists who have an interest in this predominantly non-sickle cell population.

Childhood Stroke and Arteriopathies

Sickle Cell Disease (SCD) in Children

SCD is a group of genetic disorders that result in production of hemoglobin S. Under conditions of cellular stress, hemoglobin S polymerizes, distorts the shape of red blood cells, and leads to irreversible sickling. Sickled cells have a reduced life span, which leads to an intravascular hemolytic anemia, and can cause occlusion of the microvasculature, which is believed to be the major cause of the wide range of clinical symptoms. The largest inception cohort study demonstrated an alarming stroke rate of nearly 12% by age 18 years [10]. Stroke mechanisms in children with SCD are likely multifactorial and include: microvascular occlusion as occurs in the systemic circulation; endothelial injury from a potential cell-mediated inflammatory vasculopathy and/or a potential role for platelet and/or monocyte dysfunction; and reduced nitric oxide bioavailability from chronic hemolysis and excess plasma free hemoglobin (nitric oxide has anti-inflammatory and anti-thrombotic properties) [11, 12]. Angiographic series and pathologic studies support a large artery occlusive vasculopathy as the major contributor to ischemic stroke in children with SCD [13–17].

In the 1980s, Dr. Robert J Adams used a vessel-based approach with TCD to stratify stroke risk in children with SCD. The key findings from his series of studies were: (1) TCD could distinguish children with SCD from those without SCD [18]; (2) TCD could detect stenotic lesions as seen on angiography and distinguish children with SCD with stenosis from those without steno-

sis [19]; and (3) stroke risk could be stratified by the time averaged mean of the maximum flow velocity (TAMMX) in the middle cerebral artery (MCA) or internal carotid artery (ICA) such that children with TAMMX in either artery ≥200 cm/s had a 40% risk of a first ever stroke within 3 years [1, 20].

In the Stroke Prevention Trial in Sickle Cell Anemia (STOP) study, 1934 children with SCD from age 2 to 16 years old were screened with TCD at 14 clinic sites in the United States. Children with mean flow velocity ≥200 cm/s in the MCA or ICA were randomized into two groups. Sixty-three children received regular blood transfusions every 3–4 weeks to maintain their hemoglobin S level ≤30% (intervention arm). Sixty-seven children received standard care with periodic blood transfusions (control group). The main finding was a 10% yearly stroke rate in the control group compared to a <1% stroke rate in the intervention arm, indicating a 92% relative risk reduction for a first ever stroke ($p < 0.001$) [2]. Based on the results of this study, current guidelines recommend that children between ages 2 years and 16 years with sickle cell disease should be screened with TCD annually if the study is normal (TAMMX in the MCA or ICA <170 cm/s), and quarterly if conditional (TAMMX 170–199 cm/s). Regular blood transfusions should be initiated for an abnormal TCD (TAMMX in least one artery ≥200 cm/s) [21].

Other Childhood Arteriopathies

Children with moyamoya syndrome present with ischemic stroke or transient ischemic attack due to chronic and progressive stenoses involving the arteries in the anterior cerebral circulation. Based on adult data, there may be a role for TCD as an adjunct to angiography in children with moya-moya syndrome [22]. However, validation of cerebral blood flow velocity (CBFV) thresholds in moyamoya in children that suggests clinically relevant stenoses do not exist. Rather, in children with angiographic evidence of vascular occlusion or stenosis, CBFVs may be followed over time once baseline data are procured to monitor for worsening of disease.

Children with focal cerebral arteriopathy (FCA) may be differentiated from moyamoya or cerebral vasculitis by a clinical course of improvement or stabilization over time, occasionally after a period of initial worsening. Acute central nervous system (CNS) infections from bacterial infections and herpesvirus can be associated with the development of FCA and arterial ischemic stroke in children [23–25]. While stroke mechanisms in FCA remain unclear, vessel diameter narrowing (stenosis and/or vasospasm) from contact of exudate with the vessel wall may play a role. While vascular changes are best characterized by angiography, this diagnostic study often has to be repeated frequently over weeks to months after the acute illness and may require repeated sedation and/or endotracheal intubation in young children. TCD may have a preferred role in long-term monitoring of this disease if a correlation with angiography is found.

Pediatric Critical Care Applications

Moderate to Severe TBI

In adults, TCD criteria for hypoperfusion following severe TBI have been used to guide early resuscitation [26, 27]. Similar criteria for children, however, remain unclear. In a study by Trabold et al. of 36 children with moderate to severe TBI, end diastolic cerebral blood flow velocity (Vd) <25 cm/second and pulsatility index (PI) >1.31 after the first resuscitation in the ED was associated with poor outcome, defined as Glasgow Outcome Scale 3–5 at hospital discharge (Vd: AUROC 0.91 ± 0.02, $p = 0.03$; PI: AUROC 0.89 ± 0.02, $p = 0.04$) [28]. It is important to note that in this study, mortality rate was high at 11%, and the study was not powered to perform multivariate analyses on variables besides TCD measurements, such as the Glasgow Coma Scale and other injury severity scores, that may be independent factors of poor prognosis. Other investigators have attempted to discover relationships between CBFVs and outcome, but these studies are limited by small sample sizes, retrospective study design, and

lack of rigorous, serial protocol-driven TCD measurements [29–31]. More individual level and rigorous data collection and analyses are needed.

In children with moderate to severe TBI, there has also been some work on the use of TCD for non-invasive ICP and cerebral perfusion pressure (CPP) estimation. TCD is an attractive alternative to invasive monitoring in children for 2 reasons: (1) the recommendation in the 2019 updated guidelines for management of severe TBI in children can only support class III evidence for ICP monitoring [32, 33]; and (2) there is low utilization of gold standard invasive ICP monitoring in children [34–39]. Similar to the adult literature, Vd and PI are not reliable indicators of increased ICP in children when compared to gold standard invasive ICP measurements [28, 40–42]. The main limitations in these studies are that PI measurements were often made as single, point source measurements at different timepoints following the injury in small numbers of children. A continuous, fully automated, real-time engineering approach using synchronized systemic arterial blood pressure and MCA waveforms has been recently shown to estimate ICP with similar accuracy and precision as routinely used invasive ICP monitors [43]. Validation in larger cohorts is needed. Regarding the use of TCD to estimate CPP (CPPe) in children with severe TBI, use of the formula CPPe = ABPmean*FVd (diastolic flow velocity)/Fvm (mean flow velocity) +14 as a regression equation gives limits of agreement of −17 to +25 mmHg, which is not clinically acceptable [44].

Cerebral Vasospasm

Cerebral vasospasm is a reversible reduction in the caliber of an arterial lumen of a vessel in the subarachnoid space. Arterial narrowing leads to an increase in TCD derived CBFVs and a decrease in PI with worsening spasm. If severe, vasospasm can lead to a critical reduction in cerebral blood flow and cerebral ischemia. Cerebral vasospasm has been reported following resection of brain tumors, ruptured cerebral aneurysms and arteriovenous malformations, CNS infections, and moderate to severe TBI in chil-

dren [29, 45–51]. The diagnostic accuracy of TCD for angiographic proven vasospasm when adult criteria are used in children is low, with a positive likelihood ratio of only 2.0 [52]. Using adult criteria in pediatrics has such a low positive likelihood ratio because CBFVs are higher in children compared to adults across all age groups [53]. The pediatric literature to date on this topic is limited by the use of adult criteria, lack of radiographic confirmation of elevated CBFVs and Lindegaard ratios, and small sample sizes. Thus, validated TCD thresholds for vasospasm do not exist for children. Prospective studies comparing age-related CBFV measurements and Lindegaard ratios to angiographic data in children with symptomatic vasospasm are needed. In the absence of robust pediatric data, TCD should be used as a precursor to definitive imaging when there is a suspicion for vasospasm (e.g. persistent increase in CBFVs over time, or significant day to day changes in CBFVs). Figure 1 is an example of a representative case where TCD was used to assist in the diagnosis and management of a child with cerebral vasospasm.

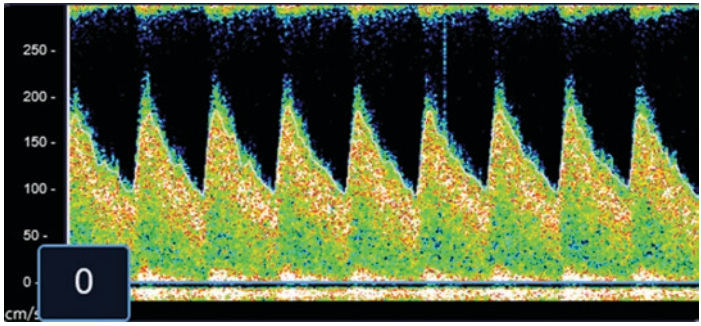

Fig. 1 24-month-old female involved in a motor vehicle accident. Transcranial Doppler ultrasound (TCD) was normal on days 1–3, but on post-injury day 4, right middle cerebral artery flow increased to 220 cm/sec with an LR of 6.9. Neurologic status declined with new left sided hemiparesis. Based on results of the TCD, angiogram was ordered and confirmed the diagnosis of cerebral vasospasm. Therapeutic interventions were undertaken, and neurologic examination improved. TCD was repeated daily with no further worsening of vasospasm and normalization of flow by post-injury day 7. Therapies were weaned with no worsening of TCD flow velocities

Monitoring During ECMO

Detection of acute brain injury that is clinically recognizable or in the subclinical phase during ECMO in a sedated and/or paralyzed child is difficult. To date, what is known about the relevance of CBFV measurements in children is that similar to adults, CBFVs and PI are lower in children supported on ECMO during the first 5 days of therapy in those who do not have acute brain injury [54]. Serial TCD monitoring has not, however, shown a reliable correlation between changes in velocity and brain ischemia or hemorrhage [54, 55]. Larger studies in this population are needed. At present, the only reliable way to detect acute brain injury during ECMO is "after the fact" by serial neurologic exams with confirmation of focal neurologic deficits by neuroimaging.

ECMO is a life-saving treatment for heart and/or lung failure, as a bridge to transplant, or as an aid to cardiopulmonary resuscitation for in hospital cardiac arrest. The use of ECMO has quadrupled in children in the last 15 years to >2500 cases in 2016 [56]. ECMO technology has improved so that avoiding acute brain injury during the course of ECMO is now key to survival and better long-term outcomes [57–61]. Acute brain injury occurs in the form of hypoxic ischemic injury, intracranial hemorrhage, and arterial ischemic stroke. Data supporting the use and effectiveness of current neuromonitoring methods on ECMO to detect acute brain injury is limited. The majority of the evidence for monitoring using neuroimaging, electroencephalography (EEG), cerebral oximetry, serum biomarkers and Doppler ultrasound is limited to mainly level 3B (case-control) and 4 (case series).

Cerebral emboli, representing air or solid matter, are one potential cause of acute brain injury during ECMO. Emboli may occur as a result of low cardiac output, or direct passage of emboli in the systemic circulation from the ECMO circuit or left heart chambers [62–64]. TCD can detect emboli as distinct high intensity signals (HITS) or microembolic signals (MES) in the Doppler spectrum. Although consensus on their signature exists in the Doppler spectrum [65], emboli monitoring has not transitioned into routine clinical care in children for the following reasons: (1) sparse pediatric literature; (2) commercial TCD software seems to generate excess false positive events and better event separation is needed

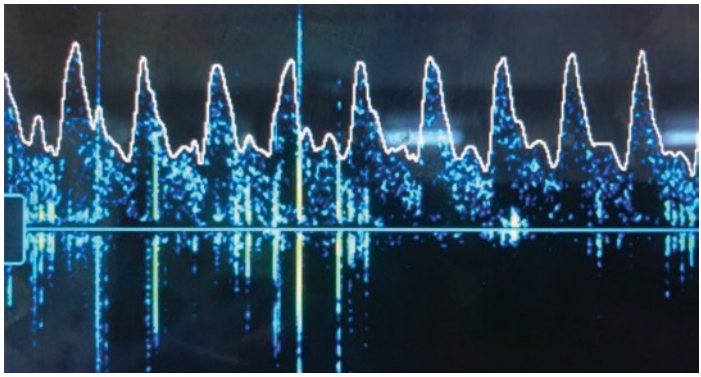

Fig. 2 7-month-old male undergoing TCD monitoring during cardiopulmonary bypass for complex congenital heart disease repair. Multiple high-intensity signals were noted throughout the case. The events were of unknown clinical significance as patient did not have any gross neurologic deficits on hospital discharge

[66]; (3) manual review is laborious and time consuming; and (4) uninterrupted signal acquisition remains a challenge due to the lack of appropriately sized headgear for infants and young children. Further technical improvements are needed to distinguish the true embolic count, size, and composition of embolic events. As a starting point to generate further data, emboli monitoring may be appropriate for infants and children on cardiopulmonary bypass while undergoing cardiac surgery [67]. Figure 2 represents embolic phenomenon identified by TCD in a child on cardiopulmonary bypass for repair of congenital heart disease.

Brain Death

Unlike adults, standards and guidelines for the TCD diagnosis of cerebral circulatory arrest do not exist for children. There are >10 cases reported in the literature of children from birth to 11 months who met clinical (loss of brainstem reflexes) and EEG criteria for brain death, but cerebral blood flow by angiography and/or TCD was detected [68, 69]. One reason for these findings may be that the elastic infant skull with open fontanelles can oppose rising ICP, allowing

for significant increases in cranial volume without a reduction in CPP (risk of false negative). False positives, on the other hand, may occur due to operator inexperience and misinterpretation of "absent" flow in infants who normally have a low diastolic flow velocity (12 ± 7 cm/sec). Accordingly, TCD is not currently recommended as an ancillary test to aid in brain death determination in children <18 years. TCD may, however, indicate the optimal timing for a perfusion study if there is clinical diagnostic uncertainty of brain death [70]. Figure 3 represents the use of TCD in a child suffering traumatic brain injury to direct timing of confirmatory brain death testing.

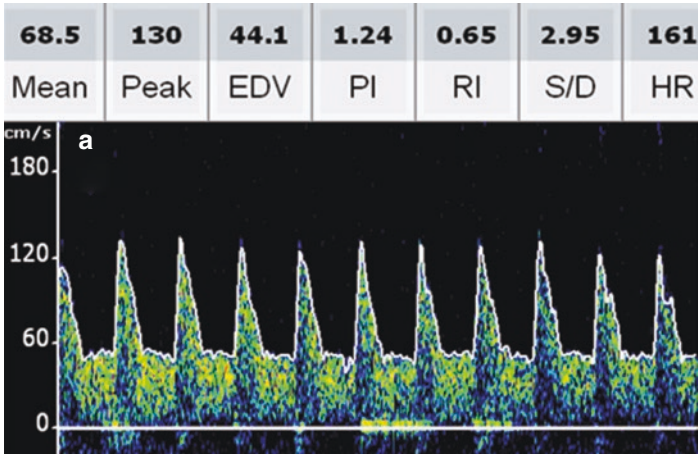

Fig. 3 8-year-old male suffering severe traumatic brain injury following a motor vehicle collision. Panel A represents his admission TCD with near normal peak systolic velocities but with flattened diastolic flow and a modestly high pulsatility index. Intracranial pressure (ICP) was 29 mmHg during the TCD examination. Despite maximal medical and surgical management, ICP continued to increase to 60 mmHg by hospital day 3. Clinical examination was concerning for brain death, but apnea testing could not be performed due to hypoxia secondary to bilateral pulmonary contusions and lacerations. Panel B represents TCD images of the middle cerebral artery acquired on hospital day 3. Trace diastolic flow was noted. Thus, given the uncertain diagnostic certainty of a confirmatory perfusion study at that time in a patient who was not clinically stable, it was deferred. Panel C represents TCD images of the middle cerebral artery acquired on hospital day 4. Systolic spikes with complete lack of diastolic flow were noted and brain death was confirmed with perfusion study following the TCD examination

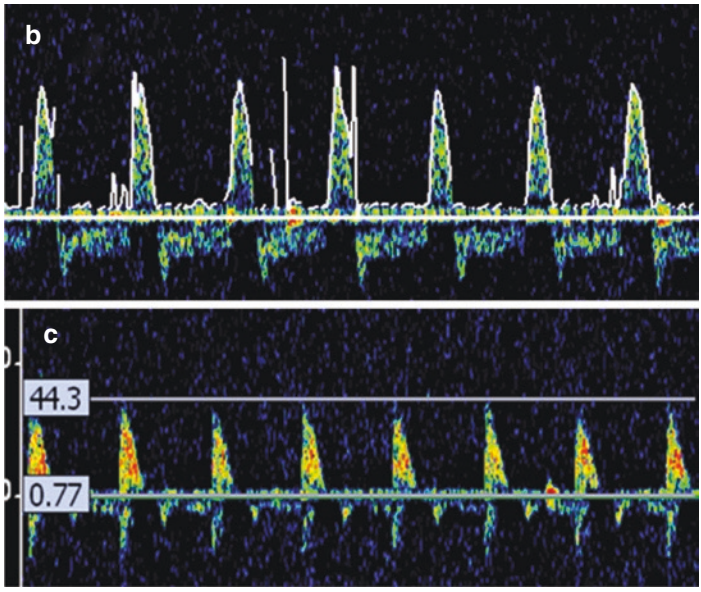

Fig. 3 (continued)

Other Conditions

One last potential unique application of TCD may be as a screening tool to aid in clinical decisions and guide therapy in children in low income countries with cerebral malaria (CM). Malaria is a global health problem resulting in >400,000 deaths annually, two-thirds of which occur in children under age 5 years [71]. CM is a severe manifestation of malaria and can be diagnosed when the child presents in coma with Plasmodium parasitemia and no other identifiable cause for coma (such as hypoglycemia, seizures, or meningitis). Severe neurologic disability (e.g. weakness/paralysis, hypotonia, spasticity, speech and language disorders, movement and gait disorders, vision impairment, epilepsy, and behavioral problems) is present in about one half of survivors [72]. Even with excellent clinical care, the mortality rate from CM is approximately 15% [73].

In a prospective observational study performed at 3 clinical sites in the Democratic Republic of the Congo between 2015 and 2017, O'Brien et al. found 5 different TCD "phenotypes" in 160 children with CM during the first 8 days of hospital admission. Interestingly, a total of 151/160 patients remained in one of the following phenotypic categories until normalization or death: hyperemia was seen in 42 cases (26%), low flow state in 46 cases (28%), microvascular obstruction in 35 cases (22%), and cerebral vasospasm in 21 cases (13%) [50]. Validation of pathophysiologic mechanisms associated with each TCD phenotype may aid in the development of individual targeted adjunctive therapies that may improve outcomes for children with CM.

Conclusions

TCD has an established clinical role in reducing a first ever stroke in children with SCD by identifying those who are high risk and benefit from blood transfusion. Beyond sickle cell disease, other potential roles for TCD are as a point of care ultrasound or neuromonitoring strategy in the PICU setting. TCD data in critically ill children should be treated as hypothesis-generating. TCD may serve as a precursor or adjunct to definitive imaging or invasive techniques. Collaboration and research is needed to advance the TCD field in pediatrics.

References

1. Adams R, McKie V, Nichols F, Carl E, Zhang DL, McKie K, et al. The use of transcranial ultrasonography to predict stroke in sickle cell disease. N Engl J Med. 1992;326(9):605–10.
2. Adams RJ, McKie VC, Hsu L, Files B, Vichinsky E, Pegelow C, et al. Prevention of a first stroke by transfusions in children with sickle cell anemia and abnormal results on transcranial doppler ultrasonography. N Engl J Med. 1998;339(1):5–11.
3. Adams RJ, McKie VC, Brambilla D, Carl E, Gallagher D, Nichols FT, et al. Stroke prevention trial in sickle cell anemia. Control Clin Trials. 1998;19(1):110–29.

4. Adams RJ, Brambilla DJ, Granger S, Gallagher D, Vichinsky E, Abboud MR, et al. Stroke and conversion to high risk in children screened with transcranial doppler ultrasound during the STOP study. Blood. 2004;103(10):3689–94.
5. Adams RJ, Brambilla D. Optimizing primary stroke prevention in sickle cell anemia trial I: discontinuing prophylactic transfusions used to prevent stroke in sickle cell disease. N Engl J Med. 2005;353(26):2769–78.
6. LaRovere KL, Tasker RC, Wainwright M, Reuter-Rice K, Appavu B, Miles D, et al. Transcranial doppler ultrasound during critical illness in children: survey of practices in pediatric neurocritical care centers. PCCM. 2020;21(1):67–74.
7. Tegeler CH, Crutchfield K, Katsnelson M, Kim J, Tang R, Passmore Griffin L, et al. Transcranial doppler velocities in a large, healthy population. J Neuroimaging. 2013;23(3):466–72.
8. O'Brien NF. Reference values for cerebral blood flow velocities in critically ill sedated children. Childs Nerv Syst. 2015;31(12):2269–76.
9. Bode H, Wais U. Age dependence of flow velocities in basal cerebral arteries. Arch Dis Child. 1988;63(6):606–11.
10. Quinn CT, Rogers ZR, Buchanan GR. Survival of children with sickle cell disease. Blood. 2004;103(11):4023–7.
11. Rothman SM, Fulling KH, Nelson JS. Sickle cell anemia and central nervous system infarction: a neuropathological study. Ann Neurol. 1986;20(6):684–90.
12. Kaul DK, Fabry ME, Nagel RL. Microvascular sites and characteristics of sickle cell adhesion to vascular endothelium in shear flow conditions: pathophysiological implications. Proc Natl Acad Sci U S A. 1989;86(9):3356–60.
13. Merkel KH, Ginsberg PL, Parker JC Jr, Post MJ. Cerebrovascular disease in sickle cell anemia: a clinical, pathological and radiological correlation. Stroke. 1978;9(1):45–52.
14. Thust SC, Burke C, Siddiqui A. Neuroimaging findings in sickle cell disease. Br J Radiol. 2014;87(1040):20130699.
15. Stockman JA, Nigro MA, Mishkin MM, Oski FA. Occlusion of large cerebral vessels in sickle-cell anemia. NEJM. 1972;287(17):846–9.
16. Powars D, Wilson B, Imbus C, Pegelow C, Allen J. The natural history of stroke in sickle cell disease. Am J Med. 1978;65(3):461–71.
17. Russell MO, Goldberg HI, Hodson A, Kim HC, Halus J, Reivich M, et al. Effect of transfusion therapy on arteriographic abnormalities and on recurrence of stroke in sickle cell disease. Blood. 1984;63(1):162–9.
18. Brass LM, Pavlakis SG, DeVivo D, Piomelli S, Mohr JP. Transcranial doppler measurements of the middle cerebral artery. Effect of hematocrit. Stroke. 1988;19(12):1466–9.
19. Adams RJ, Nichols FT, Figueroa R, McKie V, Lott T. Transcranial doppler correlation with cerebral angiography in sickle cell disease. Stroke. 1992;23(8):1073–7.

20. Adams RJ, McKie VC, Carl EM, Nichols FT, Perry R, Brock K, et al. Long-term stroke risk in children with sickle cell disease screened with transcranial doppler. Ann Neurol. 1997;42(5):699–704.
21. Nichols FT, Jones AM, Adams RJ. Stroke prevention in sickle cell disease (STOP) study guidelines for transcranial doppler testing. J Neuroimaging. 2001;11(4):354–62.
22. Lee YS, Jung KH, Roh JK. Diagnosis of moyamoya disease with transcranial doppler sonography: correlation study with magnetic resonance angiography. J Neuroimaging. 2004;14(4):319–23.
23. Fullerton HJ, Elkind MS, Barkovich AJ, Glaser C, Glidden D, Hills NK, et al. The vascular effects of infection in pediatric stroke (VIPS) study. J Child Neurol. 2011;26(9):1101–10.
24. Wintermark M, Hills NK, deVeber GA, Barkovich AJ, Elkind MS, Sear K, et al. Arteriopathy diagnosis in childhood arterial ischemic stroke: results of the vascular effects of infection in pediatric stroke study. Stroke. 2014;45(12):3597–605.
25. Elkind MS, Hills NK, Glaser CA, Lo WD, Amlie-Lefond C, Dlamini N, et al. Herpesvirus infections and childhood arterial ischemic stroke: results of the VIPS study. Circulation. 2016;133(8):732–41.
26. van Santbrink H, Schouten JW, Steyerberg EW, Avezaat CJ, Maas AI. Serial transcranial doppler measurements in traumatic brain injury with special focus on the early posttraumatic period. Acta Neurochir. 2002;144(11):1141–9.
27. Ract C, Le Moigno S, Bruder N, Vigue B. Transcranial doppler ultrasound goal-directed therapy for the early management of severe traumatic brain injury. Int Care Med. 2007;33(4):645–51.
28. Trabold F, Meyer PG, Blanot S, Carli PA, Orliaguet GA. The prognostic value of transcranial doppler studies in children with moderate and severe head injury. Int Care Med. 2004;30(1):108–12.
29. Chaiwat O, Sharma D, Udomphorn Y, Armstead WM, Vavilala MS. Cerebral hemodynamic predictors of poor 6-month Glasgow outcome score in severe pediatric traumatic brain injury. J Neurotrauma. 2009;26(5):657–63.
30. Visocchi M, Chiaretti A, Genovese O, Di Rocco F. Haemodynamic patterns in children with posttraumatic diffuse brain swelling. A preliminary study in 6 cases with neuroradiological features consistent with diffuse axonal injury. Acta Neurochir. 2007;149(4):347–56.
31. O'Brien NF, Maa T, Moore-Clingenpeel M, Rosenberg N, Yeates KO. Relationships between cerebral flow velocities and neurodevelopmental outcomes in children with moderate to severe traumatic brain injury. Childs Nerv Syst. 2018;34(4):663–72.
32. Kochanek PM, Tasker RC, Carney N, Totten AM, Adelson PD, Selden NR, et al. Guidelines for the management of pediatric severe traumatic brain injury, third edition: update of the brain trauma foundation guidelines. PCCM. 2019;20(3S Suppl 1):S1–S82.

33. Kochanek PM, Tasker RC, Carney N, Totten AM, Adelson PD, Selden NR, et al. Guidelines for the management of pediatric severe traumatic brain injury, third edition: update of the brain trauma foundation guidelines, executive summary. Neurosurgery. 2019;84(6):1169–78.
34. Alkhoury F, Kyriakides TC. Intracranial pressure monitoring in children with severe traumatic brain injury: National Trauma Data Bank-Based Review of outcomes. JAMA Surg. 2014, Jun;149(6):544–8.
35. Alali AS, Gomez D, Sathya C, Burd RS, Mainprize TG, Moulton R, et al. Intracranial pressure monitoring among children with severe traumatic brain injury. J Neurosurg Pediatr. 2015;16(5):523–32.
36. Morris KP, Forsyth RJ, Parslow RC, Tasker RC, Hawley CA, Group UKPTBIS, Paediatric Intensive Care Society Study G. Intracranial pressure complicating severe traumatic brain injury in children: monitoring and management. Int Care Med. 2006;32(10):1606–12.
37. Bennett TD, Riva-Cambrin J, Keenan HT, Korgenski EK, Bratton SL. Variation in intracranial pressure monitoring and outcomes in pediatric traumatic brain injury. Arch Pediatr Adolesc Med. 2012;166(7):641–7.
38. Dixon RR, Nocera M, Zolotor AJ, Keenan HT. Intracranial pressure monitoring in infants and young children with traumatic brain injury. PCCM. 2016;17(11):1064–72.
39. Van Cleve W, Kernic MA, Ellenbogen RG, Wang J, Zatzick DF, Bell MJ, et al. National variability in intracranial pressure monitoring and craniotomy for children with moderate to severe traumatic brain injury. Neurosurgery. 2013;73(5):746–52.
40. Figaji AA, Zwane E, Fieggen AG, Siesjo P, Peter JC. Transcranial doppler pulsatility index is not a reliable indicator of intracranial pressure in children with severe traumatic brain injury. Surg Neurol. 2009;72(4):389–94.
41. Melo JR, Di Rocco F, Blanot S, Cuttaree H, Sainte-Rose C, Oliveira-Filho J, et al. Transcranial doppler can predict intracranial hypertension in children with severe traumatic brain injuries. Childs Nerv Syst. 2011;27(6):979–84.
42. O'Brien NF, Maa T, Reuter-Rice K. Noninvasive screening for intracranial hypertension in children with acute, severe traumatic brain injury. J Neurosurg Pediatr. 2015;16(4):420–5.
43. Fanelli A, Vonberg FW, LaRovere KL, Walsh BK, Smith ER, Robinson S, et al. Fully automated, real-time, calibration-free, continuous noninvasive estimation of intracranial pressure in children. J Neurosurg Pediatr. 2019;24(5):509–19.
44. O'Brien NF, Lovett ME, Chung M, Maa T. Non-invasive estimation of cerebral perfusion pressure using transcranial doppler ultrasonography in children with severe traumatic brain injury. Childs Nerv Syst. 2020;36(9):2063–71.

45. Rao VK, Haridas A, Nguyen TT, Lulla R, Wainwright MS, Goldstein JL. Symptomatic cerebral vasospasm following resection of a medulloblastoma in a child. Neurocrit Care. 2013;18(1):84–8.
46. Pendharkar AV, Guzman R, Dodd R, Cornfield D, Edwards MS. Successful treatment of severe cerebral vasospasm following hemorrhage of an arteriovenous malformation. Case report. J Neurosurg Pediatr. 2009;4(3):266–9.
47. O'Brien NF, Reuter-Rice KE, Khanna S, Peterson BM, Quinto KB. Vasospasm in children with traumatic brain injury. Int Care Med. 2010;36(4):680–7.
48. O'Brien NF, Maa T, Yeates KO. The epidemiology of vasospasm in children with moderate-to-severe traumatic brain injury. CCM. 2014;43(3):674–85.
49. Philip S, Chaiwat O, Udomphorn Y, Moore A, Zimmerman JJ, Armstead W, et al. Variation in cerebral blood flow velocity with cerebral perfusion pressure >40 mm Hg in 42 children with severe traumatic brain injury. CCM. 2009;37(11):2973–8.
50. O'Brien NF, Mutatshi Taty T, Moore-Clingenpeel M, Bodi Mabiala J, Mbaka Pongo J, Ambitapio Musungufu D, et al. Transcranial doppler ultrasonography provides insights into neurovascular changes in children with cerebral malaria. Pediatrics. 2018;203(116–24):e113.
51. Garg K, Singh PK, Sharma BS, Chandra PS, Suri A, Singh M, et al. Pediatric intracranial aneurysms--our experience and review of literature. Childs Nerv Syst. 2014;30(5):873–83.
52. Moftakhar P, Cooke DL, Fullerton HJ, Ko NU, Amans MR, Narvid JA, et al. Extent of collateralization predicting symptomatic cerebral vasospasm among pediatric patients: correlations among angiography, transcranial doppler ultrasonography, and clinical findings. J Neurosurg Pediatr. 2015;15(3):282–90.
53. Udomphorn Y, Armstead WM, Vavilala MS. Cerebral blood flow and autoregulation after pediatric traumatic brain injury. Pediatr Neurol. 2008;38(4):225–34.
54. O'Brien NF, Buttram SDW, Maa T, Lovett ME, Reuter-Rice K, LaRovere KL. Cerebrovascular physiology during pediatric extracorporeal membrane oxygenation: a multicenter study using transcranial doppler ultrasonography. PCCM. 2019;20(2):178–86.
55. Rilinger JF, Smith CM, deRegnier RAO, Goldstein JL, Mills MG, Reynolds M, et al. Transcranial doppler identification of neurologic injury during pediatric extracorporeal membrane oxygenation therapy. J Stroke Cerebrovasc Dis. 2017;26(10):2336–45.
56. Thiagarajan RR, Barbaro RP, Rycus PT, McMullan DM, Conrad SA, Fortenberry JD, et al. Extracorporeal life support organization registry international report 2016. ASAIO. 2017;63(1):60–7.
57. Bembea MM, Felling RJ, Caprarola SD, Ng DK, Tekes A, Boyle K, et al. Neurologic outcomes in a two-center cohort of neonatal and pediatric

patients supported on extracorporeal membrane oxygenation. ASAIO. 2020;66(1):79–88.
58. Barrett CS, Bratton SL, Salvin JW, Laussen PC, Rycus PT, Thiagarajan RR. Neurological injury after extracorporeal membrane oxygenation use to aid pediatric cardiopulmonary resuscitation. PCCM. 2009;10(4): 445–51.
59. Waitzer E, Riley SP, Perreault T, Shevell MI. Neurologic outcome at school entry for newborns treated with extracorporeal membrane oxygenation for noncardiac indications. J Child Neurol. 2009;24(7):801–6.
60. Schiller RM, Madderom MJ, Reuser JJ, Steiner K, Gischler SJ, Tibboel D, et al. Neuropsychological follow-up after neonatal ECMO. Pediatrics. 2016;138(5):e20161313.
61. Bembea MM, Felling R, Anton B, Salorio CF, Johnston MV. Neuromonitoring during extracorporeal membrane oxygenation: a systematic review of the literature. PCCM. 2015;16(6):558–64.
62. Kwon HM, Park JH, Kim JM, Yoon BW. Mild left ventricular dysfunction is associated with thrombogenicity in cardioembolic stroke. Eur Neurol. 2006;56(4):217–21.
63. Yang Y, Grosset DG, Li Q, Lees KR. Identification of echocardiographic "smoke" in a bench model with transcranial doppler ultrasound. Stroke. 2000;31(4):907–14.
64. Asinger RW, Koehler J, Pearce LA, Zabalgoitia M, Blackshear JL, Fenster PE, et al. Pathophysiologic correlates of thromboembolism in nonvalvular atrial fibrillation: II. Dense spontaneous echocardiographic contrast (The Stroke Prevention in Atrial Fibrillation [SPAF-III] study). J A Soc Echocardiogr. 1999;12(12):1088–96.
65. Ringelstein EB, Droste DW, Babikian VL, Evans DH, Grosset DG, Kaps M, et al. Consensus on microembolus detection by TCD. International consensus group on microembolus detection. Stroke. 1998;29(3):725–9.
66. Imaduddin SM, LaRovere KL, Kussman BD, Heldt T. A time-frequency approach for cerebral embolic load monitoring. IEEE Trans Biomed Eng. 2019;67(4):1007–18.
67. LaRovere KL, Kapur K, McElhinney DB, Razumovsky A, Kussman BD. Cerebral high-intensity transient signals during pediatric cardiac catheterization: a pilot study using transcranial doppler ultrasonography. J Neuroimaging. 2017;27(4):381–7.
68. Sanker P, Roth B, Frowein RA, Firsching R. Cerebral reperfusion in brain death of a newborn. Case report. Neurosurg Rev. 1992;15(4):315–7.
69. Glasier CM, Seibert JJ, Chadduck WM, Williamson SL, Leithiser RE Jr. Brain death in infants: evaluation with doppler US. Radiology. 1989;172(2):377–80.
70. Bode H, Sauer M, Pringsheim W. Diagnosis of brain death by transcranial doppler sonography. Arch Dis Child. 1988;63(12):1474–8.
71. World malaria report 2018. Geneva: World Health Organization; 2018.

72. Okiro EA, Al-Taiar A, Reyburn H, Idro R, Berkley JA, Snow RW. Age patterns of severe paediatric malaria and their relationship to plasmodium falciparum transmission intensity. Malar J. 2009;8(4):1–11.
73. Taylor TE. Caring for children with cerebral malaria: insights gleaned from 20 years on a research ward in Malawi. Trans R Soc Trop Med Hyg. 2009;103(Suppl 1):S6–10.

Point of Care Transcranial Doppler

Aarti Sarwal

Introduction

Point of care Transcranial Doppler (POCUS), and POCUS TCDI (Transcranial Doppler Imaging) offers a quick non-invasive assessment for patients in the Neurocritical Care Unit, Emergency Room, Surgery Intensive Care Unit, and Medical Intensive Care Unit that can be performed at bedside. To ensure integrity of data acquired during bedside evaluation, medical personnel performing POCUS should obtain appropriate credentialing in vascular testing by appropriate agencies/governing bodies.

A. Sarwal (✉)
Neurology, Neurocritical Care, Wake Forest Baptist Medical Center, Winston Salem, NC, USA
e-mail: asarwal@wakehealth.edu

W. C. Ziai, C. L. Cornwell (eds.), *Neurovascular Sonography*,
https://doi.org/10.1007/978-3-030-96893-9_20

POCUS TCD (Transcranial Doppler Non-imaging)
Indications: See chapters "Transcranial Color Doppler Imaging for Adults" and "TCD Procedures and Protocols: Protocol for Monitoring for Emboli Detection (and with Microbubbles)" for Complete Study Protocols

- Poor neurological exam * rule out cerebral circulatory arrest (CCA) – Does the patient have positive cerebral blood flow? screening study only, suspected POCUS CCA requires full TCD examination.
- Need for evaluation of significant changes in intracranial pressure or possibility of cerebral circulatory arrest. Is perfusion deficit from high intracranial pressure contributing towards poor exam?
- Assessment of autoregulation in patients with increased ICP to determine perfusion limiting versus perfusion driven increased ICP.
- Vasospasm in subarachnoid hemorrhage

POCUS Cranial Imaging: See chapter "Cranial Ultrasound" for Complete Study Protocol

- Midline Shift
- Hydrocephalus
- Hematoma Volume

Caution

- Limited MCA assessment does NOT rule out intracranial pathology. Use clinical judgement, further diagnostic imaging including diagnostic TCDs or vascular imaging as appropriate for further assessment of cerebrovascular hemodynamics in similar fashion as other POCUS indications.

Technique- TCDI or TCD Bilateral MCA and Basilar Artery POCUS [1]

- Echo probe- for TCDI with Transcranial preset, or 2 Mhz non-imaging probe for TCD – temporal and suboccipital windows.
- Bilateral middle cerebral artery and basilar artery insonation.
- Obtain Doppler- document presence of flow during systole and diastole, and note any changes of direction of flow, pulsatile flow, elevated systolic or decreased diastolic flow.

- Pulse Doppler Gate 5–10 mm, mid – distal MCA insonation 5 cm depth – obtain spectral Doppler waveforms.
- Record- color Doppler video loop 3–4 s and spectral Doppler with sweep adjusted to 3–5 waveforms or cardiac cycles per screen.
- Note peak and end diastolic flow velocity.
- Note mean flow velocities and PIs (Pulsatility Index). To obtain PI manually measure Peak FV – end FV/mean FV = Pulsatility index. Provides information regarding increased ICP (Intracranial Pressure). See chapter "Cerebral Waveforms for Hemodynamic Assessment".

Brain Death Suspected: See chapter "Evaluation of Cerebral Circulatory Arrest" for Details

- Positive diastolic flow is not consistent with cerebral circulatory arrest at that point. Waveforms will show high resistance PI, short systolic spikes, or reverberating/oscillating flow characteristics.
- Resistive waveforms/oscillating waveforms suggest CCA. Oscillating flow in a waveform shows diastolic flow below baseline, and has a typical to- and -fro appearance and sound. Diastolic flow will appear below baseline. It is necessary to record evidence of normal windows if possible. Caution: Absent flow does not always indicate CCA, as this may be secondary to poor acoustic windows. A full diagnostic TCD per brain death protocol is required, if ancillary testing needed and TCD is pursued, or other further diagnostic imaging is necessary.

Increased ICP Evaluation [2]: See chapters "Evaluation of Cerebral Circulatory Arrest" and "Optic Nerve Sheath Diameter for Increased Intracranial Pressure" for Details

- Ocular ultrasound- papilledema or not
- ONSD – 3 mm behind the retina- serial scans, Cut off 6 mm width. Normal ONSD does not rule out ICP crisis
- Midline shift- basal cistern falx- same temporal windows for measurements on both sides
- Cranial US – scan contralateral parenchyma for obvious pathologies – subdural/epidural hemorrhage/intracranial hemorrhage

- TCD- bilateral MCA insonation – high resistance or low resistance waveforms.
  - Normal waveforms/normal velocity or Low resistance waveforms/ normal-high velocities- * Is the patients ICP being driven by increased perfusion

Resistive waveforms, high PIs >1.2 reflect increased distal resistance. Causes: distal atherosclerotic disease or increased ICP depending on clinical situation. Is there perfusion limiting increased ICP? Do I need to escalate ICP lowering therapies? Consider full diagnostic evaluation based on clinical situation.

References

1. Robba C, Goffi A, Geeraerts T, et al. Brain ultrasonography: methodology, basic and advanced principles and clinical applications. A narrative review. Intensive Care Med. 2019;45:913–27.
2. Robba C, Wong A, Poole D, Al Tayar A, Arntfield RT, Chew MS, Corradi F, Douflé G, Goffi A, Lamperti M, Mayo P. Basic ultrasound head-to-toe skills for intensivists in the general and neuro intensive care unit population: consensus and expert recommendations of the European Society of Intensive Care Medicine. Intensive Care Med. 2021;47(12):1347–67. https://doi.org/10.1007/s00134-021-06486-z.

Cerebrovascular Physiology in the Setting of Temporary and Durable Mechanical Circulatory Support

William K. Cornwell III

Introduction

Heart failure with reduced ejection fraction (HFrEF) affects approximately six million individuals in the United States [1]. The 5-year survival of HFrEF patients is approximately 50% [2–4] and is reduced to 20% for patients with end-stage, advanced disease [5]. While heart transplantation remains the gold-standard treatment algorithm [6], the demand for donor hearts far outweighs supply, and in these cases, continuous-flow (CF) left ventricular assist devices (LVADs) have emerged as an attractive alternative. CF-LVADs are used as either a "bridge-to-transplant" to support transplant-eligible patients until a suitable organ becomes available, or as "destination-therapy" for patients who are ineligible for transplantation. Newer devices, such as the Heartware VAD and Heartmate 3 CF-LVAD, are associated with

W. K. Cornwell III (✉)
Medicine-Cardiology, Advanced Heart Failure, LVAD and Cardiac Transplant, Wilderness and Environmental Medicine, University of Colorado Anschutz Medical Campus, Aurora, CO, USA
e-mail: william.cornwell@cuanschutz.edu

W. C. Ziai, C. L. Cornwell (eds.), *Neurovascular Sonography*,
https://doi.org/10.1007/978-3-030-96893-9_21

improved survival compared to medical therapy alone and previous-generation devices that are quickly becoming historical, such as the Heartmate XVE, a pulsatile pump no longer in use, and the Heartmate II, an axial-flow CF-LVAD which has become limited in use [7–9]. However, there are several complications associated with long-term use of these pumps, including nonsurgical bleeding (e.g., gastrointestinal bleeding and epistaxis), hypertension, progressive heart failure, and stroke. As will be discussed, due to certain engineering characteristics of current-generation devices, pulsatility is nonphysiologic and markedly reduced compared to normal healthy individuals. This highly unique aspect of circulatory support has important physiologic and clinical implications on end-organ function, including the brain.

Similarly, patients suffering from cardiogenic shock or fulminant respiratory failure may require stabilization in the form of veno-arterial (VA) or veno-venous (VV) extracorporeal membrane oxygenation (ECMO). ECMO may be used either as a bridge-to-recovery of the failing organ, or until definitive treatment, such as heart transplant or CF-LVAD implantation for cardiogenic shock, or lung transplant for respiratory failure, are possible. Both temporary (ECMO) and durable (CF-LVAD) forms of mechanical circulatory support impart unique physiologic challenges on the brain and are associated with an increased risk of neurovascular complications ranging from subclinical microbleeds to catastrophic and life-threatening strokes and hemorrhages.

Structural Components and Design of Left Ventricular Assist Devices

As demonstrated in Fig. 1, LVADs have historically undergone a series of technological refinements that have led to a marked improvement in survival and overall reduction in adverse events [7–9, 11]. All pumps have an inlet cannula that is surgically anastomosed to the LV, as well as an outflow cannula attached to the

aorta (typically the ascending). The Heartmate XVE pump, a pulsatile volume-displacement system, was the first widespread device used for advanced HFrEF and improved survival over medical therapy alone [12]. However, pulsatility depended on several moving parts, which broke down over approximately 18–24 months and were a major factor limiting long-term use of this pump. The Heartmate II device was the first widespread CF-LVAD that was used to treat patients with advanced HFrEF [11, 13]. Importantly, this device incorporated an axial rotor instead of a volume displacement reservoir to provide circulatory support. The rotor propels blood along its long-axis from the inlet to the

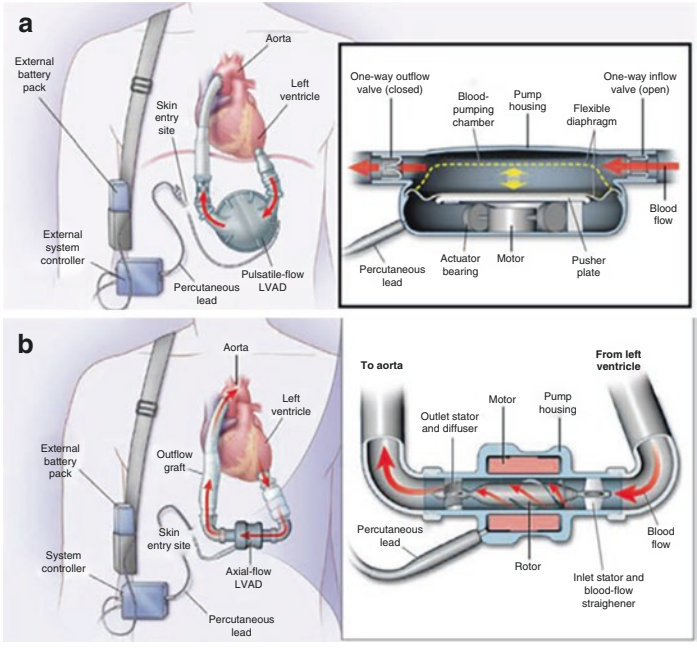

Fig. 1 Types of left ventricular assist devices (LVADs) used clinically for management of advanced heart failure. (**a**) The Heartmate VXE pulsatile pump, no longer used clinically. (**b**) The Heartmate II axial-flow pump. (**c**) The Heartware centrifugal-flow VAD. (**d**) The Heartmate 3 centrifugal-flow CF-LVAD. (Reproduced with permission from Circulation [10])

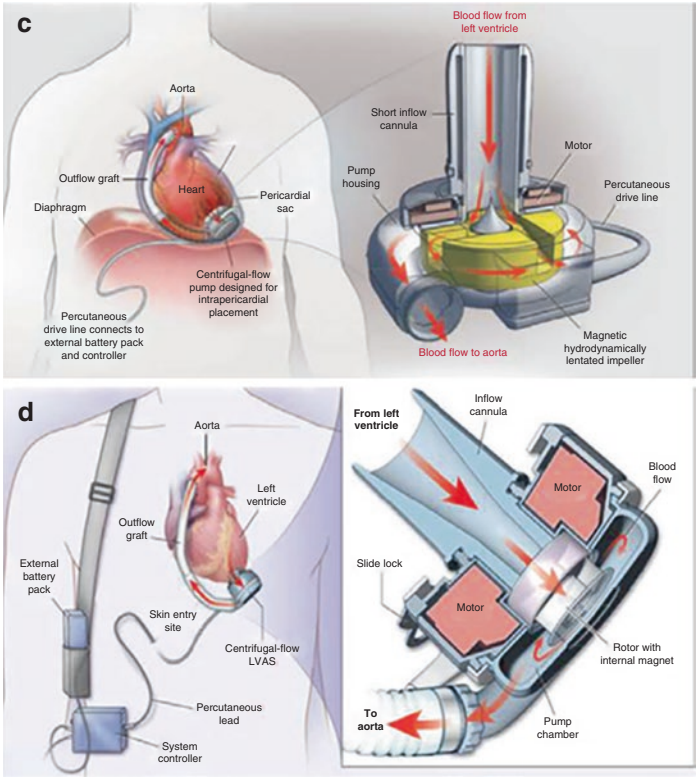

Fig. 1 (continued)

outflow cannula in a continuous fashion. The newer pumps – the Heartware VAD and Heartmate 3 CF-LVAD – incorporate a centrifugal-flow impeller which also provides circulatory support in a continuous fashion by propelling blood from the LV through the outflow cannula. The Heartware VAD is a bearingless device that utilizes magnetic and hydrodynamic levitation of the impeller. The Heartmate 3 CF-LVAD is a fully magnetically levitated device that incorporates an artificial pulse mode [14]. This artificial pulse is achieved by automated modulations in impeller speed every 2 s to reduce stasis of blood in the pump itself,

which reduces the risk of thrombus formation. While this "artificial pulse" may impart some pulsatility in the system, it does not restore a physiologic pulse throughout the body.

Stroke Incidence in the Setting of Durable Mechanical Circulatory Support

According to the Interagency Registry for Mechanically Assisted Circulatory Support (INTERMACS), ischemic stroke among CF-LVAD patients is defined as a new acute neurological deficit of any duration associated with acute infarction on imaging corresponding anatomically to the clinical deficit [15]. Acute symptomatic intracranial hemorrhage is defined as any new acute neurological deficit attributable to intracranial hemorrhage [15]. INTERMACS observational analyses have demonstrated that there is a slight predominance of ischemic strokes over hemorrhagic (51% vs. 49%) [16].

Strokes historically affect approximately 10% of individuals within the first year of support, and, between 6 and 24 months, are the primary cause of death [16–18]. The Heartmate II trials, which evaluated the first CF-LVAD that was approved by the Food and Drug Agency (FDA) for clinical use in the United States, demonstrated that the rate of disabling stroke was similar between the Heartmate II and previous-generation pulsatile devices (Heartmate XVE) over a 2-year period (17% vs. 14%, respectively, $P = 0.56$) [11]. The Heartware VAD, a centrifugal-flow LVAD currently in use, is associated with similar rates of survival compared to the Heartmate II device, but it was found to be associated with a higher stroke rate (29.7% vs. 12.1%, $P < 0.05$) over 2 years [8]. However, the Heartmate 3 CF-LVAD, another centrifugal-flow device and newest pump on the market, was found to have a much lower stroke rate than the Heartmate II pump over a 2-year period of support (10.1% vs. 19.2%, $P < 0.05$) [9]. To date, there has not been a head-to-head study comparing outcomes between the two types of centrifugal-flow devices (i.e., the Heartware VAD and Heartmate 3) which are FDA-approved and are emerging as the mainstays of CF-LVAD therapy.

Blood Pressure Considerations and Impact on Cerebrovascular Physiology and Outcomes

There are several factors that contribute to the development of hypertension in patients supported by CF-LVADs, which may also predispose to stroke and/or adverse neurological events in these patients. First, very elegant studies incorporating microneurography (to directly measure muscle sympathetic nerve traffic) have demonstrated that CF-LVAD patients have markedly abnormal levels of sympathetic tone due to arterial baroreceptor unloading in the setting of a reduced pulse [19, 20]. Second, pump flow is continuous and not gated to the cardiac cycle, which means that diastolic flow, and consequently, diastolic blood pressure is increased. This increase in diastolic blood pressure, in turn, increases mean arterial pressure and predisposes to overt hypertension (systolic blood pressure typically does not increase following CF-LVAD implantation) [20]. Finally, many HFrEF patients have concomitant hypertension as part of the natural history of their cardiovascular disease. Blood pressure variability is greater among hypertensive than normotensive individuals, which increases the risk of end-organ damage [21], as well as cardiovascular-related mortality [22].

Several studies have demonstrated that uncontrolled hypertension increases the risk of stroke, particularly with the Heartware VAD, among CF-LVAD patients [23–25]. Specifically, a mean arterial pressure above 90 mmHg is associated with an increased risk of stroke. For all of these reasons, CF-LVAD patients frequently require multiple classes of antihypertensives, in addition to standard guideline-directed medical therapy that is the cornerstone of HFrEF management [6], to maintain blood pressure within a safe margin and reduce the risk of stroke. Specifically, medical therapy is generally optimized to maintain mean arterial pressure at or below 80 mmHg [26].

Stroke Mechanisms Among Patients Supported by CF-LVADS

The combination of HFrEF and associated comorbidities, medications (primarily anticoagulants), and device-related complications all work together in an almost synergistic fashion to increase

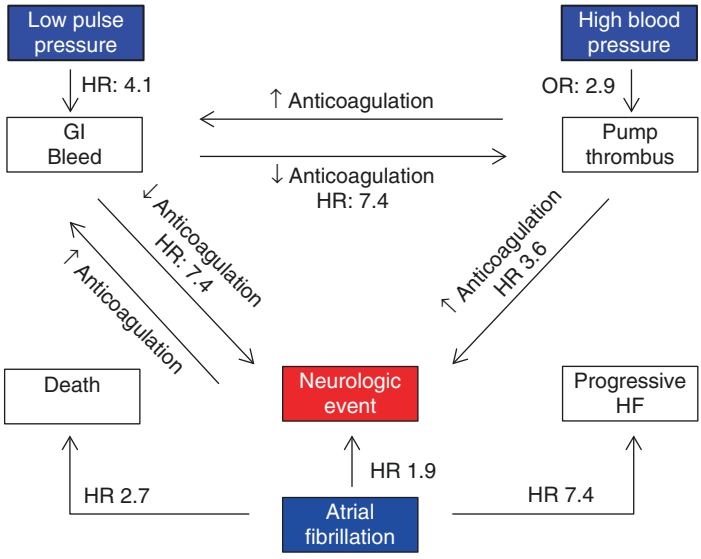

Fig. 2 Reductions in pulsatility increase the risk of nonsurgical (primarily gastrointestinal bleeding and epistaxis) by ~fourfold. Reductions in anticoagulation following a bleeding event increase the risk of development of a pump thrombus or embolic stroke by sevenfold. Hypertension increases the odds of pump thrombus formation, which more than triples the risk of a neurologic event. Approximately 25–50% of HFrEF patients have concomitant atrial fibrillation prior to CF-LVAD implantation, which if present, doubles the risk of stroke and significantly increases the risk of progressive heart failure and death. (Reproduced with permission from Stroke [17])

the risk of stroke (Fig. 2) [17]. For these reasons, cerebrovascular physiology and pathology among CF-LVAD patients cannot be considered in isolation, but it must be placed in context of what is known about the patient's overall clinical profile.

The risk of nonsurgical and more specifically gastrointestinal bleeding and epistaxis is inversely proportional to the degree of pulsatility [27], and on average, almost one-third of CF-LVAD patients will suffer from a nonsurgical bleeding event in the first year of support [18]. Since these patients are managed with both an antiplatelet and an anticoagulant to reduce the risk of pump thrombus [26], the intensity of anticoagulation may be reduced following a bleeding event. However, the benefits of this modification may be offset by the increased risk of pump thrombus or

embolic stroke [28]. In addition, these patients are inherently predisposed to bleeding events due to an acquired von Willebrand syndrome that results from cleavage of large multimers by a disintegrin and metalloproteinase with a thrombospondin type 1 motif, member 13 (ADAMTS-13) [29]. Uncontrolled blood pressure also increases the risk of pump thrombus, which when present, is associated with an increased risk of stroke [30]. Finally, approximately one-fourth of CF-LVAD individuals suffer from device-related infections [31]. For reasons that are not entirely clear, bloodstream infections increase the risk of subsequent stroke, possibly as a result of bacterial seeding causing formation of mycotic aneurysms [32].

Over one-fourth of HFrEF patients have concomitant atrial fibrillation (AF) at the time of diagnosis [33]. The combination of HFrEF and AF following CF-LVAD implantation significantly increases the rate of neurovascular complications, as well as the risk of progressive heart failure and death. The increased risk of thromboemboli is not related to inadequate anticoagulation since in one series, CF-LVAD patients with concomitant AF actually had higher international normalized ratio levels at the time of stroke than CF-LVAD patients without AF (2.70 ± 0.94 v. 1.54 ± 0.34) and for the 4-week period preceding the stroke (2.33 ± 0.65 v. 1.57 ± 0.31). Thus, it appears that the presence of AF, independent of anticoagulation, significantly increases the rate of thromboembolic stroke in these patients [17].

Impact of CF-LVAD Support on Cerebrovascular Physiology

Traditional criteria for characterizing transcranial Doppler (TCD) waveforms may not be applicable – or may require modification, for HFrEF patients supported by CF-LVADs due to a reduction pulsatility. Waveforms derived from these patients are unique and quite distinct from typical waveforms obtained from normal individuals. The degree of pulsatility within extra- and intracranial arteries is typically reduced, and the pulsatility index is typi-

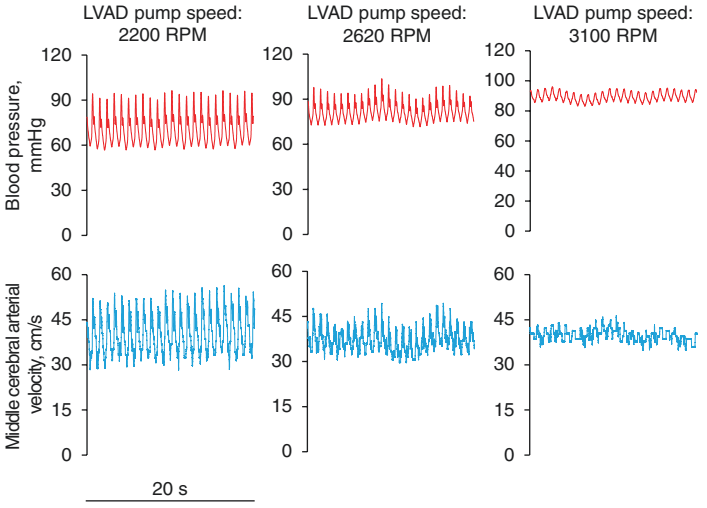

Fig. 3 Example tracings of arterial blood pressure via arterial catheterization and middle cerebral arterial velocity via transcranial Doppler from an individual supported by a Heartware VAD. Tracings obtained during spontaneous respirations during changes in pump speed. Note the increase in pulsatility at low speed (2200 RPM, left panel) and marked reduction in pulsatility at high speed (3100 RPM, right panel). (Unpublished data, courtesy of Dr. Cornwell)

cally – though not always – lower than normal reference values. However, the appearance of waveform envelopes may vary considerably between individuals, and there may be longitudinal variations within an individual over time based on several factors, such as cardiovascular loading conditions (cardiovascular preload and afterload) and changes in CF-LVAD pump speed (Fig. 3).

It is well known that cerebral perfusion is impaired in the setting of advanced HFrEF and that these individuals may experience a downward shift in the cerebral autoregulatory curve [17, 34, 35]. Longitudinal assessments evaluating how cerebral perfusion changes prior to and following CF-LVAD implantation are lacking [17]. However, it has been shown that cerebral autoregulation is normal among patients with CF-LVADs, which suggests that there is at least some improvement in cerebral perfusion following device implantation, at least under resting conditions [36].

Cerebral Microembolic Events in the Setting of CF-LVAD Support

There are little data regarding the utility of TCD for detection of microembolic signals (MES) among individuals supported by current-generation devices. MES have been reported for patients supported by older devices that are no longer in use [37, 38]. For example, patients supported by pulsatile LVADs experienced, on average, 2.3 ± 9.2 MES per 30-min monitoring period, while patients supported by CF-LVADs experienced 81 ± 443 MES per hour [37, 38]. Based on these observations, it has been suggested that patients with current-generation devices – even those who are asymptomatic and clinically stable – likely experience subclinical microbleeds [39] and microemboli [17], but this observation has not been directly observed in the form of TCD monitoring studies. Interestingly, the MES burden among patients with previous-generation CF-LVADs declined with supplemental oxygen, suggesting that these microemboli were predominantly gaseous and formed through cavitation [38, 40, 41]. Further research is necessary in this area to determine the extent of cerebral microembolization among patients supported by current-generation devices.

Extracorporeal Membrane Oxygenation, Cerebrovascular Physiology, and Outcomes

Data regarding cerebrovascular physiology on patients supported by VV- and VA-ECMO are sparse [42]. While a detailed review of the physiology associated with temporary mechanical circulatory support is beyond the scope of this chapter, it is important to recognize a few fundamental differences between VV- and VA-ECMO and the implications for circulatory support. VV-ECMO oxygenates venous blood and removes carbon dioxide but does not provide additional hemodynamic support to the body. Hence, VV-ECMO functionally bypasses the lungs but not the heart. Importantly, patients with respiratory failure supported by VV-ECMO have a physiologic pulse, with normal pulse pressure [43]. In contrast, VA-ECMO bypasses both the lungs and heart by returning oxygen-

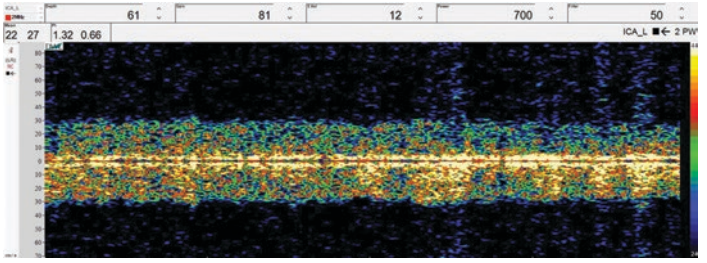

Fig. 4 Example transcranial Doppler patterns of left internal carotid arterial waveforms showing completely nonpulsatile flow in a 64-year-old male supported by VA-ECMO following an ST elevation myocardial infarction of the inferior wall complicated by free wall rupture. (Image courtesy of Ergin Bahattin and Dr. Wendy Ziai, Johns Hopkins University)

ated blood to the aorta. Since circulatory support with ECMO is provided continuously, patients with cardiogenic shock who are supported by VA-ECMO have diminished pulsatility. In these patients, pulse pressure is typically reduced (Fig. 4). Any pulsatility that is present depends on native ventricular function, or additional hemodynamic support with concomitant use of an intraaortic balloon pump. Pulsatility increases as ventricular function improves/recovers, and the return of a pulsatile arterial waveform is used clinically (along with several other factors) to justify discontinuation of VA-ECMO. These issues are relevant insomuch as they may impact the Doppler waveforms obtained while monitoring intracranial vessels. Patients supported by VV-ECMO should have TCD waveforms that are pulsatile. However, the appearance of TCD waveforms among patients supported by VA-ECMO may vary widely according to hemodynamic conditions as described.

Similar to durable mechanical circulatory support, strokes – either embolic or hemorrhagic – are common, and TCD may be incorporated to monitor the neurologic status of patients supported by VA-ECMO (Fig. 5). Bedside TCD may be particularly advantageous in these scenarios, since patients are typically intubated (which prohibits a comprehensive neurologic examination) and the degree of hemodynamic instability prohibits transportation to radiology suites for additional imaging.

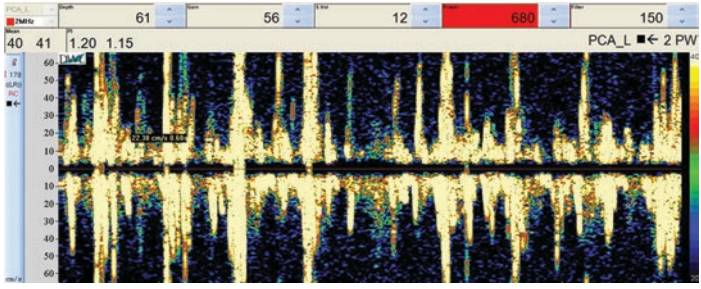

Fig. 5 Shower of emboli detected by transcranial Doppler monitoring of the left posterior cerebral artery in a 42-year-old man supported by VA-ECMO following an orthotopic heart transplant complicated by primary graft dysfunction. (Image courtesy of Ergin Bahattin and Dr. Wendy Ziai, Johns Hopkins University)

Given the abnormal TCD waveforms associated with VA-ECMO support, it may be difficult for neurosonologists/neurologists to establish brain death among patients whose clinical condition has deteriorated. It has been suggested that traditional criteria for brain death can be applied to these patients if their waveforms are pulsatile [42]. However, deciphering the presence or absence of brain death in the absence of pulsatile flow may be problematic/impossible.

Conclusion

While survival and quality-of-life among CF-LVAD patients have improved with advancements in technology, the risk of stroke remains unacceptably high and is a leading cause of death following device implantation. Several factors account for the high stroke rate, including medication effects, patient comorbidities, as well as other device-related complications, such as acquired von Willebrand syndrome, pump thrombosis, nonsurgical bleeding, and device-related infections. All of these factors work together in an almost synergistic fashion to increase the risk of stroke. Additional research is necessary to understand the implications of continuous-flow circulatory support on blood pressure regulation

and perfusion of dependent organs. Further, more information is needed to define normal TCD flow and pulsatility indices in this highly unique population.

Personal Perspective

I first became interested in CF-LVADs after learning how these devices provide circulatory support to the body – namely, that these patients lack a meaningful pulse – and the many implications that this type of flow has on the human body. From a birds-eye view, the presence or absence of a physiologic pulse may seem benign and inconsequential. However, for almost two decades now, the heart failure community has been caring for patients who are "living without a pulse" [44] and the human body's natural design is such that normal cardiovascular reflexes depend on pulsatile flow. However, these patients have shown us that chronic exposure to a nonphysiologic and reduced pulse imparts subtle responses or adaptations within the human body that manifest clinically in many forms, from cellular and tissue levels all the way up to the organ level with gastrointestinal bleeds and strokes.

The improvements in CF-LVAD technology that have occurred over the past two decades are remarkable. While these devices are not "perfect" and are associated with adverse events, they are nonetheless, lifesaving, and restore patients to a quality-of-life that they may not have enjoyed for years. Among the adverse events encountered with these devices, strokes are among the most common and are by far the most detrimental to a patient's overall survival and well-being. Much more research is necessary to understand mechanisms that account for the unacceptably high rate of stroke, which will inform clinicians on best practices for stroke prevention in this very unique population, and will also serve as a pathway to strengthen the "heart-brain connection" between the worlds of cardiology and neurology.

Disclosures Dr. Cornwell has received research funding from Medtronic Inc and is a consultant for Medtronic Inc.

References

1. Benjamin EJ, Blaha MJ, Chiuve SE, Cushman M, Das SR, Deo R, de Ferranti SD, Floyd J, Fornage M, Gillespie C, Isasi CR, Jimenez MC, Jordan LC, Judd SE, Lackland D, Lichtman JH, Lisabeth L, Liu S, Longenecker CT, Mackey RH, Matsushita K, Mozaffarian D, Mussolino ME, Nasir K, Neumar RW, Palaniappan L, Pandey DK, Thiagarajan RR, Reeves MJ, Ritchey M, Rodriguez CJ, Roth GA, Rosamond WD, Sasson C, Towfighi A, Tsao CW, Turner MB, Virani SS, Voeks JH, Willey JZ, Wilkins JT, Wu JH, Alger HM, Wong SS, Muntner P. American Heart Association Statistics C and Stroke Statistics S. Heart disease and stroke statistics-2017 update: a report from the American Heart Association. Circulation. 2017;135:e146–603.
2. Roger VL, Go AS, Lloyd-Jones DM, Benjamin EJ, Berry JD, Borden WB, Bravata DM, Dai S, Ford ES, Fox CS, Fullerton HJ, Gillespie C, Hailpern SM, Heit JA, Howard VJ, Kissela BM, Kittner SJ, Lackland DT, Lichtman JH, Lisabeth LD, Makuc DM, Marcus GM, Marelli A, Matchar DB, Moy CS, Mozaffarian D, Mussolino ME, Nichol G, Paynter NP, Soliman EZ, Sorlie PD, Sotoodehnia N, Turan TN, Virani SS, Wong ND, Woo D, Turner MB, American Heart Association Statistics C and Stroke Statistics S. Executive summary: heart disease and stroke statistics–2012 update: a report from the American Heart Association. Circulation. 2012;125:188–97.
3. Mosterd A, Cost B, Hoes AW, de Bruijne MC, Deckers JW, Hofman A, Grobbee DE. The prognosis of heart failure in the general population: the Rotterdam Study. Eur Heart J. 2001;22:1318–27.
4. Ho KK, Pinsky JL, Kannel WB, Levy D. The epidemiology of heart failure: the Framingham Study. J Am Coll Cardiol. 1993;22:6A–13A.
5. Ammar KA, Jacobsen SJ, Mahoney DW, Kors JA, Redfield MM, Burnett JC Jr, Rodeheffer RJ. Prevalence and prognostic significance of heart failure stages: application of the American College of Cardiology/American Heart Association heart failure staging criteria in the community. Circulation. 2007;115:1563–70.
6. Yancy CW, Jessup M, Bozkurt B, Butler J, Casey DE, Drazner MH, Fonarow GC, Geraci SA, Horwich T, Januzzi JL, Johnson MR, Kasper EK, Levy WC, Masoudi FA, McBride J, McMurray JV, Mitchell JE, Peterson PN, Riegel B, Sam F, Stevenson LW, Tang WHW, Tsai EJ, Wilkoff BL. 2013 ACCF/AHA Guideline for the management of heart failure: a report of the American College of Cardiology Foundation/American Heart Association Task Force on Practice Guidelines. Circulation. 2013;128:e240–327.
7. Aaronson KD, Slaughter MS, Miller LW, McGee EC, Cotts WG, Acker MA, Jessup ML, Gregoric ID, Loyalka P, Frazier OH, Jeevanandam V, Anderson AS, Kormos RL, Teuteberg JJ, Levy WC, Naftel DC, Bittman RM, Pagani FD, Hathaway DR, Boyce SW, HeartWare Ventricular Assist

Device Bridge to Transplant ATI. Use of an intrapericardial, continuous-flow, centrifugal pump in patients awaiting heart transplantation. Circulation. 2012;125:3191–200.
8. Rogers JG, Pagani FD, Tatooles AJ, Bhat G, Slaughter MS, Birks EJ, Boyce SW, Najjar SS, Jeevanandam V, Anderson AS, Gregoric ID, Mallidi H, Leadley K, Aaronson KD, Frazier OH, Milano CA. Intrapericardial left ventricular assist device for advanced heart failure. N Engl J Med. 2017;376:451–60.
9. Mehra MR, Goldstein DJ, Uriel N, Cleveland JC, Yuzefpolskaya M, Salerno C, Walsh MN, Milano CA, Patel CB, Ewald GA, Itoh A, Dean D, Krishnamoorthy A, Cotts WG, Tatooles AJ, Jorde UP, Bruckner BA, Estep JD, Jeevanandam V, Sayer G, Horstmanshof D, Long JW, Gulati S, Skipper ER, O'Connell JB, Heatley G, Sood P, Naka Y. Two-year outcomes with a magnetically levitated cardiac pump in heart failure. N Engl J Med. 2018;378:1386–95.
10. Gopinathannair R, Cornwell WK, Dukes JW, Ellis CR, Hickey KT, Joglar JA, Pagani FD, Roukoz H, Slaughter MS, Patton KK. Device therapy and arrhythmia management in left ventricular assist device recipients: a scientific statement from the American Heart Association. Circulation. 2019;139:e967–89.
11. Slaughter M, Rogers J, Milano C, Russell S, Conte J, Feldman D, Sun B, Tatooles A, Delgado R, Long J, Wozniak T, Ghumman W, Farrar D, Frazier O. Advanced heart failure treated with continuous-flow left ventricular assist device. N Engl J Med. 2009;361:2241–51.
12. Rose EAGA, Moskowitz AJ, Heitjan DF, Stevenson LW, Dembitsky W, Long JW, Ascheim DD, Tierney AR, Levitan RG, Watson JT, Meier P. Long-term use of a left ventricular assist device for end-stage heart failure. N Engl J Med. 2001;345:1435–43.
13. Miller LW, Pagani FD, Russell SD, Ranjit J, Boyle AJ, Aaronson KD, Conte JV, Naka Y, Mancini D, Delgado RM, MacGillivray TE, Farrar DJ, Frazier OH. Use of a continuous-flow device in patients awaiting heart transplantation. N Engl J Med. 2007;357(9):885–96.
14. Drazner MH. A new left ventricular assist device – better, but still not ideal. N Engl J Med. 2018;378:1442–3.
15. INTERMACS. INTERMACS User's guide 2014. Available at: https://www.uab.edu/medicine/intermacs/intermacs-documents. Accessed 26 Nov 2018.
16. Acharya D, Loyaga-Rendon R, Morgan CJ, Sands KA, Pamboukian SV, Rajapreyar I, Holman WL, Kirklin JK, Tallaj JA. INTERMACS analysis of stroke during support with continuous-flow left ventricular assist devices: risk factors and outcomes. JACC Heart Fail. 2017;5:703–11.
17. Cornwell WK III, Ambardekar AV, Tran T, Pal J, Cava L, Lawley J, Tarumi T, Cornwell C, Aaronson KD. Stroke incidence and impact of continuous-flow left ventricular assist devices on cerebrovascular physiology. Stroke. 2019;50:542–8.

18. Kirklin JK, Pagani FD, Kormos RL, Stevenson LW, Blume ED, Myers SL, Miller MA, Baldwin JT, Young JB, Naftel DC. Eighth annual INTERMACS report: special focus on framing the impact of adverse events. J Heart Lung Transplant. 2017;36:1080–6.
19. Markham DW, Fu Q, Palmer MD, Drazner MH, Meyer DM, Bethea BT, Hastings JL, Fujimoto N, Shibata S, Levine BD. Sympathetic neural and hemodynamic responses to upright tilt in patients with pulsatile and nonpulsatile left ventricular assist devices. Circ Heart Fail. 2013;6:293–9.
20. Cornwell WK 3rd, Tarumi T, Stickford A, Lawley J, Roberts M, Parker R, Fitzsimmons C, Kibe J, Ayers C, Markham D, Drazner MH, Fu Q, Levine BD. Restoration of pulsatile flow reduces sympathetic nerve activity among individuals with continuous-flow left ventricular assist devices. Circulation. 2015;132:2316–22.
21. Mancia G, Ferrari A, Gregorini L, Parati G, Pomidossi G, Bertinieri G, Grassi G, di Rienzo M, Pedotti A, Zanchetti A. Blood pressure and heart rate variabilities in normotensive and hypertensive human beings. Circ Res. 1983;53:96–104.
22. Parati G, Pomidossi G, Albini F, Malaspina D, Mancia G. Relationship of 24-hour blood pressure mean and variability to severity of target-organ damage in hypertension. J Hypertens. 1987;5:93–8.
23. Willey JZ, Boehme AK, Castagna F, Yuzefpolskaya M, Garan AR, Topkara V, Colombo PC. Hypertension and stroke in patients with left ventricular assist devices (LVADs). Curr Hypertens Rep. 2016;18:12.
24. Teuteberg JJ, Slaughter MS, Rogers JG, McGee EC, Pagani F, Gordon R, Rame E, Acker M, Kormos RL, Salerno C, Schleeter TP, Goldstein DJ, Shin J, Starling RC, Wozniak T, Malik AS, Silvestry S, Ewald GA, Jorde U, Naka Y, Birks E, Najarian KB, Hathaway DR, Aaronson KD. The HVAD left ventricular assist device. Risk factors for neurological events and risk mitigation strategies. JACC Heart Fail. 2015;3:818–28.
25. Najjar SS, Slaughter MS, Pagani FD, Starling RC, McGee EC, Eckman P, Tatooles AJ, Moazami N, Kormos RL, Hathaway DR, Najarian KB, Bhat G, Aaronson KD, Boyce SW, Investigators HBTAT. An analysis of pump thrombus events in patients in the HeartWare ADVANCE bridge to transplant and continued access protocol trial. J Heart Lung Transplant. 2014;33:23–34.
26. Slaughter MS, Pagani FD, Rogers JG, Miller LW, Sun B, Russell SD, Starling RC, Chen L, Boyle AJ, Chillcott S, Adamson RM, Blood MS, Camacho MT, Idrissi KA, Petty M, Sobieski M, Wright S, Myers TJ, Farrar DJ, HeartMate IICI. Clinical management of continuous-flow left ventricular assist devices in advanced heart failure. J Heart Lung Transplant. 2010;29:S1–39.
27. Wever-Pinzon O, Selzman CH, Drakos SG, Saidi A, Stoddard GJ, Gilbert EM, Labedi M, Reid BB, Davis ES, Kfoury AG, Li DY, Stehlik J, Bader F. Pulsatility and the risk of nonsurgical bleeding in patients supported

with the continuous-flow left ventricular assist device HeartMate II. Circ Heart Fail. 2013;6:517–26.
28. Stulak JM, Lee D, Haft JW, Romano MA, Cowger JA, Park SJ, Aaronson KD, Pagani FD. Gastrointestinal bleeding and subsequent risk of thromboembolic events during support with a left ventricular assist device. J Heart Lung Transplant. 2014;33:60–4.
29. Harvey L, Holley C, Roy SS, Eckman P, Cogswell R, Liao K, John R. Stroke after left ventricular assist device implantation: outcomes in the continuous-flow era. Ann Thorac Surg. 2015;100:535–41.
30. Kirklin JK, Naftel DC, Kormos RL, Pagani FD, Myers SL, Stevenson LW, Acker MA, Goldstein DL, Silvestry SC, Milano CA, Baldwin JT, Pinney S, Eduardo Rame J, Miller MA. Interagency Registry for Mechanically Assisted Circulatory Support (INTERMACS) analysis of pump thrombosis in the HeartMate II left ventricular assist device. J Heart Lung Transplant. 2014;33:12–22.
31. Gordon RJ, Weinberg AD, Pagani FD, Slaughter MS, Pappas PS, Naka Y, Goldstein DJ, Dembitsky WP, Giacalone JC, Ferrante J, Ascheim DD, Moskowitz AJ, Rose EA, Gelijns AC, Lowy FD, Ventricular Assist Device Infection Study G. Prospective, multicenter study of ventricular assist device infections. Circulation. 2013;127:691–702.
32. Aggarwal A, Gupta A, Kumar S, Baumblatt JA, Pauwaa S, Gallagher C, Treitman A, Pappas P, Tatooles A, Bhat G. Are blood stream infections associated with an increased risk of hemorrhagic stroke in patients with a left ventricular assist device? ASAIO J. 2012;58:509–13.
33. Wang TJ, Larson MG, Levy D, Vasan RS, Leip EP, Wolf PA, D'Agostino RB, Murabito JM, Kannel WB, Benjamin EJ. Temporal relations of atrial fibrillation and congestive heart failure and their joint influence on mortality: the Framingham Heart Study. Circulation. 2003;107:2920–5.
34. Caldas JR, Panerai RB, Haunton VJ, Almeida JP, Ferreira GS, Camara L, Nogueira RC, Bor-Seng-Shu E, Oliveira ML, Groehs RR, Ferreira-Santos L, Teixeira MJ, Galas FR, Robinson TG, Jatene FB, Hajjar LA. Cerebral blood flow autoregulation in ischemic heart failure. Am J Physiol Regul Integr Comp Physiol. 2017;312:R108–13.
35. Cornwell WK 3rd, Levine BD. Patients with heart failure with reduced ejection fraction have exaggerated reductions in cerebral blood flow during upright posture. JACC Heart Fail. 2015;3:176–9.
36. Cornwell WK 3rd, Tarumi T, Aengevaeren VL, Ayers C, Divanji P, Fu Q, Palmer D, Drazner MH, Meyer DM, Bethea BT, Hastings JL, Fujimoto N, Shibata S, Zhang R, Markham DW, Levine BD. Effect of pulsatile and nonpulsatile flow on cerebral perfusion in patients with left ventricular assist devices. J Heart Lung Transplant. 2014;33:1295–303.
37. Nabavi DG, Stockmann J, Schmid C, Schneider M, Hammel D, Scheld HH, Ringelstein EB. Doppler microembolic load predicts risk of thromboembolic complications in Novacor patients. J Thorac Cardiovasc Surg. 2003;126:160–7.

38. Thoennissen NH, Schneider M, Allroggen A, Ritter M, Dittrich R, Schmid C, Scheld HH, Ringelstein EB, Nabavi DG. High level of cerebral microembolization in patients supported with the DeBakey left ventricular assist device. J Thorac Cardiovasc Surg. 2005;130:1159–66.
39. Yoshioka D, Okazaki S, Toda K, Murase S, Saito S, Domae K, Miyagawa S, Yoshikawa Y, Daimon T, Sakaguchi M, Sawa Y. Prevalence of cerebral microbleeds in patients with continuous-flow left ventricular assist devices. J Am Heart Assoc. 2017;6:e005955.
40. Thoennissen NH, Allroggen A, Dittrich R, Ritter M, Schmid C, Scheld HH, Ringelstein EB, Nabavi DG. Can Doppler time domain analysis of microembolic signals discriminate between gaseous and solid microemboli in patients with left ventricular assist devices? Neurol Res. 2003;27:780–4.
41. Droste DW, Hansberg T, Kemeny V, Hammel D, Schulte-Altedorneburg G, Nabavi DG, Kaps M, Scheld HH, Ringelstein EB. Oxygen inhalation can differentiate gaseous from nongaseous microemboli detected by transcranial Doppler ultrasound. Stroke. 1997;28:2453–6.
42. Marinoni M, Cianchi G, Trapani S, Migliaccio ML, Bonizzoli M, Gucci L, Cramaro A, Gallerini A, Picciafuochi F, Valente S, Peris A. Retrospective analysis of transcranial Doppler patterns in veno-arterial extracorporeal membrane oxygenation patients: feasibility of cerebral circulatory arrest diagnosis. ASAIO J. 2018;64:175–82.
43. Guinot PG, Zogheib E, Detave M, Moubarak M, Hubert V, Badoux L, Bernard E, Besserve P, Causs T, Dupont H. Passive leg raising can predict fluid responsiveness in patients placed on venovenous extracorporeal membrane oxygenation. Crit Care. 2011;15:R216–24.
44. Purohit SN, Cornwell WK 3rd, Pal JD, Lindenfeld J, Ambardekar AV. Living without a pulse: the vascular implications of continuous-flow left ventricular assist devices. Circ Heart Fail. 2018;11:1–11.

Electroencephalography Versus Transcranial Doppler Ultrasonography; Indications and Applications for Intracranial Monitoring

Omar Hussein

Introduction

Bedside noninvasive non-radiological intracranial monitoring has been gaining a lot of popularity in the last few decades. Two main technologies are of high interest. Transcranial Doppler ultrasonography (TCD) uses ultrasound waves to monitor intracranial hemodynamics. Another is electroencephalography (EEG) and its more advanced form quantitative-EEG (QEEG). EEG monitors the electrical activities in the cerebral cortex. TCD and EEG can provide early and/or real-time detection of intracranial abnormalities through frequent or continuous bedside monitoring. However, both technologies still carry their own difficulties and uncertainties and require special training. TCD measures changes in the intracranial blood flow velocities, Lindegaard ratio (LR), pulsatility index (PI), and vasomotor reactivity (VMR). QEEG measures changes in the alpha/delta ratio (ADR) and/or the relative alpha variability (RAV) among others. TCD is operator-dependent while QEEG is reader-dependent. QEEG runs

O. Hussein (✉)
University of New Mexico, Albuquerque, NM, USA

W. C. Ziai, C. L. Cornwell (eds.), *Neurovascular Sonography*,
https://doi.org/10.1007/978-3-030-96893-9_22

continuously while TCD is often performed once or twice a day. This chapter will provide comparisons between TCD and EEG when used to monitor commonly known intracranial pathologies or operations based on the latest evidence and guidelines in the literature.

Transcranial Doppler (TCD) measures peak systolic velocity (PSV), end-diastolic velocity (EDV), and mean flow velocity (MFV) in the large intracranial vessels. The main formulas produced include:

- Lindegaard ratio (LR = middle cerebral artery (MCA) MFV/Ipsilateral extracranial carotid artery MFV) is used to differentiate between hyperemia and vasospasm/vasoconstriction. An increased LR indicates vasospasm/vasoconstriction [1].
- Pulsatility index (PI = PSV – EDV/MFV; measured at the proximal MCA) is another parameter that measures the flow resistance. Pulsatility index directly correlates with intracranial pressure and negatively correlates with cerebral perfusion pressure (CPP), especially when CPP falls below 70 mmHg. A normal PI value is 1. PI >3 is associated with increased intracranial pressure (ICP) and low CPP. PI >6 is associated with cerebral circulatory arrest [2].
- Vasomotor reactivity (VMR = [$MFV_{hypercapnea}$ – $MFV_{hypocapnea}$]/MFV at rest × 100; measured at the MCA). If low (<33%), it indicates poor reactivity and imparied auto-regulation. If reserved, blood pressure augmentation can be used to enhance cerebral perfusion and oxygenation and vice versa. This is helpful during the management of cerebral perfusion pressure and brain oxygenation [1]. In addition, it can be used to identify patients at higher risk of stroke among those with asymptomatic carotid stenosis or previously symptomatic carotid occlusion [3].

However, these measures are not a direct measure of cerebral or cortical dysfunction.

A raw-EEG measures the electrical conduction within the cortical tissue and thus, can directly detect dysfunction. QEEG measures long term trends over time. Many parameters are recognized

including band power, band variability, and band to band ratio. Of these, a few parameters are most reliable:

- Declining Alpha/Delta Ratio (ADR) (8–13 Hz power divided by 1–4 Hz power)
- Declining Relative Alpha Variability (RAV) (8–12 Hz power divided by 1–20 Hz power)
- Detection of new or increasing periodic or rhythmic discharges on raw-EEG

However, caution upon reviewing the QEEG should be made as confounders like age, state change, sedation, or artifacts may give false-positive results. Furthermore, a patient might have severe focal vasospasm but the QEEG changes might be delayed due to good collateral circulation.

The current guidelines [4], published by the joint committee of The American Society of Neurophysiologic Monitoring (ASNM) and The American Society of Neuroimaging (ASN) in 2010, recommended the use of TCD in the following situations (Class II and III evidence, Type B recommendation):

1. Cerebral vasomotor reactivity and autoregulation assessment;
2. The circle of Willis functional status assessment;
3. Relative cerebral hypo- and hyperperfusion identification;
4. Cerebral emboli detection. (low to moderate quality evidence, Moderate (type B-C) recommendations except for vasospasm watch in aneurysmal SAH associated with good clinical grade and stroke screening for sickle cell patients which carries high-quality evidence and strong (type A) recommendations:

Nevertheless, two indications for the use of TCD have emerged as Class I evidence, Type A recommendation since then:

1. Vasospasm watch in aneurysmal subarachnoid hemorrhage associated with good clinical examination.
2. Screening for ischemic stroke among sickle cell children.

Here are more specifications on how TCD might be helpful:

1. Perioperative assessment of the cerebral hemodynamics:

Preoperative TCD assessment is essential for intra- and/or post-operative comparisons. This is because it might be influenced by many factors. These factors might be age, gender, race, chronic conditions like anemia, hypertension, nicotine consumption, and/or diabetes mellitus. Others factors include anesthesia and vasopressors [4, 5].

Surgeries or interventions that benefit from TCD include:

(a) Carotid Endarterectomy: Following the MCA-MFV intraoperatively or the embolic load postoperatively can detect early complications [6].
(b) Post carotid stenting and/or mechanical thrombectomy: TCD assesses the intracranial hemodynamics after mechanical thrombectomy of an acute large vessel occlusion (LVO) stroke. An abnormal MCA signal with 72 h post-thrombectomy is an independent predictor of poor outcome at 90 days [7].
(c) Some intracranial aneurysm repairs: TCD can detect the hemispheric dependence on the flow from the ipsilateral hemisphere during carotid artery sacrifice associated with giant aneurysms. This is done by performing endovascular carotid balloon occlusion test with continuous intracranial monitoring [8].
(d) Cardiopulmonary bypass: TCD is used to watch for impending cerebral ischemia when ≥80% decline from the MFV at baseline occurs [9, 10].

2. Assessment of the intracranial hemodynamics:

Examples include:

- Assessment of cerebral blood flow velocities and Lindegaard ratio in case of vasospasm associated with conditions like aneurysmal subarachnoid hemorrhage (SAH). This is likely the most common indication for the use of TCD currently and has the strongest level of recommendation.

- Assessment of the cerebral blood flow velocities after an acute ischemic stroke with or without administering a thrombolytic which might show recanalization, hypoperfusion, hyperperfusion (≥50% of normal), or reocclusion [11].
- Assessment of the cerebral blood flow velocities before an acute ischemic stroke occurs in children with sickle cell disease who are at high risk of developing acute ischemic stroke.
- Assessment of the collateral circulation in the brain using the cerebral blood flow direction which might demonstrate flow reversal if collaterals are present after an ischemic stroke, or flow diversion if the vessel is obstructed without adequate collaterals [11].
- Assessment of the cerebral blood flow velocities in chronic hypoperfusion conditions such as severe carotid stenosis or positional basilar artery stenosis [12, 13]
- Assessment of changes between the peak-systole and the end-diastole velocities. This might indicate venous obstruction or intracranial hypertension [14].
- Detection and quantification of micro-emboli with or without a bubble-challenge provides a way of detection of cardiac emboli in cardio-embolic or cryptogenic strokes or even during carotid procedures [15].
- Assessment of the cerebral autoregulation and vasomotor reactivity in patients with traumatic brain injury can help refining treatment for better cerebral perfusion.

On the other hand, the guidelines for QEEG in monitoring vasospasm or cerebral ischemia carry class III evidence and moderate-level (type C) recommendation including those for vasospasm watch in aneurysmal SAH. This is based mainly on a few retrospective studies and expert opinion [16–20]. Thus, it can be used as an adjunctive method in high-risk patients for ischemia. For SAH, monitoring should start at or before day-3 post-bleeding before the risky period for vasospasm starts (post-bleed days 4–14) to establish a baseline reading. Readers should review the QEEG at least 3–4 times a day. For other cerebral ischemic conditions like crescendo transient ischemic attacks or post carotid endarterectomy, it should start immediately and last for up to 24–48 h. Readers should review QEEG at a more frequent rate especially during sleep [20].

TCD Versus EEG in Common Clinical Scenarios

1. Acute Subarachnoid Hemorrhage (SAH):

According to the recommendations from the Neurocritical Care Society's multidisciplinary consensus published in 2011 [21], TCD is considered a good test bridging between physiological (cerebral microdialysis and brain tissue oxygenation) and radiological studies (CT angiogram). It has high specificity but moderate sensitivity. In general, daily monitoring for vasospasm and delayed cerebral ischemia clinically or by using TCD in patients with good-grade aneurysmal SAH is recommended and if suspicious, should be followed by confirmatory neuroimaging of the cerebral vessels and/or perfusion (Class I evidence, Strong recommendation).

Degree of vasospasm as determined by the MCA mean flow velocities and Lindegaard ratio:

- A MFV of <120 cm/s or MCA/ICA LR <3 indicates absent vasospasm.
- A MFV = 120–159 cm/s and LR of 3–6 are indicative of mild vasospasm.
- A MFV = 160–199 cm/s and LR of 3–6 are indicative of moderate vasospasm.
- MFV ≥200 cm/s and LR >6 are indicative of severe vasospasm.

Degree of vasospasm as determined by the basilar artery (BA) mean flow velocity and $BA/VA_{extracranial}$ (BA/ECVA) ratio:

- A MFV of <70 cm/s or BA/ECVA <2 indicates absent vasospasm
- A MFV of ≥70 cm/s and BA/ECVA of 2–2.49 are indicative of mild vasospasm
- A MFV of ≥85 cm/s and BA/ECVA of 2.5–2.99 are indicative of moderate vasospasm
- A MFV of ≥85 cm/s and BA/ECVA of ≥3 are indicative of severe vasospasm

Similarly, using the relative alpha variability on QEEG [17, 18] or using the intracortical EEG [22] individually or as part of a multimodal approach is of some value especially in high-grade patients like in SAH Hunt & Hess score of 3–5 and Fischer score

of ≥3 (Class III evidence, moderate [type C] recommendation). Three most reliable measures are usually followed:

- Alpha/Delta ratio (ADR): A decrement (focal, hemispheric, or diffuse) can predict delayed cerebral ischemia (DCI) as follows:
  - ADR decrease of 10% below baseline lasting 6 consecutive hours (100% sensitive and 76% specific).
  - ADR decrement of at least 50% below baseline lasting one or more hours (89% sensitive and 84% specific)
- Relative Alpha Variability (RAV): relies on qualitative visual inspection of the variability of the relative alpha power:
  - Poor RAV (Figs. 1 and 2)
  - Fair RAV (Fig. 3)

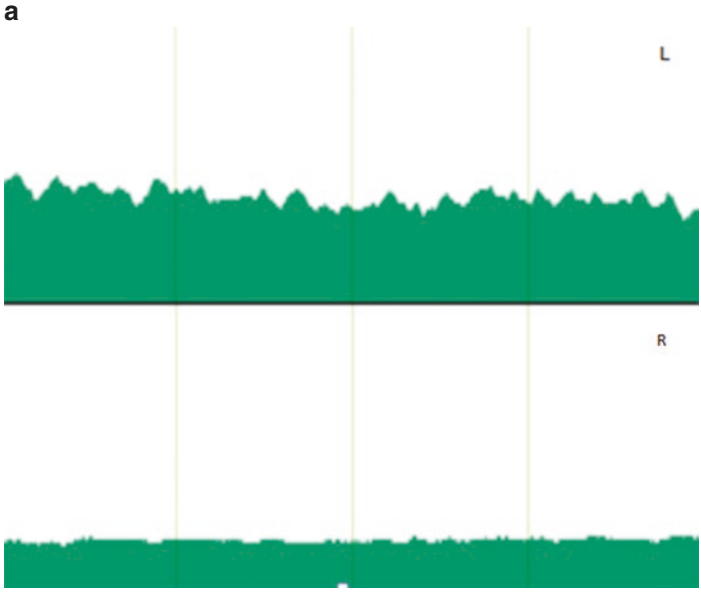

Fig. 1 (**a**) Example of a quantitative EEG showing a **good relative alpha variability (good-RAV)** – moderate amplitude peaks above the trough- on the left and **poor relative alpha variability (poor-RAV)** – No variability (peaks) above the trough on the right in a patient with aneurysmal (right MCA) SAH (Hunt Hess 2 Modified Fischer 3). (**b**) Correlating TCD of the middle cerebral artery (MCA) and basilar artery (BA) mean flow velocities at post-bleed day 7 showing severe vasospasm in the right MCA (MFV = 199 cm/s with Lindegaard ratio of 8.96). The left MCA and the basilar artery show normal velocities

b

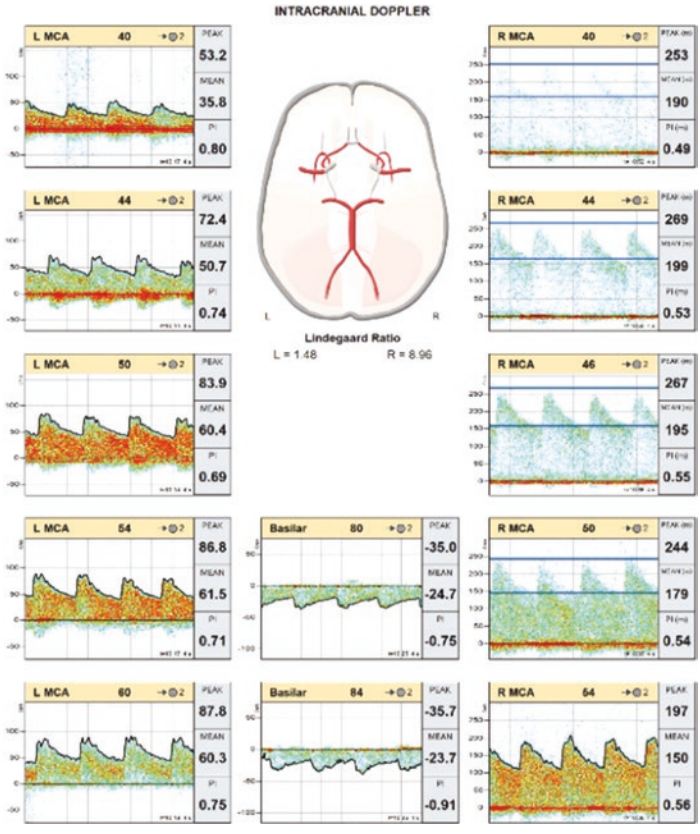

Fig. 1 (continued)

– Good RAV (Fig. 1)
– Excellent RAV (Figs. 3 and 4)

A persistent drop by one or more grades is considered alarming (Figs. 5 and 6). However, based on the author's experience, a drop from excellent to good falls within the normal variation and should be interpreted with caution. Also a persistent drop is defined as one degree drop for 6 consecutive hours or two degree drop for more than 1 h.

Fig. 2 Example of a quantitative EEG showing a **poor relative alpha variability (poor-RAV)** – minimal variability (peaks) above the trough that start to show some improvement at the end of recording. Of Note, this patient had aneurysmal subarachnoid hemorrhage post-bleed day 10 (Hunt Hess 2 Modified Fischer 4). Improvement was a response to a fluid bolus and increasing vasopressor requirement that helped raise the blood pressure. This is an example of real time management of vasospasm

- New or increasing periodic or rhythmic (epileptiform) discharges on the raw-EEG: These are lateralized periodic discharges (LPD), generalized periodic discharges (GPD), lateralized rhythmic delta activity (LRDA), or LRDA with bilateral asymmetry (LRDA-BA). Generalized rhythmic delta activity (GRDA) is usually less epileptogenic and unless associated with other epileptogenic modifiers should not be considered alarming.

These QEEG abnormalities could be focal, hemispheric, or diffuse. QEEG readers should be aware and look for confounders before rushing for a conclusion. Looking at the raw-EEG is important especially to rule out artifacts. In addition, making sure that the patient did not receive any sedation during this period of change is important. In addition, when the change is diffuse, it could be due to state change. In this situation, looking at the RAV is important.

An important study of patients with SAH compared TCD-PSV to EEG ADR, RAV, and new periodic and rhythmic discharges for the accuracy of detection of DCI. Worsening RAV had the highest odds

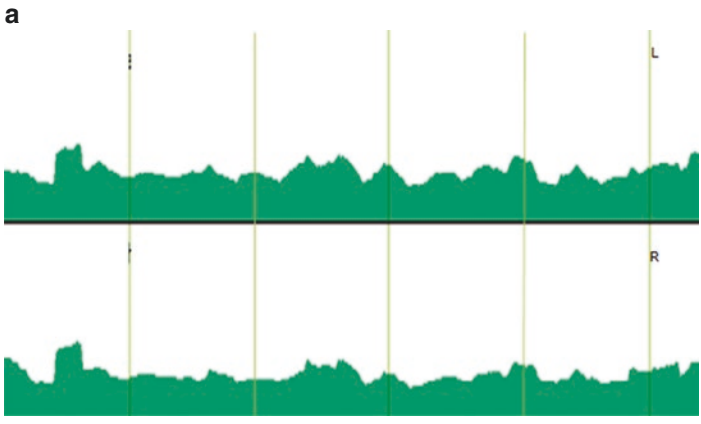

Fig. 3 (**a**) Example of a quantitative EEG showing an **excellent relative alpha variability (Excellent-RAV)** in a patient with aneurysmal subarachnoid hemorrhage (Hunt Hess 1 Modified Fischer 4) post-bleed day 5: Continuous variability (peaks of high amplitude above the trough). (**b**) Correlating TCD findings of the patient described above at post-bleed day 5 showing bilateral MCAs and basilar artery mean flow velocities below the threshold for vasospasm. Lindegaard ratio was <3 bilaterally. BA/ECVA ratio <2. (**c**) Example of a quantitative EEG showing a **fair relative alpha variability (fair-RAV)**: few low amplitude spikes (peaks) above the trough. This is the same patient described above at post-bleed day 10 (5 days later). It shows persistent two grade drop that correlated with a decline in the clinical examination and moderate to severe vasospasm on the conventional angiogram. (**d**) Correlating mean flow velocities of the bilateral MCAs and the BA showing mild to moderate diffuse vasospasm (MCA: mean flow velocities between 120 and 160 cm/s with Lindegaard ratio of 4.0 on the left and 3.7 on the right – BA: mean flow velocities ≥85 cm/s with BA/ECVA ratio of 2.85)

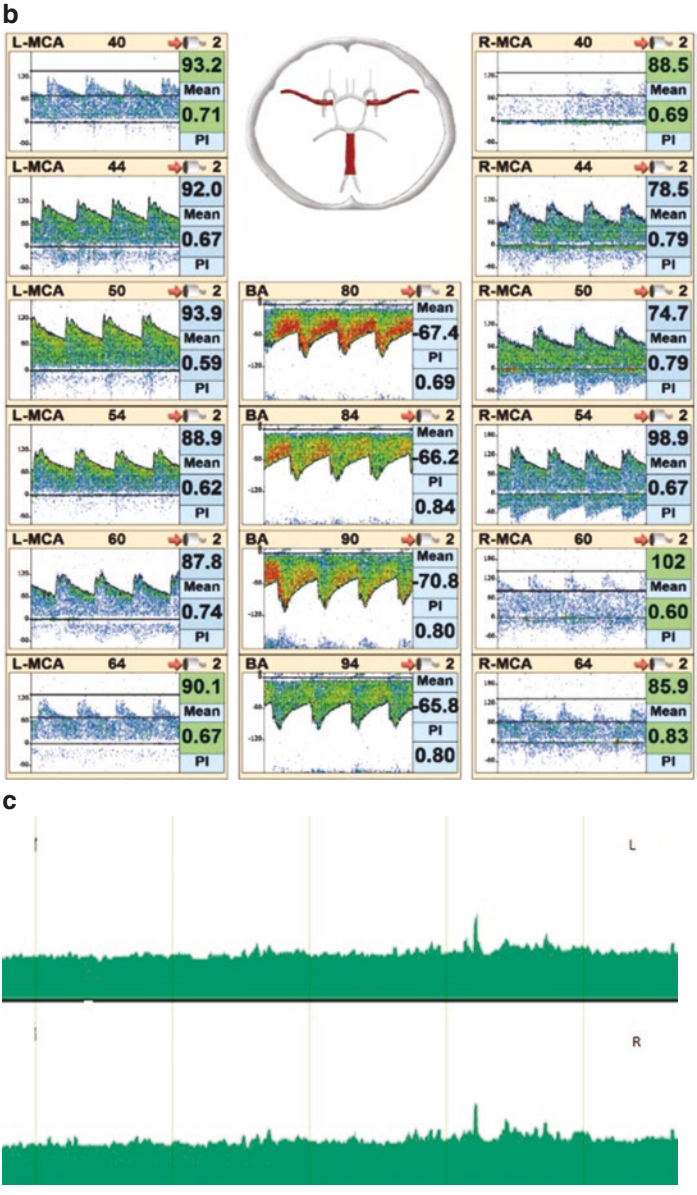

Fig. 3 (continued)

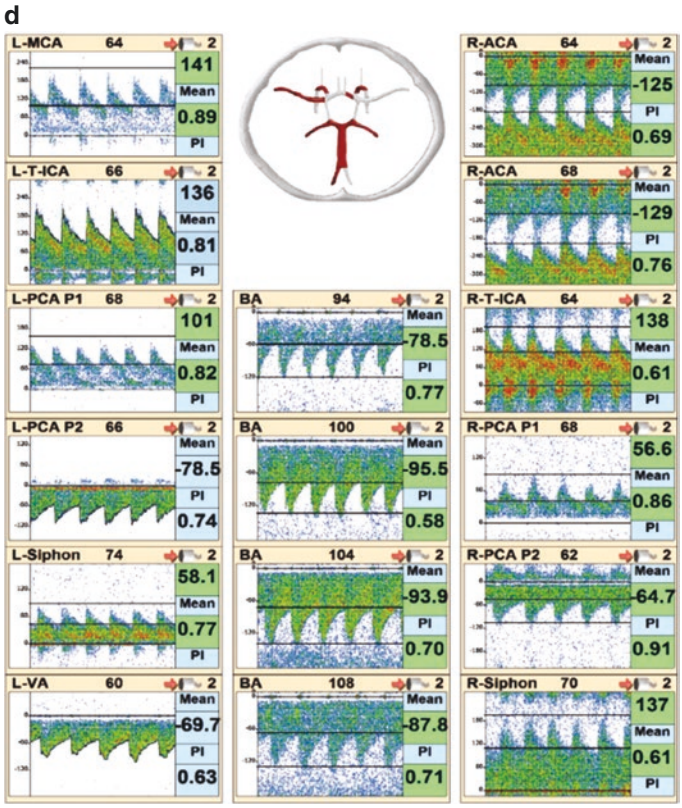

Fig. 3 (continued)

ratio followed by the appearance of new or increasing periodic or rhythmic discharges (Table 1) [23]. However, these have not made their way to the guidelines yet as larger prospective studies are needed.

In the author's opinion, whichever technique is available should be done along with frequent clinical exams and as needed radiological testing. However, if both techniques are available, TCD is more appropriate (once a day is sufficient if the clinical exam is reliable) for good-grade aneurysmal SAH and QEEG is more appropriate (runs continuously if clinical exam is unreliable) for poor-grade aneurysmal SAH [24].

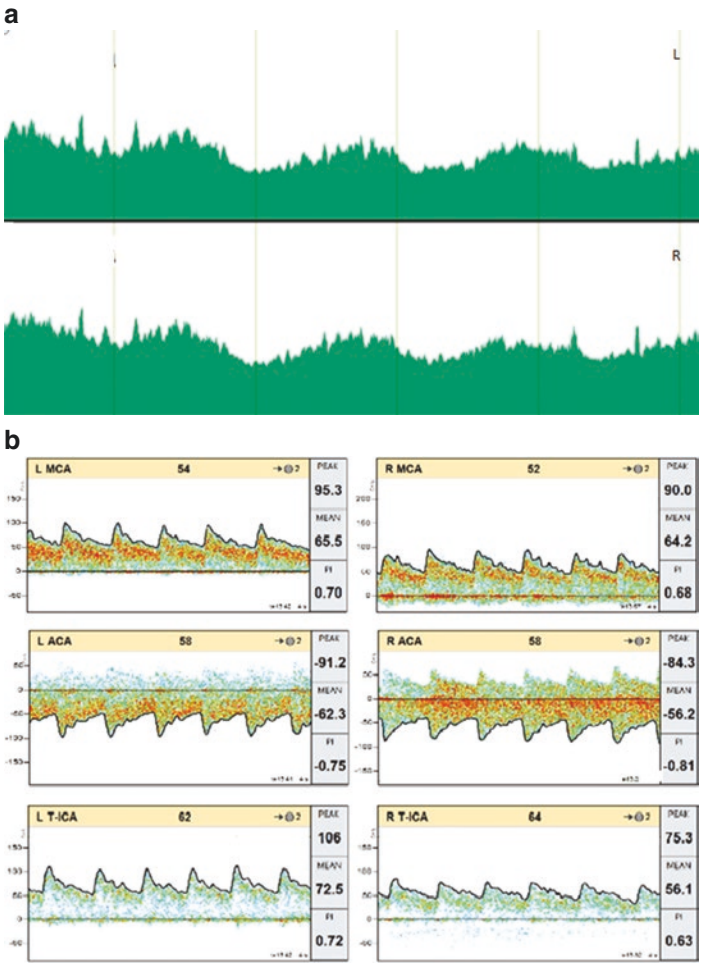

Fig. 4 (**a**) Example of a quantitative EEG showing an **excellent relative alpha variability (Excellent-RAV)** in a patient with aneurysmal subarachnoid hemorrhage (Hunt Hess 1 Modified Fischer 2): Continuous small spikes superimposed over larger peaks of high amplitude above the trough. (**b**) Correlating TCD mean flow velocities from the bilateral MCAs, ACAs, and terminal internal carotid arteries (T-ICA) of the same patient. Lindegaard ratio (LR) on the left is 1.46 and on the right is 1.19

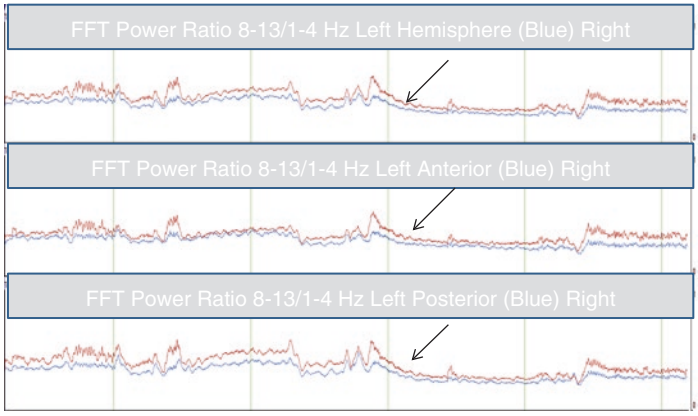

Fig. 5 A quantitative EEG showing an Alpha/Delta Ratio display in a patient with aneurysmal diffuse subarachnoid hemorrhage – It shows a sudden diffuse drop in the ratio (black arrows). Each segment (between green lines) represent one hour and twelve minutes

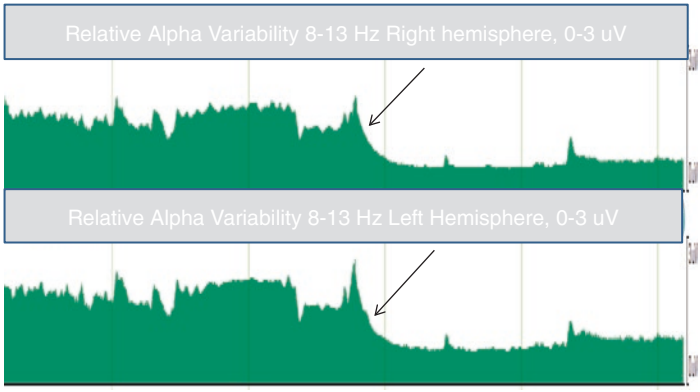

Fig. 6 A quantitative EEG showing a Relative alpha variability (RAV) display in the same patient described in Fig-5. It shows a sudden diffuse drop in the ratio (black arrows). Of note, the drop occurred several minutes before it happens with the ADR [69]. Each segment (between green lines) represent one hour and twelve minutes

Table 1 Comparison between accuracy of TCD and EEG parameters

	No DCI (n = 52)	DCI (n = 51)	OR	p-value
PSV >200 cm/s	45%	75%	3.65	<0.01
PSV > 250 cm/s	33%	58%	2.73	0.01
PSV >300 cm/s	20%	31%	1.8	0.14
Worsening ADR	10%	33%	4.47	<0.01
Worsening RAV	2%	42%	36.7	<0.01
New periodic or rhythmic discharges	8%	64%	20.4	<0.01

DCI delayed cerebral ischemia, *OR* odds ratio, *PSV* peak systolic velocity, *ADR* Alpha/Delta Ratio, *RAV* Relative Alpha Variability

2. Acute Intracerebral Hemorrhage (ICH):

TCD can detect some ICH as homogenous hyperechogenic foci that can be clearly distinguished from the surrounding brain tissue. Unlike acute ischemic strokes, it is not associated with absent or damping signal along a major intracerebral vessel. The detection of ICH using TCD is limited by the location of the ICH. It can detect 53% of the deep structure ICH and 33% of the cortico-subcortical lobar ICH. In addition, it is difficult to detect intraventricular hemorrhages (IVH) due to similar echogenicity with calcified choroid plexus and cerebellar tentorium. Furthermore, tumors, arteriovenous malformation, and cerebral microangiopathies can mimic ICH on TCD [25].

Elevated PI calculated from TCD flow velocities can predict elevation in the intracranial pressure (ICP) and midline shift. This is because high ICP lowers end-diastolic flow velocity. Specifically, elevated PI from the unaffected side has been considered an independent predictor of mortality in ICH (sensitivity 80%, specificity 94%). Additionally, if the MCA PI of the unaffected hemisphere ≥ 1.055, it might be associated with hematoma expansion. Those with radiologically proven hematoma expansion had MCA PI of the unaffected side increase by 48% from the baseline [26].

As for QEEG, it is not specific for the detection of ICH as a primary diagnostic tool. However, ADR was found to be an independent prognostic factor in ICH. In a study which combined PI/TCD & ADR/QEEG together, the accuracy of the combined technique increased the predictive prognostic value (i.e. prediction of mortality) than when each was done separately (area under curve AUC = 0.949 compared to 0.822 for PI/TCD alone and 0.860 for QEEG alone) [27].

3. Acute Ischemic Stroke (AIS):

Similar to ICH, Elevated PI/ TCD is indicative of increased ICP. Additionally, TCD can be used earlier to detect large vessel occlusion by detecting absent or diminished cerebral blood flow signals in a major intracerebral vessel. In middle cerebral artery occlusion, there is a hyperechogenic signal of the MCA with absent, minimal, damped, or blunted CBF throughout the artery with a diverted signal from the distal ICA, ACA, and PCA. Anterior and posterior cerebral artery LVO is defined by absent or minimal CBF. This should be associated with an asymmetry index ≥21%. This method has a sensitivity of 68–100% and a specificity of 78–99%. The utility of this method can be most useful in the prehospital setting where it can streamline patient care and allow direct transfer to a comprehensive stroke center with endovascular capabilities. However, such a protocol still needs to be further investigated. Of note, lacunar strokes or distal branch strokes are difficult to detect by TCD [25].

Furthermore, TCD can provide information about the status of the collateral circulation through the detection of flow reversal (good collaterals) or flow diversion (poor collaterals) [11].

TCD also can detect microemboli (microembolic signals MES) in different clinical scenarios like during CEA or carotid artery stenting (CAS), during cardiac surgery, symptomatic carotid stenosis, or cardioembolic strokes. MES is defined as unidirectional, >3 dB in intensity above background signal, <300 ms in duration, and accompanied by a characteristic pop sound. Large emboli are characterized by those of >12 dB in intensity above the back-

ground signal [28]. This technique is used by some to direct therapy for symptomatic carotid stenosis with dual antiplatelet drugs if MES are found versus monotherapy if MES are not found [29].

Additionally, paradoxical cerebral venous or fatty emboli with patent-foramen-ovale (PFO) can be diagnosed using TCD with a bubble (agitated saline) challenge. According to the number of emboli, the PFO can be classified as poor (<30 emboli) group or high (≥30 emboli) conductance shunt [30].

QEEG is not a specific marker for detecting acute ischemia. However, ADR & RAV within 72 h post-stroke were predictors of short and long term outcomes. Additionally, a research parameter called the brain symmetry index (BSI) which compares the spectral power of the two hemispheres and estimates the magnitude of the asymmetry, is found to be helpful in prognostication of acute ischemic stroke. It provides a scale from zero to one. Zero means perfect symmetry and one means maximum asymmetry. Unlike with ICH, The BSI in ischemic stroke was significantly increased and thus can differentiate between acute stroke and transient ischemic attack (TIA) [31, 32]. The inconsistent results between ICH and AIS in terms of BIS prediction of mortality is assumingly related to contralateral hemispheric swelling during ICH and not AIS making the asymmetry less evident in ICH [33]. Additionally, upon detection of diminished ADR and RAV on QEEG, it might be worth looking at the raw EEG for detection of RAWOD (Regional Attenuation Without Delta). The pattern and sequence of abnormality on raw EEG with acute ischemia is as follows:

- CBF 35–70 (ml/100 g/min) → Normal EEG → Intact neurons
- CBF 25–35 (ml/100 g/min) → Loss of fast beta activity (RAWOD) → Reversible neuronal injury
- CBF 18–25 (ml/100 g/min) → Background slowing 5–7 Hz → Potentially reversible neuronal injury
- CBF 12–18 (ml/100 g/min) → Background slowing 1–4 Hz → Potentially reversible neuronal injury
- CBF <8–10 (ml/100 g/min) → Suppression of all frequencies → Neuronal cell death [34]

RAWOD is a marker of early changes in acute ischemia. Practically, detecting RAWOD is most valuable during Carotid Endarterectomy after clamping. However, patients with high-risk of acute stroke-like in SAH, subdural hematoma (SDH) [35], or recent acute stroke might benefit from looking for RAWOD if continuous EEG is placed early enough or following TCD CBFV and PI. Also, the effect of blood pressure augmentation can be monitored with these parameters.

Additionally, there is growing interest for using both TCD and EEG in the post thrombectomy or post carotid stenting period to detect relative changes identifying reocclusion or hyperperfusion injuries. This might guide blood pressure management in the post thrombectomy period as well [36].

4. Carotid Endarterectomy (CEA):

Monitoring the cerebral blood flow and/or the cerebral activity during clamping of the carotid artery gives important guidance for the need for shunt placement during the procedure. Clinical change might not always be as early as these parameters. Clinical changes can actually happen in the postoperative period without any postoperative flow changes but rather after intraoperative alteration in these parameters. TCD blood flow changes (diminished or absent) are likely to be detected earlier than EEG changes. Furthermore, TCD can detect emboli after unclamping the carotid artery [37, 38].

EEG changes are similar to those discussed in AIS. Usually, raw-EEG is used rather than QEEG as immediate changes are looked for rather than changes over time. However, QEEG-BSI changes ≥ 0.6 during test clamping correlated with raw-EEG changes while BSI <0.3 had no associated raw-EEG changes [39].

5. Traumatic brain injury

There is a lot of enthusiasm regarding the role of TCD in intracranial monitoring after traumatic brain injuries. TCD is used to monitor various flow velocities, and measure LR for vasospasm

watch, PI for intracranial pressure (ICP) and cerebral perfusion pressure (CPP) monitoring, and vasomotor (VMR) for autoregulation monitoring. In a recent meta-analysis, patients with TBI who had abnormal TCD (MFV >120 cm/s or MFV <35 cm/s + PI >1.2 had a significant 3-fold increase in having poor outcome and a significant 9-fold increase in mortality [40]. In another study that tested early TCD-guided treatment to increase CPP and decrease cerebral edema for severe TBI where TCD studies were applied within 18 ± 11 min from admission, there was a reduction in the extent of hypoperfusion and secondary ischemic events [41].

The role of QEEG monitoring in severe TBI, aside of seizure detection, is still under investigation. Several parameters have been suggested for outcome prediction. These include declining variability of the faster frequencies (theta, alpha, and beta powers) as poor predictive parameters [42–44]. Additionally, a high bispectral index (BIS) was associated with good outcomes [45]. BIS simplifies EEG into a single number that is used to monitor the depth of anesthesia (2–4 pads applied to the forehead). When QEEG was combined with SSEP, it had better predictive values [46, 47].

As for mild traumatic brain injury, QEEG in the acute phase (up to first 2 weeks) showed a decrease in the alpha, theta, and delta powers with reduced ADR and alpha/theta ratio (ATR). In the subacute phase (weeks – 6 months), there was diffuse slowing, especially in the left temporal region. In the chronic phase, there was a persistent decrease in the alpha power and an increase in the delta power compared to controls [48].

6. Cardiac Surgery:

Brief cerebral hypoperfusion episodes are common during cardiac surgery. However, prolonged hypoperfusion episodes are concerning. Arterial blood pressure monitoring and cerebral oximetry might not provide an accurate measurement of cerebral hypoperfusion.

Interest in TCD for cerebral monitoring during cardiac surgeries is growing. TCD monitoring during cardiac surgeries is mainly focused on the MFV in the MCAs. During the pulsatile flow phase, a reduction of MFV by 60% from baseline or loss of diastolic flow is indicative of cerebral hypoperfusion. During the non-pulsatile phase, a reduction of the MFV by 80% is indicative of cerebral hypoperfusion. During the circulatory arrest phase, TCD can be used to monitor antegrade and retrograde flow in the MCA to evaluate selective cerebral perfusion. Additionally, TCD can monitor microemboli during surgery [49, 50].

On the other hand, EEG technology that is commonly used during cardiac surgeries is the BIS. Over-suppression, defined as BIS <40 for a prolonged time, correlates with prolonged recovery time, poor neurological outcome, and higher one-year mortality rate. In the deep hypothermic circulatory arrest phase, complete suppression is desired. In the rewarming phase, over-stimulation should be avoided [49, 51, 52].

7. Post-cardiac arrest:

In the first 24 h, TCD could identify patients who have progressed to irreversible neurological damage. In patients who remain comatose 2 h after return of spontaneous circulation (ROSC), persistent diffuse hypodynamic TCD patterns (Low MFV and high PI) or diffuse hyperdynamic TCD patterns (high MFV and low PI) are also associated with poor prognosis because of progression to intracranial hypertension and brain death. These could be of early prognostic value to avoid therapeutic futility.

The presence of a mix of hypodynamic, normal, and hyperdynamic TCD patterns may indicate the presence of hypoperfused regions in the brain. Thus, serial TCD examinations in comatose patients after ROSC can detect and guide treatment of early changes in cerebral hemodynamics which can decrease the likelihood of secondary neurological damage.

An advantage of TCD is that it can be performed irrespective of the effect of sedation, paralytics, and/or hypothermia [53].

On the other hand, raw-EEG has a great prognostic role in the post-cardiac arrest scenarios according to recent studies. Post-cardiac arrest patients are divided into: Predicted poor outcome and indeterminate outcome.

For the predicted poor outcome group, they should have any of the first-line criteria or at least two of the second-line criteria.

- First-line criteria: Bilateral absence of N20 wave on SSEP and/or absent both pupillary and corneal reflexes.
- Second-line criteria: Presence of at least two of the following:
  (a) Status myoclonicus ≤48 h after resuscitation.
  (b) Diffuse anoxic brain injury on CT and/or MRI.
  (c) Peak serum Neuron-specific-enolase (NSE) >75 μg/L.
  (d) Unreactive EEG with burst suppression and/or status epilepticus after rewarming.

For the indeterminate outcome group: EEG finding at Day 2 are divided into the following:

- Highly malignant (suppression, suppression with periodic discharges, burst suppression)
- Malignant (periodic or rhythmic patterns, pathological or non-reactive background)
- Benign (none of the malignant features)

If the EEG is not showing highly malignant patterns, then it has a sensitivity of 99.5%, a specificity of 8.5%, a positive predictive value (PPV) of 66.1%, and a negative predictive value (NPV) of 91% for predicting good neurological outcomes in 3 months. If combined with NSE <33 μg/L, then it has a sensitivity of 84.4%, a specificity of 46.6%, a PPV of 74%, and a NPV of 62.5% for predicting good neurological outcomes in 3 months.

If the EEG is showing a highly malignant pattern, then it has a sensitivity of 8.5%, a specificity of 99.5%, a PPV of 91%, a NPV of 66.1% for predicting poor neurological outcomes in 3 months. If combined with NSE >75 μg/L, then the specificity increases to 100% [54, 55].

8. Brain Death:

Both TCD and EEG are ancillary tests for brain death evaluation. Both are not needed if the clinical evaluation of brain death (full cranial nerve reflexes and apnea test) is successfully completed. However, if the clinical evaluation cannot be fully assessed or is inconclusive, an ancillary test should be performed. Several ancillary tests are available. According to several studies, the validity of these tests is as follows: TCD 57–92%, EEG ~94%, CTA ~94%, SSEP ~82%, and auditory evoked potentials (AEP) 2–32%. However, due to technical difficulties and artifacts, these tests are still not strongly reliable. Brain perfusion scintigraphy is currently considered the most sensitive and specific test and the most trusted by many physicians [56, 57].

TCD finding in brain-dead patients is the absence of a flow signal (cerebral circulatory arrest). Of note, a baseline TCD before perfusion cessation is vital for TCD interpretation. This is because the lack of an ultrasound window can lead to a false picture mimicking absent flow signals (false-positive; 10–20%). Additionally, TCD can provide false-negative results due to residual cerebral flow in patients with skull defects and CSF drainage. Furthermore, Other TCD findings like oscillation, reversed diastolic flow, or sharp peak waveforms were considered early signs of brain death and lack of response to treatment (Fig. 7). However, these conclusions were found to have exceptions [58].

On the other hand, EEG should be set on the double distance montage. It shows electrocerebral silence or inactivity (ECI) in case of brain death (no cerebral electrical activity >2μV without any variability or reaction to external stimuli). While a good quality 30 min EEG recording with ECI is sufficient, other protocols exist. These include two EEG recordings separated by a four-hour observation period especially if the quality of the EEG is not optimal [59].

Of note, all ancillary tests should be performed under all conditions mandatory for performance of the apnea test which include no sedation, no paralysis, SBP >90 mmHg (even with the aid of

a

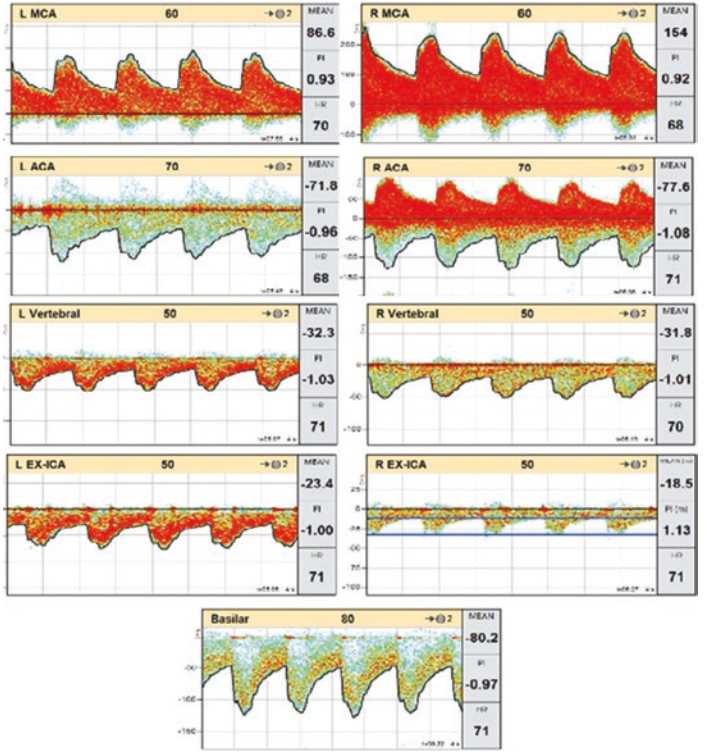

Fig. 7 (**a**) TCD findings of a 66-year-old female patient who presented with aneurysmal subarachnoid hemorrhage (Hunt Hess 4 Modified Fischer 4) – These velocities were obtained on post-bleed day six showing normal pulsatility index (<1). (**b**) On post-bleed day seven, her exam worsened and her head CT scan showed extensive cerebral edema with herniation. A repeat TCD exam showed evidence of brain death (oscillations and sharp peak waveforms). This was confirmed by a brain death exam

b

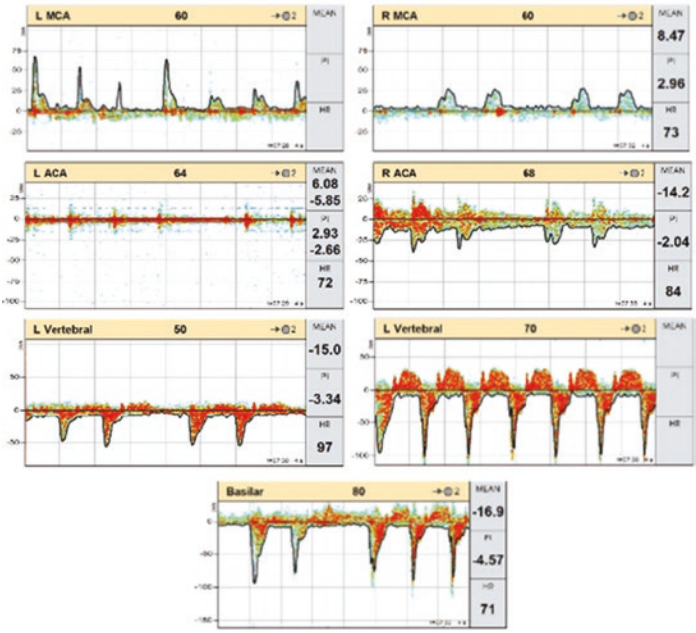

Fig. 7 (continued)

vasopressors), temp >36° Celsius, normocapnea, serum sodium <160 meq/L. If the patient is still under the effects of sedation or paralysis, TCD and CTA might have an advantage over EEG and SSEP.

9. Cerebral Venous Sinus Thrombosis (CVST)

TCD or Transcranial color-coded duplex sonography (TCCS) have a limited role in diagnosing CVST. Lack of the color signal on TCCS can point towards the diagnosis but cannot differentiate thrombotic occlusion from aplasia or hypoplasia. Incidental findings on TCD like a prominent venous signal (increased velocities of the cerebral veins) or significant side differences (>50%) can

also point towards the diagnosis and trigger further investigations like CT venogram [60]. This prominent signal is usually due to presence of collateral venous flow. Another finding that can hint towards the diagnosis of cerebral venous sinus thrombosis (CVST) is the presence of a retrograde flow in a vein like the basal vein which can indicate straight sinus thrombosis. Another maneuver that sonographers occasionally use for detection of abnormality in the transverse sinus is contralateral compression of the jugular vein (Fig. 8). This is expected to produce a decent increase in the flow velocity of the tested sinus. However, no or poor rise in the velocity (especially when compared to the other side) might suggest an abnormality in this sinus and warrant further investigations [61]. It is important to note that a normal exam does not rule out the diagnosis [62]. Table 2 provides a normal range of flow velocities in each cerebral sinus from different insonation windows. In severe cases where there are hemorrhagic sequelae and/or brain ischemia, measuring the PI may reflect an ICP elevation.

The role of EEG in CVST is limited except for the detection of early seizures. Early seizures were associated with worse early, but not late, outcomes [63]. This might guide physicians towards more aggressive treatment during the course of the disease.

10. Sickle cell Disease

TCD can be used as a good and effective screening test for the detection of brain ischemia in patients with sickle cell anemia. When correlated with MRI-FLAIR findings, Increased TCD-PSV in the middle cerebral artery had 73% sensitivity and 81% specificity. PSV ≥200–<250 cm/s or time average maximum mean velocity (TAMV or TAMM) ≥170–<200 cm/s is considered conditionally elevated and it requires increased surveillance (3–6 months) while PSV ≥250 cm/s or TAMV ≥200 cm/s is considered abnormal and high risk of cerebrovascular involvement [64, 65]. The Stroke Prevention Trial in Sickle Cell Anemia (STOP) concluded that in children with at least two

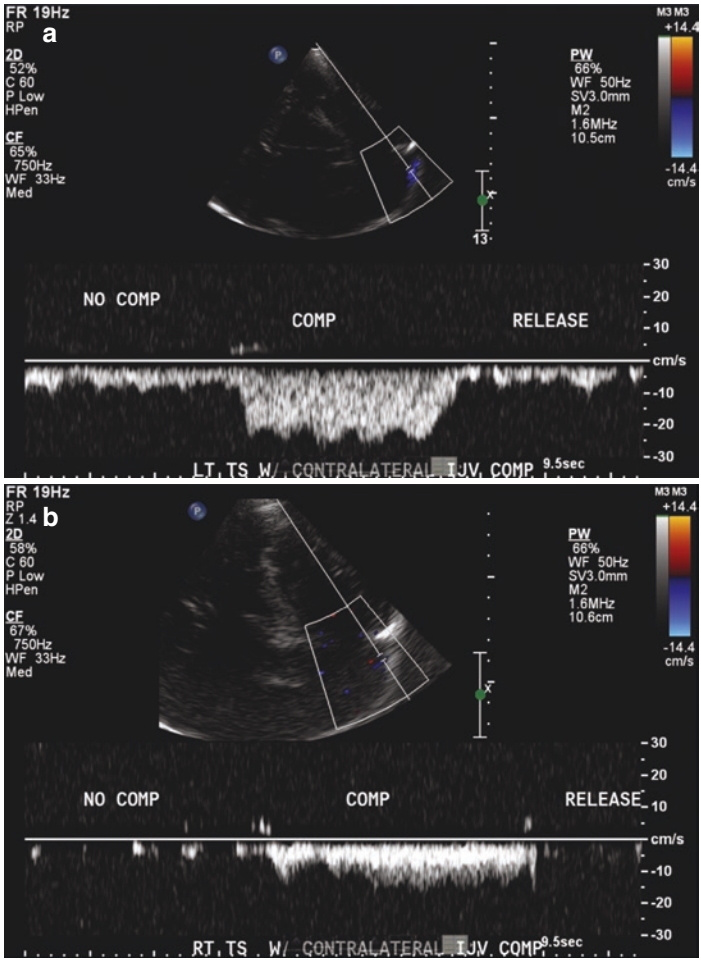

Fig. 8 (**a**) TCD of the left transverse sinus through a temporal bone window while applying compression on the right jugular vein – It shows significant increase in the blood flow velocity in the left transverse sinus. (**b**) TCD of the right transverse sinus through a temporal bone window while applying compression on the left jugular vein – It shows modest increase in the velocity in the right transverse sinus. While this can be due to partial occlusion (thrombosis), hypoplasia cannot be ruled out – Only neuroimaging (CT venogram) confirmed the diagnosis of partial right transverse sinus thrombosis

Table 2 Normal flow velocities of the cerebral veins and sinuses [61]

Cerebral Vein or Sinus	Flow Velocities[a]	Detection Rate
TCCS (temporal bone window) n[b] = 250		
dMCV	4–15/3–11	0.53–0.95
BV	7–20/5–15	0.85–1.0
GCV	6–32/4–25	0.84–0.94
SRS	6–39/4–27	0.23–0.82
TS	6–56/5–38	0.20–0.84
SSS	6–20/3–14	0.38–0.67
TCCS (temporal bone window) n = 43		
SPaS + SPS	27 ± 17	0.84
TCCS (occipital and frontal bone windows) n = 120, 75 respectively		
GCV	12–34/7–26	0.20–0.34
SRS	7–64/2–43	0.50–0.81
ICV	7–22/4–16	0.13–0.60
TCD (transforaminal bone window) n = 80		
IPS	20 ± 9	0.78

TCCS Transcranial Color-coded Duplex Sonography, *dMCV* deep Middle Cerebral Vein, *BV* Basal Vein, *GCV* Great Cerebral Vein of Galen, *SRS* Straight Sinus, *TS* Transverse Sinus, *SSS* Superior Sagittal Sinus, *SPaS* Sphenoparietal Sinus, *SPS* Superior Petrosal Sinus, *ICV* Internal Cerebral Veins, *IPS* Inferior Petrosal Sinus

[a]Flow velocities are demonstrated in range of systolic/diastolic values

[b]n number of tested individuals in each window

elevated TCD-PSV, receipt of chronic blood transfusions reduced the risk of stroke by 92% compared with standard care. Eleven percent of sickle cell children will have an ischemic stroke by the age of 20 years [65–67].

The role of EEG in sickle cell anemia is potentially promising in pain assessment and management. Few studies showed that there was increased theta power in areas related to pain processing. This can lead to using the EEG in grading pain objectively and not subjectively, which can help in pain management [68].

Conclusion

TCD and EEG are two contemporary technologies for intracranial monitoring that should be used in conjunction rather than competing with each other. Although both modalities occasionally have common indications, the increasing workload will force both into practice. An example of that is the use of TCD for vasospasm watch in post aneurysmal SAH cases presenting with good clinical exam while using EEG for the same indication when the exam is poor. Nonetheless, both modalities currently lack enough evidence to be utilized as the standard of care. Additionally, both modalities lack enough training and resources to be practiced in a wide-scale fashion although scientific societies and hospital administrations are starting to put more effort and resources into these two promising noninvasive technologies. Large randomized controlled studies are needed to activate these roles.

Quality of Level Rating

1. Class I: Evidence obtained from one or more well-designed prospective, controlled, blinded studies.
2. Class II: Evidence obtained from one or more well designed clinical studies.
3. Class III: Evidence obtained from expert opinion(s), case series, or case reports.

Strength of Recommendation Rating

1. Type A (strong): Based on class I or overwhelming class II evidence.
2. Type B (moderate): Based on class II evidence.
3. Type C (moderate): Based on a strong consensus of class III evidence.
4. Type D (weak): Based on inconclusive or conflicting class II or III evidence.
5. Type E (weak): Based on lack of efficacy evidence.

Acknowledgement The author would like to thank Jashua D Waks, BS, RVT for performing and providing the TCD studies and images provided in this chapter.

References

1. Sharma AK, Bathala L, Batra A, Mehndiratta MM, Sharma VK. Transcranial doppler: techniques and advanced applications: part 2. Ann Indian Acad Neurol. 2016;19(1):102–7.
2. Bellner J, Romner B, Reinstrup P, Kristiansson KA, Ryding E, Brandt L. Transcranial doppler sonography pulsatility index (PI) reflects intracranial pressure (ICP). Surg Neurol. 2004;62(1):45–51. discussion 51
3. Silvestrini M, Vernieri F, Pasqualetti P, Matteis M, Passarelli F, Troisi E, et al. Impaired cerebral vasoreactivity and risk of stroke in patients with asymptomatic carotid artery stenosis. JAMA. 2000;283:2122–7.
4. Edmonds HL Jr, Isley MR, Sloan TB, Alexandrov AV, Razumovsky AY. American Society of Neurophysiologic Monitoring and American Society of Neuroimaging joint guidelines for transcranial doppler ultrasonic monitoring. J Neuroimaging. 2011;21(2):177–83.
5. Bass A, Krupski WC, Schneider PA, Otis SM, Dilley RB, Bernstein EF. Intraoperative transcranial doppler: limitations of the method. J Vasc Surg. 1989;10(5):549–53.
6. Spencer MP, Thomas GI, Moehring MA. Relation between middle cerebral artery blood flow velocity and stump pressure during carotid endarterectomy. Stroke. 1992;23:1439–45.
7. Kneihsl M, Niederkorn K, Deutschmann H, Enzinger C, Poltrum B, Horner S, et al. Abnormal blood flow on transcranial duplex sonography predicts poor outcome after stroke thrombectomy. Stroke. 2018;49(11):2780–2.
8. Schneweis S, Urbach H, Solymosi L, Ries F. Preoperative risk assessment for carotid occlusion by transcranial doppler ultrasound. J Neurol Neurosurg Psychiatry. 1997;62(5):485–9.
9. Edmonds HL Jr. Advances in neuromonitoring for cardiothoracic and vascular surgery. J Cardiothorac Vasc Anesth. 2001;15(2):241–50.
10. Edmonds HL Jr. Protective effect of neuromonitoring during cardiac surgery. Ann N Y Acad Sci. 2005;1053:12–9.
11. Martínez-Sánchez P, Tsivgoulis G, Lao A, Sharma V, Alexandrov AV. Ultrasound in acute ischemic stroke. Neurologia. 2009;24(1):59–68.
12. Park JH, Song J, Shin J, Jang HS, Seo WK. Teaching neuroimages: vertebral artery compression by head tilt around the roll axis diagnosed by transcranial doppler. Neurology. 2018;91(17):e1657–8.
13. Zachrisson H, Fouladiun M, Blomstrand C, Holm J, Volkmann R. Functional assessment of high-grade ICA stenosis with duplex ultra-

sound and transcranial doppler. Clin Physiol Funct Imaging. 2012;32(3):241–6.
14. Hassler W, Steinmetz H, Gawlowski J. Transcranial doppler ultrasonography in raised intracranial pressure and in intracranial circulatory arrest. J Neurosurg. 1988;68(5):745–51.
15. Babikian VL, Wijman CA. Brain embolism monitoring with transcranial doppler ultrasound. Curr Treat Options Cardiovasc Med. 2003;5(3):221–32.
16. Vespa PM, Nuwer MR, Juhasz C, et al. Early detection of vasospasm after acute subarachnoid hemorrhage using continuous EEG ICU monitoring. Electroencephalogr Clin Neurophysiol. 1997;103:607–15.
17. Claassen J, Hirsch LJ, Kreiter KT, et al. Quantitative continuous EEG for detecting delayed cerebral ischemia in patients with poor-grade subarachnoid hemorrhage. Clin Neurophysiol. 2004b;115:2699–710.
18. Muniz CF, Shenoy AV, O'Connor KL, Bechek SC, Boyle EJ, Guanci MM, et al. Clinical development and implementation of an institutional guideline for prospective EEG monitoring and reporting of delayed cerebral ischemia. J Clin Neurophysiol. 2016;33(3):217–26.
19. Nuwer M. Assessment of digital EEG, quantitative EEG, and EEG brain mapping: report of the American Academy of Neurology and the American Clinical Neurophysiology Society. Neurology. 1997;49(1):277–92.
20. Herman S, Abend NS, Bleck TP, Chapman KE, Drislane FW, Emerson RG, et al. Consensus statement on continuous EEG in critically ill adults and children, part I: indications. J Clin Neurophysiol. 2015 Apr;32(2):87–95.
21. Diringer MN, Bleck TP, Claude Hemphill J, Menon D, Shutter L, Vespa P, et al. Critical care management of patients following aneurysmal subarachnoid hemorrhage: recommendations from the Neurocritical Care Society's Multidisciplinary Consensus Conference. Neurocrit Care. 2011 Sep;15(2):211–40.
22. Stuart RM, Waziri A, Weintraub D, Schmidt MJ, Fernandez L, Helbok R, et al. Intracortical EEG for the detection of vasospasm in patients with poor-grade subarachnoid hemorrhage. Neurocrit Care. 2010 Dec;13(3):355–8.
23. Rosenthal ES, Biswal S, Zafar SF, O'Connor KL, Bechek S, Shenoy AV, et al. Continuous electroencephalography predicts delayed cerebral ischemia after subarachnoid hemorrhage: a prospective study of diagnostic accuracy. Ann Neurol. 2018 May;83(5):958–69.
24. Hong JH, Bang JS, Chung JH, Han MK. Protocol based real-time continuous electroencephalography for detecting vasospasm in subarachnoid hemorrhage. J Korean Neurosurg Soc. 2016 Mar;59(2):154–7.
25. Antipova D, Eadie L, Macaden AS, Wilson P. Diagnostic value of transcranial ultrasonography for selecting subjects with large vessel occlusion: a systematic review. Ultrasound J. 2019;11(1):29.

26. Kesav P, Khurana D, Prabhakar SK, Ahuja CK, Khandelwal N. Transcranial doppler and hematoma expansion in acute spontaneous primary intracerebral hemorrhage. Ann Indian Acad Neurol. 2019;22(2):195–8.
27. Chen Y, Xu W, Wang L, Yin X, Cao J, Deng F, et al. Transcranial doppler combined with quantitative EEG brain function monitoring and outcome prediction in patients with severe acute intracerebral hemorrhage. Crit Care. 2018;22(1):36.
28. Consensus Committee of the Ninth International Cerebral Hemodynamic Symposium. Basic identification criteria of doppler microembolic signals. Stroke. 1995;26(6):1123.
29. Markus HS, Droste DW, Kaps M, Larrue V, Lees KR, Siebler M, et al. Dual antiplatelet therapy with clopidogrel and aspirin in symptomatic carotid stenosis evaluated using doppler embolic signal detection: the Clopidogrel and Aspirin for Reduction of Emboli in Symptomatic Carotid Stenosis (CARESS) trial. Circulation. 2005;111(17):2233–40.
30. Spencer MP, Moehring MA, Jesurum J, Gray WA, Olsen JV, Reisman M. Power m-mode transcranial doppler for diagnosis of patent foramen ovale and assessing transcatheter closure. J Neuroimaging. 2004 Oct;14(4):342–9.
31. Cuspineda E, Machado C, Galán L, Aubert E, Alvarez MA, Llopis F, et al. QEEG prognostic value in acute stroke. Clin EEG Neurosci. 2007 Jul;38(3):155–60.
32. Sheorajpanday RV, Nagels G, Weeren AJ, van Putten MJ, De Deyn PP. Reproducibility and clinical relevance of quantitative EEG parameters in cerebral ischemia: a basic approach. Clin Neurophysiol. 2009;120(5):845–55.
33. Zazulia AR, Videen TO, Diringer MN, Powers WJ. Poor correlation between perihematomal MRI hyperintensity and brain swelling after intracerebral hemorrhage. Neurocrit Care. 2011 Dec;15(3):436–41.
34. Schneider AL, Jordan KG. Regional attenuation without delta (RAWOD): a distinctive EEG pattern that can aid in the diagnosis and management of severe acute ischemic stroke. Am J Electroneurodiagnostic Technol. 2005 Jun;45(2):102–17.
35. Alkhachroum AM, Fernandez-Baca Vaca G, Sundararajan S, DeGeorgia M. Post-subdural hematoma transient ischemic attacks: hypoperfusion mechanism supported by quantitative electroencephalography and transcranial doppler sonography. Stroke. 2017 Mar;48(3):e87–90.
36. Schleiger E, Wong A, Read S, Coulthard A, Finnigan S. Improved cerebral pathophysiology immediately following thrombectomy in acute ischaemic stroke: monitoring via quantitative EEG. Clin Neurophysiol. 2016 Aug;127(8):2832–3.
37. Jansen C, Moll FL, Vermeulen FE, van Haelst JM, Ackerstaff RG. Continuous transcranial doppler ultrasonography and electroencephalography during carotid endarterectomy: a multimodal monitoring sys-

tem to detect intraoperative ischemia. Ann Vasc Surg. 1993 Jan;7(1):95–101.
38. Costin M, Rampersad A, Solomon RA, Connolly ES, Heyer EJ. Cerebral injury predicted by transcranial doppler ultrasonography but not electroencephalography during carotid endarterectomy. J Neurosurg Anesthesiol. 2002 Oct;14(4):287–92.
39. van Putten MJ, Peters JM, Mulder SM, de Haas JA, Bruijninckx CM, Tavy DL. A brain symmetry index (BSI) for online EEG monitoring in carotid endarterectomy. Clin Neurophysiol. 2004 May;115(5):1189–94.
40. Fatima N, Shuaib A, Chughtai TS, Ayyad A, Saqqur M. The role of transcranial doppler in traumatic brain injury: a systemic review and meta-analysis. Asian. J Neurosurg. 2019 Jul-Sep;14(3):626–33.
41. Ract C, Le Moigno S, Bruder N, Vigué B. Transcranial doppler ultrasound goal-directed therapy for the early management of severe traumatic brain injury. Intensive Care Med. 2007 Apr;33(4):645–51.
42. Tolonen A, Särkelä MOK, Takala RSK, Katila A, Frantzén J, Posti JP. Quantitative EEG parameters for prediction of outcome in severe traumatic brain injury: development study. Clin EEG Neurosci. 2018 Jul;49(4):248–57.
43. Vespa PM, Boscardin WJ, Hovda DA, McArthur DL, Nuwer MR, Martin NA, et al. Early and persistent impaired percent alpha variability on continuous electroencephalography monitoring as predictive of poor outcome after traumatic brain injury. J Neurosurg. 2002 Jul;97(1):84–92.
44. Moulton RJ, Marmarou A, Ronen J, Ward JD, Choi S, Lutz HA, et al. Spectral analysis of the EEG in craniocerebral trauma. Can J Neurol Sci. 1988 Feb;15(1):82–6.
45. Dunham CM, Ransom KJ, McAuley CE, Gruber BS, Mangalat D, Flowers LL. Severe brain injury ICU outcomes are associated with cranial-arterial pressure index and noninvasive bispectral index and transcranial oxygen saturation: a prospective, preliminary study. Crit Care. 2006;10(6):R159.
46. Carter BG, Butt W. Are somatosensory evoked potentials the best predictor of outcome after severe brain injury? A systematic review. Intensive Care Med. 2005 Jun;31(6):765–75.
47. Carter BG, Butt W. Review of the use of somatosensory evoked potentials in the prediction of outcome after severe brain injury. Crit Care Med. 2001 Jan;29(1):178–86.
48. Haneef Z, Levin HS, Frost JD Jr, Mizrahi EM. Electroencephalography and quantitative electroencephalography in mild traumatic brain injury. J Neurotrauma. 2013;30(8):653–6.
49. Grocott HP. Monitoring the brain in cardiac surgery–an evolving area for research. Anaesthesia. 2012 Mar;67(3):216–9.
50. Doblar DD. Intraoperative transcranial ultrasonic monitoring for cardiac and vascular surgery. Semin Cardiothorac Vasc Anesth. 2004 Jun;8(2):127–45.

51. Willingham M, Ben Abdallah A, Gradwohl S, Helsten D, Lin N, Villafranca A, et al. Association between intraoperative electroencephalographic suppression and postoperative mortality. Br J Anaesth. 2014 Dec;113(6):1001–8.
52. Oliveira CR, Bernardo WM, Nunes VM. Benefit of general anesthesia monitored by bispectral index compared with monitoring guided only by clinical parameters. Systematic review and meta-analysis. Braz J Anesthesiol. 2017;67(1):72–84.
53. Álvarez-Fernández JA. Transcranial doppler ultrasound use in post-cardiac arrest coma. Rev Neurol. 2011;53(9):545–54.
54. Westhall E, Rossetti AO, van Rootselaar AF, Wesenberg Kjaer T, Horn J, Ullén S, et al. Standardized EEG interpretation accurately predicts prognosis after cardiac arrest. Neurology. 2016;86(16):1482–90.
55. Bongiovanni F, Romagnosi F, Barbella G, Di Rocco A, Rossetti AO, Taccone FS, et al. Standardized EEG analysis to reduce the uncertainty of outcome prognostication after cardiac arrest. Intensive Care Med. 2020;46(5):963–72.
56. Welschehold S, Boor S, Reuland K, Thömke F, Kerz T, Reuland A, et al. Technical aids in the diagnosis of brain death: a comparison of SEP, AEP, EEG, TCD and CT angiography. Dtsch Arztebl Int. 2012 Sep;109(39):624–30.
57. Robbins NM, Bernat JL. Practice current: when do you order ancillary tests to determine brain death? Neurol Clin Pract. 2018 Jun;8(3):266–74.
58. Li Y, Liu S, Xun F, Liu Z, Huang X. Use of transcranial doppler ultrasound for diagnosis of brain death in patients with severe cerebral injury. Med Sci Monit. 2016 Jun;6(22):1910–5.
59. Szurhaj W, Lamblin MD, Kaminska A, Sediri H. Société de Neurophysiologie Clinique de Langue Française. EEG guidelines in the diagnosis of brain death. Neurophysiol Clin. 2015 Mar;45(1):97–104.
60. Wardlaw JM, Vaughan GT, Steers AJ, Sellar RJ. Transcranial doppler ultrasound findings in cerebral venous sinus thrombosis. Case report. J Neurosurg. 1994 Feb;80(2):332–5.
61. Caso V, Agnelli G, Paciaroni M, editors. Handbook on cerebral venous thrombosis. Frontiers of neurology and neuroscience. S. Karger AG; 2007.
62. Canhão P, Batista P, Ferro JM. Venous transcranial doppler in acute dural sinus thrombosis. J Neurol. 1998;245(5):276–9.
63. Uluduz D, Midi I, Duman T, Yayla V, Karahan AY, Afsar N, et al. Epileptic seizures in cerebral venous sinus thrombosis: subgroup analysis of VENOST study. Seizure. 2020;3(78):113–7.
64. Jones A, Granger S, Brambilla D, Gallagher D, Vichinsky E, Woods G, et al. Can peak systolic velocities be used for prediction of stroke in sickle cell anemia? Pediatr Radiol. 2005;35:66–72.
65. Naffaa LN, Tandon YK, Irani N. Transcranial doppler screening in sickle cell disease: the implications of using peak systolic criteria. World J Radiol. 2015;7(2):52–6.

66. Adams RJ, McKie VC, Hsu L, Files B, Vichinsky E, Pegelow C, et al. Prevention of a first stroke by transfusions in children with sickle cell anemia and abnormal results on transcranial doppler ultrasonography. N Engl J Med. 1998;339(1):5–11.
67. Nichols FT, Jones AM, Adams RJ. Stroke prevention in sickle cell disease (STOP) study guidelines for transcranial doppler testing. J Neuroimaging. 2001;11(4):354–62.
68. Case M, Shirinpour S, Zhang H, Datta YH, Nelson SC, Sadak KT, et al. Increased theta band EEG power in sickle cell disease patients. J Pain Res. 2018;11:67–76.
69. Hussein O. Relative alpha variability changes precede alpha-delta ratio changes in cerebral ischemia. J Stroke Cerebrovasc Dis. 2020;29(11):105262. https://doi.org/10.1016/j.jstrokecerebrovasdis.2020.105262. PMID: 33066936.

Moyamoya Disease

Deepak Gulati

Moyamoya disease (MMD) is characterized by chronic progressive steno-occlusion at the terminal portion of the internal carotid artery, proximal portion of the anterior cerebral artery, and the middle cerebral artery (MCA) with concomitant abnormal collateral networks. The insidious development of a network of compensatory enlarged collateral vessels at the base of the brain appear as a puff of smoke ('moyamoya') on angiography. It is called moyamoya syndrome when a moyamoya-like pattern of obstruction and collateral formation develops in the setting of another condition (eg. atherosclerosis) [1]. In 1969, Suzuki and Takaku named this novel disorder "moyamoya disease", because "moyamoya" means "puff of smoke" in Japanese [2].

Epidemiology

Moyamoya is a rare disease. It is discovered throughout the world, especially in East Asian countries such as Japan, Korea and China. Moyamoya arteriopathy is ten times higher in Asian countries and

D. Gulati (✉)
The Ohio State University Wexner Medical Center, Columbus, OH, USA
e-mail: Deepak.gulati@osumc.edu

W. C. Ziai, C. L. Cornwell (eds.), *Neurovascular Sonography*,
https://doi.org/10.1007/978-3-030-96893-9_23

more common in females. It has a bimodal age of distribution, 5–10 years and 40–50 years. The familial forms account for 15% of patients with this disease [3].

Moyamoya is the most common pediatric cerebrovascular disease in Japan, with a prevalence of 3 cases per 100,000 children. The incidence among all patients with moymoya in Europe appears to be about 1/10th of that observed in Japan. Results from a 2005 American review suggest an incidence of 0.086 case per 100,000 persons [4].

Etiology

Two plausible mechanisms underlying MMD with ischemic stroke – (1) hemodynamic compromise, and (2) artery-to-artery embolism, have been suggested. Both mechanisms have been assumed to coexist and thus, are complementary in MMD with ischemic stroke.

The exact pathogenesis of moyamoya disease is unknown, partly due to the lack of animal models. The stenotic vessels show eccentric fibro-cellular thickening of the intima from abnormal proliferation of smooth-muscle cells, thinned media, tortuous or duplicated internal elastic lamina and absence of atheromatous involvement. The majority of dilated vessels are fibrotic, have thinned media, and often segmentation of the elastic lamina and microaneurysms.

There is increased prevalence of autoimmune disease in patients with moyamoya disease. There might be a genetic predisposition for moyomoya as suggested by strong regional differences (high occurrence in Asia), higher incidence in females in familial cases and lower age of onset (11.8 years as compared to 30.8 years). There is noted to be an association with some heritable disorders (Down syndrome, Neurofibromatosis 1, sickle disease).

Genetic factors are most likely involved but the causative genes have still to be identified (mostly in Western countries). A recent study has identified RNF213 as the first gene associated with moyamoya [5]. The proportion of patients who have affected first-

degree relatives is reported to be 10% in Japan, while one US study found a rate of 6% [6].

Clinical Features

Hypoperfusion has been considered as a cause of transient ischemic attack or ischemic stroke in MMD. However, increasing evidence supports the notion that artery-to-artery embolism may also contribute to ischemic events.

The clinical picture of moyamoya disease is complex. Patients develop different symptoms in relation to age and geographical distribution.

Symptoms are due to the following –

1. Steno-occlusive disease: manifesting as TIA/stroke in carotid artery territory, seizures or cognitive disorders
2. Compensatory mechanisms and development of collateral vessel network: Intracranial hemorrhage/subarachnoid hemorrhage or headache.

Children present mainly with ischemic events while adults present with ischemic or hemorrhagic stroke. TIA is more frequent in children. There is a lower rate of hemorrhages in Western countries. Bleeding typically occurs in the frontal horn of the lateral ventricle, basal ganglia, and thalamus, leading to severe headache, vomiting and focal neurological deficit. The rate of hemorrhage among adults is approximately seven times as high as the rate among children in the United States [7].

Atypical presentations include headache, seizures, cognitive impairment, and dementia, but MMD can also be asymptomatic.

It has been reported that the annual risk of ischemic stroke can be 1.4% even in the hemodynamically stable patients presenting with hemorrhagic strokes [8]. The annual risk of developing ischemic stroke in incidental MMD patients has been reported to be 0.8% in the literature [8, 9].

Headache (from dilated transdural collaterals) is one of the serious symptoms associated with moyamoya disease, particu-

larly in pediatric patients. Typically, headache is migraine-like in quality and refractory to medical therapies; it persists in up to 63% of patients, even after successful surgical revascularization. In addition, epilepsy and involuntary movements are important clinical presentations in moyamoya disease: involuntary movements are mostly seen in pediatric patients.

The natural history of moyamoya disease is not fully understood because there have been only a few studies on the progression of the disease.

Differential Diagnosis

Because MMD is a rare cause of complicated headache syndrome with a variable symptomatology, moyamoya can masquerade as migraine. Other differentials include intracranial atherosclerosis, radiation vasculopathy, CNS vasculitis and sickle cell disease

Role of Transcranial Doppler

Although digital subtraction angiography (DSA) has been regarded as the diagnostic gold standard, the potential complications often limit its usefulness. Transcranial Doppler sonography (TCD) is a noninvasive, reliable method to evaluate intracranial stenosis or occlusion. TCD is easier to perform and less expensive.

Transcranial Doppler sonography criteria for the diagnosis of intracranial stenosis include circumscribed flow velocity increase, distal signal damping, and side-to-side differences in velocity. Mild (<50%) stenoses are not reliably detected by these criteria [10].

In MMD, stenosis usually starts at the terminal internal carotid and proximal portions of the ACAs and MCAs. The collateral channels including moyamoya vessels develop as the stenosis progresses and subsequently fade away as the occlusive changes become more severe. The morbidity of MMD is directly related to the changes of cerebral blood flow, and it is therefore important to detect the vascular status in clinical practice.

Increasing evidence supports the notion that artery-to-artery embolism may also contribute to ischemic events [11, 12]. As a potential indicator of artery-to-artery embolism, microembolic signals (MES), also known as high-intensity transient signals detected by transcranial Doppler (TCD), are thought to represent solid emboli (HITS) composed of thrombi and platelet aggregates [13]. The clinical role of MES in MMD has yet to be identified.

Rating the angiographic findings according to the Suzuki and Takaku criteria [2], which classify the angiographic stage of MMD as narrowing of carotid fork (stage I); initiation of MMD (dilated major cerebral artery and a slight moyamoya vessel network, stage II); intensification of MMD (disappearance of the middle and anterior cerebral artery, and thick and distinct moyamoya vessels, stage III); minimization of moyamoya (disappearance of posterior cerebral artery and narrowing of individual moyamoya vessels, stage IV); reduction of the moyamoya (disappearance of all main cerebral arteries from the internal carotid artery system, further minimization of the moyamoya vessels and an increase in the collateral pathways from the external carotid artery system, stage V); and disappearance of the moyamoya (disappearance of the moyamoya vessels, with cerebral blood flow derived only from external carotid artery and vertebrobasilar artery system, stage VI) [14].

Early stage MMD (eg. Suzuki stage I and II) are more likely to have high MFVs. Symmetric high MFVs and low PI on TCD without color Doppler image are characteristic features of MMD. However, these features are not specific to MMD and are observed in other conditions such as migraine, anemia and diffuse hyperperfusion.

Internal Carotid Artery

Velocities in terminal ICA are higher in early stages while very low-flow velocity values were still detected even though both supraclinoid ICAs were hardly opacified on angiograms in later stages. This discrepancy might have been caused by the very prolonged regional circulation time in moyamoya vessels; the con-

trast medium did not reach the "stenotic but patent" vessels on time. Angiography is not necessarily accurate, since the opacification of a particular vessel and its direction of flow depend on the pressure of contrast injection.

Middle Cerebral Artery

Normally, the MCA has the highest flow velocity among the basal cerebral arteries. Mild to moderate stenosis increases flow velocity, and this increase is inversely correlated to the residual lumen's diameter. Decreased flow velocity occurs distal to the stenotic segment when the stenosis exceeds 60%–80%.

With progressive stenotic lesions of ICA, the mean flow velocities of the MCAs are found to be lower than those of the ipsilateral ICAs. The presence of stenotic lesions proximal to the insonated vessels, that is, arterial segment proximal to the supraclinoid ICA, leads to low flow velocity of the distal ICAs and the MCAs, only if the stenosis was very severe.

MFV was higher and PI was lower in moderate stenosis (>50% stenosis with intact distal segment), and MFV was lower and PI was higher in severe steno-occlusion (severe stenosis with no apparent distal segment) compared with normal or mild stenosis (<50% stenosis). These results suggest that MFV might increase and PI decrease with progression from normal to stenosis, while MFV might decrease and PI increase with progression from stenosis to occlusion.

There are few reports related to TCD diagnosis of MMD, and the results are complex and variable. Flow velocities of proximal or distal MCA were reduced or increased with dampened waveforms, reversed flow, or musical murmurs [15]. One study comparing TCD and DSA showed low flow velocity in stenosis and very low flow velocity in occlusion. Takase et al. classified TCD findings of MMD as a high-high pattern, high-low pattern, or low-low pattern, which was correlated with the age of patients and the severity of disease [16]. These variable results seem to be inevitable because the number of cases was small and the cases were mixed with variable stages of the disease.

Posterior Cerebral Artery

Significantly higher flow velocity of the PCAs in children are found as compared to that of adults, demonstrating the more important role performed by the PCAs as collateral circulation to the ischemic brain in children than in adult cases. The higher incidence of aneurysm in the vertebrobasilar system, especially at basilar bifurcation in Moyamoya patients may be explained by the presence of hemodynamic stress caused by the very high flow velocity at the bilateral PCAs.

When a vessel narrows, regardless of the cause, the velocity of the blood flow increases to allow the same volume of blood to pass the narrowed lumen. This "law of continuity" is the basis for the compensatory flow velocity increase found in vascular spasm after aneurysmal subarachnoid hemorrhage. Velocity also increases when there is augmentation due to collateral contribution to other vessels' territories. This latter reason applies for the abnormally high flow velocity of the PCAs in children, and of the ophthalmic arteries in adult Moyamoya cases, since no stenotic lesion was observed in those insonated arterial segments.

MMD may be suspected in young adults whose TCD findings show symmetrical high MFV and low PI in basal arteries. Careful interpretation with clinical correlation is required. In general, high MFV (MCA > 85 cm/s, ACA > 80 cm/s, PCA > 60 cm/s) and low PI (<0.60) suggested moderate stenosis, while low MFV (MCA < 50 cm/s) suggested severe steno-occlusion.

Microembolic Signals (MES) in Moyamoya

MES on TCD examination are typically visible and audible (click, chirp, whistle), short-duration, unidirectional, high-intensity signal (≥5 dB) within the Doppler flow spectrum with its occurrence at random in the cardiac cycle.

Recent studies found that microembolic signals (MES), also called high-intensity signals (HITS), could be detected by transcranial Doppler (TCD) in MMD patients, and they were associated with rapid progression of middle cerebral artery (MCA) stenosis.

The presence of MES was confirmed to be an independent predictor of future stroke in atherosclerotic occlusive cerebrovascular diseases, however, the clinical significance of MES in MMD, a non-atherosclerotic disease, remains unknown [17, 18].

There is no consistency about the presence of MES in relation to Suzuki staging among various studies. In one study, MES were found to be common in patients with MMD and were associated with both recent ischemic symptoms and subsequent cerebral ischemic events [12]. In the 19 hemispheres with ischemic events within 3 months, the rate of MES detection was up to 26.3%. The increasing stages did not appear to reduce the presence of MES. MES were present in both early and late stages of MMD, from Suzuki stage II to stage VI. Horn et al. performed MES monitoring in 24 patients with angiographic features of MMD (21 bilateral and three unilateral), whose clinical symptoms were heterogeneous, including not only stroke, TIA, but also headache, seizures and cognitive impairment etc. MES were detected in three (6.6%) hemispheres, which were all in early stages of MMD [18]. They assumed artery-to-artery embolism was an important mechanism of cerebral ischemia in MMD, but the progression of MMD might lead to a reduction of embolism. In another study, Kraemer et al. reported that MES were detected in three of 14 MMD patients, all of them with previous ischemic events [17].

It is unclear if the detection of MES might be helpful for further stratifying the patients with revascularization surgery or antiplatelet therapy. MES detection may be of potential clinical value in the management of patients with MMD.

Autoregulation and Vasomotor Reactivity

Cerebral hemodynamics have been intensively studied in MMD suggesting that a decreased cerebrovascular reserve predicts an increased risk of ischemic events [19].

Cerebral arterial autoregulation is accomplished by resistance changes that occur at the level of cerebral arteries of 400 micrometer in diameter or less. Transcranial Doppler sonography

evaluation of large basal conducting vessels, which remain relatively constant in diameter during moderate pressure fluctuations, can provide an index of relative flow changes in response to small blood pressure changes and assess the autoregulatory response of the distal bed.

Vasomotor reactivity can be assessed with TCD by measuring changes in flow velocities in response to acetazolamide injection, hyperventilation, or C02 inhalation. The C02 method of testing is preferred as there is less risk, the effect is stronger, and there is greater certainty regarding which arterial segments are affected. In healthy patients, flow velocities may drop 35% with hyperventilation and increase 50% with hypercapnia. The response to dilatory stimuli is reduced in the setting of severe carotid disease because the resistance bed is presumed to be dilated at baseline. Vasomotor reactivity may be as low as 30% distal to occluded, symptomatic internal carotid arteries and it may approach 60% in arteries that had occluded asymptomatically. Vasomotor reactivity is calculated as the percentage change of MBFV.

Identification of decreased reactivity may cause physicians to allow blood pressure to remain higher after internal carotid artery severe stenosis or occlusion, and to select patients with decreased reactivity for extracranial-intracranial bypass surgery [10].

Other Procedures

TCD is a noninvasive technique that is quite available and can be performed at the bedside. However, it is very operator dependent and prone to spurious results. It can be used to measure blood flow volume in the ICA as a correlate for CBF in the corresponding hemisphere. However, this hemispheric CBF is an estimation based on the ICA blood flow volume measurement. It has poor spatial resolution because it cannot relay information on focal CBF impairments [20].

Other procedures used to evaluate cerebral hemodynamics and metabolism in patients with moyamoya disease include Xenon (Xe-133) CT, SPECT and PET.

EEG is used to demonstrate “re-build-up” phenomenon which is the return of high voltage slow waves 30–60 seconds following hyperventilation.

Cerebral angiography is the gold standard for the diagnosis of moyamoya disease.

Magnetic resonance angiography (MRA) is also useful to diagnose moyamoya disease in a non-invasive way, however, the possibility of overestimation of accuracy should always be taken into account because of the imaging quality. MRI and MRA are non-invasive methods that can be repeated after surgery.

Recently, new neurovascular imaging modalities such as high-resolution vessel wall imaging (HR-VWI) have led to advancements in the diagnosis of MMD. Features such as small and concentric narrowing or occlusion of intracranial arteries constitute the distinguishing features of MMD.

Treatment

For adults with ischemic MMD, antiplatelet agents (mostly aspirin) can be recommended especially in the setting of acute ischemic stroke. However, the long- term use of antiplatelet agents for preventing ischemic events may also increase the risk of hemorrhagic events [21]. Revascularization surgery is an option recommended to consider in patients with ischemic MMD and even with hemorrhagic or asymptomatic MMD depending on the hemodynamic status [1].

The preventive role of antiplatelet treatment in MMD remains to be determined in clinical trials. The use of antiplatelet agents may be considered in ischemic MMD but not in hemorrhagic or incidental MMD because of presumed risk of future hemorrhagic risk [1, 21].

Overall, there are no effective medical therapies for moyamoya disease. Through the provision of collateral pathways, surgical revascularization is the most successful therapy to improve cerebral hemodynamics, and to reduce the risk of subsequent stroke. Surgical

procedures for moyamoya disease can be classified into three categories: direct bypass, indirect bypass, and combined bypass.

Case 1

A young adult female presented with right lower extremity weakness. MRI brain showed left ACA/MCA watershed stroke. DSA-showed stenosis of terminal ICA along with left MCA and ACA, stage 1 Suzuki classification (Fig. 1).

Case 2

A young adult female presented with right sided weakness. MRI brain showed left basal ganglia stroke. DSA- severe moyamoya disease with stage III Suzuki classification. TCD demonstrated severe diminished cerebrovascular reserve bilaterally (Fig. 2).

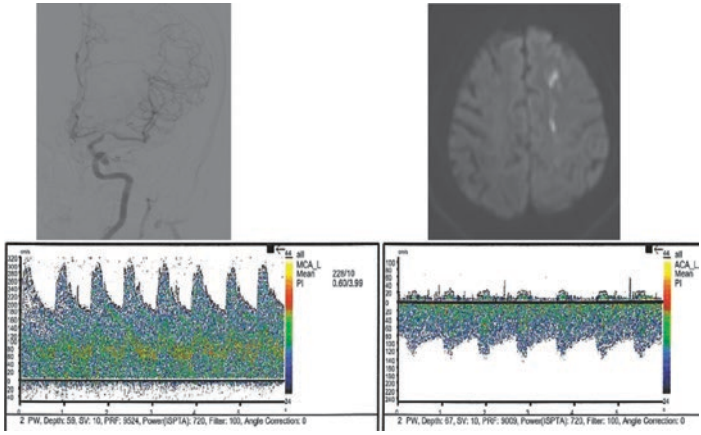

Fig. 1 Top left – DSA shows narrowing of terminal ICA along with left MCA and ACA, stage I Suzuki classification. Top right – DWI MRI brain – left ACA/MCA watershed stroke. Bottom – Increase MFV in left MCA and ACA, indicative of underlying stenosis

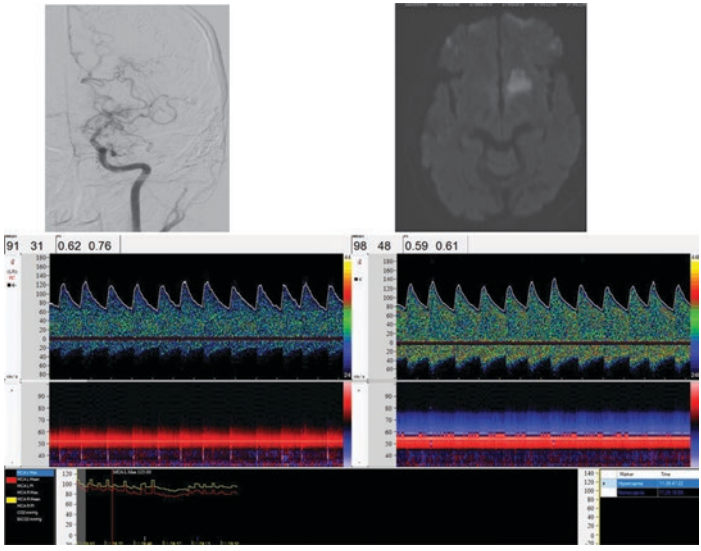

Fig. 2 Top left- Digital Subtraction Angiography showing severe stenosis of left terminal ICA, ACA and MCA with moyamoya changes (collateral pattern), stage III Suzuki classification. Top right. DWI MRI – Left basal ganglia hyperintensity, indicative of stroke. Bottom. TCD vasomotor reactivity (CO2 test) showing severely reduced autoregulation bilaterally

References

1. Scott RM, Smith ER. Moyamoya disease and moyamoya syndrome. N Engl J Med. 2009;360(12):1226–37.
2. Suzuki J, Takaku A. Cerebrovascular "moyamoya" disease. Disease showing abnormal net-like vessels in base of brain. Arch Neurol. 1969;20(3):288–99.
3. Wakai K, Tamakoshi A, Ikezaki K, Fukui M, Kawamura T, Aoki R, et al. Epidemiological features of moyamoya disease in Japan: findings from a nationwide survey. Clin Neurol Neurosurg. 1997;99(Suppl 2):S1–5.
4. Uchino K, Johnston SC, Becker KJ, Tirschwell DL. Moyamoya disease in Washington State and California. Neurology. 2005;65(6):956–8.
5. Fujimura M, Sonobe S, Nishijima Y, Niizuma K, Sakata H, Kure S, et al. Genetics and biomarkers of moyamoya disease: significance of RNF213 as a susceptibility gene. J Stroke. 2014;16(2):65–72.
6. Starke RM, Crowley RW, Maltenfort M, Jabbour PM, Gonzalez LF, Tjoumakaris SI, et al. Moyamoya disorder in the United States. Neurosurgery. 2012;71(1):93–9.

7. Hallemeier CL, Rich KM, Grubb RL Jr, Chicoine MR, Moran CJ, Cross DT 3rd, et al. Clinical features and outcome in North American adults with moyamoya phenomenon. Stroke. 2006;37(6):1490–6.
8. Cho WS, Chung YS, Kim JE, Jeon JP, Son YJ, Bang JS, et al. The natural clinical course of hemodynamically stable adult moyamoya disease. J Neurosurg. 2015;122(1):82–9.
9. Kuroda S, Hashimoto N, Yoshimoto T, Iwasaki Y. Research committee on moyamoya disease in J. Radiological findings, clinical course, and outcome in asymptomatic moyamoya disease: results of multicenter survey in Japan. Stroke. 2007;38(5):1430–5.
10. Babikian VL, Feldmann E, Wechsler LR, Newell DW, Gomez CR, Bogdahn U, et al. Transcranial Doppler ultrasonography: year 2000 update. J Neuroimaging. 2000;10(2):101–15.
11. Jeon C, Yeon JY, Jo KI, Hong SC, Kim JS. Clinical role of microembolic signals in adult moyamoya disease with ischemic stroke. Stroke. 2019;50(5):1130–5.
12. Chen J, Duan L, Xu WH, Han YQ, Cui LY, Gao S. Microembolic signals predict cerebral ischaemic events in patients with moyamoya disease. Eur J Neurol. 2014;21(5):785–90.
13. Babikian VL, Hyde C, Pochay V, Winter MR. Clinical correlates of high-intensity transient signals detected on transcranial Doppler sonography in patients with cerebrovascular disease. Stroke. 1994;25(8):1570–3.
14. Suzuki J, Kodama N. Moyamoya disease--a review. Stroke. 1983;14(1):104–9.
15. Muttaqin Z, Ohba S, Arita K, Nakahara T, Pant B, Uozumi T, et al. Cerebral circulation in moyamoya disease: a clinical study using transcranial Doppler sonography. Surg Neurol. 1993;40(4):306–13.
16. Takase K, Kashihara M, Hashimoto T. Transcranial Doppler ultrasonography in patients with moyamoya disease. Clin Neurol Neurosurg. 1997;99(Suppl 2):S101–5.
17. Kraemer M, Heienbrok W, Berlit P. Moyamoya disease in Europeans. Stroke. 2008;39(12):3193–200.
18. Horn P, Lanczik O, Vajkoczy P, Daffertshofer M, Bueltmann E, Werner A, et al. Hemodynamic reserve and high-intensity transient signals in moyamoya disease. Cerebrovasc Dis. 2005;19(3):141–6.
19. So Y, Lee HY, Kim SK, Lee JS, Wang KC, Cho BK, et al. Prediction of the clinical outcome of pediatric moyamoya disease with postoperative basal/acetazolamide stress brain perfusion SPECT after revascularization surgery. Stroke. 2005;36(7):1485–9.
20. Lee M, Zaharchuk G, Guzman R, Achrol A, Bell-Stephens T, Steinberg GK. Quantitative hemodynamic studies in moyamoya disease: a review. Neurosurg Focus. 2009;26(4):E5.
21. Kraemer M, Berlit P, Diesner F, Khan N. What is the expert's option on antiplatelet therapy in moyamoya disease? Results of a worldwide survey. Eur J Neurol. 2012;19(1):163–7.

Vertebral Steal

Sanjeev Sivakumar and Ryan Hakimi

Introduction

The subclavian steal phenomenon was first reported in the 1960s, with coining of the term by Fisher in 1961 [1–3]. The phenomenon involves flow reversal in a branch of the subclavian artery, usually the vertebral artery, which results from a hemodynamically significant ipsilateral occlusion or severe stenosis of the proximal subclavian artery. Blood siphons from the contralateral vertebral artery into the vertebral artery ipsilateral to subclavian stenosis, thus "stealing" blood from the basilar artery [3]. Subclavian stenosis is often asymptomatic. In some patients however, subclavian steal syndrome is symptomatic, manifesting as transient brain ischemia [4]. Determination of blood pressure differences between the arms and identification of retrograde flow in the vertebral artery are features that diagnose this syndrome [5, 6]. Retrograde flow and subclavian steal has been well studied with Doppler ultrasound [7–23].

S. Sivakumar
USC School of Medicine-Greenville, Greenville, SC, USA
e-mail: Sanjeev.sivakumar@prismahealth.org

R. Hakimi (✉)
Neuro ICU and TCD Services Prisma Health-Upstate, Department of Medicine (Neurology) University of South Carolina School of Medicine-Greenville, Greenville, SC, USA
e-mail: ryan.hakimi@prismahealth.org

W. C. Ziai, C. L. Cornwell (eds.), *Neurovascular Sonography*,
https://doi.org/10.1007/978-3-030-96893-9_24

This chapter will provide a brief neuroanatomical overview of vertebrobasilar arterial system and Doppler ultrasound characteristics of vertebral-subclavian steal syndrome.

Brief Anatomy of the Vertebrobasilar Arterial System and Antegrade Flow

The posterior circulation also known as the vertebrobasilar arterial system supplies blood to the cerebellum, brainstem, thalami, posterior parietal lobes, posterior inferior temporal lobes and occipital lobes. The right and left subclavian arteries originate from the brachiocephalic trunk and the aortic arch, respectively. The subclavian arteries course outward as they turn from the superior mediastinum towards the sub-clavicular fossa. The vertebral arteries arise from the top of the subclavian arteries at the apex of this lateral curve.

The vertebral artery is typically divided into four segments. The extracranial vertebral artery is comprised of the V_1–V_3 segments and while the V_4 segment forms the intracranial vertebral artery. The V1 (extraosseous) segment travels medially then upwards from its origin, to enter the transverse foramina of the cervical spine at the C5 or C6 level, but can be as high as the C3 level [24]. The V2 (foraminal) segment continues from the lowest traversed transverse foramen (usually C6 vertebrae), cranially to the C1 level. The V3 (extraspinal) segment extends from the C1 transverse foramen to the foramen magnum. The intracranial V4 segment is also termed the intradural segment.

The cervical vertebral arteries give off muscular branches (to deep cervical muscles) and spinal branches that supply the spinal cord, cervical spinal meninges and cervical vertebra [8]. Intracranially, the two V4 segments give off a posterior meningeal artery, posterior and anterior spinal arteries, perforating arteries and a posterior inferior cerebellar artery (PICA), after which they unite to form the basilar artery. The basilar artery is usually straight, but can be tortuous in some patients. The basilar artery gives off multiple perforating branches, the anterior inferior cerebellar arteries (AICAs), superior cerebellar arteries (SCAs) before terminating in the posterior cerebral arteries (PCAs) in

most patients. In approximately 20% of patients, the embryonic fetal condition can persist on one side [8]. In this case, the PCA is derived primarily from the ipsilateral internal carotid artery via a prominent posterior communicating artery (PComA) with a small ipsilateral P1-PCA segment. This is known as "fetal origin" or "fetal configuration" of the PCA (Fig. 1).

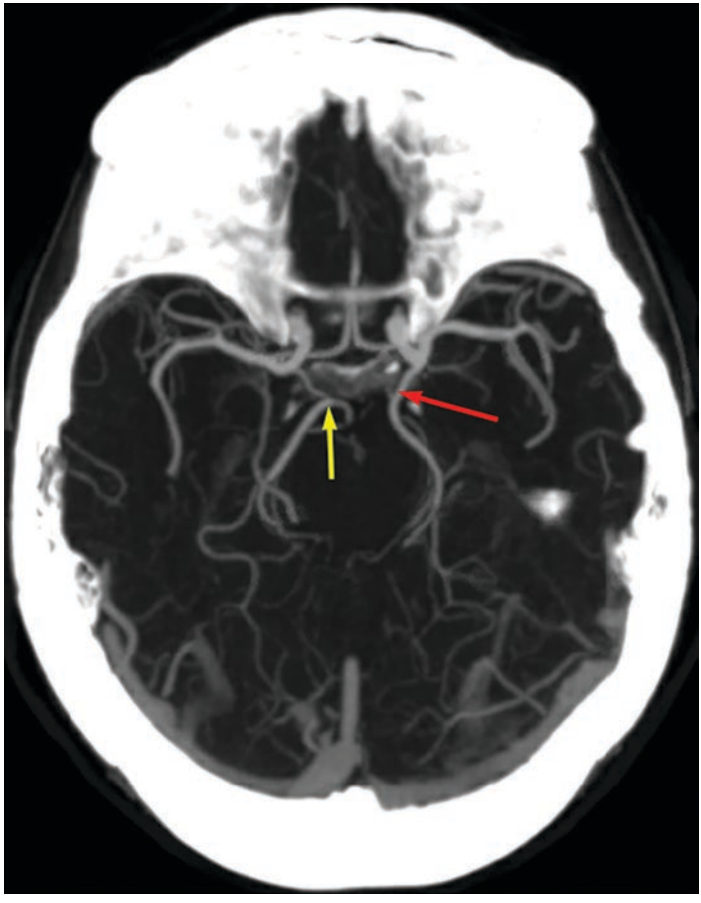

Fig. 1 The right PCA (yellow arrow) originates from the basilar artery. The left PCA is derived primarily from the ipsilateral internal carotid artery via a prominent posterior communicating artery (red arrow); this is known as "fetal origin" or "fetal configuration" of the PCA

The vertebral arteries can be asymmetrical. Up to 15% of the population have one vertebral artery that is atretic. The smaller vertebral artery often functionally terminates as the posterior inferior cerebellar artery (PICA), with an atretic segment between the PICA origin and the V4 confluence. Approximately 50–60% have a dominant left vertebral, 25% a dominant right vertebral and 25% have both vertebral arteries of similar caliber [25, 26]. Fenestrations, which are duplicate, endothelially lined parallel lumens, are common in vertebral arteries [8].

Normal antegrade flow in the posterior circulation consists of blood flow from the subclavian artery to the vertebral arteries, and then to the basilar artery. This is represented by flow directed away from the probe, when insonating the vertebral arteries and the basilar artery via the suboccipital window. Posterior circulation vessels, however, can recruit collateral flow. Most important among them being the reversed basilar arterial flow, when the dominant vertebral artery is occluded [27]. In this case, basilar flow descends from the top of the basilar artery (flow towards probe) towards cerebellar branches, which is supplied via the posterior communicating arteries (PComAs).

Subclavian-Vertebral Artery Steal Syndrome (SSS)

Subclavian-vertebral artery steal syndrome (SSS) is a hemodynamic phenomenon of blood flow reversal in the vertebral artery due to significant stenosis or occlusion of the proximal subclavian artery or innominate artery that may result in significant vertebrobasilar ischemia [1–3]. Ipsilateral upper extremity claudication, or coronary insufficiency (among patients with internal mammary artery bypass grafts) are other clinical features that may be caused by subclavian steal phenomenon [28]. The prevalence varies from 3–4% in patients evaluated with diagnostic cardiac catheterization, to up to 11–18% in patients with peripheral vascular disease [29, 30].

The pathophysiology involves stenosis or occlusion of proximal to the origin of vertebral artery-segment take-off from the subclavian or innominate artery. This causes hypoperfusion of the

ipsilateral arm leading to a pressure gradient and flow diversion from the ipsilateral vertebral to subclavian artery. The vertebral artery contributes to the blood supply of upper extremity via the contralateral vertebral artery with or without other collaterals and at times the basilar artery. Thus blood is "stolen" from the posterior circulation, and this phenomenon is aggravated during physical activity involving muscles of the arm [31]. In SSS, the left subclavian artery is more frequently affected by atheromatosis [31], however, Takayasu and giant cell arteritis can cause SSS [12]. Vertebrobasilar insufficiency can be attributed to blood flow steal from high output arteriovenous graft (AVG), and can be detected using Duplex ultrasonography [23].

Subclavian stenosis is seldom symptomatic. When symptomatic, it usually indicates widespread atherosclerosis in the aortic branches. The most important predictive factor is the magnitude of blood pressure difference between the upper extremities [32]. Symptomatic SSS can manifest as paroxysmal vertigo, syncope, diplopia, ataxia and ipsilateral arm claudication or paresthesia.

When steal is present at rest, the key findings are a difference in blood pressure of ≥20 mmHg between arms and systolic flow reversal (an alternating flow signal or absent diastolic flow) in the "stealing" vertebral artery. This is often accompanied by a low resistance flow in the donor artery. When the inter-arm blood pressure difference is 10–20 mmHg and with absence of steal waveforms at rest or when flow reversal is incomplete, the hyperemia test or the ischemic cuff test can be performed to provoke the steal and to augment flow reversal. Here, the blood pressure cuff is inflated to about 20 mm Hg greater than the patient's own systolic blood pressure, and flow reduction to the arm is maintained for 60–90 seconds (maximum 3 min, if tolerated by patient). This induces ischemia in the arm. During this process, the ipsilateral vertebral artery is monitored using TCD by insonating the vertebral artery in the sub occipital window. The cuff is then rapidly deflated, resulting in rapid reperfusion of the arm. The increased metabolic demand induced by the short period of ischemia augments the steal. This can manifest as varying degrees of flow reversal or alternating flow for a short period of time, in the recipient vertebral artery confirming the diagnosis of SSS (Figs. 2, 3 and 4).

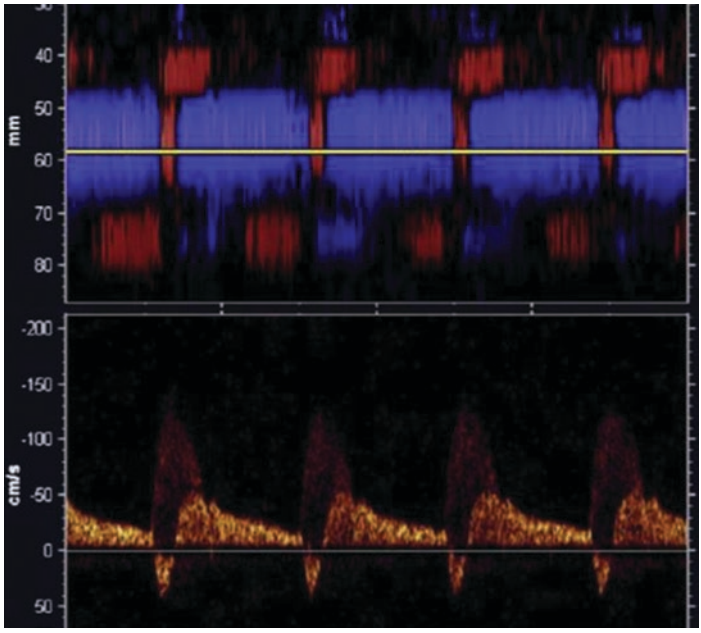

Fig. 2 Alternating flow signal in the vertebral artery (VA). PMD display: on the yellow line, red color signal, steal direction/toward the probe in systole; blue, away (normal direction) in diastole. Spectral display: negative and positive waveforms corresponding with direction changes. (Reproduced with permission from Hakimi et al. [35])

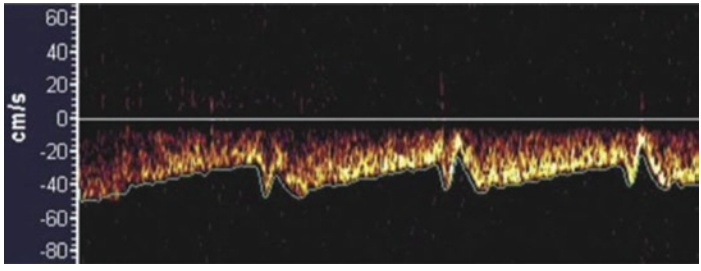

Fig. 3 Abnormal waveform in the VA indicates subclavian steal phenomenon. V-shaped cutout is the first form of the alternating flow signal. (Reproduced with permission from Hakimi et al. et al. [35])

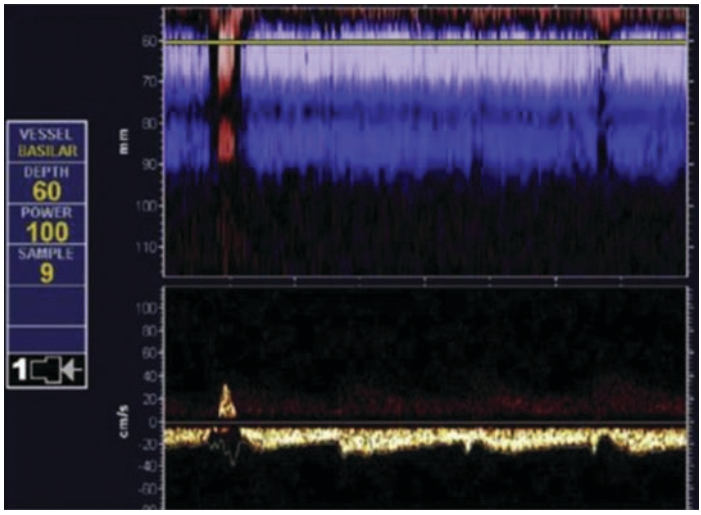

Fig. 4 Hyperemia test: overinflated blood pressure cuff released, flow reversal (*red signal*) in the vertebral-basilar system, and various waveforms returned to baseline (spectral display). (Reproduced with permission from Hakimi et al. [35])

Steal phenomenon can also be identified by alternating flow signatures on a motion mode display. Dissection of the intracranial vertebral artery is a differential diagnosis that must be considered. In patients with known or suspected disease, a subclavian artery flow velocity exceeding 240 cm/s on Doppler ultrasound has been validated to be predictive of significant subclavian stenosis [33].

Computed tomography or magnetic resonance angiography can confirm the presence and degree of severity of subclavian stenosis. Angiographic confirmation is necessary since vertebral artery waveforms suggestive of steal can be seen in the absence of subclavian stenosis among patients with hypoplastic vertebral arteries with or without fetal-type posterior vertebral arteries [34]. Most commonly these patients are treated with medical therapy (antiplatelets and statins) and a cardiovascular evaluation. In more advanced cases, subclavian artery angioplasty and stenting is required.

Conclusions

Subclavian-vertebral steal syndrome is a phenomenon of varying degrees of blood flow reversal in the vertebral artery, which is often asymptomatic or can be associated with symptoms of vertebrobasilar ischemia. Doppler ultrasound is a non-invasive bedside tool, which can be used to demonstrate reversed vertebral artery flow and to confirm the diagnosis.

References

1. Contorni L. The vertebro-vertebral collateral circulation in obliteration of the subclavian artery at its origin. Minerva Chir. 1960;15:268–71.
2. Reivich M, Holling HE, Roberts B, Toole JF. Reversal of blood flow through the vertebral artery and its effect on cerebral circulation. N Engl J Med. 1961;265:878–85.
3. Fisher CM. A new vascular syndrome - "the subclavian steal". New Eng J Med. 1961;265:912–3.
4. Fields WS, Lemak NA. Joint study of extracranial arterial occlusion. VII. Subclavian steal--a review of 168 cases. JAMA. 1972; 222(9):1139–43.
5. Tan TY, Schminke U, Lien LM, Tegeler CH. Subclavian steal syndrome: can the blood pressure difference between arms predict the severity of steal? J Neuroimaging. 2002;12(2):131–5.
6. von Reutern GM, Pourcelot L. Cardiac cycle-dependent alternating flow in vertebral arteries with subclavian artery stenoses. Stroke. 1978;9(3):229–36.
7. Voigt K, Kendel K, Sauer M. Subclavian steal syndrome. Bloodless diagnosis of the syndrome using ultrasonic pulse echo and vertebral artery compression [German]. Fortschr Neu- rol Psychiatr Grenzgeb. 1970;38:20–33.
8. Alexandrov AV. Cerebrovascular ultrasound in stroke prevention and treatment. 2nd ed. Blackwell Publishing Ltd ISBN: 978–1–405-19576-8; 2011.
9. Grossman BL, Brisman R, Wood EH. Ultrasound and the subclavian steal syndrome. Radiology. 1970;94(1):1–6.
10. Reutern GM, Budingen HJ, Freund HJ. The diagnosis of obstructions of the vertebral and subclavian arteries by means of directional Doppler sonography (author's transl). Arch Psychiatr Nervenkr (1970). 1976;222(2–3):209–22.

11. von Reutern GM, Budingen HJ. Doppler sonographic study of the vertebral artery in subclavian steal syndrome. Dtsch Med Wochenschr. 1977;102(4):140–1.
12. Yoneda S, Nukada T, Tada K, Imaizumi M, Takano T. Subclavian steal in Takayasu's arteritis. A hemodynamic study by means of ultrasonic Doppler flowmetry. Stroke. 1977;8(2):264–8.
13. Pourcelot L, Ribadeau-Dumas JL, Fagret D, et al. Contribution of the Doppler examination to the diagnosis of subclavian steal syndrome [French]. Rev Neurol (Paris). 1977;133:309–23.
14. Walker DW, Acker JD, Cole CA. Subclavian steal syndrome detected with duplex pulsed Doppler sonography. AJNR Am J Neuroradiol. 1982;3(6):615–8.
15. Ringelstein EB, Zeumer H. Delayed reversal of vertebral artery blood flow following percutaneous transluminal angioplasty for subclavian steal syndrome. Neuroradiology. 1984;26(3):189–98.
16. Ackerstaff RG, Hoeneveld H, Slowikowski JM, Moll FL, Eikelboom BC, Ludwig JW. Ultrasonic duplex scanning in atherosclerotic disease of the innominate, subclavian and vertebral arteries. A comparative study with angiography. Ultrasound Med Biol. 1984;10(4):409–18.
17. Kuperberg EB, Grozovskii IL, Agadzhanova LP. Functional test of reactive hyperemia in the diagnosis of the vertebro-subclavian steal syndrome using ultrasonic dopplerography. Zh Nevropatol Psikhiatr Im S S Korsakova. 1986;86(1):28–34.
18. Bornstein NM, Norris JW. Subclavian steal: a harmless haemodynamic phenomenon? Lancet. 1986;2(8502):303–5.
19. Ackermann H, Diener HC, Seboldt H, Huth C. Ultrasonographic follow-up of subclavian stenosis and occlusion: natural history and surgical treatment. Stroke. 1988;19(4):431–5.
20. Rossum AC, Steel SR, Hartshorne MF. Evaluation of coronary subclavian steal syndrome using sestamibi imaging and duplex scanning with observed vertebral subclavian steal. Clin Cardiol. 2000;23(3):226–9.
21. Iino T, Yamanaka T, Sato W, Iino K, Watanabe H. Manifestation of coronary subclavian steal phenomenon using reactive hyperemia in the ipsilateral forearm. Echocardiography. 2019;36(10):1956–8.
22. de Deus M, Passos LMA, de Jesus PC, Junqueira LF Jr, Vasconcelo DF. An update on Doppler ultrasound of vertebral arteries: subclavian steal syndrome. Arq Bras Cardiol: Imagem cardiovasc. 2016;29(2):58–62.
23. Kargiotis O, Siahos S, Safouris A, Feleskouras A, Magoufis G, Tsivgoulis G. Subclavian steal syndrome with or without arterial stenosis: a review. J Neuroimaging. 2016;26(5):473–80.
24. Matula C, Trattnig S, Tschabitscher M, Day JD, Koos WT. The course of the prevertebral segment of the vertebral artery: anatomy and clinical significance. Surg Neurol. 1997;48(2):125–31.

25. Khan S, Cloud GC, Kerry S, Markus HS. Imaging of vertebral artery stenosis: a systematic review. J Neurol Neurosurg Psychiatry. 2007;78(11):1218–25.
26. Tay KY, UK-I JM, Trivedi RA, Higgins NJ, Cross JJ, Davies JR, et al. Imaging the vertebral artery. Eur Radiol. 2005;15(7):1329–43.
27. Ribo M, Garami Z, Uchino K, Song J, Molina CA, Alexandrov AV. Detection of reversed basilar flow with power-motion Doppler after acute occlusion predicts favorable outcome. Stroke. 2004;35(1):79–82.
28. Potter BJ, Pinto DS. Subclavian steal syndrome. Circulation. 2014;129(22):2320–3.
29. English JA, Carell ES, Guidera SA, Tripp HF. Angiographic prevalence and clinical predictors of left subclavian stenosis in patients undergoing diagnostic cardiac catheterization. Catheter Cardiovasc Interv. 2001;54(1):8–11.
30. Gutierrez GR, Mahrer P, Aharonian V, Mansukhani P, Bruss J. Prevalence of subclavian artery stenosis in patients with peripheral vascular disease. Angiology. 2001;52(3):189–94.
31. Osiro S, Zurada A, Gielecki J, Shoja MM, Tubbs RS, Loukas M. A review of subclavian steal syndrome with clinical correlation. Med Sci Monit. 2012;18(5):RA57-63.
32. Clark CE, Taylor RS, Shore AC, Ukoumunne OC, Campbell JL. Association of a difference in systolic blood pressure between arms with vascular disease and mortality: a systematic review and meta-analysis. Lancet. 2012;379(9819):905–14.
33. Mousa AY, Morkous R, Broce M, Yacoub M, Sticco A, Viradia R, et al. Validation of subclavian duplex velocity criteria to grade severity of subclavian artery stenosis. J Vasc Surg. 2017;65(6):1779–85.
34. Kocak B, Korkmazer B, Islak C, Kocer N, Kizilkilic O. Endovascular treatment of extracranial vertebral artery stenosis. World J Radiol. 2012;4(9):391–400.
35. Hakimi R, Alexandrov AV, Garami Z. Neuro-ultrasonography. Neurol Clin. 2020;38:215–29.

Transcranial Doppler in Acute Bacterial Meningitis

Eder Caceres

Cerebral Metabolism in Acute Bacterial Meningitis

Patients with meningitis usually hyperventilate spontaneously and cerebrospinal fluid (CSF) shows signs of metabolic acidosis (low CO2, low bicarbonate and elevated lactate) [1]. This is probably not only related to the presence of inflammation in the meninges but also a systemic phenomenon related to sepsis [2]. A correlation between CSF pH and cerebral blood flow (CBF) support the fact that brain interstitial fluid pH and CSF pH are key factors determining CBF and involved in the hemodynamic and metabolic derangements observed in meningitis [1]. However, the metabolic activity of the brain in cases of meningoencephalitis and therefore variables like CBF, oxygen consumption (VO2), lactate efflux, and cerebral metabolic rate (CMR) seem to rely on more factors, not fully understood, related to a pattern of non-ischemic metabolic distress and mitochondrial dysfunction [3] leading to an uncoupling between oxygen delivery (DO2) and VO2 that is the process behind impaired autoregulation,

E. Caceres (✉)
Translational Science in Infectious Disease and Critical Care Research Group, Clínica Universidad de La Sabana, Chía, Cundinamarca, Colombia
e-mail: edercr@clinicaunisabana.edu.co

W. C. Ziai, C. L. Cornwell (eds.), *Neurovascular Sonography*,
https://doi.org/10.1007/978-3-030-96893-9_25

vasoreactivity and the so-called luxury perfusion. The key in this scenario seems to be an individualized approach guided by monitoring modalities including TCD [4]. Besides these local vascular and metabolic phenomena there is also a systemic inflammatory response with releasing of cytokines that leads to disruption of brain blood barrier (BBB) and altered neurotransmission. Septic patients from a source other than SNC often have an impaired cerebral autoregulation and the level of PaCO2 can affect the ability of the patient to adjust CBF to changes in mean arterial pressure (MAP) which implies a risk of ischemia or hyperemia [2]. Ultimately the patient with meningoencephalitis is septic and exposed to the systemic repercussions that contribute to the presentation of sepsis associated encephalopathy.

Cerebral Blood Flow in Acute Bacterial Meningitis

Nuclear imaging, SPECT, have been used to evaluate variations of CBF caused by changes in microcirculation. Compared to healthy volunteers, the group of patients with bacterial meningoencephalitis had a decreased global perfusion assessed by SPECT and increased asymmetry between brain regions in the same patient. The highest level of asymmetry was found in the frontotemporal region and may represent zones of hypoperfusion or hyperperfusion. On top of these, a decreased perfusion and higher asymmetry was related to worse mental status and focal signs on presentation [5]. Areas of hypoperfusion often correspond to focal clinical symptoms but not to signs of ischemia in the non-contrast computed tomography (CT) and not always to detectable abnormalities on cerebral angiography (DSA), probably related to an alteration of small vessels or at a metabolic level. A follow up examination with SPECT 3 to 45 weeks after the acute disease revealed improvement or disappearance of these abnormalities. This suggests a functional and reversible disorder not necessarily related to structural injury detectable on CT [9]. Cerebral angiogram (DSA) can sometimes demonstrate the presence of arterial narrowing and stenosis at the base but also dilation of surface

arteries [8]. These alterations can be secondary to arterial narrowing from vasculitis as well as microvascular and metabolic changes as mentioned above [6, 7] however, histopathological inflammatory changes compatible with vasculitis or thrombosis are not always present suggesting vasospasm plays also an important role [10].

Transcranial Doppler and Evaluation of Cerebrovascular Involvement

TCD has been used as a reliable and noninvasive tool to detect hemodynamic changes early in the disease and alert the team about the risk of stroke and hypoperfusion. These hemodynamic changes are thought to be related to arterial narrowing secondary to vasospasm and/or inflammation of the arterial wall. There is a correlation between CSF concentration of proinflammatory cytokines (IL-1B IL-6), leucocyte count and high systolic CBFv in middle cerebral artery (MCA) in cases of meningitis [14, 15].

Some studies have proposed a classification of the severity of vasospasm in meningitis based on previous physiologic studies [12] (Table 1). Resistance Index (RI) > 0.6 was also used as a sign of increased vascular resistance and increased intracranial pressure (ICP).

After evaluation of anterior cerebral artery (ACA), middle cerebral artery (MCA), internal carotid artery (ICA), posterior cerebral artery (PCA) and basilar artery (BA), 43% (n = 94) of patients with ABM had increased systolic blood flow velocities

Table 1 Grades of cerebrovascular involvement

Grade	SBFV MCA
0	≤140 cm/s
Ia	140–170 cm/s
Ib	170–210 cm/s
II	210–280 cm/s
III	>280 cm/s

SBFV MCA Systolic Blood Flow Velocity in the Middle Cerebral Artery

(SBFv) mostly within the first week of therapy but, could happen later. SBFv greater than 150 cm/s was considered high in this study. 63% of these patients had increased SBFv in anterior and posterior circulation and 35% only in anterior circulation. Vasospasm or stenosis does not always correlate to findings in DSA, MRA or CT angiography [11]. Serial measurement showed that the highest CBFv occurs during day 3–6 after onset of symptoms and normalization of flow is observed within 3 weeks. CBFv was commonly asymmetrical and patients with velocities in Grade II and III had a lower Glasgow Coma Scale on presentation and higher frequency of stroke and fatal outcome [13, 17].

It remains unclear which threshold of cerebral blood flow velocity (CBFv) is pathologic in meningitis but there is definitely a correlation between these values and increased occurrence of ischemic stroke and worse outcomes. Increased SBFv was associated with an odds ratio of 9.15 (95% CI: 1.96 to 42.67) for ischemic stroke diagnosed by MRI and an increased incidence of unfavorable outcome defined by Glasgow Outcome Scale (GOS) 1,2 or 3 [11]. Correlation between TCD and other imaging techniques like Magnetic Resonance Angiography (MRA) and DSA is debatable and each study has its own pitfalls [12].

In case of clinical signs of elevated ICP there is a direct correlation between decreased MFV in the MCA probably as a sign of global hypoperfusion. This was also related to increased pulsatility index (PI). Lower GOS was also related to decreased MFV and increased PI [18].

To summarize, there is an increase in CBFv in ABM probably related to vasospasm and/or vasculitis, the highest velocities occur within the first week of symptoms and patients with a higher grade of vasospasm may be more obtunded on presentation and have increased frequency of stroke and worse functional outcomes. However, patients with elevated ICP and lower cerebral perfusion pressure (CPP) may have decresed CBFv. There are only a few studies with heterogeneous populations and different TCD criteria, this limits our ability to draw any definitive conclusions about risk factors or establish standardized criteria in this setting however, it does tell us the potential role of routine TCD examination for this population.

Cerebral Autoregulation in Acute Bacterial Meningitis

Patients with acute bacterial meningitis are often critically ill and require use of vasopressors to maintain organ perfusion. Impairment of cerebral autoregulation leads to dependency of cerebral blood flow (CBF) and cerebral blood volume (CBV) on mean arterial pressure (MAP) exposing the patient to the risk of hypoperfusion or hyperperfusion and vasogenic edema develops. In this setting, increased MAP can cause elevated ICP secondary to higher CBF and CBV; if the critical care team is not aware of this phenomenon it would be tempted to prescribe specific interventions (i.e. hyperoncotic therapy) aimed to lower the ICP instead of adjusting MAP and CPP which could be an effective measure.

For evaluation of autoregulation a study performed in Denmark used elevated MAP induced by norepinephrine and simultaneous measurement of mean flow velocity (MFV) in the MCA by TCD as well as arterial to jugular oxygen saturation difference (a-vDO2). In conditions of a constant cerebral metabolic rate of oxygen (CMRO2), an increase or decrease in CBF would result in an inversely proportional change of a-vDO2 (Eqs. 1 and 2):

$$\mathrm{CMRO2} = \mathrm{CBF} \times \left(\mathrm{CaO2} - \mathrm{CvO2}\right) \tag{1}$$

CBF: Cerebral blood flow, CaO2: arterial content of oxygen, CvO2: venous content of oxygen

$$\begin{aligned} \mathrm{CaO2} &= \left(\mathrm{Hg} \times 1.34 \times \mathrm{SaO2}\right) + \left(0.0031 \times \mathrm{PaO2}\right) \\ \mathrm{CvO2} &= \left(\mathrm{Hg} \times 1.34 \times \mathrm{SvO2}\right) + \left(0.0031 \times \mathrm{PvO2}\right) \end{aligned} \tag{2}$$

CaO2: arterial content of oxygen, CvO2: venous content of oxygen, PaO2: arterial pressure of oxygen, PvO2: venous pressure of oxygen, Hg: hemoglobin.

The initial autoregulation study was performed within the first 24 h after lumbar puncture and measurement of MAP and MFV was recorded simultaneously. On average, 6 studies were

performed per patient (16 patients). MFV in the MCA increased by a median of 36% (10% to 81%) when MAP was raised by 46% (25% to 93%). Simultaneous measurement of a-vDO2 decreased by 37% (10% to 51%). The proportional increase in MAP and MFV tells us about the loss of autoregulation in these patients and a lower a-vDO2 is a sign of constant CMRO2 and metabolic uncoupling [16].

A second study confirmed these results using the gold standard for quantitative perfusion, the Kety-Schmidt technique with Xe as radiotracer. They found results consistent with an increase in CBF directly proportional to an elevated MAP after norepinephrine infusion within the first 48 h of diagnosis of ABM. CMRO2 remained unchanged in patients and controls. No cerebral net flux of norepinephrine was found in patients or controls; this answered the question whether leakage of norepinephrine into interstitium could be affecting CMRO2 or metabolism and biasing results. They did also evaluate these variables after propofol infusion founding that propofol decreased CMRO2 and a-vDO2 but CBF remained unchanged, supporting also the idea of vascular and metabolic uncoupling [16].

To summarize, cerebral autoregulation is impaired in patients with ABM; recognition of an individualized plateau as well as multimodality monitoring may be of value when optimizing hemodynamic variables and to guarantee an adequate perfusion and oxygen delivery. TCD is again a bedside and non-invasive method to evaluate changes in CBF related to systemic pressures.

Vasoreactivity in Acute Bacterial Meningitis

The presence of arterial narrowing of the arteries of the base is often accompanied by arteriolar dilation and loss of tone which probably hinders the ability of the cerebral vasculature to adjust to changes in cerebral perfusion. However, the arterial vasorreactivity to carbon dioxide seems to be partially preserved. One study evaluated the change in CBF in ventilated patients with ABM after dropping the PaCO2 by 7.5 mmHg from baseline for 30 minutes and its relation to autoregulation. A computer program vali-

dated for this purpose created a slope of autoregulation and fitted a lower and upper limit of autoregulation according to recorded measurements. Autoregulation was defined as MVF increase ≤10% per increase in MAP of 30 mmHg (slope of linear regression line ≤0.33%/mmHg). Norepinephrine was used to increase MAP and changes in MFV in the MCA were recorded by TCD. During normoventilation, 8 out of 9 patients were found to have impaired autoregulation. After hyperventilation, 4 patients had autoregulation recovered. Global cerebral ischemia was not present during normoventilation or hyperventilation when evaluated by SjvO2 [19]. However, this effect may last a few hours and compensatory mechanisms will push CBF toward baseline despite persistent hypocapnia [18].

A different study using the Kety-Schmidt technique and SPECT-Xe in patients with ABM confirmed that compared to healthy subjects, ABM patients have a higher variability of CBF and CO2 reactivity. The pH at baseline for patients with ABM was normal despite slight spontaneous hyperventilation which means that hypocapnia had been already compensated and its effect on CBF was not present anymore. That could explain the similar CBF between controls and patients and suggest that correcting PaCO2 to normal values for baseline hypocarbic patients may lead to transitory vasodilation and rebound hyperperfusion [19].

Summary

- Cerebrovascular complications in patients with ABM are frequent, well recognized and have an impact on clinical outcomes.
- The metabolic activity of the brain in cases of bacterial meningoencephalitis (CBF, VO2, lactate efflux, and CMR) seems to rely on several factors not fully recognized and is related to a pattern of non-ischemic metabolic distress and mitochondrial dysfunction that leads to DO2 - VO2 uncoupling.
- Nuclear imaging has demonstrated asymmetry in the perfusion of the brain in ABM that represents changes at a macro and microvascular level. This is reversible most of the time.

- Increased MFV in the MCA recorded through TCD could be secondary to arterial narrowing (vasospasm, vasculitis) or to a hyperdynamic state. Higher MFVs are associated with increased incidence of stroke and worse functional outcomes.
- SBFv in the MCA greater than 150 cm/s seems to have a good sensitivity to identify patients at risk of stroke or poor outcome. There are no validated scales for the severity of vasospasm in ABM.
- Impairment of cerebral autoregulation is frequent in ABM and identification of upper and lower limits of autoregulation could be critical when dealing with ICP issues and hemodynamic management.
- Vasoreactivity is partially preserved in ABM and could be a short term measure for control of intracranial hypertension. Correcting PaCO2 to normal values in hypocapnic patients can cause a transient rebound of CBF.

References

1. Paulson OB, Brodersen P, Hansen EL, Kristensen HS. Regional cerebral blood flow, cerebral metabolic rate of oxygen, and cerebrospinal fluid acid-base variables in patients with acute meningitis and with acute encephalitis. Acta Med Scand. 1974;196(3):191–8. https://doi.org/10.1111/j.0954-6820.1974.tb00994.x.
2. Taccone FS, Castanares-Zapatero D, Peres-Bota D, Vincent JL, Berre' J, Melot C. Cerebral autoregulation is influenced by carbon dioxide levels in patients with septic shock. Neurocrit Care. 2010;12(1):35–42. https://doi.org/10.1007/s12028-009-9289-6.
3. Kofler M, Schiefecker A, Beer R, et al. Neuroglucopenia and metabolic distress in two patients with viral meningoencephalitis: a microdialysis study. Neurocrit Care. 2016;25(2):273–81. https://doi.org/10.1007/s12028-016-0272-8.
4. Møller K, Strauss GI, Thomsen G, et al. Cerebral blood flow, oxidative metabolism and cerebrovascular carbon dioxide reactivity in patients with acute bacterial meningitis. Acta Anaesthesiol Scand. 2002;46(5):567–78. https://doi.org/10.1034/j.1399-6576.2002.460515.x.
5. Merkelbach S, Müller M, Huber G, Schimrigk K. Alteration of cerebral blood flow in patients with bacterial and viral meningoencephalitis. AJNR Am J Neuroradiol. 1998;19(3):433–8.

6. Igarashi M, Gilmartin RC, Gerald B, Wilburn F, Jabbour JT. Cerebral arteritis and bacterial meningitis. Arch Neurol. 1984;41(5):531–5. https://doi.org/10.1001/archneur.1984.04050170077022.
7. Pfister HW, Koedel U, Haberl RL, et al. Microvascular changes during the early phase of experimental bacterial meningitis. J Cereb Blood Flow Metab. 1990;10(6):914–22. https://doi.org/10.1038/jcbfm.1990.148.
8. Förderreuther S, Tatsch K, Einhäupl KM, Pfister HW. Abnormalities of cerebral blood flow in the acute phase of bacterial meningitis in adults. J Neurol. 1992;239(8):431–6. https://doi.org/10.1007/bf00856807.
9. Davis DO, Dilenge D, Schlaepfer W. Arterial dilatation in purulent meningitis. Case report. J Neurosurg. 1970;32(1):112–5. https://doi.org/10.3171/jns.1970.32.1.0112.
10. Klein M, Koedel U, Pfefferkorn T, Zeller G, Woehrl B, Pfister HW. Arterial cerebrovascular complications in 94 adults with acute bacterial meningitis. Crit Care. 2011;15(6):R281. https://doi.org/10.1186/cc10565.
11. Rother, et al. Middle cerebral artery Stenoses: assessment by magnetic resonance angiography and transcranial Doppler ultrasound. Cerebrovasc Dis. 1994;4:273–9.
12. Ries S, Schminke U, Fassbender K, Daffertshofer M, Steinke W, Hennerici M. Cerebrovascular involvement in the acute phase of bacterial meningitis. J Neurol. 1997;244(1):51–5. https://doi.org/10.1007/s004150050050.
13. Fassbender K, Ries S, Schminke U, Schneider S, Hennerici M. Inflammatory cytokines in CSF in bacterial meningitis: association with altered blood flow velocities in basal cerebral arteries. J Neurol Neurosurg Psychiatry. 1996;61(1):57–61. https://doi.org/10.1136/jnnp.61.1.57.
14. Berg RM, Strauss GI, Tofteng F, et al. Circulating levels of vasoactive peptides in patients with acute bacterial meningitis. Intensive Care Med. 2009;35(9):1604–8. https://doi.org/10.1007/s00134-009-1515-3.
15. Møller K, Qvist T, Tofteng F, et al. Cerebral blood flow and metabolism during infusion of norepinephrine and propofol in patients with bacterial meningitis. Stroke. 2004;35(6):1333–9. https://doi.org/10.1161/01.STR.0000128418.17312.0e.
16. Haring HP, Rötzer HK, Reindl H, et al. Time course of cerebral blood flow velocity in central nervous system infections. A transcranial Doppler sonography study. Arch Neurol. 1993;50(1):98. https://doi.org/10.1001/archneur.1993.00540010092024.
17. Müller M, Merkelbach S, Hermes M, Schimrigk K. Transcranial Doppler sonography at the early stage of acute central nervous system infections in adults. Ultrasound Med Biol. 1996;22(2):173–8. https://doi.org/10.1016/0301-5629(95)02029-2.
18. Møller K, Skinhøj P, Knudsen GM, Larsen FS. Effect of short-term hyperventilation on cerebral blood flow autoregulation in patients with

acute bacterial meningitis. Stroke. 2000;31(5):1116–22. https://doi.org/10.1161/01.str.31.5.1116.

19. Raichle ME, Posner JB, Plum F. Cerebral blood flow during and after hyperventilation. Arch Neurol. 1970;23(5):394–403. https://doi.org/10.1001/archneur.1970.00480290014002.

TCD Equipment, Lab Accreditation, Reimbursement, and Practice Issues

Pam Young, Amanda K. Phillips, and Ryan Hakimi

Introduction

There are two types of non-invasive ultrasound used for intracranial vessel interrogation (TCD and TCCD). TCD is a non-invasive, portable, bedside tool for assessment of cerebral hemodynamics. With TCD, the sonographer must rely on the audible Doppler signal as well as the spectral waveform display. With TCCD, the sonographer can see the vessels with color Doppler and has the ability to angle correct. This visualization allows the sonographer to be sure which vessel they are insonating,

P. Young
Vascular Lab Services, Prisma Health–Upstate, Greenville, SC, USA
e-mail: pam.young@prismahealth.org

A. K. Phillips
Vascular Sonographer Sr., Vascular Lab, Prisma Health–Upstate, Greenville, SC, USA
e-mail: Amanda.phillips2@prismahealth.org

R. Hakimi (✉)
Neuro ICU and TCD Services Prisma Health-Upstate, Department of Medicine (Neurology) University of South Carolina School of Medicine-Greenville, Greenville, SC, USA
e-mail: ryan.hakimi@prismahealth.org

W. C. Ziai, C. L. Cornwell (eds.), *Neurovascular Sonography*,
https://doi.org/10.1007/978-3-030-96893-9_26

thereby eliminating the uncertainty of correct vessel insonation. As such, TCCD requires less training and technical skill than TCD. Once the exams are completed, both types of equipment should have the ability to send images directly into a picture archiving system (PACS). Serial examination is needed for subarachnoid hemorrhage patients as changes from day to day as well trends guide patient management. Therefore, TCD/TCCD must be made available seven days per week in order to provide optimal care. The most common study, the TCD/TCCD complete requires evaluation of the right and left anterior circulation by the transtemporal approach as well as the posterior circulation by the suboccipital approach which must include the vertebral and basilar arteries. There are a select group of indications for which TCD/TCCD is approved, and a specific indication must be listed in each study report. Ideally, every TCD/TCCD laboratory should be accredited by the Intersocietal Accreditation Commission, every sonographer within the lab be certified to perform TCD/TCCD via the NVS (Neurovascular Specialist) designation, and every interpreting physician should carry the RPNI credential from the American Society of Neuroimaging or its equivalent, to ensure accuracy, safety, and quality neuroimaging.

There are two types of non-invasive ultrasound used for intracranial vessel interrogation. The starting point for determining the equipment your transcranial Doppler ultrasound (TCD) laboratory will need is to determine whether you will be using non-imaging/blind TCD, herein referred to as TCD or imaging TCD herein referred to as TCCD (transcranial color coded duplex)/transcranial color coded sonography). From a cost perspective, which type of system (TCD vs TCCD) depends on the type of existing equipment the laboratory has and whether there is availability to use the equipment.

TCD

TCD is a non-invasive, portable, bedside tool for assessment of cerebral hemodynamics [1]. With TCD, the sonographer must rely on the audible Doppler signal as well as the spectral waveform display. The presence of power-motion mode (PMD) allows

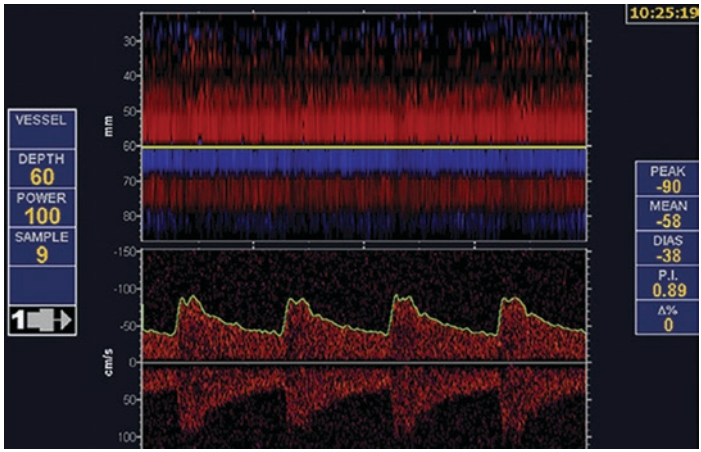

Fig. 1 Normal TCD signals on Power M-Mode screen: middle cerebral artery (MCA) (red: 40–60 mm), anterior cerebral artery (ACA) (blue: 60–70 mm), contralateral ACA (red: 70–80 mm), and contralateral MCA (blue: 80–90 mm). (*From* Hakimi R, Alexandrov AV, Garami Z. Neuroultrasonography. Neurol Clin. 2020 Feb;38(1):215–229; with permission)

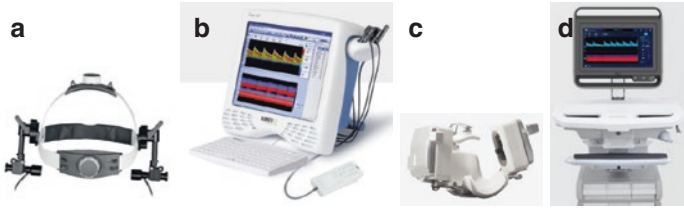

Fig. 2 From https://rimed.com/products/auto-track/. Accessed September 21, 2020. (**a**, **b**). From: https://novasignal.com/solutions/lucid-tcd/. Accessed September 21, 2020. (**c**, **d**)

the spectral waveforms to represent the depth, direction, and intensity of the blood flow through the intracranial vasculature (Fig. 1).

There are several TCD manufacturers who typically provide two 2 MHz Doppler probes and a headframe allowing the operator to affix two probes for bilateral continuous insonation in a hands-free fashion. Some examples are shown in Fig. 2.

The blind TCD equipment is much smaller than the imaging equipment and costs thousands of dollars less. The equipment is easier to move and maneuver when used for portable exams. However, one disadvantage is that greater training and skill is required as the sonographer has to depend on the coordinated movements of the probe, assessing the audible signal, and analyzing the waveform morphology in one synchronous process.

TCCD

The second type of non-invasive ultrasound used to evaluate the vessels of the brain is TCCD. With this type of testing, the sonographer uses an ultrasound cart that can also be used for other vascular ultrasound testing. This test and equipment is usually deemed easier by the sonographer as most sonographers have experience using this equipment for other studies such as echocardiography, peripheral vascular ultrasound, and carotid duplex imaging. In addition, most medical facilities already have this equipment and thus only have to purchase a software package or separate probe to be able to perform these studies. The total TCCD equipment cost can be in excess of $100,000. The equipment is also bigger and is difficult to maneuver into small spaces such as the emergency department or in most ICUs.

With TCCD, the sonographer can see the vessels with color Doppler and has the ability to angle correct. This visualization allows the sonographer to be sure which vessel they are insonating. As such, TCCD requires less training and technical skill than TCD. In contrast to the TCD exam, the TCCD exam does not allow for continuous monitoring as to date there are no existing headframes for TCCD thereby essentially precluding its use for emboli detection or intraoperative monitoring.

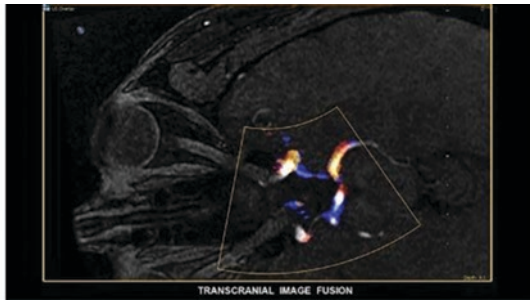

1. From: https://www.usa.philips.com/healthcare/solutions/ultrasound/all-ultrasound-products#filters=FG_HC_US_SYSTEM%3AShow%20All%2CFG_HC_US_CLINICAL_SEGMENT%3AFK_HC_US_INTERVENTIONAL_RADIOLOGY. Accessed September 22, 2020.
2. From: https://www.usa.philips.com/healthcare/resources/landing/ultrasound-article-pages/interventional-radiology. Accessed September 22, 2020.

Image Storage and Retrieval

Once the exams are completed, both types of equipment should have the ability to send images directly into a picture archiving system (PACS). There are many different PACS systems to choose from which allow for image review from multiple locations. This makes it very convenient for physicians and other medical staff to review images quickly and communicate the report to the ordering provider. In some cases, physicians can see the PACS images remotely while off-campus. All worksheets and images showing the waveform analyses should be stored in a PACS system for easy retrieval and comparison study review with any future exams. In addition, it is incumbent on the laboratory to be able to produce not only the interpretation reports but also the raw images for accreditation bodies and insurance carriers during (re)accreditation or audits, respectively.

Reporting

For consistent and organized reporting, consider a structured reporting software system. Some manufacturers provide this with their equipment, while others choose to utilize the reporting structure of their electronic medical record system. This type of software allows standardized reporting with consistent and clear reports. Reports can be created by selecting from a set of preprogrammed report statements that coordinate with the diagnostic criteria for each vessel. Structured reporting also allows a chart to be inserted into the report that lists all velocities making it quicker and easier for the interpreting physician to review the study. These structured reports also ensure compliance with the Intersocietal Accreditation Commission (IAC) guidelines [2].

Examination

The TCD exams generally take between 30 minutes to one hour to perform. Schedulers should also account for the time that it takes for the sonographer to verify all images are in the PACS system and a preliminary structured report has been completed. If the sonographer is scheduled to work an eight-hour day, one should expect approximately seven complete TCD exams to be completed during that time frame. Most providers prefer that TCD exams be performed in the early morning hours. For inpatients, this allows treating teams the opportunity to make treatment decisions based on the findings of the study, while also allowing enough time for the patient to be sent for additional studies or procedures that may be needed.

For many patients, serial examination is needed. Such is the case for subarachnoid hemorrhage patients. In such patients changes from day to day as well as trends guide patient management decisions as opposed to isolated mean flow velocity measurements. Therefore, TCD/TCCD must be made available seven days per week in order to provide optimal care [1, 3].

Accreditation

In the United States, the Intersocietal Accreditation Commission (IAC) offers standards and guidelines for vascular and neuroimaging labs [2]. Guidelines provide requirements including the credentials of the imaging and interpreting personnel, the extent of supervision including proper training, experience and continuing medical education (CME); facility and facility safety requirements including transducer cleaning, control of infectious disease, as well as staff safety which includes information on avoidance of work-related musculoskeletal disorders.

Information must also include policies on patient confidentiality, patient complaints, and primary source verification; multiple site labs, examinations and procedures; examination reports and records. IAC requires written protocols for the vascular lab regarding equipment, testing procedure protocols, and documentation. Written protocols must be in place at each facility for equipment, technique, complete versus limited exams, anterior and posterior circulation, technique including power reduction for transorbital exams, and documentation.

A medical director must be properly trained and credentialed for interpretation with the Registered Physician Vascular Interpretation (RPVI) credential or the Registered Physician in Neurovascular Interpretation (RNPI) certification from the American Society of Neuroimaging if interpreting *only* extracranial and intracranial examinations. The medical director must maintain a minimum of fifteen relevant Category 1 continuing medical education credits (CME's) for every three years.

The technical director and other sonographers are required to be a Registered Vascular Technologist (RVT), Registered Vascular Specialist (RVS), Registered Technologist Vascular Sonography [RT(VS)], or a Neurovascular Specialist (NVS) from the American Society of Neuroimaging for extracranial and intracranial testing only. Fifteen relevant CME's every three years must be obtained for each individual. The technical director has the additional responsibility for the daily operations including but not limited to quality, technical training, and compliance to IAC standards.

The equipment used for intracranial evaluation must be appropriate for the intracranial vessels including but not limited to proper frequencies, audible feedback and visual display. It must be able to differentiate bi-directional flow and the visual display should be saved as a permanent record of the examination. Equipment upkeep must be maintained with records including routine cleaning, safety inspections, as well as any needed validation of automated software packages.

Facility specific protocols determine the proper technique with support of published criteria when available. Protocols should include information about patient positioning and preparation, transducer selection and positioning, and appropriate sample volume size, depth, and positioning. The protocol should discuss proper identification of vessels, spectral Doppler angle, and spectral velocity measurements. Supplemental imaging such as color Doppler and power Doppler will require a description of use. Abnormalities found require additional documentation. Each type of examination must have a separate written protocol (complete TCD, emboli detection, vasomotor reactivity, etc.).

The facility specific protocol determines the vessels insonated with a minimum of proximal M1, A1, terminal ICA (TICA), P1 or P2, carotid siphon, terminal VA, proximal and distal basilar artery. When appropriate, the ophthalmic artery and distal ICA at the skull base should also be interrogated. When detectable, cross filling via the anterior communicating artery or the posterior communicating artery should be evaluated.

The final report must include the exam performed, exam indication, performing sonographer, exam findings and physician interpretation. Interpretation must include spectral Doppler waveforms and velocity, as well as grayscale and color Doppler if used. When abnormal findings are present, documentation must include the severity, location, extent, and etiology when possible. The diagnostic criteria can be formed from published criteria or internally-validated results. The study and report should be retained for 5–7 years, based on federal guidelines, and therefore should be a form of media suitable for long-term storage.

Reimbursement

Each study has an associated technical fee and a professional fee [4]. Each institution will need to work with their local Medicare carrier and third-party providers to determine the appropriate charge for each study as they vary widely from region to region. In addition, there are other variables which impact reimbursement including the TCD being part of a global procedure fee, being part of the diagnostic related group (DRG) for inpatient care, etc. There are currently five Current Procedural Terminology (CPT) codes that are reimbursable [4, 5] which are listed in Table 1.

The most common study, the TCD complete requires evaluation of the right and left anterior circulation by the transtemporal approach as well as the posterior circulation by the suboccipital approach which must include the vertebral and basilar arteries. Each study must list at minimum the depth, mean flow velocity, and pulsatility index for each of the insonated vessels as well as the Lindegaard Ratio for the right and left anterior circulation [5] which are listed in Table 2.

Table 1 TCD/TCCD CPT Codes

CPT Code	Study Name
93886	TCD intracranial, complete
93888	TCD intracranial, limited
93890	Vasoreactivity study
93892	Embolus detection without bubbles
93893	Embolus detection with bubbles

Table 2 Common components of a complete TCD/TCCD study

Right	Left	Basilar
Vertebral artery	Vertebral artery	
M1	M1	Proximal
M2	M2	Mid
ACA	ACA	Distal
TICA	TICA	
PCA	PCA	
Carotid siphon	Carotid siphon	
Ophthalmic artery	Ophthalmic artery	
Extracranial ICA	Extracranial ICA	

It is important to note that if all of the components of a complete study are attempted, but not successfully insonated, the study can still be designated as a complete study. However, in such a case, the sonographer must document that all of the vascular segments necessary for a complete study were attempted, to indicate which vessels were not successfully insonated, and why.

In contrast, if any of the components of a complete study were not attempted, the study will be designated as a limited TCD and should be billed as such [5].

Each study must list the indication for the study. Common indications for TCD are listed in Table 3 [5].

Table 3 Approved indications for TCD/TCCD

Assessing collateral blood flow and embolization during carotid endarterectomy
Assessing patterns and extent of collateral circulation in persons with known regions of severe stenosis or occlusion, including persons with Moya Moya syndrome
Assessing persons suspected of having patent foramen ovale/paradoxical embolism (symptoms include visual disturbance, weakness, hemiplegia, or slurred speech)
Assessing persons with suspected brain death
Assessing stroke risk of children (2 to 16 years of age) with sickle cell anemia (although the optimal time is unknown, accepted guidelines state that re-screening should be considered approximately every 6 months)
Detecting arterio-venous malformations (AVMs) and studying their supply arteries and flow patterns
Detecting noncardiac right-to-left shunts
Detecting microemboli in cerebral artery embolism
Detecting severe stenosis in the major basal intra-cranial arteries for patients who have neurological signs or symptoms or carotid bruits
Diagnosing and monitoring of reversible cerebral vasoconstriction syndrome
Diagnosing dissection of vertebral artery
Evaluating and following persons with vasoconstriction of any cause, especially after subarachnoid hemorrhage
Evaluating very low birth weight preterm infants with gestational age less than 30 weeks

Table 4 wRVUs for each TCD/TCCD study

CPT Code	Study Name	wRVU
93886	TCD intracranial, complete	0.91
93888	TCD intracranial, limited	0.50
93890	Vasoreactivity study	1.00
93892	Embolus detection without bubbles	1.15
93893	Embolus detection with bubbles	1.15

In many practices, physician productivity is tracked through work relative value units (wRVUs), wherein each task a physician performs has an associated wRVU, the sum of which is used to track their productivity on a monthly, quarterly or annual basis. The wRVUs for each TCD/TCCD study are listed in the Table 4 below [6].

Certification of Interpreting Physicians

The American Society of Neuroimaging offers certification of physicians in TCD through the RPNI (Registered Physician in Neurovascular Interpretation) credential. To be eligible, a physician must be certified in their primary specialty, have the requisite CME in TCD or have recently graduated from a fellowship program where the program director is able to provide a letter certifying that the physician was exposed to TCD interpretation during their training, and pass both the ultrasound physics and the TCD portions of the neurosonology examination [7]. One additional certifying body for physicians is the American Registry for Diagnostic Medical Sonography (ARDMS) [8].

Conclusions

TCD/TCCD allow for non-invasive intracranial vascular imaging. The choice between the two systems is dependent on a number of variables unique to each institution. Safety and quality are best ensured by having a laboratory accredited by the IAC, having

every sonographer within the lab be certified to perform TCD/TCCD via the NVS (Neurovascular Specialist) designation, and every interpreting physician carry the RPNI credential from the American Society of Neuroimaging or its equivalent, to ensure accuracy, safety, and quality neuroimaging.

References

1. Hakimi R, Alexandrov AV, Garami Z. Neuro-ultrasonography. Neurol Clin. 2020;38(1):215–29.
2. Available at: https://www.intersocietal.org/vascular. Accessed 21 Sept 2020.
3. Kumar G, et al. Vasospasm on transcranial Doppler is predictive of delayed cerebral ischemia in aneurysmal subarachnoid hemorrhage: a systematic review and meta-analysis. J Neurosurg. 2016;124(5):1257–64.
4. Available at: https://clarius.com/wp-content/uploads/2020/04/CPT-2020-MKTG-00084-Rev-3.pdf. Accessed 22 Sept 2020.
5. Available at: http://www.aetna.com/cpb/medical/data/300_399/0353.html. Accessed 21 Sept 2020.
6. Available at: https://www.aan.com/siteassets/home-page/tools-and-resources/practicing-neurologist%2D%2Dadministrators/billing-and-coding/medicare-fee-for-service/18medicarevalues_tr.pdf. Accessed 21 Sept 2020.
7. Accessed at: https://www.asnweb.org/i4a/pages/index.cfm?pageid=3309. Accessed 22 Sept 2020.
8. Accessed at: https://www.ardms.org/get-certified/. 22 Sept 2020.

Use of Transcranial Doppler in the Outpatient Ultrasound Lab

Richard Genova

Abbreviations

ACA	Anterior cerebral artery
AD	Alzheimer's Disease
BA	Basilar artery
Carotid duplex	A type of ultrasound study with standardized protocol and diagnostic criteria
CAS	Carotid artery stent
CBF	Cerebral blood flow
CEA	Carotid endarterectomy
CTA	Computed tomography angiography
ESUS	Embolic Stroke of Undetermined Source
IAC	Intersocietal Accreditation Commission
ICA	Internal carotid artery
JVU	Journal for Vascular Ultrasound published by the SVU
MCA	Middle cerebral artery

R. Genova (✉)
Neurovascular Ultrasound Laboratory, Weill Cornell Medicine—New York Presbyterian Hospital, New York, NY, USA
e-mail: rig7007@med.cornell.edu

W. C. Ziai, C. L. Cornwell (eds.), *Neurovascular Sonography*,
https://doi.org/10.1007/978-3-030-96893-9_27

MOST-CA	Mechanisms of Ischemic Stroke In Patients with Cancer (NCT02604667)
MRA	Magnetic resonance angiography
NINDS	National Institute of Neurological Disorders and Stroke
NVUL	Neurovascular ultrasound lab
OA	Ophthalmic artery
PCA	Posterior cerebral artery
SRUCC	Society of Radiologists in Ultrasound
STOP	Stroke Prevention Trial in Sickle Cell Anemia
SVM	Society for Vascular Medicine
SVU	Society for Vascular Technology
TCD	Transcranial Doppler
TIA	Transient ischemic attack
t-ICA	Terminal internal carotid artery aka distal internal carotid artery [non-cervical]
TOAST	Trial of ORG 10172 in Acute Stroke Treatment
TTW	Transtemporal window
VA	Vertebral artery
VaD	Vascular dementia
VCI	Vascular cognitive impairment
VMJ	Vascular Medicine Journal
WML	White matter lesions

The outpatient neurovascular ultrasound lab (NVUL) must be an integral component for secondary stroke prevention by the vascular neurology service and stroke clinicians. In addition, prevention of first-ever stroke is also part of the NVUL's mission. A special category of patients for TCD exams to prevent first-ever stroke are pediatric sickle cell patients. Almost 25 years ago, The Stroke Prevention Trial in Sickle Cell Anemia (STOP), led by Dr. Robert Adams, demonstrated how to reduce first-time stroke in children with sickle cell anemia by 70% through the administration of prophylactic transfusion therapy [1]. The study design was based on the clinical observation that if hemoglobin S (HbS) levels are maintained at or below 30% in children who have had a

stroke, the incidence of recurrence can be reduced from 80% to approximately 10% with periodic exchange or simple transfusions.

Subsequently, the 2002 NIH recommendations and 2014 consensus experts panel's guidelines called for annual TCD screening for children with sickle cell disease [2, 3]. The clinical screening of those pediatric sickle cell carriers at highest risk of stroke is done with a modified TCD complete protocol that any competent neurosonologist can learn quickly. Almost always, these pediatric patients have transtemporal acoustic windows that are easily insonated. (Pearl: Don't settle for the first great window that you find, because these pediatric patients often have multiple easily found transtemporal windows; be sure to find the TTW with the highest velocity.) Ensure that your lab is in contact with pediatrics and hematology departments to get all pediatric sickle cell patients referred for annual TCD screenings [3–5] (see chapter "Applications of Transcranial Doppler Ultrasonography in Sickle Cell Disease, Stroke, and Critical Illness in Children").

The use of STOP screening protocols for all potential pediatric stroke victims was promoted in a *New York Times* (*NYT*) article in May 2021 which shared a distressing story about missed opportunities to prevent two sisters' devastating pediatric strokes and the simple, painless test that could be preventative [6].

Not infrequently, adult patients at high risk for first-time stroke are seen in the NVUL whose risk factors were discovered incidentally. The NVUL is therefore an important factor in primary stroke prevention for adults, too. The ability of the competent neurosonologist to perform both extracranial and intracranial exams for these patients is another strength of the outpatient NVUL combining evaluation of extracranial and intracranial hemodynamics and detection of spontaneous microemboli reaching the cerebral vasculature.

Moreover, the use of TCD in peripheral vascular labs that perform carotid duplex exams on patients who appear with (or without) symptoms for cerebral ischemia can be extremely valuable to resolve discrepancies between carotid duplex, cerebral angiography and presenting symptoms [7]. Of note, in early 2021, the U.S. Preventive Services Task Force (USPSTF) updated its 2014 recommendation against general population screening for carotid

artery stenosis in patients without prior stroke or ischemic attack. Among the key points in the update is a warning that although carotid duplex screening itself does not impart harm, subsequent testing and interventions can lead to harm, including excess risk for stroke or death [8].

TCD in the Dedicated Neurovascular Ultrasound Lab

There are estimated to be less than three dozen Intersocietal Accreditation Commission (IAC) accredited and dedicated NVULs in the United States[1]. In a typical lab, many of the patients presenting for exams are transient ischemic attack (TIA) and stroke survivors faring relatively well, but needing regular surveillance. Another large subset of these patients has had a so-called "cryptogenic stroke" and neurovascular specialists are trying to determine the best methods of surveillance and secondary stroke prevention.

There are also individuals who are at high risk of stroke with their risk discovered incidentally during another encounter with the healthcare system. Embolic strokes and TIAs are not the only concern. Full TCD complete diagnostic exams are done for patients with vasculitis and reversible cerebral vasoconstriction syndrome (RCVS) among outpatients as well. The author's lab is part of an academic medical center and the affiliated hospital is a comprehensive stroke center that must have TCD and carotid duplex imaging available; therefore many outpatients have had hospital stays previously and will have TCD and carotid duplex exams available for comparison. This means the outpatient neuro-

[1]Information supplied by the marketing department of the IAC in February 2019 in a private communication with this author. The IAC identified 32 sites that were dual accredited in extracranial and intracranial vascular testing but only in those two peripheral vascular modalities. The number of NVULs did not change during the past year (March 2020 – June 2021) of COVID-19 pandemic that depressed outpatient services across the board. In June 2021, the IAC marketing department confirmed that the number of sites had decreased by only one, to 31 sites [9, 10].

vascular lab should have easy access to the patient's full medical and relevant clinical history.

Despite the small number of accredited and dedicated outpatient NVULs that currently exist, there is a growing need for neurosonologists who can perform quality carotid duplex and TCD exams on all of these types of patients. The American Society of Neuroimaging (ASN) has a new Neurovascular Specialist (NVS) certification available for those candidates who demonstrate competency knowledge and have acquired the skill set for performing high-quality carotid duplex and TCD exams (see the certification chapter by Bennett, Rinsky and Douville). The Society for Vascular Ultrasound has commendably taken some initiatives to encourage more registered vascular technologists (RVTs) to acquire good TCD exam skills. Other chapters in this handbook describe and explain how to build a NVUL equipped with non-imaging and/or imaging TCD and ultrasound machines with the appropriate ultrasound transducers and how to start the process for IAC accreditation.

An Indispensable Tool for Clinical and Academic Medical Center Research

Whether the patient is in the lab for prevention of first-ever stroke or is there for follow-up on a chronic condition, the neurosonologist is using technology that is noninvasive and uniquely can provide calibrated prognostic information that can determine the true extent of the ischemic disease and the proper course of treatment (if one exists). So, what do these cases look like? How are spectral Doppler parameters and waveform morphology applied to diagnose and treat outpatients for secondary stroke prevention? What are some of the particular collateral pathways of compensation in the setting of a cervical or an intracranial stenosis that increase the odds of a stroke or ischemic compromise of brain perfusion?

Always start with the A&P—anatomy and physiology. The well-known stroke clinicians David Liebeskind, MD and Louis Caplan, MD explain: "As each imaging modality provides a

depiction that combines anatomy and flow physiology, it is important to interpret each image with a solid understanding of typical arterial anatomy and corresponding collateral routes. Compensatory collateral perfusion and downstream flow status have recently emerged as pivotal variables in the clinical management of patients with atherosclerosis" [11].

The four major pathways that have been identified and have developed TCD exam criteria to identify the collateral or compensatory flow channels in ischemic stroke and chronic impaired brain perfusion cases are (1) collateral flow via the Circle of Willis; (2) reversed ophthalmic artery flow; (3) reversed vertebrobasilar flow; and (4) leptomeningeal collaterals in middle cerebral artery occlusions. These are all discussed in several other chapters of this handbook as well.

Here is the case of patient A, who has been followed for secondary stroke prevention starting 5 years ago in 2016, when A was first diagnosed with a TIA (see Figs. 1, 2, 3, 4, and 5).

On XX/XX/2016, A was getting ready for work and noticed that A's right hand felt numb, A could not hold a cup. Also noted right

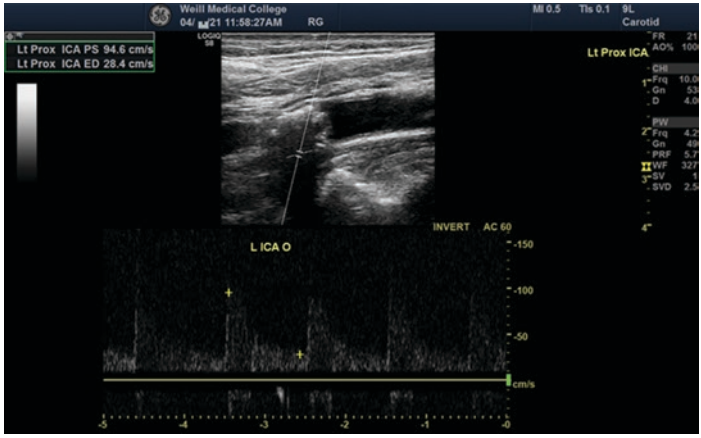

Fig. 1 Left ICA, proximal to the dampened flow squeezing through in the right image (Fig. 2)

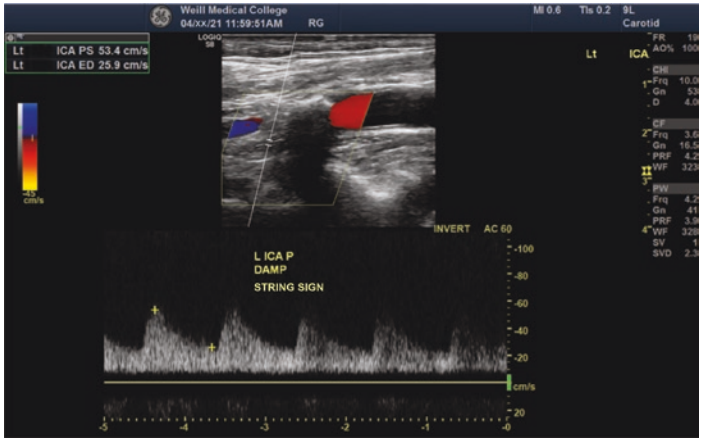

Fig. 2 CTA confirmed that this flow was consistent with a string sign. CEA is planned

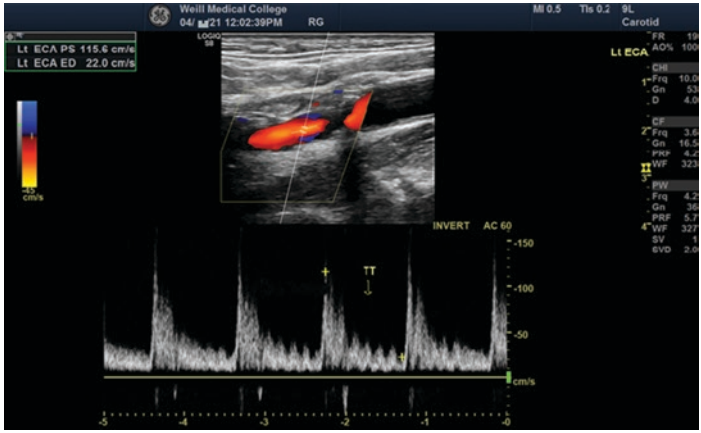

Fig. 3 Temporal Tap (TT) in the left ECA helps to confirm correct anatomical notation (however, it's not definitive evidence because there are reports of TTs reflected in true ICAs)

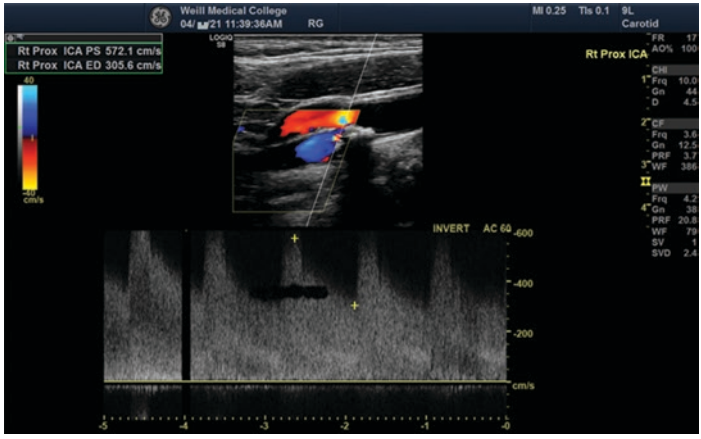

Fig. 4 This severe stenosis (70–99%) in the right ICA is contralateral to the left sided string sign ICA. It is graded >70% with the SRU 2003 Consensus Criteria, but it obviously doesn't matter whether the PSV was 500 or 600 cm/s to know that this is a hemodynamically severe stenosis

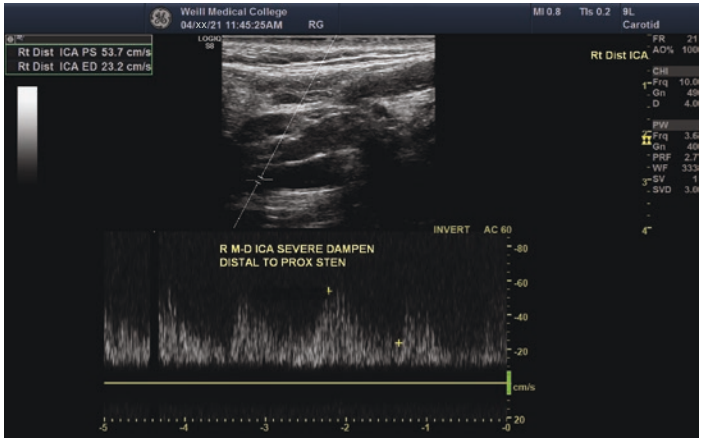

Fig. 5 If somehow the high-grade focal stenosis was missed initially during the scan, but the sonographer later saw this waveform, it should suggest investigating to find the proximal source of this dampened waveform

facial numbness and a right facial droop when looking in the mirror. A called 911 and was taken to Hospital X. Symptoms resolved in 10–15 minutes on their own, A was diagnosed with a TIA and found to have 100% blockage of the left carotid and 80% blockage of the right. A was transferred to Hospital Y and found to have a small left precentral gyrus acute stroke. At first, the plan was to place a left ICA stent but then it was found to be completely occluded and they decided to continue maximal medical management. A was discharged and is currently taking Atorvastatin 80 mg, Aspirin 81 mg and Plavix 75 mg.

A has been on a regimen of medical management since the 2016 TIA. As a patient in the outpatient lab, A's vascular neurologist is focused on secondary stroke prevention and has followed up with A by regularly scheduling same-day carotid duplexes, non-imaging complete TCD exams and TCD monitoring for spontaneous microemboli during A's office visits with the care team. A's carotid duplex exams and TCD exams provide evidence of the existence of two of the four major collateral flow pathways for adequate brain perfusion. From the final TCD and carotid duplex reports in 2021 before a planned surgical intervention:

The final carotid duplex report using Society of Radiologists in Ultrasound 2003 Consensus Criteria (SRUCC) velocity criteria, plaque morphology and clinical medical history stated that "The left internal carotid artery has abnormal dampened flow consistent with a severe stenosis or near occlusion. The right internal carotid artery has heterogeneous plaque producing a 70–99% proximal stenosis" (see Figs. 4 and 5).

At the time of this writing, two major papers have appeared that affect clinical interpretations of carotid duplex exams for diagnosing and reporting of carotid stenosis. First, in July 2020, two clinical vascular societies, the Society for Vascular Medicine (SVM) and the Society for Vascular Ultrasound (SVU), jointly published the first consensus-based nomenclature for arterial and venous waveforms in their respective journals, *Vascular Medicine* (*VMJ*) and the *Journal for Vascular Ultrasound* (*JVU*). The primary intent of this consensus statement was to "improve

communication amongst all practitioners who care for vascular patients" [12].

In addition to proposed standardized nomenclature, this consensus statement produced a comprehensive document with many examples of waveforms to illustrate the use of standardized terminology and to help implement the findings in clinical practice. Although the SVU/SVM document includes guidance for extracranial vascular sonography and hemodynamics, there is no guidance for intracranial sonography because the intracranial vasculature system was recognized as qualitatively different from the rest of the periphery and required a separate treatment.

Second, in May 2021, the IAC commissioned research (2014) into optimizing duplex velocity criteria for diagnosis of internal carotid artery stenosis. This was published in the SVM journal and offers important discussion and changes for those labs using the SRUCC for their lab reports and diagnostic interpretations. Importantly, this document reported that "use of SRUCC overestimated the degree of ICA stenosis and identified potential opportunities for modifications that can enable greater accuracy and consistency in ICA interpretation across vascular laboratories" [13, 14].

Their conclusion was that "laboratories currently using SRU Consensus Criteria should consider modification of existing criteria to incorporate more stringent and accurate parameters for ICA stenosis greater than 50% by increasing the peak systolic velocity (PSV) threshold to ≥180 cm/s or requiring the ICA/CCA PSV ratio 2.0 in addition to PSV of ≥125 cm/s." The IAC Vascular Testing group promised to disseminate a white paper summarizing the study results and providing guidance to vascular laboratories for implementation of criteria and further steps toward standardization across the vascular testing community. By the time this handbook is published it is likely that the planned IAC white paper will have appeared. These two research papers together are highly important and should be discussed and incorporated into the outpatient NVUL's work.

A's TCD Narrative

TCD Summary Findings (see Figs. 6, 7, 8, 9, 10, 11, 12, and 13)**:**

1. There is evidence of a >50% stenosis of the right middle cerebral artery (>100 cm/s).
2. There is evidence of narrowing (possibly severe) for the left middle cerebral artery.
3. There is evidence of narrowing for the terminal ICAs bilaterally (>70 cm/s).
4. There is evidence of narrowing for the right anterior cerebral artery (>80 cm/s).
5. There is evidence of a >50% stenosis of the left vertebral artery (>80 cm/s).
6. There is evidence of a >50% stenosis of the basilar artery (>80 cm/s).

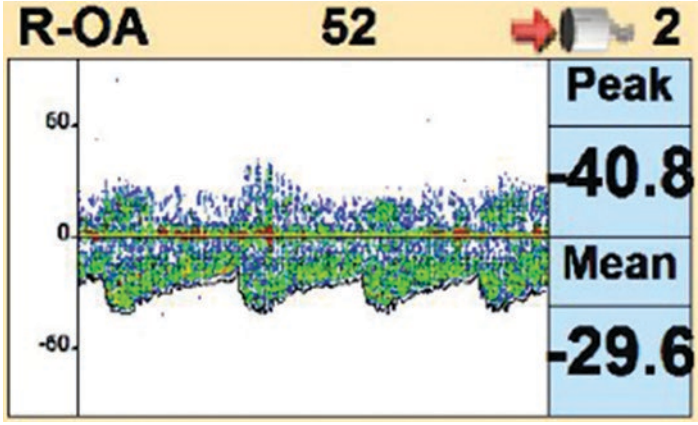

Fig. 6 Both ophthalmic arteries have bi-directional flow with a strong retrograde component

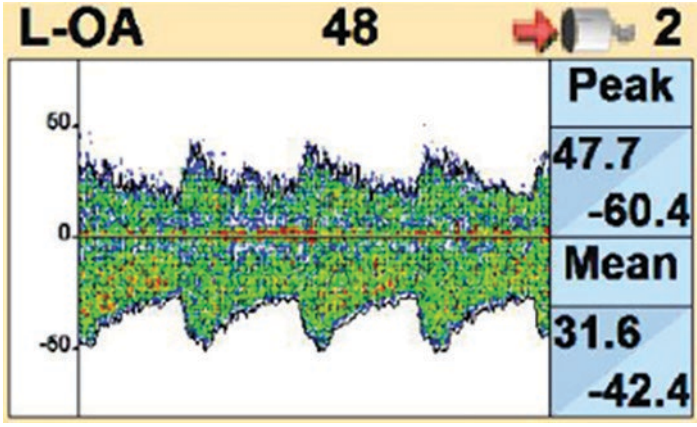

Fig. 7 The carotid duplex exam revealed that both cervical ICAs have severe proximal stenosis

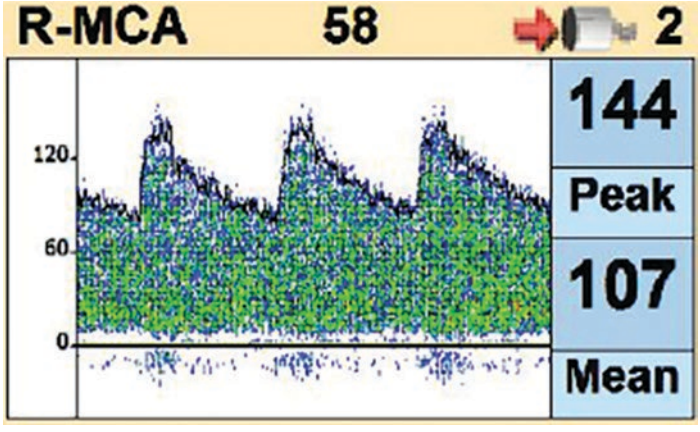

Fig. 8 The right cervical ICA has a >70% proximal stenosis and the left ICA has a string sign. The mean flow velocity is elevated in the right middle cerebral artery (>100 cm/s) consistent with a >50% stenosis. N.B. Imaging TCD uses a different scale of velocity criteria

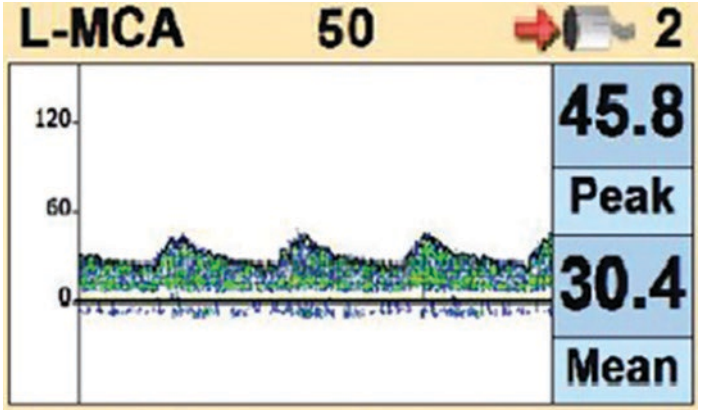

Fig. 9 Quite a significant variation from the right MCA

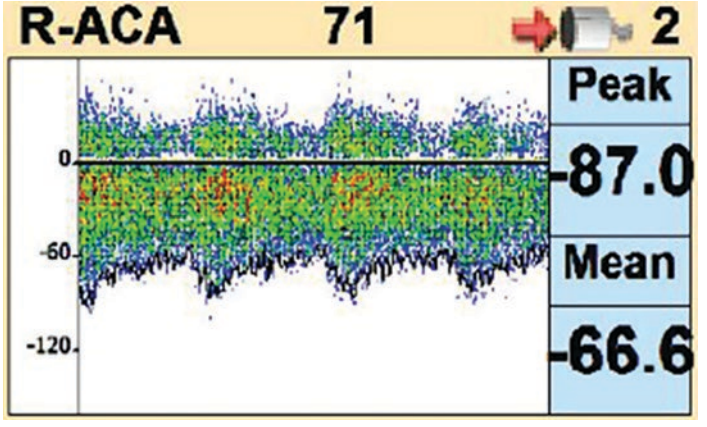

Fig. 10 Turbulent flow and "spectral bruits" in right ACA

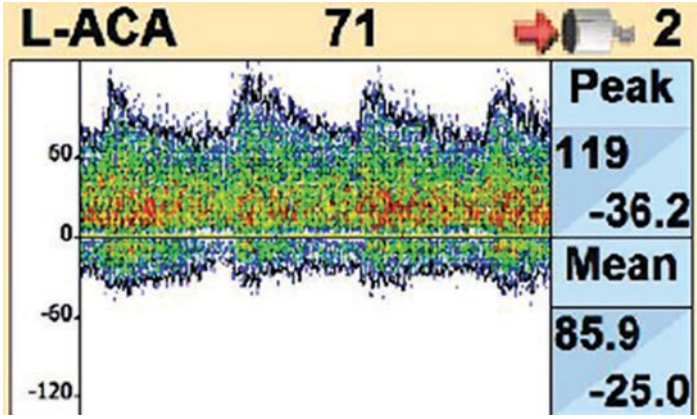

Fig. 11 Notice the flow reversal in the left ACA

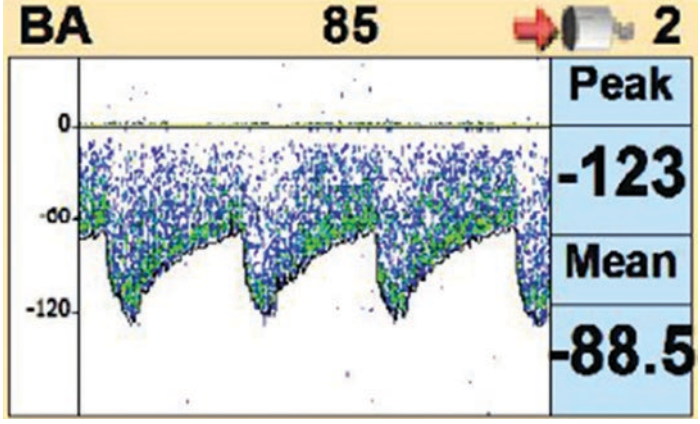

Fig. 12 The CTA also confirmed stenosis in the posterior circulation

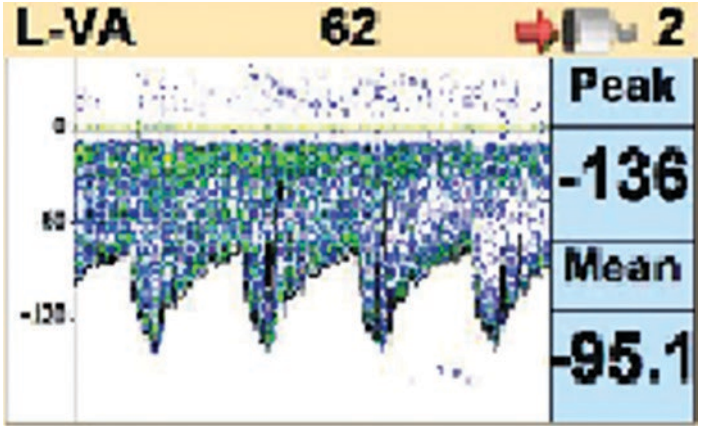

Fig. 13 The mean flow velocities are highly elevated in the left vertebral and basilar arteries

TCD Reading Physician Interpretation (see Figs. 6, 7, 8, 9, 10, 11, 12, and 13):

1. There is evidence for anterior intracranial stenoses of the middle cerebral arteries, the terminal internal carotid arteries, and the posterior intracranial stenoses in the left vertebral and basilar arteries.
2. The increased velocities in the left VA and the BA though could also be explained in part by collateral flow from the posterior to the anterior circulation in this patient with severe bilateral cervical carotid disease.
3. Increased MFV in the right anterior cerebral artery could reflect narrowing of the artery but could also reflect abnormal collateral flow.
4. Dampened waveforms in the left middle cerebral artery and in the left anterior cerebral artery likely reflect the severe bilateral cervical ICA stenoses.

5. Retrograde flow in the OAs reflect abnormal collateral flow from the external carotid arteries to the cervical internal carotid arteries in the patient with severe ICA stenoses bilaterally.

   Reviewed and Interpreted by Attending Physician: Dr. X, MD, RPNI

   Date Signed: xx/xx/2021

Here is the edited narrative from A's xx/xx/2021 visit with a neurosurgeon who confirmed the results of A's most recent NVUL visit and exams in xx/xx/2021:

> CTA [xx/xx/2021 post-carotid duplex and TCD exams] demonstrates a tight left ICA (string sign). Dr. X [A's vascular neurologist] is recommending A have a left CEA prior to lung surgery.
>
> Serial vessel wall imaging (CTA) indicates progressive stenosis on the right side which is now greater than 90% and severe stenosis on the left with a string sign. Physical exam currently is relatively unremarkable. The plaque on both sides is very calcified and circumferential. Thus, A is not an excellent stent candidate. Moreover, the thoracic surgeons want to proceed with resection of A's lung mass and placement of stents [which] would require anticoagulation and thereby hold up surgical intervention.
>
> I discussed the case with Dr. X and we agreed that initially a left carotid endarterectomy should be performed as that was A's symptomatic side and A still has a string sign. Subsequently, a week or so later we would perform a right carotid endarterectomy given the degree of severe stenosis.

ESUS and Cryptogenic Stroke

Although most strokes are ischemic, up to a third of these ischemic strokes do not have a known cause after a standard evaluation. Cryptogenic stroke is the term for a category of ischemic stroke for which a thorough diagnostic evaluation could not find a probable cause. The National Institute of Neurological Disorders and Stroke (NINDS) Stroke Data Bank research and the TOAST trial led clinicians to start using the term in clinical practice as

they work to find the optimal management strategy related to their patient's underlying stroke mechanism. In 2014 the term "embolic stroke of undetermined source" (ESUS) was coined to replace the term "cryptogenic stroke." Since 2014, hundreds of published studies have appeared to try to shed light on the underlying mechanisms of ESUS, its natural history and secondary prevention of an embolic stroke. It is now realized that there may be multifactorial occult embolic mechanisms in play, confounding treatment strategies based on antiplatelet and/or anticoagulation therapies [15, 16].

A *Journal of the American College of Cardiology* review article by Dr. George Ntaios, MD, PhD in 2020 laid out the importance of the neurovascular imaging modalities for this future research. It's fair to predict that much of this research should take place in the outpatient lab. He noted, "The high prevalence of ESUS patients, the considerable stroke risk, the availability of sophisticated diagnostic modalities, the establishment of novel antithrombotic strategies (like the combination of low-dose rivaroxaban/aspirin), and the development of novel classes of oral anticoagulants (like the FXIa inhibitors) highlight ESUS as an important priority in stroke research in the coming years" [17]. In particular, the embolic detection capability of TCD (see Fig. 14) makes it an important research and clinical tool in unraveling ESUS and finding effective treatments and prophylactic stroke prevention.

The prevalence of the two major modern killers worldwide, cancer and stroke—while individually bad enough for those afflicted patients—dually affect many patients with both active cancer and an acute or recurrent stroke. This too is an important research frontier for the outpatient lab that is now a part of broader work to better understand and treat all ESUS subgroups. The MOST-Cancer Trial (NCT02604667) ended in 2020 and the results and discussion appeared in June 2021 in the *Annals of Neurology* [18]. An outpatient NVUL performed the TCD microemboli detection studies cited for this prospective cross-sectional study, which ran from 2016 to 2020 at two hospitals (n = 150 with three groups of 50 adult participants).

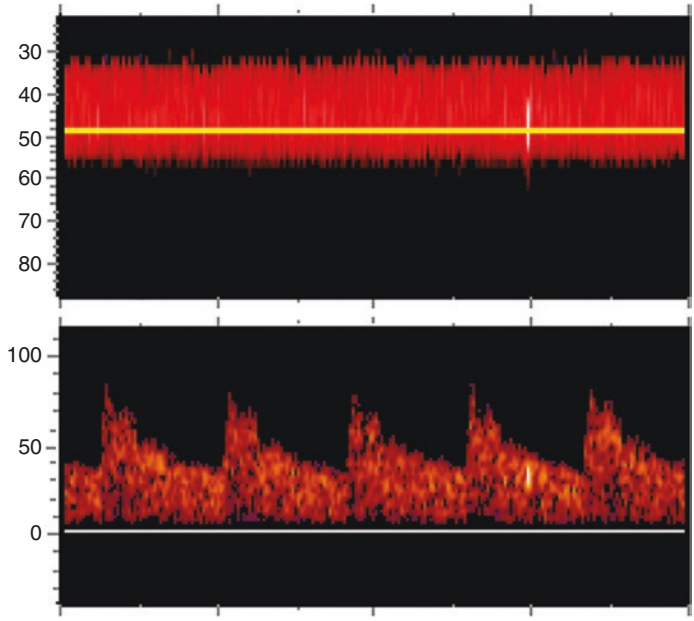

Fig. 14 An example of a HITS (high intensity transient signal) with transcranial Doppler from the MOST-Cancer Trial. (With permission of author)

MOST-Cancer researchers found that "Transcranial Doppler microemboli were detected in 32% of patients with cancer-plus-stroke, 16% of patients with stroke-only, and 6% of patients with cancer-only ($p = 0.005$)" [18]. The researchers concluded that "patients with cancer-related stroke have higher markers of coagulation, platelet, and endothelial dysfunction, and more circulating microemboli, than matched controls" [18]. Future studies are needed to evaluate whether the identified biomarkers can predict the risk of incident and recurrent stroke and the response to antithrombotic treatment in patients with solid tumor cancers.

The MOST-Cancer conclusion is that "clinicians should explore prothrombotic and embolic pathophysiologies in patients with cancer and stroke, especially when the stroke mechanism is undetermined after standard evaluation" [18].

Research into ESUS and other stroke sources and mechanisms are not the only frontiers for the outpatient NVUL. In other related medical fields, there is a need for TCD technology and for studies that can be easily performed in the outpatient lab. For example, there is now a significant body of literature investigating the pathophysiology of vascular cognitive impairment (VCI) and mild cognitive impairment (MCI). VCI is thought to be the most common cognitive disorder in the elderly. However, the exact relationships between vascular lesion, cognition, and neuroplasticity are not completely understood. Recent findings point out the possibility to identify a panel of markers to predict cognitive deterioration in the "brain at risk" for vascular or mixed dementia. Interested researchers and leaders in this field note the role of TCD:

> TCD is a non-invasive and feasible neurosonological technique able to evaluate CBF [cerebral blood flow] velocity, arterial perfusion integrity, and intracranial small vessel compliance. The microangiopathy, demonstrated both in VaD [vascular dementia] and AD [Alzheimer's Disease], might lead to arteriolosclerosis, vasoconstriction, and vascular stiffness, thus resulting in decreased arterial diameter and CBF. In a recent TCD study, mild VCI patients showed a hemodynamic pattern of cerebral hypoperfusion and enhanced vascular resistance, likely arising from small vessels and then extending to larger arteries. This result provides evidence of the occurrence and severity of small vessel disease and executive dysfunction in elderly patients at risk of future dementia. It has been also demonstrated that a similar hemodynamic dysfunction might play a pathogenic role in the development of cognitive impairment in patients with vascular depression and predominant WML [white matter lesions]. Further studies aiming at a direct TCD comparison between AD and VaD, and their preclinical stages (i.e., MCI and VCI, respectively), are warranted. [19]

The outpatient NVUL is a valuable tool for the stroke team of doctors and clinicians but it should be equally valuable to those in functional neuroscience research as well as clinical or translational research from the neurophysiology and neuro-oncology departments. This handbook provides a compendium of information, reference standards, resources and tips and tricks that are needed to develop a sound and innovative neurovascular ultrasound lab.

Conflict of Interest The author declares no potential conflicts of interest with respect to the research, authorship, and/or publication of this chapter

References

1. Adams RJ, Brambilla DJ, Granger S, Gallagher D, Vichinsky E, Abboud MR, et al. Stroke and conversion to high risk in children screened with transcranial Doppler ultrasound during the STOP study. Blood. 2004;103(10):3689–94.
2. The management of sickle cell disease. NIH Publication No. 02-2117. Revised June 2002. 4th ed. https://www.nhlbi.nih.gov/files/docs/guidelines/sc_mngt.pdf.
3. Evidence-based management of sickle cell disease, expert panel report 2014. NIH (National Heart, Lung and Blood Institute). https://www.nhlbi.nih.gov/sites/default/files/media/docs/sickle-cell-disease-report%20020816_0.pdf.
4. DeBaun MR, Jordan LC, King AA, Schatz J, Vichinsky E, Fox CK, et al. American Society of Hematology 2020 guidelines for sickle cell disease: prevention, diagnosis, and treatment of cerebrovascular disease in children and adults. Blood Adv. 2020;4(8):1554–88.
5. Transcranial ultrasound in pediatric patients with sickle cell disease. SVU vascular technology professional performance guidelines. 2019. https://www.svu.org/practice-resources/professional-performance-guidelines/.
6. Kolata G. These sisters with sickle cell had devastating, and preventable, strokes. New York Times. 2021 May 23. https://www.nytimes.com/2021/05/23/health/sickle-cell-black-children.html.
7. Alexander TH Jr, Collins L, Harrison P, Hostetler W, Rountree S, Ulrich R. Transcranial Doppler will resolve discrepancies between extracranial vascular test results, angiography, and clinical symptomatology—a case study. J Vasc Technol. 1998;22(4):209–12.
8. USPSTF recommends (again) against screening for carotid artery stenosis in asymptomatic patients, Comment by Thomas L. Schwenk. NEJM Journal Watch-General Medicine. 2021;1(5).
9. Sloper T, CMP, Director of IAC Marketing/Communications, email to the author. 2019 February 21.
10. Sloper T, CMP, Director of IAC Marketing/Communications, email to the author. 2021 June 21.
11. Kim JS, Caplan LR, Wong KS, editors. Intracranial atherosclerosis: pathophysiology, diagnosis and treatment. Front Neurol Neurosci, vol. 40. Basel: Karger; 2016. p. 1–20.
12. Kim ES, Sharma AM, Scissons R, Dawson D, Eberhardt RT, Gerhard-Herman M, et al. Interpretation of peripheral arterial and venous Doppler waveforms: a consensus statement from the Society for Vascular Medicine and Society for Vascular Ultrasound. Vasc Med. 2020;25(5):484–506.

13. Lally M, Sloper T. IAC News Release. Study exploring optimization of duplex velocity criteria for diagnosis of internal carotid artery (ICA) stenosis published online today. 2021 May 19. https://www.intersocietal.org/vascular/forms/IACVascularTesting_ICADiagCriteria_News%20Release.pdf.
14. Gornik HL, Rundek T, Gardener H, Benenati JF, Dahiya N, Hamburg NM, et al. Optimization of duplex velocity criteria for diagnosis of internal carotid artery (ICA) stenosis: a report of the Intersocietal Accreditation Commission (IAC) Vascular Testing Division Carotid Diagnostic Criteria Committee. Vasc Med. 2021;26(5):515–25.
15. Strambo D, Sirimarco G, Nannoni S, Perlepe K, Ntaios G, Vemmos K, Michel P. Embolic stroke of undetermined source and patent foramen ovale: risk of paradoxical embolism score validation and atrial fibrillation prediction. Stroke. 2021;2021(52):1643–52. https://doi.org/10.1161/STROKEAHA.120.032453.
16. Prabhakaran S, Elkind MS. Cryptogenic stroke. UpToDate (accessed 7/7/21), last topic update 5/25/21. https://www.uptodate.com/contents/cryptogenic-stroke?search=Elkind%20cryptogenic%20stroke.
17. Ntaios G. Embolic stroke of undetermined source. JACC review topic of the week. J Am Coll Cardiol. 2020;75(3):333–40.
18. Navi BB, Sherman CP, Genova R, Mathias R, Lansdale KN, LeMoss NM, et al. Mechanisms of ischemic stroke in patients with cancer: a prospective study. Ann Neurol. 2021;90(1):159–69.
19. Vinciguerra L, Lanza G, Puglisi V, Fisicaro F, Pennisi M, Bella R, et al. Update on the neurobiology of vascular cognitive impairment: from lab to clinic. Int J Mol Sci. 2020;21(8):2977.

Part I

Protocols

Transcranial Doppler Non-Imaging for Adults

Christy L. Cornwell

Introduction

There are two methods of insonating the intracranial vessels. There are advantages and disadvantages of both modalities. Non-imaging Transcranial Doppler (TCD) (Fig. 1). provides a smaller transducer to place in the window, and easier accessibility to locate Doppler signals, however it is based on the examiners' ability to recognize the distinct sound of each vessel segment. Transcranial Color Doppler Imaging (TCDI) (Fig. 2) provides a color map of the circle of Willis (CoW), which is helpful to visualize the vessels in color using Doppler to obtain waveforms. However, since the probe used for TCDI is a 2 Mhz cardiac probe, the foot of the probe is often too large and often only segments of the vessels are seen. Regardless of which modality is used, the final impression is based on waveform morphology. TCD is performed in multiple specialties including Neurovascular, Cardiology, Monitoring in OR, Vascular Surgery, and Research labs. Other uses of TCD such as emboli detection, vasoreactivity, and evaluation of patent foramen ovale (PFO) can be found in

C. L. Cornwell (✉)
Neurosonology Consultant, Cardiovascular Ultrasound Services, Inc., Columbus, OH, USA

W. C. Ziai, C. L. Cornwell (eds.), *Neurovascular Sonography*,
https://doi.org/10.1007/978-3-030-96893-9_28

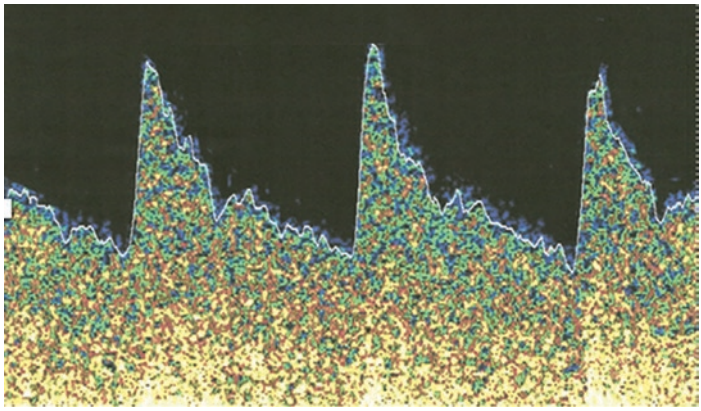

Fig. 1 TCD Non-imaging

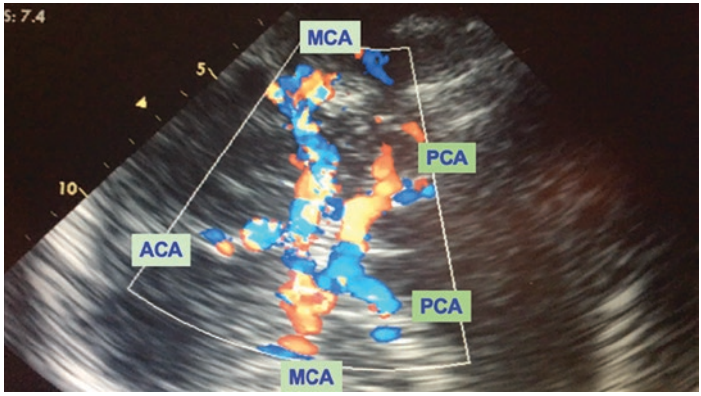

Fig. 2 Transcranial Doppler Color Imaging (TCDI)

other chapters. The protocol for TCDI is addressed in the following chapter. This chapter will focus on non-imaging freehand Doppler assessment of the CoW.

Purpose To provide non-invasive assessment of the intracranial vessels in the circle of Willis using non-imaging Doppler. Time

Average Mean Velocity (TAMV) is used to assess physiologic information from averaging all peaks within a cardiac cycle. The protocol includes a complete bilateral study.

Indications for Transcranial Doppler

- Monitoring of vasospasm following subarachnoid hemorrhage
- Intracranial occlusive disease
- Effects of extracranial stenosis on intracranial hemodynamics
- Evaluation of flow following head trauma
- Assess degree of intracranial stenosis in the major basal cerebral arteries
- Assessment of the vertebrobasilar (posterior) circulation
- Monitoring of reperfusion therapies in acute stroke
- Sickle cell disease
- Detection of cerebral emboli
- MoyaMoya disease
- Cerebral circulatory arrest

Equipment

Dedicated Transcranial Doppler Machine

- 2Mhz pulsed wave transducer for spectral analysis with M-Mode software
- A direction sensitive Doppler blood flow meter
- Doppler waveform monitor that displays bidirectional flow and signal intensity
- Audible output and permanent recording of the waveform
- Evidence of validation for the intended application will be provided if software is used for emboli detection
- Ultrasound gel
- Wash cloths, towels to support patient's head
- Gloves
- Masks

Equipment Quality Control

- Equipment used for diagnostic testing will be maintained in good operating condition
- Equipment maintenance includes preventative maintenance checks quarterly by the vendor

Limitations

- Patient is uncooperative
- Post-operative dressings
- Poor positioning of patient
- Inadequate windows

Procedure

Patient Positioning

If the patient is in the Neurocritical Care unit and not able to follow commands, it is sometimes necessary to prop their head for proper positioning in order to assess the transtemporal window, as frequently the patient will turn their head to one side. For an out-patient, position the patient comfortably in supine position on the exam table, with head supported for transtemporal exam, and turned to side with neck flexed to optimize foramen magnum for suboccipital approach.

- Explain procedure. Obtain patient history by reviewing the patient's medical records and interviewing the patient or patient representative. Record age, gender, race, and current medical status. Document symptoms, relevant risk factors, and pertinent lab values.
- Risk factors may include but are not limited to: smoking, diabetes, hypertension, peripheral vascular disease, coronary artery disease.
- Lab values should include hematocrit, hemoglobin, heart rate, cardiac output, blood pressure, PaCO2, and intracranial pressure [1].
- Set up equipment.

TCD Acoustic Windows

We use acoustic windows which are the natural indentations in the temporal bone that allow us to assess the intracranial arteries [1] (Fig. 3).

Begin Procedure with Insonation of the Middle Cerebral Artery (MCA)

Begin procedure at the right Middle Cerebral Artery (RMCA), in the mid transtemporal window. Set the depth at 50–55 mm which is the M1 segment. (Tables 1 and 4). Place a generous amount of gel above the zygomatic arch on the temporal region of the patient's cranium. Before applying the probe on the patient, use the index finger to slide across the temporal windows to palpate the natural indentations in the skull in the temporal window. Place

Fig. 3 CD Acoustic Windows. Transcranial Doppler windows for acquisition of the anterior Circle of Willis. 1 = mid-temporal window; 2 = anterior window; 3 = posterior window [1]

Table 1 Criteria for MCA vasospasm

MFV cm/s	Lindegaard ratio	Interpretation
<120	<3	Hyperemia
>80	3–4	Hyperemia + possible mild spasm
≥120	3–4	Mild spasm + hyperemia
≥120	4–5	Moderate spasm + hyperemia
>120	5–6	Moderate spasm
≥180	6	Moderate to severe spasm
≥200	≥6	Severe spasm
>200	4–6	Moderate spasm + hyperemia
>200	3–4	Hyperemia + mild/residual spasm
>200	<3	Hyperemia

See Refs. [1, 2, 4]

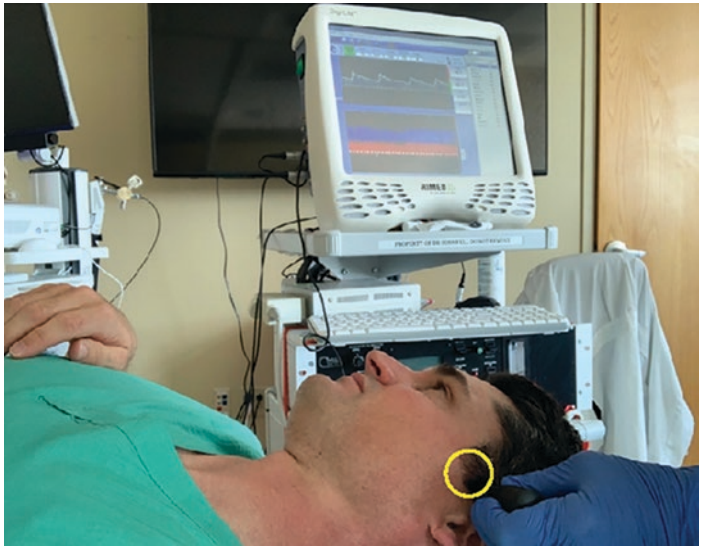

Fig. 4 Mid transtemporal window with TCD display of MCA flow toward the probe

the probe in the mid temporal window, (Fig. 4) and aim slightly upward and anteriorly, listening for the strongest signal. If the signal is difficult to locate, move the probe without lifting it out of

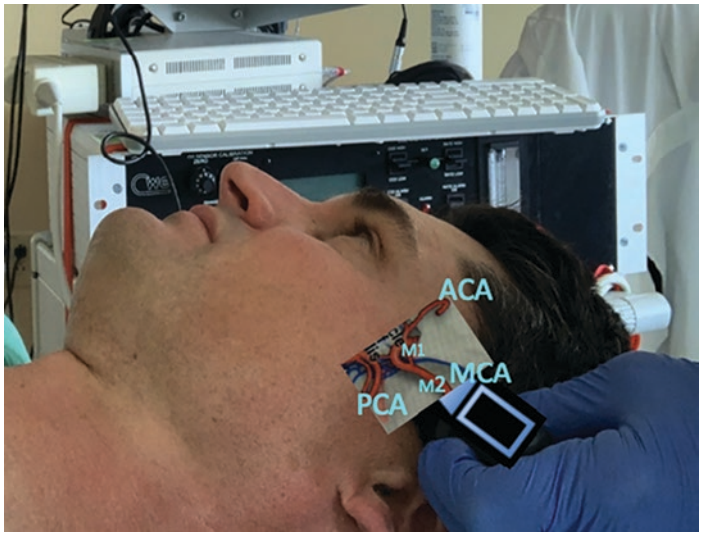

Fig. 5 From the temporal window, the MCA, ACA, and PCA can be insonated [1]

the window into the posterior temporal window. Use caution to be sure you are insonating the MCA, and not the PCA (see Fig. 10).

While insonating the MCA, the flow will be toward the transducer, which will appear above the baseline on your screen (Fig. 5).

Document the spectral MCA waveform. Move the probe in very small circular motion without lifting the probe out of the window, to be sure you have the strongest signal. After obtaining a clear signal, (Fig. 6a) decrease the depth in intervals to 30–40 mm, insonating the M2 segment. (Tables 1 and 4). The M2 segment is also toward the transducer and will be above the baseline (Fig. 6b). Again, move the probe in a very small circular motion without lifting the probe and follow the sound listening for the highest mean velocity. Take several samples of both M1 and M2 at multiple depths (Fig. 6, Tables 1 and 4) [1].

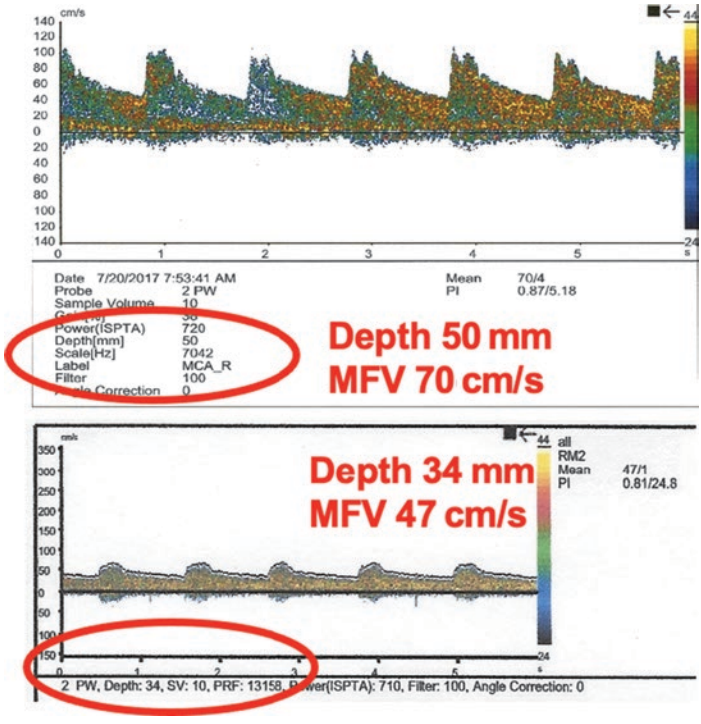

Fig. 6 MCA (M1) depth and MCA (M2) depth

ACA/MCA Bifurcation

Continue to follow sound angling the probe anteriorly while increasing the depth until flow becomes bi-directional (both above and below baseline), to insonate the MCA/ACA bifurcation. (Fig. 7). If a signal is lost while scanning other vessels, return to the bifurcation as this is a landmark area. Store sample of bifurcation [1].

Depth: 55–65 mm
Flow direction: Bidirectional
Spatial relationship: Anterior and posterior
Flow velocity not assigned as this is a landmark area Fig. 7

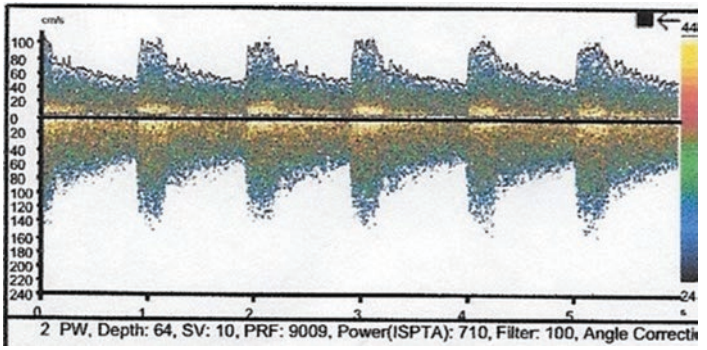

Fig. 7 ACA/MCA Bifurcation

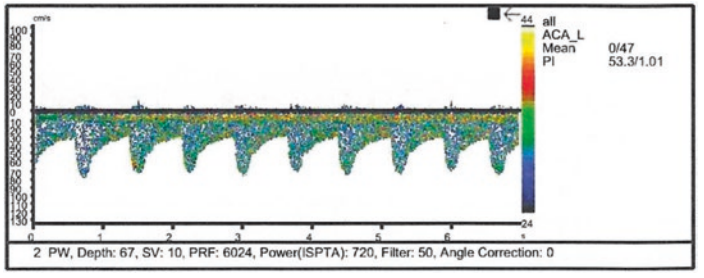

Fig. 8 Anterior Cerebral Artery (ACA) waveform

Anterior Cerebral Artery (ACA)

Continue to follow sound through the bifurcation, continuing to increase depth to 60–65 mm insonating the ACA (Fig. 8) [4]. The flow will be going away from the probe so will appear on the screen below baseline. Take several samples of the A1 segment and store waveforms at multiple depths up to 75 mm. Note that only A1 can be insonated due to the angle of the A2 segment of the ACA (Tables 3 and 4).

Depth: 60–80 mm

Flow direction: Away from the transducer

Spatial Relationship: Anterior mean velocity: 50 ± 11 cm/s

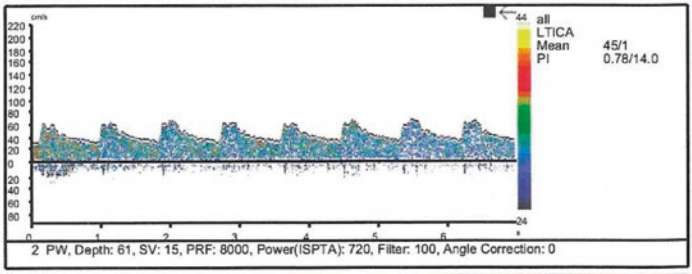

Fig. 9 Terminal internal carotid artery

Terminal Internal Carotid Artery (tICA)

Return to M1 at a depth of 60 mm, moving the probe slightly inferior to insonate the terminal internal carotid artery (tICA) (Fig. 9), and store the sample. The terminal ICA signal is located just inferior to the bifurcation at 60–65 mm. The sound will be lower and more pulsatile than the MCA (Tables 3 and 4).

Depth: 60–65 mm
Flow direction: Toward transducer
Spatial Relationship: Inferior to MCA/ICA bifurcation
Mean velocity: 39 ± 9 cm/s.

Posterior Cerebral Artery (PCA)

Return to the landmark bifurcation and move probe slightly posteriorly. Continue to move very slowly posteriorly while at a depth of 60 mm. Slowly turn the transducer posteriorly by 10–30 degrees, (usually there is a sound of flow gap) between the bifurcation and the PCA (Fig. 10). The PCA signal will have a lower velocity and will become bi-directional as you follow sound increasing depth into the P2 segment. Take a sample at P1 and P2 and store images (Tables 3 and 4).

Depth: 60–80 mm
Flow direction: PCA (P1) toward transducer, PCA (P2) away

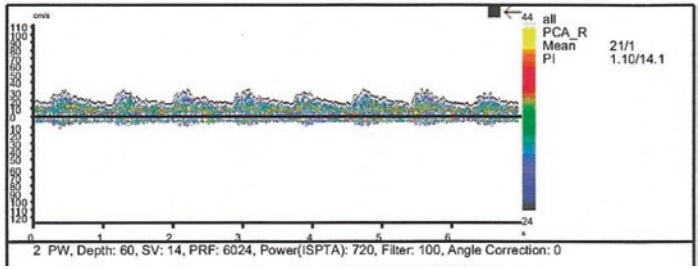

Fig. 10 Posterior cerebral artery (PCA)

Spatial Relationship: Posterior and inferior to MCA/ACA bifurcation

Mean velocity: 39 ± 10 cm/s

Obtain Lindegaard Ratio

The Lindegaard ratio is used to determine the severity of vasospasm, and to differentiate elevated mean flow velocity from hyperemia. This ratio is obtained by measuring the mean flow velocity of the ipsilateral MCA / mean flow velocity of the extracranial ICA from the submandibular window (Fig. 11). A ratio of 3–6 is indicative of mild / moderate vasospasm, and greater than 6 is indicative of severe vasospasm. Elevated mean flow velocities with a Lindegaard ratio of less than 3.0 are suggestive of hyperemia [2] (Table 1).

Vertebral Arteries and Basilar Artery Can Be Insonated in the Suboccipital Window

For insonation of the vertebrobasilar system, if possible, turn the patients' head slightly to locate the suboccipital window. Before placing the probe on the patient, using a generous amount of gel, place the index finger to palpate the foramen magnum, just below

Fig. 11 Submandibular window for insonation of the extracranial Internal Carotid Artery (ICA)

the hairline to locate the suboccipital window (Fig. 12). Place transducer depth at 60 mm and aim probe toward the patient's eyes. Move probe in a small circular movement and locate a vertebral artery (VA) at a depth of 60 mm. The flow will be below baseline, as flow is moving away from the probe. Move the probe slowly from left to right to determine which vertebral artery you

Fig. 12 Suboccipital window for insonation of Vertebral Arteries and Basilar Artery

are on. Continue on the right side. Take sample waveforms of the right VA (RVA) once you have determined you are on the right side. Keep the transducer on the RVA, and while following the sound, continue to increase the depth from 60 to 75 mm to identify the distal RVA (Fig. 13a). Continue to follow sound increasing depth to 80 mm to insonate the proximal basilar artery (BA). (Fig. 13b). Continue to follow the sound, and store several samples, while increasing depth to the mid BA at 90 mm. Store sample of mid BA. Continue to increase depth to 100 mm or greater to insonate at the distal BA. Store several samples. While still holding the transducer on the BA, begin to decrease the depth slowly and follow the sound back to the left VA. Take multiple samples and store at depth of 75 mm for distal VA and 60 mm for proximal VA [1, 3, 5] (Table 2).

The Sviri ratio is obtained by dividing the mean flow velocities of basilar artery (BA) by those of extracranial vertebral artery [2] (Table 2).

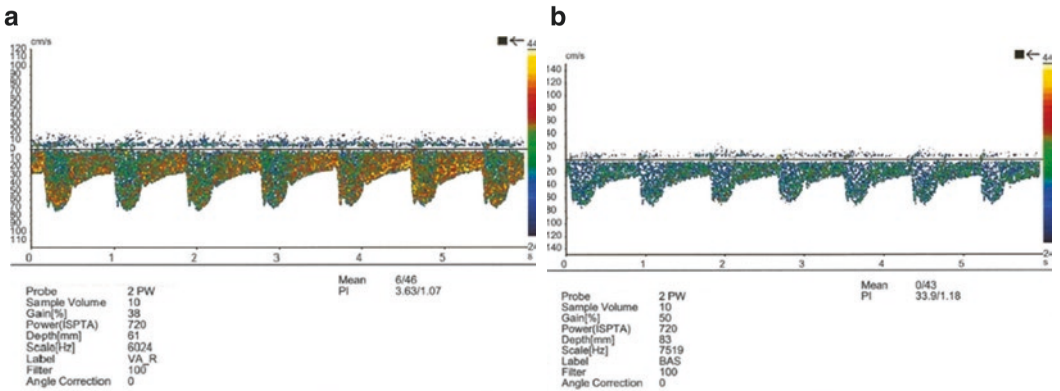

Fig. 13 (**a**) Vertebral Artery (VA). Depth: 60–75 mm, Flow direction: Away from transducer, Mean velocity: 38 ± 10 cm/s. (**b**) Basilar Artery (BA). Depth: 80–120 mm, Flow direction: Away from transducer, Mean velocity: 41 ± 10 cm/s

Table 2 Criteria for basilar artery vasospasm

MFV cm/s	Sviri ratio	Interpretation
>70	>2	Vasospasm
>85	>2.5	Moderate or severe vasospasm
>85	>3	Severe vasospasm

See Ref. [3]

To calculate Sviri Ratio [3] (Table 2):

$$\text{Basilar}\left(\text{mean flow velocity}\right)/\left(\text{Right Vertebral Artery} + \text{Left Vertebral Artery}\right)/\ 2$$

Transorbital Window for Insonation of the Ophthalmic Artery and Carotid Siphon

NB: reduce power to 10% to avoid retinal damage

Place transducer over eyelid, angle medially

Depth: Ophthalmic artery: located 45–52 mm (Figs. 14 and 15)

Carotid Siphon located 60–64 mm (Fig. 16, Tables 3 and 4) [1].

It is important to watch for flow direction, as small branches can collateralize with distal branches of the External Carotid Artery (ECA).

Flow direction in the ophthalmic artery is toward the probe, appearing on the screen above baseline. Flow direction in the siphon may be bidirectional. Watch for increased velocities and store images.

Vasospasm

The most widely used procedure for TCD is for noninvasively monitoring vasospasm following patients with subarachnoid hemorrhage and is a required procedure in comprehensive stroke centers. Mean flow velocities (mFV) are monitored daily, for approximately 15 days, and each study is compared to the previ-

Fig. 14 Transorbital window for insonation of the Ophthalmic artery and Carotid Siphon

ous study. It is necessary to obtain Lindegaard ratios (LR), and Sviri ratios in order to determine whether or not elevated mFV is due to vasospasm, hyperemia, or both (Tables 1 and 2).

Example of typical pattern of vasospasm, including anterior and posterior system beginning on day 3–5, with highest mFV on day 7, and returning to baseline normal by day 15 (Fig. 17).

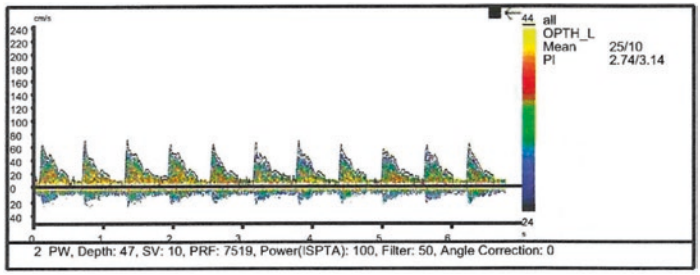

Fig. 15 Ophthalmic artery waveform

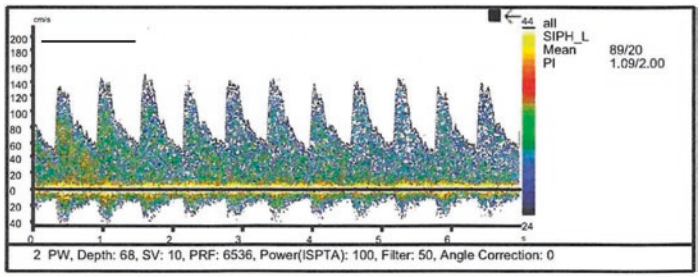

Fig. 16 Carotid siphon waveform

Table 3 Grading criteria for ACA, ICA, PCA & VA vasospasm

	Possible vasospasm	Probable vasospasm	Definite vasospasm
Artery	MFV cm/s	MFV cm/s	MFV cm/s
ICA	>80	>110	>130
ACA	>90	>110	>120
PCA	>60	>80	>90
VA	>60	>80	90

See Ref. [4]

Table 4 Criteria for intracranial stenosis

Artery	Depth (mm)	MFV (cm/s)	MFV ≥50% stenosis (cm/s)	MFV ≥70% stenosis (cm/s)
M1–M2 MCA	30–65	≥80	≥100 (use 1:2 ratio)	≥128 (1:4 ratio)
A1 ACA	60–75	≥80	N/A	N/A
ICA Siphon	60–65	≥70	≥90 (use 1:2 ratio)	≥128 (1:4 ratio)
PCA	60–72	≥50	N/A	N/A
BA	80–100+	≥60	≥80 (use 1:2 ratio)	≥119 (1:4 ratio)
VA	40–80	≥50	≥80 (use 1:2 ratio)	≥119 (1:4 ratio)

See Ref. [1]

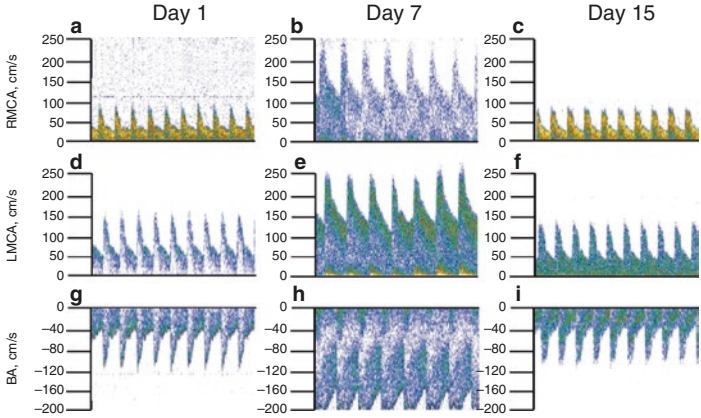

Fig. 17 Vasospasm. (**a–c**) correspond with RMCA days 1, 7 and 15, respectively (**d–f**) correspond with LMCA days 1, 7 and 15, respectively (**g–i**) correspond with BA days 1, 7, 15, respectively

Documentation

Documentation will include grayscale images, Doppler waveforms, depth ranges, and velocity measurements of the following segments [1]

- MCA at M1 and M2
  - ACA

  - Cross-filling via anterior cerebral communicating artery (when detectable)
  - Terminal ICA (tICA) when detectable
  - Collateral flow via PCA when detectable
  - PCA at P1 or P2
  - Ophthalmic artery when appropriate
  - Internal carotid artery (ICA siphon)
  - Terminal vertebral artery (VA)
  - Proximal, mid and distal basilar artery
  - Pulsatility Index (PI)

- Areas of suspected stenosis or obstruction will include Doppler waveforms and velocity measurements at and distal to the stenosis or obstruction.
- Lindegaard and Sviri ratios for vasospasm in SAH patients.
- Store all abnormal waveforms, which may include delayed systolic upstroke, increased pulsatility, high or low diastolic flow, oscillating or reverberating waveforms, short systolic spike, hyperemia, hyperdynamic, or stenosis.

Review of the Diagnostic Exam Findings

- Review data to ensure that a complete exam has been performed and documented.
- Record all technical findings required to complete the final diagnosis on a worksheet so that the measurements can be classified according to the laboratory diagnostic criteria.
- Record all findings in the logbook including date, tech, indication, software, ordering physician, and any other necessary information.
- For SAH patients Lindegaard and Sviri index and include findings from previous study [1–5].

- TCD normal values
- Criteria for MCA, ACA, and PCA vasospasm
- Criteria for Basilar, and Vertebral Artery vasospasm

Spectral Doppler Waveform Examples

Normal waveform

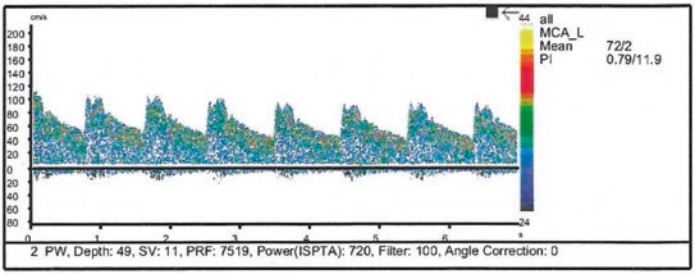

Mild Vasospasm

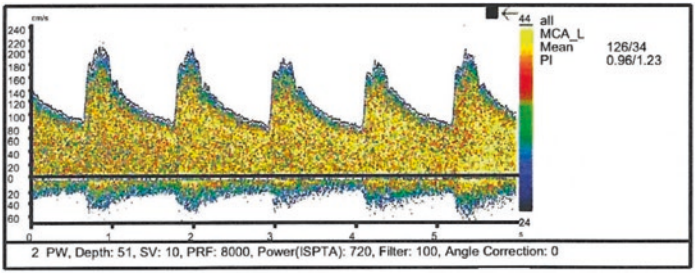

Moderate Vasospasm

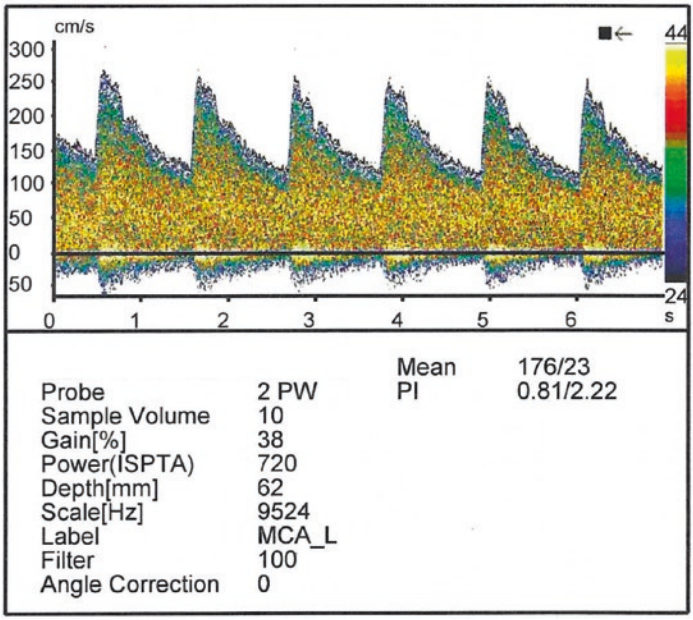

Severe Vasospasm M1 (depth 51 mm)

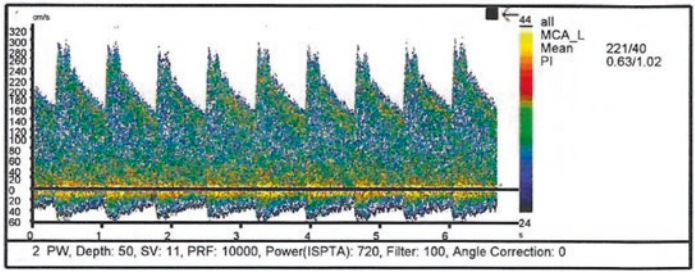

Severe Vasospasm M2 (depth 41 mm)

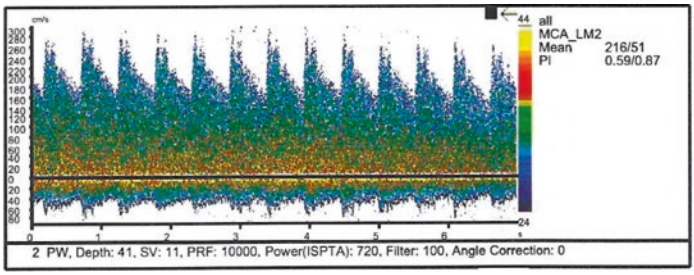

Hyperdynamic waveform

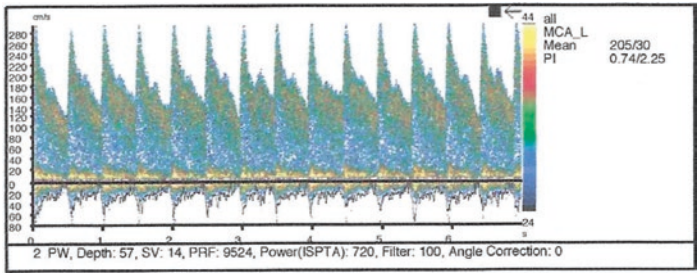

Elevated Pulsatility Index (P.I.). Decreased diastolic flow due to increased Intracranial Pressure (ICP)

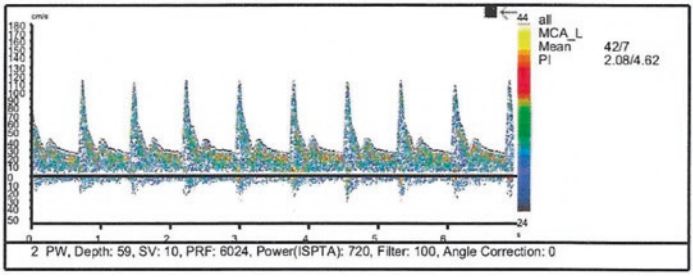

Elevated ICP resulting in impending Cerebral Circulatory Arrest

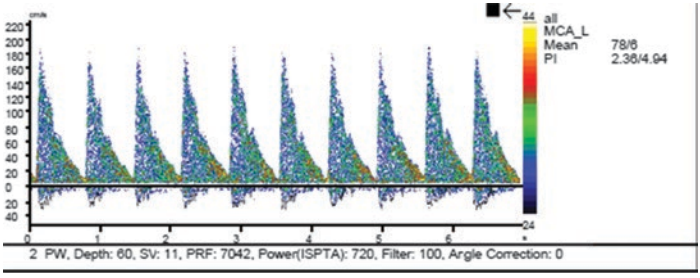

Cerebral Circulatory Arrest. Oscillating flow. Diastolic flow is below baseline

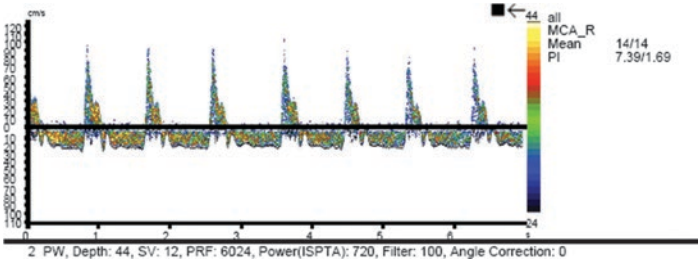

MCA stenosis with elevated velocity, turbulence, and bruit

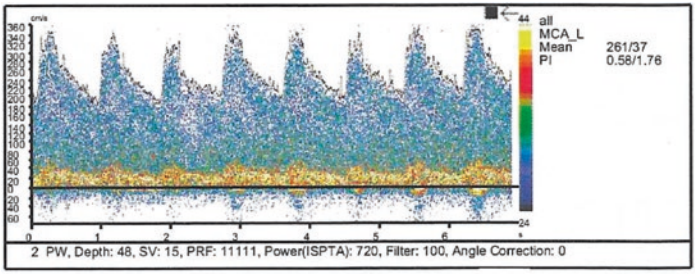

Meningitis with elevated velocity secondary to vasospasm or inflammation of arterial wall

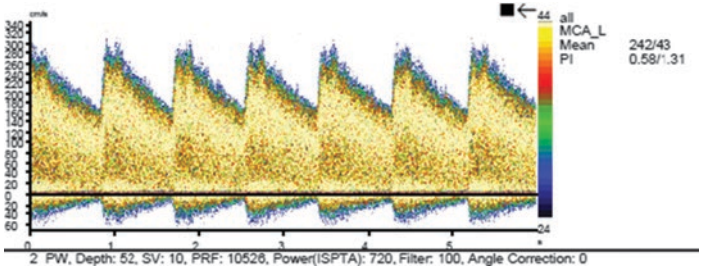

References

1. Alexandrov AV. Cerebrovascular ultrasound in stroke prevention and treatment. 2nd ed. Oxford, Hoboken: Blackwell Publishing Ltd; 2011.
2. Lindegaard KF, Nornes H, Bakke SJ, Sorteberg W, Nakstad P. Cerebral vasospasm diagnosis by means of angiography and blood velocity measurements. Acta Neurochir. 1989;100:12–24.
3. Sviri GE, Ghodke B, Britz GW, et al. Transcranial Doppler grading criteria for basilar artery vasospasm. Neurosurgery. 2006;59:360–6.
4. Kumar G, Alexandrov AV. Vasospasm surveillance with transcranial Doppler sonography in subarachnoid hemorrhage. J Ultrasound Med. 2015;34:1345–50.
5. Britz GW, Sviri GE. Vertebrobasilar vasospasm after aneurysmal subarachnoid hemorrhage: review. J Neurol Stroke. 2018;8. https://doi.org/10.15406/jnsk.2018.08.00278.

Transcranial Color Doppler Imaging for Adults

Colleen Douville

Abbreviations

ACA 2	Anterior cerebral artery (post-communicating)
ACA	Anterior cerebral artery (pre-communicating)
ACOA	Anterior communicating artery
BA	Basilar artery
C1-terminal, C2-supraclinoid, C3 genu, C4 parasellar, C5- proximal cavernous	Internal carotid artery
EC-ICA	Extracranial internal carotid artery
IAC	Intersocietal Accreditation Commission
MCA 1	Middle cerebral artery main trunk
MCA 2	Middle cerebral artery proximal branches
OA	Ophthalmic artery
PCA 1	Posterior cerebral (pre-communicating)

C. Douville (✉)
Swedish Vascular Ultrasound, Swedish Neuroscience Institute, Swedish Health Services, Seattle, WA, USA
e-mail: Colleen.douville@swedish.org

W. C. Ziai, C. L. Cornwell (eds.), *Neurovascular Sonography*,
https://doi.org/10.1007/978-3-030-96893-9_29

PCA 2	Posterior cerebral artery (post-communicating)
PCOA	Posterior communicating artery
PICA	Posterior inferior cerebellar artery
SCA	Superior cerebellar artery
SMW	Submandibular window
SOW	Suboccipital window
TICA	Terminal internal carotid artery
TOW	Transorbital window
TTW	Transtemporal window
VA (V3)	Vertebral artery at atlas loop
VA (V4)	Vertebral artery intracranial

Introduction

Transcranial Doppler Imaging (TCDI) is a non-invasive ultrasound study of cerebral arteries that can be performed at bedside or in the outpatient setting. TCDI diagnostic exams provide real-time flow information for patients with a variety of cerebrovascular diseases and can be repeated serially. Good technique and an understanding of ultrasound technology and cerebral hemodynamics are required to produce valid results. Once the technique to perform a complete study of the basal cerebral arteries has been mastered, abbreviated exams directed at the vessel/s of interest can be rapidly achieved in an acute clinical scenario.

Procedure and Purpose

Transcranial Doppler Imaging (TCDI) is used in the clinical management of patients with a variety of intracranial cerebrovascular abnormalities. It provides physiologic data in real time complementing computed tomography with contrast (CTA), magnetic resonance imaging with contrast (MRA) and cerebral angiography. Exams can be repeated serially demonstrating the complex and often changing dynamics of blood flow.

Accurate vessel identification, a shortened learning curve, and potential expanded applications are advantages of TCDI. This

technique provides B-mode visualization of boney and parenchymal anatomic landmarks and color flow mapping of blood vessels in contrast to the purely physiological information acquired using TCD. Arterial tortuosity, branch points and the confluence of the vertebral and basilar arteries are easily appreciated. Power Doppler is a feature that can be used to enhance acquisition of flow signals and is readily available on duplex ultrasound machines.

Indications

The diagnosis of intracranial vascular disease using TCDI includes vasospasm secondary to subarachnoid hemorrhage [1, 2] intracranial stenosis, thrombosis, occlusion [2, 3], circle of Willis collateral flow [4–6], significant changes in intracranial pressure and cerebral circulatory arrest [7–9] (as secondary, supportive evidence), and pediatric sickle cell disease [10–12]. Assessment of venous thrombosis, arteriovenous malformations and abnormalities of the parenchyma is possible; however, the utility and reliability of these applications are still unknown [2].

Accurately interpreting intracranial findings requires knowledge of the extracranial carotid and vertebral arteries because hemodynamically significant obstructive disease will greatly influence intracranial hemodynamics [3]. Modalities to obtain this information include carotid duplex ultrasound, CTA, MRA and DSA.

Limitations

Due to the large footprint of a phased array transducer, access through the temporal and foramen magnum approaches may be limited and in patients with very small bone windows non-imaging TCD will perform better than TCDI. Monitoring applications easily done using TCD by attaching the transducer to the patient's head using a head frame and acquiring signals continuously is not performed using TCDI. Duplex ultrasound transducers are too large to attach to a head frame, have not been validated

for these applications and may not be FDA cleared for continuous insonation. Excluded indications are emboli monitoring, right to left cardiac shunt detection and any intraprocedural monitoring including carotid endarterectomy, stenting or cardiac surgery. Some equipment may not have approval for transorbital evaluation. There are fewer diagnostic criteria available for detection and grading of intracranial disease with TCDI.

Evaluation of flow velocities requires placing the sample volume gate to obtain spectral waveforms within the vessel color map at different depths. Due to tortuosity and branching of blood vessels the color image may not display in a single plane and the operator must have the skill and anatomical knowledge to place the sample volume correctly even in the absence of color Doppler. The accuracy of velocity detection, the primary quantitative characteristic of the spectral Doppler waveform, is dependent on achieving a low angle of insonation (zero degree) to flow. This is facilitated by listening for the highest pitch of the Doppler signal and making small adjustments to decrease the angle in accordance with pitch change. Developing the skill to acquire and understand audible feedback from the Doppler signal improves the quality and accuracy of the examination.

Equipment

A standard duplex vascular ultrasound machine, software specifically designed for TCDI and a broadband, 1–5 MHz with 2 MHz range Doppler frequency, phased array transducer is required for this examination (Fig. 1).

Supplies

Acoustic coupling gel to conduct the sound effectively from the transducer into the body.

Utilization of hospital gloves is standard for performing ultrasound procedures.

Sterile transducer sleeves and sterile gel for use on broken skin or open wounds.

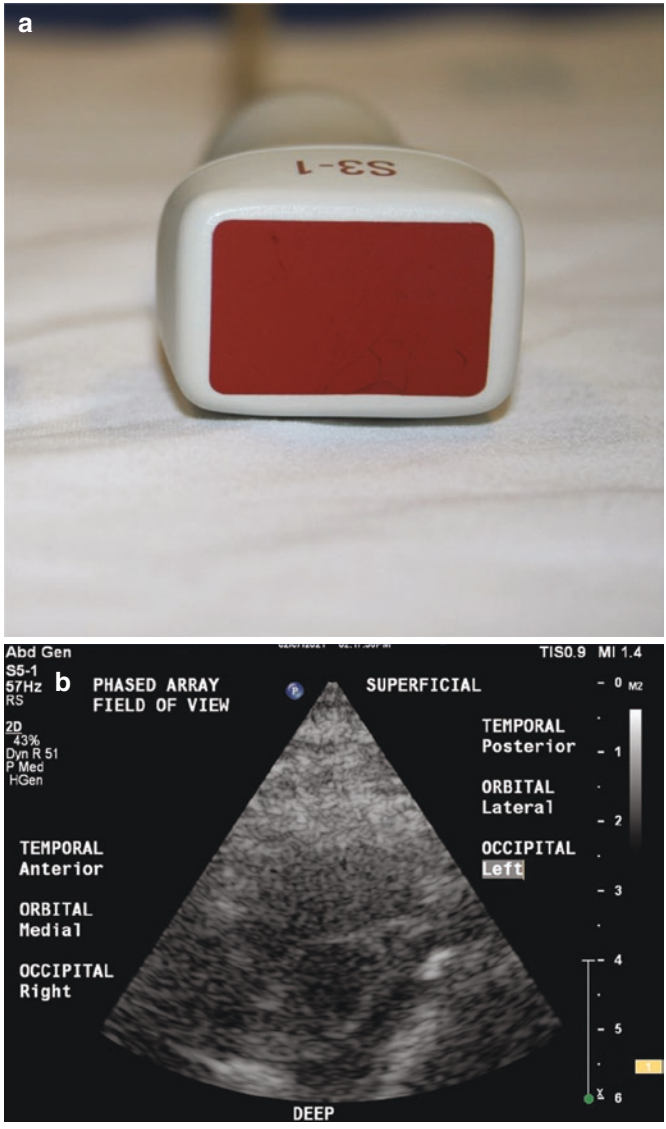

Fig. 1 (**a**) Phased array transducer (**b**) The shape of the display on the monitor is determined by the transducer. Phased array transducers have a curved near field with sloped sides

Disinfectants for transducer cleaning post use as recommended by the machine manufacturer. Some disinfectants can cause the transducer face to deteriorate so it is important to consult the equipment company's specific guidance on products to use.

The body of the ultrasound machine is cleaned using standard hospital protocols and isolation precautions.

Equipment Quality and Control

The ultrasound instrument should be checked every 6 months by biomedical engineering for electrical safety. Purchasing a service contract once the warranty has expired is recommended to maintain optimal function and receive software updates.

Patient Assessment and Communication

There are multiple established indications for performance of diagnostic TCDI studies and locations for the study range from outpatient laboratories to bedside in a critical care ward. Patient assessment and preparation are guided by the indication, venue and the person performing the study which may be an attending physician or a sonographer. A full diagnostic exam of the basal cerebral arteries, both anterior and posterior, or a limited study of one artery, for example post clot lysis, to determine the results of the procedure, may be required.

If the patient is alert and oriented explain the test and the non-invasive nature of it to relieve anxiety about the procedure. Instruct them to rest quietly and not speak during the test. If unknown, take a relevant history either from the patient and/or from the medical record.

In all patients it is important to take or record the blood pressure. In the ICU additional physiologic parameters to record are hematocrit, CO_2, intracranial pressure and cerebral perfusion pressure as these can impact waveform velocities and produce alterations that inform the final exam interpretation.

Performance Protocol and Technique

The optimal patient position for TCDI is supine with the head minimally elevated for all but the occipital approach. Removing the pillow and replacing it with a rolled towel provides the sonographer with better range of motion. A semi dark room facilitates patient relaxation and improves the image on the monitor screen.

To obtain information on the vertebrobasilar arteries a lateral decubitus position supporting the head with a small pillow provides good access. If the patient cannot be put into this pose, their head can be turned to the right and left providing access to the foramen magnum via a lateral approach.

Sonographer positioning can be either from the head or side of the bed-exam table (Table 1).

TCDI convention defines color Doppler maps with flow towards the transducer depicted as red and flow away from the

Table 1 Arteries identifiable utilizing each of the four acoustic windows

TTW Vessels	TOW Vessels	SOW Vessels	SMW Vessels
Carotid siphon, OA (coronal) TICA (axial) MCA 1, MCA 2 (proximal segments) ACA 1, ACA 2 (proximal segment) ACOA (when acting as collateral) PCA 1, PCA 2 (proximal segment) PCOA (when acting as collateral)	Ophthalmic artery ICA – siphon *Check with manufacturer for FDA approval (M.I. ≤ 0.23)	Vertebral artery – V3, V4 PICA BA	Submandibular ICA (EC-ICA)

transducer blue. There are changes in color Doppler direction when the physiologic direction of flow changes, for example with collateral flow through the circle of Willis. When arteries are recruited as collateral, physiologic flow direction will change in any non-end artery (ACA1, ICA, PCA1, VA & BA). When physiologic flow direction changes the color map will change accordingly.

Changes in color Doppler also occur in tortuous or anatomically curving vessels, such as the cavernous internal carotid artery. In this case, physiologic flow direction (antegrade/retrograde) is unchanged but the direction of flow relative to the transducer and ultrasound beam does.

Comments on Angle Correction

Non-imaging transcranial Doppler always assumes a zero degree angle of insonation for all vessel segments. TCDI allows for angle corrected flow velocity measurements which will always introduce a variable in the Doppler equation ($V = c(Fd)/2f(\cos\theta)$) and velocity calculation. It is therefore important to use angle correction only when the sample volume can be placed in a vessel segment that is long enough to trace the main flow vector and positioned to obtain the lowest possible angle [3] (Table 2).

Table 2 Ultrasound equipment control settings for B-mode, color Doppler and spectral Doppler

B-Mode
Select 1.0–5.0 MHz range phased array sector transducer and presets for TCD exam
B-mode gain increases or decreases image brightness
Color Doppler
Select a high setting for *color persistence*
Keep *color Doppler box (gate)* width as narrow as necessary to improve the frame rate and color flow signal acquisition
Increase *color Doppler gain* to increase color fill or decrease if the color is bleeding outside presumed vessel walls
Set *color scale*/PRF low for slow flow and high for fast flow
Inverting the color scale changes the way negative and positive Doppler shifts (flow direction and color) are represented on the image

Table 2 (continued)

Spectral Doppler
Use *spectral Doppler sample volume* (SV) size between 3.0 and 10.0 mm; SV depth and position are adjusted to acquire vessels at different depths or locations
Set spectral Doppler *velocity scale* to normal values; adjust baseline and scale to record higher or lower velocities so the waveform occupies two-thirds of the area without touching the top or bottom of the display
Optimize *spectral gain* so the waveform is easily visible without background noise on the display
Angle correction set at zero degrees unless vessel is >45 degrees off axis avoids overestimation of velocities.
Other settings
Sweep speed is adjustable, for best analysis of waveform morphology display about four cardiac cycles per sweep. To appreciate changes over time or during provocation use a slow sweep speed.
Invert changes the display of the direction of the flow waveform. Convention has flow towards above and flow away below the baseline
Enlarge an area of interest using the *zoom* function
Use the ALARA (as low as reasonably achievable) principle to adjust *power output*

Finding the Temporal Bone Window

The quality of the exam using the TTW is dependent on the thickness of the temporal bone and approximately 10% of patients will have incomplete or absent identification of the basal cerebral vessels due to hyperostosis [3].

The left and right hemispheres should each be studied from the ipsilateral side unless there is access only on one side. Crossing midline to insonate contralateral vessels will diminish signal strength and make the assessment of Doppler angles challenging (Fig. 2).

Apply gel and place the transducer just above the zygomatic arch and in front of the external auditory canal. Begin using B-mode only with a depth setting of 8–10 cm. Observe the B-mode image of the skull base. If there is an adequate acoustic window bright boney landmarks will be seen forming a crescent shape at the depth of approximately 5 cm. These bright reflections represent the lesser wing of the sphenoid bone (anterior) and the petrous ridge of the temporal bone (posterior). If all reflections are homogenous there may be no ultrasonic window.

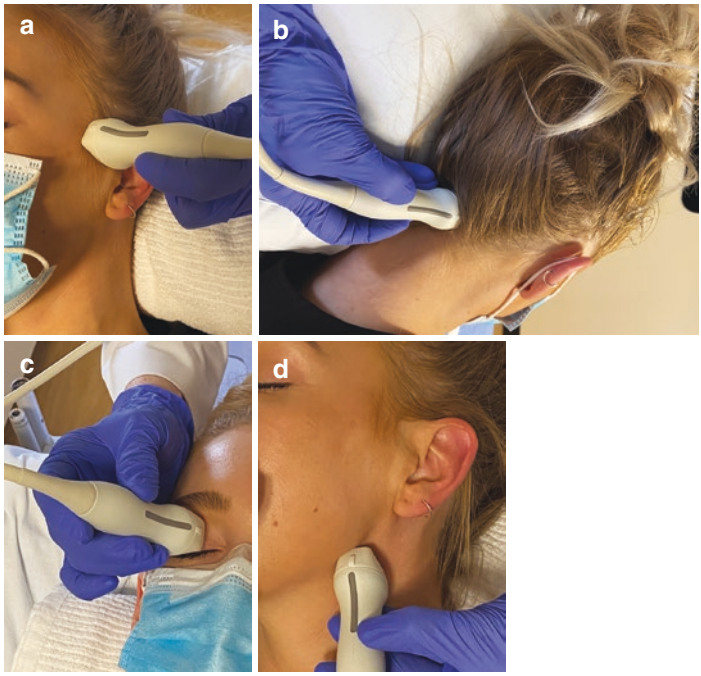

Fig. 2 (**a**) TOW: transducer placed above zygomatic arch; orientation marker anterior/up (**b**) SOW: transducer placed below foramen magnum; orientation marker to the right (**c**) TOW: transducer directly over closed eye; orientation marker medial/nose (**d**) SMW: transducer below angle of jaw; orientation marker anterior/up

Continue using B-mode only, increase depth to 15–16 cm and aim directly parallel to the zygomatic arch. This produces an image of mesencephalic structures: cerebral peduncle, midline, optic chiasma tract and the contralateral skull (Figs. 3 and 4; Tables 3 and 4).

Identifying the terminal ICA

1. Reduce B-mode depth to 8–10 mm to study the ipsilateral hemisphere
2. Use the base of skull scan plane
3. Turn on color Doppler, center the color box gate over the anterior clinoid process around which the ICA courses. TICA (C1) will appear in cross section as a small circle of color.

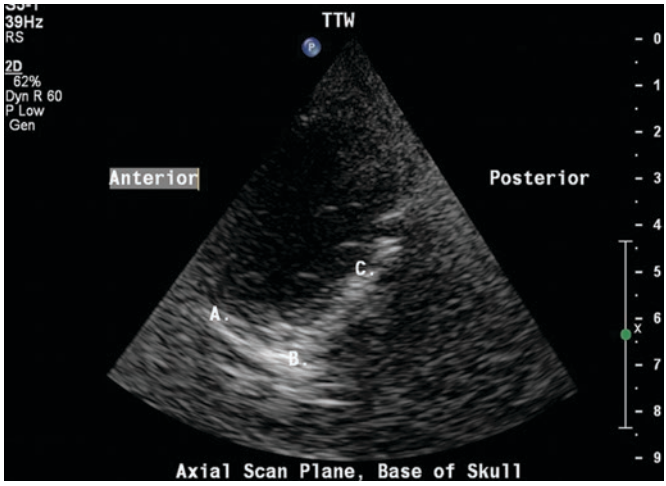

Fig. 3 Axial scan plane at the base of skull level showing bright reflections from bone (A) lesser wing of sphenoid, (B) anterior clinoid process (C) petrous ridge

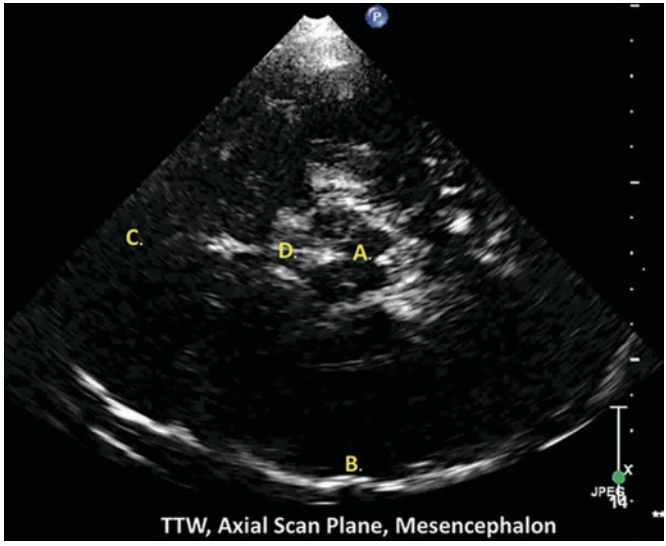

Fig. 4 Axial scan plane at the level of the mesencephalon (A) cerebral peduncle, (B) contralateral skull (C) midline (D) optic chiasma, tract

Table 3 Temporal window axial scan planes and anatomy

Scan plane	Transducer level	B-mode anatomy
Base of skull	Tilt inferior	Lesser wing of sphenoid bone, petrous ridge, anterior clinoid process
Mesencephalon	Parallel to zygomatic arch	Midbrain, peduncles (butterfly shaped)

4. Obtain a spectral Doppler waveform from the TICA and document the highest velocity. The angle of insonation may be suboptimal due to the perpendicular course of this artery relative to the sound beam and resultant velocities may be lower than expected due to this technical limitation.
5. Change the transducer orientation to coronal opening the vessel longitudinally. The ICA is tortuous, and color may appear blue, red or both due to its course. This approach provides access to the cavernous carotid segments with better insonation angles (Fig. 5).

Identifying the MCA

1. Increase the color box size and position above the lesser wing of the sphenoid bone; the MCA courses parallel and above this boney landmark, is flowing towards the transducer and will appear as color Doppler red.
2. Tilt the transducer superior/upwards to see the proximal M2 segments which may appear blue in color as they course up into the sylvian fissure and flow away from the transducer.
3. Place the spectral Doppler sample volume in the distal M2 segment/s. Sample the MCA in 2.0–5.0 mm increments obtaining spectral waveforms at each depth.
4. Document the M2 branches, distal, mid and proximal segments of the main trunk of the MCA 1. Record the highest velocities at each segment.

The Bifurcation Landmark

The terminal ICA bifurcates into the middle and anterior cerebral arteries and can function as a landmark to use for orientation to the other arteries of the circle of Willis. Flow is divided at this

Table 4 Approach, depths, color/flow direction and mean velocities for normal adults [13–16]

Approach	Artery	Depth range (mm)	Flow direction relative to transducer	Color flow map	TCD, TCDI: Normal mean velocity (cm/s) No angle correction, All ages	TCDI: Normal mean velocity (cm/s) Angle corrected Age 20–39	TCDI: Normal mean velocity (cm/s) Angle corrected Age 40–59	TCDI: Normal mean velocity (cm/s) Angle corrected Age ≥ 60
Temporal	MCA 1	35–60	Towards	Red	51 (24–79)	74 (71–76)	72 (69–76)	58 (55–61)
Temporal	MCA 2	25–35	Towards or Away	Red/ Blue				
Temporal	TICA (coronal plane)	60–70	Towards or Away	Red/ Blue	41 (37–45)			
Temporal	TICA Bifurcation	60–70	Towards or Away	Red/ Blue				
Temporal	ACA 1	60–75	Away	Blue	45 (24–67)	60 (57–62)	61 (57–64)	51 (48–54)
Temporal	ACA 2	65–75	Away	Blue				
Temporal	ACOA	65–75	Indeterminate					
Temporal	PCA 1	60–75	Towards	Red	37 (19–55)	53 (51–55)	49 (48–51)	42 (40–45)
Temporal	PCA 2	60–65	Away	Blue		47 (45–49)	48 (46–51)	42 (39–45)
Temporal	PCOA	60–65	Indeterminate					

(continued)

Table 4 (continued)

Approach	Artery	Depth range (mm)	Flow direction relative to transducer	Color flow map	TCD, TCDI: Normal mean velocity (cm/s) No angle correction, All ages	TCDI: Normal mean velocity (cm/s) Angle corrected Age 20–39	TCDI: Normal mean velocity (cm/s) Angle corrected Age 40–59	TCDI: Normal mean velocity (cm/s) Angle corrected Age ≥ 60
Occipital	VA-3 (atlas)	40–50	Both (tortuous)	Blue				
Occipital	VA-4	60–90	Away	Blue	38 ± 10	44 (42–47)	40 (38–43)	33 (30–36)
Occipital	PICA	60–90	Towards	Red				
Occipital	BA	70–120	Away	Blue	41 ± 10	50 (47–53)	44 (39–48)	35 (31–40)
Submandibular	Extracranial ICA	35–80	Away	Blue	30 ± 9			
Orbital	OA	35–55	Towards	Red	21 ± 5			
Orbital	ICA (C4, C3, C2)	65–80	C4 Towards, C3 Bidirectional, C2 Away	C4 Red, C3 Red/Blue, C2 Blue	C4 47 ± 14 C2 41 ± 11			

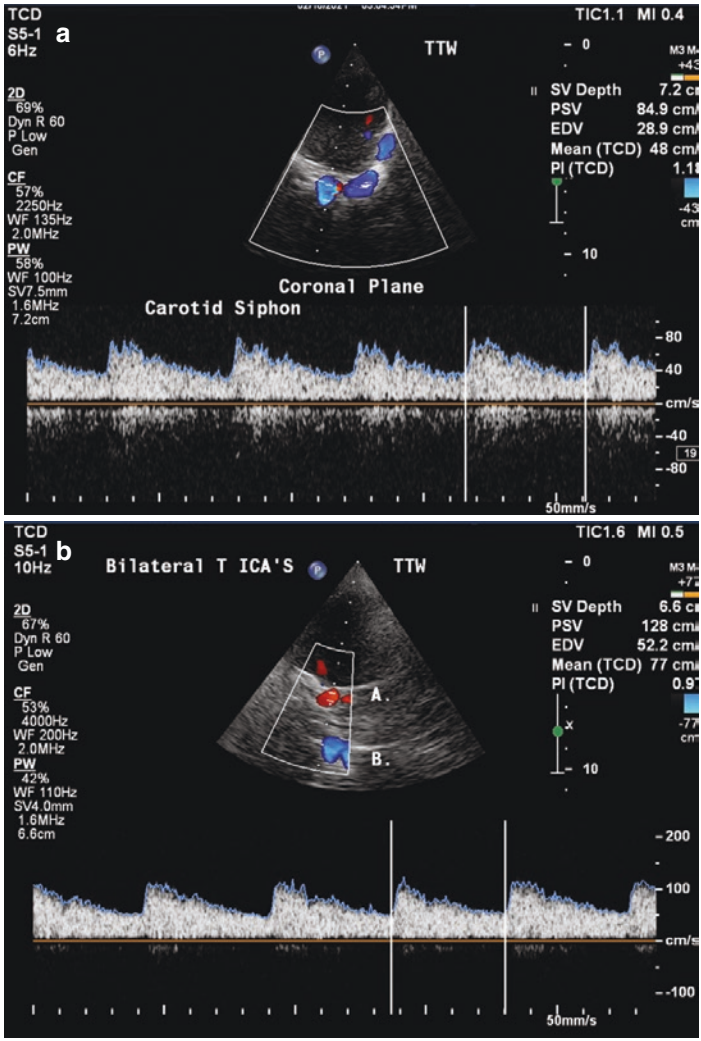

Fig. 5 Left: TTW axial scan plane (**a**) ipsilateral TICA (**b**) contralateral TICA. Right: TTW, coronal scan plane, color box placed over cavernous carotid, spectral waveform from supraclinoid ICA

location to supply the MCA (towards/red) and the ACA (away/blue). The TICA is inferior to, and the PCA posterior to this landmark.

Identifying the ACA

1. The ACA (A1) is close to midline and often anterior (to the left of the screen) to the landmark bifurcation. Normal flow direction is away from the transducer. Moving the transducer into a coronal plane often provides good visualization of the ACA. The zoom function may be used to help focus on this short ACA 1 segment. The ACA 2 portion is seen at midline, anterior and perpendicular to the ACA 1. Obtain spectral waveforms from each segment, document the highest velocity.
   - Tip: there should be no bright bone reflections around the ACA; if seen the artery is the TICA- move the transducer superior to correct.
   - Tip: if there is no color fill try placing the spectral Doppler in the region where the ACA would normally be located (Fig. 6).

Identifying the PCA

1. Locate the mesencephalic brainstem using B-mode.
2. Place the color box over the peduncles, which are encircled by the PCA's. The PCA1 and proximal PCA2 will appear as red (flowing towards the transducer). As the PCA 2 curves around the peduncles the flow orientation changes to away from the transducer (blue)
3. To differentiate between PCA 1 and PCA 2 segments, open the color box to include the TICA simultaneously with the PCA. Draw an imaginary line between these two arteries- this will be the location of the PCOA. If large, serving as collateral or of fetal origin it will color fill and spectral Doppler signals can be obtained, however, due to the poor angle of insonation it may not be positively identified.
4. Obtain spectral Doppler signals from PCA1 and PCA2 (Fig. 7).

Finding the Transorbital Window

Considerations

Determine if equipment manufacturer has FDA approval for orbital imaging then select the machine's preset for transorbital testing which will have limited, approved power output. The study

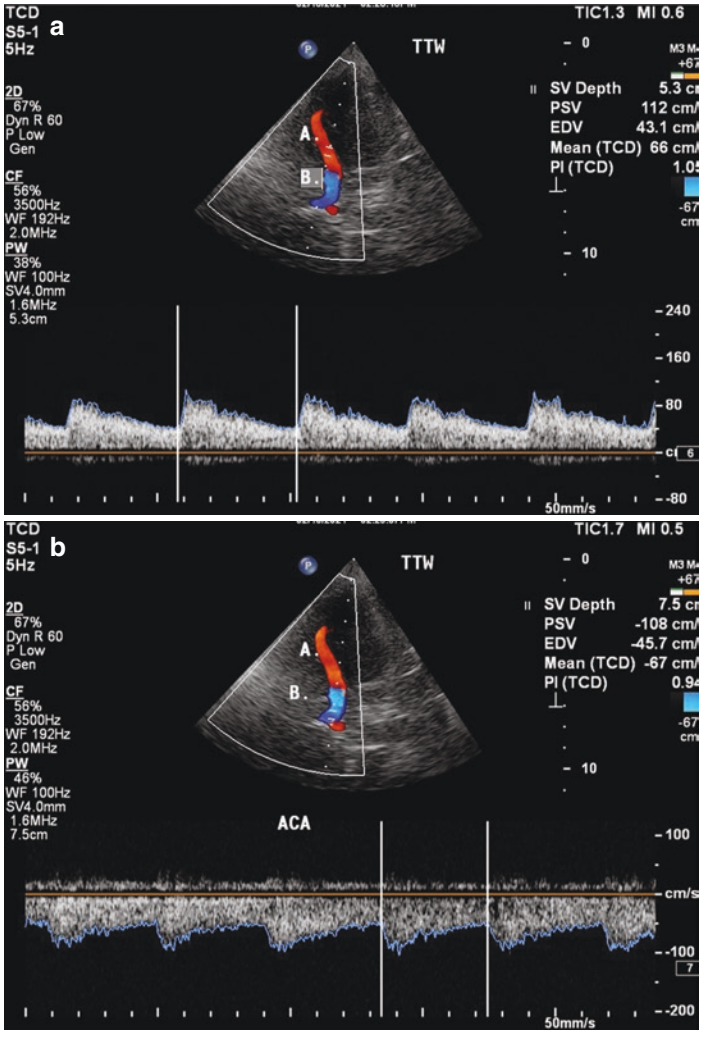

Fig. 6 (**a**) A. MCA main trunk with spectral waveform B. ACA 1 segment, color only. (**b**) A. MCA main trunk, color only B. ACA 1 segment with spectral waveform

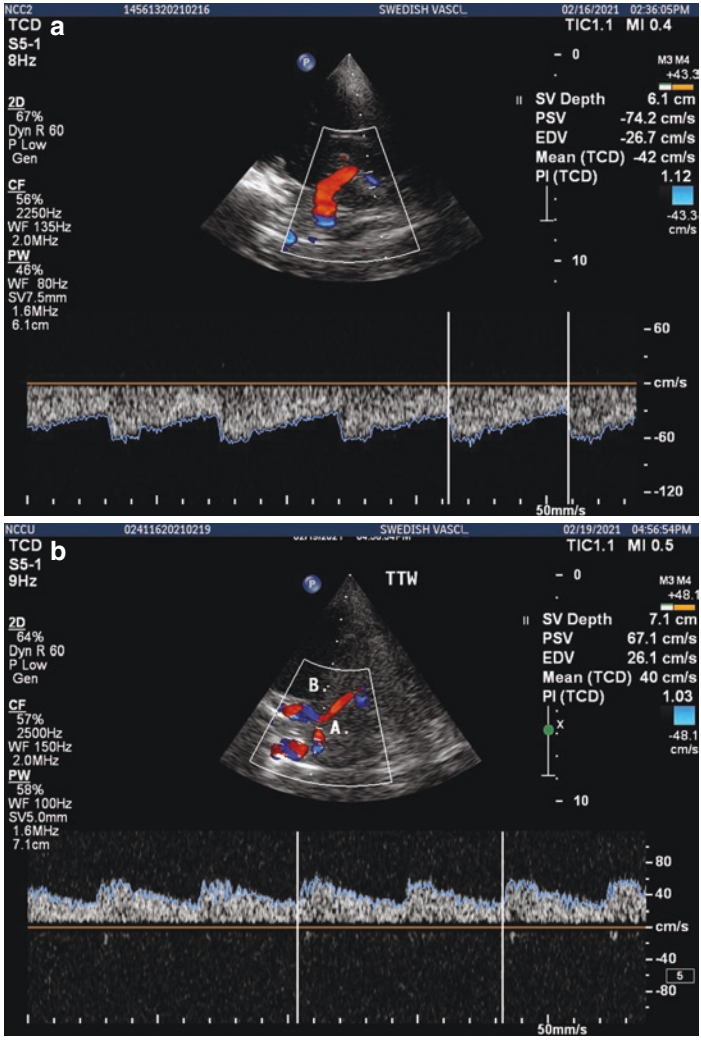

Fig. 7 (**a**) Ipsilateral PCA1 with spectral waveform (**b**) ipsilateral TICA, PCOA and PCA2 flowing away from transducer

must be done at a lowered power setting with a mechanical index not greater than 0.23 to prevent ocular injury [17].

Recent unhealed trauma or surgery to the eye and artificial eyes are contraindications for this approach

Use minimal gel, the salt compounds in the gel may be irritating or cause eye discomfort. Have patient keep eyelids shut throughout exam.

Do not apply pressure to the eye.

Remove gel before the patient reopens their eyes

1. The transducer orientation marker is pointed towards the nose (on both right and left sides). The screen will display medial to the left and lateral to the right
2. Gently place the transducer centered on the eyelid
3. Start with a B-mode depth of 6.0 cm
4. Place a thin layer of gel on the transducer and position in a horizontal scan plane with an anterior to posterior orientation
5. Identify the globe of the eye in the near field and the acoustic shadow of the optic nerve behind the globe.

Identifying the OA

1. Rotate the transducer aiming the sound beam about 15–20 degrees medial. The optic nerve shadow will distort or disappear. Turn on color Doppler and orient the color box below the posterior aspect of the globe and over the optic nerve shadow at a depth of 3–6 cm
2. The OA is lateral to the optic nerve before it crosses over it and then courses medial sending off branches. It is flowing towards the transducer and appears red.
3. Spectral Doppler signals are taken at depths ranging from 3.0 to 6.0 cm depending on the level of best visualization. The characteristic OA waveform has high resistance. Evaluate the direction of flow, waveform morphology and velocity and document.

Identifying the ICA (carotid siphon)

1. Set B-mode depth to 8.0 cm and locate the B-mode echogenic reflections arising from the medial and lateral rectus muscles which form a V shape deep to the orbit.
2. Place the color box at 6.0–7.0 cm depth and slowly sweep the color box from the left to the right of the screen. This part of the ICA is tortuous, and flow may appear as blue (away) or red (towards) the transducer and represents the parasellar, genu and supraclinoid ICA segments.

3. Spectral Doppler: Sample all visible segments documenting the highest velocities (Fig. 8).

Finding the Suboccipital Window

1. Place the transducer below foramen magnum with the orientation marker to the patient's right (this orients the right vertebral on the left of the screen)
2. Position transducer two finger widths below the skull base, at midline, aiming the ultrasound beam towards the nasion. Alternatively, the transducer may be placed slightly lateral to midline and aimed at the contralateral orbit.
3. B-mode appearance of the foramen magnum appears as an anechoic circular shape surrounded by bright reflections from the occipital bone at a depth of about 5.0 cm.

Identifying the VA's and BA

1. Place the color box at a depth of 5.0–9.0 cm. In the near field (depths of 5.0–5.5 cm) color Doppler will be bidirectional caused by the artery changing course as it moves from the atlas through the foramen magnum and continues as the V4 segment which travels away from the transducer (blue). Both VA's may or may not be seen simultaneously depending on their course, plane and tortuosity.
2. The two VA's confluence at depths ranging from 7.0 to 9.0 cm depending on body habitus. They meet and form a V shape which extends into a Y shape as the basilar artery is observed at a greater depth. The PICA is often seen as a branch coming off prior to the VA confluence and usually flows towards the transducer (red).
3. Spectral Doppler signals are obtained in 2–5 mm increments from proximal to distal.
4. To identify the BA, narrow the color box and place between 7.0 and 10.0 cm depth. It is often curving (C shape) to the left/right of the screen. Slide the transducer slightly inferior and aim superior to open up the mid-distal portions. If no color signal is seen use the spectral Doppler to locate a signal in the expected area of the vessel course.

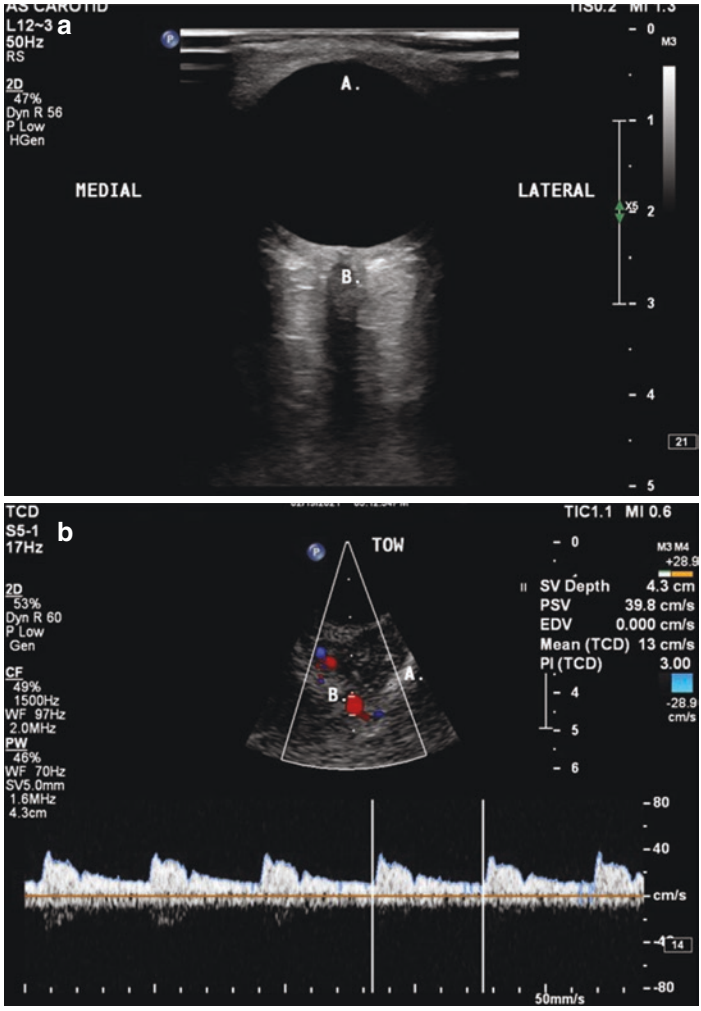

Fig. 8 (**a**) A. Eye globe B. optic nerve (**b**) ophthalmic artery (**c**) carotid siphon

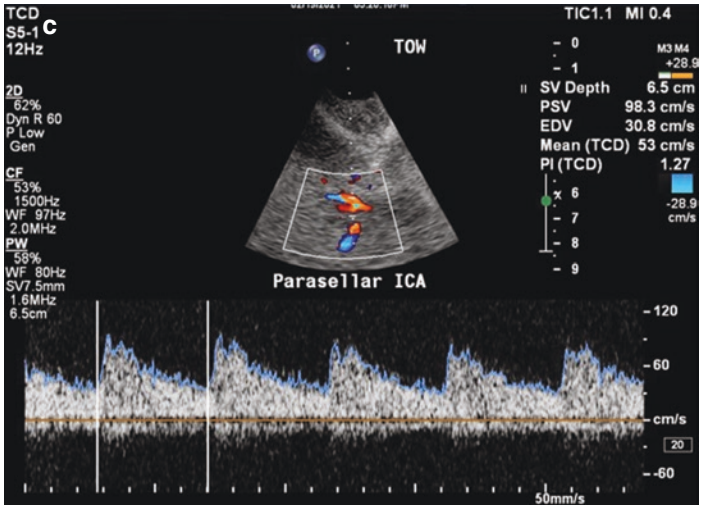

Fig. 8 (continued)

5. When possible obtain and document proximal, mid and distal spectral Doppler signals, from the right and left VA's and BA; always seeking to acquire the highest velocity (Fig. 9).

Finding the Submandibular Window

This approach is useful to obtain the retromandibular, extracranial ICA in patients with subarachnoid hemorrhage in order to calculate the Lindegaard ratio. Obtaining this ratio differentiates high MCA velocities caused by vasospasm from high MCA velocities caused by hyperdynamic flow. It may also be useful for intracranial stenosis, feeding vessels to arteriovenous malformations and fistulae and other etiologies of increased cerebral blood flow. Identifying the EC-ICA using this technique can also be used to identify distal EC-ICA dissections and narrowing secondary to fibromuscular dysplasia.

Power can be reduced since no bone penetration occurs with this approach. Depth is set at 7.0 cm.

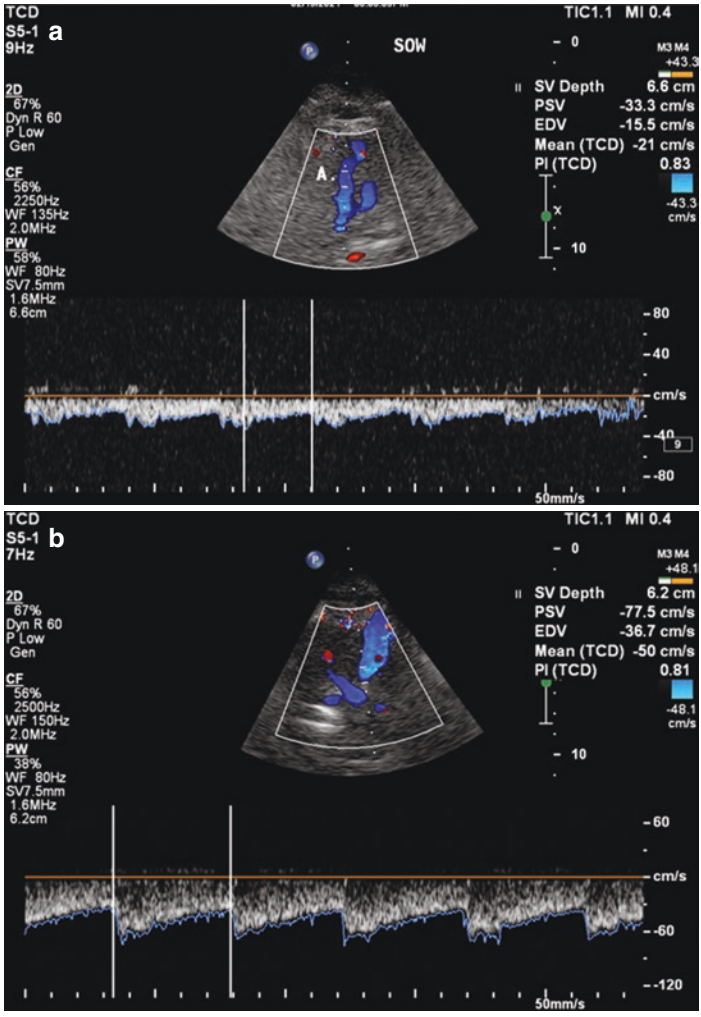

Fig. 9 (**a**) Suboccipital window, left VA (**b**), right VA (**c**) BA

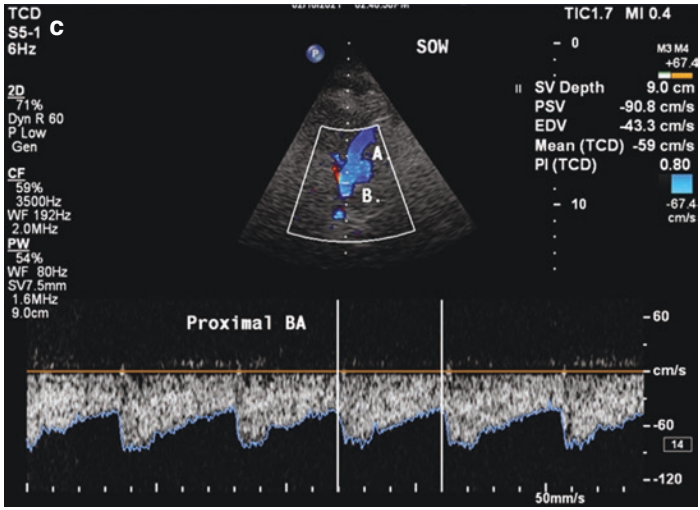

Fig. 9 (continued)

Place the transducer orientation marker anterior and use a zero degree angle of insonation for the spectral Doppler. Do not use a lateral approach as is the convention for carotid duplex studies.

Place transducer at the angle of the jaw directing the ultrasound beam superior with a slight medial and posterior orientation. The EC-ICA will appear in the near field, coursing from the right to the left side of the screen, flowing away from the transducer. Obtain the spectral Doppler at depths of 4.0–5.0 cm where a zero-degree angle can be obtained. Take the highest velocity signal; failure to achieve the highest velocity because of poor technique can cause false positive Lindegaard ratio results (Fig. 10).

Documentation

IAC standards for documentation for a full TCDI study include B-mode, color and spectral Doppler waveforms from the following arteries: Proximal MCA1, ACA1, ACOA when cross filling, TICA, PCA1 or PCA2, PCOA when collateralizing, OA, ICA

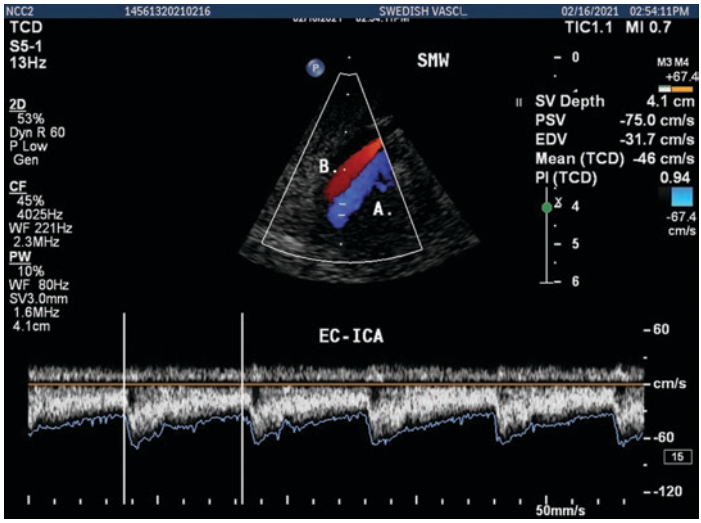

Fig. 10 (A) EC-ICA flowing away from the transducer (B) internal jugular vein flowing towards the transducer

(siphon), VA4, BA proximal and distal, EC-ICA when used for Lindegaard ratio [18].

A permanent record of all images representative of the interpretation along with any incidental findings are recorded and stored. Images should be labeled with patient and facility identification, date of exam, and side (right or left) of the anatomy. A formal report of the findings should be placed into the patient's medical record. Retention of these records should comply with clinical and legal requirements [17].

Diagnostic Findings (Fig. 11)

There are four main features of the Doppler spectral waveform used for the interpretation of the intracranial hemodynamics. They are velocity, pulsatility, systolic upstroke and spectral distribution.

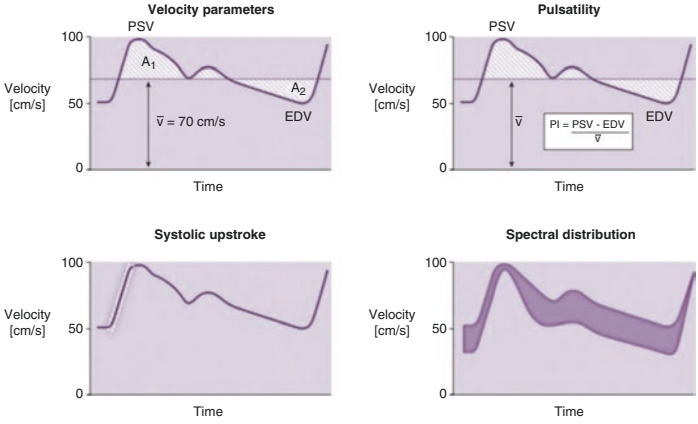

Fig. 11 Waveform analysis. (Adapted from: Douville [20])

Velocity

Waveform analysis requires quantification of velocity and the convention for TCDI is to use the "mean" velocity defined as the time mean of the peak velocity envelope or the tracing of all peak flow velocities as a function of time. The mean velocity is calculated and displayed automatically and can be relied on only when there is visual confirmation that the envelope trace is accurately following the spectral waveform. This may require adjusting the Doppler gain settings and in some instances a manual trace will be required to achieve accurate values [19].

Pulsatility

Describes the amount of variability in the velocity between systole and diastole as a result of the pulsatile nature of the heart. The more similar these values are the lower the pulsatility, and conversely the greater the difference, the higher the pulsatility. Goslings pulsatility is normally used in the adult population and is influenced by distal resistance in the brain and proximal effects, commonly from the heart [19].

Systolic Upstroke

The initial slope of the peak velocity envelope during acceleration phase of systole creates a steep slope with short time from onset

to peak systole. This becomes delayed when distal to a lesion in a supply vessel [19].

Spectral Distribution

Refers to the velocity distribution within the spectral waveform, also called bandwidth. A narrow bandwidth demonstrates high amplitude concentrated in the upper part of the waveform and is consistent with laminar flow. When the amplitude migrates across the waveform and is greatest around the baseline it represents turbulent flow [19].

Report Example

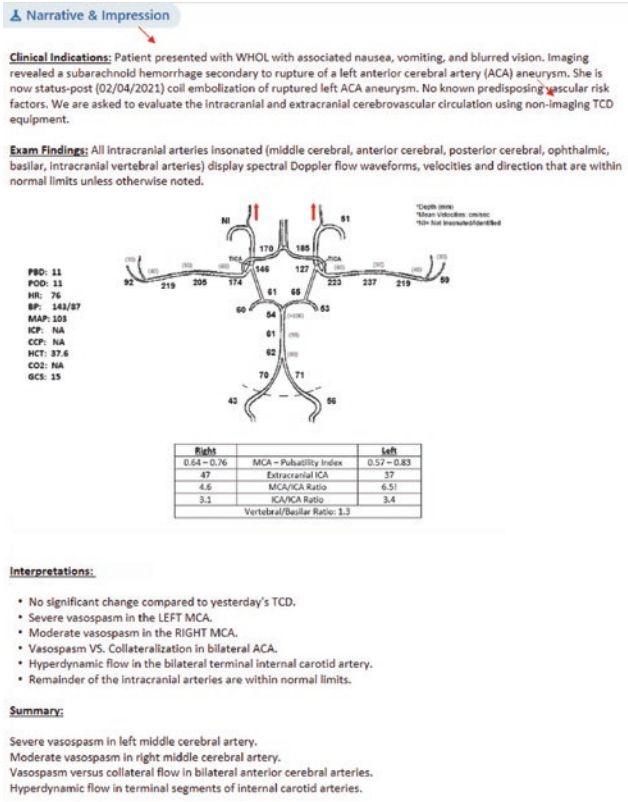

Narrative & Impression

Clinical Indications: Patient presented with WHOL with associated nausea, vomiting, and blurred vision. Imaging revealed a subarachnoid hemorrhage secondary to rupture of a left anterior cerebral artery (ACA) aneurysm. She is now status-post (02/04/2021) coil embolization of ruptured left ACA aneurysm. No known predisposing vascular risk factors. We are asked to evaluate the intracranial and extracranial cerebrovascular circulation using non-imaging TCD equipment.

Exam Findings: All intracranial arteries insonated (middle cerebral, anterior cerebral, posterior cerebral, ophthalmic, basilar, intracranial vertebral arteries) display spectral Doppler flow waveforms, velocities and direction that are within normal limits unless otherwise noted.

PBO: 11
POD: 11
HR: 76
BP: 143/87
MAP: 103
ICP: NA
CCP: NA
HCT: 37.6
CO2: NA
GCS: 15

Right		Left
0.64 – 0.76	MCA – Pulsatility Index	0.57 – 0.83
47	Extracranial ICA	37
4.6	MCA/ICA Ratio	6.5!
3.1	ICA/ICA Ratio	3.4
Vertebral/Basilar Ratio: 1.3		

Interpretations:

- No significant change compared to yesterday's TCD.
- Severe vasospasm in the LEFT MCA.
- Moderate vasospasm in the RIGHT MCA.
- Vasospasm VS. Collateralization in bilateral ACA.
- Hyperdynamic flow in the bilateral terminal internal carotid artery.
- Remainder of the intracranial arteries are within normal limits.

Summary:

Severe vasospasm in left middle cerebral artery.
Moderate vasospasm in right middle cerebral artery.
Vasospasm versus collateral flow in bilateral anterior cerebral arteries.
Hyperdynamic flow in terminal segments of internal carotid arteries.

References

1. Krejza J, Kochanowicz J, Mariak Z, Lewko J, Melhem ER. Middle cerebral artery spasm after subarachnoid hemorrhage: detection with transcranial color-coded duplex US. Radiology. 2005;236(2):621–9.
2. Baumgartner RW. Transcranial color duplex sonography in cerebrovascular disease: a systematic review. Cerebrovasc Dis. 2003;16:4–13.
3. Nedelmann M, Stolz E, Gerriets T, Baumgartner RW, Malferrare G, Seidel G. Consensus recommendations for transcranial color-coded duplex sonography for the assessment of intracranial arteries in clinical trials on acute stroke. Stroke. 2009;40:3238–44.
4. Baumgartner RW, Baumgartner I, Mattle HP, Schroth G. Transcranial color-coded duplex sonography in the evaluation of collateral flow through the circle of Willis. AJNR Am J Neuroradiol. 1997;18(1):127–33.
5. Sallustio F, Kern R, Gunther M, Szabo K, Greibe M, Meairs S, et al. Assessment of intracranial collateral flow by using dynamic arterial spin labeling MRA and transcranial color-coded duplex ultrasound. Stroke. 2008;39:1894–7.
6. Saqqur M, Khan K, Derksen C, Alexandrov A, Shuaib A. Transcranial Doppler and transcranial color duplex in defining collateral cerebral blood flow. J Neuroimaging. 2018;28(5):455–76.
7. Krejza J, Baumgartner RW. Clinical applications of transcranial color-coded duplex sonography. J Neuroimaging. 2004;14(3):215–25.
8. Blanco P. Cerebral circulatory arrest detected by transcranial color-coded duplex sonography: a feasible diagnosis for intensivists. J Ultrasound Med. 2015;34:1337–40.
9. Chang JJ, Tsivgoulis G, Katsanos AH, Malkoff MD, Alexandrov AV. Diagnostic accuracy of transcranial Doppler for brain death confirmation: systematic review and meta-analysis. AJNR Am J Neuroradiol. 2016;37:408–14.
10. Bulas DI, Jones A, Seibert JJ, Driscoll C, O'Donnell R, Adams RJ. Transcranial Doppler (TCD) screening for stroke prevention in sickle cell anemia: pitfalls in technique variation. Pediatr Radiol. 2000;30(11):733–8.
11. Krejza J, Rudzinski W, Pawlak MA, Tomaszewski M, Ichord R, Kwiatkowski J, et al. Angle-corrected imaging transcranial Doppler sonography versus imaging and nonimaging transcranial Doppler sonography in children with sickle cell disease. AJNR Am J Neuroradiol. 2008;28:1613–8.
12. McCarville MB. Comparison of duplex and nonduplex transcranial Doppler ultrasonography. Ultrasound Q. 2008;24(3):167–71.
13. Barrientos-Guerra JD, Flores-Silva F, Cantú-Brito C, Chiquete E. Evaluation of cerebral hemodynamics with color-coded duplex sonog-

raphy: normative values with correction of insonation angles. J Stroke Cerebrovasc Dis. 2020;29(3):104595.
14. Martin PJ, Evans DH, Ar N. Transcranial color-coded sonography of the basal cerebral circulation: reference data from 115 volunteers. Stroke. 1994;25(2):390–6.
15. Valaikiene J, Schlachetzki F, Hoelscher T, May A, Bogdahn U. Transcranial color-coded duplex sonography of the carotid siphon, the coronal approach. J Clin Imaging. 2002;26:81–5.
16. Nabavi DG, Otis SM, Ringelstein EB. Ultrasound assessment of the intracranial arteries. In: Zweibel WJ, Pellerito JS, editors. Introduction to vascular ultrasonography. Philadelphia: Elsevier Saunders; 2005. p. 225–50.
17. American College of Radiology (ACR), Society for Pediatric Radiology (SPR), Society of Radiologists in Ultrasound (SRU). AIUM practice guideline for the performance of a transcranial Doppler ultrasound examination for adults and children. J Ultrasound Med. 2012;31(9):1489–500.
18. IAC Standards and Guidelines for Vascular Testing Accreditation (Published November 1, 2020) 31 ©2020 Intersocietal Accreditation Commission. All Rights Reserved.
19. Fujioka KA, Douville CM. Anatomy and freehand examination techniques. In: Newell DW, Aaslid R, editors. Transcranial Doppler. New York: Raven Press; 1992. p. 9–31.
20. Douville CM. Intracranial cerebrovascular examination. In: Kupinski AM, editor. The vascular system. Philadelphia: Wolters Kluwer; 2018. p. 123–50.

TCD Procedures and Protocols: Protocol for Monitoring for Emboli Detection (and With Microbubbles)

Larry N. Raber

Transcranial Doppler monitoring for emboli will be performed using the blind Doppler technique.

A dedicated TCD unit should be used with 2 MHz pulsed Doppler transducers.

The examination will be explained to the patient.

Patient is supine with head in the neutral position.

The vessel to be insonated for emboli detection will be identified. The middle cerebral artery is the easiest vessel to utilize for this purpose. Either bilateral or unilateral MCA monitoring will be performed depending on the suspected embolic source. If a central embolic source is suspected (cardiac, A-fib, aortic arch pathology) bilateral monitoring will be performed. If carotid pathology is the suspected source of emboli unilateral monitoring can be performed on the ipsilateral MCA.

As with the diagnostic TCD examination the MCAs will be identified using the transtemporal approach. The MCA is

L. N. Raber (✉)
Clinical Manager Ultrasound-Neurovascular Laboratory, Imaging Institute, Cleveland Clinic, Cleveland, OH, USA
e-mail: Raberl@ccf.org

W. C. Ziai, C. L. Cornwell (eds.), *Neurovascular Sonography*,
https://doi.org/10.1007/978-3-030-96893-9_30

insonated at depths of 45–65 mm for the skin surface. The direction of flow of the MCA in normal pathology will be towards the transducer. The lowest power settings will be used that will provide optimal penetration. Spectral gain will be optimized.

It is easier to identify the optimal temporal acoustic window using the diagnostic 2 MHz transducer first before placing the head band on the patient. This will give you a good idea of where to place the monitoring probe and the best angle to direct the monitoring probe to insonate the MCA for an optimal spectral signal. Some facilities will put a small mark on the patient's skin after locating the optimal spectral window with the diagnostic probe to help locating the best window with the monitoring probes attached to the head band.

After localizing the optimal temporal acoustic windows the head band will be placed on the patient with the monitoring probes attached according to the manufacture of the head bands recommendations. The proper placement of the head band and monitoring probes is demonstrated Fig. 1.

The MCAs will be monitored at the same depth bilaterally for a set amount of time that is established by your institution. If a MCA stenosis is suspected the monitoring depth should be set distal to the stenosis if possible to detect emboli.

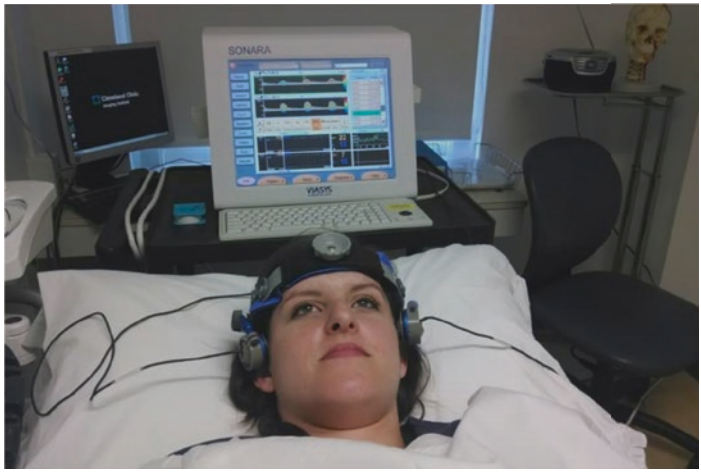

Fig. 1 Proper placement of the monitoring head band

Routinely the MCAs are monitored continuosly for 30–60 min. Depending on the patients clinical presentation a longer monitoring time may sometimes be required.

The automatic emboli detection software on your unit will be enabled and the entire examination saved on hard drive for review.

All suspected emboli will be recorded for later visual and auditory review. Number of emboli will be counted and documented on the final report. Showers or curtain of emboli will be reported as the duration of the shower measured in seconds. Criteria for the identification of emboli have been established and should be followed. Emboli have characteristic signals. They occur sporadically within the cardiac cycle. They are usually transient (.01–.1 s) in duration. They can, however, be seen in showers giving prolonged rough signal similar to artifact. They have intensities which are 3 dB greater than the background Doppler signal. Emboli may have variable signal intensities in the same patient. The sound produced by an embolus is harmonic and described as chirps, whistles or plops.

Consensus committee of the ninth International Cerebral Hemodynamics Symposium. Basic identification criteria of Doppler microembolic signal. *Stroke*. 1995;26:1123

Reporting

The number of embolic events will be reported bilaterally. The mean flow velocity and PI within the insonated depth of the MCA will be reported. An asymmetry >20% within the mean flow velocities or PIs may require a complete TCD diagnostic exam to be performed.

Agitated Saline Protocol: TCD Bubble Study

The TCD bubble study will be performed using the blind Doppler technique.

Dedicated TCD unit will be used with 2 MHz pulsed Doppler transducers.

Transcranial Doppler is a simple method to detect a right-to-left shunt as a Patent Forman Ovale or pulmonary AVM. Patients with a possible stroke risk factor from a paradoxical embolism can be easily identified by this examination.

The examination is explained to the patient.

Patient is supine with the head in the neutral position.

Optimal MCA spectrums will be obtained using the documented conventional TCD protocol.

The Transcranial Doppler head band will be positioned on the patient using same protocol as the when performing bilateral TCD monitoring for emboli.

The middle cerebral arteries will be identified bilaterally and monitored continuously during the procedure. Intravenous access will be established by a caregiver trained in venipuncture.

Automated emboli detection software will be enabled and entire examination saved on hard drive for review.

Set up for the examination will include:

1. Two 10 cc syringes
2. One 3 way stopcock
3. 9 cc normal saline

The set up used for the TCD bubble study, Fig. 2, one 10 cc syringe is filled with 9 cc normal saline and attached to the 3-way stop cock. The other empty 10 cc syringe is attached to the other port of the stop cock.

One syringe is filled with 9 cc of normal saline solution. The second syringe is filled with 1 cc of air. Using the saline filled syringe, several drops of the patient's blood will be withdrawn to act as an emulsifier.

The solution will be agitated by withdrawing and injecting between the two syringes with the stopcock turned off to the patient. Once the solution is agitated to satisfaction (usually withdrawing and injecting between the two syringes 10 times). After agitating the saline the saline is collected into a single syringe, the stopcock is turned on to the patient and injected into the venous

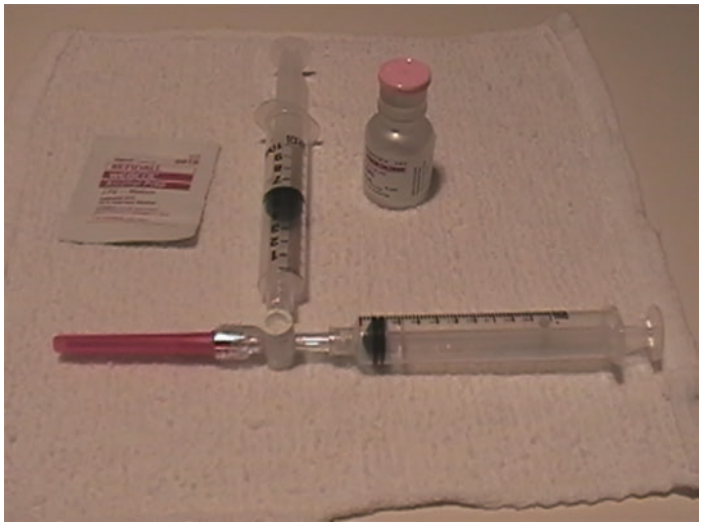

Fig. 2 Set-up for the TCD bubble study

access of the patient. Immediately after injection the patient is asked to perform a Valsalva maneuver to provoke right-to-left shunting. It helps to explain the Valsalva maneuver to the patient before the procedure to be sure it is done correctly. Any air emboli will be detected and recorded.

Reporting

Air emboli will be detected and recorded. Emboli will be counted and classified as detected with injection, Valsalva, and post Valsalva. The number of air emboli detected in the MCAs will be reported individually. If a shower or curtain of emboli is detected it will be reported in seconds of duration. If emboli only detected post Valsalva, late in the cardiac cycle, this may suggest pulmonary shunting vs. cardiac. Examination is reported as negative, no evidence of right to left shunt if no embolic events are detected.

Protocol for Procedures: How to Obtain Measurements of the Optic Nerve Sheath Diameter in Adults and Children Utilizing Point-of-Care Ophthalmic Ultrasonography

Becky J. Riggs and Megan F. Hunt

Purpose: Non-invasive diagnostic and monitoring tool to detect intracranial hypertension.

Indications: Clinical exam or pathology suggestive of possible intracranial hypertension. Suggested pathology is traumatic brain injury, brain tumor, stroke, liver failure, diabetic ketoacidosis, cerebral edema, and ventriculoperitoneal shunt failure. See chapters "Clinical Application of Cerebrovascular Physiology" and "Optic Nerve Sheath Diameter for Increased Intracranial Pressure" for expanded clinical applications of ultrasound guided ONSD measurements.

Equipment: bedside ultrasound machine, linear array ultrasound probe, ophthalmic safe eye gel or Tegaderm™ with ultrasound gel.

B. J. Riggs (✉)
Oregon Health Science University, Doernbecher Children's Hospital, Portland, OR, USA
e-mail: riggsbe@ohsu.edu

M. F. Hunt
School of Medicine, Johns Hopkins, Baltimore, MD, USA

W. C. Ziai, C. L. Cornwell (eds.), *Neurovascular Sonography*,
https://doi.org/10.1007/978-3-030-96893-9_31

Introduction

Rapid assessment of intracranial pressure is essential in the diagnosis and management of acute intracranial insults. A recent review of the literature concluded that optic nerve sheath diameter (ONSD) and transcranial Doppler are the most superior non-invasive tools clinically proven to detect intracranial hypertension [1]. Bedside ultrasound measurements of the ONSD is an accurate, non-invasive, radiation-free, and easily repeated method of detecting intracranial hypertension in adults and children [2–11]. As part of the central nervous system, the optic nerve is surrounded by cerebrospinal fluid which is encased within the optic nerve sheath [12–14]. Fluctuations in intracranial pressure are transmitted through the subarachnoid space causing the pliable retrobulbar segment of the optic nerve sheath to distend or deflate in response to changes in intracranial pressure [12–14]. Ophthalmic ultrasound detection and monitoring of changes of the ONSD in response to intracranial hypertension has been extensively studied and is reliably reproducible in children and adults [2–5, 8–11]. This chapter details training, equipment needed, suggestions for setting up your equipment and patient, step wise directions on how to obtain, measure, and interpret ultrasound guided ONSD measurements. For further information concerning the physiologic premise for ONSD measurements, clinical applications, methods for interpreting results, and limitations in obtaining ultrasound guided ONSD measurements are detailed in chapter "Optic Nerve Sheath Diameter for Increased Intracranial Pressure" of this book.

Suggested Training for Obtaining Ultrasound Guided ONSD Measurements

There is a general understanding that obtaining the skills to perform ultrasound guided ONSD measurements safely, effectively, and accurately takes minimal training; however, the exact extent of that training is debatable. Some have suggested that experienced ultrasonographers can be taught by an expert how to take images of the ONSD followed by 10 supervised examinations to become proficient, while the inexperienced ultrasonographer

requires at least 25 supervised examinations to become proficient [3, 15]. Others suggest that 25 measurements should be the universal standard learning curve for ultrasound guided ONSD measurements [16, 17]. Vigilant training and regular practice at obtaining ultrasound guided ONSD measurements is advised. Several studies have reported a high inter-rater reliability with ultrasound guided ONSD measurements obtained after training with 15–25 observed exams [18–20].

How to Set Up the Ultrasound and the Patient

High frequency (10—22 mHz) linear array probes are ideal for ophthalmic ultrasound; however, low frequency (6–13 mHz) linear array probes often referred to as "vascular probes" are more commonly used due to their availability [21]. To safely perform ophthalmic point-of-care ultrasound, after connecting the linear array probe, the ultrasound machine must either be placed in "ophthalmic safety mode" or the power (<30%), mechanical index (<0.23), and thermal index (<1) must be manually decreased below safety thresholds [21–24]. To protect the cornea, the degree of heat (thermal index) and vibration (mechanical index) produced by the ultrasound soundwaves must be reduced. Animal studies have suggested that if the heat and vibration are not decreased, the cornea can be injured [25–27]. The cornea and lens of the eye contain a large amount of collagen which can absorb heat during ultrasound exposure that if prolonged can lead to transient chemosis, conjunctival injection, lens opacities, corneal clouding, reduction in intraocular tension, or permanent destruction of the ciliary body [24, 28]. Contact your ultrasound vender for instructions on how to manually decrease the power below 30%, the mechanical index below 0.23, and the thermal index below 1 [29–31]. All pre-programed "ophthalmic safety modes" for bedside ultrasound machines automatically decrease the power, mechanical index, and thermal index below the above listed safety thresholds. To locate the "ophthalmic safety mode" push the exam button and scroll through the exam options available, often the "ophthalmic safety mode" is embedded within the "small parts," "ED," or "other" exam modalities. If you are unable

to find the "ophthalmic safety mode," contact your ultrasound vender for further assistance. The duration of the ophthalmic ultrasound exam should always be minimized, especially when Doppler flow analysis is performed as to shorten the exposure of high frequency soundwaves to the vulnerable cornea [25–27]. The fragile nature of the cornea puts it at risk for thermal injury when prolonged ocular ultrasounds are performed even when in "ophthalmic safety mode" [27, 32]. Never perform ophthalmic ultrasound if there is a concern for glaucoma, penetrating or direct eye trauma.

Always perform bedside ophthalmic ultrasonography through a closed eyelid. Never allow the ultrasound probe to come in contact with an open eye, as this can cause corneal abrasions and puts the patient at risk for ocular infection. Only highly trained ophthalmic ultrasonographers with specialized equipment and training should perform ocular ultrasound through an opened eyelid (A-mode scanning). To protect your patient's eyes, either apply a generous amount of ophthalmic safe eye gel to the ultrasound probe (instead of ultrasound gel), or place a Tegaderm™ over a closed eye and then cover the Tegaderm™ with ultrasound gel [17, 33]. Two commonly used over the counter ophthalmic safe lubricating gels are GenTeal® eye lubricant (Novartis Pharmaceuticals Corporation, East Hanover, NJ) and Systane® eye lubricant (Alcon laboratories, Inc., Fort Worth, TX). A thick layer of gel must be applied over the closed upper eyelid and or directly over the footprint of the ultrasound probe prior to probe placement.

ONSD images are most easily obtained with the patient lying supine at 15–30° to horizontal [3, 17, 34]. Ideally, have your patient's neck straight with their head and eyes facing forward, understanding that this is often not possible to achieve with young pediatric patients [3, 19, 35, 36]. Optimal alignment of the optic nerve can be achieved by having your patient close the eye being imaged while the other eye focuses on an object straight ahead. However, ONSD measurements can be obtained from any patient position if the orbits can be easily accessed with the ultrasound probe. The ultrasound machine should be placed in two-

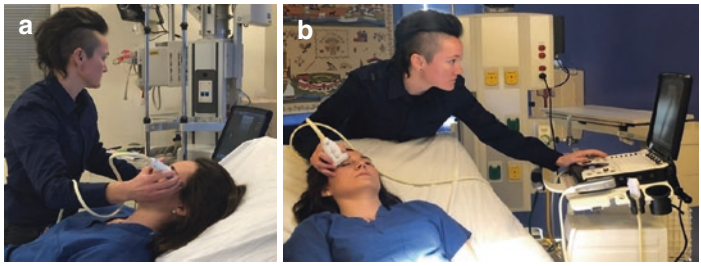

Fig. 1 (**a**) Ultrasonographer using a high frequency linear array ultrasound probe gently placed over the closed left eyelid in the transverse position to obtain ophthalmic ultrasound images while facing the patient. Ultrasonographer's right hand is securely anchored on the patient's left mandible to minimize pressure placed on the left eye and maximize control of the probe while scanning. (**b**) Ultrasonographer is standing behind the patient in the more traditional approach to obtaining ophthalmic ultrasound images. Ultrasonographer has a high frequency linear array ultrasound probe placed over the closed right eyelid in the transverse position, while her hand is securely anchored on the patient's right forehead to minimize pressure placed on the eye

dimensional B-mode with ophthalmic safety settings and set at a depth of 2.0–3.5 cm in children and 3–4.5 cm in adults. At these depths, ideally the entire globe of the eye and 0.5–1 cm of the optic nerve should be in view. The high frequency linear array probe should be cleaned, and either ophthalmic safe eye gel should be utilized or a Tegaderm™ directly placed over the closed eye covered in ultrasound gel should be utilized. The ultrasonographer should sit or stand behind the patient's head and the probe-cable should have minimal tension to maximize fine movements [17], see Fig. 1b. While less ideal, some prefer to perform the examination while facing their patients (Fig. 1a). Always securely ground the hand holding the ultrasound probe on your patient's face (forehead, cheek, nose, or orbital ridge) hold the probe delicately between your thumb and forefinger to minimize the pressure placed on the eye through the closed eyelid (Figs. 1, 2, and 3). If unable to ground your hand on your patient's face, place a firm pillow or rolled up towel next to their face to stabilize your hand to prevent pressure on the closed eye (Fig. 2c).

Fig. 2 (**a**) High frequency linear array ultrasound probe covered in ophthalmic eye gel and placed over the closed left eye in the sagittal position. The probe is gently held like a pen, with the hand of the ultrasonographer anchored to the patient's left cheek and forehead to stabilize the transducer and prevent any pressure to the eye from the probe. (**b**) Proper probe placement to obtain sagittal views of the patient's right eye. (**c**) Ultrasonographer is standing behind the patient obtaining sagittal ophthalmic ultrasound images of the patient's right eye, while her hand is securely anchored on a rolled up towel next to the patient's face to prevent pressure on the closed eye

How to Obtain Optic Nerve Sheath Diameter Images

Gently place the ultrasound probe midline over the closed eye in either the sagittal (vertical) (Fig. 2) or transverse (horizontal) position (Fig. 3) with minimal pressure on the closed eye. Patients are instructed to look straight ahead while relaxing their eyes during the exam [17]; however, if compliance is not possible, the ultrasonographer must gently track the optic nerve until the ultrasound beam is exactly parallel to the straight and symmetric optic nerve, or until a perfect 90° transection of the optic nerve just behind the orbit is obtained. The position of the probe is adjusted to give a suitable angle for displaying the entry of the optic nerve into the globe. To assure an accurate 90° transection of the optic nerve, a double circle or "bullseye" appearance of the optic nerve must be obtained (Fig. 5). Ideally, 3 quality "bullseye" images (Fig. 5) in the transverse plane (Fig. 3) and 3 quality "bullseye" images in the sagittal plane (Fig. 2) should be taken and saved for measurements. To assure that the ultrasound beam is exactly parallel to the optic nerve, the image must be straight with the lens/cornea of the eye aligning with the optic nerve, which appears straight and symmetric (Fig. 4). If an accurate 90° transection or

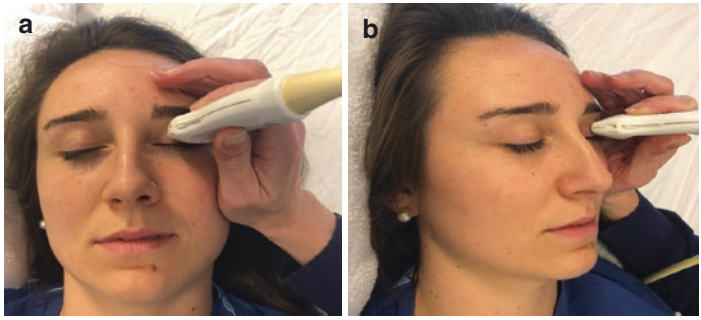

Fig. 3 (**a**) High frequency linear array ultrasound probe covered in ophthalmic eye gel and placed over the closed left eye in the transverse position. The probe is gently held like a pen, with the hand of the ultrasonographer anchored to the patient's left cheek and forehead to stabilize the transducer and prevent any pressure to the eye from the probe. (**b**) Proper probe placement to obtain transverse views of the patient's left eye

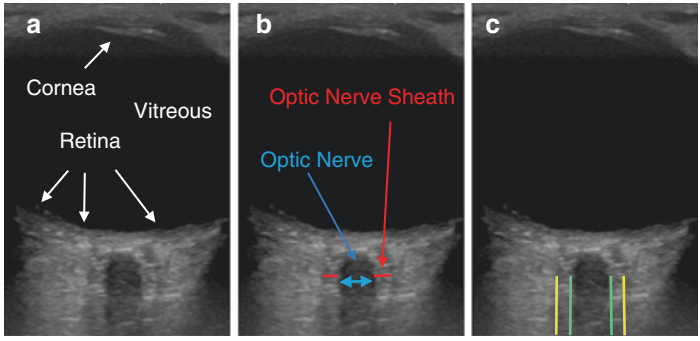

Fig. 4 (**a**) Normal ophthalmic ultrasound images obtained in the transverse view with the anterior cornea of the eye facing upwards and the hypoechoic optic nerve (dark) attaching posteriorly. (**b**) The same ultrasound image showing a symmetric and straight longitudinal section of the optic nerve (blue arrow) surrounded by a symmetric and straight hyperechoic optic nerve sheath (red lines). (**c**) The same image with straight green lines along the edge of the optic nerve and optic nerve sheath and yellow lines on the external border of the optic nerve sheath reinforcing the straight and symmetric alignment of the optic nerve and nerve sheath

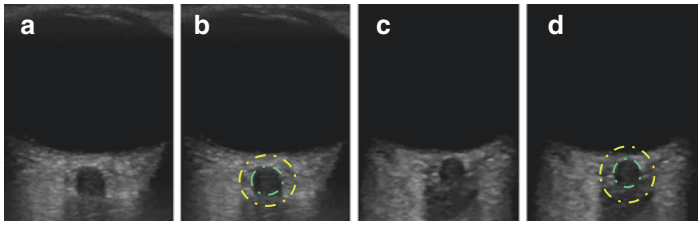

Fig. 5 (**a**) Normal ophthalmic ultrasound images obtained in the transverse view showing a circular cross-section of the optic nerve (dark circle) surrounded by the optic nerve sheath mimicking a bullseye. (**b**) The same image with green dotted lines outlining the outer edge of the optic nerve and yellow dotted lines outlining the outer edge of the optic nerve sheath to emphasize the appropriately aligned bullseye appearance. (**c**) Ophthalmic ultrasound images obtained in the transverse view showing a circular cross-section of the optic nerve surrounded by the optic nerve sheath mimicking a bullseye. (**d**) The same image with green dotted lines outlining the outer edge of the optic nerve and yellow dotted lines outlining the outer edge of the optic nerve sheath

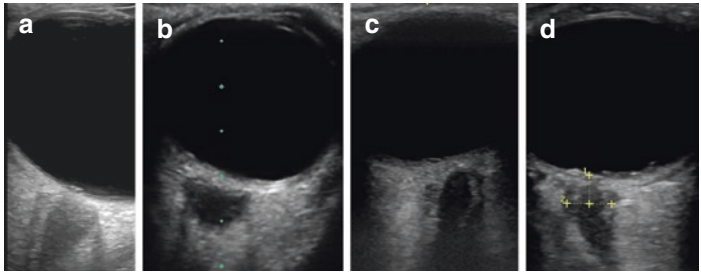

Fig. 6 (**a**–**d**) All images of poorly aligned, asymmetric, and crooked images of the hypoechoic or dark optic nerve surrounded by the hyperechoic or lighter optic nerve sheath with the outermost boarder of the optic nerve sheath appearing hypoechoic or black where the cerebral spinal fluid flows through the subarachnoid space. (**d**) Inaccurate measurement of the optic nerve sheath diameter (due to poor alignment) measured 3 mm behind the orbit

an exactly parallel image of the optic nerve cannot be obtained, the ONSD measurements will not be accurate, and the study should be aborted. See Fig. 6 for examples of inaccurate optic nerve images that cannot be accurately measured.

How to Measure the ONSD from Saved Images

Obtaining measurements of the ONSD can occur in real time by obtaining an accurate image, "freezing" the image, and utilizing the electronic measurement calipers of the ultrasound machine to obtain immediate results. This must be repeated three times for each eye to assure an accurate interpretation of the ONSD [3, 19]. If time allows, it is encouraged to obtain three accurate ONSD images or short video clips of each eye saving each image or clip to the ultrasound machine immediately followed by sequential measurements of all six images at once. The latter of these two measuring approaches is slightly more time consuming; however, it minimizes the time actually spent with the ultrasound machine taking up valuable real-estate at the critically ill patient's bedside. The average of three measured ONSD values of each eye is calculated and serves as the ONSD value for that eye. This average reduces the intra-observer variability and serves as a quality check assuring all three measurements are similar [3, 19]. Most studies reported in the literature do not show a significant difference between the right and left eye ONSD measurements of patients; therefore, in the rare case where time will not allow for six measurements, some studies would suggest that obtaining the average value of 3 quality ONSD measurements of one eye could suffice. However, standard practice for determining the ONSD of a patient should be to obtain the average measurement of 3 quality images per eye for a final ONSD value for each eye [3, 19]. The ONSD of each eye should be extremely similar in measurement. If there is a significant difference in the ONSD measurements of each eye, the study should be aborted due to inaccurate technique, unless the patient's genetics or underlying pathology explains why a difference should exist between the ONSD in each eye.

Prior to measuring the ONSD, assure that accurate images are obtained. Accurate axial cuts through the eye and optic nerve should include a straight longitudinal section of the optic nerve (Fig. 4). Accurate transection of the optic nerve, which is often an approach obtained in uncooperative pediatric patients, shows a double circle or "bullseye" appearance of the optic nerve (Fig. 5). Examples of inaccurate crooked optic nerve images are reflected

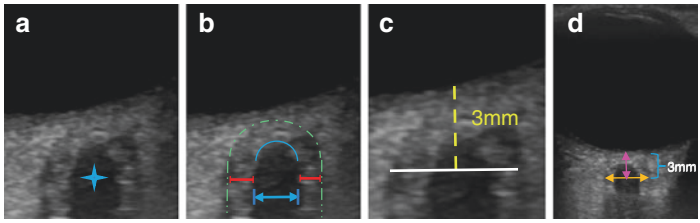

Fig. 7 (**a**) Normal ophthalmic ultrasound image zoomed in focusing on the posterior chamber of the eye where the optic nerve (blue star) meets the orbit often referred to as the papilla. (**b**) The same ultrasound image with a blue line with arrows showing a cross-section of the optic nerve. Blue lines along the pia mater enhance the separation of the optic nerve (hypoechoic) from the internal edge of the optic nerve sheath (hyperechoic). Red lines show the distance between the internal and external edges of the optic nerve sheath. Green dashed lines along the external edge of the optic nerve sheath or the outer hyperechoic borders of the subarachnoid space internal to the hypoechoic (light) dura mater. (**c**) The same image with a yellow dashed line measuring 3 mm behind the papilla with a white line transecting the optic nerve sheath measured from the distance between the external edges of the subarachnoid space. (**d**) Pink line measuring 3 mm up the optic nerve from the papilla with orange line measuring the optic nerve sheath diameter between the external edges of the subarachnoid space

in Fig. 6. To obtain measurements of the ONSD from your saved images, first measure 3mms directly posterior to where the orbit and the optic nerve meet see Fig. 7b, c [3, 29, 30]. Next, measure the optic nerve sheath in a straight line from one end of the sheath to the other while transecting the optic nerve at 90° crossing the 3 mm mark (Fig. 7b, c). Studies have proven that at 3 mm behind the optic disc, the optic nerve sheath is subject to maximum diameter fluctuations due to ICP changes. It is also at the 3 mm mark that shadowing artifact is at a minimum [17, 29, 30, 36].

Most published cut-off values for diagnosing ICH are based on measurements obtained from the external edge of the optic nerve sheath or the outer hyperechogenic (dark) borders of the subarachnoid space internal to the hypoechogenic (light) dura mater [17, 35, 37, 38]. Therefore, the correct way to measure ONSD is the distance inside the dura mater, not the distance outside the dura mater see Fig. 7. Some studies have published data incorrectly measuring from the internal edges of the optic nerve sheath,

or the distance between the outer edges of the pia mater. Measurements taken from the internal edge of the ONSD will be smaller than those taken from the external edge, which can lead to inconsistent data [35, 38]. Several studies also exist where the ONSD was incorrectly obtained by measuring the distance between the outer hypoechogenic borders of the dura mater, leading to falsely enlarged ONSD values [38, 39]. Therefore, it is important when evaluating the literature to identify exactly how the ONSD measurements were obtained.

Interpretation of ONSD Measurements for Adult Patients

Once the image is acquired and the measurement determined, the ONSD must be interpreted and used as a complementary technique combined with the clinical exam and standard neuro-imaging findings to guide the care of the patient. In 2011, Dubourg et al. conducted a systematic review and meta-analysis of adult patients finding a pooled sensitivity of 0.90 (95% CI 0.8–0.95), specificity of 0.85 (95% CI 0.73–0.93), and diagnostic odds ratio of 51 (95% CI 22–121) with the area under the SROC curve of 0.94 (95% CI 0.91–0.96) [11]. However, the cutoff thresholds for optimal ONSD to identify ICH from normal ICP ranged from 5.0 to 5.9 mm in this systematic review. Eight years later, Koziarz et al. provided an updated systematic review and meta-analysis with over ten times the studies compared to Dubourge et al. including both pediatric and adult studies. Koziarz group also separated data based on traumatic brain injury and non-traumatic brain injury, finding pooled sensitivity and specificity of ONSD ultrsonography to identify ICH in patients with traumatic brain injury to be 97% (95% CI, 92–99%) and 86% (CI, 74–93%) respectively [2]. For patients with non-traumatic brain injuries the pooled sensitivity was 92% (CI, 86–96%) and specificity was 86% (CI, 77–92%). The SROC curve of all patients showed a pooled sensitivity and specificity of 94% (CI, 91–96%) and 87% (CI, 82–91%), respectively [2]. Koziarz et al. was the first systematic review and meta-analysis to compare variable cut off values and calculation methods to determine that 5.0 mm is the optimal cutoff to diagnose ICH in adult

patients [2]. However, other studies have shown that an ONSD of 5.5 mm can be a normal finding in adults stating that a more reliable cutoff value to predict ICH is 5.7–6.0 mm showing sensitivity of 87–95% and specificity of 79–100% [37, 40–43].

Further questions exist in the global meaning of these ONSD measurements. Individual trends are trusted more than absolute numbers regarding the ONSD. We recommend averaging at least three measurements, as the average best accommodates for technique, anomalies in images, and anatomic differences [3, 19]. There also remains controversy regarding the validity of ONSD measurements in acute versus chronic changes of intracranial pressure. Acute changes have been more robustly studied, and it has been suggested that chronically elevated ICP may undergo a decrease in optic nerve sheath distensability such that measurements will not reflect accurately the clinical context. Ensure that the duration of intracranial pathology is a consideration with interpretation of the ONSD measurements.

Interpretation of ONSD Measurements for Pediatric Patients

Despite the limited number of pediatric specific studies compared to adult studies investigating ultrasonographic measurements of ONSD in detecting intracranial hypertension, the first suggested cutoff value for children was published nearly 25 years ago, suggesting a cutoff of 5.0 mm based on 39 children all over the age of 4 years old [30, 36]. Three years later, Ballantyne et al. created generalized normative pediatric ONSD based on optic nerve growth curves from 102 children ages 0–15 years proposing far lower cut off values of 4 mm for infants <1 year old and 4.5 mm for children >1 year old [44]. These same lower cutoff values were reproduced several times over the following 10 years [4, 5, 29, 45, 46], with the addition of Moretti and Pizzi suggesting a cutoff of 4.0 mm for children ≤1 year old, 4.5 mm for children 1–4 years old, and 5.0 mm for children >4 years old [18]. However, Le et al., calculated the accuracy of the 4 mm and 4.5 mm cutoff points and found a sensitivity of 83% and specificity of 38% based on 64 pediatric patients [47]. Beare et al., published a study including 51 pediatric

patients >1 year old using a cutoff value of 4.2 mm, finding the sensitivity and specificity of ONSD to diagnose ICH to be 100% and 86% respectively [6]. Young et al. was less keen on a direct cut-off that could be applied across pediatric cohorts. Instead, they indicated that <4.9 mm was unlikely to correlate with increased ICP suggesting an optimal cut off of 6.1 mm with a sensitivity of 77%, specificity of 91%, and area under the ROC curve of 0.85 [48]; however, this was only based on 36 patients with an average age of 8 years old. Padayachy et al. reported a cutoff of 5.16 mm for children ≤1 year old and 5.75 mm for children >1 year old and an overall cutoff for their entire cohort of 5.5 mm based on 174 patients [7, 49]. Steinborn et al. has also suggested a significantly higher ONSD cutoff value be used in children to suggest ICH [50].

In the past few years, it has been argued that the optic nerve growth curve must be more heavily considered when establishing ONSD cutoff values in relation to children as their visual pathways are developing through childhood [51]. The development of the nervous system and the visual pathway has a rapid initial growth phase significantly slowing by age 4 with continued very slow development until the age of 8–10 years old [51, 52]. Therefore, it has been suggested that age stratification is essential when interpreting ONSD in children. Fontanel et al. developed an optic nerve growth curve for normal children 4–18 years of age based on 165 children, which showed progressive increase of the optic nerve up to approximately 10 years of age; therefore, they calculated cutoff values for children between 4 and 10 years and between 11 and 18 years old separately based on 29 children with ICH and 165 healthy children [53]. They reported an optimal cut off value of 4.1 mm for the 4–10 year old subgroup and a cutoff of 4.4 mm for the 11–18 year old subgroup both cutoffs had a 100% sensitivity with specificity ranging from 83.9% to 98.8%. Fontanel et al. also evaluated a cutoff of 5.0 mm in their 29 children with ICH finding a sensitivity of 28.6% with 100% specificity [53], thus reinforcing lower cut off values. Never before have such low cutoff thresholds been suggested. A possible limitation of Fontanel and associates is that all patients had non-traumatic chronic ICH (pseudotumor 52%, cerebral tumors 38.5%, and cerebral venous sinus thrombosis 10%), and ICH was defined as having an opening pressure on LP > 28 cm H_2O, though no absolute or average opening pressures were reported by the study.

To our knowledge, there are no pediatric studies that have determined optic nerve growth curves or more precise age stratification of ONSD measurements for neonates, babies, and children <4 years old. Along with the rapid growth of the optic nerve within the first year of life, it has also been suggested that having an open fontanel might affect accurate readings of ONSD measurements [49, 54]. Research has shown that patency of the anterior fontanelle can be used to help stratify patients into different ICP cutoff values [49]. With infants experiencing such profound growth of their optic nerves and closure of their fontanelles in the first year of life, it would be worthwhile to develop normative values and ONSD cut-off points with tighter age stratification cohorts such as: 0–6 months, 6–12 months, 12–24 months, 2–3 years, 3–4 years. Specifically, with the pediatric population the recent variability in reported cutoff thresholds without consensus suggests that caution should be used when interpreting ONSD measurements in children. It is imperative that ONSD measurements are interpreted in conjunction with physical exam and other imaging modalities when making clinical decisions. It appears that the application of ONSD measurements in the pediatric population is most likely primarily utilized in research as opposed to daily clinical practice.

Conclusion

Because this bedside tool allows for fast and safe real time assessment of conditions associated with elevated intracranial pressure, we propose routine inclusion of ONSD measurements in the multimodal monitoring of patients in adult and pediatric neurocritical care. Ultrasound guided ONSD measurement should be used in conjunction with invasive ICP monitoring for patients with neurological conditions at risk for developing ICH. Ultrasound guided ONSD measurements should be used as a complementary technique at identifying and monitoring ICH but should not substitute current standard techniques of measuring ICP. The technique can also provide interval monitoring to follow responses of ICP to therapy or disease progression. Caution should be used when applying universal cutoff values to determine ICH. While further research is warranted to elucidate further granularity and application of the technique, clinicians

should utilize optic nerve sheath diameter in the diagnostic workup of pediatric patients with suspected intracranial pathology, especially in emergency settings.

References

1. Narayan V, Mohammed N, Savardekar AR, Patra DP, Notarianni C, Nanda A. Non-invasive intracranial pressure monitoring for severe traumatic brain injury in children: a concise update on current methods. World Neurosurg. 2018;114:293–300.
2. Koziarz A, Sne N, Kegel F, Nath S, Badhiwala JH, Nassiri F, Mansouri A, Yang K, Zhou Q, Rice T, Faidi S, Passos E, Healey A, Banfield L, Mensour M, Kirkpatrick AW, Nassar A, Fehlings MG, Hawryluk GWJ, Almenawer SA. Bedside optic nerve ultrasonography for diagnosing increased intracranial pressure: a systematic review and meta-analysis. Ann Intern Med. 2019;171(12):896–905.
3. Lochner P, Czosnyka M, Naldi A, Lyros E, Pelosi P, Mathur S, Fassbender K, Robba C. Optic nerve sheath diameter: present and future perspectives for neurologists and critical care physicians. Neurol Sci. 2019;40(12):2447–57.
4. Newman WD, Hollman AS, Dutton GN, et al. Measurement of optic nerve sheath diameter by ultrasound: a means of detecting acute raised intracranial pressure in hydrocephalus. Br J Ophthalmol. 2002;86:1109–13.
5. Malayeri AA, Bavarian S, Mehdizadeh M. Sonographic evaluation of optic nerve diameter in children with raised intracranial pressure. J Ultrasound Med. 2005;24:143–7.
6. Beare NA, Kampodeni S, Glover SJ, Molyneux E, Taylor TE, Harding SP, Molyneux ME. Detection of raised intracranial pressure by ultrasound measurement of optic nerve sheath diameter in African children. Tropical Med Int Health. 2008;13(11):1400–4.
7. Padayachy LC, Padayachy V, Galal U, Gray R, Fieggen AG. The relationship between transorbital ultrasound measurement of the optic nerve sheath diameter (ONSD) and invasively measured ICP in children: part I: repeatability, observer variability and general analysis. Childs Nerv Syst. 2016;32(10):1769–78.
8. Lee SH, Kim HS, Yun SJ. Optic nerve sheath diameter measurement for predicting raised intracranial pressure in adult patients with severe traumatic brain injury: a meta-analysis. J Crit Care. 2020;56:182–7.
9. Kim EJ, Koo BN, Choi SH, Park K, Kim MS. Ultrasonographic optic nerve sheath diameter for predicting elevated intracranial pressure during laparoscopic surgery: a systematic review and meta-analysis. Surg Endosc. 2018;32(1):175–82.
10. Lochner P, et al. B-mode transorbital ultrasonography for the diagnosis of idiopathic intracranial hypertension: a systematic review and meta-analysis. Ultraschall Med. 2019;40(2):247–52.

11. Dubourg J, Javouhey E, Geeraerts T, Messerer M, Kassai B. Ultrasonography of optic nerve sheath diameter for detection of raised intracranial pressure: a systematic review and meta-analysis. Intensive Care Med. 2011;37(7):1059–68.
12. Khan M, Shallwani H, Khan M, Shamim M. Noninvasive monitoring intracranial pressure? A review of available modalities. Surg Neurol Int. 2017;8(1):51.
13. Hansen HC, Helmke K. The subarachnoid space surrounding the optic nerves: an ultrasound study of the optic nerve sheath. Surg Radiol Anat. 1996;18(4):323–8.
14. Hayreh SS. Pathogenesis of oedema of the optic disc. Doc Ophthalmol. 1968;24(2):289–411.
15. Tayal VS, Neulander M, Norton HJ, Foster T, Saunders T, Blaivas M. Emergency department sonographic measurement of optic nerve sheath diameter to detect findings of increased intracranial pressure in adult head injury patients. Ann Emerg Med. 2007;49:508–14.
16. Zeiler FA, Ziesmann MT, Goeres P, Unger B, Park J, Karakitsos D, et al. A unique method for estimating the reliability learning curve of optic nerve sheath diameter ultrasound measurement. Crit Ultrasound J. 2016;8:9.
17. Aspide R, Bertolini G, Albini Riccioli L, Mazzatenta D, Palandri G, Biasucci DG. A proposal for a new protocol for sonographic assessment of the optic nerve sheath diameter: the CLOSED protocol. Neurocrit Care. 2020;32(1):327–32.
18. Moretti R, Pizzi B, Cassini F, Vivaldi N. Reliability of optic nerve ultrasound for the evaluation of patients with spontaneous intracranial hemorrhage. Neurocrit Care. 2009;11:406.
19. Bauerle J, Lochner P, Kaps M, Nedelmann M. Intra- and interobsever reliability of sonographic assessment of the optic nerve sheath diameter in healthy adults. J Neuroimaging. 2012;22(1):42–5.
20. Lochner P, Coppo L, Cantello R, Nardone R, Naldi A, Leone MA, et al. Intra- and interobserver reliability of transorbital sonographic assessment of the optic nerve sheath diameter and optic nerve diameter in healthy adults. J Ultrasound. 2016;11:406.
21. Shah S, Kimberly H, Marill K, Noble V. Ultrasound techniques to measure the optic nerve sheath: is a specialized probe necessary? Med Sci Monit. 2009;15:63–8.
22. Fowlkes JB, Holland CK. Mechanical bioeffects from diagnostic ultrasound: AIUM consensus statements. American Institute of Ultrasound in Medicine. J Ultrasound Med. 2000;19:69–72.
23. Toms DA. The mechanical index, ultrasound practices, and the ALARA principle. J Ultrasound Med. 2006;25:560–1.
24. Ertl M, Gamulescu M-A, Schlachetzki F. Application of orbital sonography in neurology. In: Thoirs K, editor. Sonography. Rijeka: InTech; 2012.
25. Rosenberg RS, Purnell EW. Effects of ultrasonic radiation to the ciliary body. Am J Ophthalmol. 1967;63:403–9.
26. Moore CH, Herrick JF, Martens TG. Some effects of ultrasonic energy on the rabbit eye. AMA Arch Ophthalmol. 1955;54:922–30.

27. Murano N, Ishizaki M, Sato S, Fukuda Y, Takahashi H. Corneal endothelial cell damage by free radicals associated with ultrasound oscillation. Arch Ophthalmol. 2008;126:816–21.
28. Shankar H, Pagel PS. Potential adverse ultrasound-related biological effects: a critical review. Anesthesiology. 2011;115:1109–24.
29. Hansen HC, Helmke K. Validation of the optic nerve sheath response to changing cerebrospinal fluid pressure: ultrasound findings during intrathecal infusion tests. J Neurosurg. 1997;87:34–40.
30. Helmke K, Hansen HC. Fundamentals of transorbital sonographic evaluation of optic nerve sheath expansion under intracranial hypertension II. Patient study. Pediatr Radiol. 1996;26:706–10.
31. Liu D, Li Z, Zhang X, Zhao L, Jia J, Sun F, Wang Y, Ma D, Wei W. Assessment of intracranial pressure with ultrasonographic retrobulbar optic nerve sheath diameter measurement. BMC Neurol. 2017;17:188.
32. Silverman RH, Lizzi FL, Ursea BG, Cozzarelli L, Ketterling JA, Deng CX, Folberg R, Coleman DJ. Safety levels for exposure of cornea and lens to very high-frequency ultrasound. J Ultrasound Med. 2001;20(9):979–86.
33. Roque PJ, Hatch N, Barr L, Wu TS. Bedside ocular ultrasound. Crit Care Clin. 2014;30:227–41.
34. Romagnuolo L, Tayal V, Tomaszewski C, Saunders T, Norton HJ. Optic nerve sheath diameter does not change with patient position. Am J Emerg Med. 2005;23:686–8.
35. Bauerle J, Schuchardt F, Schroeder L, Egger K, Weigel M, Harloff A. Reproducibility and accuracy of optic nerve sheath diameter assessment using ultrasound compared to magnetic resonance imaging. BMC Neurol. 2013;13:187.
36. Helmke K, Hansen HC. Fundamentals of transorbital sonographic evaluation of optic nerve sheath expansion under intracranial hypertension. I. Experimental study. Pediatr Radiol. 1996;26:701–5.
37. Ertl M, Barinka F, Torka E, Altmann M, Pfister K, Helbig H, Bogdahn U, Gamulescu MA, Schlachetzki F. Ocular color-coded sonography – a promising tool for neurologists and intensive care physicians. Ultraschall Med. 2014;35(5):422–31.
38. Topcuoglu M, Arsava EM, Bas DF, Kozak HH. Transorbital ultrasonographic measurement of optic nerve sheath diameter in brain death. J Neuroimaging. 2015;25(6):906–9.
39. Krogias C, Ayzenberg I, Schroeder C, Gruter T, Gold R, Yoon MS. Transorbital sonography in CIDP patients: no evidence for optic nerve hypertrophy. J Neurol Sci. 2016;362:206–8.
40. Soldatos T, Karakitsos D, Chatzimichail K, et al. Optic nerve sonography in the diagnostic evaluation of adult brain injury. Crit Care. 2008;12:R67.
41. Geeraerts T, Launey Y, Martin L, et al. Ultrasonography of the optic nerve sheath may be useful for detecting raised intracranial pressure after severe brain injury. Intensive Care Med. 2007;33:1704–11.
42. Watanabe A, Kinouchi H, Horikoshi T, et al. Effect of intracranial pressure on the diameter of the optic nerve sheath. J Neurosurg. 2008;109:255–8.

43. Geeraerts T, Merceron S, Benhamou D, et al. Non-invasive assessment of intracranial pressure using ocular sonography in neurocritical care patients. Intensive Care Med. 2008;34:2062–7.
44. Ballantyne J, Hollman AS, Hamilton R, Bradnam MS, Carachi R, Young DG, Dutton GN. Transorbital optic nerve sheath ultrasonography in normal children. Clin Radiol. 1999;54(11):740–2.
45. Körber F, Scharf M, Moritz J, Dralle D, Alzen G. Sonography of the optical nerve – experience in 483 children. Rofo. 2005;177(2):229–35.
46. McAuley D, Paterson A, Sweeney L. Optic nerve sheath ultrasound in the assessment of paediatric hydrocephalus. Childs Nerv Syst. 2009;25(1):87–90.
47. Le A, Hoehn ME, Smith ME, Spentzas T, Schlappy D, Pershad J. Bedside sonographic measurement of opticnerve sheath diameter as a predictor of increased intracranial pressure in children. Ann Emerg Med. 2009;53:785–91.58.
48. Young AMH, Guilfoyle MR, Donnelly J, Scoffings D, Fernandes H, Garnett M, et al. Correlating optic nerve sheath diameter with opening intracranial pressure in pediatric traumatic brain injury. Pediatr Res. 2017;81(3):443–7.
49. Padayachy LC, Padayachy V, Galal U, Pollock T, Fieggen AG. The relationship between transorbital ultrasound measurement of the optic nerve sheath diameter (ONSD) and invasively measured ICP in children. : Part II: age-related ONSD cut-off values and patency of the anterior fontanelle. Childs Nerv Syst. 2016;32(10):1779–85.
50. Steinborn M, Friedmann M, Makowski C, Hahn H, Hapfelmeier A, Juenger H. High resolution transbulbar sonography in children with suspicion of increased intracranial pressure. Childs Nerv Syst. 2016;32:655–60.
51. De Bernardo M, Vitiello L, Rosa N. Optic nerve sheath diameter ultrasound: optic nerve growth curve and its application to detect intracranial hypertension in children. Am J Ophthalmol. 2019;208:438.
52. Yu DY, Cringle SJ, Balaratnasingam C, Morgan WH, Yu PK, Su EN. Retinal ganglion cells: energetics, compartmentation, axonal transport, cytoskeletons and vulnerability. Prog Retin Eye Res. 2013;36:217–46.
53. Fontanel L, Pensiero S, Ronfani L, Rosolen V, Barbi E. Optic nerve sheath diameter ultrasound: optic nerve growth curve and its application to detect intracranial hypertension in children. Am J Ophthalmol. 2019;208:439.
54. Kerscher SR, Schöni D, Hurth H, Neunhoeffer F, Haas-Lude K, Wolff M, Schuhmann MU. The relation of optic nerve sheath diameter (ONSD) and intracranial pressure (ICP) in pediatric neurosurgery practice – part I: correlations, age-dependency and cut-off values. Childs Nerv Syst. 2020;36(1):99–106.

Protocol for Extracranial Carotid Examination

William K. Cornwell

Introduction

The carotid duplex exam has become the standard noninvasive diagnostic test to determine the presence of flow limiting stenosis in the extracranial carotid arteries. It is the recommended test for symptomatic and asymptomatic patients with suspected or known carotid occlusive disease. Elevated velocities obtained by the carotid exam can be used to estimate the degree of stenosis in the carotid arteries. In the hands of a credentialed technologist using a state-of-the-art duplex scanner, this exam can readily identify irregular plaques, stenosis, and occlusion of the carotid arteries.

The Carotid Arterial Examination

Indications

The following are indications for which noninvasive assessment of the carotid arteries is indicated:

- Cervical bruits
- Cerebrovascular accident

W. K. Cornwell (✉)
Cardiovascular Ultrasound Services, Inc., Columbus, OH, USA

W. C. Ziai, C. L. Cornwell (eds.), *Neurovascular Sonography*,
https://doi.org/10.1007/978-3-030-96893-9_32

- Transient ischemic attacks
- Visual disturbances
- Pulsatile neck mass
- Neck trauma
- Amaurosis fugax
- Post-op or post-intervention
- Vertebral insufficiency
- Follow up of known stenosis

Equipment

- Duplex imaging system with color flow and transducer frequencies from 4 to 10 MHz.
- Ultrasound gel [1].

Description of Procedure

The exam is routinely performed as a bilateral study unless ordered as a limited exam. The procedure should be explained to the patient and any questions answered. The patient should lie on an exam table or in bed in a supine position with the head slightly elevated, chin raised, and head turned slightly away from the sided being scanned (Fig. 1).

The exam usually begins on the right side. It is helpful to start by making a grey scale sweep through the entire carotid system in

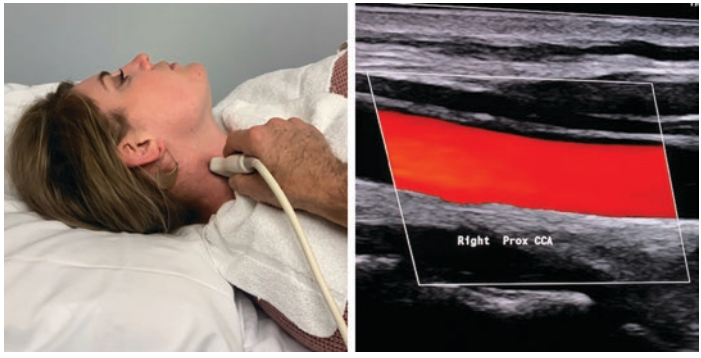

Fig. 1 Patient position and probe placement for the carotid exam

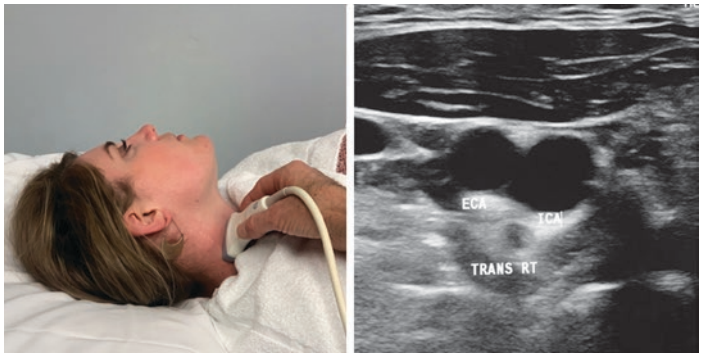

Fig. 2 Transverse view of the bifurcation

a transverse view. This will allow for identification of unusual anatomy or pathology. Begin at the base of the neck with the proximal common carotid artery (CCA) as low on the neck as possible. Scan through the CCA, bifurcation (Fig. 2), bulb, proximal external carotid artery (ECA) and proximal, mid and distal segments of the internal carotid artery (ICA). Make note of the location and extent of any plaque observed.

After completing the transverse scan, follow the same sequence in the longitudinal view starting with the CCA at the base of the neck [2].

During the scan the technologist should continually optimize the image by adjusting the grey scale display, color, depth and focal zone.

Anatomic Variations

Normally the bifurcation occurs in the mid portion of the neck with the ICA taking a posterior lateral course and the ECA branching more medial and anterior. Occasionally the bifurcation may occur either very low or very high in the neck making multiple Doppler samples of the CCA or ICA very difficult. In rare cases only the distal CCA or proximal ICA may be able to be sampled. The position of the ICA and ECA may also be reversed. In this case the ICA may be identified by its low resistant flow pattern compared to the high resistant waveform of the ECA. A temporal tap or identification of the superior thyroid artery can also help identify the ECA.

Documentation

Document the study by obtaining loops or still frame images including grey scale, color and Doppler spectral waveforms according to the facility protocol.

Example:

- In the long view document in grey scale the:
  - CCA in the proximal and mid-distal segments (Fig. 3)
  - Carotid bulb
  - Proximal ECA
  - Proximal, mid and distal segments of the ICA
- In the long view document in color the:
  - Carotid bulb
  - Proximal, mid and distal segments of the ICA (Fig. 4)
  - Proximal ECA

Fig. 3 Long view mid-distal CCA

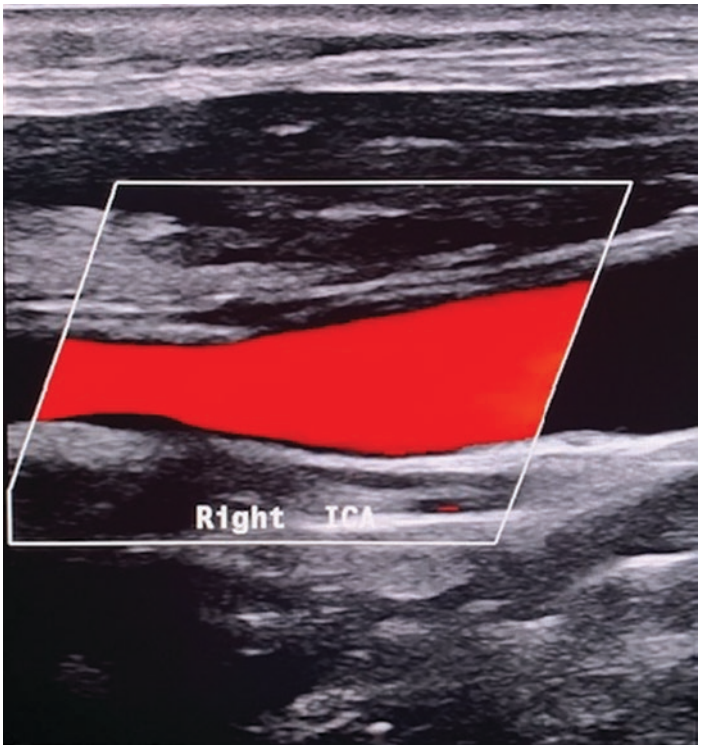

Fig. 4 Long view proximal ICA

- In the long view obtain a spectral Doppler waveform measuring peak systolic (PSV) and end diastolic velocities (EDV) of the:
  - CCA in the proximal and mid-distal segments
  - Carotid bulb
  - Proximal ECA (peak systolic only)
  - ICA in the proximal, mid and distal segments (Fig. 5).
  - Vertebral (as near the origin as possible) (Fig. 6).

For interpretation areas of stenosis should include the highest velocity measurements at the stenosis and a waveform just distal to the stenosis to document post stenotic turbulence.

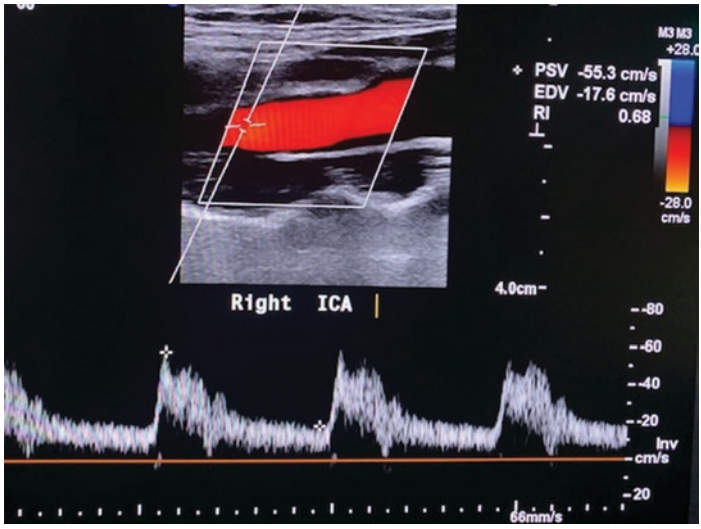

Fig. 5 Proximal ICA velocities

If a stent is present velocity measurements should be obtained in the proximal, mid and distal segments of the stent as well as the native artery just proximal to and distal to the stent. Grey scale images should be taken in the long view of the proximal and distal ends of the stent [2].

As with imaging the Doppler display should be optimized during the scan in regard to scale, gain, sample size and angle (60 degrees or less).

The technologist performing the exam should use his/her discretion to obtain a combination of loops, still frame grey scale and color images (transverse and longitudinal) and spectral waveforms to adequately portray pathology to the reader.

Interpretation

Carotid Doppler velocities along with a visual estimation of the degree of stenosis of the plaque (Figs. 7 and 8) are used to categorize percent stenosis. The PSV and EDV of the ICA are the

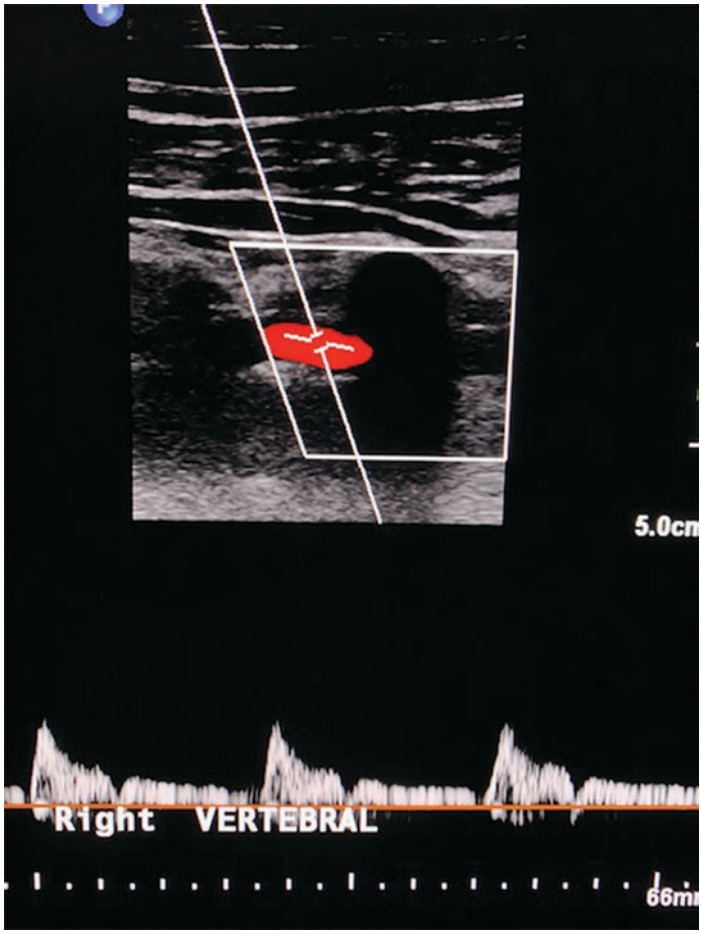

Fig. 6 Antegrade flow in the Right Vertebral Artery

primary criteria (Figs. 9 and 10). Additionally, the ICA/CCA ratio may be used. Although there is variability of carotid interpretation criteria, each lab should use either one of the accepted criteria (Table 1) or internally developed and validated velocity criteria [1].

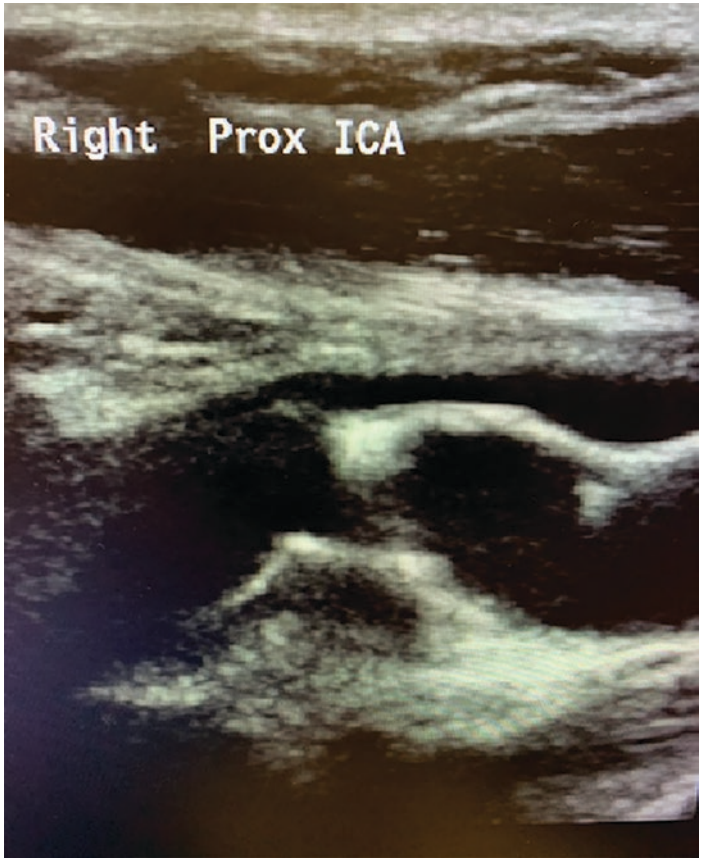

Fig. 7 ICA Stenosis – Greyscale

Stent criteria is also variable. The peak systolic velocity of the stenotic segment of the stent has been found to be the best predictor of in-stent restenosis compared to the end diastolic velocity or the ICA/CCA ratio. An example of in-stent restenosis criteria is as follows:

- PSV of greater than or equal to 154 cm/s = greater than 30% stenosis

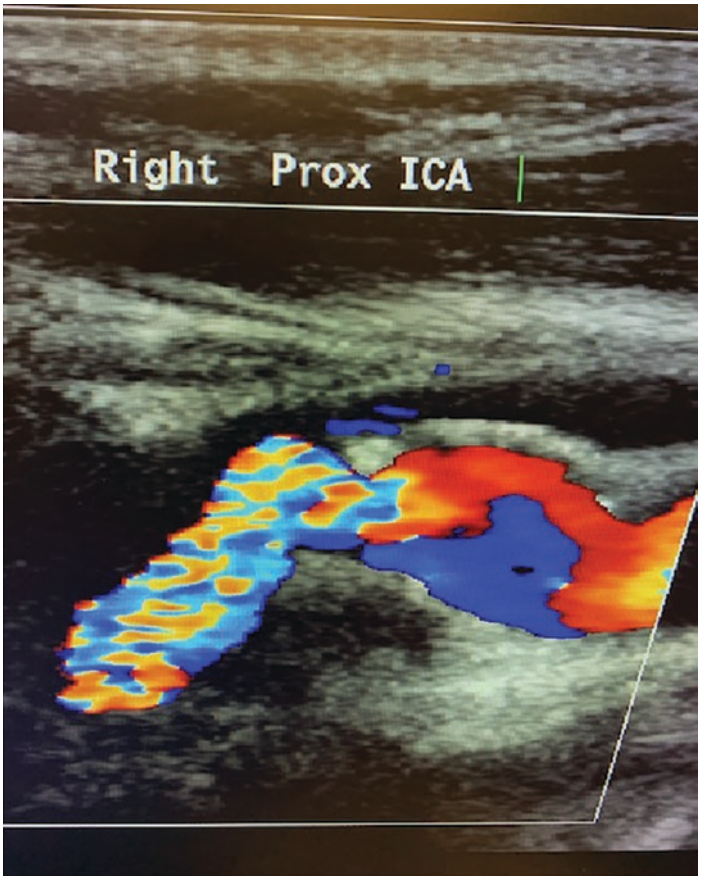

Fig. 8 ICA Stenosis – Color

- PSV of greater than or equal to 222 cm/s = greater than 50% stenosis
- PSV of greater than or equal to 325 cm/s = greater than 80% stenosis

Interpretation normally includes at minimum an estimate of the percent stenosis of the right and left carotid systems as well as a description of the plaque. Plaque may be described as being

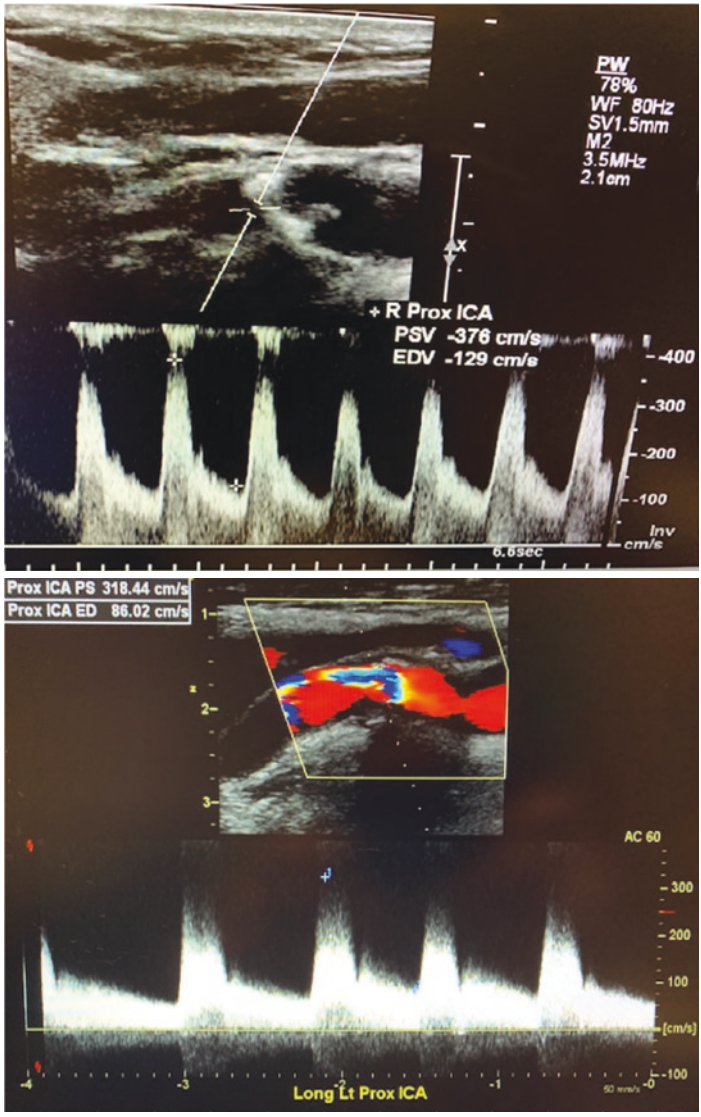

Figs. 9 and 10 Elevated velocities in the proximal ICA

Table 1 Society of Radiologists in ultrasound consensus criteria for carotid stenosis

Degree of stenosis, %	Primary parameters		Secondary parameters	
	ICAPSV, cm/s	Plaque estimate, %[a]	ICA/CCA PSV ratio	ICA EDV, cm/s
Normal	<125	None	<2.0	<40
<50	<125	<50	<2.0	<40
50–69	125–230	>50	2.0–4.0	40–100
≥70 but less than near occlusion	>230	>50	>4.0	>100
Near occlusion	High, low, or undetectable	Visible	Variable	Variable
Total occlusion	Undetectable	Visible, no detectable lumen	Not applicable	Not applicable

[a]Plaque estimate (diameter reduction) with grayscale and color Doppler ultrasound

homogenous (of similar characteristics or echogenicity), or heterogenous (of mixed characteristics or echogenicity) and whether the plaque surface is smooth or irregular in contour [3]. A comment should also be included on whether vertebral flow is absent, antegrade, retrograde or some variation.

The SRUCC criteria (Table 1) are among the most widely used for classification of carotid stenosis [4]. In October 2021 the Intersocietal Accreditation Commission (IAC) recommended modifications to the SRUCC velocity criteria [5]. The recommendation followed a more than 6 year study by IAC involving accredited labs validating the SRU's velocity criteria. In general, the study found that the SRU criteria tended to overestimate the degree of stenosis for moderate (50–69%) stenosis compared to angiography. The IAC recommended raising the PSV for 50–69% stenosis to 180 cm/s. Table 2 displays the revised criteria. Laboratories should perform center-specific validation studies by correlating results derived from ultrasonography with angiographic findings, to determine which criteria are most appropriate for their facility.

Table 2 Intersocietal Accreditation Commission (IAC) recommended modifications to the SRUCC velocity criteria

Degree of stenosis, %	Primary parameters		Secondary parameters	
	ICA PSV, cm/s	Plaque estimate, %[a]	ICA/CCA PSV ratio	ICA EDV, cm/s
Normal	<180	None	<2.0	<40
<50	<180	<50	<2.0	<40
50–69	180–230	>50	2.0–4.0	40–100
≥70 but less than near occlusion	>230	>50	>4.0	>100
Near occlusion	High, low, or undetectable	Visible	Variable	Variable
Total occlusion	Undetectable	Visible, no detectable lumen	Not applicable	Not applicable

[a]Plaque estimate (diameter reduction) with grayscale and color Doppler ultrasound

References

1. IAC Standards and guidelines for vascular testing accreditation. Intersocietal Accreditation Commission; 2020. p. 1–70.
2. Alexandrov AV. Neurovascular examination. Wiley Blackwell. West Sussex; 2013.
3. AbuRahma AF, Abu-Halimah S, Bensenhaver J, Scott Dean L, Keiffer T, Emmett M, Flaherty S. Optimal carotid duplex velocity criteria for defining the severity of carotid in-stent restenosis. J Vasc Surg. 2008;48:589–94.
4. Grant EG, Benson CB, Moneta GL, Alexandrov AV, Baker JD, Bluth EI, Carroll BA, Eliasziew M, Gocke J, Hertzberg BS, Katanick S, Needleman L, Pellerito J, Polak JF, Rholl KS, Wooster DL, Zierler RE. Carotid artery stenosis: gray-scale and Doppler US diagnosis – Society of Radiologists in Ultrasound Consensus Conference. Radiology. 2003;229:340–6.
5. Gornik HL, Rundek T, Gardener H, Benenati JF, Dahiya N, Hamburg NM, Kupinski AM, Leers SA, Lilly MP, Lohr JM, Pellerito JS, Rholl KS, Vickery MA, Hutchisson MS and Needleman L. Optimization of duplex velocity criteria for diagnosis of internal carotid artery (ICA) stenosis: a report of the Intersocietal Accreditation Commission (IAC) Vascular Testing Division Carotid Diagnostic Criteria Committee. Vasc Med. 2021:1358863X211011253.

Index

W. C. Ziai, C. L. Cornwell (eds.), *Neurovascular Sonography*,
https://doi.org/10.1007/978-3-030-96893-9